GROUNDWATER AND HEAT FLOW IN SOUTHEASTERN MANITOBA: IMPLICATIONS TO WATER SUPPLY AND THERMAL ENERGY

by

Grant Andrew George Ferguson

A Thesis
Submitted to the Faculty of Graduate Studies
In Partial Fulfillment of the Requirements for the Degree of

Doctor of Philosophy

Department of Civil Engineering
University of Manitoba
Winnipeg, Manitoba

2004

THE UNIVERSITY OF MANITOBA

FACULTY OF GRADUATE STUDIES
*****
COPYRIGHT PERMISSION

Groundwater and Heat Flow in Southeastern Manitoba:
Implications to Water Supply and Thermal Energy

BY

Grant Andrew George Ferguson

A Thesis/Practicum submitted to the Faculty of Graduate Studies of The University of

Manitoba in partial fulfillment of the requirement of the degree

Of

DOCTOR OF PHILOSOPHY

Grant Andrew George Ferguson © 2004

DEDICATION

This thesis is dedicated to my family, especially to my parents who have supported me throughout my education. They created an environment for me to learn from an early age and have always encouraged me in my education. My parents have instilled me with the work ethic and perseverance that I have needed to complete this thesis.

Dulcius ex asperis.

ACKNOWLEDGEMENTS

ABSTRACT

The study of groundwater and heat flow can provide an understanding of the sustainability of groundwater supplies and geothermal energy in southeastern Manitoba. In areas where temperatures are significantly altered by groundwater flow, it is sometimes possible to estimate specific discharges. This approach has been applied in the Sandilands region of southeastern Manitoba, which is a major recharge area to regional bedrock aquifers. Temperature data have been used to estimate recharge rates to these aquifers. Subsurface heat flow in the Winnipeg area was also of interest in this study due to the exploitation of the Carbonate Rock Aquifer for air conditioning and industrial cooling. Aquifer temperatures beneath the City of Winnipeg are currently several degrees Celsius greater than those found in surrounding rural areas. Numerical modeling conducted during this study indicates that increases in temperature of up to 5 °C can be attributed to heat loss from buildings. The bulk of this increase in temperatures occurs over the first few decades after building construction. Injection of thermal wastewater into the aquifer causes temperature increases of a similar magnitude, but the rate of temperature increase in the subsurface is much greater. In most thermal developments of the aquifer, the temperature at the production well increases by a few degrees Celsius in the first few years of operation. This increase in temperature makes current practises unsustainable and future development should include plans to prevent further increases in the temperature of the Carbonate Rock Aquifer.

TABLE OF CONTENTS

LIST OF TABLES

LIST OF FIGURES

LIST OF SYMBOLS AND ABBREVIATIONS

a	Fitting constant in Reiter's (2001) solution	Dimensionless
A	Average fluid potential	Pa
B	Fluid potential above average fluid potential at x = 0	Pa
c	Specific heat capacity	kJ kg^{-1} °C^{-1}
c_{cr}	Specific heat capacity of confining layer	kJ kg^{-1} °C^{-1}
c_f	Fluid specific heat capacity	kJ kg^{-1} °C^{-1}
c_r	Rock specific heat capacity	kJ kg^{-1} °C^{-1}
c_{sat}	Specific heat capacity of saturated porous medium	kJ kg^{-1} °C^{-1}
DCM	Dual continuum model	N/A
D	Distance between production and injection wells in a doublet	m
EPM	Equivalent porous media model	N/A
g	Acceleration due to gravity	m^2/s
GSC	Geological Survey of Canada	N/A
h	Hydraulic head	m
H	Aquifer thickness	m
H_e	Enthalpy	kJ kg^{-1}
j_o	Coefficient in Toth's (1962) solution	Dimensionless
j_i	Coefficient in Toth's (1962) solution	Dimensionless
K	Hydraulic conductivity	m s^{-1}
k	Permeability	m^2
L	Length	m
N	Number of fractures per unit distance	m^{-1}
N_{Pe}	Peclet number	Dimensionless
P	Pressure	kPa
q	Heat flux	W m^{-2}
$\hat{q}$	Mean heat flux	W m^{-2}
Q	Pumping rate	m^3 s^{-1} or L s^{-1}
$\overline{Q}$	Fluid source term	kg m^{-2} s^{-1}
r	Radius	m
REV	Representative elementary volume	N/A
RMS	Root mean square error	Units of associated measurement
S_s	Specific storage	m^{-1}
T	Temperature	°C
T'	Perturbation in temperature	°C
$\hat{T}$	Mean temperature	°C
T_{abs}	Absolute temperature	K
$T_{predicted}$	Temperature predicted by model	°C

T_o	Temperature at top of semi-confining layer	°C
$T_{observed}$	Observed temperature	°C
T_z	Temperature at a given depth of a semi-confining layer	°C
T_L	Temperature at the bottom of a semi-confining layer	°C
t	Time	s
u	Internal energy	kJ
v	Darcy flux (specific discharge)	m s^{-1}
V_i	Mass fraction of phase i present in a rock mass	Dimensionless
z	Elevation	m
z_o	Depth of basin	m
α	Volumetric coefficient of thermal expansion	°C^{-1}
β	Mass fraction of second phase present in a rock mass	Dimensionless
γ	Mass fraction of third phase present in a rock mass	Dimensionless
δ	Fractional change in temperature gradient	Dimensionless
Γ	Temperature gradient	°C m^{-1}
Γ_h	Vertical temperature gradient	°C m^{-1}
Γ_z	Horizontal temperature gradient	°C m^{-1}
$\Gamma_{z(critical)}$	Critical temperature gradient	°C m^{-1}
Φ	Fluid potential	m^2 s^{-2}
η	Porosity	Dimensionless
θ	Angle between aquifer and the horizontal	Degrees
Θ	Expected heat flux	W m^{-2}
κ	Thermal conductivity	W m^{-1} °C^{-1}
κ'	Perturbation in thermal conductivity	W m^{-1} °C^{-1}
$\hat{\kappa}$	Mean value of thermal conductivity	W m^{-1} °C^{-1}
κ_d	Effective thermal conductivity based on dispersed model	W m^{-1} °C^{-1}
κ_e	Effective thermal conductivity	W m^{-1} °C^{-1}
κ_p	Effective thermal based on parallel model	W m^{-1} °C^{-1}
κ_r	Rock thermal conductivity	W m^{-1} °C^{-1}
κ_s	Effective thermal conductivity based on series model	W m^{-1} °C^{-1}
μ	Viscosity	kg m^{-1} s^{-1}
μ_k	Kinematic viscosity	m^2 s^{-1}
ρ	Density	kg m^{-3}
ρ_{cr}	Density of geologic unit overlying an	kg m^{-3}

	aquifer	
ρ_f	Fluid density	kg m^{-3}
ρ_r	Density of rock	kg m^{-3}
ρ_{sat}	Density of saturated porous medium	kg m^{-3}
$\overline{\rho}_f$	Molar density of fluid	mols m^{-3}
σ	Mass fraction of first phase present in a rock mass	Dimensionless
ψ	Pressure head	m
λ	Thermal diffusivity	m^2 s^{-1}
∇	Del operator	N/A

CHAPTER 1: INTRODUCTION

1.1 General Overview

The subjects of heat flow and groundwater flow are linked in many environments and are of interest in a wide range of disciplines including hydrogeology, solid earth geophysics, climate change and geothermal energy development. The union of these two subjects occurs because of the capability of groundwater to transport heat and perturb the temperature distribution from a conductive temperature profile, which is typical in most geologic environments (Smith and Chapman, 1983). Understanding both heat transport and groundwater flow in southeastern Manitoba is important in assessing the sustainability of groundwater supplies and geothermal energy use in the area.

The quality and quantity of groundwater available is of interest in Manitoba due to quality concerns related to increased development in southeastern Manitoba (Betcher et al., 1995; Kennedy, 2002). Possible climate change scenarios have also raised questions about the sustainability of groundwater resources in Manitoba (e.g. Chen et al., 2002; Ferguson and St. George, 2003). These issues have increased the need for an improved understanding of groundwater flow systems in southeastern Manitoba and temperature measurements may provide valuable insight into these systems. The spatial variability of temperatures in the Winnipeg Formation and Carbonate Rock Aquifer in Manitoba could reveal important characteristics of the regional groundwater flow systems that they host and the sustainability of

current groundwater withdrawals. In the Sandilands area of southeastern Manitoba, traditional methods of estimating recharge rates to bedrock aquifers have been only marginally successful due to the depth of the aquifers and the age of the groundwater. Measuring temperature profiles and using these data to estimate Darcy velocities may provide a fast and cost effective method of determining the amount of recharge to the bedrock aquifers in this region.

Interest in groundwater as an energy source and an energy storage medium has grown in recent years due to increased concern for the environment and rising energy prices. Despite the renewed interest in geothermal energy and geothermal energy storage, little attention has been given to the design of open loop heat pumps and their impact on groundwater and heat flow in aquifers. In an open loop heat pump system, groundwater is extracted from an aquifer and passed through a heat exchanger. The resulting heated water (hereafter referred to as thermal wastewater) is then discharged to the aquifer, sewer or surface water body. In the Winnipeg area, groundwater is used for air conditioning and industrial cooling and in most cases the resulting thermal wastewater is injected back into the aquifer to prevent loss of hydraulic head and reduce stress on the City of Winnipeg's sewer system (Render, 1981; Render, 1983; Betcher et al., 1995). This practise has been occurring since the 1940's (Render, 1970) with little planning occurring during the initial stages of development. At that time, little was known about regional hydrogeology and heat flow in the region and

2

despite studies on both of these subjects during the past 60 years, the interplay between groundwater and heat flow has received only limited attention. Other sources of heat at the ground surface will also affect the subsurface temperature field and have an effect on geothermal resources in the Winnipeg area. These problems are somewhat different than those encountered in conventional geothermal reservoir engineering due to the relatively shallow depth of the aquifer involved and its use for cooling as opposed to heating. Heat loss from buildings also has the potential to significantly affect subsurface heat flow and can affect the efficiency of any thermal exploitation of groundwater. Climate change, from local to global scales, may also have an impact the sustainability of current thermal uses of groundwater in the Winnipeg area and throughout Canada.

1.2 Hypotheses and Objectives

1.2.1 Hypotheses

1. Background temperatures and heat fluxes in the subsurface of Manitoba are not significantly impacted by groundwater flow in most areas. However, vertical profiles of temperatures are capable of providing information on recharge rates in the Sandilands area.

2. The subsurface temperature field beneath Winnipeg has been significantly affected by heat losses from buildings. Smaller changes in temperature can be attributed to changes in surface cover and climate change.

3

3. The use of groundwater in cooling applications is largely unsustainable if current practises are maintained due to the inability of the aquifers to dissipate the introduced heat from thermal wastewater. The addition of heat in the subsurface due to heat losses from buildings, changes in surface cover and climate change are also decreasing the efficiency of groundwater as a coolant.

1.2.2 Objectives and Methodology

1. Background temperatures and heat flow in the Winnipeg area will be described. This will be accomplished by measuring temperature profiles in monitoring wells in this area and estimating heat flow rates from these measured profiles and measurements of thermal conductivity. Simple models will be used to explain the impact of regional aquifers on the background heat flow. Darcy velocities will be estimated from temperature profiles where simple inversion techniques are applicable. A particular area of interest is the Sandilands Moraine, which is known to be an important recharge area to regional bedrock aquifers in southeastern Manitoba.

2. Subsurface temperature changes associated with heat loss from buildings will be estimated. This will be accomplished by creating generic numerical models using geology typical of the Winnipeg area along with typical hydrogeologic and thermal parameters. The results of these generic models will be compared with temperature profiles in the Winnipeg area.

4

3. The sustainability of current practises using groundwater as a coolant in the Winnipeg area will be examined using analytical and numerical models. This endeavour will involve a sensitivity analysis describing the effects of variations in thermal and hydrogeologic parameters. The impact of regional groundwater flow will also be studied though numerical modeling. Numerical models of groundwater and heat flow will also be created for specific areas of Winnipeg to determine if the results of the synthetic models are reasonable.

CHAPTER 2: REVIEW OF GROUNDWATER AND HEAT FLOW

2.1 Groundwater Flow

2.1.1 Darcy's Law

Groundwater flow in porous media is described by Darcy's Law, which can be stated as the following in the case of vertical flow:

$$v_z = -K \frac{\partial h}{\partial z} \qquad (2.1)$$

where v_z is the specific discharge, K is hydraulic conductivity and h is hydraulic head (Freeze and Cherry, 1979). Hydraulic conductivity can be described mathematically as follows:

$$K = \frac{k \rho_f g}{\mu} \qquad (2.2)$$

where k is permeability, ρ_f is fluid density, g is acceleration due to gravity and μ is viscosity (Hubbert, 1956). Hydraulic conductivity is dependent on the temperature of the fluid involved, because of the relationships between temperature each of and fluid density and fluid viscosity. Hydraulic conductivity is a scale-dependent macroscopic property and is only applicable if a large enough volume of the porous media is examined. The minimum volume required to apply the concept of hydraulic conductivity is normally termed the representative elementary volume (REV) (Bear, 1972).

2.1.2 Hydraulic Head and Fluid Potential

The concept of hydraulic head was arrived at empirically in Darcy's experiment and it was not until a century later that Hubbert (1956) explained this concept from first principles. Working in terms of fluid potential (Φ), Hubbert (1940) provided the following relationship:

$$\Phi = gz + \frac{P}{\rho_f} \quad (2.3)$$

where z is the elevation above a datum or elevation head and P is gauge pressure. Dividing this equation through by g, the following relationship is obtained:

$$h = z + \frac{P}{\rho_f g} = z + \psi \quad (2.4)$$

where ψ is pressure head (Freeze and Cherry, 1979).

2.1.3 Differential Equations Describing Groundwater Flow

The differential equation describing transient groundwater flow in an anisotropic saturated porous medium is:

$$\frac{\partial}{\partial x}\left(K_{xx}\frac{\partial h}{\partial x}\right) + \frac{\partial}{\partial y}\left(K_{yy}\frac{\partial h}{\partial y}\right) + \frac{\partial}{\partial z}\left(K_{zz}\frac{\partial h}{\partial x}\right) = S_s \frac{\partial h}{\partial t} \quad (2.5)$$

where K_{xx}, K_{yy} and K_{zz} are the components of the hydraulic conductivity tensor in the principle directions of the coordinate system and S_s is specific storage. Specific storage is defined as the volume of water that a unit volume of aquifer releases from storage under a unit decline in hydraulic head (Freeze and Cherry, 1979). Equation 2.5 assumes that anisotropy in hydraulic conductivity is aligned with the co-ordinate system. Changes in hydraulic

conductivity due to changes in temperature can be accounted for in this equation but the role of buoyancy forces cannot be described by this form. A more general form of the groundwater flow equation for non-isothermal conditions can be written for the three-dimensional case as:

$$\nabla \cdot \left[\frac{k\rho_f}{\mu} \left(\nabla P + \rho_f g \nabla z \right) \right] = \frac{\partial (\eta \rho_f)}{\partial t} \quad (2.6)$$

where ∇ is the del operator, P is pressure and η is porosity (e.g. Bear, 1972).

2.2 Heat Flow

2.2.1 Heat Transfer Mechanisms

Heat transfer in geological environments occurs by conduction, advection and radiation. These three mechanisms are all important in porous media but only conduction and advection are of interest in this study as radiation only becomes important at extremely high temperatures and at the ground-atmosphere interface.

Conductive heat transfer occurs due to crystal lattice interactions (Schon, 1996) and for vertical conduction this is described by Fourier's Law (eg. Jessop, 1990)

$$q_z = -\kappa \frac{\partial T}{\partial z} \quad (2.7)$$

where q_z is heat flux, κ is the thermal conductivity of the material and T is temperature. The differential equation describing conductive flow of heat in a solid is given by Carslaw and Jaeger (1959) as:

8

$$\frac{\partial^2 T}{\partial^2 x} + \frac{\partial^2 T}{\partial^2 y} + \frac{\partial^2 T}{\partial^2 z} = \frac{c_r \rho_r}{\kappa} \frac{\partial T}{\partial t} \quad (2.8)$$

where c_r is specific heat capacity and ρ_r is density of the solid.

The thermal conductivity of a material describes the ability of a substance to conduct heat. Conduction occurs by two fundamental processes: 1) electron-conductivity; and 2) lattice-conductivity (Schon, 1996). In silicates and most rocks, lattice-conductivity is dominant (Horai, 1971). Lattice-conduction occurs due to motions of the crystal lattice and this is related to the mineral composition of the rock.

Many sedimentary rocks, such as limestone and sandstone, are sufficiently porous that fluids occupying the pore spaces significantly alter the thermal conductivity of the medium. In these cases, the bulk thermal conductivity at the REV scale can be calculated as follows:

$$\kappa_e = \eta \kappa_f + (1 - \eta)\kappa_r \quad (2.9)$$

where κ_e is bulk thermal conductivity, κ_f is the thermal conductivity of the fluid and κ_r is the thermal conductivity of the solid (Slattery, 1972). Several other models describing the effective thermal conductivity of a composite medium exist and several of these models will be discussed in Chapter 4.

Advective heat transfer occurs when heat is transported by the relative motion of portions of the heated body (Schon, 1996). In the case of fluid flow in a porous media, heat can be transported with the moving fluid as a result of hydraulic gradients. This process can occur independently of temperature gradients and is often referred to as forced convection. Heat transport can

also occur by free or natural convection, which occurs when fluid motion occurs due to density differences that arise due to temperature gradients.

Stallman (1963) proposed a differential equation that describes the flow of heat in a porous medium. This can be written for three dimensional flow of groundwater and heat in a homogeneous media as:

$$\kappa_e \left[\frac{\partial^2 T}{\partial x^2} + \frac{\partial^2 T}{\partial y^2} + \frac{\partial^2 T}{\partial z^2} \right] - \frac{c_f \rho_f}{\kappa_e} \left[\frac{\partial(v_x T)}{\partial x} + \frac{\partial(v_y T)}{\partial y} + \frac{\partial(v_z T)}{\partial z} \right] = c_{sat} \rho_{sat} \frac{\partial T}{\partial t} \qquad (2.10)$$

where T is temperature, c_f is the specific heat of water, ρ_f is the density of water, v_x, v_y and v_z are the x, y and z components of specific discharge, c_{sat} is the specific heat capacity of the saturated porous medium and ρ_{sat} is the density of the saturated porous medium. Equation 2.10 assumes that there is no difference in temperature between solid and fluid phases. This state is commonly referred to as thermal equilibrium. In equation 2.10 the first term is the conductive component of heat flow, the second is the advective component, and the term on the right hand side of the equation describes heat storage in the geologic medium.

2.2.2 Heat Flow in Geological Environments

Since the 18th century, it has been recognized that heat flows to the surface of the Earth from the Earth's interior (Bullard, 1965). This heat originates primarily from the cooling of the Earth since its original accretion 4.5 billion years ago and by decay of radioactive isotopes of potassium, uranium and thorium within the Earth's crust (e.g. Lowrie, 1997). Calculation of heat flow values began in the early 20th century with the advent of thermal

conductivity measurements. Heat flow rates vary from 20 to 90 mW m^{-2} over most areas of the Earth, except in areas of extreme heat flow as found in areas of active tectonism and over hot spots (Pollack et al., 1993). The heat flow value for an area is related to the type and age of the given geological environment, with Precambrian cratons tending to have the lowest heat flow rates and young sedimentary basins tending to have higher heat flow rates (Jessop, 1990).

2.2.3 Measurement of Subsurface Temperatures

Care must be taken to ensure that temperatures measured in boreholes and wells are representative of the surrounding geologic formations. Mechanisms that can lead to deviation between the temperature in the borehole or well and the surrounding formation include: 1) free convection within the well; 2) hydraulic, and thus thermal, short circuiting of the well; and 3) presence of disequilibrium conditions due disturbances to the fluid column, drilling or the setting of grout around the well casing.

Hales (1937) provides the following equation to determine the critical geothermal gradient required for the onset of free convection within a borehole:

$$\Gamma_{z(critical)} = \frac{g\alpha T_{abs}}{c_f} + \frac{B\mu_k\lambda}{g\alpha r^4} \quad (2.11)$$

where $\Gamma_{zcritical}$ is the critical geothermal gradient, g is acceleration due to gravity, α is the volume coefficient of thermal expansion, T_{abs} is absolute temperature, B is a constant (216 for wells where the depth is much greater

than the diameter of the well), μ_k is kinematic viscosity, λ is thermal diffusivity of the fluid and r is the radius of the well. Gretener (1967) suggested that this critical value is actually too low in most cases because many wells with geothermal gradients greater than the critical geothermal gradient are stable for practical purposes.

Short circuiting of fluid with a well occurs when fluid flow results from the connection of otherwise unconnected fractures or permeable zones in the geologic section; the connection occurring as a result of drilling a vertical conduit that acts to connect the naturally separated zones. This fluid flow can cause an unnatural flow of heat by advection, which causes a deviation from the background temperature field. In instances where the well has been cased off, this effect can be minimised by sealing the annulus of wells with bentonite to prevent flow along the outside of the casing. Disequilibrium in the thermal state of boreholes can be caused by various mechanisms. Drilling introduces a significant amount of heat into the ground and this may take several months to dissipate (Gretener, 1981).

Proper temperature logging equipment and logging techniques are also required to obtain high quality temperature data. Temperature measurements made during this research were conducted with a Seabird™ SBE38 digital temperature probe with an overall resolution of ±0.00025 °C and an accuracy of ±0.001 °C in the range of -5 to 35 °C. The temperature measurements made by this probe are digitized downhole and received by a personal computer at the surface. This accuracy provided by this equipment

is beyond the level of stability that can be expected within a borehole (Gretener, 1967). The digitization of temperatures at depth by the SB38 and this ensures that the there is no distortion of an analog signal along the length of the cable. To ensure accurate temperature measurements, readings must be taken as the instrument is being lowered through the water column. This procedure minimises disturbances in the temperature profile that occur due to agitation of the water column upon advancement of the probe.

2.3 Modeling Groundwater and Heat Flow

2.3.1 General Modeling Philosophy

Groundwater modeling, although a relatively new field in the geological sciences and engineering, has had a number of protocols proposed during the last decade outlining the method for creating groundwater models (e.g. Anderson and Woessner, 1992; Spitz and Moreno, 1996). Although these protocols were provided for use in groundwater flow modeling and contaminant transport, they are equally applicable to heat flow.

Establishing a purpose is the first issue that must be addressed in the creation of any hydrogeologic model. The purpose of the modeling exercise will establish the level of accuracy required, and thus, the detail needed in the model.

Following this, the creation of a conceptual model is the second step in the creation of a hydrogeological model. The hydrogeological model provides a summary of the hydrogeologic data available, combined with a geological interpretation. This allows hydraulic properties to be assigned to

hydrostratigraphic units, which are assigned shapes and thicknesses in the model. Boundary conditions must also be assigned to the edges of the model. Assigning boundary conditions to positions within the model, such as wells, is also possible. There are three boundary conditions that are available for use in groundwater modeling: Dirichlet or specified head boundary conditions; Neuman or specified flux boundary conditions, and Cauchy or mixed boundary conditions (Anderson and Woessner, 1992). These are also applicable to heat flow models as specified temperature (Dirichlet) and specified heat flux boundaries (Neuman). Temperature-dependent flux boundary conditions (Cauchy) are also possible but are not typically used.

Following the creation of the conceptual model, a mathematical model must be chosen to solve the governing differential equations. Both analytical and numerical methods are available to perform this task. Analytical models generally offer a much faster calculation and have the advantage of producing continuous solutions. However, analytical solutions are restricted to simple boundary conditions and sources and sinks, homogeneous material properties and idealized problem geometries.

Numerical models are much more flexible, allowing for variations in boundary conditions and sources and sinks, heterogeneous material properties and complex geometries. Numerical models provide a piecewise solution; solving for the required potential, such as head or temperature, at discrete points within the model domain. These drawbacks are usually

outweighed by the ability of numerical models to more accurately examine complex problems.

Once the mathematical model is created, it must be calibrated. Calibration is generally accomplished by using a trial-and-error technique in which model parameters are varied within acceptable ranges to produce a match between the model results and observations. The match is evaluated using a predetermined calibration criterion and once this condition is met the model is deemed to be calibrated. The most commonly used calibration criterion is the root mean square error of the model (Anderson and Woessner, 1992). The R^2 calibration coefficient of the best fit line of a scatterplot of observed and modeled values also provides a measure of model accuracy. Ideally, the regressed line should have a slope of one and an intercept of zero and if it is significantly different from this ideal case, it may indicate short-comings in the model. In this study, differences between the regressed line and the ideal fit will be assessed at 95% confidence level. However, results that indicate that the regressed line is significantly different do not necessarily constitute a failure to calibrate the model.

A calibrated model must be validated before it can be used in a predictive manner. This can be accomplished by comparing the calibrated model's performance against a second set of observations or by a select number of observations that have been withheld from the dataset used for calibration. This process helps to establish that the model reacts in the same way that the natural system does to a given "stress" that the natural system

15

does. However, it should be noted that a model cannot ever be validated for every possible stress (Bredehoeft and Konikow, 1993). In reality, it is only possible to invalidate a model.

2.3.2 Modeling Flow in Fractured Rock

Groundwater flow in fractured rock can be treated in various manners in accordance with the scale examined and the degree of uniformity in the fracture system. Bear (1993) suggested that four levels of study are possible in fractured geological bodies: 1) the very near field, where interest is focused on an individual fracture and possibly the adjacent porous block; 2) the near field, where flow is considered in a relatively small domain that consists of a few well defined fractures; 3) the far field, where flow can be visualized as occurring in two overlapping media; a network of fractures and a series of porous blocks, known as the dual continuum approach; and 4) the very far field, where the entire fractured porous medium can be treated as a single continuum, also known as the equivalent porous medium approach. This idea was further simplified by Berkowitz (2002), who suggested that all models fall under the two broad categories of discrete fracture models or continuum models. Discrete fracture models can explicitly account for the effects of an individual fracture on fluid flow or transport. These types of models are generally applied to very near field and near field problems, where fracture locations and properties can be at least moderately constrained. These models require a great deal of data for calibration purposes.

16

Continuum models can be used where a fracture network is dense and an REV can be defined. This group of models includes equivalent porous media models (EPMs) or single continuum models and dual continuum models (DCMs), which are commonly applied to far field and very far field problems. These approaches cease to be valid in cases where the fracture network is not well connected and where a REV cannot be defined.

Stochastic models have been useful in some of these cases. It should also be recognized that fracture permeabilities are heterogeneous in most situations. Stochastic treatments have provided valuable insight into the behaviour of transport in a medium where a spectrum of fracture permeabilities exist (Doughty and Karasaki, 2002). Stochastic modeling of fractured rock is not currently common practice and will not be examined in this thesis.

In cases where it is possible to treat the fractured medium as an equivalent porous medium approach, the equilvalent or bulk hydraulic conductivity of the fractured media, based on the premise that a set of planar fractures exist, can be written as follows:

$$K = \frac{\rho_f g N b^3}{12\mu} \qquad (2.12)$$

where N is the number of fractures per unit distance across the face of the rock mass and b is the fracture aperture (Snow, 1968). This equation can be used to describe the equivalent hydraulic conductivity (or permeability) of an aquifer where groundwater flow is parallel to a set of planar fractures.

2.3.3 Modeling Subsurface Heat Transport

Subsurface heat transport models solve for the temperature field by considering the governing equation for heat transport (equation 2.10). However, groundwater velocities, which are obtained by solving for the hydraulic head field, are required in the solution of equation 2.10. In cases where density and viscosity do not vary appreciably, it may be possible to have a decoupled model where groundwater flow and heat flow are dealt with separately. However, many applications do not allow for this assumption and the solutions to 2.6 and 2.10 must be coupled to provide an accurate solution.

2.3.4 MULTIFLO/METRA

Numerical models created in this study used METRA, which is a submodule of the MULTIFLO program developed by Lichtner et al. (2000). METRA is a three-dimensional nonisothermal flow simulator that allows for heat flow by advection and/or conduction. METRA solves mass balance equations for water and air, and energy. In this thesis, only saturated conditions are considered and the governing equations for mass balance and energy balance simplify considerably over the more general equations given by Lichtner (2000). The equation for total mass balance can be written as follows:

$$\frac{\partial}{\partial t}\left[\eta \bar{\rho}_f\right] + \nabla \bullet \left[v\bar{\rho}_f\right] = \bar{Q} \qquad (2.13)$$

where $\bar{\rho}_f$ is the molar density of water and $\bar{Q}$ is a fluid source term. The simplified energy balance equation is:

$$\frac{\partial}{\partial t}\left[\eta \overline{\rho}_f u\right] + \nabla \bullet \left[v \overline{\rho}_f H_e\right] + \frac{\partial}{\partial t}\left[(1-\eta)c_r \rho_r T\right] = \nabla \bullet \kappa \nabla T + E \quad (2.14)$$

where u is internal energy, H_e is enthalpy, c_r is the specific heat capacity of the rock, ρ_r is the density of the rock and E is an energy source term. MULTILFLO uses a fully-implicit integral-finite volume approach to solve these equations and uses a block centred grid for the discretisation of the model domain. The code solves the governing equations for groundwater flow and heat flow iteratively so that the appropriate fluid density and viscosity are used in each cell of the model. Thus, heat and groundwater flow are coupled.

METRA is capable of using all boundary conditions for fluid flow but it is somewhat limited in how heat flow boundary conditions are specified. Specified temperature boundary conditions are possible but only in conjunction with specified pressure boundary conditions. Specified heat flux boundary conditions cannot be declared explicitly in the model. Sources and sinks can be specified for an input or extraction of a given amount of energy or mass of water and its associated energy.

METRA's correctness has been verified through its use at the Southwest Research Institute. The code has been used to study the flow of solutes, heat and groundwater near Yucca Mountain, Nevada (Lichtner, 1996; Painter et al., 2001), where the United States plans to dispose of nuclear waste. During the current study, METRA was further verified by comparing its results to well known analytical solutions, such as the solutions to equation 2.10 provided for steady-state conditions in one dimension (Bredehoeft and Papadopulos, 1965) and two dimensions (Domenico and Palciauskas, 1973).

Simulations produced by METRA can be based on either conventional porous media or dual continuum approaches. The dual continuum approach in METRA is a dual permeability approach where fluid flow is allowed in both the fractures and the matrix blocks. This is implemented in the programs through the use of two discrete continua that are represented by two overlapping grid blocks at each node in space. The input parameters required by METRA in this formulation are the fracture volume and the matrix block dimensions. The fracture aperture and interfacial surface areas are calculated from these parameters through a series of equations described by Lichtner (2000). Darcy's law is used to model fluid flow in the fractures of the dual continuum models and thus modeling of fractures that deviate from the assumptions of Darcy's law is not possible.

CHAPTER 3: GEOLOGY, HYDROGEOLOGY AND HEAT FLOW IN SOUTHEASTERN MANITOBA

3.1 Geological Environment of Southeastern Manitoba

3.1.1 Precambrian Geology

The Precambrian rocks forming the Canadian Shield, which is exposed in eastern and northern Manitoba (Figure 3.1), also extends beneath the Phanerozoic sedimentary rocks found in the Prairie Provinces of Canada. Beneath much of southern Manitoba, these rocks are Archean in age and belong to the Superior Province of the Canadian Shield (Card and Poulsen, 1998).

Precambrian rocks of the Canadian Shield outcrop approximately 80 kilometres east of Winnipeg (Figure 3.2) and occur at a depth of 150 to 180 metres beneath the City of Winnipeg (Figure 3.3). In this area, these rocks consist of granitic gneisses and granite (McCabe, 1971). Overlying the Precambrian basement throughout southeastern Manitoba is a number of Paleozoic sedimentary units that dip gently to the southwest at a rate of approximately 5 metres per kilometre (McCabe, 1971).

3.1.2 Phanerozoic Bedrock Geology

The eastern edge of the Western Canada Sedimentary Basin (WCSB) occurs in southeastern Manitoba (Figure 3.4). The WCSB is the general name given to a wedge of sedimentary rocks extending from the Canadian Shield to the Rocky Mountains, with the deepest part of the basin occurring in the west. The WCSB contains two major sub-basins, the Alberta Basin and

the Williston Basin, which are separated by the Sweetgrass Arch (Osadetz and Haidl, 1989). The Williston Basin is centred in southeastern Saskatchewan and northern North Dakota and extends over much of southern Manitoba, Saskatchewan, southeastern Alberta and into the adjacent areas of the United States as far south as Wyoming and South Dakota. In the centre of the basin in northern North Dakota, the total thickness of sediments exceeds 4500 metres (Porter et al., 1982).

In Manitoba, the Williston Basin consists of sedimentary rocks ranging in age from Cambrian to Tertiary (Figure 3.5), but most formations were deposited between the Ordovician Period and the Devonian Period (McCabe, 1971). The basal unit present in the area is the Winnipeg Formation, which consists of sandstone and shale deposited during an expansion of the Williston Basin during the early Ordovician Period. The Winnipeg Formation ranges up to 50 metres in thickness (McCabe, 1978). Beneath Winnipeg, this formation consists of a lower sandstone unit, an intermediate shale unit and an upper sandstone unit. Also, a layer of shale that is thought to be laterally continuous, occurs at the top of the Winnipeg Formation and this unit acts as a hydraulic barrier, separating the sandstones from the overlying Paleozoic carbonate rocks.

The Winnipeg Formation is overlain by the Red River Formation, which is the first in a series of carbonate-evaporite sequences that were deposited between the middle Ordovician and the Devonian Periods. The units of this sequence are formally referred to as the Bighorn Group (Osadetz and Haidl,

22

1989). The Red River Formation is up to 170 metres thick beneath Winnipeg and forms the uppermost bedrock unit in an area extending from the Sandilands area to the an area beneath western Winnipeg, where it is overlain by the Stony Mountain Formation. Paleokarst features are present in many areas of the Red River Formation (Render, 1970; Ford, 1984). The Stony Mountain Formation, which overlies the Red River Formation, is also an Ordovician carbonate unit. This unit is the uppermost bedrock unit throughout the western portion of the Winnipeg area, except where it is overlain by the Amaranth Formation, a Jurassic shale unit (McCabe, 1971).

3.1.3 Surficial Geology

Quaternary sediments dominate the surficial geology of southern Manitoba. These sediments include tills and glaciofluvial sediments deposited during the Wisconsinan Glaciation, glaciolacustrine sediments deposited by Lake Agassiz and alluvium and organic sediments deposited during the Holocene.

During the late Wisconsinan Glaciation, the Laurentide and Keewatin Ice Sheets advanced across Manitoba from the northeast and northwest respectively (Teller and Fenton, 1980). During this time, till was deposited over the bedrock formations in most of southern Manitoba (Teller and Fenton, 1980). These tills have thicknesses ranging from 1 to 50 metres beneath Winnipeg but are approximately 5 metres thick on average (Render, 1970). In the Winnipeg area, the tills are dominated by silt-sized particles and are

derived primarily from the Paleozoic and Mesozoic rocks located to the northwest of Winnipeg (Teller and Fenton, 1980).

Near the end of the Wisconsinan Glaciation, several glaciofluvial complexes were formed in the vicinity of the boundary between the Canadian Shield and the Williston Basin, including the Sandilands Interlobate Moraine, the Belair Moraine and the Birds Hill glaciofluvial complex, and a large buried esker north of the Sandilands moraine.

Lake Agassiz was formed at the end of the last glaciation as glacial meltwater was impounded by ice sheet to the north (Teller and Clayton, 1983). During this time, large thicknesses of clay and silt were deposited in southern Manitoba, forming an aquitard over the sedimentary bedrock aquifers of the area. These clay deposits have been divided into a lower unit consisting of unweathered massive clay and an upper unit consisting of weathered silty clay (Teller and Clayton, 1983). Pach (1994) also noted this distinction based on hydrogeological properties.

3.2 Hydrogeology of Southeastern Manitoba

3.2.1 Hydrogeology of the Western Canada Sedimentary Basin

The regional hydrogeology of southeastern Manitoba cannot be completely understood without looking beyond Manitoba's borders to examine the hydrogeology of the WCSB as a whole. Although smaller-scale regional flow systems are present east of the Red River and in the Interlake area, west of Winnipeg groundwater flow emanates from areas in the western and southwestern portions of the Williston Basin. Recharge areas include the

Cypress Hills in Saskatchewan (Hitchon, 1969) and the Black Hills area of South Dakota and Wyoming (Grasby et al., 2000). The Paleozoic carbonate units found in Manitoba are continuous to this area, as is the basal clastic unit that includes the Winnipeg Formation (Simpson et al., 1987; Grasby et al., 2000).

3.2.2 Winnipeg Formation Sandstone Aquifer

The basal aquifer in southeastern Manitoba is the sandstone aquifer of the Winnipeg Formation. This aquifer has transmissivities ranging from 3.6 x 10^{-2} to 5.2 x 10^{-5} m²/s but this aquifer is not used in the Winnipeg area for domestic or agricultural water supply because it contains saline water flowing up dip from deeper areas of the Williston Basin to the west (Figure 3.3; Betcher, 1986). To the east of the Red River, this aquifer contains freshwater resulting from both modern and late Pleistocene recharge (Betcher, 1986; Grasby et al., 2000). This aquifer is currently recharged where it subcrops beneath several glaciofluvial complexes in southeastern Manitoba (Betcher, 1986).

3.2.3 Carbonate Rock Aquifer

The Paleozoic carbonate formations of southern Manitoba form a regional aquifer that is often referred to as the Carbonate Rock Aquifer. In the Winnipeg area the Carbonate Rock Aquifer is often divided into two regional aquifers, known locally as the Lower Carbonate Aquifer and Upper Carbonate Aquifer. The Lower Carbonate Aquifer occurs in the lower 7.5 to

15 metres of the Red River Formation and generally has a low transmissivity (Render, 1970). This aquifer contains marginal quality water in the Winnipeg area and is generally not used for water supply, except to supplement the capacity of industrial wells. The Upper Carbonate Aquifer is the primary aquifer for groundwater supply in the Winnipeg area. Kennedy (2002) reported a mean transmissivity of 7.4×10^{-4} m^2/s for the Carbonate Rock Aquifer based on 2711 measurements throughout southern Manitoba. However, Kennedy (2002) also showed that the transmissivity in the Winnipeg area is above the mean value for the aquifer, with transmissivities exceeding 4.1×10^{-3} m^2/s in most areas. In a detailed study of the Carbonate Rock Aquifer in the Winnipeg area, Render (1970) reports transmissivities ranging from 2.9×10^{-2} m^2/s to 2.9 m^2/s in the Winnipeg area. The highest permeabilities occur in regions where the carbonate rock is extensively fractured and jointed or where solution channels exist (Render, 1970). The majority of groundwater production in high yield wells comes from one or more discrete fractures or solution features, ranging from 3 centimetres to greater than 30 centimetres in aperture (McCabe et al. 1993). In the Upper Carbonate Aquifer, the fracture network generally consists of orthogonal fractures spaced at approximately 1 metre in every direction (Render, 1970). These fractures are generally thought to occupy approximately 5% of the total rock mass (Render, 1970; Kennedy, 2002).

The clays and tills overlying the Upper Carbonate Aquifer in the Winnipeg area act as a semi-confining layer. The Upper Carbonate Aquifer

receives some recharge through these sediments, largely through fractures (Day, 1977; Pach, 1994). Most recharge to the Upper Carbonate Aquifer occurs through the thin layer of till in the Interlake area, through the coarse grained tills and glaciofluvial sediments east of Winnipeg and through the Birds Hill glaciofluvial complex northeast of Winnipeg (Render, 1970). Recharge from these areas is the source of the freshwater found in the Carbonate Rock Aquifer to the east and north of Winnipeg. Saline waters exist to the west of Winnipeg as a result of water flowing up dip from deep within the Williston Basin (Grasby and Betcher, 2002). The Red River is approximately coincident with the transition from fresh to saline groundwater in the Upper Carbonate Aquifer, as it defines a discharge area for waters flowing from both the east and west (Render, 1970; Grasby and Betcher, 2002; Kennedy, 2002).

3.3 Heat Flow in Southeastern Manitoba

3.3.1 Background Heat Flow and Climate

Jessop and Judge (1971) reported a heat flow of 35 mW m^{-2} in the Precambrian basement beneath Winnipeg based on temperatures measured from a deep borehole beneath the University of Manitoba campus and corresponding thermal conductivity measurements (Figure 3.6). This value is low but typical of older Precambrian environments (Lowrie, 1997). The geothermal gradient found in the Precambrian rocks at this location beneath Winnipeg is approximately 0.01°C m^{-1}. There has been essentially no prior heat flow research performed on the Phanerozoic units in the Winnipeg area.

However, there have been a large number of heat flow investigations performed in parts of the Williston Basin further west, especially in areas of known hydrocarbon reserves (e.g. Majorowicz and Jessop, 1981). Heat flow rates in southwestern Manitoba and southeastern Saskatchewan are much greater than those observed in the Winnipeg area, with values as high as 84 mW m^{-2} observed near Weyburn, Saskatchewan (Majorowicz and Jessop, 1981). These heat flow estimates are based on thermal conductivity estimates and temperature measurements made in geologic formations that are of Mississippian age. In a geothermal study beneath Regina, Saskatchewan, the temperature of the Winnipeg Formation was found to be approximately 85 °C (Hutchence et al., 1986). This temperature is significantly higher than the Winnipeg Formation beneath Winnipeg. There is a gap between the oil producing area near Virden and Wascada in southwestern Manitoba and Winnipeg where no heat flow estimates exist. Unfortunately, the transition from relatively high heat flow values to low heat flow values occurs in this area. No firm data exists to determine the location of this transition but Majorowicz and Jessop (1981) suggest that it may correspond to the boundary between the Churchill and Superior Provinces in the Precambrian basement. They also provide references to other types of geophysical evidence, such as the existence of a low velocity layer and a zone of low electrical conductivity at a depth of approximately 40 kilometres.

Temperatures in the tills and glaciolacustrine clays in the Winnipeg area are affected by seasonal variations in surface temperatures, as are

temperatures in the Upper Carbonate Aquifer in some areas in the northwestern portion of the city. This aquifer is occurs at a much shallower depth in this part of the city than in other areas. The mean annual air temperature in the Winnipeg area is 2.3°C and the overall range of temperatures seen throughout the year is quite large, with a mean temperature of 19.5°C during July and a mean temperature of -17.8°C during January. In an average winter, the depth of frost penetration is approximately 1.8 meters in the Winnipeg area (Baracos et al., 1983).

3.3.2 Climate Change in Manitoba

Climate change may also contribute to increases in subsurface temperatures, as the mean annual temperature has increased by approximately 1.0 °C over the last century (Figure 3.7). Results of the Canadian Coupled Climate Model suggest that the global mean temperature will increase between 1.4 and 5.8 °C over the next century based on coupled general circulation models, simple climate models and various emission scenarios (McBean et al., 2001). Further heat loading to the subsurface will occur based on the amount of increase in surface temperature.

In a study of borehole temperatures in northern Manitoba and northern Saskatchewan, inversion of the borehole temperatures to estimate past ground surface temperatures suggested that there has been a warming trend beginning in approximately 1920 was noted (Guillou-Frottier et al., 1998). The inversions from the same study showed a cooling trend from approximately 1400 to 1800, corresponding to the Little Ice Age, followed by

29

an increase back to the estimated temperature in 1400 by the beginning of the 20th century. A study using 246 sites across Canada by Beltrami et al. (2003) found that ground surface temperatures generally increased in Canada over the last century. However, the magnitude and timing of this increase varied with location. No temperature profiles in that study corresponded to the area of the current study. In a study in North Dakota and two boreholes in the Turtle Mountain area of southwestern Manitoba, Harris and Gosnold (1998) reported a rise of 1.5 °C in ground surface temperatures over the past century but warn that this rise in ground surface temperature does not necessarily have a direct linear relationship with air temperatures. The relationship between ground surface temperatures and air temperatures is an area of active research (e.g. Schmidt et al., 2001; Beltrami, 2001). Changes in surface cover due to agriculture and forestry may have caused an increase in ground surface temperature over the past century (e.g Lewis and Wang, 1998). These changes in surface cover change the amount of solar radiation that an area received and also affect the amount of evapotranspiration, and thus the relative humidity and groundwater flow. Advective effects must also be considered in the relationship between ground surface temperatures and air temperatures. The presence of thick units of relatively permeable tills and highly permeable sands and gravels in some areas of southeastern Manitoba may have a pronounced effect on the relationship between subsurface temperatures and air temperatures.

3.3.3 Anthropogenic Heat Loading

Anomalously high subsurface temperatures have been measured beneath Winnipeg, Manitoba since the early 1980's (Render, 1981; Render, 1983). One of the primary causes for increases in subsurface temperatures is the non-consumptive use of groundwater from the Upper Carbonate Aquifer in air conditioning and industrial cooling, where thermal wastewater is injected back into the aquifer to prevent excessive drawdown. The injection of this warm water has resulted in the creation of plumes of warm water in the Upper Carbonate Aquifer (Render, 1983).

3.4 Summary

The bedrock geology of southeastern Manitoba is characterized by Paleozoic sediments that overlie a Precambrian Basement. The Winnipeg Formation, which is the basal sedimentary unit in the region, forms an extensive sandstone aquifer. The carbonate rocks that overlie the Winnipeg Formation also contain a regional aquifer, known as the Carbonate Rock Aquifer. This unit is overlain by clays and tills that form a semi-confining layer over most of the region.

Subsurface heat flow in the area is low and temperatures in the Paleozoic and Quaternary sediments of the region are also generally quite low. The relative importance of advective and conductive heat flow in the distribution of these temperatures will be evaluated in Chapter 5 of this thesis. Temperatures in the subsurface beneath some areas of Winnipeg are several

degrees above background values. The reasons for these elevated temperatures will be examined in Chapters 6 through 10.
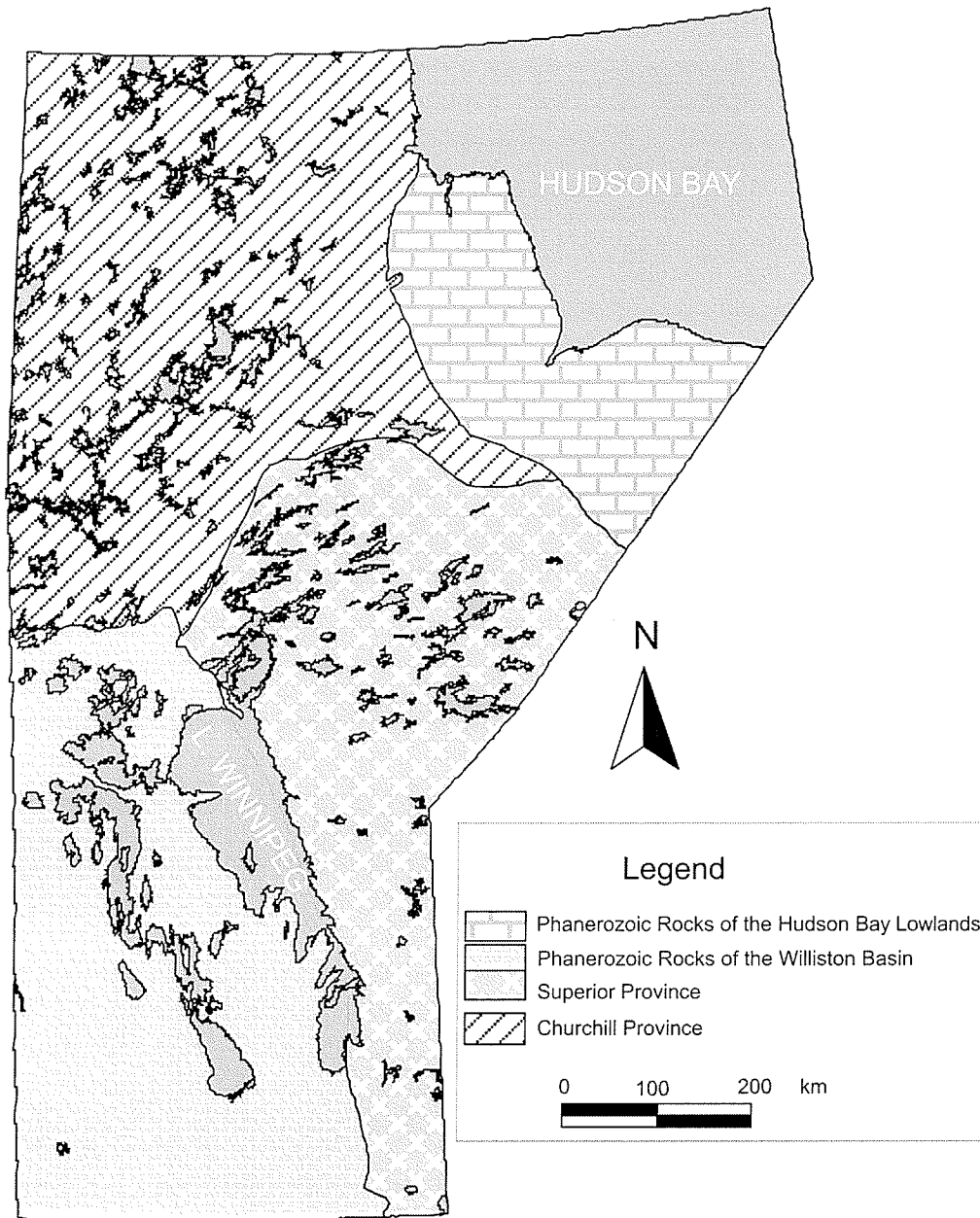
Figure 3.1: Precambrian bedrock provinces in Manitoba (after Hoffman, 1989).
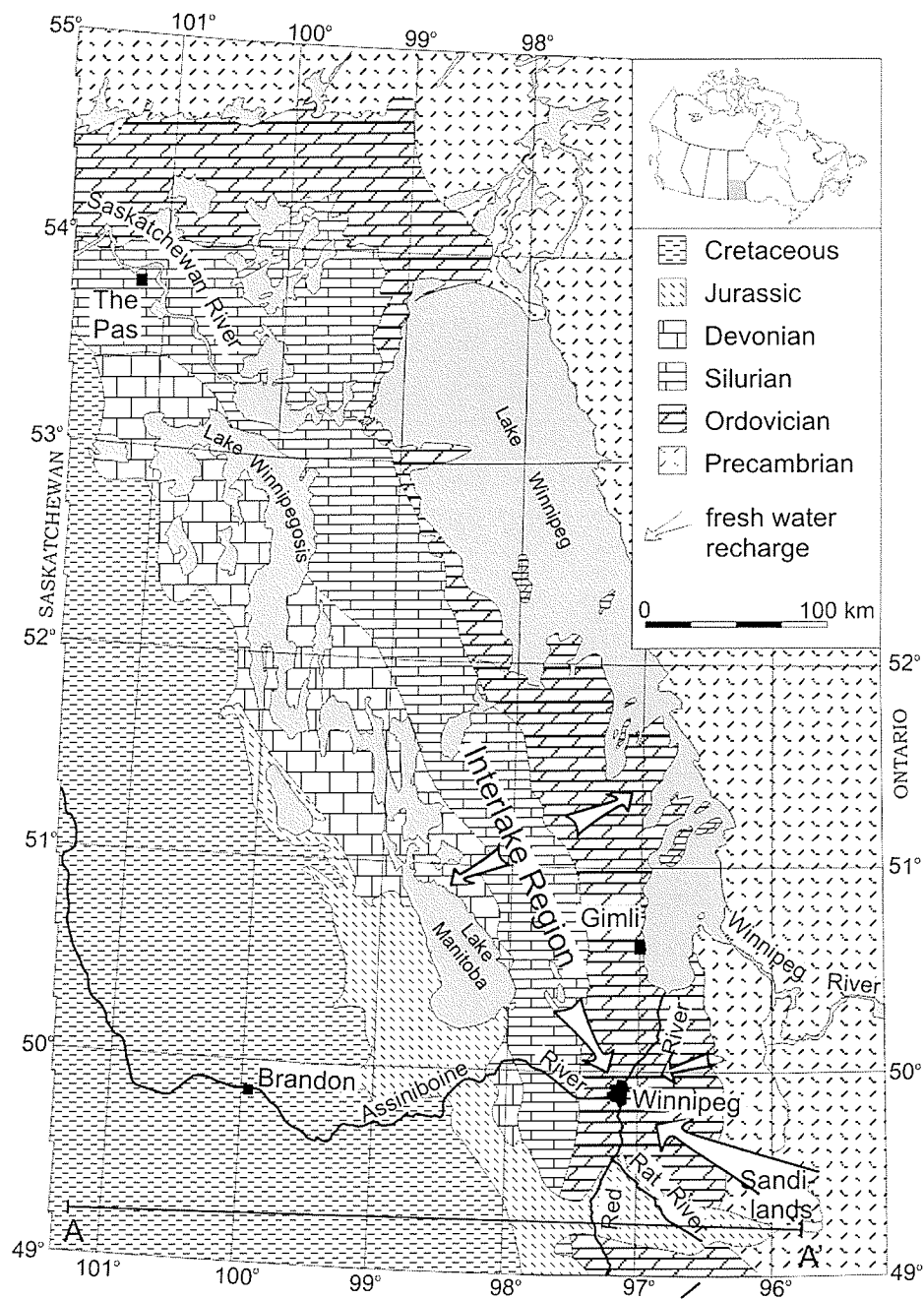
Figure 3.2: Geology of southern Manitoba with direction of regional groundwater flow in the Carbonate Rock Aquifer shown by arrows (adapted from Simpson et al., 1987; Grasby and Betcher, 2002). A to A' indicates location of cross-section given in Figure 3.3.
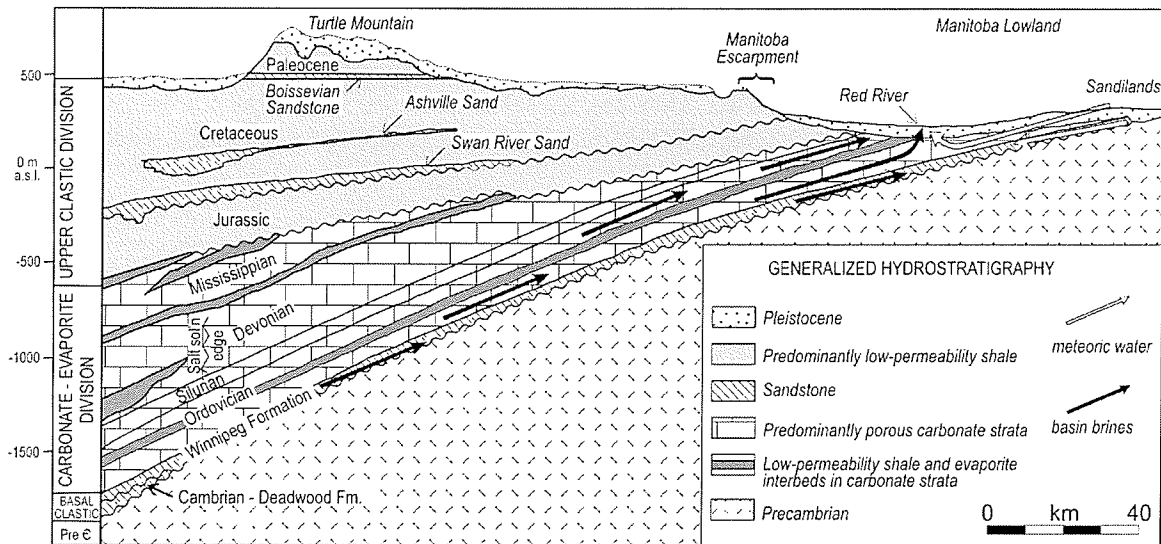
Figure 3.3: Cross-section of southeastern Manitoba geology (adapted from Simpson et al., 1987; Grasby and Betcher, 2002). Direction of regional groundwater flow shown as arrows (adapted from Betcher et al., 1995). Location of cross-section indicates figure given by A to A' in Figure 3.2.
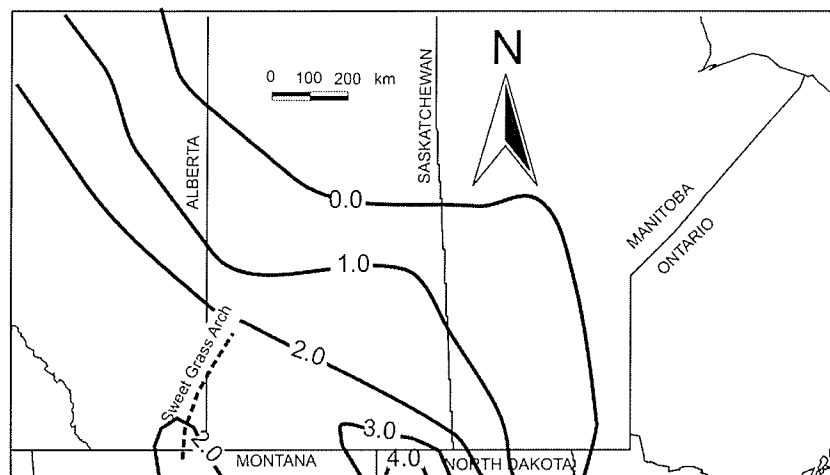
Figure 3.4: Contours showing thickness of basin fill in the eastern Western Canada Sedimentary basin. Isopachs of basin fill are given in kilometres (after Aitken, 1989).
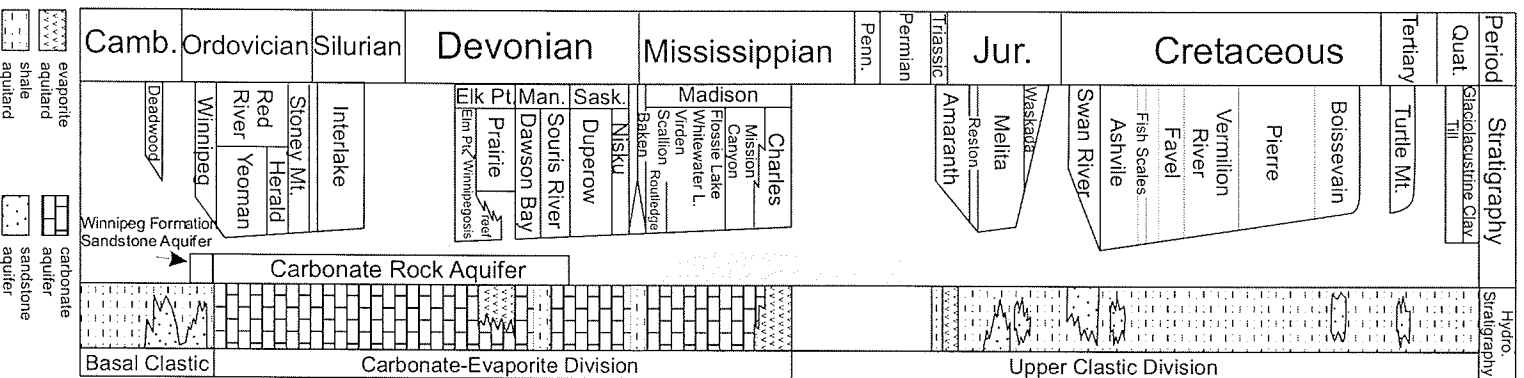
Figure 3.5: Stratigraphic column of the Williston Basin showing major aquifers of southern Manitoba (adapted from Grasby and Betcher, 2002).

37
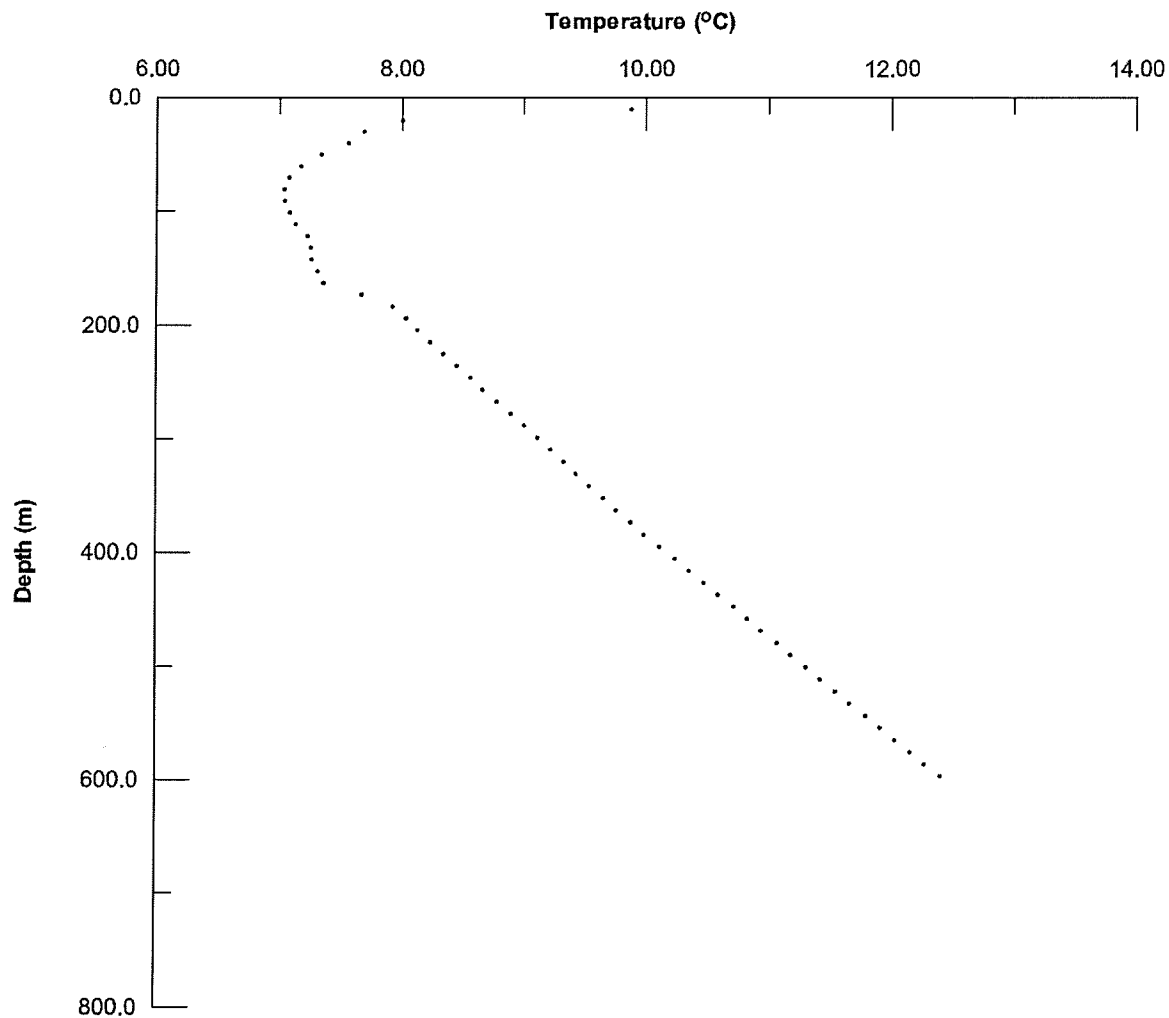
Figure 3.6: Temperature log from GSC borehole 7001 from which Jessop and Judge (1971) made their heat flow estimate for the Winnipeg area (Source: Geological Survey of Canada).
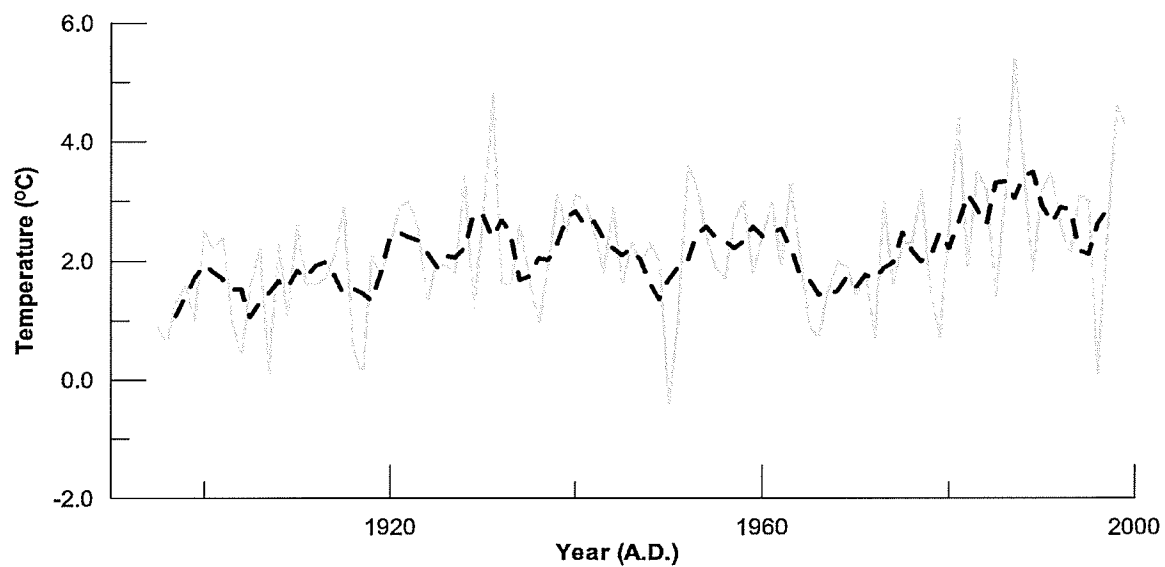
Figure 3.7: Mean annual temperature for Winnipeg, Manitoba (solid line) shown with five year moving average of mean annual temperature for Winnipeg, Manitoba (dashed line) (Source: Environment Canada).

CHAPTER 4: ASSESSMENT OF THERMAL CONDUCTIVITY OF CARBONATE ROCK IN THE CARBONATE ROCK AQUIFER

4.1 Introduction

Knowledge of thermal conductivity is necessary for the estimation of conductive heat flow as described by equation 2.7. Methods of obtaining thermal conductivity data for heat flow calculations range from intensive laboratory testing of hundreds of samples and in situ measurements to the use of literature values. The appropriateness of different methods of obtaining thermal conductivity values for carbonate rock is addressed in this study, with particular attention paid to spatial variation.

Thermal conductivity is subject to considerable variability, even within similar rock types. For example, Schon (1996) provided ranges of mean values of thermal conductivity of limestone from three different sources (Dortman, 1976; Cermak and Rybach, 1982; and Jessop, 1990), all of which were based on sample populations of greater than 200 (Table 4.1). Mean values and ranges reported by Dortman (1976) and Cermak and Rybach (1982) are quite similar. However, results reported by Jessop (1990) have a mean value that is approximately 1.0 W m^{-1} $°C^{-1}$ greater than that of the other compilations. Values reported for dolostone by Schon (1996) show similar levels of variability. This variability is present not only between different geologic units but also within the same geologic unit. If unaccounted for, variability in thermal conductivity results in geologic 'noise' in measured temperatures (Conway and Beck, 1977). This noise can have a notable effect

on heat flow calculations and geothermal studies in general. Variations in thermal conductivity are of particular interest in the study of transient heat flow to recover ground surface temperatures, where a variation in thermal conductivity could cause an apparent climate signal. Shen et al. (1995) suggest that variations in thermal conductivity are more problematic than other sources of error in transient heat flow models.

To address the problem of variability in thermal conductivity, many researchers have attempted to find correlations between thermal conductivity and petrological and geophysical parameters. If applicable, such techniques may provide information related to the variation of thermal conductivity within a geologic unit. Blackwell and Steele (1989) summarize a number of attempts to produce empirical models for predicting thermal conductivities from various geophysical well logs. Although some of these attempts were found to produce reasonable predictions, the models were applicable only to certain lithologies or limited geographic areas. In sedimentary rocks, bulk density and porosity are commonly found to have a statistically meaningful correlation with thermal conductivity. This is largely due to the difference in the thermal conductivities of the fluid occupying the pore spaces and the thermal conductivity of the rock (e.g. Beck, 1976). However, this relationship does not always produce a strong enough correlation to accurately predict thermal conductivities (Schon, 1996). Brigaud et al. (1990) suggested that lithology and mineralogy have the greatest impact on the thermal conductivity of a rock. However, predicting thermal conductivities from mineral contents

has produced only moderately successful results, primarily because thermal conductivities of minerals are generally not constant (Beck, 1965; Jessop, 1990). Other factors, such as the structure, presence of residues in pore spaces and thermal resistance between crystal faces (Jessop, 1990), can affect thermal conductivity and these are not always easily examined or quantified.

Both thermal conductivity, and other parameters that may be used to estimate thermal conductivity, are subject to variations arising from the heterogeneity that is ubiquitous in geological environments (Bachu, 1991). As a result, a large number of measurements may be required to determine a representative value of thermal conductivity for a geologic unit. The use of conventional statistics and geostatistics may be of use in the design of a testing program and in the interpolation of data. Conventional statistics can be used to determine the number of samples required to determine the mean value of a population of samples within a specified degree of certainty. The use of geostatistics, which is common in other branches of the geosciences, such as hydrogeology and economic geology, addresses the spatial variability of geological parameters. Geostatistics is of interest in the field of heat flow because thermal conductivity is subject to spatial variations, which in turn affects temperature profiles. The degree of spatial correlation present is an important factor to consider when determining the spacing of samples tested for thermal conductivity and may also aid in the development of effective thermal conductivity models.

4.2 Background: Effective Parameters

Many applications require primary information, such as average fluxes, as a prelude to more complex calculations. For example, the effective thermal conductivity is the thermal conductivity, which when multiplied by the mean thermal gradient, produces the total heat flow through a column. In order to produce a mean heat flow equation one first has to alter the form of equation 2.7 to account for the presence of materials with differing thermal conductivity within a given rock mass. Models describing thermal conductivity have been formulated for scales ranging from microscopic to macroscopic. One of the most common examples of an effective thermal conductivity model is the one developed to account for the difference between the thermal conductivities of the rock and fluid in a porous media. Perhaps the most commonly used equation to describe the effect of porosity on effective thermal conductivity is equation 2.9. However, other models, which may be more appropriate in various situations, also exist.

Woodside and Messmer (1961) proposed the use of the Maxwell model to estimate the impact of porosity on bulk thermal conductivity. In this model, spheres of one phase are dispersed in another continuous phase, such that the thermal effect of one sphere cannot be "seen" by other spheres. This results in the following equation describing bulk thermal conductivity:

$$\kappa_d = \kappa_s \left[\frac{2 \kappa_r / \kappa_f + 1 - 2\eta\left(\kappa_r / \kappa_f - 1 \right)}{2 \kappa_r / \kappa_f + 1 + \eta\left(\kappa_r / \kappa_f - 1 \right)} \right] \quad (4.1)$$

Brailsford and Major (1964) expanded the two-phase dispersive model developed by Woodside and Messmer (1961) to incorporate a third phase, which can be either fluid or mineral. This model is described by the following equation:

$$\kappa_d = \frac{\sigma + A\kappa_b + B\kappa_c}{\left(\sigma / \kappa_a\right) + A + B} \qquad (4.2)$$

$$A = 3\beta /(2\kappa_a + \kappa_b)$$

$$B = 3\gamma /(2\kappa_a + \kappa_c)$$

where κ_d is the dispersive thermal conductivity, σ, β and γ are the fractions of the first, second and third phases present in the rock mass respectively and κ_a, κ_b and κ_c are the thermal conductivities of the three phases present in the model. This model can be applied to a porous media where the third phase is the fluid. Series (equation 4.3) and parallel (equation 4.4) models have also been used to model effective thermal conductivities (e.g. Schon, 1996):

$$\kappa_s^{-1} = \sum_{i=1}^{n} V_i \kappa_i^{-1} \qquad (4.3)$$

$$\kappa_p = \sum_{i=1}^{n} V_i \kappa_i \qquad (4.4)$$

where κ_p and κ_s represent effective thermal conductivities based on parallel and series models and V_i is the percentage of a given phase in the rock . It should be noted that equation 2.9 is a specific case of 4.4. The models described by equations 4.3 and 4.4 can be used not only to describe the

arrangement of mineral and fluid phases in a small sample but also the macroscopic structure of a geologic formation.

However, a paradigm in the geosciences suggests that geological parameters are best represented as random space functions and thus stochastic approaches are needed to formulate effective parameters (e.g. Gelhar, 1993). Gelhar's (1993) derivation of effective hydraulic conductivity based on a perturbation in hydraulic head can be altered for use with any physical law described by Laplace's equation. In this study, it will be altered for use with equation 2.7.

Beginning with the steady-state heat flow equation in one dimension let:

$$\kappa = \hat{\kappa} + \kappa' \qquad (4.5)$$

$$T = \hat{T} + T' \qquad (4.6)$$

where $\hat{\kappa}$ is the mean thermal conductivity, κ' is the perturbation in thermal conductivity, $\hat{T}$ is the mean temperature and T' is the perturbation in temperature. As a consequence of these definitions, the expected values of the perturbations in thermal conductivity and temperature are both zero. The expression for vertical heat flow considering perturbations can be written as:

$$q_z = \left[\hat{\kappa} + \kappa' \right] \left[\frac{\partial \hat{T}}{\partial z} + \frac{\partial T'}{\partial z} \right] \qquad (4.7)$$

which can be expanded to produce the following:

$$q_z = \hat{\kappa} \frac{\partial \hat{T}}{\partial z} + \kappa' \frac{\partial \hat{T}}{\partial z} + \hat{\kappa} \frac{\partial T'}{\partial z} + \kappa' \frac{\partial T'}{\partial z} \qquad (4.8)$$

By taking expected values, the following is derived:

$$\hat{q}_z = \Theta = \hat{\kappa}\frac{\partial \hat{T}}{\partial z} \qquad (4.9)$$

where Θ is the expected heat flux. Effective thermal conductivity can thus be written as:

$$\kappa_e = \frac{\Theta}{\dfrac{\partial \hat{T}}{\partial z}} \qquad (4.10)$$

and therefore, by definition:

$$\kappa_e = \hat{\kappa} \qquad (4.11)$$

The current study will examine the applicability of the above deterministic and stochastic models to samples from the Paleozoic carbonate sequence from beneath Winnipeg, Manitoba. Deterministic models will be applied to the individual samples in an attempt to explain variations in thermal conductivity within the Red River Formation. Deterministic and stochastic effective thermal conductivities will be explored in an attempt to scale the laboratory measurements to field scale applications.

4.3 Field Program and Testing

During this study, rock core from the Red River Formation obtained from a borehole in southern Winnipeg (Figure 4.1) was analysed. This rock core consisted of dolomitic limestone, with minor gypsum beds less than 2 millimetres thickness present at various locations in the core. In addition to this core, other samples obtained from a site in central Winnipeg were also analysed. The analyses were conducted using the method outlined by MacLeod (1997) and theory described by Jessop (1990). The rock core

obtained in this study was 63.5 millimetres in diameter and had to be cored again in the laboratory to allow for testing with the GSC's divided bar apparatus. Plugs, 25 millimetres in diameter, were drilled with their axes positioned vertically and at spacings ranging from 0.005 to 1.2 metres. The spacing of samples was erratic due to the presence fractures in the core. These plugs were then cut into discs that were 10 to 15 millimetres thick. The flat sides of the discs were sanded and polished to allow for good thermal contacts in the divided bar apparatus. The discs were then saturated with water by placing them in a beaker of deionised water in a bell jar, which was placed under a pressure of 25 kPa for 48 hours. The samples were then tested for thermal conductivity using a divided bar apparatus with the temperatures between the two water baths kept at 18 and 28 °C. Individual samples were run for 10 minutes each, allowing for thermal equilibrium to be achieved. Samples were weighed after saturation and then again after they had been dried in an oven maintained at 105 °C for 48 hours. These wet and dry weights, along with measurements of the dimensions of the samples, were used to determine the densities and porosities of the samples. At least three runs were performed for each disc, with discs being dried and then saturated again between runs. The contact resistance of the divided bar was determined prior to testing of samples and was treated as a constant value in this study according to the method outlined by Jessop (1990).

4.4 Results of Testing and Statistical Analysis

4.4.1 Statistics and Distributions

Forty three thermal conductivity estimates were obtained for samples from borehole W8 during this study (Appendix A). This population had a mean value of 2.22 W m^{-1} °C^{-1} with a standard deviation of 0.54 W m^{-1} °C^{-1} (Table 4.2) and these samples appear to approximately follow a normal distribution (Figure 4.2). Other distributions may also provide a reasonable fits to the data. The 95% confidence interval for the mean was ±0.165 W m^{-1} °C^{-1} and the approximate accuracy of individual readings was ±4%. Of these samples, 32 were cut with their axes in a vertical orientation and 11 were cut with their axes in a horizontal orientation to provide some indication of the presence of anisotropy. The mean value of the vertically cut samples was 2.32 W m^{-1} °C^{-1} with a standard deviation of 0.54, while the horizontally cut samples had a mean value of 1.92 W m^{-1} °C^{-1} and a standard deviation of 0.44 W m^{-1} °C. These means are not statistically different at the p=0.05 level. Another five samples from the Red River Formation beneath central Winnipeg at the Provencher Bridge site (Figure 4.1) were also subjected to thermal conductivity testing. Other results based on testing of samples from a borehole beneath the University of Manitoba campus performed by the Geological Survey of Canada during the 1960's (GSC7001) have also been incorporated into the overall statistics for the Red River Formation given in this study. In summary, the overall population of 66 samples from the Red

River Formation had a mean value of 2.36 W m^{-1} °C^{-1} with a standard deviation of 0.69 W m^{-1} °C^{-1}.

Seventy two porosity measurements were also made from samples from borehole W8 during this study (Appendix A). The mean porosity found in these tests was 0.095 with a standard deviation of 0.035 (Table 4.2). The differences between the vertical and horizontal samples were not compared because porosity is a scalar quantity. The porosities sampled in this study also appear to have a normal distribution (Figure 4.3). An additional two measurements were available from the borehole at the University of Manitoba, having values of 0.13 and 0.065 and another six samples from central Winnipeg were also tested. Porosities were calculated from the measured dry and saturated densities of the samples tested. Measured dry densities ranged from 2150 to 2710 kg m^{-3}, with a mean value of 2520 kg m^{-3} and saturated densities ranged from 2460 to 2740 kg m^{-3}, with a mean value of 2620 kg m^{-3}. Solid phase densities were also calculated from the measured saturated and dry masses for all samples analyzed in this study. The measured solid phase densities ranged from 2730 to 2850 kg m^{-3}.

4.4.2 Spatial Variation

Within the core examined from borehole W8, there is an apparent trend of decreasing vertical thermal conductivity from 17 to 24 metres (Figure 4.4). This is followed by a slight increase in thermal conductivity from 24 to 28 metres. Similar trends in horizontal thermal conductivity were not as obvious due to greater variability in the data, which was more sparse for horizontal

49

measurements. Porosity exhibited an apparent increase from approximately 19 to 24 metres, followed by an apparent decrease from 24 to 29 metres (Figure 4.5). However, R^2 correlation coefficients of regressions between depth and thermal conductivity indicate that there is not a statistically significant relationship for less than third order polynomials. Porosity and depth trends also lack significant relationships for polynomials lower than third order.

A semi-variogram was constructed for thermal conductivity measured in borehole W8 (Figure 4.6). To account for the variability in sampling interval, the moving window semi-variance estimator proposed by Li and Lake (1993) was utilised. The resulting semi-variogram indicated that samples located at lags 5 and 10 metres are somewhat correlated and that adjacent samples have a slightly higher semi-variance than those at greater lags. Thermal conductivity tests conducted on samples spaced within a few millimetres of each other often varied by greater than 1.0 W m^{-1} $^{\circ}$C^{-1} (Figure 4.4). This implies that there is very little correlation between samples at shorter lags. The moving window semi-variance estimator was also used to construct a variogram for porosity at W8 (Figure 4.7). This semi-variogram had approximately the same shape as those constructed for thermal conductivity. Porosity is more highly correlated at lags of 5 and 10 metres but it differs from the semi-variograms constructed for thermal conductivities in that it the semi-variance tends to increase at greater lags. There is apparently very little or no correlation at shorter lags. Spatial aliasing may be

present in the semi-variograms constructed for thermal conductivity and porosity at shorter lags.

The spatial distribution of thermal conductivities can have an effect on the overall conductivity of a geologic unit. Due to the tendency of geologic units to occur in horizontal beds, the bed with the lowest thermal conductivity will exert the greatest control on heat flow if heat flow is perpendicular to bedding. If a weighted harmonic mean model (Equation 4.2) is employed using the moving window estimated values (Figure 4.4), the resulting effective thermal conductivity is 2.12 W m^{-1} °C^{-1}, which is 91.4% of the value based on the stochastic derivation (Equation 4.11).

4.4.3 Potential for Empirical and Deterministic Modeling of Thermal Conductivity

Correlations of rock density, saturated density, dry density, porosity and bulk thermal conductivity were assessed. The only statistically significant relationship found at the p = 0.01 level was between porosity and saturated density (Table 4.3). The next highest correlation coefficients were between bulk thermal conductivity and porosity and bulk thermal conductivity and saturated density. These relationships were not significant at the p = 0.05 level, but suggest that porosity and density might be useful for predicting thermal conductivity values when appropriately conditioned or when combined with other data.

In order to better understand the relationship between bulk thermal conductivity and porosity, the parallel model (Equation 2.9), dispersed model

51

(Equation 4.1) and series model (Equation 4.3) were used to estimate the thermal conductivity based on a two phase system. The thermal conductivity of the mineral component was assumed to be 3.6 W m^{-1} $°C^{-1}$, which is the approximate thermal conductivity of calcite (Schon, 1996). Based on this estimate of thermal conductivity, the series model produced the lowest root mean square error (RMS) while the two-phase series, parallel and dispersed models all produced the same R^2 correlation coefficient with the observed data (Table 4.4). A regression analysis was conducted to minimize the RMS error in all models by finding an optimal thermal conductivity for the rock. This produced approximately the same results for the series model, while reducing the RMS error in the parallel model and dispersed model was not able to reduce the RMS to lower than 0.50 W m^{-1} $°C^{-1}$. The optimal values of thermal conductivity found in the parallel and dispersed models were much less than that found for the series model.

The relationship between density and thermal conductivity may also be due in part to mineralogy, which in this case was expected to be related to the relative percentages of calcite and dolomite present in a given sample. Dolomite is slightly more dense than calcite and has a thermal conductivity which is nearly twice as great as calcite (Schon, 1996). To test this theory, three models that attempt to estimate bulk thermal conductivity were examined, including a dispersive model (Equation 4.2), a parallel model (4.3) and a series model (4.4). These models were all based on three phases, which were assumed to be calcite, dolomite and water. The relative

percentages of calcite and dolomite present in the samples tested in this study were estimated based on density and the amount of water present was deduced from the porosity. There were a few samples where the rock density was a few percent less than calcite and in these samples it was assumed that the rock was composed entirely of calcite.

In the first part of this analysis, thermal conductivities from of 3.6 and 5.5 W m^{-1} °C^{-1} were assigned to calcite and dolomite, respectively, based on values reported by Schon (1996). The series model produced the best results in this case (Table 4.4), with an RMS error of 0.59 W m^{-1} °C^{-1} and an R^2 correlation coefficient of 0.100. The RMS errors found in the other models were approximately three times greater at 1.47 and 1.68 W m^{-1} °C^{-1}, respectively, and the R^2 correlation coefficients were approximately zero.

To investigate the possibility that the thermal conductivities of the minerals are incorrect, an analysis was performed to find the values of thermal conductivity that would produce the lowest RMS error for each of the three models. This was done using the complex method of Box (e.g. Woodbury et al., 1988). The RMS error was reduced to approximately 0.5 in all cases after the optimal thermal conductivities were found but the series model still produced the best R^2 correlation coefficient. The thermal conductivity of calcite estimated by this analysis was greater than that assigned to dolomite in all three models. In the parallel and dispersed models, the optimal thermal conductivity of calcite was less than the value stated by Schon (1996) by more than 20% and the optimal value of dolomite

was less than the Schon's (1996) value by greater than 40%. The optimal thermal conductivities produced suggest that the problem is not adequately constrained or that there is a fundamental problem in the model.

4.5 Discussion

The vertical variation in thermal conductivity found in this study had a relatively wide variation, with the moving window average having a range of approximately 1.0 W m^{-1} °C^{-1} over the length of the sampling interval, which is approximately one third of the overall range of thermal conductivity. There is essentially no spatial correlation in the data at the scale examined in this study. This suggests that thermal conductivity data are subject to considerable random variations over short distances. This level of variability is problematic because in most cases temperature measurements are made at a higher spatial frequency than thermal conductivity measurements. Uncertainty in the spatial variation of thermal conductivity reduces the amount of certainty that can be placed on interpretations of apparent anomalies in temperature profiles and suggests that in some cases greater attention should be given to the characterization of the distribution of thermal conductivity.

Porosity measurements made in this study suggest that porosity is subject to a considerable degree of variation in the Red River Formation. However, there is a stronger degree of spatial correlation in the porosity data than in the thermal conductivity data, at least vertically. There is some similarity between the two semi-variograms, which is to be expected as the bulk thermal conductivity and porosity are correlated. However, these semi-

variograms are somewhat deceiving because they do not use data at lags shorter than 1 metre. There is little correlation at these short lags, which is apparent from the amount of variability found in closely spaced samples.

In this study, thermal conductivity is not sufficiently correlated with porosity to warrant the use of an empirical model to estimate thermal conductivity. The use of deterministic models to predict bulk thermal conductivity from porosity and an assumed rock thermal conductivity is also questionable. The RMS errors found in the models produced in this study suggest that it might be possible to estimate an average value of thermal conductivity for the section of rock examined using an appropriate model. The RMS errors suggest that it would be able to estimate the average thermal conductivity within approximately 20%, which would provide a crude estimate for use in heat flow studies and geothermal resource analysis. However, it does not appear to be possible to capture the variability in thermal conductivity present and this is supported by the R^2 correlation coefficients, none of which were significant at the $p = 0.05$ level. Of the deterministic models produced, the series models had the lowest RMS error. This suggests that the porosity may be present in the form of horizontal microfractures. Some of these features are likely naturally occurring and others were probably introduced during drilling and sample preparation. Alternatively, horizontal layering in the sedimentary structure may be causing this behaviour.

Of the models that used mineralogical data, the series model appears to be the most representative of the data in this study. However, the RMS was still 0.59 W m^2 s^{-1} and the R^2 correlation coefficient was not significant at the p = 0.05 level. The optimal thermal conductivities for the two mineral phases present in the rock mass were not representative of calcite and dolomite, suggesting that the models may not account for all phases present in the rocks. Gypsum, which has a thermal conductivity of approximately 1.05 to 1.3 W m^{-1} °C^{-1}, is known to be present in the Red River Formation. However, gypsum's density is approximately 2300 kg m^{-3}, which suggests that it is only a minor component of the rock and therefore, should not have a major impact on thermal conductivity. Clay minerals, which have highly variable thermal conductivities and densities, might be responsible for the low thermal conductivities measured in the Red River Formation relative to other limestones. Although not noted in the examination of the rock samples, clay minerals have been incorporated in to the Red River Formation during at least three different geologic time periods. Shale is interbedded with carbonates and evaporites in some parts of the formation (McCabe, 1971) and it is not unreasonable to suppose that trace amounts of clay minerals are present in the samples analysed in this study. Also, the Red River Formation is karstic in many areas and shales were deposited in many of the fractures and solution cavities during the Mesozoic (McCabe et al., 1971). Finally, many of the fractures and solution features were infilled with till during the Wisconsinan glaciation (McCabe et al., 1993). Till was observed in the upper

reaches of the core used in this study but it was not possible to obtain samples from this part of the core because it was so intensely fractured. The presence of shales and clays complicates the construction of any model involving mineralogy due to the number of minerals that may be present, many of which have poorly characterized thermal properties (Brigaud et al., 1990).

In addition to uncertainty as to which deterministic model is most appropriate and the roles of different minerals in the prediction of thermal conductivity, there are other factors that can affect thermal conductivities. The thermal conductivities of many minerals are variable and can be affected by the presence of impurities, which are quite common in nature (Beck, 1965; Jessop, 1990). The presence of thermal resistance at the contacts between crystal faces can also cause a reduction in the overall thermal conductivity of a sample, as can the presence of any residues within the pore spaces (Jessop, 1990). These factors are difficult to account for and their influence likely varies between different locations. Extensive petrographic analysis of samples may provide some insight into all of the above mentioned issues but was beyond the scope of this study.

The inability to characterize the distribution of thermal conductivity from other parameters suggests that the treatment thermal conductivity as a random space function is realistic, at least for this dataset. However, this does not preclude the use of petrophysical and mineralogical data in the Red River Formation to estimate thermal conductivity. Variations in porosity and

saturated density were able to explain some of the variability in the thermal conductivity data and although they should not be used alone to estimate thermal conductivity they may be useful in helping to constrain estimates of thermal conductivity. Other parameters not examined in this study may be sufficiently correlated to allow for estimation of thermal conductivity. Alternatively, researchers could choose to accept a certain level of 'noise' in temperature data and deal with it by other means, such as using the variance of thermal conductivity to place bounds on predicted results.

4.6 Summary

Thermal conductivity measurements made in this study exhibit a considerable amount of variability, even over short distances. This spatial variability cannot be accounted for by models produced in this study. This is contrary to other studies (e.g. Beck, 1965; Brigaud et al., 1990), which suggest that it may be possible in some cases to formulate an empirical model to predict thermal conductivity from other parameters. However, these models are really only applicable to certain lithologies or locations (e.g. Blackwell and Steele, 1989). The inability to produce an empirical model to predict thermal conductivity in this study suggests that such relationships are indeed site specific and models developed for specific sites should be validated prior to their use. Deterministic models also performed poorly in this study, and although mineralogical data were lacking in this study, there are several other factors that are not accounted for in these models that lead to poor performance. The use of stochastic methods and geostatistics may

provide the means for a more realistic treatment of the spatial variability in thermal conductivity. Both stochastic and empirical methods generally provide better results when more data are available and every attempt should be made to make a sufficient number of thermal conductivity measurements in heat flow studies. Based on the results of thermal conductivity testing and the stochastic treatment of the data, the most appropriate value for use in analytical and numerical models of the Paleozoic carbonates in southeastern Manitoba is the mean value found in this study, which 2.4 W m^{-1} °C^{-1}.

Reference	Number of Samples	Minimum Thermal Conductivity $(W^{-1} \, ^\circ C^{-1})$	Maximum Thermal Conductivity $(W \, m^{-1} \, ^\circ C^{-1})$	Mean Thermal Conductivity $(W \, m^{-1} \, ^\circ C^{-1})$
Dortman, 1976	216	0.92	4.40	2.40
Cermak and Rybach, 1982	445	0.62	4.40	2.29
Jessop, 1990	487	1.30	6.26	3.44

Table 4.1: Thermal conductivity of limestone samples as reported by Schon (1996).

	Effective Thermal Conductivity (W m^{-1} °C^{-1})				Porosity	
	Horizontal	Vertical	W8	Overall	W8	Overall
Mean	1.92	2.32	2.22	2.36	0.10	0.09
Standard Error	0.13	0.09	0.08	0.09	0.00	0.00
Median	1.92	2.39	2.27	2.35	0.10	0.09
Standard Deviation	0.44	0.54	0.54	0.69	0.04	0.03
Sample Variance	0.20	0.29	0.28	0.48	0.00	0.00
Kurtosis	2.91	0.30	0.49	6.60	-1.10	-1.10
Skewness	-1.07	-0.18	-0.13	1.55	0.12	0.25
Range	1.71	2.55	2.69	4.67	0.14	0.14
Minimum	0.87	1.01	0.87	0.87	0.03	0.03
Maximum	2.58	3.56	3.56	5.54	0.17	0.17
Count	11	32	43	66	72	80

Table 4.2: Statistics describing the distribution of the thermal conductivity and porosity in borehole W8 and overall in the Red River Formation (includes Provencher Bridge and U of M samples).

	Mineral Density	Saturated Density	Porosity	Bulk Thermal Conductivity
Bulk Thermal Conductivity	0.031	0.189	0.230	1.000
Porosity	0.043	0.790	1.000	
Saturated Density	0.002	1.000		
Mineral Density	1.000			

Table 4.3: R^2 correlation coefficients between parameters measured in this study.

Model	Literature Values		Optimized Values				
	RMS (W m^{-1} °C^{-1})	R^2 correlation coefficient	RMS (W m^{-1} °C^{-1})	R^2 correlation coefficient	κ_a (W m^{-1} °C^{-1})	κ_b (W m^{-1} °C^{-1})	κ_r (W m^{-1} °C^{-1})
2 phase parallel	1.02	0.144	0.53	0.144	N/A	N/A	2.42
2 phase dispersed	1.16	0.144	0.51	0.144	N/A	N/A	2.51
2 phase series	0.08	0.144	0.08	0.144	N/A	N/A	3.17
3 phase dispersed	1.47	0.002	0.51	0.147	2.7	2.17	N/A
3 phase series	0.59	0.100	0.48	0.151	3.73	3.17	N/A
3 phase parallel	1.68	-0.001	0.49	0.129	2.74	2.39	N/A

Table 4.4: Comparison of the deterministic models used in this study. Thermal conductivity of calcite is represented by κ_a, while κ_b is the thermal conductivity of dolomite and κ_r is the thermal conductivity of the minerals within the rock mass.
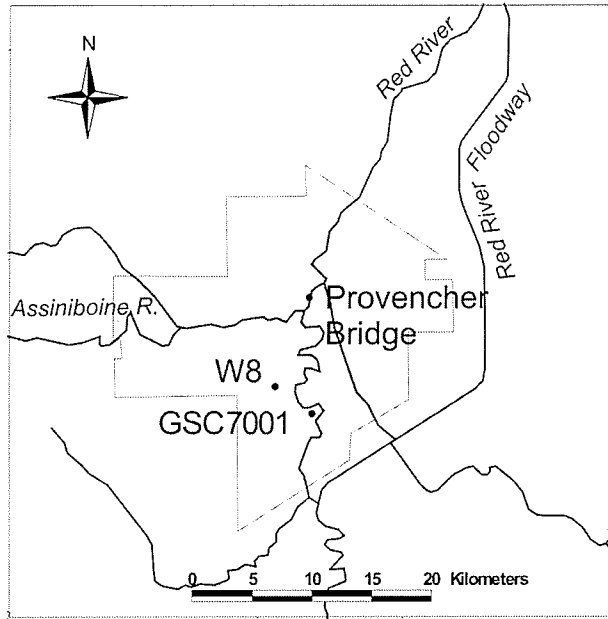
Figure 4.1: Map of the Winnipeg area showing locations of boreholes W8 and GSC7001 along with the Provencher Bridge site where samples were obtained. Winnipeg city limits are shown in grey.
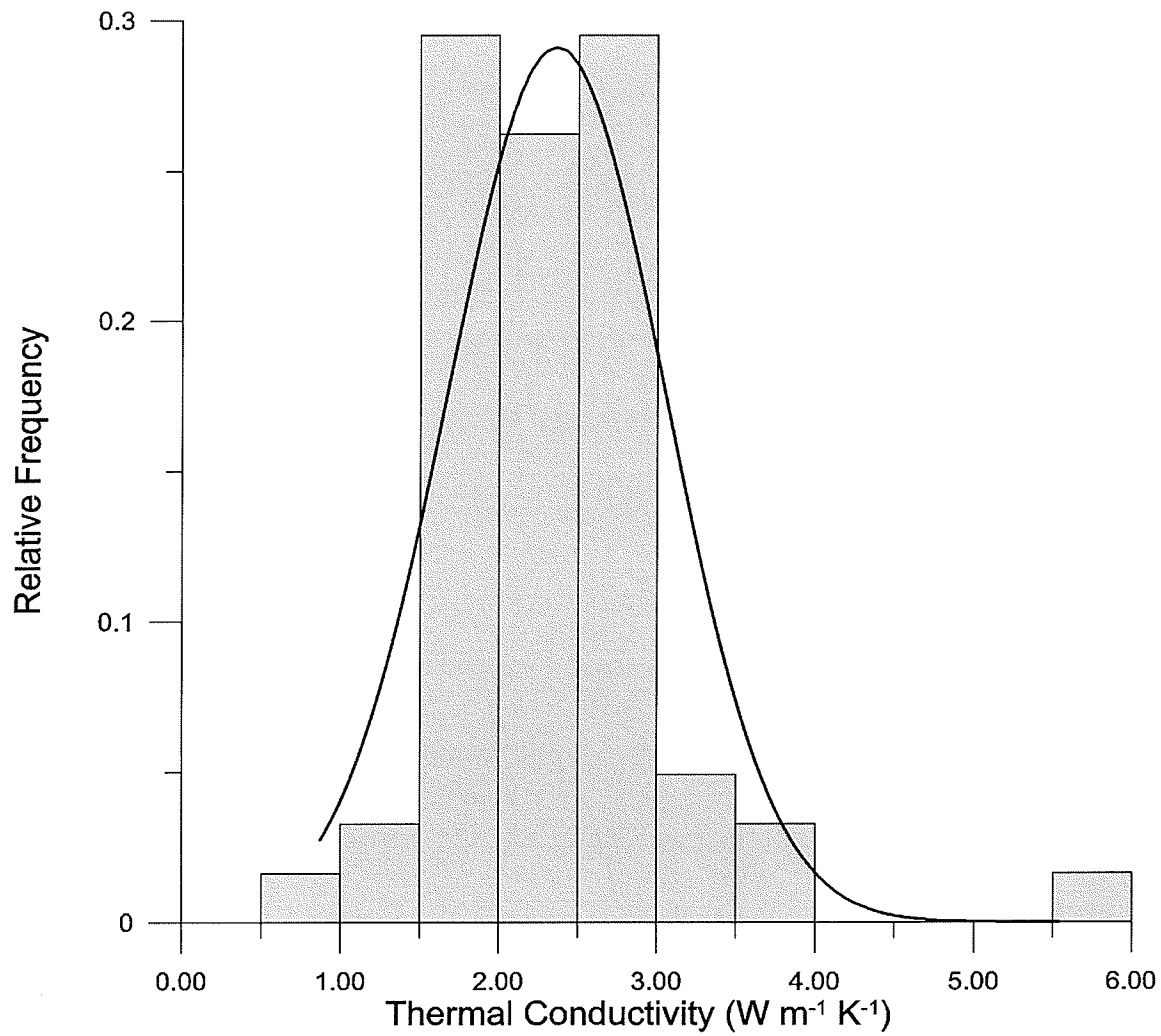
Figure 4.2: Thermal conductivity distribution in borehole W8 beneath Winnipeg, Manitoba with the solid line representing the Gaussian fit to the data.
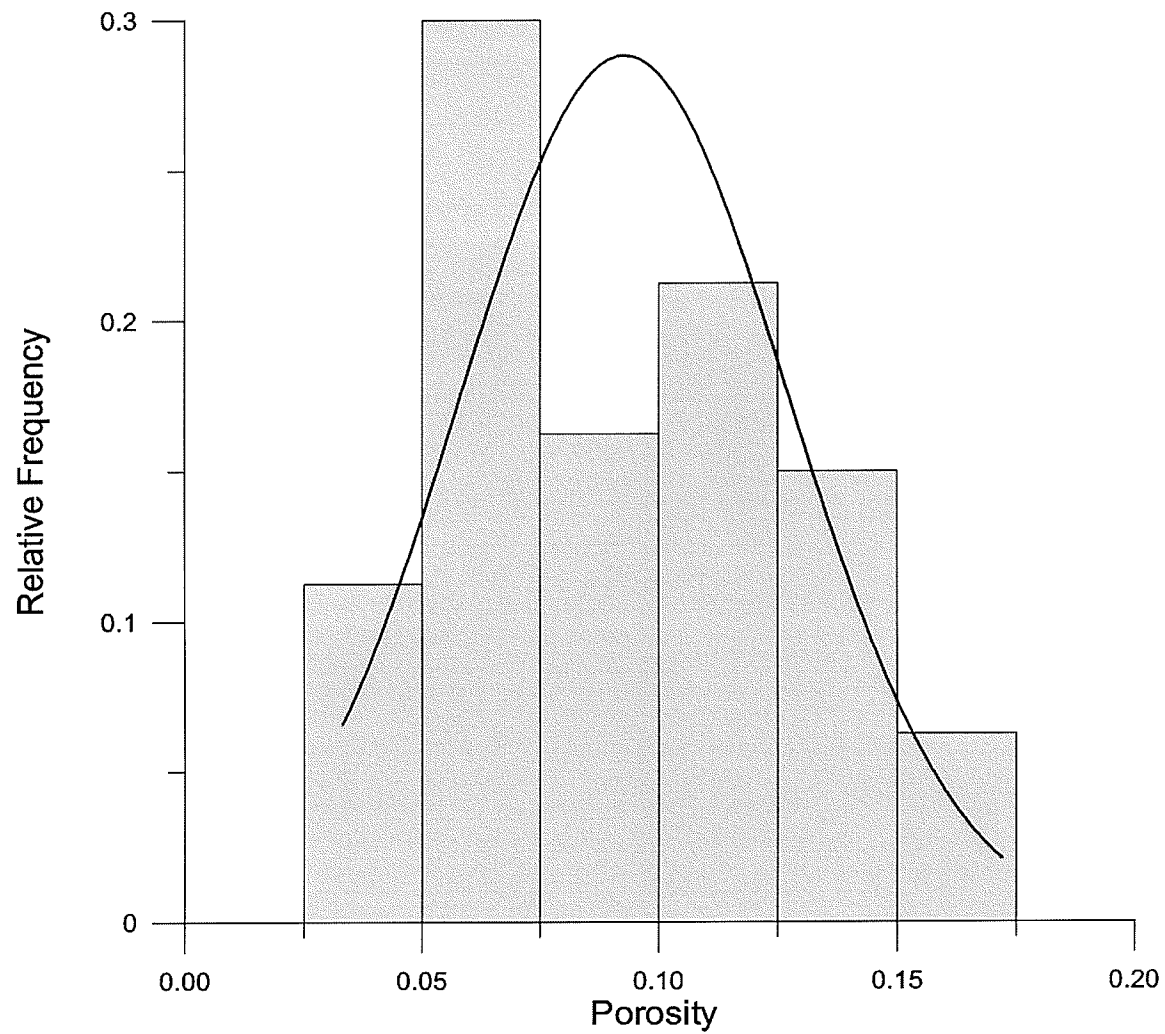
Figure 4.3: Porosity distribution for Red River Formation in borehole W8 with the solid line representing the Gaussian fit to the data.
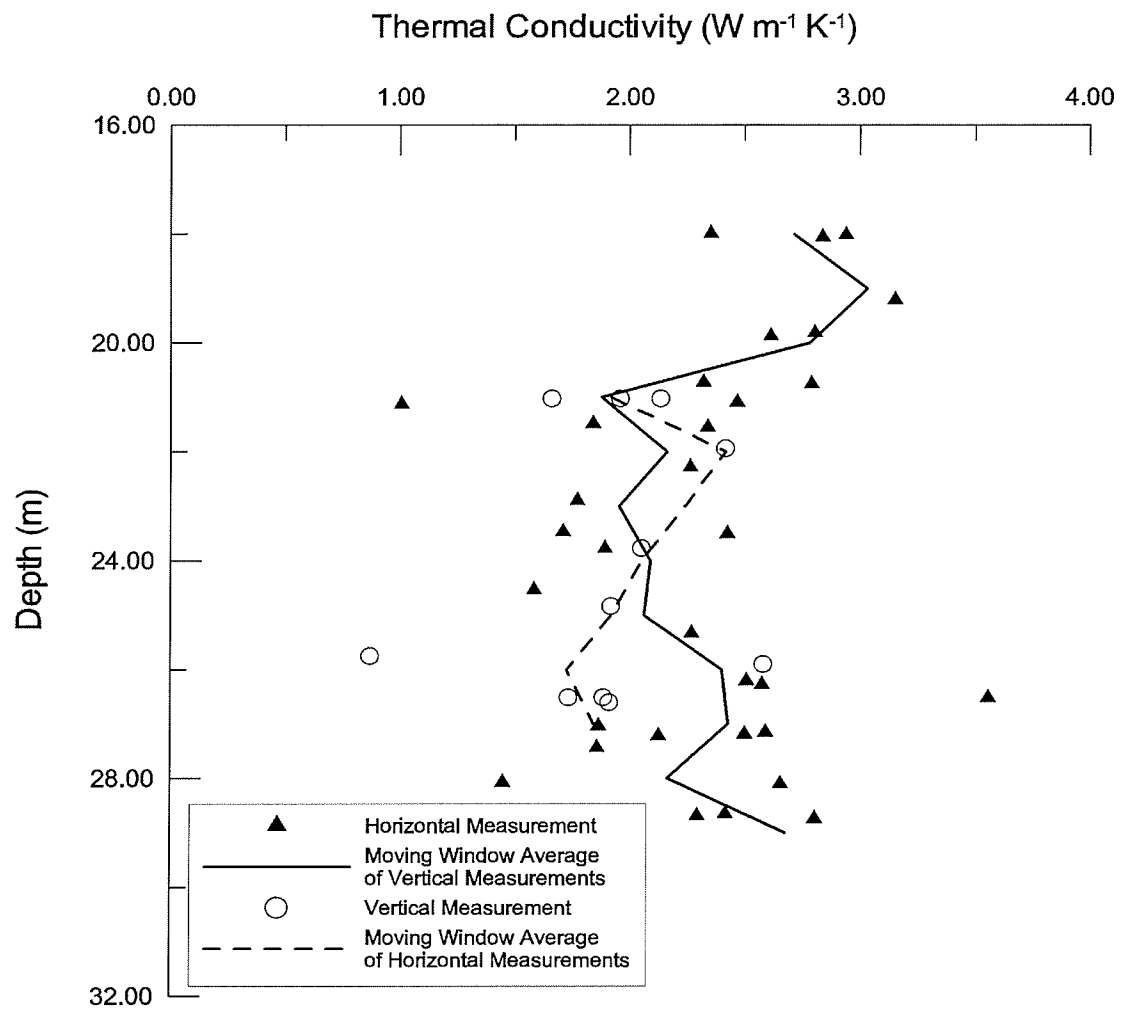
Figure 4.4: Variation of thermal conductivity with depth for borehole W8 in southern Winnipeg.
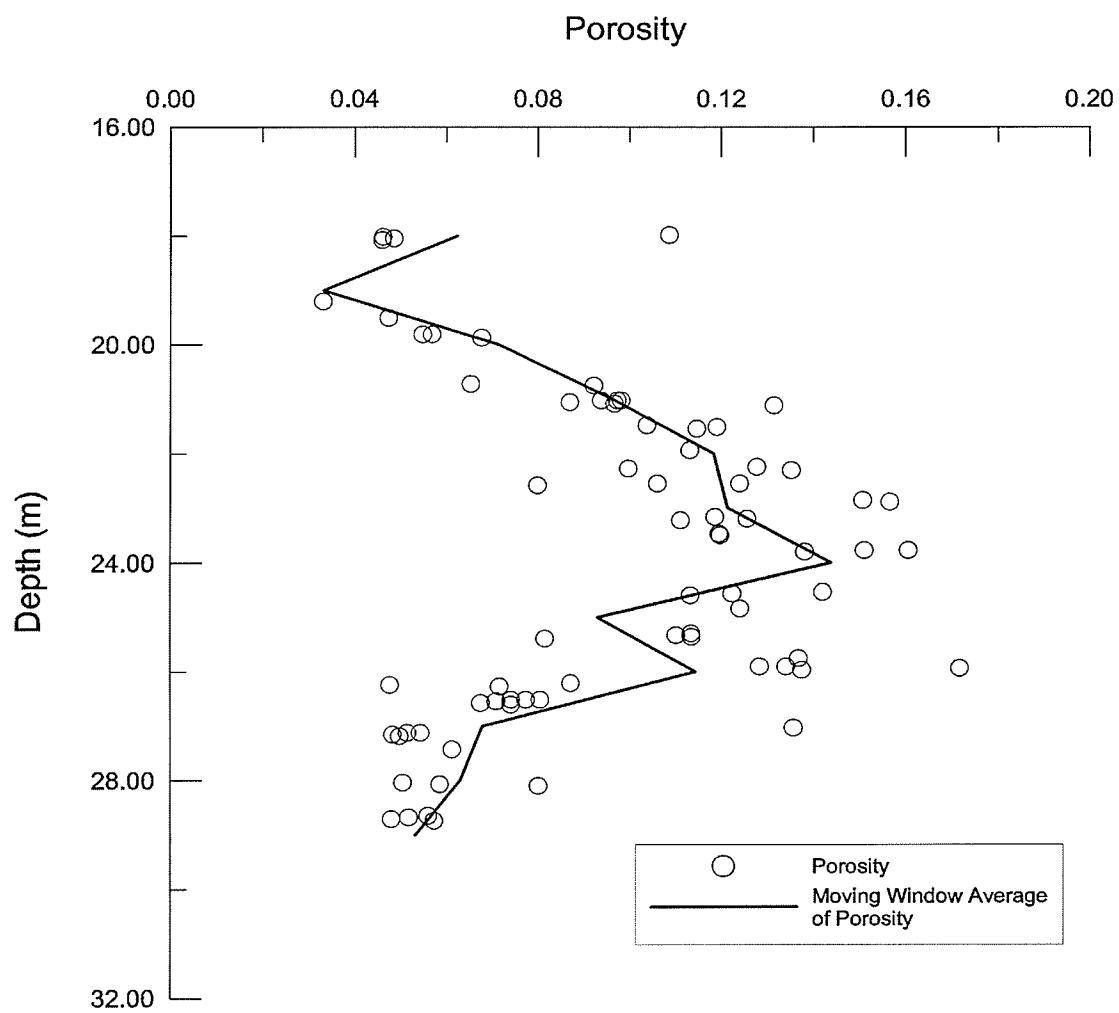
Figure 4.5: Variation in porosity with depth at borehole W8.
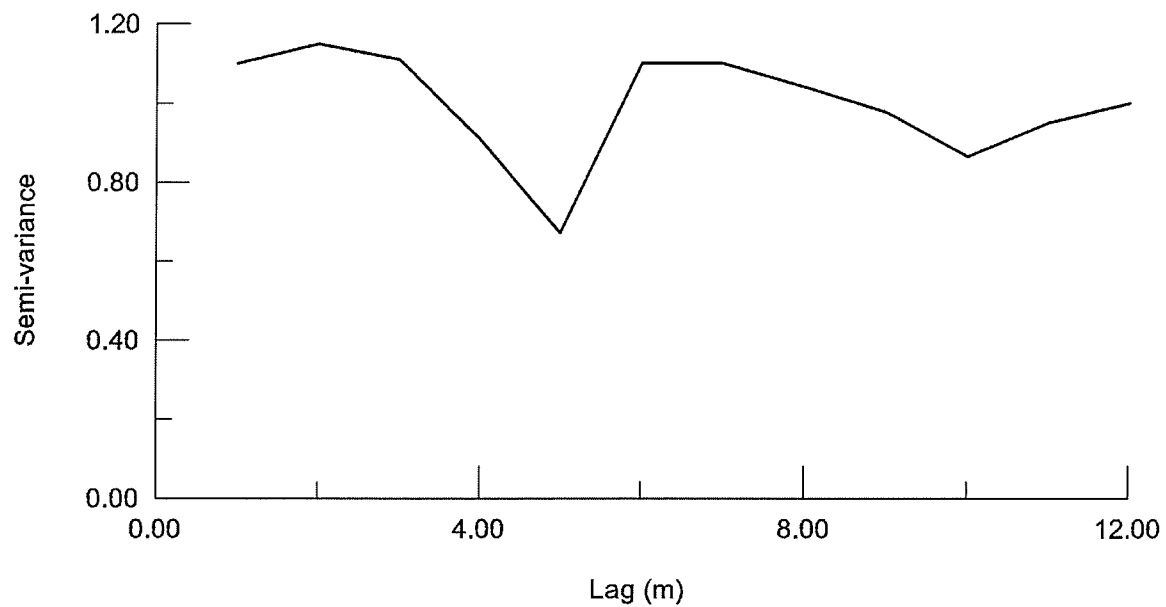
Figure 4.6: Variogram for thermal conductivity measurements made from samples taken from borehole W8.
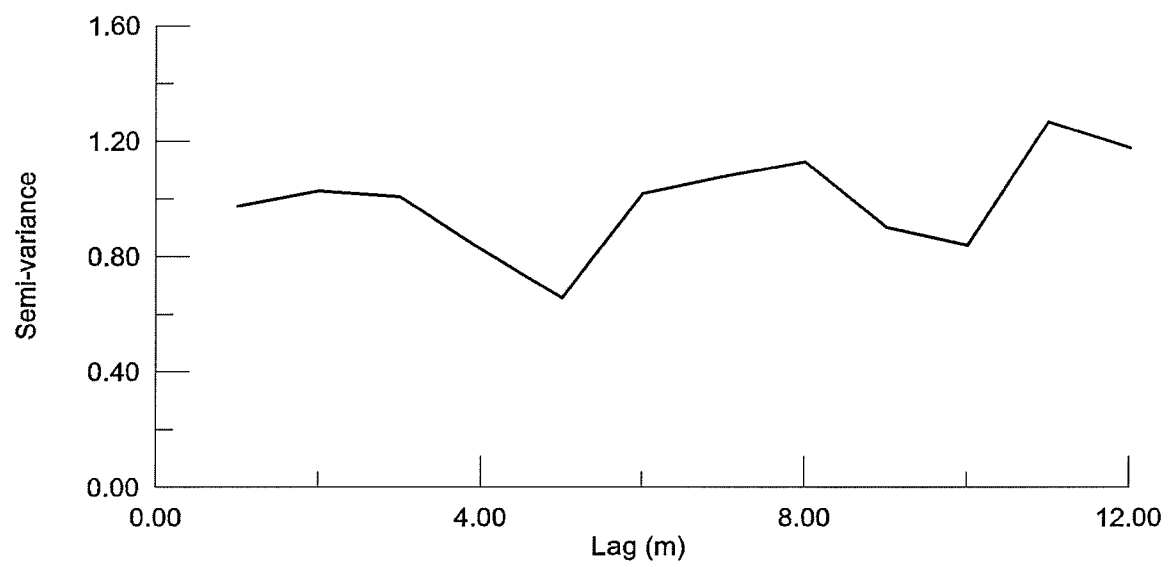
Figure 4.7: Variogram for porosity at borehole W8.

CHAPTER 5: INTERACTIONS BETWEEN REGIONAL HEAT AND GROUNDWATER FLOW IN MANITOBA

5.1 Introduction

The distribution of heat flow in sedimentary basins is often affected by groundwater flow. Lachenbruch and Sass (1977) stated that groundwater flow is the greatest obstacle to accurately determining heat flow conditions at depth from shallow measurements. Among the first researchers to examine the effect of groundwater flow on temperature distributions were Stallman (1963) and Bredehoeft and Papadopulos (1965), who both examined perturbations in temperature in groundwater recharge and discharge areas. These studies showed that in recharge areas isotherms are depressed and in discharge areas isotherms are elevated. Domenico and Palciauskas (1973) extended this work by producing a two-dimensional model of the temperature distribution in a closed sedimentary basin due to groundwater flow. They also found that recharge areas have depressed isotherms and discharge areas have elevated isotherms but showed that this only occurs when a critical depth-to-length ratio is exceeded. Betcher (1977) furthered this research by studying the behaviour of groundwater in deep flow systems with finite element models. Later studies by Smith and Chapman (1983) and Woodbury and Smith (1985) examined the effect of hydrogeology on subsurface temperatures in a range of situations through numerical modeling.

Conversely, because of the coupled nature of groundwater flow and heat flow, temperature measurements may also provide valuable insight into

71

groundwater flow. Temperature measurements can be easily taken in standpipe piezometers or boreholes along with hydraulic head measurements. Typically, the number of hydraulic head measurements is limited in a vertical borehole and in most cases only one such measurement is available in an individual piezometer. Temperatures, however, can be profiled continuously along the entire length of a borehole or standpipe, thus greatly increasing the number of temperature data compared to hydraulic head data that can be collected (e.g. Woodbury et al., 1991). The relative ease of making temperature measurements makes the use of heat flow in groundwater flow investigations very attractive.

In this chapter, the interaction between groundwater flow and heat flow in southeastern Manitoba is examined. The possibility that regional groundwater flow redistributes substantial amounts of heat in southeastern Manitoba will be addressed. Temperature measurements are also used to estimate recharge rates to bedrock aquifers in the Sandilands area.

5.2 Temperature and Heat Flow Data in the Eastern Williston Basin

5.2.1 Subsurface Temperatures in Southeastern Manitoba

Most temperature measurements made during this study were taken east of the Red River, which defines a groundwater divide in the Carbonate Rock Aquifer of Manitoba (Render, 1970; Grasby and Betcher, 2002; Kennedy, 2002). Temperatures measured at the upper surface of the Red River Formation in this area range from less than 5 °C to greater than 15 °C

(Figure 5.1; Appendix B). Outside of the City of Winnipeg, the highest temperatures observed in the upper few metres of the Carbonate Rock Aquifer are less than 6.5 °C, with the highest temperatures occurring in the southeastern portion of the study area and the coolest in the northeastern portion of the study area. The temperature of the Winnipeg Formation was only measured at four locations (Figure 5.2). The temperature measured in the southeastern portion of the study area, which was from a well beneath the Sandilands Moraine, was higher than any of those measured in the other three wells, which were all located in the City of Winnipeg. Based on these measured temperatures profiles (Appendix B) and thermal conductivity estimates provided in the previous chapter, estimated heat flow in southeastern Manitoba ranges from 21 to 29 mW/m^2 in the Paleozoic carbonate formations. The highest heat flow values occur outside the City of Winnipeg or near the base of the carbonate sequence in some parts of the Winnipeg area. Heat flow in the Precambrian basement is estimated to be approximately 35 mW m^{-2} in the Winnipeg area (Jessop and Judge, 1971).

5.2.2 Estimating the Importance of Regional Groundwater Flow Using Analytical Models

Domenico and Palciauskus (1973) provided an approximate solution to the differential equation describing heat flow within a closed sedimentary basin with a rectangular geometry in cross-section:

$$T(x,z) = T_1 + \Gamma_z(z - z_o) + \Gamma_z \frac{K}{\lambda} \sum_{n=1}^{\infty} j_n \cos\left(\frac{n\pi x}{L}\right) \left[(z - z_o)\cosh\left(\frac{n\pi z}{L}\right) + \frac{L\sinh\left[\frac{n\pi(z - z_o)}{L}\right]}{n\pi \cosh\left(\frac{n\pi z_o}{L}\right)} \right]$$

(5.1)

where z_o is the depth of the basin, Γ_z is the vertical geothermal gradient, λ is thermal diffusivity, and L is the length of the basin. The groundwater flow regime incorporated into this equation is based on Toth's (1962) solution to the groundwater flow equation for small unconfined basins, which can be written as follows:

$$\Phi(x,z) = j_o + \sum_{n=1}^{\infty} j_n \cosh\frac{n\pi z}{L} \cosh\frac{n\pi x}{L}$$ (5.2)

where j_o and j_n are coefficients determined by the position of the water table. Domenico and Palciauskas (1973) provided the following relationships for the general solution to equation 5.2:

$$j_o = A$$ (5.3)

$$j_1 = \frac{-B}{\cosh\left(\frac{\pi z_o}{L}\right)}$$ (5.4)

$$j_i = 0 \text{ for } I > 1$$ (5.5)

where A is the average fluid potential and B is the fluid potential above the average fluid potential at x = 0 and below the average fluid potential at x = L. By applying these relationships, equation 5.2 becomes:

74

$$\Phi(x,z) = A - \left[\frac{B\cosh\left(\dfrac{\pi z}{L}\right)}{\cosh\left(\dfrac{\pi z_o}{L}\right)} \right]\cosh\left(\frac{\pi x}{L}\right) \qquad (5.6)$$

This model assumes homogeneous material properties and allows for recharge and discharge along the entire upper surface. These assumptions of homogeneous material properties are violated by the Carbonate Rock Aquifer, as is the model geometry. However, a model based on estimates of typical parameters for the Paleozoic carbonate sequence in the Williston Basin and the dimensions of the basin will still provide some indication of the relative importance of advective and conductive heat transport.

The distance between the recharge and discharge areas of the Carbonate Rock Aquifer is required in the application of equation 5.1. The Carbonate Rock Aquifer is recharged in the Black Hills of South Dakota and adjacent areas of Wyoming and discharges into the large lakes of southern and central Manitoba and the Red and Rat Rivers (Grasby et al., 2000; Grasby and Betcher, 2002). This geometry represents drop in elevation of approximately 1800 metres over a distance of approximately 800 kilometres. In the model it was assumed the hydraulic head drops linearly according to this drop in elevation. A basin depth of 4500 metres was used (Aitken, 1989). Other parameters used in this model are outlined in Table 5.1. The results of this model indicate that advection has essentially no impact on the geotherms present in the basin (Figure 5.3). Other values of hydraulic conductivity and thermal conductivity were also considered but these had very little impact on

the results. The Winnipeg Formation is subject to roughly the same parameters, suggesting that advective heat flow will play only a minor role in determining the position of the geotherms within the aquifer. This is in agreement with the findings of Domenico and Palciauskus (1973), which suggests that groundwater flow will have little impact on the distribution of temperatures in a basin if the basin's length is very long, compared its depth.

The possibility of advective perturbations to the temperature field in the Williston Basin between the recharge area in the Sandilands area and the discharge areas of the Red River and Lake Winnipeg was also investigated. The parameters used in this model are outlined in Table 5.1. The temperature field estimated by this model indicates that advection should have a negligible effect on temperatures in the Carbonate Rock Aquifer between the Sandilands and the Red River (Figure 5.4). When considering these results, it becomes apparent that the recharge entering the Carbonate Rock Aquifer in the Sandilands, Bird's Hill and Interlake areas will not have a noticeable impact on the temperature distribution in the subsurface because of the shallow depth of these flow systems compared to their length.

In addition to the rectangular model of Domenico and Palciauskas (1973), a model with a wedge-shaped geometry, which estimates the change in heat flow of a sedimentary basin above a basal aquifer, can be used (Figure 5.5; Jessop, 1989). The model is based on one developed by Lewis and Beck (1977) to estimate that change in temperature gradient above a

fracture with active groundwater flow. Jessop (1989) replaced the fracture with an aquifer in his model estimate and derived the following equation:

$$\kappa\delta = \frac{v}{\eta} H \rho_f c_f g \sin(\theta) \qquad (5.7)$$

where δ is the fractional change in temperature gradient, $\frac{v}{\eta}$ is groundwater velocity, H is the thickness of the aquifer and θ is the angle between the aquifer and the horizontal. This model is perhaps more applicable than Domenico and Palicauskas' (1973) model to many sedimentary basins that have a wedge shape, such as the WCSB.

The wedge model was used to examine the possibility that groundwater flow in the Winnipeg Formation could be affecting subsurface temperatures in southeastern Manitoba. Using parameters outlined in Table 5.2, the temperature gradient is predicted to change by less than 1% across the Winnipeg Formation according to equation 5.7. This finding is consistent with measured temperatures, which are not significantly different between the Sandilands and Winnipeg areas.

The change in heat flow from the deepest part of the Williston Basin to the Red River in the Paleozoic carbonate sequence was also examined using this equation. Assuming parameters outlined in Table 5.2, the temperature gradient is predicted to increase by 11%. However, temperature gradients and heat fluxes present in the Winnipeg area are lower than those observed deeper in the basin. This result suggests that the assumptions made in equation 5.7 concerning aquifer geometry are not met in this portion of the

77

Williston Basin. Groundwater velocities are likely lower than 1.0 m yr^{-1} and the Paleozoic sequence decreases in thickness from greater than 1000 metres at the centre of the Williston Basin to less than 200 metres in the Winnipeg area. Also, the geometry of the problem is not completely consistent with the model described by equation 5.7. However, Jessop (1989) does provide a basin example as an example of the utility of his model suggesting that it may provide some insight in the current context.

5.2.3 Discussion of Heat Flow in the Eastern Williston Basin

Regional groundwater flow does not appear to have a major impact on the distribution of subsurface temperatures in southeastern Manitoba. This is supported by the temperature measurements and analysis. Subsurface temperatures in southeastern Manitoba appear to be primarily a result of conductive heat flow. Variations in temperature at a given depth from location to location appear to be a function of elevation and amount of surface cover. Temperatures in the bedrock aquifers in the Sandilands are approximately the same as those that occur at lower elevations to the west. However, the amount of sediment cover is generally greater in the Sandilands area than in area near the Red River.

5.3 Estimating Recharge Rates in the Sandilands Area Using Temperature Profiles

5.3.1 Introduction

While topographically-driven groundwater flow does not appear to affect regional heat flow in southeastern Manitoba, it does have the potential to cause systematic deviations in the Sandilands area, where relatively large amounts of water recharge the underlying bedrock aquifers. These deviations in temperature may allow for estimation of groundwater recharge rates, which is one of the most important parameters necessary for groundwater resource management (Scanlon and Cook, 2002). Although field techniques exist to estimate recharge, such as infiltrometers, environmental isotopes, and Darcy's law estimates; recharge remains an elusive quantity to measure and is subject to large degrees of uncertainty and spatial variability.

The Sandilands area of southeastern Manitoba is thought to be a major area of recharge to a regional sandstone aquifer based on its elevated topography, the permeability of its surficial sediments, regional water chemistry data and hydraulic head distribution within the sandstone aquifer (Betcher, 1986). Recharge rates in the shallow sands and gravels of the Sandilands have been estimated using environmental isotopes and chlorofluorocarbon dating (Cherry, 2000). However, there is a thick till layer that separates the highly permeable surficial sediments from the underlying

sandstone aquifer, indicating that further research is required to determine the amount of recharge to the sandstone aquifer in this region. The current study attempts to quantify the amount of recharge to the sandstone aquifer by analysing temperature profiles of monitoring wells and boreholes in the region.

In the past, shallow groundwater flow systems have been studied using temperature measurements. For example, Cartwright (1970) used temperature profiles in monitoring wells to examine vertical groundwater movement in Illinois. Parsons (1970) utilised temperature measurements to study groundwater flow within a glaciofluvial complex in northern Ontario. Various researchers (e.g. Lachenbruch and Marshall, 1986; Harris and Chapman, 1997) have noted that climate change can have a significant impact on subsurface temperatures. Most of these studies were conducted in areas of minimal groundwater flow but it is possible that transient heat flow due to climate change could create spurious estimates of groundwater recharge rates. This issue of increases in ground surface temperature due to climate change has been addressed by Taniguchi et al. (1999) in a study where subsurface temperatures were used to estimate recharge rates in Japan. However, a linear increase in surface temperature was assumed in that study and this limits the applicability of their method.

5.3.2 Geology of the Sandilands Area

The Quaternary geology of the Sandilands area is complex and includes glacial, glaciofluvial and glaciolacustrine deposits (Figure 5.6). The dominant feature of the area is a large ridge composed mainly of sand, gravel and silt diamicton (Figure 5.7), which is underlain by several silty till formations. The ridge was formed in an interlobate position when the Rainy Lake Lobe and the Red River Lobe of the Laurentide Ice Sheet retreated and separated during the late Wisconsinan Glaciation and is classified as an interlobate moraine in accordance with guidelines provided by Prest (1967). This interlobate moraine is coincident with the subcrop belt of the Winnipeg Formation. Within the moraine are several outwash fans that have coalesced and to the north of the ridge, sand and gravel were deposited as an esker, which has since been buried by till during later advances of Pleistocene ice. Subsequent readvances of the ice sheet deposited a silty sand till known as the Marchand Formation by reworking the previously deposited outwash (Teller and Fenton, 1980). During this deposition, the ice sheet did not have enough energy or thickness to flow over the ridge and, as a result, this silty sand till occurs only on the flanks of the ridge. The ridge existed as an island in Glacial Lake Agassiz at the end of the Wisconsinan Glaciation. Sand and gravel were deposited as beaches on the slopes of the moraine during this period.

5.3.3 Hydrogeology of the Sandilands Area

The Sandilands area is an important area of recharge to both the Winnipeg Formation sandstone aquifer (Betcher, 1986) and the Carbonate Rock Aquifer (Grasby and Betcher, 2002; Kennedy, 2002). However, only a portion of the recharge infiltrating the surficial sediments reaches these bedrock aquifers. Just to the east of the axis of the moraine, a groundwater divide is present (Cherry, 2000; Hinton, 2003) and groundwater to the east of this divide flows eastward into the tills that surround the moraine. This water does not enter any large-scale regional flow system due to the lack of bedrock aquifers in this area and likely discharges into the wetlands east of the moraine.

Limited data exist on the hydrogeologic properties of the Sandilands area. Cherry (2000) conducted slug tests, which suggested that the hydraulic conductivities range from 2.4×10^{-4} to 8.2×10^{-6} m s^{-1} for the sands of the area and from 6.8×10^{-6} to 8.3×10^{-9} m s^{-1} for the underlying tills. Betcher (1986) reported hydraulic conductivities of the sandstone ranging from 10^{-3} to 10^{-6} m s^{-1}, with most values falling between 10^{-5} to 10^{-6} m s^{-1}. The hydraulic conductivities of surficial sands in the Sandilands area range from 1.3×10^{-4} to 1.5×10^{-5} m s^{-1} based on a limited number of constant head permeameter tests conducted in the current study. The lower hydraulic conductivity of the tills implies that the flow rate within the tills controls the recharge rate to the sandstone aquifer beneath the moraine.

5.3.4 Analytical Methods of Estimating Groundwater Velocities from Temperature Profiles

Solutions to equation 2.10, which can be used to estimate specific discharges, have existed for many years. However, the application of these solutions has yet to become common practice in hydrogeology. The solutions examined in this study are those of Bredehoeft and Papadopulos (1965) and Reiter (2001).

Bredehoeft and Papadopulos (1965) provided the following solution to equation 2.10 assuming uniform vertical flow of both heat and groundwater:

$$T_z = T_o + [T_L - T_o][\exp(N_{Pe} (z/L))-1]/[\exp(N_{Pe})-1] \quad (5.8)$$

where T_z is the temperature at a given depth along the profile, T_o is the temperature at the top of a semi-confining layer, T_L is the temperature at the bottom of a semi-confining layer, N_{Pe} is the Peclet number for porous media, z is the depth along the profile and L is the length of the temperature profile over the semi-confining unit. Following Domenico and Schwartz (1998) the Peclet number for porous media is defined as:

$$N_{Pe} = \rho_f c_f v_z L/\kappa_e \quad (5.9)$$

A curve matching procedure can be applied to determine the Peclet number and the specific discharge can be calculated within a hydrostratigraphic unit of uniform and steady flow.

Reiter (2001) solved the differential equation describing heat flow in porous media using an approach that decouples the horizontal and vertical components of the differential equation. By assuming steady-state conditions,

uniform groundwater flow velocities, and $\partial^2 T/\partial z^2 \gg \partial^2 T/\partial x^2$ equation 2.10

becomes:

$$\frac{d^2 T}{dz^2} = \frac{c_f \rho_f}{\kappa_e} v_x \frac{dT}{dx} + \frac{c_f \rho_f}{\kappa_e} v_z \frac{dT}{dz} \qquad (5.10)$$

Equation 5.10 can then be integrated to produce the following equation:

$$\Gamma_z = a + bz + cT \qquad (5.11a)$$

where:

$$b = (c_f \rho_w / \kappa_e) \; v_x \frac{dT}{dx} \qquad (5.11b)$$

$$c = (c_f \rho_w / \kappa_e) v_z \qquad (5.11c)$$

and a is a fitting constant and Γ_x is the horizontal temperature gradient.

By creating a three-dimensional plot of vertical temperature gradient versus temperature and depth, it is possible to obtain a unique estimate of vertical specific discharge. When a plane is fit to the data, the temperature slope of the plane is used in equation 5.11c to calculate a vertical specific discharge. Equation 5.11b can be used to provide an estimate of horizontal specific discharge if the horizontal temperature gradient is known. If horizontal temperature gradient data are unavailable, the slope provides the product of horizontal specific discharge and horizontal temperature gradient.

5.3.5 Methodology

Temperature measurements were taken in existing monitoring wells in the Sandilands area (Figure 5.6) in June 2000, August 2000 and November

2001. Based on equation 2.11, free convection within wells and boreholes used in this study is not significant because observed temperature gradients were less than the critical value. All installations had diameters of less than 0.125 metres, which allowed for critical gradients much higher than the gradients measured in the area.

Two boreholes, TH1 and TH2 (Figure 5.6), were used in this study in addition to the monitoring wells. These boreholes were installed in October 2000 specifically for thermal measurements by placing a 0.125 metre diameter polyvinyl chloride (PVC) casing in a 0.20 metre diameter borehole. The annulus was sealed with bentonite over the entire length of the casing and the casing was then filled with a mixture of water and glycol, to prevent the top of the column from freezing during the winter. Gretener (1981) suggested that temperature anomalies associated with drilling will dissipate to a few percent within days of drilling. However, the temperature profile in these boreholes was not measured until November 2001 to ensure that the temperature of the water in the wells was representative of groundwater in surrounding formations.

The stratigraphy of the tills is highly variable and there are at least two units present in the tills underlying the subaqueous outwash (Figure 5.7). In some of the lithological logs these units could not be distinguished and as a result of the complex stratigraphy temperatures at different depths ere analysed in each borehole using equations 5.8 and 5.11. Generally, temperatures within the entire till sequence beneath the moraine or a more

85

clay-rich lower till unit, which is assumed to be a semi-confining layer, were analysed.

The methods proposed by Bredehoeft and Papadopulos (1965) and Reiter (2001) both assume that changes in climate do not affect the temperatures used to estimate recharge rates. Cherry (2000) measured temperatures at several depths over a period of 12 months in a piezometer near GSC9901. Temperatures at that location were found to vary by less than 0.1°C beneath a depth of 10 metres. Temperatures measured in this study suggest that temperatures variations beneath a depth of 35 metres are less than 0.05 °C between May 2000 and November 2001.

To assess possible affects of changes in climate over longer periods of time, a series of synthetic models were created using an assumed ground surface temperature history (Figure 5.8) based on Environment Canada's record for Winnipeg (Figure 3.7). In most cases, ground surface temperature histories appear to be a damped version of surface air temperature histories (Majorowicz et al., 1999) and thus a five-year moving average filter was applied to the temperature record for Winnipeg. Also, it should be noted that the relationship between ground surface temperatures and air temperatures is not fully understood and depend on a number of factors (e.g. Schmidt et al., 2001; Beltrami, 2001: Majorowicz et al., 1999). Majorowicz et al. (1995) found that ground surface temperature and surface air temperature histories in grassland sites in western Canada were more highly correlated than those in forested areas, which suggests that ground surface temperature variability

may not be strongly correlated with climate in the Sandilands area. However, the simulations examined should provide an indication of the importance of variability in ground surface temperature in recharge studies that use temperature measurements. Recharge rates used in these simulations were 7.9×10^{-10} m s^{-1}, 3.2×10^{-9} m s^{-1} and 1.3×10^{-8} m s^{-1}, which extend over the range of recharge rates expected in the area. Saturated conditions were assumed over the entire thickness examined.

These simulations predict that a wide range of temperatures in the upper portion of the profiles during the past century (Figure 5.9). This variability makes it difficult to distinguish the characteristic concave downward shape in the temperature profiles in the case where recharge was only 7.9×10^{-10} m s^{-1} (Figure 5.9a). However, this curvature was obvious in the two higher recharge rate cases (Figure 5.9b and c). Temperature profiles at depths of 40 to 140 metres and 60 to 140 metres were then analysed using equation 5.8 to examine deviations in the estimated recharge rate for the actual recharge rate resulting from variation in ground surface temperature.

Recharge rates estimated from the synthetic profiles showed a considerable amount of variation over time (Figure 5.10). The estimated recharge rates were most highly correlated with ground surface temperature with a lag of 10 to 20 years but these correlations were not significant at the p = 0.05 level. In each case, the mean of the estimated recharge rates was significantly different than the actual recharge rate in the model at a 95% confidence level (Table 5.3). The ratio of the standard deviation to the

recharge rate decreased with increasing recharge rate. The results suggest that where higher recharge rates are estimated, the estimates are more likely to be accurate. The results using the portion of the profile from 60 to 140 metres also appear to be considerably more accurate than those that utilised temperatures from 40 to 140 metres depth. The Sandilands area thus provides a situation where it should be possible to estimate specific discharge from temperature profiles. However, estimates in areas surrounding the moraine may be less accurate due to the depth of the aquifers in these areas.

In the analysis of temperatures measured in this study, Bredehoeft and Papadopulos' (1965) solution was fit to the temperatures within the hydrostratigraphic unit of interest and plots of dimensionless temperature versus dimensionless depth were created. The measured temperatures at the top and bottom of the unit of interest were assigned T_o and T_L respectively. Peclet numbers were obtained from these dimensionless plots by using a regression analysis that maximized the R^2 correlation coefficient between observed and modeled temperatures (Table 5.4). Peclet numbers obtained from modeling were then used to estimate vertical specific discharge from equation 5.8. The specific heat capacity and density values required for the calculation were those of water at approximately 6 °C. Limited thermal conductivity testing was performed on till samples due to difficulties encountered in the handling of specimens. Two tests of till thermal conductivity were performed during this study and these had a mean value of 0.4 W m^{-1} °C^{-1}. Poor contact between the divided bar apparatus and sample

may have decreased the measured thermal conductivity. Also, these tests were conducted under unsaturated conditions because the samples did not remain intact once saturated. However, if we examine the thermal conductivity of the major components of this till, which are clay and clasts of carbonate rock, a slightly higher value is estimated. Domenico and Schwartz (1998) state that the range of thermal conductivity for clay is 0.5 to 0.8 W m^{-1} °C^{-1} and testing in this study produced a mean value of 2.4 W m^{-1} °C^{-1} for the Red River Formation, which is the source of much of the carbonate material in the tills of this region (Teller and Fenton, 1980). Based on the results of the two tests and the expected range values, an effective thermal conductivity of 1.0 W m^{-1} °C^{-1} was used in the modeling performed in this study for all profiles modeled. Although thermal conductivity likely varies with depth in each profile and between profiles, the overall range of plausible thermal conductivities is reasonably small and likely fall within a factor of approximately five according to the assumption about the properties of the tills. The estimated specific discharges should have approximately the same level of accuracy as the thermal conductivity estimates. This method therefore provides a greater degree of certainty than would be possible for recharge estimates requiring estimation of hydraulic conductivity, which is known to vary over several orders of magnitude.

The plane fitting method of estimating vertical specific discharge proposed by Reiter (2001) was also applied to each of the profiles over the same hydrostratigraphic sections as those analysed with the Bredehoeft and

89

Papadopulos (1965) solution. This was also accomplished with a regression analysis that maximized the correlation coefficient between observed and modeled temperatures, where modeled temperatures were calculated by using vertical temperature gradient and depths in equation 5.11a. The product of horizontal specific discharge and horizontal temperature gradient was calculated using equation 5.11b to estimate the ratio of horizontal specific discharge to vertical specific discharge. If this ratio is less than 0.01 horizontal gradients are negligible (Lu and Ge, 1996) and permits valid results to be obtained from the curve matching solution provided by Bredehoeft and Papadopulos (1965).

5.3.6 Results

All wells and boreholes were measured repeatedly during the study and in the sections studied no significant transient effects (> 0.05 °C) were observed at depths of greater than 35 metres. The absence of sinusoidal trends in the temperature profiles at this depth is in agreement with the findings of Cherry (2000). In that study, monthly measurements were made with thermistors at various depths ranging from 1 to 18 metres deep at location near GSC 9901. During a complete year of measurements temperatures at depths of greater than 10 metres varies by less than 0.1 °C. In the current study, temperature profiles of GSC9901, GSC9902, TH1, TH2 and Woodridge (Figures 5.11 to 5.15) showed a convex downward temperature profile over at least part of the temperature profiles suggesting

90

downward movement of groundwater in these areas. The temperature profile observed at OH20 exhibited a decrease in temperature with depth, indicating this monitoring well may be located in a discharge area (Figure 5.16).

All wells but OH20 produced R^2 correlation coefficients between modeled and observed temperatures greater than 0.995 for the one-dimensional solution (Table 5.4). Vertical recharge rates between 1.2×10^{-9} and 1.3×10^{-8} m s^{-1} were obtained with this solution. The two-dimensional plane-fitting method of estimating specific discharges given by Reiter (2001) suggested that recharge rates ranged from 1.2×10^{-8} to 1.6×10^{-8} m s^{-1}. R^2 correlation coefficients for this model were lower, ranging from 0.897 to 0.996 (Table 5.4). The products of horizontal specific discharge and horizontal temperature gradient calculated from equation 5.10b in these wells varied from 1.2×10^{-10} to 1.6×10^{-10} °C s^{-1}. Measurements from closely spaced piezometers suggested that the maximum horizontal temperature gradient was approximately 0.01 °C m^{-1}. Using this horizontal temperature gradient, the horizontal specific discharges are of the same order of magnitude as the vertical specific discharges, which may render the one-dimensional results invalid according to the criterion of Lu and Ge (1996). However, this cannot be proved or disproved because horizontal temperature gradient data was only available at a few locations and only at depths of less than 50 metres. Also a lack of accurate geodetic surveying of monitoring wells in the area places further uncertainty of horizontal temperature gradient estimates.

Monitoring wells in the areas surrounding the moraine often had complex hydrostratigraphies, which made analysis impractical in many cases. For example, analysis of the temperature profile of OH20 using the one-dimensional method produced an upward vertical specific discharge of 2.4 x 10^{-10} m s^{-1} and an R^2 correlation coefficient of 0.657 (Table 5.4). Analysis using the plane fitting procedure was possible with Reiter's method and this was performed for a portion of the temperature log that had the best linear fit when temperature was plotted against vertical temperature gradient (Figure 5.16). The results indicated an upward specific discharge of 1.3 x 10^{-8} m s^{-1} and a product of horizontal specific discharge and horizontal geothermal gradient of 3.1 x 10^{-11} $^{\circ}$C m^{-1}. The product of the horizontal specific discharge and horizontal temperature gradient suggests that the solution given by Bredehoeft and Papadopulos (1965) is invalid in this case if a horizontal temperature gradient at that location is less than 0.02 $^{\circ}$C m^{-1}.

5.3.7 Discussion

The results obtained from equation 5.8 suggest that groundwater flow has a downward component ranging from 1.2 x 10^{-9} m s^{-1} to 6.5 x 10^{-9} m s^{-1} (37 to 210 mm yr^{-1}) in areas where outwash is exposed at the surface in this study. Alternatively, if equation 5.11 is used the estimated Darcy flux is approximately 1.4 x 10^{-8} m s^{-1} (420 mm yr^{-1}) throughout areas where outwash is exposed at the surface in the study area. The range of recharge rates estimated by equation 5.8 is appealing because it is closer to estimates

produced in other studies. However, horizontal groundwater flow is likely present in some areas, suggesting that equation 5.11 is more appropriate. There is no statistical difference between the fits of the two models at a 99% confidence level and it is not obvious which model is more accurate. Monitoring wells GSC9901, GSC9902, TH1 and TH2 all exhibit extremely good correlations between modeled and observed temperatures within the till units for both methods used. Over the range of depths examined, these recharge rates estimates are most likely accurate according to the synthetic models produced earlier in this chapter. The ability to achieve a good fit over the till section indicates that flow is relatively uniform over these intervals, as this is a requirement of the application of equations 5.8 and 5.11a. Recharge to the Winnipeg Formation occurs mainly along the axis of the ridge in the vicinity of wells GSC9901, GSC9902, TH1 and TH2. All of these wells except TH2 overlie or penetrate the sandstone of the Winnipeg Formation.

At Woodridge1, recharge in at till layer approximately 35 to 46 metres deep is estimated at approximately the same rate as GSC9901, GSC9902, TH1 and TH2. Groundwater flow in deeper till formations at this location were not conducive to modeling at this location, likely due to a change in flow direction with depth, which violates the assumptions of both equation 5.8 and 5.11. Flow in the area of Woodridge1 is expected to become increasingly more horizontal with depth due to the presence of low permeability Precambrian rocks beneath the till. Groundwater in these deeper till formations presumably flows with a strong horizontal component towards the

Winnipeg Formation. Similar trends are likely present in the area of TH2 near the Precambrian basement but no temperature or hydraulic head data are available to corroborate this idea.

In a study using tritium and chlorofluorocarbon (CFC) groundwater dating techniques, Cherry (2000) reported surficial recharge rates varying between 1.4×10^{-9} and 5.5×10^{-9} m s^{-1} (44 to 173 mm/yr. Traditional groundwater hydraulics suggest recharge rates in the Sandilands area range from 10^{-7} to 10^{-10} m s^{-1} but these estimates are poorly constrained due to a lack of hydraulic conductivity data for the tills. Using the average hydraulic conductivity and distribution of equipotentials given by Betcher (1986), the Darcy velocity within the Winnipeg Formation is approximately 10^{-9} m s^{-1}.

Groundwater flow in the surficial sediments overlying the Winnipeg Formation north of the outwash becomes largely horizontal and the temperature profile suggests that there may be upward from of groundwater at OH20. Grasby and Betcher (2002) suggested that flow within the Carbonate Rock Aquifer is from east to west at this location and emanates from the Sandilands area. The analysis of OH20's temperature profile indicates that groundwater is discharging from the Carbonate Rock Aquifer in this area, implying that not all of the recharge received in the vicinity of the moraine becomes part of the larger regional flow systems. Due to the depth of the temperatures analysed at this location, there is a considerable amount of uncertainty associated with this estimate of the Darcy velocity.

5.3.8 Conclusions on Sandilands Recharge

Analysis of temperature profiles is an effective method of estimating recharge rates in the Sandilands area, giving estimates of recharge rates and the direction of flow. However, care must be taken when selecting the method of analysis of temperature profiles. The one-dimensional solution to the flow of groundwater and heat derived by Bredehoeft and Papadopulos (1965) can produce excellent fits even when the presence of horizontal flow of groundwater precludes the model's application. This suggests that methods, such as Reiter's (2001) plane fitting method, which account for a horizontal component of groundwater and heat flow may be necessary to effectively use temperature data. However, because Reiter's (2001) method is capable a producing a wider variety of curves, it is more likely that this method could match a signal influenced by climate. The influence of variations in ground surface temperature should also be considered because variations in climate can cause deviations in temperature profiles that are similar to advectively influenced profiles.

Results from this study are in agreement with previous results from other studies in the area that utilized other methods to estimate recharge and provided better resolution than traditional groundwater hydraulics and results for depths greater than those of environmental tracers. The use of temperature logs to examine groundwater flow is highly efficient because field installations are simple and large amounts of data can be derived from individual monitoring wells and boreholes. Piezometer nests required for

most chemical tracer studies and for measurement of hydraulic gradients are not required for thermal investigations and temperature data obtained in the field require no laboratory analysis, making thermal methods both time and cost efficient. Less certainty is required for parameters in this case because the effective thermal conductivity of geological materials varies over less than one order of magnitude (Domenico and Schwartz, 1998), while hydraulic conductivity can vary over as many as thirteen orders of magnitude (Freeze and Cherry, 1979).

The use of temperature measurements can be a more powerful technique than environmental isotopes and other groundwater age dating techniques in some studies. Age dating techniques are generally only useful back to times dictated by half-lives, whereas temperature measurements are not subject to these age limitations. For example, tritium and chlorofluorcarbon dating would be of little use for estimating specific discharge through the tills of the Sandilands because groundwater at the bottom of the tills is likely at least 200 years old. However, over the depths where tritium and chlorofluorocarbon dating can be used, temperature profiles appear to be dominated by variations in climate and may produce erroneous estimates of recharge. The difficulties associated with determining recharge rates suggest that estimates should be made using several different techniques. The use of temperature profiles is an attractive method for estimating recharge because it provides an average estimate over a given depth interval, which is of interest to long-term water resource management

planning. Temperature analysis can also be used to estimate discharge rates, which is generally not possible with environmental isotopes in regional flow systems.

5.4 Conclusions on the Interaction between Groundwater Flow and Heat Flow in Southeastern Manitoba

On a regional scale, topographically-driven groundwater flow does not appear to have a significant effect on the thermal regime in southeastern Manitoba. Temperatures present in the bedrock aquifers of the area are largely a result of the magnitude of the basal heat flux from the Precambrian basement and factors related to elevation and sediment cover. A complete understanding of groundwater flow does not add significantly to our understanding of heat flow in southeastern Manitoba. However, subsurface temperature measurements are able to add to our knowledge of groundwater flow. The lack of heat transport from southwestern Manitoba to the Winnipeg area indicates that groundwater velocities in the Winnipeg Formation and in the overlying carbonate rock are low in that area. In the Sandilands area, advective disturbances to temperature profiles in the Sandilands areas provide a cost-efficient method of estimating deep recharge rates. The temperature field in southeastern Manitoba is not significantly affected by regional groundwater flow and heat flow appears to fairly uniform. The following chapters will use this information in the treatment of perturbations in the temperature field due to anthropogenic activities.

	Williston Basin from Black Hills to Red River	Williston Basin from Sandilands to Red River
Thermal Conductivity $(W\ m^{-1}\ {}^{\circ}C^{-1})$	3.6_1	2.4
Difference in Hydraulic Head based on topography (m)	1770	145
Depth of Flow System (m)	5000	150
Distance from Recharge to Discharge (km)	800	80
Geothermal Gradient $({}^{\circ}C\ m^{-1})$	0.015_1	0.010

References:
1. Majorowicz et al.,1986

Table 5.1: Parameters used in regional heat flow models produced using equation 5.2.

	Williston Basin from Black Hills to Red River	Williston Basin from Sandilands to Red River
Thermal Conductivity $(W\ m^{-1}\ ^\circ C^{-1})$	3.6_{1}	2.4
Darcy Velocity $(m\ y^{-1})$	1.0_{2}	1.0_{3}
Aquifer Thickness (m)	500	50
Dip Angle (degrees)	0.13	0.11
Change in Heat Flux	11%	1%

References:
1. Majorowicz et al., 1986
2. Hitchon, 1969
3. Betcher, 1986

Table 5.2: Parameters used in regional heat flow models produced using equation 5.7.

Recharge Rate (m s^{-1})	Average Recharge Rate from Temperature Data (m s^{-1})		Standard Deviation of Recharge Rate from Temperature Data (m s^{-1})		95% Confidence Interval of Mean Recharge Rate Estimates (m s^{-1})	
	40-140 m Depth	60-140 m Depth	40-140 m Depth	60-140 m Depth	40-140 m Depth	60-140 m Depth
7.9×10^{-10}	7.3×10^{-10}	5.1×10^{-10}	1.2×10^{-9}	7.0×10^{-10}	5.1×10^{-10}	3.2×10^{-10}
3.2×10^{-9}	4.7×10^{-9}	3.7×10^{-9}	2.3×10^{-9}	1.1×10^{-10}	1.0×10^{-9}	5.1×10^{-10}
1.3×10^{-8}	1.5×10^{-8}	1.2×10^{-8}	3.6×10^{-9}	1.6×10^{-9}	1.6×10^{-9}	7.0×10^{-10}

Table 5.3: Statistics of apparent recharge rate estimates from temperature profiles shown in Figure 5.9.

Well	Interval Analyzed (m)	Bredehoeft and Papadopulos' Method			Reiter's Method		
		N_{Pe}	v_z (m s^{-1})	R^2	$(v_x)(\Gamma_x)$ (^{O}C s^{-1})	v_z (m s^{-1})	R^2
GSC9901	65-130	0.32	1.2×10^{-9}	0.999	2.3×10^{-10}	1.6×10^{-8}	0.995
GSC9902	51-88	0.90	6.5×10^{-9}	0.988	1.9×10^{-10}	1.4×10^{-8}	0.897
TH1	63-127	0.66	2.5×10^{-9}	0.993	2.3×10^{-10}	1.5×10^{-8}	0.995
TH2	48-94	0.30	1.5×10^{-9}	0.997	1.9×10^{-10}	1.2×10^{-8}	0.993
Wood-ridge1	38-48	0.43	1.3×10^{-9}	0.996	2.3×10^{-10}	1.2×10^{-8}	0.994
OH20	35-56	-.07	-2.4×10^{-10}	0.657	3.1×10^{-10}	-1.3×10^{-8}	0.837

Table 5.4: Results of analysis of temperature logs using both Bredehoeft and Papadopulos' (1965) model and Reiter's (2001) model along with depths analyzed in each profile and times each well was logged. Downward groundwater velocities are indicated as positive values and upward groundwater velocities are indicated as negative values.
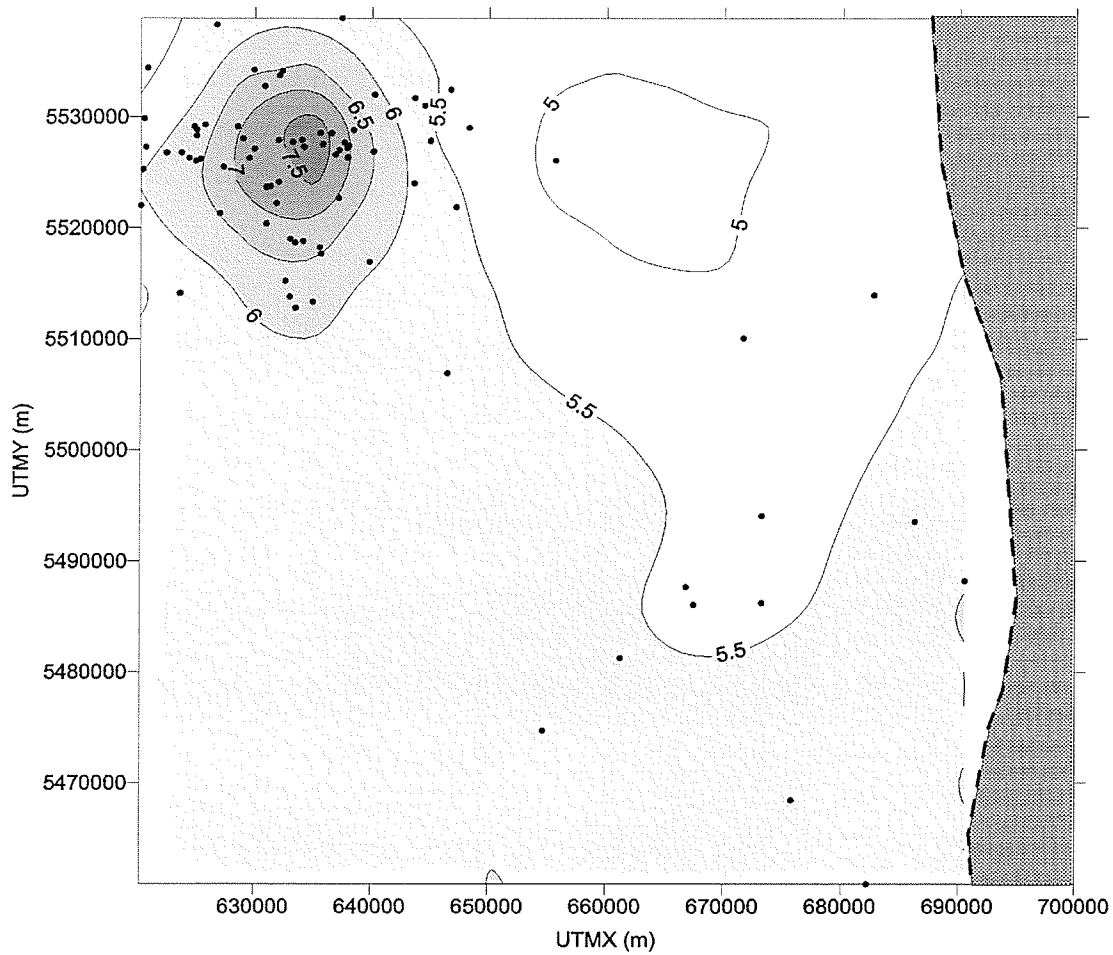
Figure 5.1: Temperature distribution in the carbonate rock aquifer of southeastern Manitoba. Dashed line indicates the eastern extent of the Paleozoic carbonates in the region and dots represent the location of wells where temperature measurements were made.
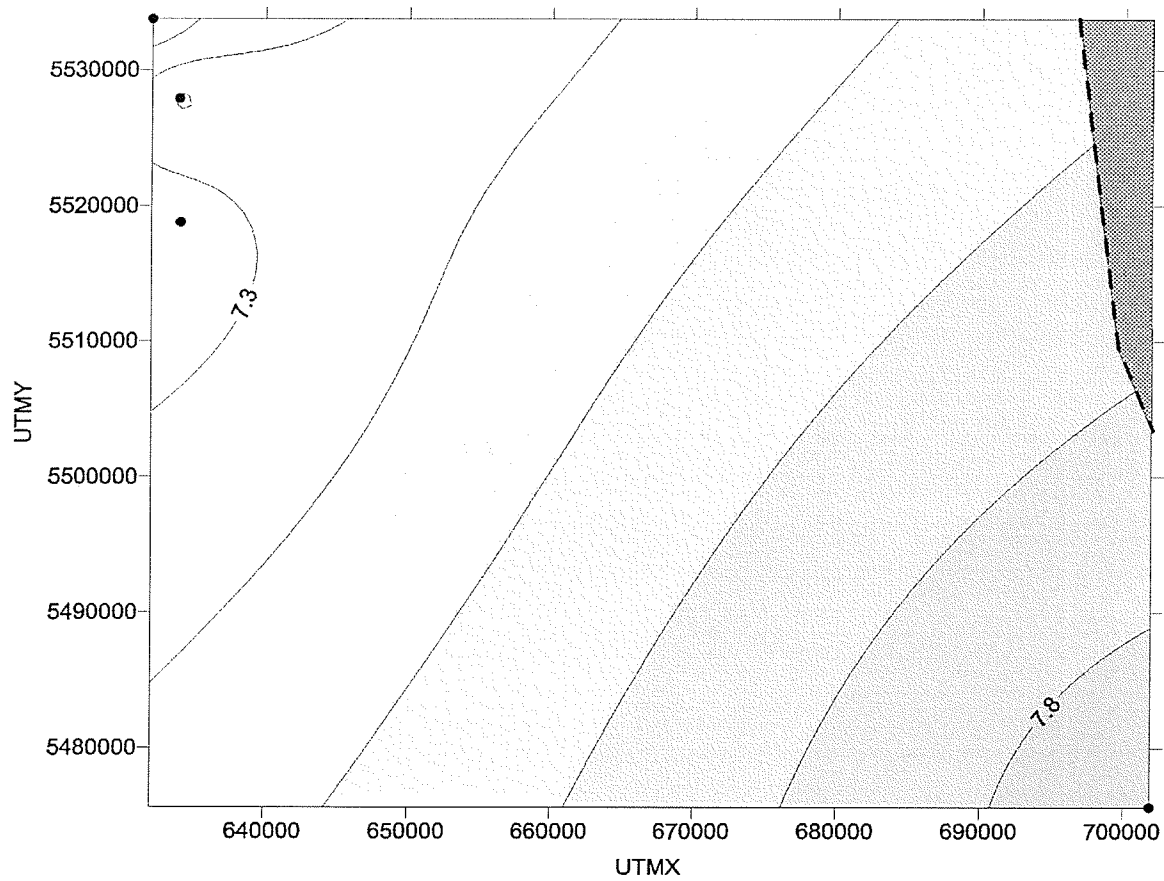
Figure 5.2: Temperature distribution in the Winnipeg Formation of southeastern Manitoba. Dashed line indicates the eastern extent of the Winnipeg Formation in the region and dots represent the location of wells where temperature measurements were made.
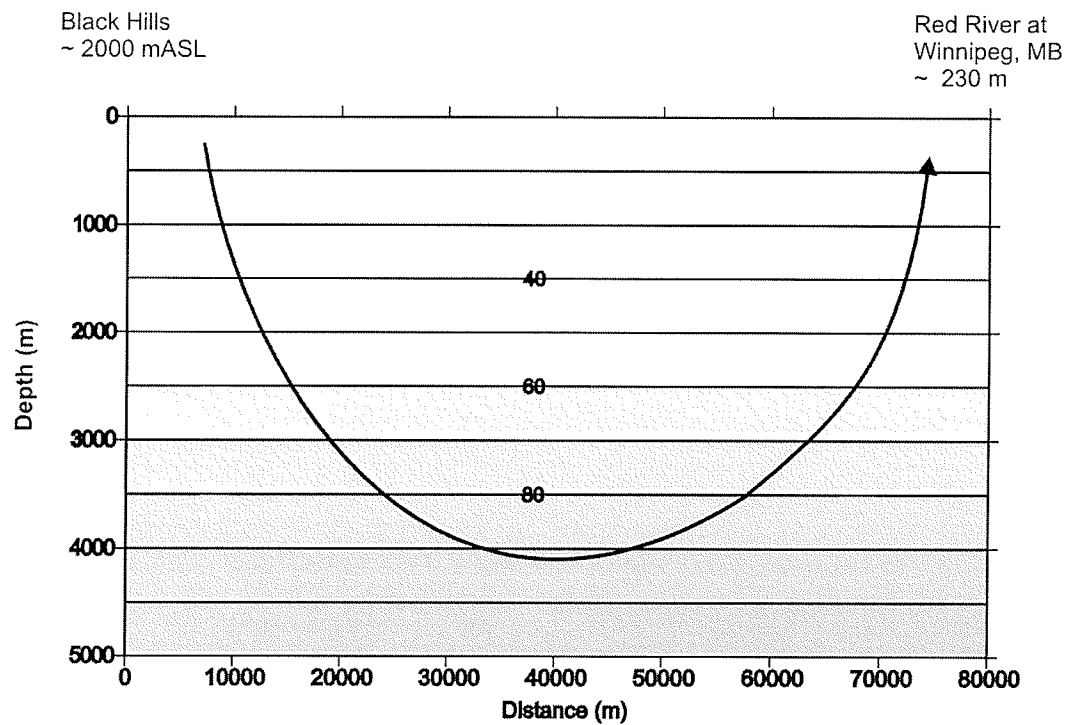
Figure 5.3: Temperature distribution estimated by the model produced by Domenico and Palciauskas (1973) for the Williston Basin between the Black Hills in South Dakota and the Red River in Manitoba. Arrow shows approximate groundwater flow direction in this model.
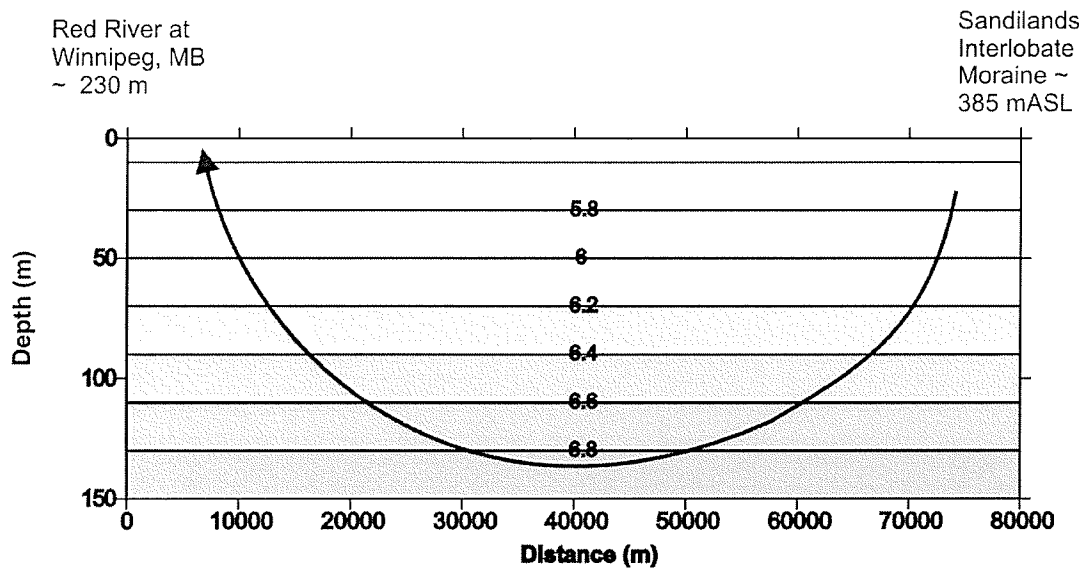
Figure 5.4: Temperature distribution estimated by the model produced by Domenico and Palciauskas (1973) for the Williston Basin between the Sandilands and the Red River in Manitoba. Arrow shows approximate groundwater flow direction in this model.
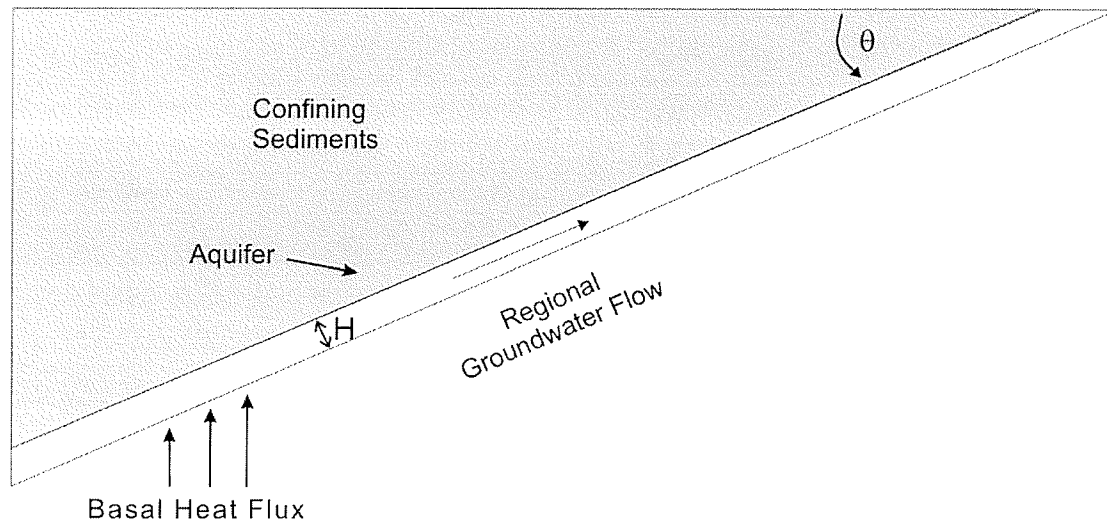
Figure 5.5: Wedge shaped model to estimate influence of groundwater flow on heat flow developed by Jessop (1990).

NONGLACIAL SEDIMENTS

1. ORGANIC DEPOSITS

REWORKED GLACIAL SEDIMENTS

2. GLACIAL LAKE SHORELINE SEDIMENTS

   2b. sand and gravel beach ridges;

   2a. sandy nearshore sediments.

SORTED GLACIAL SEDIMENTS

3. FINE GRAINED GLACIOLACUSTRINE SEDIMENTS

4. SUBAQUEOUS OUTWASH

UNSORTED GLACIAL SEDIMENTS

5. TILL.
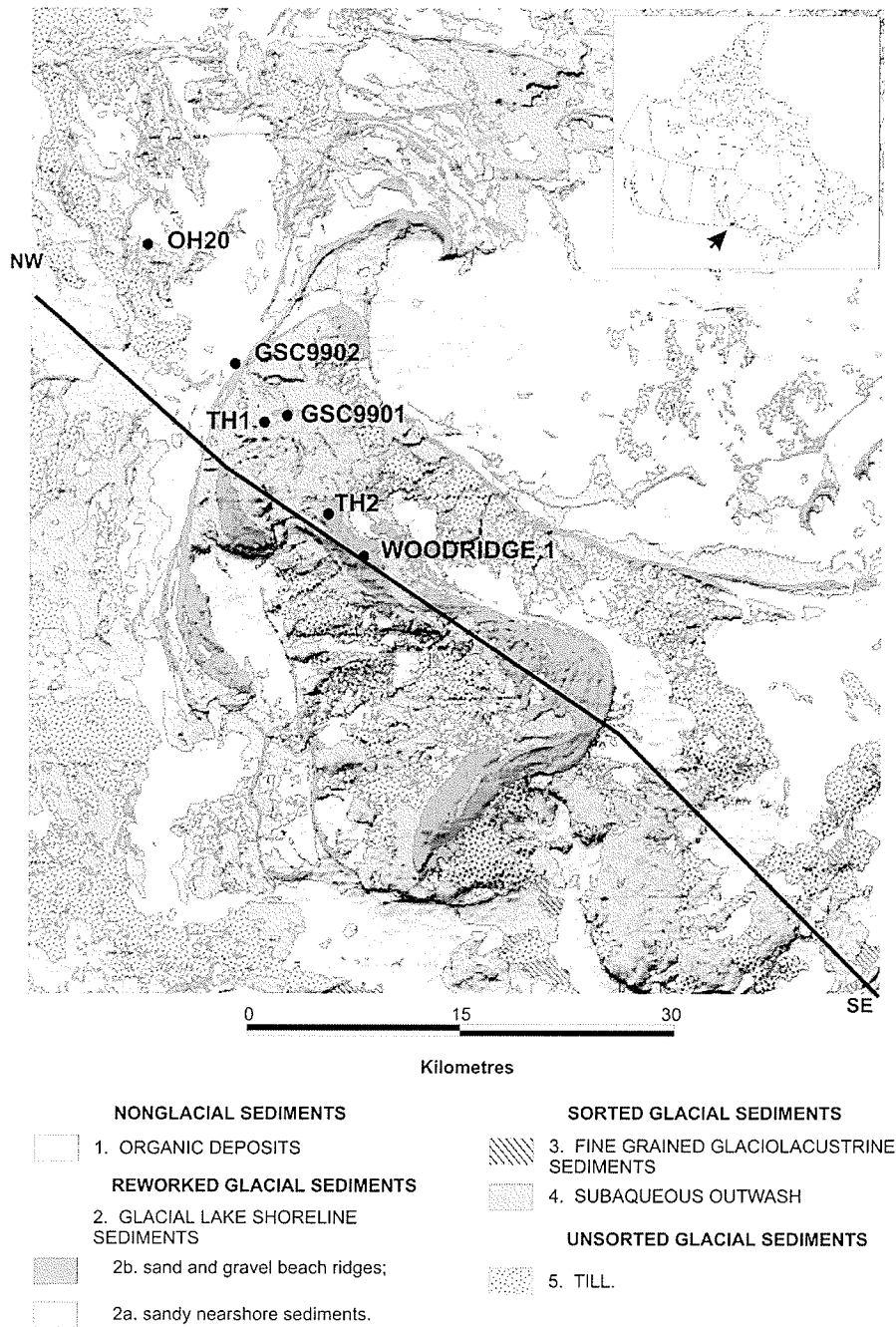
Figure 5.6: Digital elevation model of the Sandilands area draped with surficial geology of the Sandilands. Points indicate monitoring wells and boreholes analyzed in this study. Inset shows location of Sandilands area in Canada and line labeled NW-SE shows trace of cross-section shown in Figure 5.7 (Source: Manitoba Geological Survey).
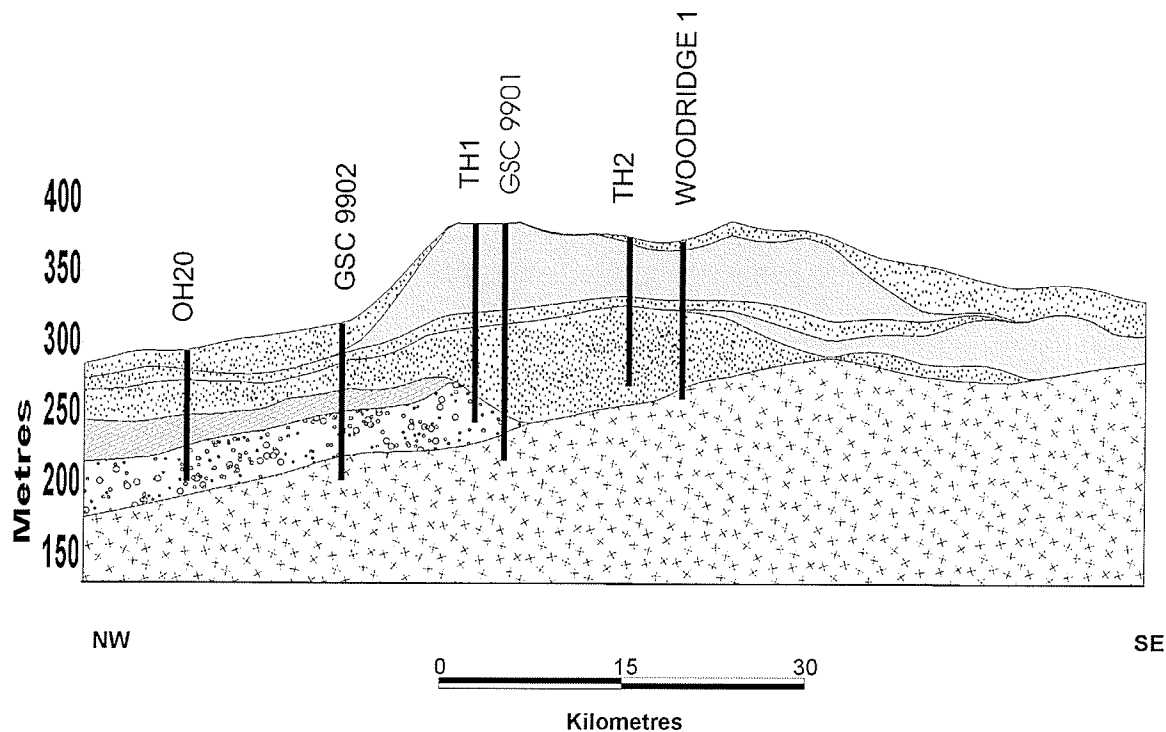
107

Figure 5.7 Cross section of the Sandilands area showing various geological units and approximate locations of monitoring wells and boreholes used in this study. Units not shown in the legend are equivalent to those used in Figure 5.6. Stratigraphy of the cross section is derived from a regional model compiled from a provincial database of all wells in the area and has a resolution of 5 km. Location of the cross section is indicated by the northwest-southeast trace on Figure 5.6 (Source: Manitoba Geological Survey).
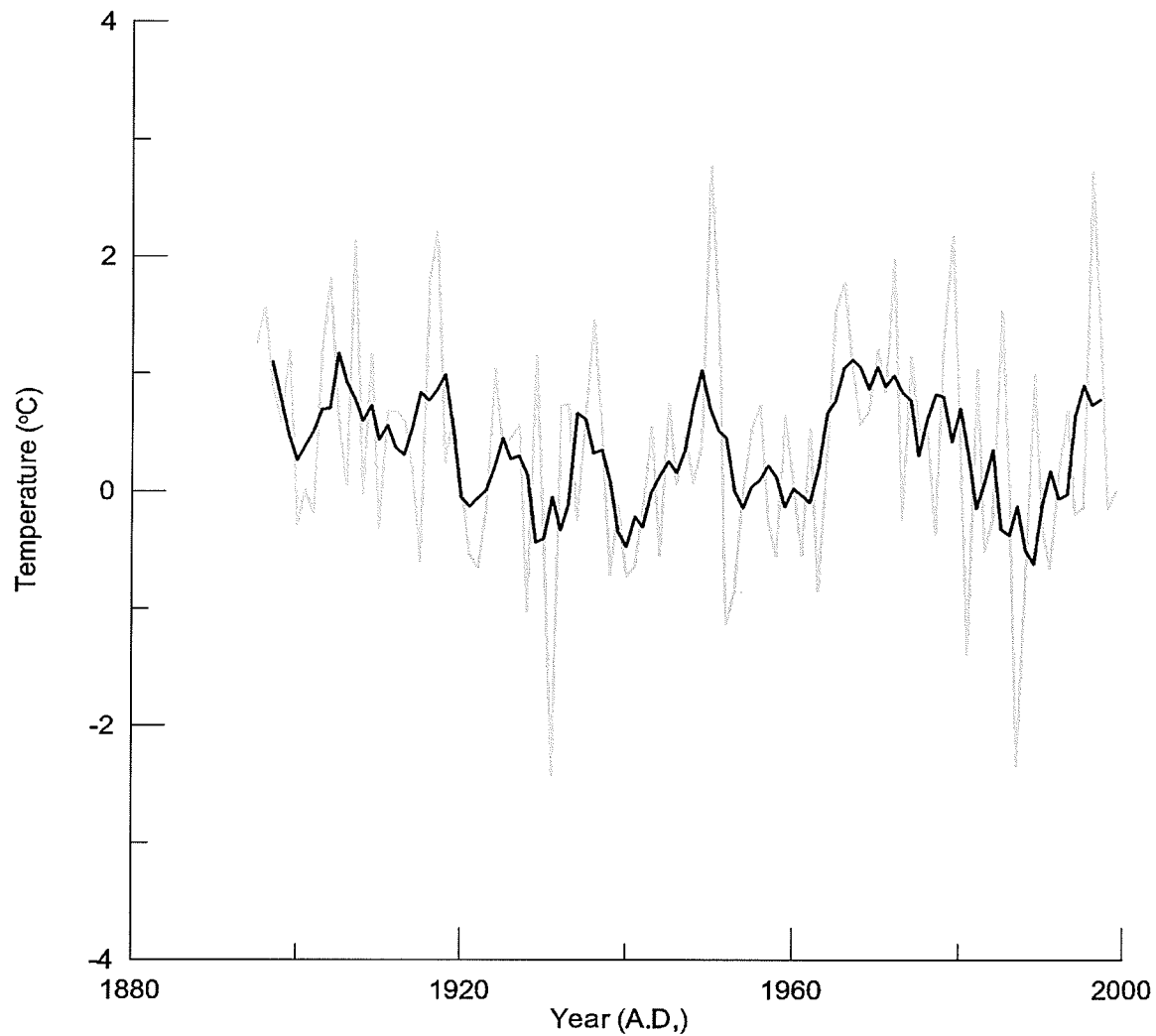
Figure 5.8: Ground surface temperature based on Environment Canada's record for Winnipeg used in the creation of synthetic heat flow models used to examine the impact of variability in ground surface temperature on recharge rates.
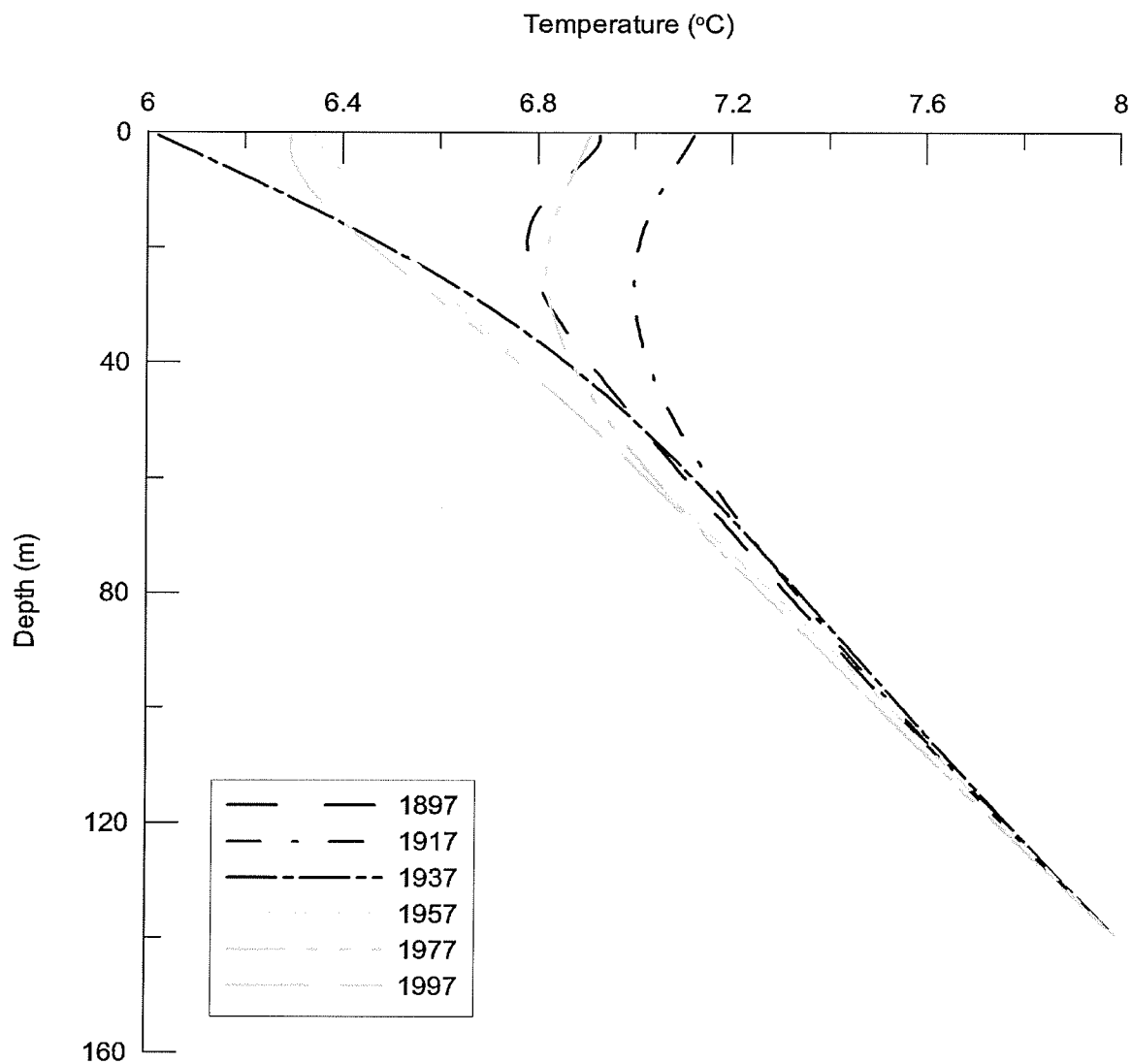
Figure 5.9a: Range of synthetic temperature profiles created with recharge rate of 7.9 x 10^{-10} m s^{-1} and the ground surface temperature history shown in Figure 5.8 over time period from 1895 to 2000.
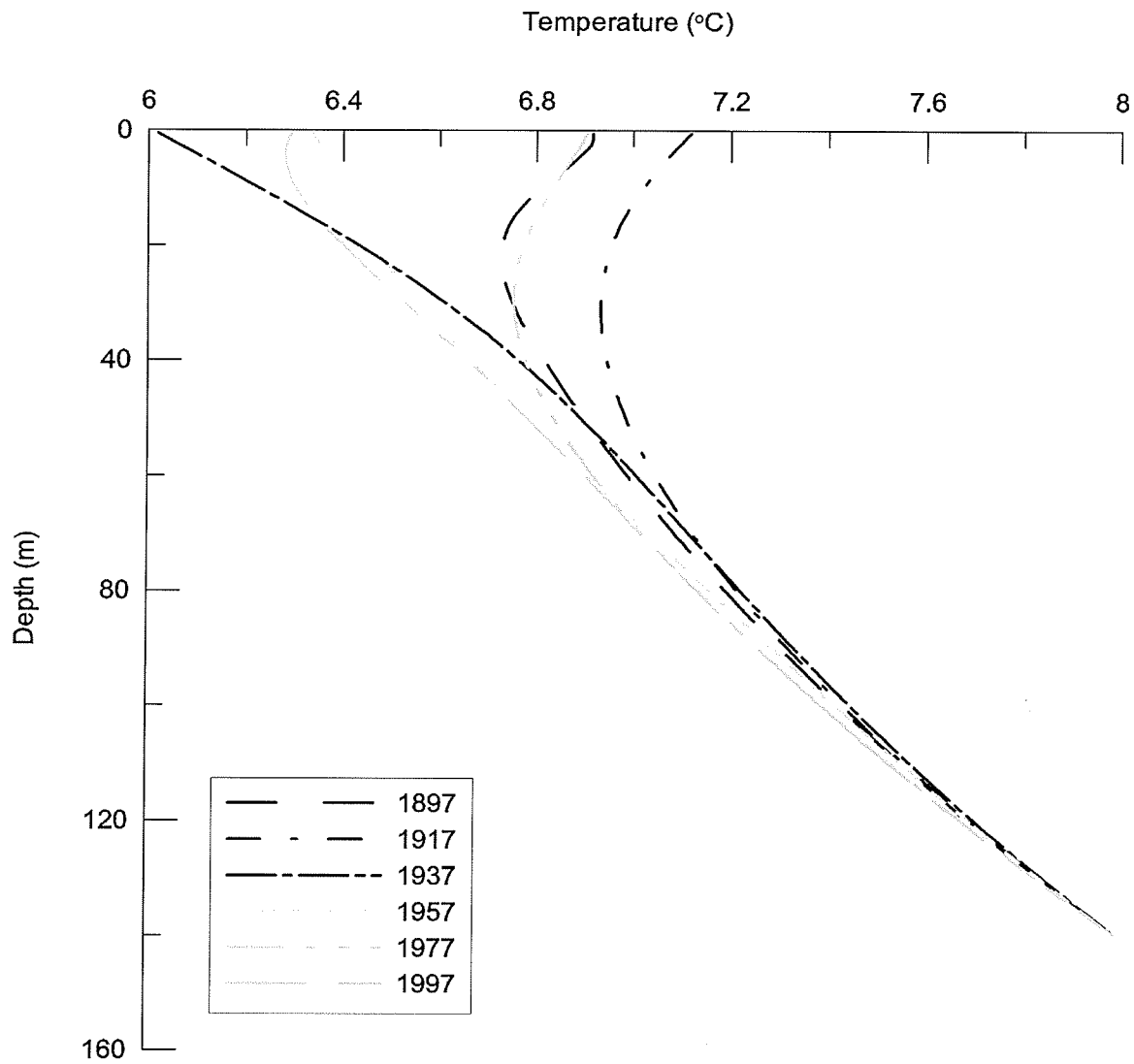
Figure 5.9b: Range of synthetic temperature profiles created with recharge rate of 3.2 x 10^{-9} m s^{-1} and the ground surface temperature history shown in Figure 5.8 over time period from 1895 to 2000.
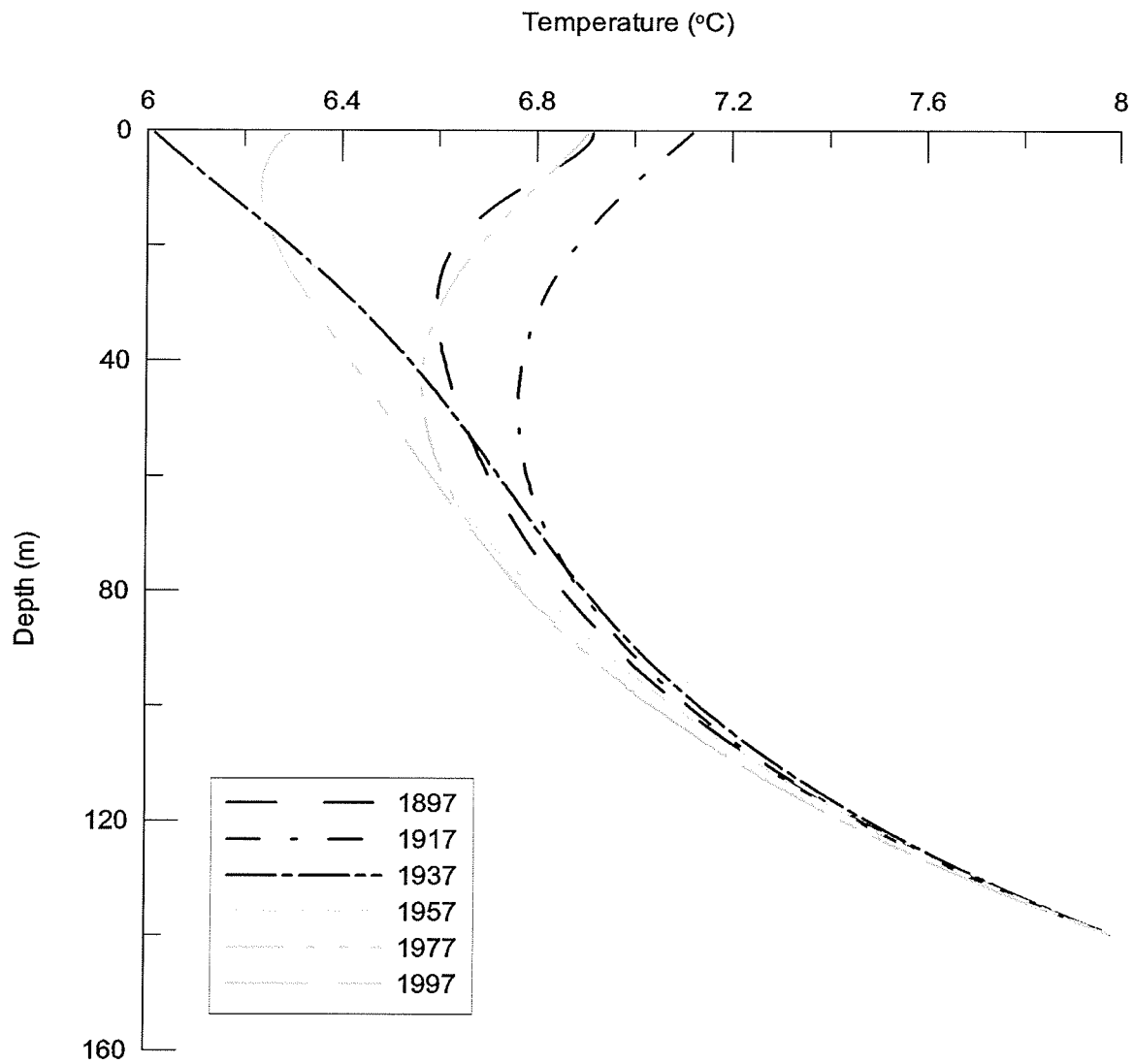
Figure 5.9c: Range of synthetic temperature profiles created with recharge rate of 1.3 x 10^{-8} m s^{-1} and the ground surface temperature history shown in Figure 5.8 over time period from 1895 to 2000.
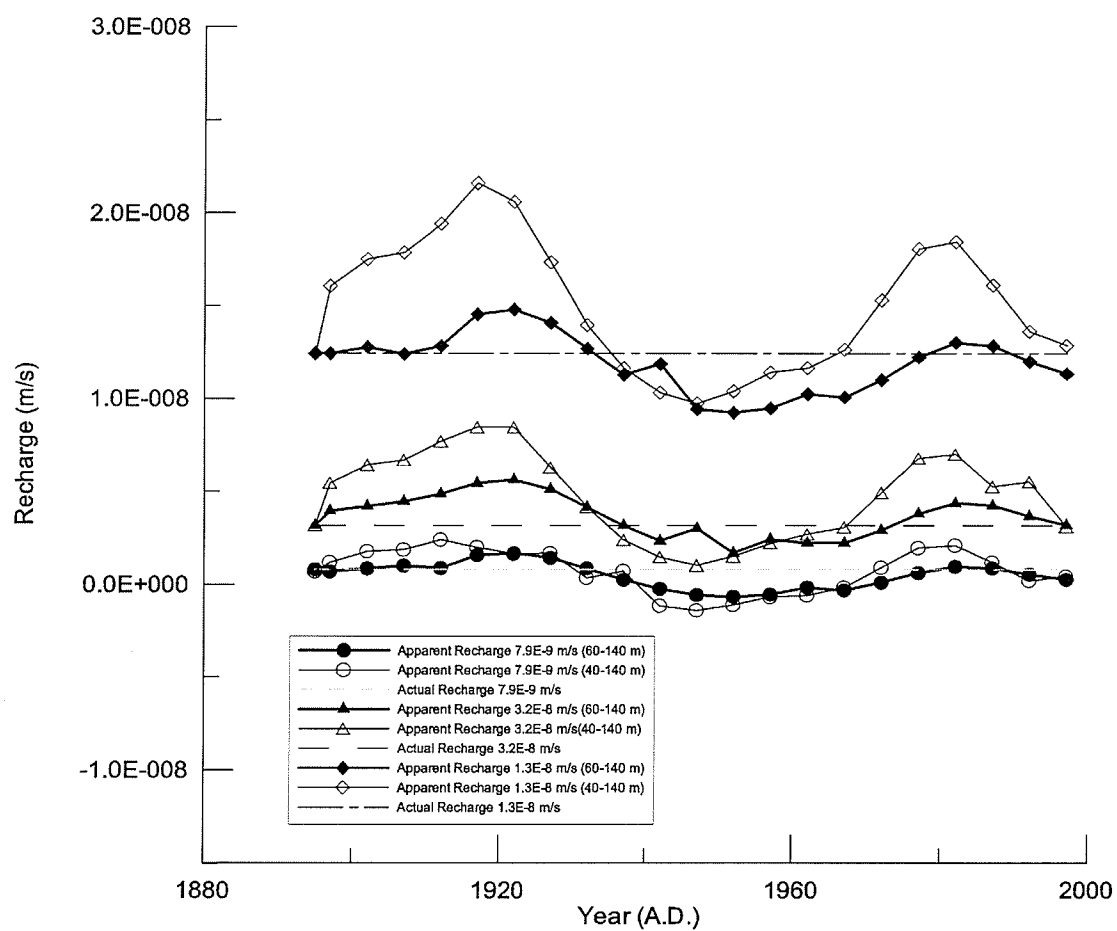
Figure 5.10: Variability in apparent recharge estimates over time due to variations in ground surface temperature.

113
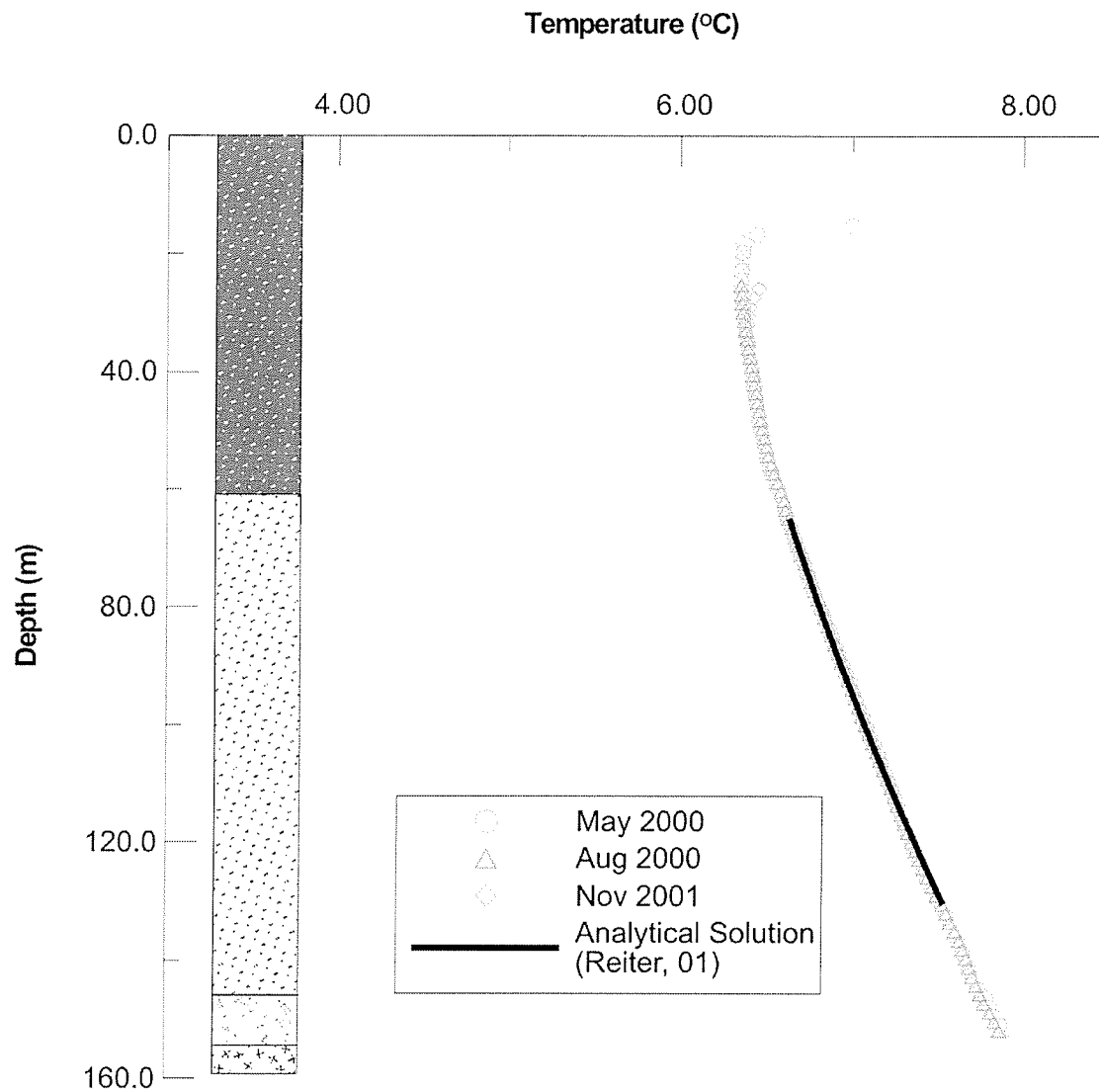
Figure 5.11: Temperature profile and geological log for well GSC 9901. Legend for lithological units is equivalent to that of Figures 5.6 and 5.7. Results of Reiter's (2001) analytical solution for groundwater and heat flow are shown on the graph as solid line, while measured points are shown as diamonds.
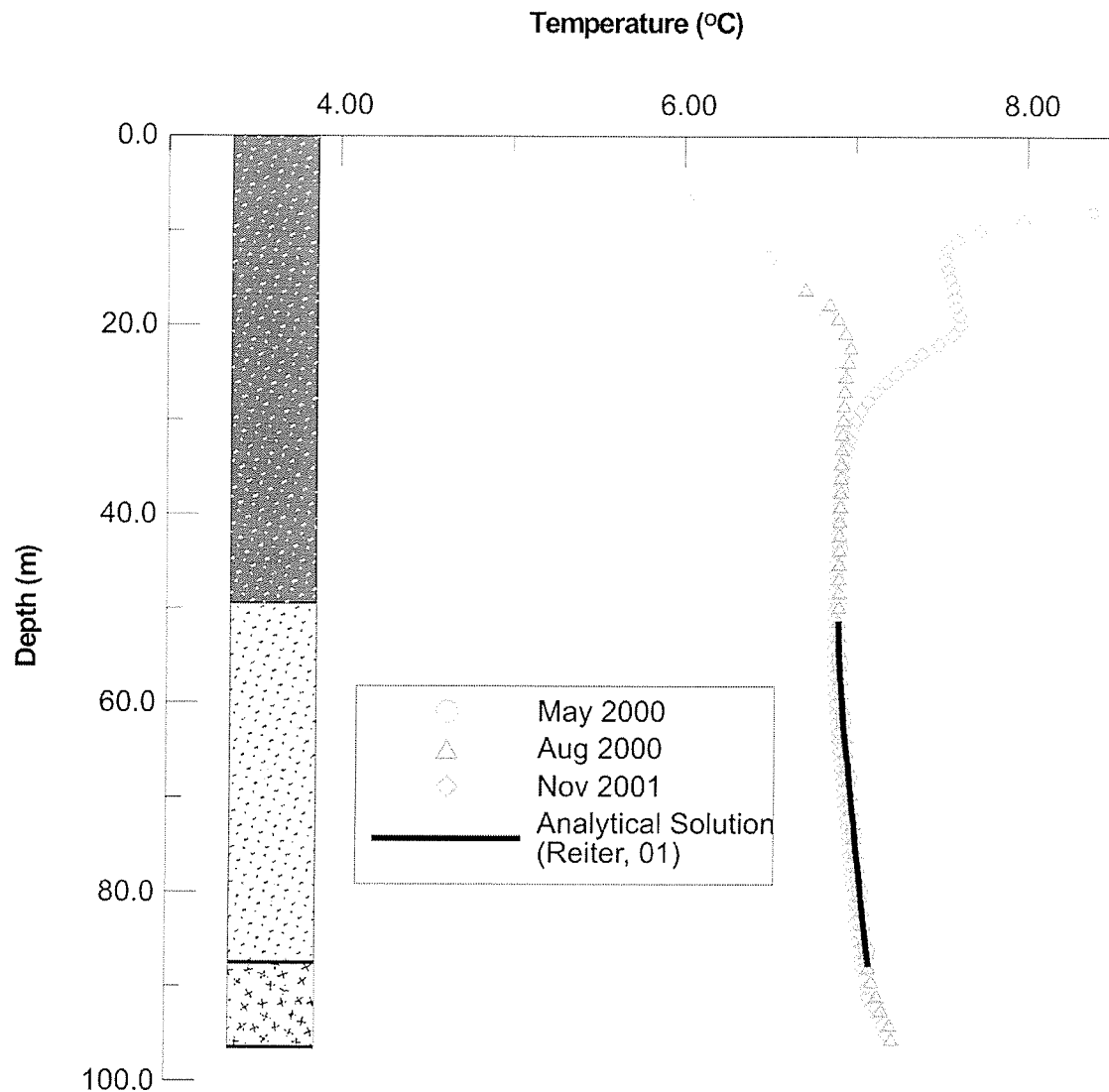
Figure 5.12: Temperature profile and geological log for well GSC 9902 Legend for lithological units is equivalent to that of Figures 5.6 and 5.7. Results of Reiter's (2001) analytical solution for groundwater and heat flow are shown on the graph as a solid line, while measured points are shown as diamonds.
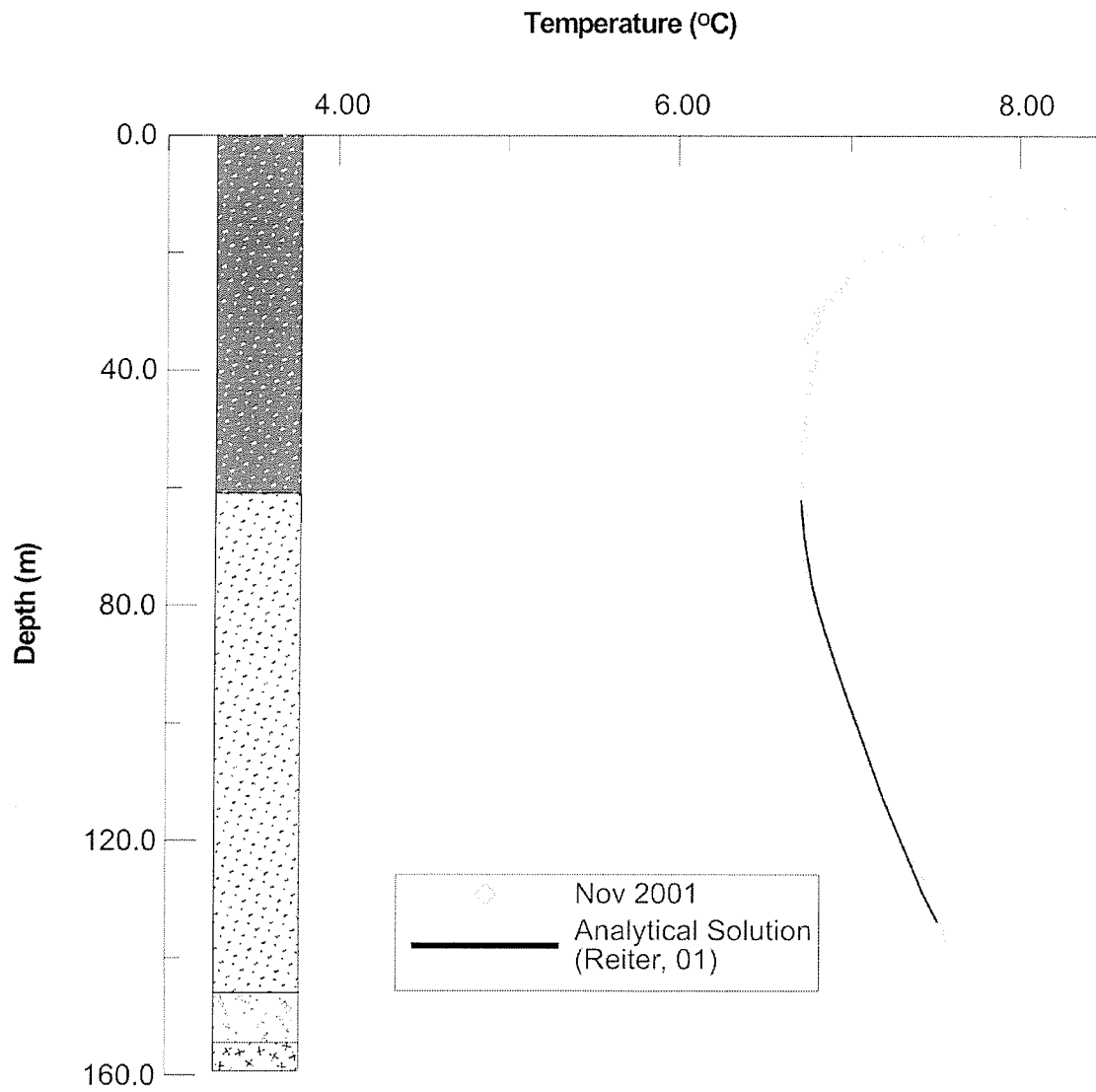
Figure 5.13: Temperature profile and geological log for borehole TH1. Legend is equivalent to that of Figures 5.6 and 5.7. Results of Reiter's (2001) analytical solution for groundwater and heat flow are shown on the graph as solid line, while measured points are shown as diamonds.
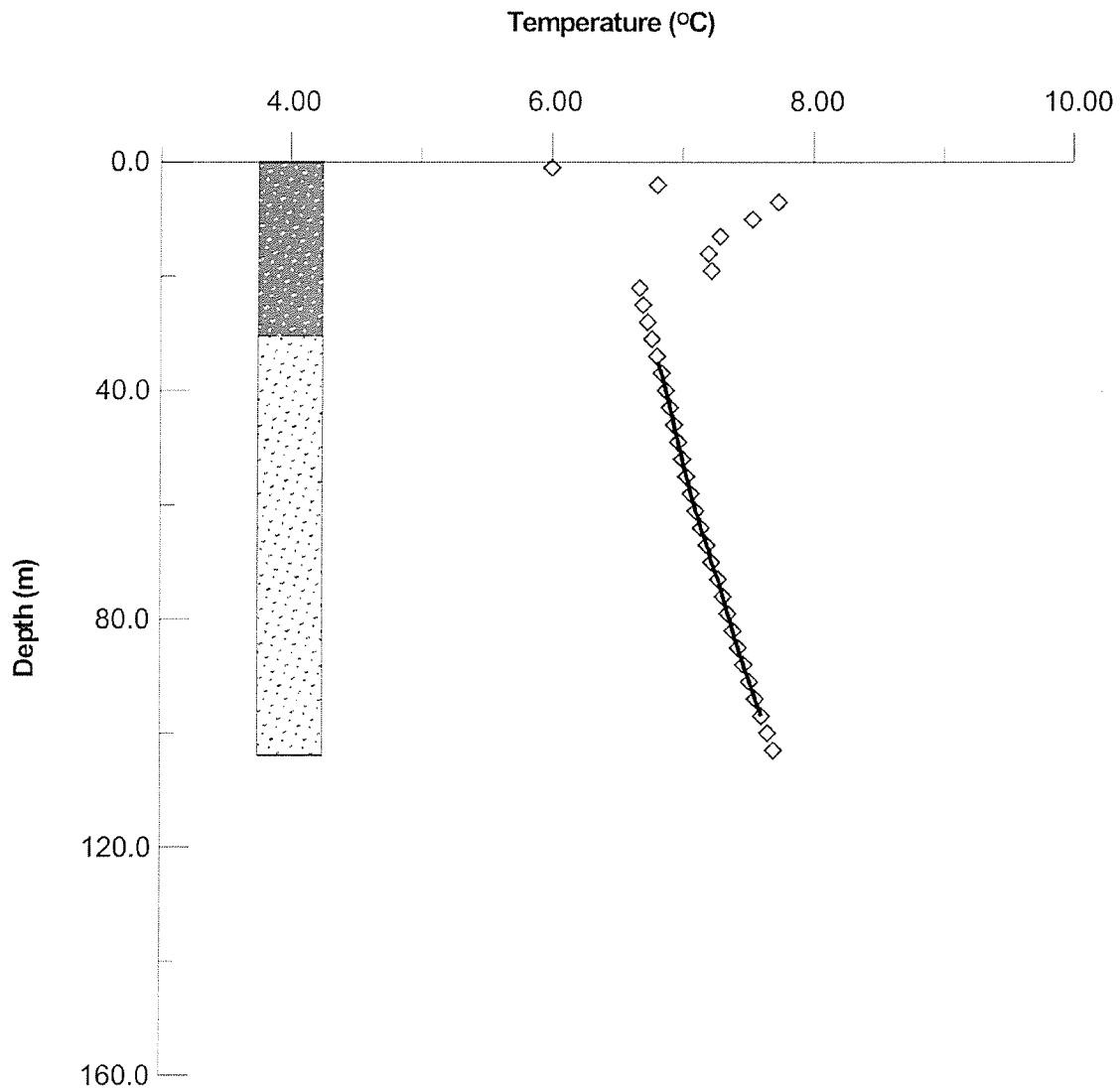
Figure 5.14: Temperature profile and geological log for borehole TH2. Legend for lithological units is equivalent to that of Figures 5.6 and 5.7. Results of Reiter's (2001) analytical solution for groundwater and heat flow are shown on the graph as a solid line, while measured points are shown as diamonds.
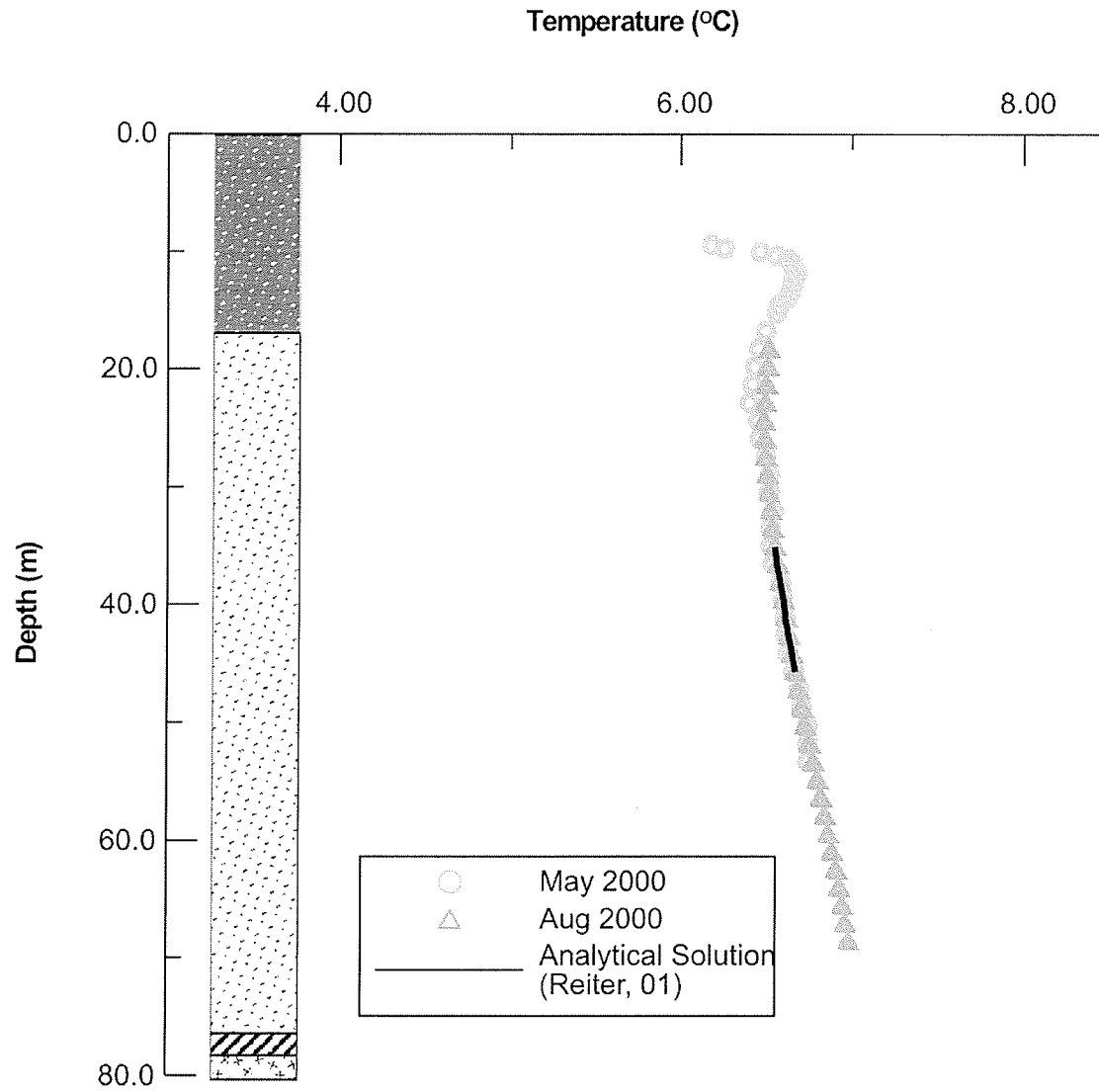
Figure 5.15: Temperature profile and geological log for well Woodridge. Legend for lithological units is equivalent to that of Figures 5.6 and 5.7. Results of Reiter's (2001) analytical solution for groundwater and heat flow are shown on the graph as a solid line, while measured points are shown as diamonds.

118
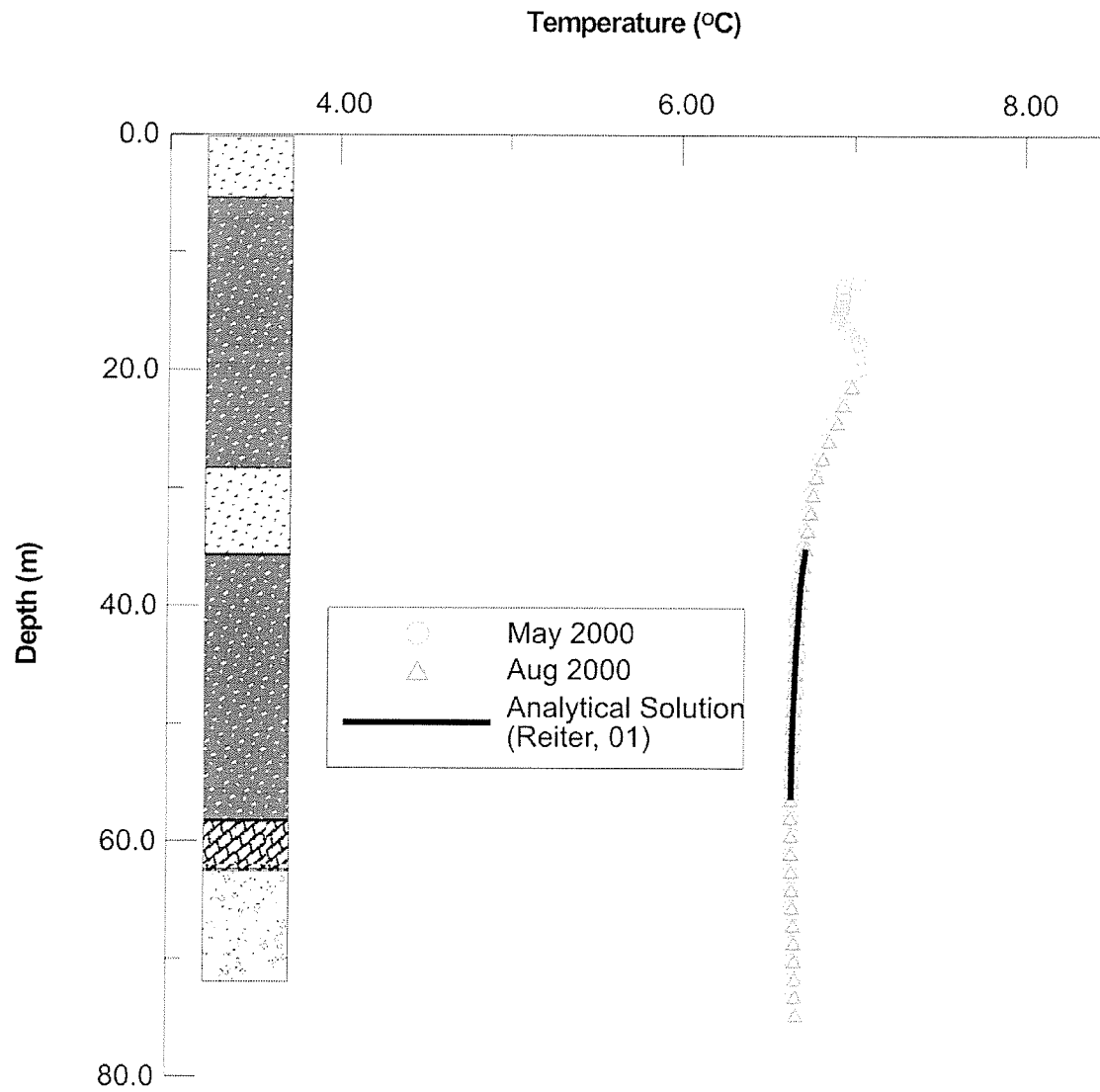
Figure 5.16: Temperature profile and geological log for well OH20. Legend for lithological units is equivalent to that of Figures 5.6 and 5.7. Results of Reiter's (2001) analytical solution for groundwater and heat flow are shown on the graph as a solid line, while measured points are shown as diamonds.

CHAPTER 6: SUBSURFACE URBAN HEAT FLOW

6.1 Introduction

Birch (1948) noted that changes in surface temperature during the Pleistocene had a noticeable effect on subsurface temperatures and a correction was required to calculate heat flow rates from the Earth's interior. Lachenbruch and Marshall's (1986) study of subsurface temperatures in Alaska showed that climate change over the last few centuries has also had a significant effect on subsurface temperatures. Since that time there has been a great deal of interest in using subsurface temperature to study climate change (eg. Chapman, 1995; Beltrami and Harris, 2001). However, the impact of the development urban areas on subsurface temperatures has received little attention in the literature. Terrestrial heat flow studies also generally avoid urban areas due to the impacts of heat loss from buildings, changes in surface cover and mesoclimate change (Jessop, 1990).

Manley (1958) defined an urban heat island as an area having closed isotherms separating the city from the general temperature field. The change in temperature generally manifests itself as an increase in the daily mean temperature and decrease in the daily minimum temperature. This increase has been found to be proportional to the population of a given city (Karl et al., 1988). These temperature changes are related to microclimate changes within an urban environment and are largely due to changes in the radiative balance (Landsberg, 1981). This change in radiative balance will have an impact on the subsurface temperatures, but conductive heat loading will also

have a significant impact on the subsurface, particularly beneath temperature-controlled buildings. Warming of the subsurface in an urban environment was considered by Taniguchi et al. (1999) in a study of groundwater recharge in Japan. However, there was no study of the mechanisms causing the warming in that study and a constant rate of surface temperature increase was used in the analysis of the temperature measurements. By understanding the sources of increases in temperature in an urban environment it may be possible to use temperatures from boreholes and monitoring wells in urban areas to study climate change. Examining the processes that have caused increases in subsurface temperatures may also allow for a more complete evaluation of geothermal resources.

During the current study, temperature profiles were measured in various locations throughout the city of Winnipeg. Generic numerical simulations of heat loss from temperature-controlled buildings are used to predict the resulting subsurface temperature field, which is then compared with measured temperature profiles. These simulations will provide estimates of the extent, magnitude and timing of temperature increases in the subsurface in the Winnipeg area. Numerical simulations are also used to determine the importance of groundwater flow in a shallow aquifer on the resulting temperature field. Groundwater flow is shown to have only a secondary effect in determining the subsurface temperature field in the Winnipeg area. The impact of climate change on the subsurface temperature is also considered in this study.

6.2 Field Survey

6.2.1 Methodology

Measurements were made in monitoring wells maintained by the University of Manitoba and the Manitoba Water Branch at intervals of approximately 1 metre beneath the water surface in the borehole. The majority of these monitoring wells were conventional installations consisting of 0.125 m diameter polyvinyl chloride (PVC) pipe installed in a 0.2 metre diameter borehole through the clay and till, and a 0.11 m diameter open borehole through the underlying bedrock. The annulus between the PVC pipe and edge of the borehole in these installations is normally backfilled with cuttings. In the 15 monitoring wells maintained by the University of Manitoba, the annulus was filled with bentonite pellets, rather than cuttings, to decrease the potential for advective heat flow in the annulus of the monitoring wells.

6.2.2 Measured Temperatures

Temperature data obtained from temperature logging conducted in this study and from point measurements provided by Manitoba Water Branch were used to construct a map of temperatures in the Upper Carbonate Aquifer beneath Winnipeg. The temperature at a depth of 20 metres below ground surface, which roughly corresponds to the temperature of the Upper Carbonate Aquifer, was determined from temperature profiles measured during this study (Appendix B). Temperature measurements were also obtained from Manitoba Water Branch and the measurement were generally conducted at a depth of a few metres below the top of the aquifer. Variations

in temperature with depth in the Upper Carbonate Aquifer are generally less than few tenths of a degree Celsius in individual boreholes and therefore the depth of the measurement will have little impact on the resulting map (Figure 6.1). This map was produced using a kriging algorithm routine with a grid spacing of 500 metres. The observed temperatures in the aquifer range from 5.4 to 13.8 °C. It should be noted that among the locations monitored for temperature by Manitoba Water, the majority are at production wells in systems where groundwater is being used for thermal purposes. Manitoba Water Branch also monitors temperatures at injection wells but these have not been included in the construction of the map because they will introduce a significant amount of bias into the map. Temperatures in this aquifer outside of the urbanized area are generally below 6.0 °C. These temperatures will be referred to hereafter as background temperatures. The exception to the limit of 6.0 °C for background temperature occurs where temperatures in the Carbonate Rock Aquifer are affected by seasonal temperature variations. The highest temperatures are within a few hundred metres of sites where thermal wastewater is injected into the aquifer (Figure 6.1). In areas not within a few hundred metres of injection wells, the highest observed temperature is 9.6 °C and this occurred at OJ28, which is in an area where the aquifer has a very low permeability (Render, 1970). At this location, daily readings made at a thermistor at a depth of 20 metres indicate that aquifer temperature only varies by ±0.1 °C throughout the year.

Temperature profiles measured in Winnipeg show a range of subsurface temperatures and heat flow rates (Figure 6.2). The background temperature gradient in the lower permeability rocks between the Upper Carbonate Aquifer and the Winnipeg Formation increases with depth from 0.005 °C m^{-1} directly beneath the Upper Carbonate Aquifer to a nearly constant 0.010 °C m^{-1} between a depth of 80 metres and the top of the Winnipeg Formation, giving a heat flow rate of approximately 24 mW/m^2. The Winnipeg Formation appears to have a near constant temperature of 7.2 °C throughout the study area but this estimate is based on limited data.

Beneath urban areas of Winnipeg, geothermal gradients observed in deeper monitoring wells are reversed, with temperatures decreasing at rates as great as 0.05 °C m^{-1} with increasing depth. Decreasing temperatures are observed to depths as great as 150 metres in some locations. This type of temperature profile is present in a 690 metre deep borehole (GSC 7001), drilled by the GSC at the University of Manitoba campus. Temperature profiles have been measured in this borehole several times since the 1960's by the Earth Physics Branch of Natural Resources Canada, and later by the Geological Survey of Canada (Figure 6.3). This borehole was installed 8 metres away from a building that was constructed in 1913 and its temperature profile shows decreasing temperatures down to approximately 100 metres below ground surface and a gradual shift to warmer temperature in the upper 110 metres since 1967. Temperatures in the Upper Carbonate Aquifer at this location reached approximately 8.0 °C by 1985, approximately 2.0 °C above

background measurements. This borehole has since been capped and was not accessible during the current study.

6.3 Numerical Modeling

6.3.1 Possible Sources of Heat to Winnipeg's Subsurface

Possible reasons for the anomalous temperatures observed in the Winnipeg area include: climatic forcing; injection of thermal wastewater; changes in surface cover; variations in thermal conductivity; and heat loss from buildings. The magnitude of the temperature anomalies beneath Winnipeg is in excess of what would be expected purely under climatic influences. The average annual air temperature in Winnipeg has increased by approximately 1.0°C over the last century (Figure 3.6) and can only be responsible for a small portion of the observed anomalies. Injection of thermal wastewater at temperatures of up to 16°C is known to occur in the Winnipeg area and this influx of heat is capable of causing significant increases in subsurface temperatures. However, it should be noted that the observations shown in Figure 6.1 suggest that the temperature anomaly resulting from injection of water heat is generally confined to an area extending less than 500 metres from an injection well. The number of injection wells and their distribution (Figure 6.1) cannot explain the widespread anomaly observed beneath Winnipeg. The effects of changes in surface cover are more difficult to quantify due to the range of surfaces present in the urban environments and their complex distribution. Changes in surface cover due to deforestation have been found to cause increases in ground surface temperatures of a few

degrees (e.g. Murtha and Williams, 1986; Cermak et al., 1992; Lewis and Wang, 1998). However, changes in surface cover in the Winnipeg area do not appear to have caused changes of this magnitude. Temperature measurements located several hundred metres from heated buildings or injection wells, but still in the vicinity of roads or parking lots, tend to be within a few tenths of a degree Celsius of background temperatures. Variations in thermal conductivity may be responsible for some of the variation in temperatures observed in the Winnipeg area but are likely not of the magnitude that could explain discrepancies of several degrees Celsius. If vertical heat flow is assumed to be at a rate of 35 mW/m^2 and the mean temperature at the ground surface is assumed to be 5.5 °C, the effective thermal conductivity of the upper 20 metres of the geologic section would have to be 0.35 W m^{-1} C° $^{-1}$ to produce a temperature of 7.5°C at a depth of 20 metres. This estimated thermal conductivity is well beyond the range observed for geologic materials (e.g. Jessop, 1990). Heat loss from buildings is a likely source of much of the excess heat present in the subsurface beneath Winnipeg, Manitoba. Space heating and air conditioning keeps the majority of these structures at a temperature of approximately 20 °C throughout the year and they are present throughout the urban environment, often at a high density. Heat loss from buildings, which most commonly do not have insulated basements, will be examined through numerical modeling to determine the magnitude, extent and timing of development of associated subsurface temperature anomalies.

6.3.2 Model Construction

Generic two-dimensional heat transport models were used to estimate the subsurface temperature field associated with heat loss from buildings. Models were created with METRA and a geological cross-section typical of the Winnipeg area. Thermal and hydrogeologic properties of the Paleozoic carbonates and till determined as part of this research were used in combination with estimates based on literature values (Table 6.1). The initial conditions of the models were set using an estimate of the background temperature profile based on that measured in monitoring well OJ30, which is assumed to be representative of subsurface heat flow prior to urban development. The resulting model used fixed temperatures of 5.0 °C at the surface based on an extrapolation of background temperature profiles to the surface and 7.2 °C at the base of the Red River Formation. The fixed temperature used as the upper boundary condition is approximately 2.7 °C higher than the corresponding temperature in the Winnipeg area but this difference has been observed in studies in other locations. For example, in a study of soil temperatures in North Dakota, the mean annual air temperature was found to be at least 2 °C less than the average mean annual temperature in the upper few metres of the soil column (Schmidt et al., 1999). Beltrami (2001) found a similar difference between air and ground surface temperatures in Nova Scotia. This effect can generally be attributed to the difference in heat capacities of the air and ground. Next, the top of the Winnipeg Formation, which appears to have a relatively constant temperature

throughout the study area, was used as the lower condition to the boundary value problem. Lateral boundaries were placed 2500 metres away from the centre of the building or in the case of the two building model, the midpoint between the two buildings and were assigned a zero-flux heat flow boundary. At this distance, the addition of a heat source at the surface had a negligible effect on subsurface temperatures. These conditions were used to create a steady-state model that was the starting point for transient modeling.

Transient modeling looked at three cases: 1) heat loss from an individual building; 2) heat loss from two buildings; and 3) heat loss beneath two buildings with horizontal groundwater flow in an aquifer in the geologic section. The second and third simulations were produced to examine the impacts between two buildings, which is a typical situation in an urban environment. For each of these cases buildings were conceptualized as a constant temperature boundary condition of 20 °C at the surface over a horizontal width of 50 metres. The actual heat source is likely a variable heat flux boundary condition at a depth of 1 to 5 metres, depending on the depth of the basement. However, the fixed boundary condition was assumed to be sufficient in this model to demonstrate the potential effects of heat loss from buildings on the subsurface. All other boundary conditions used in the transient simulation were the same as the steady-state model. For the case considering groundwater flow, the Upper Carbonate Aquifer was given a permeability of 10^{-11} m^2, which is typical of this aquifer (Render, 1970). A horizontal hydraulic gradient of 0.0002 was imposed within the aquifer by

placing fixed head boundary conditions on the lateral boundaries of the aquifer that were 1 metre greater at the left side of the problem than the right. The effects of climate and surface cover changes over the last century were not considered in these models.

6.3.3 Modeling Results

Heat loss from an individual building resulted in the creation of a bulb-shaped area of elevated subsurface temperatures (Figure 6.4a). After 100 years, the temperature anomaly extended to a depth of approximately 130 metres and temperatures as great as 8.0°C, an increase in temperature of over 2.0°C, extended approximately 50 metres laterally outwards from the building. The rate of heat loss directly beneath a building is estimated to be about 2.0 W m^{-2}.

The case where two buildings were examined showed a slightly greater downward penetration of the temperature anomaly and also showed that the entire region between the two buildings was impacted (Figure 6.4b). In the area between the two buildings a large zone of elevated temperatures from 4.0 to over 5.0 °C above background temperatures is present in the Quaternary sediments after 100 years and temperatures decrease with depth to a depth of approximately 130 metres.

In the model where groundwater flow was considered, horizontal Darcy velocities of approximately 2.0×10^{-8} m s^{-1} occurred within the aquifer but in the rest of the modeled area the maximum Darcy velocities predicted were less than 10^{-11} m s^{-1}. Vertical Darcy velocities ranged between 10^{-10} and 10^{-12}

m s^{-1} throughout the model, with the lowest values occurring in the clay unit. Only a slight shift in the direction of groundwater occurred in the temperature anomaly beneath the buildings when groundwater flow was considered (Figure 6.4c). This shift was less than 5 metres in the horizontal direction after 100 years, despite movement of groundwater on the order of several hundred metres during this time period. The depth of the anomaly in this model was approximately the same as the purely conductive case in the area directly beneath the building. However, the depth of the anomaly was approximately 50 metres shallower on its lateral edges.

The timing of the temperature changes is quite similar for the cases where two buildings are considered (Figure 6.5). At a point situated midway between the two buildings 22.5 metres deep, the temperature reaches 8.0°C approximately 50 years after the building is constructed. During the next 50 years, the temperature at this point is expected to rise less than 1.0°C, suggesting that equilibrium conditions are being approached. The same trend is noted for the case where only one building is considered.

The results of the simulations agree well with observed temperature profiles in most cases with respect to their position relative to buildings and the age of the buildings. The temperature profiles observed in OJ26 and OJ28 provide two of the best demonstrations of this agreement (Figure 6.6). OJ26 is located approximately 20 metres away from the nearest building, which was constructed during the 1960's and it is compared with the temperature profile 18 metres away from a single building forty years after the

construction of that building. These temperature profiles compare very well for temperatures below 20 metres depth, having an RMS of 0.13 °C and an R^2 correlation coefficient of 0.89. OJ28 is situated less than two metres away from a building that was built in 1911 and approximately 40 metres away from another building constructed in 1909. These results were compared with the temperature profile produced by the generic model of the temperature field beneath two buildings 2 metres away from one building and 48 metres away from the other at a time of 90 years. The results are in good agreement, having and RMS of 0.25 °C and an R^2 correlation coefficient of 0.90 between measured and predicted profiles below 20 metres depth. However, the slopes and intercepts of regressions in both models are significantly different at a 95% confidence level than a line with a slope of one passing through the origin, indicating that this model may have limited predictive capabilities. The use of site specific geometries, development histories and thermal properties may provide more accurate modeling results. Modeling GSC7001 was also considered because of its age and the existence of multiple temperatures logging episodes. However, this borehole is located in an area of the University of Manitoba where the neighboring buildings have a complex geometry and are of various ages.

6.4 Discussion

Temperature profiles predicted by the generic simulations of heat loss from buildings created in this study are similar to observed temperature profiles in the Winnipeg region. However, it is difficult to model site-specific

locations due to variability in material properties, differences in heating history, variation in basement depths and the presence other heat sources affecting the subsurface. These data are lacking in many parts of the Winnipeg area but the results of the generic simulations suggest that conductive heat loss from buildings is largely responsible for the observed increases in subsurface temperatures throughout the Winnipeg area. This suggests that temperature contours produced in Figure 6.1 should be interpreted with caution. Although temperatures are likely representative of average conditions in beneath most areas of the City of Winnipeg, it should be noted that there may be variations of up to a few degrees observed over the space of several metres in some areas.

Time of construction plays a major role in the size of the temperature anomaly observed. The temperature profile observed at monitoring well OJ28, which shows the greatest penetration of downward heat flow of all temperature profiles measured in this study. This monitoring well was installed in an area of Winnipeg which was among the first to be settled. The monitoring well is less than 3 metres away from a building that was constructed in 1911 and is approximately 40 metres away from a building constructed in 1909. Monitoring wells W3 and W4 occur in residential areas where development took place at approximately the same time. These temperature profiles were both taken in monitoring wells installed approximately 5 metres away from a smaller building. Other buildings were more than 50 metres away in both cases. The smaller anomaly observed in

these locations may be due to the presence of shallower basements, smaller building footprints and more green space in residential areas. Monitoring well OJ26 was installed approximately 40 metres away from a building constructed in 1968. Downward heat flow at this location occurs to a depth of 73 metres. Temperature profiles observed on the University of Manitoba campus also support the conjecture of conductive heat loading causing the temperature disturbance. The temperature profile measured at GSC7001 shows a significant amount of downward heat flow and a temperature of approximately 8 °C in the Upper Carbonate Aquifer.

Due to a lack of multiple boreholes surrounding any individual building in this study, the predicted effects of groundwater flow on heat transport beneath a building were not verified by field measurements in this study. However, those advective effects may be important in the background temperature field. This is supported by the change in estimated heat flow from 35 mW m^{-2} in the Precambrian basement to approximately 24 mW m^{-2} in the overlying Paleozoic rocks. Models of regional groundwater and heat flow produced by Smith and Chapman (1983) suggest that thermal regimes become advectively dominated above a threshold permeability of 10^{-17} m^2. The permeability of the Upper Carbonate Aquifer is several orders of magnitude higher than this threshold value (Render, 1970). The Winnipeg Formation also has a permeability which is above this threshold value. However, in areas affected by heat loss from buildings the temperature field appears to be dominated by conductive heat transport. When an aquifer was

placed beneath the buildings in the generic model it had little effect on the simulated subsurface temperature field during the period examined. The magnitude of the imposed heat flux resulting from heat loss from a building is much greater than any of the regional scenarios examined by Smith and Chapman (1983), who explored basal heat fluxes ranging from 40 to 80 mW m^{-2}, which are typical of many geologic environments. In the current study, the estimated heat flux immediately below a building is nearly two orders of magnitude greater, implying that the threshold value of permeability required for advective heat transport to become dominant will be much greater in urban environments.

Temperatures measured in the Upper Carbonate Aquifer in monitoring wells situated less than 1000 metres away from borehole GSC7001 were only 6.0 °C. These monitoring wells were situated more than 200 metres away from the nearest heated building, supporting the results of the models produced in this study. The presence of these areas of low temperatures in the subsurface is somewhat similar to the presence of low air temperatures observed in urban heat islands. Oke (1979) found that the pattern of temperature, changes in urban heat islands is often dominated by local features related to land use and building density. These near background temperatures suggest that it may be possible to derive some information on past climates from subsurface temperatures in specific areas of the city. However, changes in surface cover are present throughout almost the entire urban environment and it is unlikely that the associated noise can be resolved

to a point where detailed information on past climates can be recovered from subsurface temperatures. In areas that are at a several hundred metres from a building or area where the surface cover has changes significantly, it may be possible to interpret a climate change signal associated with the urban heat island. The Winnipeg area is not a good location to test this hypothesis because the presence of the two regional aquifers beneath Winnipeg also causes a departure from the conductive environment that is desired in the analysis of subsurface temperatures to study past climates.

The increases in subsurface temperature in the Winnipeg area are only a few degrees Celsius but could have important implications in some geothermal energy applications. For cooling purposes, the observed and predicted increases in temperature could cause significant reductions in efficiency. This is an especially important consideration in Winnipeg, where there are nearly 100 users of groundwater for cooling purposes. Conversely, an increase in temperature of this magnitude will increase the efficiency of heat pumps for space heating. The spatial relationships between subsurface temperature distribution and building locations may help to improve the design of these systems in the future.

Although this study was conducted exclusively in Winnipeg, Canada, the results are likely applicable to other urban areas in temperate and sub-arctic climates to varying extents. Areas where space heating is necessary during winter months will experience heat loss from buildings to the subsurface. Although many newer buildings have insulated basements, this is

a relatively new practice and a significant amount of heat loss will have already occurred. Also, Winnipeg is a fairly young city when compared to many cities in northern Europe and Asia. Cities in these locations may be experiencing downward heat flow to greater depths than observed in the current study. The findings of this study may also have implications that extend beyond the potential for geothermal energy use, particularly to geotechnical engineering where depth of frost penetration and freeze-thaw cycles are of interest.

6.5 Conclusions

Heat loss from buildings is having a noticeable impact on the distribution of subsurface temperatures in the Winnipeg area. The resulting distribution of temperatures is dependent primarily on the following factors: 1) the duration of heat loading; 2) distance from a given temperature measurement point to a building; and 3) density of buildings in a given area. The amount of heat lost beneath a building is approximately 50 to 100 times greater than the amount of heat flowing upwards from the Precambrian basement in the Winnipeg area. Heat loss from buildings in addition to other lesser sources of increased heat flow to the subsurface, such as changes in surface cover and climate change due to the urban heat island effect, make subsurface temperatures in urban areas higher than surrounding rural areas. This increase in subsurface temperatures generally precludes the use of temperature profiles in urban environments for high resolution studies of past

climates and should also be noted in the development of geothermal energy resources.

Geological Unit	Thermal Conductivity $(W\ m^{-1}\ ^{\circ}C^{-1})$	Porosity	Permeability (m^2)
Lake Agassiz Clay	1.2_1	0.55 to 0.60_2	$10^{-14}{}_2$
Till	1.5	0.10 to 0.30_2	$10^{-10}{}_3$
Upper Carbonate Aquifer	2.4	0.10	$10^{-11}{}_4$
Paleozoic Carbonates	2.4	0.05	$10^{-14}{}_5$

Sources:
1. Domenico and Schwartz, 1998
2. Pach, 1994
3. McMillan et al., 1994
4. Render, 1970
5. Freeze and Cherry, 1978

Table 6.1: Model parameters used in heat flow modeling for area beneath a building. Values lacking references were measured during this study.
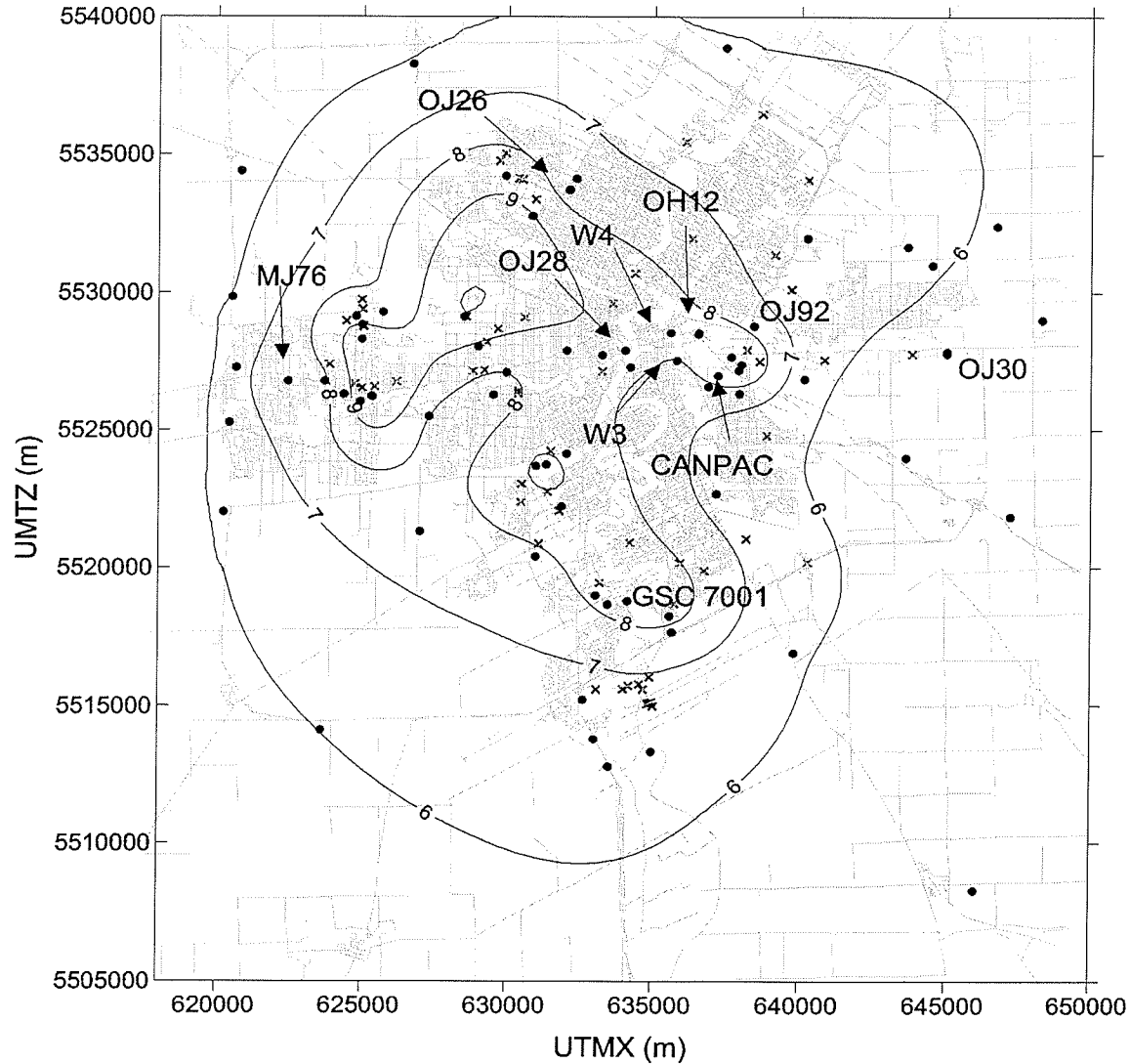
Figure 6.1: Contour map of Winnipeg area showing temperatures in degrees Celsius in the Carbonate Rock Aquifer beneath Winnipeg at a depth of 20 metres. The locations of temperature measurements (circles) and injection wells (x's). Roads are shown in the background as grey lines to give an indication of the amount of urban development in a given area.
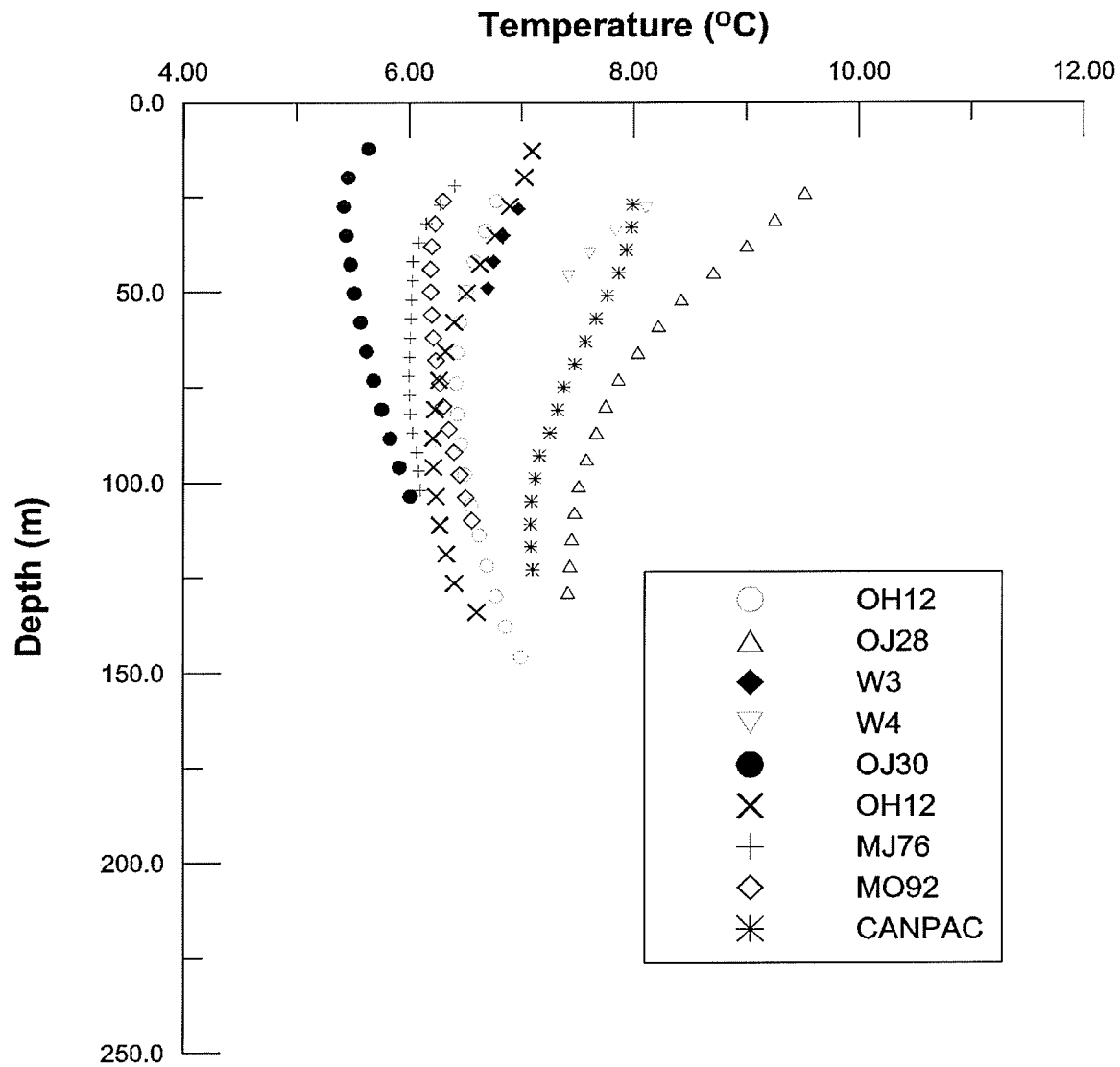
Figure 6.2: Measured temperature profiles showing downward heat flow in the Winnipeg area. OJ30 is shown as an example of a temperature profile outside of the urban environment.
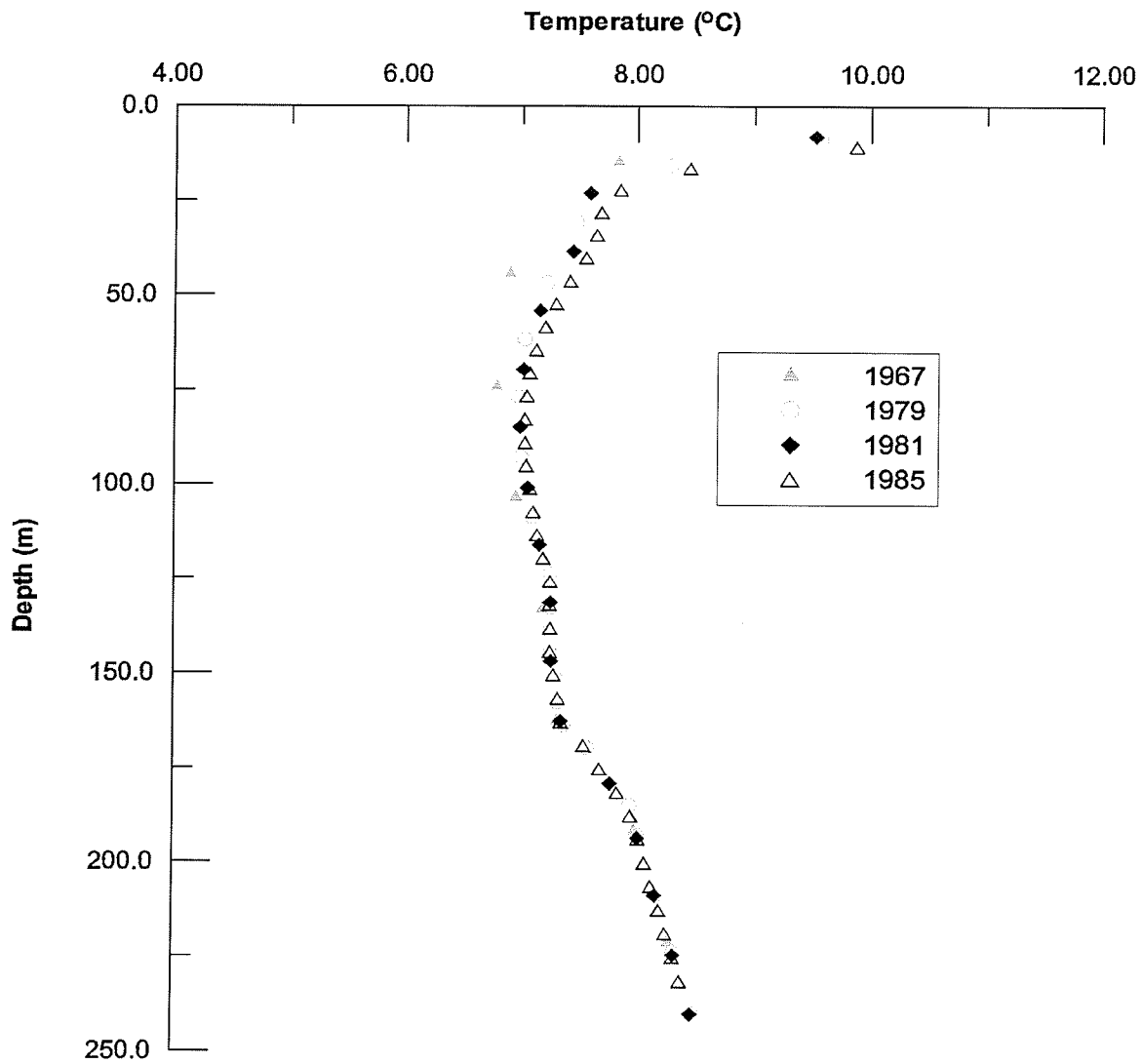
Figure 6.3: Temperature profiles measured in GSC Borehole 7001 at the University of Manitoba campus by the GSC.
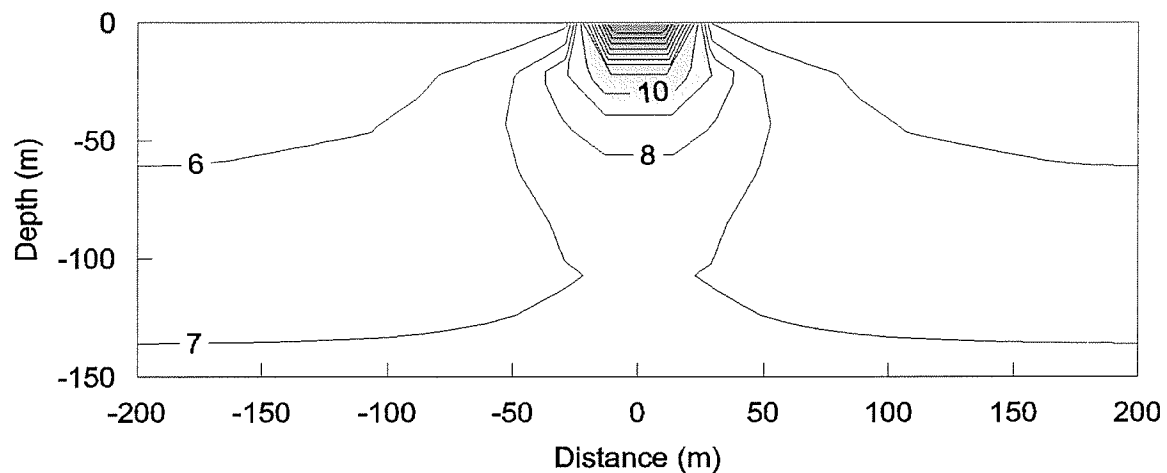
Figure 6.4a: Modeled subsurface temperature field a region beneath a single uninsulated building 100 years after construction. Contours of temperature are shown for every ! °C for temperatures greater than 10 °C.
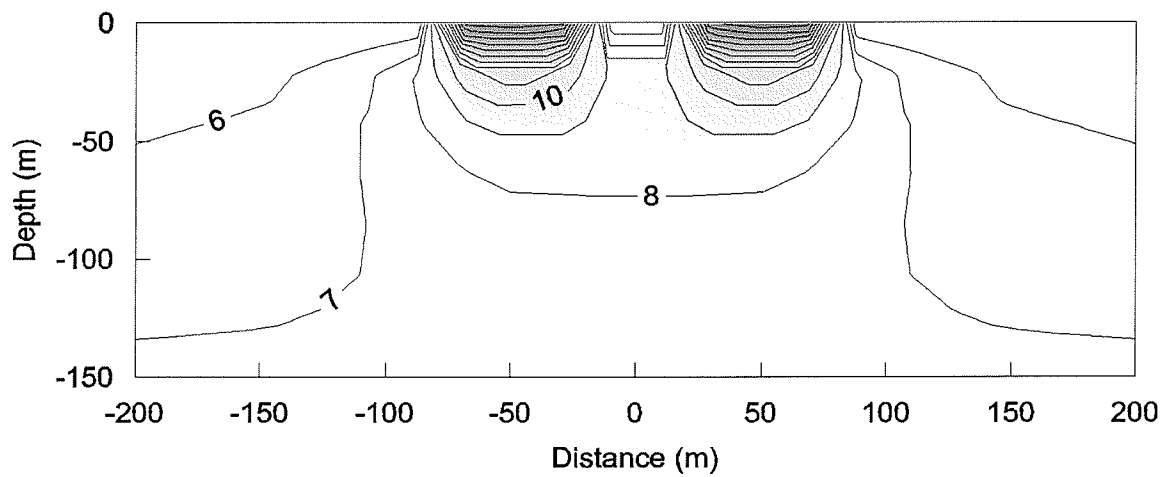
Figure 6.4b: Modeled subsurface temperature field for a region beneath two uninsulated buildings 100 years after construction. Contours of temperature are shown for every 1 °C for temperatures greater than 10 °C.
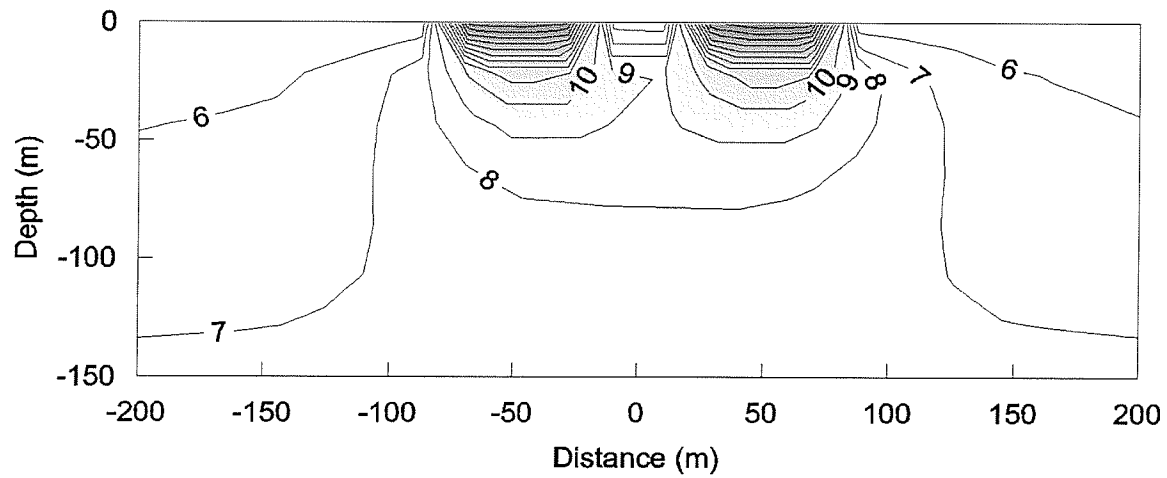
Figure 6.4c: Modeled subsurface temperature field for a region beneath two uninsulated building 100 years after construction with groundwater flow in an aquifer 15 metres deep. Contours of temperature are shown for every 1 °C for temperatures greater than 10 °C.
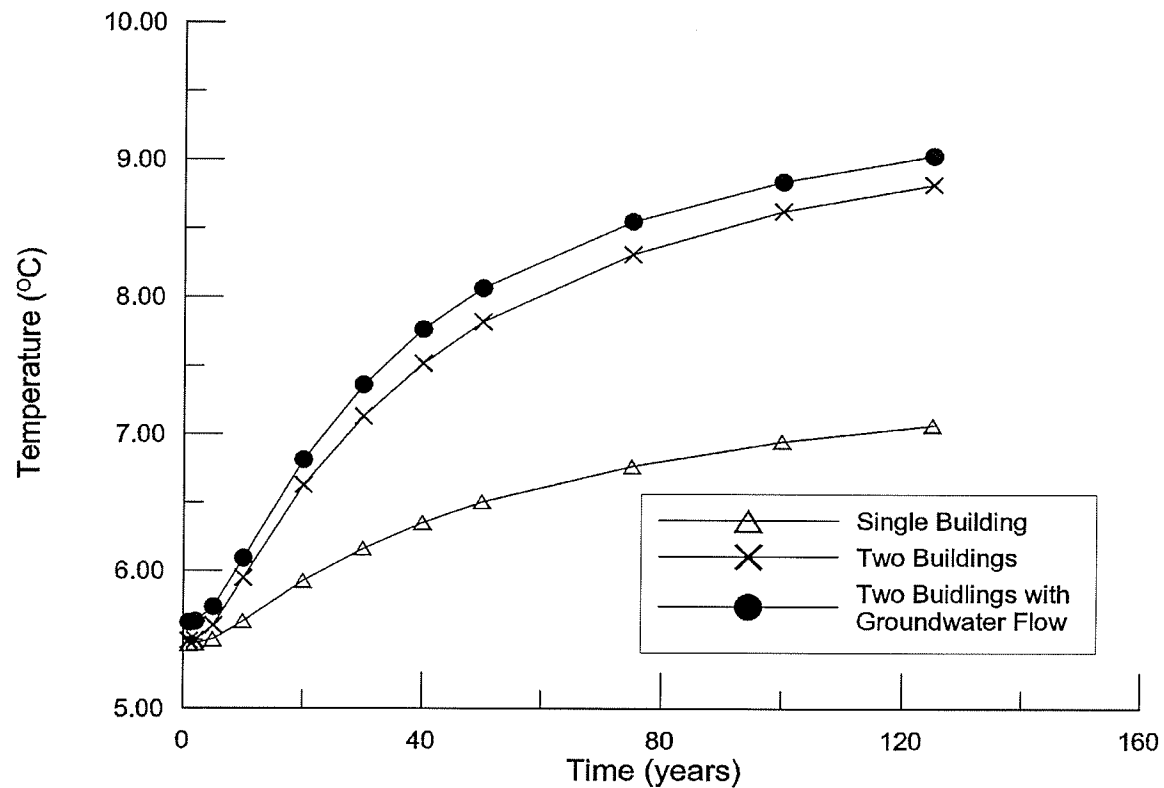
Figure 6.5: Modeled temperature in the generic aquifer located 25 metres away horizontally from a single building (triangles). Also, modeled temperature midway between two buildings for case not considering groundwater flow (x's) and the case where groundwater flow is considered (circles).
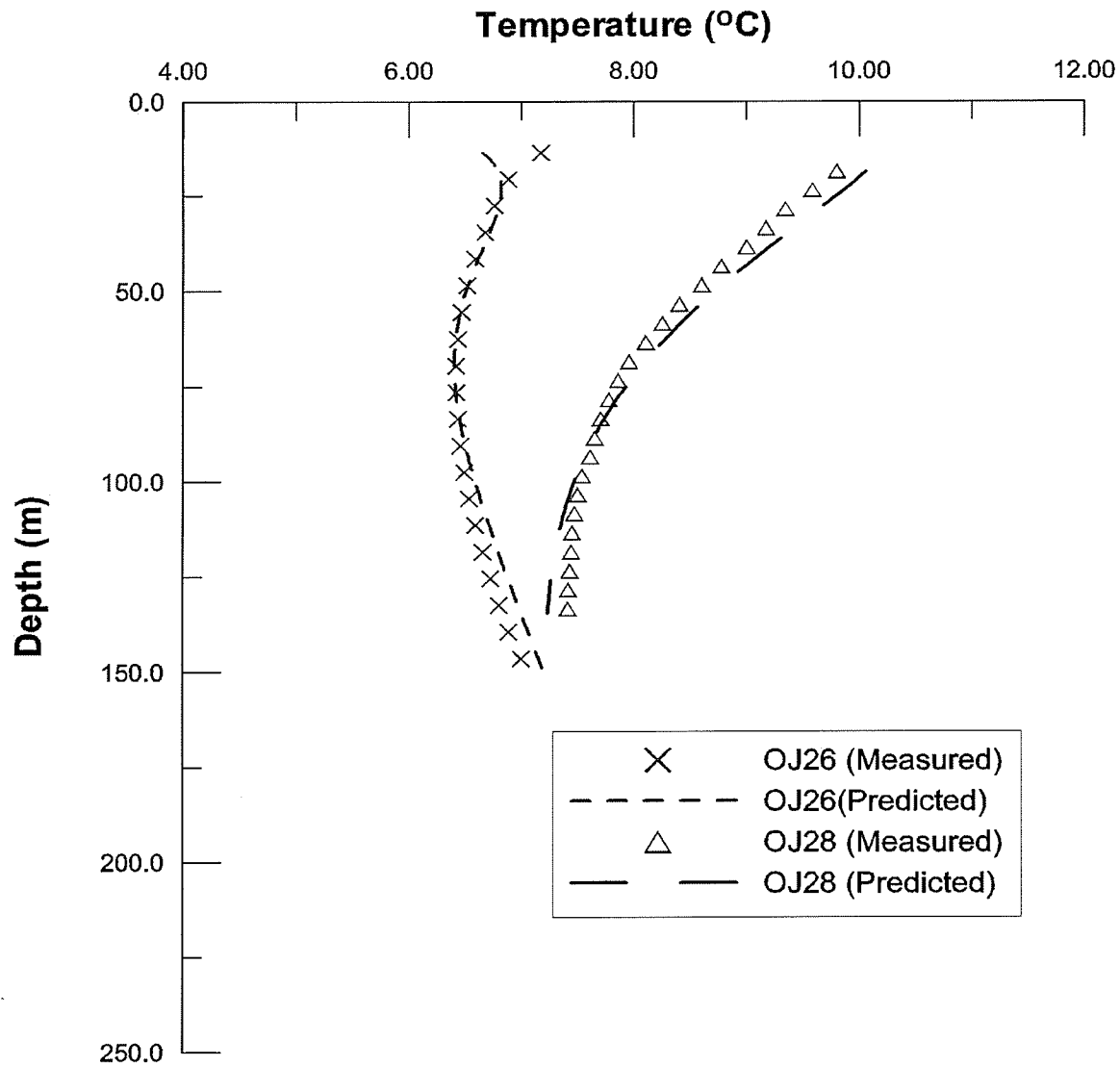
Figure 6.6: Comparison of observed profiles to those produced by the synthetic models. Observed temperature profile for OJ26 is compared to modeled temperature profile 18 metres away from a single building 40 years after construction of the building. OJ28 is compared to temperature profile situated 2 metres away from one building and 48 metres away from another, 90 years after construction of the buildings.

CHAPTER 7: GEOTHERMAL ENERGY AND SUBSURFACE HEAT STORAGE AND DISPOSAL

7.1 Introduction

The use of geothermal energy for space heating has a long history dating back several centuries, with early use occurring in areas of high crustal heat flow. The French village of Chaudes-Aigues Cantal began using geothermal energy for space heating in the fourteenth century (Bloomquist, 2003). Geothermal energy was first used to generate electricity in Tuscany in 1913 and the first major regional use of geothermal energy for space heating was in Iceland in 1930 (Bloomquist, 2003). Geothermal energy and geothermal energy storage have increased in popularity substantially during the past thirty years. Much interest occurred during the 1970's energy crisis and there is currently a renewed interest in this technology today with growing environmental awareness and increasing energy prices (Huttrer, 2001). The advent of the heat pump, which allows extraction of energy from low temperature water or soil, has enabled geothermal energy to be used in low heat flow areas. By 2000, approximately 30,000 heat pumps were operating in Canada (Lund and Freeston, 2000).

In addition to heat pumps, aquifer thermal energy storage (ATES) systems are in use in several provinces (Allen et al., 2000). In an ATES system, heated water from an external source is injected into an aquifer and the resulting warm water is then pumped from the aquifer for use in heating at a later date (e.g. Sauty et al., 1982). In some cases it has been possible to

146

use ATES to provide both space heating and space cooling. In this scheme, groundwater is used for air conditioning during the summer and the resulting warm wastewater is injected back into the aquifer. This warm water is pumped from the aquifer from the winter for space heating. In some cases, direct use of groundwater for cooling is performed without the intent of recovering the waste heat at a later time. This is more popular than the use of geothermal energy for cooling but statistics on the number of systems or amount of energy saved by using such systems are not readily available. Note that the International Association of Geothermics does not recognize this practise as the use of geothermal energy. Typically, heat is transferred to cool groundwater and in many cases this water is then injected back into the subsurface to prevent excessive drawdown. This process adds heat to the subsurface rather than extracting it but the physics of this process are similar to geothermal energy exploitation in many respects.

Sustainability is an important consideration for both extracting heat from the subsurface or disposing of heat in the subsurface. Bruntland (1987) provided the following statement defining sustainable development: "Sustainable development seeks to meet the needs and aspirations of the present without compromising the ability to meet those of the future." For management of groundwater resources for thermal purposes, sustainability is related to the ability to maintain both fluid temperatures and an adequate supply of water (Gringarten and Sauty, 1975). However, in many cases geothermal reservoirs are subjected to excessive stresses in their

development because of economic factors which lead to undesirable changes in temperature and pressure (Rybach, 2003). Such developments are not good for the viability of geothermal energy and geothermal energy storage and utilisation schemes should be designed so that these changes in temperature and pressure are minimized.

Other issues are related to the sustainability of systems that extract or add heat to the subsurface. Rybach (2003) listed the following environmental impacts that may be temporary or irreversible: changes to landscape and use; emissions to the atmosphere, surface water and groundwater; noise created by the conversion of geothermal energy to other forms of energy; land subsidence and seismicity; and solid waste. In most cases where the subsurface is used for energy storage or dissipation, the primary environmental concern is related to changes in water quality. Clearly care must be taken to ensure that any water injected into an aquifer should not contain harmful contaminants. Also, any poor quality groundwater used for thermal purposes should not be disposed in an aquifer or surface water body that is used as a drinking water supply or is important ecologically. Problems can also occur due to chemical incompatibilities between injected water and native groundwater. Changes in the solubility of certain minerals with temperature can also cause problems. In a field experiment of aquifer thermal energy storage (ATES) in Alabama, reduction of permeability occurred in the test as a result of clogging due to suspended solids present in injected water and chemical reactions between the injected water and native

groundwater (Molz et al., 1979). Other studies in Ontario (Palmer and Cherry, 1984) and Minnesota (Perlinger et al., 1987) have examined geochemical aspects of ATES development. These studies found problems associated with the retrograde solubility of carbonate minerals, particularly within the immediate vicinity of the injection well.

7.2 Design and Analysis of Geothermal Reservoir Developments

Flow of groundwater and heat during the utilization of groundwater for thermal purposes is governed by the differential equations describing groundwater flow (Equation 2.6) and heat flow (Equation 2.10). Both analytical and numerical models have been used to study the changes in temperature that result from the extraction or injection of hot or cold water into aquifers.

Much of the early research into the exploitation of aquifers for geothermal energy examined the situation with a single production well and a single injection well, known as a doublet. The groundwater velocity field in a doublet was examined by Grove et al. (1970). Gringarten and Sauty (1975) looked at heat transport in the same configuration as Grove et al. (1970) and derived the following equation to estimate the separation between two wells required to achieve a desired reservoir lifetime:

$$D = \sqrt{\frac{2Q\Delta t}{\left[\left(\eta + (1-\eta)\frac{\rho_{cr}c_{cr}}{\rho_f c_f}\right)h + \left(\left(\eta + (1-\eta)\frac{\rho_{cr}c_{cr}}{\rho_f c_f}\right)^2 H^2 + 2\frac{\kappa_{cr}\rho_{cr}c_{cr}}{\rho_f c_f}\Delta t\right)^{1/2}\right]}}$$

(7.1)

where Q is the rate of withdrawal and injection, D is the distance between the injection and withdrawal well, H is the thickness of the aquifer, ρ_{cr} is the density of the geologic unit confining the aquifer, c_{cr} is the specific heat capacity of the confining unit, κ_{cr} is the thermal conductivity of the confining geologic unit and Δt is the time prior to thermal breakthrough, also defined as reservoir lifetime. This equation is the solution to equations 2.6 and 2.10 with several simplifying assumptions. Within the aquifer, heat flow is entirely due to horizontal advection and only vertical conductive heat flow is assumed in the units underlying and overlying the aquifer. In this context, reservoir lifetime is also often referred to as the time of thermal breakthrough, which is defined as the time when the first temperature increase is observed at the production well.

Gringarten (1978) provides an additional solution to equations 2.6 and 2.10 for the case where no heat loss to the surrounding geologic units:

$$\frac{\rho_f c_f}{\rho_{sat} c_{sat}} \frac{Q \Delta t}{D^2 H} = \frac{\pi}{3} \quad (7.2)$$

Equations 7.1 and 7.2 are of limited use because they only provide an estimate of the timing of thermal breakthrough and give no indication of the magnitude of the temperature increase that can be expected nor the spatial extent of the thermal anomaly.

These solutions do not account for many of the complexities present inherent in most geological environments, such as variations in hydrogeological and thermal properties, thicknesses of geologic units and the presence of fractures. The analytical models presented in equations 7.1 and

7.2 also assume that the units above and below the aquifer are impermeable. This may be a reasonable assumption if the aquifer is several orders of magnitude greater than these surrounding units but this is not always the case. The analytical models also assume a simple configuration for the production and withdrawal wells, allowing for only two wells that both fully penetrate the aquifer being exploited. Many systems attempt to increase the effective well spacing by installing these wells at different depths. This situation requires the use of a numerical model for the solution of equation 2.10. The analytical models are also incapable to dealing with irregular usage patterns. Numerical models of heat transport related to thermal use of groundwater are created with METRA in this study.

7.3. Thermal Use of Groundwater in the Winnipeg Area

7.3.1 History of Thermal Use of Groundwater in the Winnipeg Area

Groundwater has been used for heating and cooling purposes in Winnipeg, Manitoba since the early part of the 20th century when groundwater was used as a coolant in meat packing plants and for air conditioning in some theatres. Early use was consumptive, with wastewater produced from cooling discharged to the sewer system. This put an excessive stress on the City of Winnipeg's sewer system and during the 1940's a groundwater sewage tax was implemented to limit the disposal of thermal wastewater to the Winnipeg's sewer system (Render, 1970). In the time period between 1940 and 1960, Render (1970) stated that 8 injection systems came into use, although none of these wells are listed in the Province of Manitoba's well

151

database, GWDrill. The number of heating systems disposing of thermal wastewater by injecting it into the Upper Carbonate Aquifer has increased to 73 as of 1997 (Figure 7.1). These wells are located throughout the City of Winnipeg, with the highest concentrations occurring in an area surrounding the Winnipeg International Airport in St. James (Figure 7.2). Several high volume users of groundwater for refrigeration were formerly present in the St. Boniface area but with downscaling of the meat packing industry in Winnipeg some of these wells have been decommissioned. Another high volume user in this area of the Winnipeg has recently converted to consumptive use.

The development of groundwater resources for thermal purposes in the Winnipeg area is still quite active, with a number of systems currently being planned or developed. Recently completed systems include a groundwater source heat pump for a commercial building in downtown Winnipeg and the conversion of a groundwater source air conditioning system to a conjunctive use space heating/air conditioning system for a hotel in western Winnipeg. Systems in the planning stages include an air conditioning system for a large commercial building in southern Winnipeg, a potential heating and/or cooling system for a large office building in downtown Winnipeg and a system being designed to cool hydroelectric transformers west of Winnipeg.

7.3.2 Typical Development

All wells drilled for thermal purposes in the Winnipeg area are completed in the carbonate rock sequence beneath the city. Although the

bulk of the permeability is present in the upper fractured portion of the sequence, known locally as the Upper Carbonate Aquifer, most wells are completed through a considerable thickness of the less permeable carbonate rock underlying the aquifer. In most cases wells are completed into the lower part of the carbonate sequence to supplement the capacity of the wells but in some cases this has been done in an attempt to delay thermal breakthrough. In other cases where insufficient capacity is obtained from a single well, one or more additional production or injection wells are drilled.

The majority of these systems are licensed to produce and inject groundwater at a rate of approximately 10 L s^{-1}, although some of the larger systems are licensed for rates in excess of 50 L s^{-1}. The majority of these systems are using groundwater for air conditioning and are used predominantly during the summer. Other systems are used for industrial cooling and are required throughout the year. Some of the larger industrial cooling systems involve more complex disposal schemes involving multiple injection wells. Spacing of production and injection wells is constrained by the size of the property and is generally less than 100 metres.

7.3.3 Effect on Subsurface Temperatures

Temperature anomalies within the aquifer related to injection of thermal wastewater are found in many locations in the City of Winnipeg. The largest anomalies have been noted in an industrial area of St. Boniface in eastern Winnipeg and in an area where there are several apartment buildings and hotels that use groundwater for air conditioning in the St. James area of

153

western Winnipeg (Figure 7.2). Rises in temperature noted at production wells are variable, ranging from virtually no change in temperature (Figure 7.3) to changes of several degrees Celsius (Figure 7.4). Thermal breakthrough generally occurs in the first few years of operation and varying increases in temperature are observed following this event. In some cases the temperature of the injection well and the production well become approximately equal after thermal breakthrough (Figure 7.5) while in others the temperature rise observed at the production well is only a fraction of the temperature difference between the native groundwater and injected water (Figure 7.6). The reasons for these increases will be examined through generic and site specific models in Chapters 8 and 9 of this thesis.
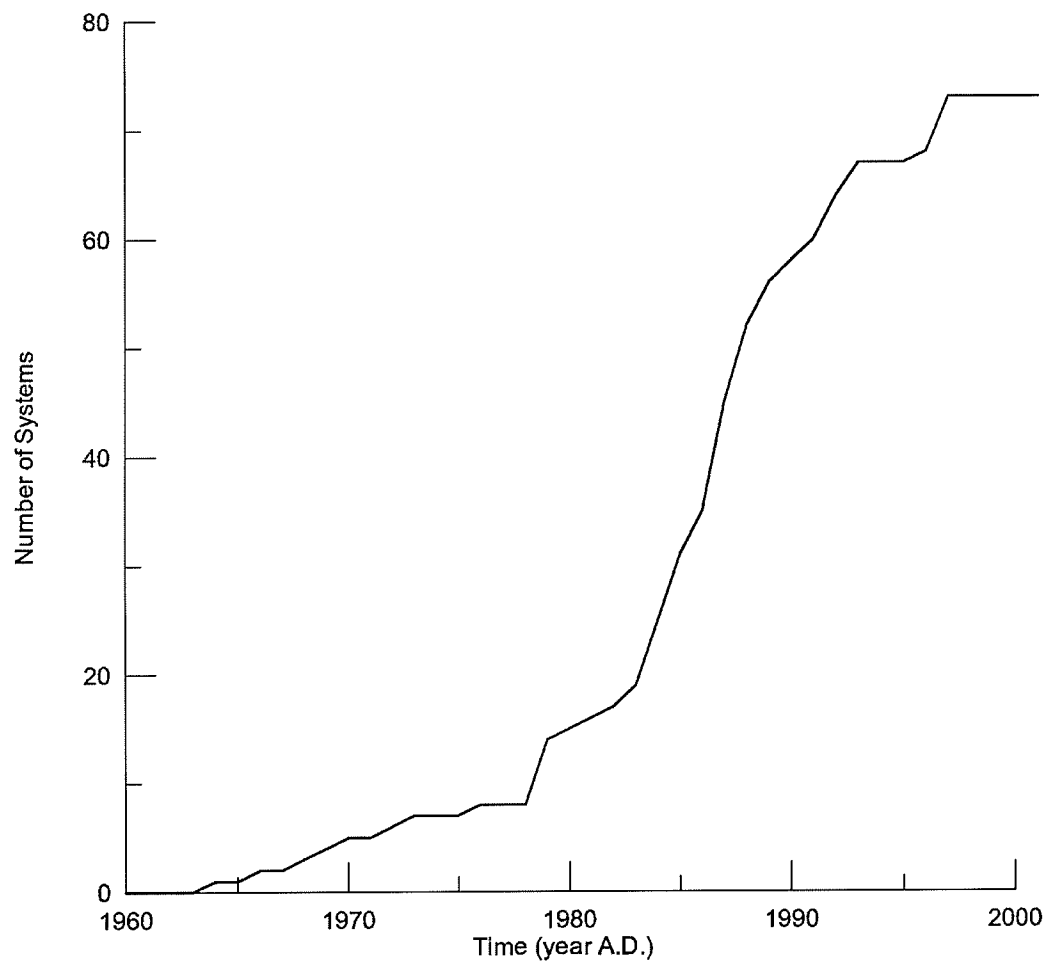
Figure 7.1: Cumulative number of injection wells installed for geothermal purposes in Winnipeg (Source: GWDrill).
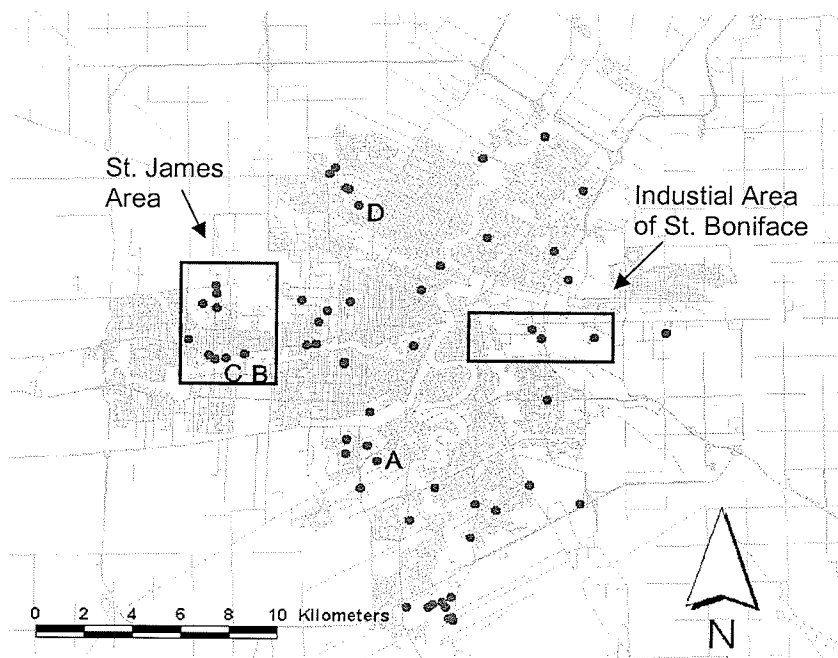
Figure 7.2: Location of injection wells in the Winnipeg area. The wells denoted A, B, C and D represent the locations of the wells shown in figures 7.3, 7.4, 7.5 and 7.6 respectively.
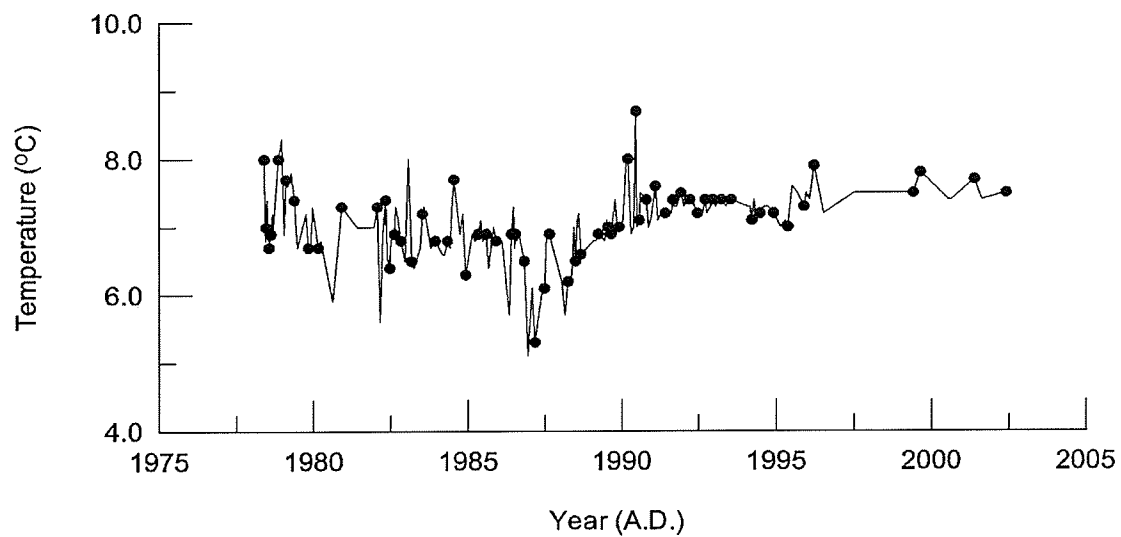
Figure 7.3: Temperature record for the production well at a building using groundwater for air conditioning in southern Winnipeg. Location of this system is denoted in Figure 7.2.
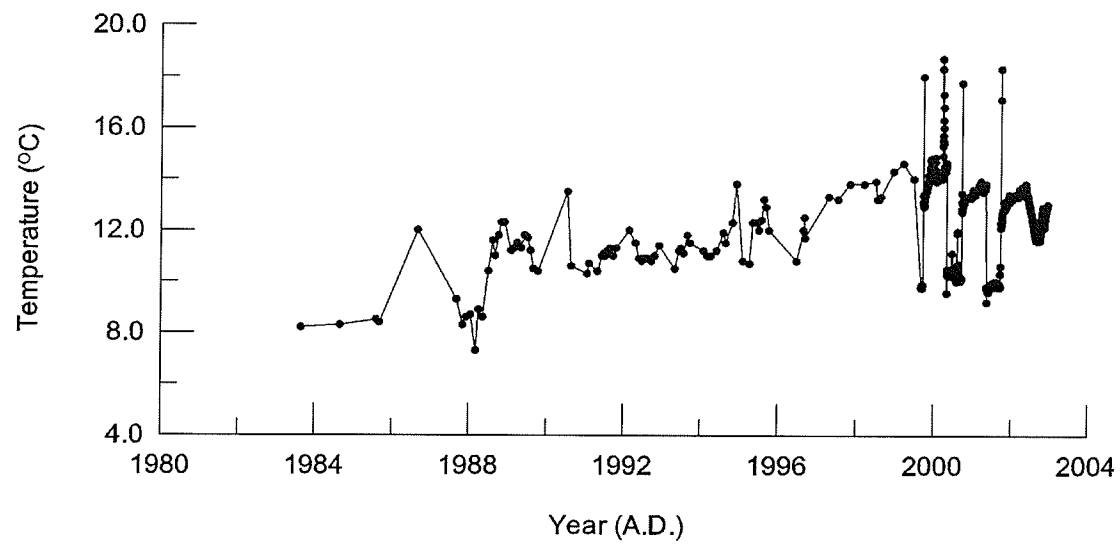
Figure 7.4: Temperature record for the production well at a building using groundwater for air conditioning in the St. James are of western Winnipeg. Location of this system is denoted in Figure 7.2.

Figure 7.5: Temperature records for the injection (hollow circles) and production (solid circles) wells at a building using groundwater for air conditioning in the St. James area of western Winnipeg. Location of this system is denoted in Figure 7.2.
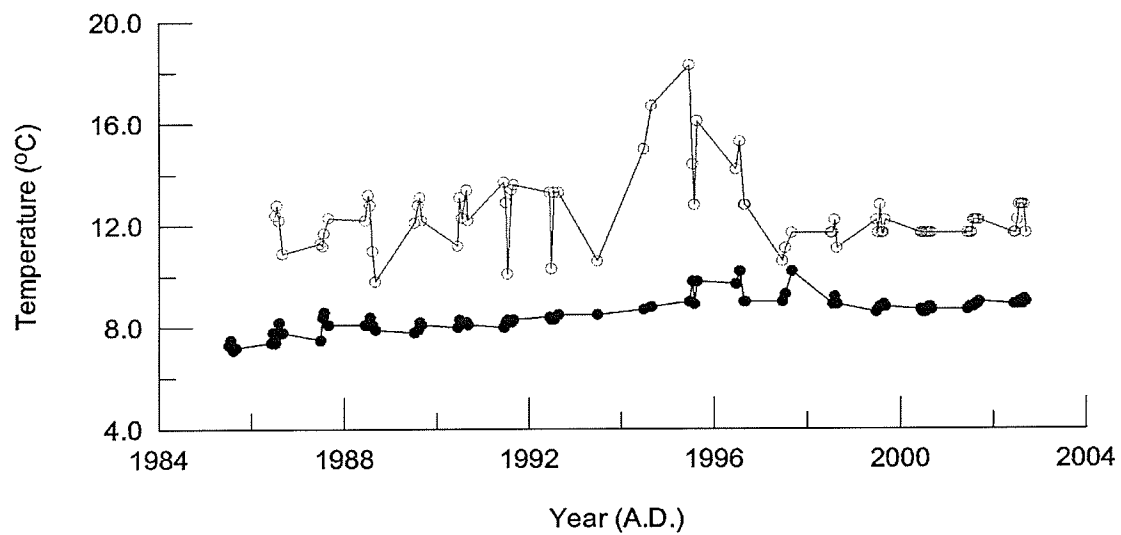
Figure 7.6: Temperature records for the injection (hollow circles) and production (solid circles) wells at building using groundwater for air conditioning in northern Winnipeg. Location of this system is denoted in Figure 7.2.

160

CHAPTER 8: GENERIC MODELS OF THERMAL DEVELOPMENT IN THE WINNIPEG AREA
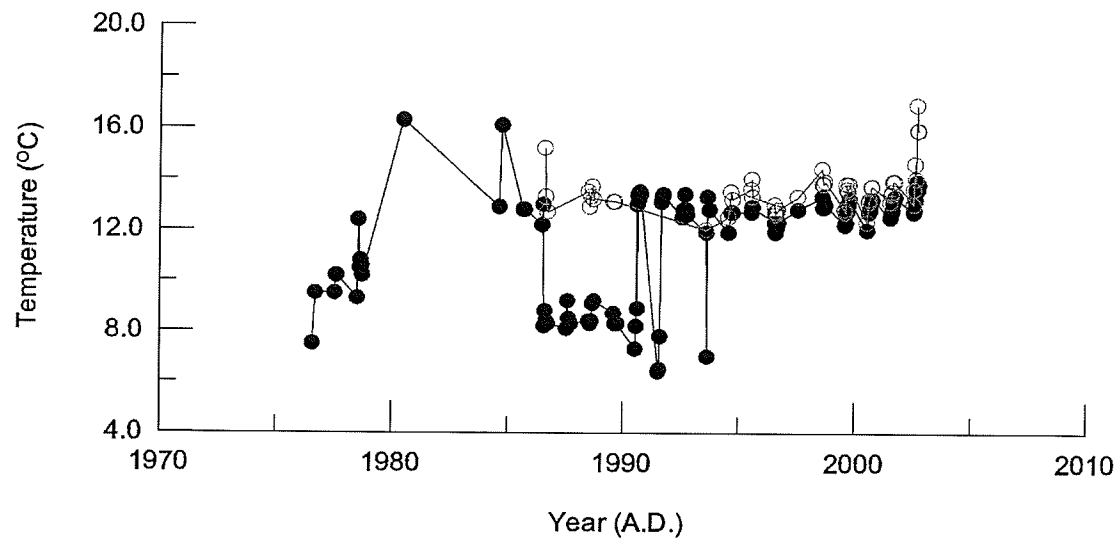
8.1 Motivation for Generic Modeling

Due to the number of systems using groundwater for cooling purposes in the Winnipeg area, modeling of all cases would be a daunting task. Generic modeling provides an efficient method for examination of typical development scenarios in the Carbonate Rock Aquifer over a range of hydrogeological situations. The importance of various parameters can be analysed and suggestions for thermal development of the aquifers underlying Winnipeg can be made for different situations that may be encountered. Generic modeling will also be used to determine the areal extent of thermal anomalies that result from the injection of thermal wastewater, both in the absence and presence of regional groundwater flow. These results will be used to establish the value of regional modeling in this thesis. Also, the role of fractures in the Carbonate Rock Aquifer has long been debated (e.g. Render, 1970; McCabe et al., 1993; Kennedy, 2002). Generic models created in this study will examine both conventional porous media (single continuum) and dual continuum models to address whether or not there is an advantage to either model formulation.

8.2 Upper Carbonate Aquifer

8.2.1 Analytical Models Applied to the Upper Carbonate Aquifer

Gringarten's (1978) model (Equation 7.2) was applied to the Upper Carbonate Aquifer to predict the time of thermal breakthrough for the case where there is no heat loss to the units above and below the aquifer (Figure 8.1). Densities and heat capacities outlined in Table 8.1 were used along with an aquifer thickness of 10 metres for various pumping rates and well spacings. The results indicate that in cases where the pumping rate is greater than 2.5 L s^{-1}, thermal breakthrough will occur in less than two years for all well spacings examined. For pumping rates less than 1.0 L s^{-1}, breakthrough times can be much longer, reaching approximately 10 years for wells spaced at 200 metres.

To examine the case where heat flow is allowed to occur in the units above and below the aquifer, Gringarten and Sauty's (1975) model (Equation 7.2) was manipulated to calculate the expected times for thermal breakthrough in the Upper Carbonate Aquifer for various well spacings and for various withdrawal and injection rates (Figure 8.2). These calculations indicate that accounting for heat loss to the confining bed does not significantly retard the movement of the thermal front.

Temperature data from doublets in operation in the Winnipeg area indicate that these results are plausible in some areas of the Upper Carbonate Aquifer. However, the magnitude of temperature increases at the production well is variable in different systems (Figure 7.3 to 7.6). The need

162

to understand of timing and magnitude of temperature increases that result from the operation of injection-withdrawal doublets suggests that more complex numerical models are required.

8.2.2 Numerical Models Applied to the Upper Carbonate Aquifer

8.2.2.1 Introduction

Generic numerical models of the Upper Carbonate Aquifer produced in this study were constructed using parameters typical of the Winnipeg area (Table 8.1) in combination with typical hydrostratigraphy. Fracture permeabilities were estimated using equation 2.12 along with geological and hydrogeological data provided by Render (1970), McCabe et al. (1993) and Kennedy (2002). Specific heat capacity and matrix permeability data were not available for the Carbonate Rock Aquifer and in their place literature values were used (Table 8.1). The models produced using these parameters will be referred to as the base models for the conventional porous media and dual continuum formulations hereafter. These models were used to conduct a sensitivity analysis of parameters involved in the modeling of doublets in the Winnipeg area in both conventional porous media and dual continuum approaches. In both approaches the effects of well spacing, aquifer thickness, thermal conductivity, specific heat capacity, porosity, pumping rate and permeability of the rock underlying the aquifer were examined. In the dual continuum model, the effect of increasing or decreasing the volume of the aquifer occupied by fractures was examined, in addition to the effect of matrix permeability variations.

163

In the generic withdrawal-injection doublet, water was injected at a constant rate of 3.8 L s^{-1} at 11°C; corresponding to a rise in temperature of 5°C, for the duration of the model. A rise in temperature of injected water after breakthrough of injected water at the production well was not considered in this study although it has been observed in some injection-withdrawal doublets in the Winnipeg area. In the first set of models produced, regional groundwater flow was neglected by imposing equal fixed head boundary conditions on all sides of the model, which were placed at a distance of nearly 2000 metres from the wells in all directions. Changes in hydraulic head due to pumping of the aquifer were not predicted at this distance from the wells by the numerical models. Block sizes in the numerical model ranged from 10 x 10 metres across in the area between and immediately surrounding the production and injection wells to 500 x 500 metres across near the boundaries of the models. Only the Paleozoic carbonate sequence was examined in these models because the incorporation of the overlying till and clay into the model was found to have minimal impact on the results while making the models much more computationally expensive. The background temperature gradient was neglected in this model and a uniform background temperature of 6.0 °C was assumed. The use of a constant temperature is likely reasonable even in cases where wells are located near buildings because the rates of temperature change due to conductive heat losses from buildings are relatively slow compared to the rates of temperature change related to advective heat flow due to withdrawals and injection.

The impact of regional groundwater flow is addressed by a second set of models that impose a hydraulic gradient over the model by imposing a fixed hydraulic head at opposite ends of the model. These models use the same hydraulic and thermal parameters used in the first set of models.

8.2.2.2 Conventional Porous Media Models

In the base model, water with elevated temperatures is predicted to breakthrough at the production well during the first six months of operation (Figure 8.3). A temperature of 6.2°C is predicted at this time and the temperature is predicted to be 8.3°C after two years of operation. During the next 10 years, an increase of slightly less than 1.0°C is predicted. This increase in temperature following breakthrough can be attributed to arrival of heat along different streamlines at various times during the first few years of operation. After this time, conduction becomes a more important mechanism of heat transport. Conductive heat transport has some effect on the temperatures observed at the production well but is more important in the growth of the area of influence of the doublet regionally (Figure 8.4). The areal extent of a predicted temperature increase of greater than 1.0°C is approximately 250 metres in the direction parallel to the axis of the doublet and approximately 200 metres perpendicular to the doublet. The isotherms are more closely spaced in the vicinity of the production well than they are near the injection well.

In the less permeable rock underlying the aquifer, advective transport is reduced due to a decrease in permeability; however temperature increases

are still observed. Increases in temperature of 1.0°C are predicted at approximately 30 metres below the aquifer after only 3 months of operation (Figure 8.5). This depth increases slowly following the first few months of operation, reaching a depth of over 40 metres after ten years of operation.

The spacing of the injection and production wells had a significant effect on the temperatures at the production well. Reducing the spacing of the wells to 50 metres resulted in an increase in the predicted temperature of 0.6°C compared to the base model at the production well after 10 years of operation, while increasing the spacing to 200 metres resulted in a decrease in temperature of approximately 1.3°C at the production well compared to the base model after 10 years of operation (Figure 8.3). The increase in spacing also increased the amount of time prior to thermal breakthrough, keeping temperatures below 6.1°C during the first two years of operation. Conversely, decreasing the spacing resulted in a reduction in the time of thermal breakthrough, as a temperature increase of 0.7°C was observed during the first three months of operation. Changing the spacing between the injection and production wells is predicted to have a significant effect on the area of the aquifer that experiences increases in temperature (Figure 8.6). If the spacing is decreased to 50 metres, the area of the anomaly, as defined by the 7°C isotherm, decreases to an area of less than 200 metres across, both parallel and perpendicular to the axis of the doublet. The anomaly is predicted to become much larger and elongated for a well spacing of 200 metres. Increases in temperature of greater than 1°C are predicted over an area of

nearly 400 metres in length in the direction parallel to the axis of the doublet and approximately 300 metres in length in the direction perpendicular to the doublet.

In the conventional porous media model, increasing the pumping rate by a factor of two caused an increase in the temperature at the production well of approximately 0.5°C after 10 years (Figure 8.7). A reduction in pumping rate to 50% of the base case resulted in a decrease in predicted temperature at the production well of approximately 0.6°C relative to the base case. Varying the pumping rate did not greatly affect the timing of thermal breakthrough but the shape of the breakthrough curve was affected. At the lower pumping rate, the predicted increase in temperature is more gradual than that predicted at the higher rates. An examination of seasonal pumping rates was conducted by restricting production and injection to a three month period of every year, while maintaining the same amount of pumping per annum (Figure 8.8). The results showed that there is some seasonal variation in temperature but the longer-term trend in temperatures can be approximated by using a constant pumping rate that reflects the total volume of water produced and injected in a year. The areal extent of predicted anomalous temperatures does not vary much with changes in pumping rate (Figure 8.9). A slight decrease in the size of the affected area relative to the base case is predicted for the lower pumping rate as the width of the anomaly decreases in size to fewer than 200 metres, as defined by the 7°C isotherm. A slight increase in size is predicted if the pumping rate is doubled. The

length of the anomaly along the axis of the doublet is approximately the same size as that predicted in the base case but in the direction perpendicular to the doublet, the size of the anomaly increases to encompass an area of approximately 250 x 250 metres.

The thickness of the aquifer had a smaller impact on predicted temperatures at the production well. By increasing or decreasing the thickness of the generic aquifer between 5 and 15 metres, the predicted temperatures vary within about 0.3°C with the higher temperatures predicted for the thinner aquifers (Figure 8.10). The slope of the breakthrough curve is slightly more gradual for the thicker aquifer. The predicted areal distribution of anomalous temperatures did not change appreciably with increases or decreases in aquifer thickness.

In the unit underlying the aquifer, an increase in the permeability of an order of magnitude above the base case value had little impact on predicted temperatures at the production well (Figure 8.11). However, an increase of two orders of magnitude had a significant impact, reducing the predicted temperatures by approximately 0.5°C (Figure 8.11). The increase in advective heat transport in the unit beneath the aquifer caused an increase in the depth of penetration of the temperature anomaly. A temperature of 7.0 °C is predicted to reach a depth of over 50 metres beneath the aquifer if the underlying unit has a permeability of 10^{-12} m^2 (Figure 8.12).

An examination of the sensitivity of predicted temperatures to the permeability of the aquifer showed that increasing permeabilities within the

aquifer has no effect. Also, reducing the permeabilities in the aquifer by an order of magnitude had very little effect. Simulations for lower permeabilities were not representative of systems in operation in the Carbonate Rock Aquifer because predicted changes in hydraulic head were much greater than observed changes. The sensitivity of temperatures at the production well to the porosity of the generic aquifer was also assessed. Porosity values of 0.05 and 0.11 were found to produce temperatures that were different by less than 0.1°C, indicating that the rate of heat transport is relatively insensitive to porosity over the range observed in the aquifer.

Thermal conductivity was shown to have an impact on the predicted temperatures, but only after thermal breakthrough had occurred. Thermal conductivities of 1.0, 2.4 (the base case), and 5.0 W m^{-1} $°C^{-1}$ were examined and all three simulations had temperatures that were quite similar during the first year (Figure 8.13). However, increases in temperature occurred more rapidly in lower thermal conductivity cases over the next two years because heat built up more readily. The temperatures after five years were approximately 0.1°C less in the 5.0 W m^{-1} $°C^{-1}$ than in the base case and approximately 0.25°C greater in the 1.0 W m^{-1} $°C^{-1}$ case than in the base case.

Different specific heat capacities were also considered in this analysis of heat transport. Changing specific heat capacity had a greater effect on the predicted temperatures at the production well than varying thermal conductivity. Increasing specific heat capacity of the carbonate rock by 50%

reduced predicted temperatures throughout the period modeled, with predicted temperatures of approximately 0.5°C less than that of the base model after one year of operation (Figure 8.14). Temperatures were generally approximately 0.2°C less than those of the base model at later times. For the case where specific heat capacity was reduced by 50%, the temperatures are predicted to rise more rapidly at production well than in the base model. Temperatures predicted for times greater than two years are approximately 0.2 °C greater than those predicted in the base model.

8.2.2.3 Dual Continuum Models

The base dual continuum model predicts that breakthrough will occur slightly sooner than in the porous media model, with a predicted temperature increase of 0.06 °C occurring at the pumping well during the first few months (Figure 8.15). Temperatures increase more rapidly during the first year and after two years of operation a temperature of 8.0°C is predicted at the production well. This value is slightly less than the predicted temperature for the base model in the porous media case. Drawdown in the dual continuum model was similar to the porous media model, with a hydraulic head for the grid cell containing the production well that is approximately 0.2 metres greater than that predicted in the porous media model.

The thermal anomaly resulting from the operation of the doublet, as defined by the 7°C isotherm, is predicted to cover a nearly circular area with a radius of approximate 50 metres after three months of operation (Figure 8.16). The anomaly tends to grow in the direction of the production well over

the next several months and water 1°C above the background temperature is expected to reach the production well after one year of operation. The predicted temperature field between the injection and production wells appears to reach an approximately steady state during the first five years of operation but the anomaly continues to grow outward slowly.

Well spacing and pumping rate were found to be the most important variables in the dual continuum model (Figures 8.15 and 8.17). The changes associated with changing well spacing and pumping rates produced differences in the predicted temperatures similar to those predicted in the porous media model.

Changes in aquifer thickness in the dual continuum model are predicted to have only a slight effect on predicted temperatures. Increasing the thickness of the aquifer is predicted to cause a later breakthrough of heated water at the production well (Figure 8.18). However, after two years of production, higher temperatures at the production well are predicted if the aquifer is 15 metres thick as opposed to 10 metres thick. The difference between predicted temperatures between these two models is very small and does not exceed 0.1°C following ten years of operation. Reducing the thickness of the generic aquifer to 5 metres results in a slightly earlier thermal breakthrough at the production well and slightly lower predicted temperatures than the base model after two years of operation. After ten years of operation, the temperature at the production well is predicted to be more than

171

0.2°C less in the model with the 5 metre aquifer than in the base model, which had a 10 metre thick aquifer.

The predicted temperatures at the production well increase with an increase in the volume of the aquifer occupied by fractures. This volume is also referred to as fracture porosity. Increasing the fracture porosity from 0.05 to 0.10 results in an increase in predicted temperature of slightly greater than 0.2°C after 1 year (Figure 8.19). The difference in predicted temperature between the models decreases slightly over the next nine years of the model. Thermal breakthrough at the production well occurs at approximately the same time in both models and the rate of temperature increase is not appreciably different. Reducing the fracture porosity to 0.01 is predicted to cause temperature increases of approximately 0.8°C less than those predicted for a 10 metre thick aquifer at the production well. The rate of temperature increase observed at the production well is much lower for the case of a 5 metre thick aquifer.

Higher temperatures at the production well are predicted in cases in which lower fracture porosities are assigned to the underlying rock (Figure 8.20). When the fracture porosity of the underlying rock is increased to 0.01 from the base model value of 0.005, temperatures at the production well are predicted to decrease by approximately 0.2°C relative to the base model following thermal breakthrough. For the case where the fracture porosity of the underlying rock is given a value of 0.001, the temperatures at the production well are predicted to be approximately 0.2°C higher than those

predicted in the base model. The time of thermal breakthrough at the production well does not change noticeably with changes in the fracture porosity of the rock underlying the aquifer.

8.2.2.4 Effect of Regional Groundwater Flow

The permeability of a homogeneous aquifer is predicted to have no effect in the absence of regional groundwater flow by potential field theory (Grove et al., 1971; Gringarten and Sauty, 1975) but permeability becomes an important parameter when regional groundwater flow is significant. The effect of permeability and regional groundwater flow were examined in the numerical models using conventional porous media and dual continuum approaches. The hydrostratigraphy and associated hydrogeologic and thermal parameters used in these models were identical to that of the base models created in the previous sensitivity analysis where regional groundwater flow was neglected. A regional hydraulic gradient was imposed by placing fixed head boundary conditions at the east and west ends of the modeled domain, with a two metre drop in head over the 5000 metre length of the domain. The doublet was placed in a north-south orientation in order to represent the most neutral case. If the doublet was placed parallel to the direction of regional groundwater flow, regional groundwater flow could act to increase or decrease the time of thermal breakthrough, depending on the relative locations of the injection and production wells.

Conventional porous media models predict the formation of extensive plumes of heated water affected by regional groundwater flow when aquifer

173

permeabilities exceed $10^{-9}\,\text{m}^2$. At a permeability of $10^{-8}\,\text{m}^2$, temperatures 1°C greater than the background temperature are predicted at a distance of approximately 2000 metres from the injection well (Figure 8.21). For a generic aquifer with a permeability of $10^{-9}\,\text{m}^2$, the shape of the resulting temperature anomaly is only slightly affected by regional groundwater flow. Temperatures 1°C above background temperatures are predicted 300 metres downstream of the injection well after five years of operation. If the generic aquifer is given a permeability of $10^{-10}\,\text{m}^2$, the temperature anomaly is approximately symmetric about the injection well in the north-south direction, indicating that regional groundwater flow has a minimal impact on heat transport.

The magnitude of the temperature increase observed at the production well is inversely related to the distance that the plume of heat can travel from the injection well. No increase in temperature is predicted at the production well if the generic aquifer has a permeability of greater than $10^{-8}\,\text{m}^2$ and an increase to a temperature of just over 7 °C is predicted for a generic aquifer with a permeability of $10^{-9}\,\text{m}^2$ (Figure 8.22). For the $10^{-9}\,\text{m}^2$ case, it should be noted that the predicted rate of temperature increase at late times is much slower than the rate predicted in the absence of regional groundwater flow. Predicted temperature increases in a generic aquifer with a fracture permeability of $10^{-10}\,\text{m}^2$ are nearly identical to those predicted in the absence of regional groundwater flow during the first two years of operation. However, temperature increase predicted at the production well at later times are a few

tenths of a degree Celsius greater than those predicted in the case where regional hydraulic gradients are not considered.

The dual continuum models predict the formation of extensive plumes of heated water controlled by regional groundwater flow at fracture permeabilities greater than 10^{-8} m^2. At a fracture permeability of 10^{-7} m^2, groundwater with a temperature of 1°C above the background temperature is predicted at a distance of approximately 2000 metres from the injection well (Figure 8.23). For a generic aquifer with a fracture permeability of 10^{-8} m^2, regional groundwater flow only has a small effect on the shape of the temperature anomaly. Temperatures of 7°C are predicted 300 metres downstream of the injection well after five years of operation. If the fractures in the generic aquifer are given a permeability of 10^{-9} m^2, the regional groundwater flow appears to have no effect on the shape of the temperature anomaly.

In general, predicted production temperatures in the dual continuum models are less in more permeable aquifers under the influence of a regional hydraulic gradient (Figure 8.24). Temperature is predicted to remain at the background level in a generic aquifer with a fracture permeability of 10^{-7}m^2 and an increase to a temperature of just under 7 °C is predicted for a generic aquifer with a fracture permeability of 10^{-9} m^2. For the 10^{-8} m^2 case, temperatures at the production well increase very slowly following the initial thermal breakthrough. The temperatures predicted at the production well for a generic aquifer with a fracture permeability of 10^{-9} m^2 are essentially the

same those predicted in the absence of regional groundwater flow during the first two years of operation. At later times, temperatures predicted at the production well are slightly less when regional groundwater flow is present.

8.3 Winnipeg Formation Sandstone Aquifer

8.3.1 Analytical Models Applied to the Winnipeg Formation

The analytical solutions produced by Gringarten (1978) (Equation 7.1) and Gringarten and Sauty (1975) (Equation 7.2) were used to estimate thermal breakthrough times for the Winnipeg Formation if it were to be used for as a source of groundwater for cooling applications. Equation 7.1 predicts that thermal breakthrough will occur in only 1.3 years for the same situation (Figure 8.25). Equation 7.2 predicts that for a pumping rate of 3.8 L s^{-1}, an aquifer thickness of 30 metres and a well spacing of 100 metres, thermal breakthrough will occur in approximately 4.0 years (Figure 8.26).

8.3.2 Numerical Models Applied to the Winnipeg Formation

Numerical models were created to estimate the temperature field resulting from the use of groundwater from the Winnipeg Formation for cooling. Fewer variables were examined in the analysis of the Winnipeg Formation because many of the factors that could affect heat transport in the Carbonate Rock Aquifer are not as much of an issue in the Winnipeg Formation. The overlying shale and underlying Precambrian rock are several orders of magnitude less permeable than the sandstone of the Winnipeg Formation, making the assumptions about aquitard impermeability realistic

based on the findings of the previous generic models. Uncertainty in porosity is estimated to have little effect on the Winnipeg Formation as large variations in porosity were found to have only a small effect on predicted temperatures in the more heterogeneous Upper Carbonate Aquifer. Other than spacing and pumping rates, the variations in the thickness of the Winnipeg Formation will have the largest impact on the behaviour of this formation when subjected to geothermal development. Betcher (1986) indicated that the Winnipeg Formation ranges in thicknesses from 6.1 to 42.8 metres. To estimate the behaviour of injected water in the Winnipeg Formation, numerical simulations were conducted with typical and estimated parameters for the Winnipeg Formation (Table 8.2) for a pumping rate of 3.8 L s^{-1} and an injection temperature of 13°C, which is 5°C greater than the uniform assumed in situ temperature of 8.0°C. The thickness of the Winnipeg Formation was varied between 10 and 40 metres in these simulations.

As in the previous models of the generic aquifer resembling the Carbonate Rock Aquifer, block sizes in the numerical model ranged from 10 x 10 metres in the area between and immediately surrounding the production and injection wells to 500 x 500 metres near the boundaries of the model. Fixed head boundary conditions were placed on the lateral boundaries of the aquifer at a distance where hydraulic head was not affected by pumping. The upper and lower boundaries of the model were treated as impermeable boundaries to reflect the presence of the crystalline Precambrian rock below and the continuous shale unit above this sandstone aquifer.

Temperatures at the production well are predicted to increase from 1.7 to 2.7°C after 10 years of operation, with the greatest temperature increase occurring in the case with the 10 metre thick aquifer (Figure 8.27). Predicted thermal breakthrough occurred within the first year of operation for each case but the predicted rise in temperature is much more dramatic for thinner aquifers. The temperature at the production well is predicted to increase to 9.3 °C by the end of the first year of operation for the case a 10 metre thick aquifer. The predicted temperature increase is less than 0.1°C for the 40 metre thick aquifer.

The spatial extent of the anomaly created by injection grows slowly (Figure 8.28). In the first two years of operation, the anomaly remains centred on the injection well and it is only after this time that the anomaly becomes asymmetric, with isotherms most closely spaced around the injection well. The anomaly, as defined by the 9°C isotherm, is approximately 200 metres across in the direction perpendicular to the axis of the doublet after 5 years. At the same time, the 9°C isotherm is located approximately 120 metres away from the injection well on the side containing the production well and approximately 200 metres away from the injection well along the axis of the doublet in the other direction. In the next five years there is not a substantial change observed in the position of isotherms between the injection and production wells.

8.4 Discussion

8.4.1 Comparison of Generic Models

The comparison of analytical and numerical models is somewhat difficult due to the levels of information provided by the two types of models. However, the time of thermal breakthrough in the numerical models can be compared to the results of the analytical models. In the conventional porous media model, temperature increases were observed at the pumping well within the first 0.5 years of operation. For the same aquifer, thermal breakthrough predicted by equations 7.1 and 7.2 occurs at approximately 0.4 years in both models. These numbers are in reasonable agreement but the timing of thermal breakthrough is only one aspect of the sustainability of the use of groundwater as a coolant in the Winnipeg area.

The conventional porous media model and the dual continuum model produced similar results in many respects. The base models for both cases predicted similar temperature increases in the early and late stages of operation. The dual continuum model predicts a slightly more rapid thermal breakthrough and a marginally lower temperature at later times. The area that experiences elevated temperatures is slightly larger for the dual continuum case, with the anomaly, as defined by the 7 °C isotherm (Figures 8.4 and 8.16). The predicted anomaly in the dual continuum model extends an additional 20 metres in the x-direction on the injection well side of the anomaly and increasing in size by approximately 50 metres perpendicular to the axis of the doublet after five years of operation.

179

The sensitivity of porosity in the different models was quite different. The conventional porous media model was largely insensitive to porosity, while changes in the fracture porosity had a noticeable impact on the timing of temperature increases at the production well and the magnitude of these increases. However, bulk permeability is directly linked to fracture porosity in the dual continuum formulation because the volume of rock occupied by fractures is assigned a higher permeability. This link between permeability and fracture porosity is also important in the understanding of the behaviour of temperatures in the model in which fracture porosity was increased in the rock underlying the aquifer. No threshold value of fracture porosity was noticed because the fractures were given a uniform permeability throughout the dual continuum models and fractures were included in the lower unit in all model runs.

8.4.2 Implications of Generic Modeling Results

The results of the generic models imply that rises in temperature at a generic production well are inevitable in doublet style systems that use groundwater for cooling. The only exception to this would occur in areas where large areas with a bulk permeability of over 10^{-8} m^2 occur in combination with a regional hydraulic gradient of over 0.0002. Such conditions are not apparent in the Carbonate Rock Aquifer in the Winnipeg area (Render, 1970; Kennedy, 2003). Of the parameters required in the design of these systems, well spacing and pumping rate, have the greatest impact on the timing and magnitude of temperature increase observed at the

production well. Pumping rates in these systems are normally dictated by the amount of water required to operate a cooling system or by the sustainable amount that can be produced from the aquifer. Spacing of wells is not usually determined by the needs of the cooling system because it is restricted by the size of the property on which the system is to be installed. Due to the relatively large impact that well spacing has on the efficiency of groundwater as a coolant, every effort should be made to increase the amount of space between the injection and production wells. This may preclude the use of groundwater for thermal purposes in the current fashion by owners of smaller properties.

Geological conditions are predicted to be much less influential in the behaviour of heat flow in the operation of a doublet. In the absence of regional groundwater flow, aquifer permeability and porosity are of less importance in the behaviour heat in a doublet if the aquifer is homogeneous. However, vertical variations in hydraulic properties in both the aquifer and underlying aquitard can cause differences in behaviour. In the Carbonate Rock Aquifer, these variations are primarily due to differences in the fracture network. In the conventional porous media models, the variations in permeability cause noticeable differences in the estimated temperature field and porosity was not found to be important. In the dual continuum models, variations in fracture porosity are expected to have a significant impact on heat transport. Fracture porosity is directly related to the volume of the aquifer that is assigned a higher permeability in the dual continuum

formulation and therefore this is linked to the overall permeability of the medium.

The impacts of individual users of groundwater for thermal purposes are not predicted to affect a large area. Even in the case of injecting water constantly at 7.6 L s^{-1}, the impacted area was only a few hectares in size. Except when systems are placed within a few hundred metres of each other, they will not affect each other. Therefore regional modeling of the Upper Carbonate Aquifer is not absolutely necessary to understand heat flow in the subsurface of Winnipeg or the behaviour of heat flow in injection-withdrawal doublets installed for thermal purposes.

The Winnipeg Formation has not been developed for thermal purposes but under the same pumping rates and difference between background aquifer temperature and injection temperature, the Winnipeg Formation may be a better source of groundwater for thermal purposes. In this formation, temperature increases at the production well are predicted be much more gradual than the rate predicted for the generic aquifer used to simulate the Upper Carbonate Aquifer. At a thickness of 30 metres, the overall predicted temperature increase is less than that predicted by the generic models representing the Upper Carbonate Aquifer. McCabe (1978) suggested that the Winnipeg Formation is slightly thicker than 30 metres beneath Winnipeg but a small portion of the total thickness does not act as an aquifer. Despite the potential for later thermal breakthroughs and lesser increases in production well temperatures, the increased cost of drilling deep wells and

problems associated with the water quality of this aquifer likely preclude the use of the Winnipeg Formation for thermal purposes.

8.5 Summary

Based on the predictions of the generic models created, rises in temperature at production wells are unavoidable during the operation of a typical doublet in to the Carbonate Rock Aquifer. Despite the inevitability of increases in the temperature of produced water, doublets can be designed in such a way that thermal breakthrough at the pumping well is delayed and the temperature increase is minimised. The most important of these design parameters appears to be well spacing and this may severely limit the ability for some property owners to install efficient doublets on their properties. The generic models also suggest that a reduction in pumping rate can slightly delay thermal breakthrough and lead to smaller increases in temperature at the production well.

Generic modeling suggests that the presence of greater permeability in the carbonate rock underlying the aquifer, whether in the form of a porous media or increase in fracture volume, will slightly increase the time required for thermal breakthrough at the pumping well. The resulting temperatures after thermal breakthrough will also be less. These findings signify that the current practise of installing wells through the Upper Carbonate Aquifer and the underlying less permeable rock to increase production capacity may actually have thermal benefits. The generic models predict that other hydrogeologic and thermal parameters are likely of minimal importance in the

thermal development of the Upper Carbonate Aquifer. Regional groundwater flow is also something that can be neglected in most situations.

The greater thickness of the Winnipeg Formation appears to make it an attractive source of groundwater for thermal purposes. However, the increase in the expected life of the system is not substantially greater and other costs associated with the development of this aquifer may outweigh the potential benefits.

The results of the generic modeling should be used with caution as they may oversimplify actual situations. Permeability is extremely variable within this aquifer and large changes in permeability can occur of very short distances (Render, 1970; Kennedy, 2002). Also, pumping rates and injection temperatures are rarely constant and can be subject to variations on a variety of time scales. These complexities should be examined on a site-specific basis during the design stage of any new geothermal developments in the Winnipeg area.

	Porous Media Model		Dual Continuum Model	
	Upper Aquifer	Lower Unit	Upper Aquifer	Lower Unit
Matrix Permeability (m^2)	$10^{-10}{}_1$	$10^{-13}{}_2$	$10^{-13}{}_2$	$10^{-13}{}_2$
Fracture Permeability (m^2)	N/A	N/A	$10^{-9}{}_1$	$10^{-13}{}_2$
Matrix Porosity	0.095	0.095	0.095	0.095
Fracture Porosity	N/A	N/A	0.05_3	$0.005_{3,4}$
Thermal Conductivity ($W\ m^{-1}\ {}^\circ C^{-1}$)	2.4	2.4	2.4	2.4
Specific Heat Capacity ($J\ kg^{-1}\ {}^\circ C^{-1}$)	1200_5	1200_5	1200_5	1200_5

References:
1. Render, 1970
2. Freeze and Cherry, 1979
3. Kennedy, 2002
4. McCabe et al., 1993
5. Schon, 1996

Table 8.1: Parameters used in the creation of the baseline conventional porous media and dual continuum generic models for heat transport between a production well and injection well in the Upper Carbonate Aquifer.

	Winnipeg Formation
Matrix Permeability (m^2)	10^{-11}[1]
Fracture Permeability (m^2)	N/A
Matrix Porosity	0.08[1]
Fracture Porosity	N/A
Thermal Conductivity $(W\ m^{-1}\ °C^{-1})$	5.5[2]
Heat Capacity $(J\ kg^{-1}\ °C^{-1})$	1200[3]

References:
1. Betcher, 1986
2. Hutchence et al., 1986
3. Schon, 1996

Table 8.2: Parameters used in the creation of the models for heat transport between a production well and injection well in the Winnipeg Formation.
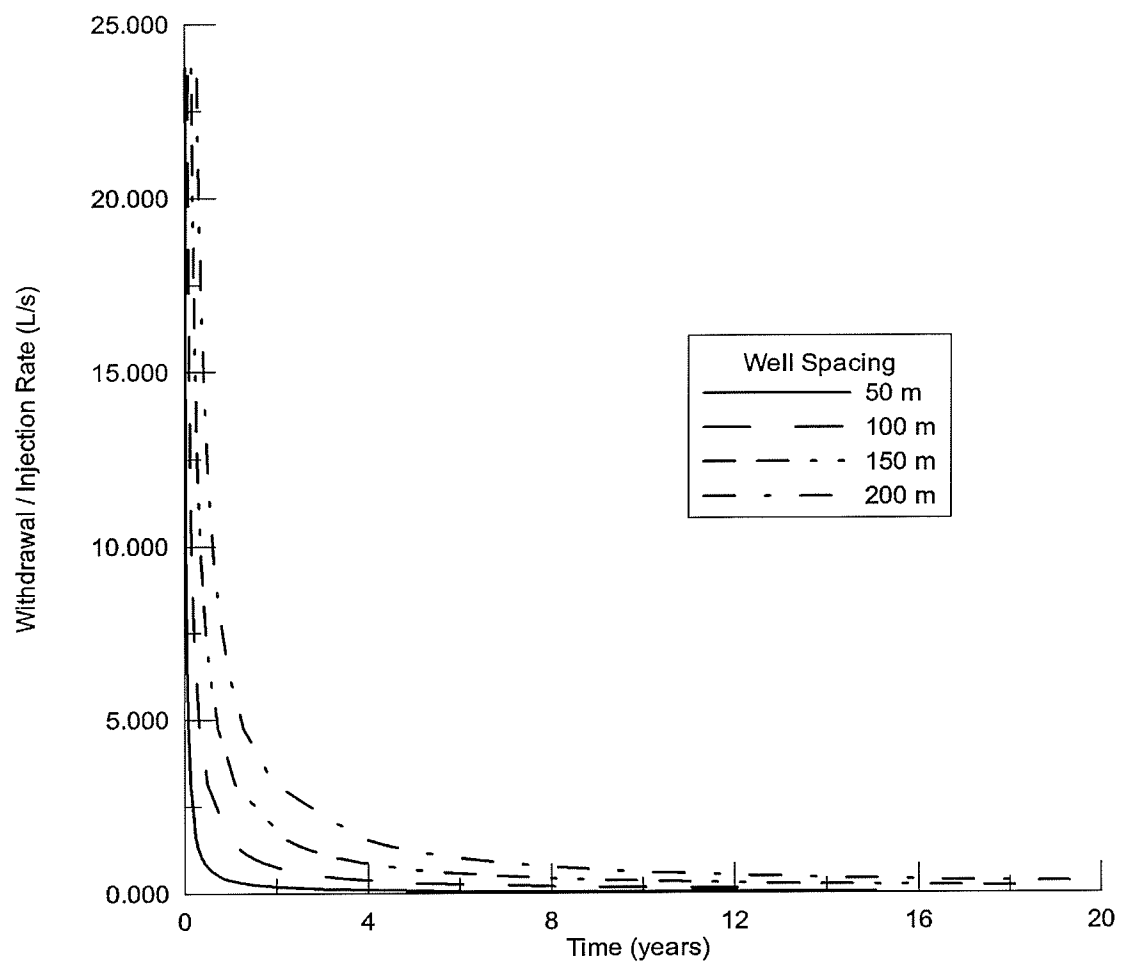
Figure 8.1: Breakthrough times in the Upper Carbonate Aquifer predicted by Gringarten's method (1978) as a function of injection rate, plotted for various well spacings.
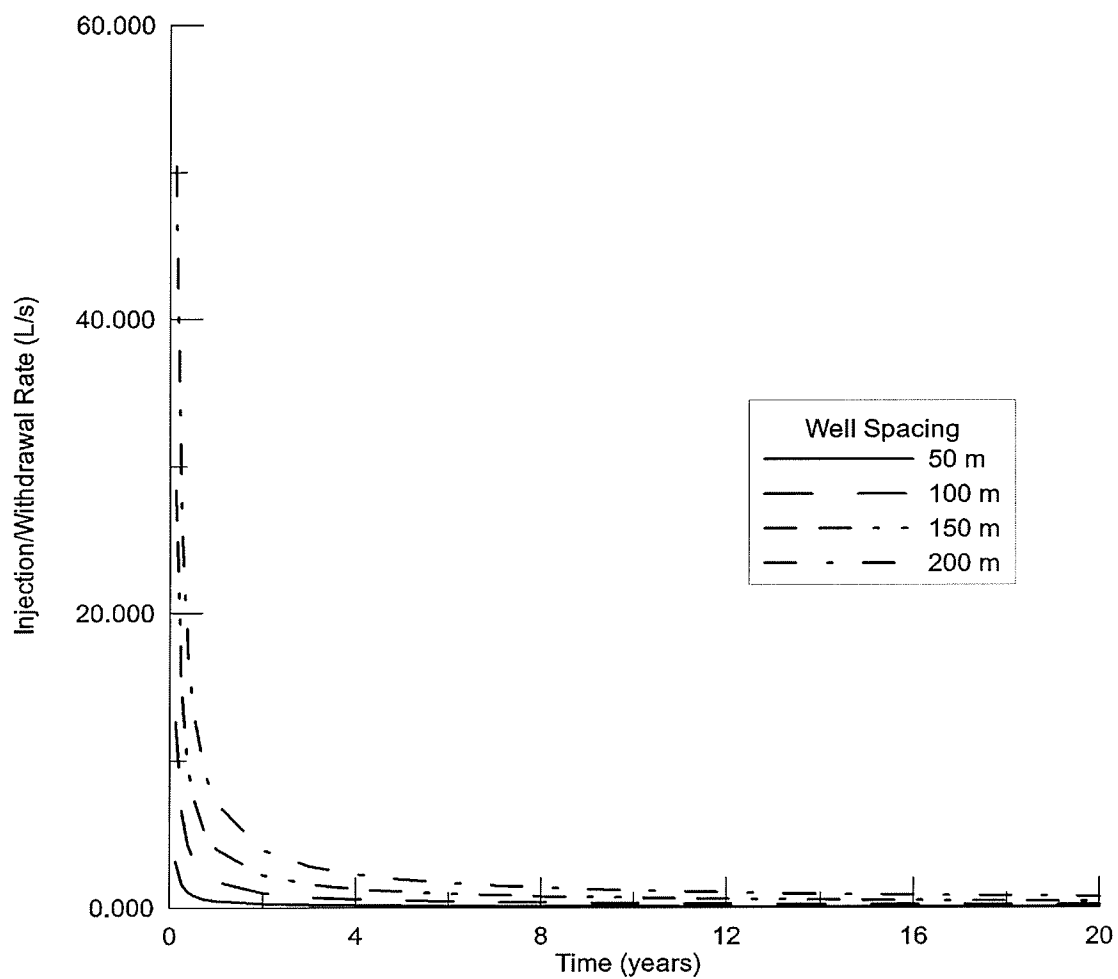
Figure 8.2: Breakthrough times in the Upper Carbonate Aquifer predicted by Gringarten and Sauty's method (1975) as a function of injection rate, plotted for various well spacings.
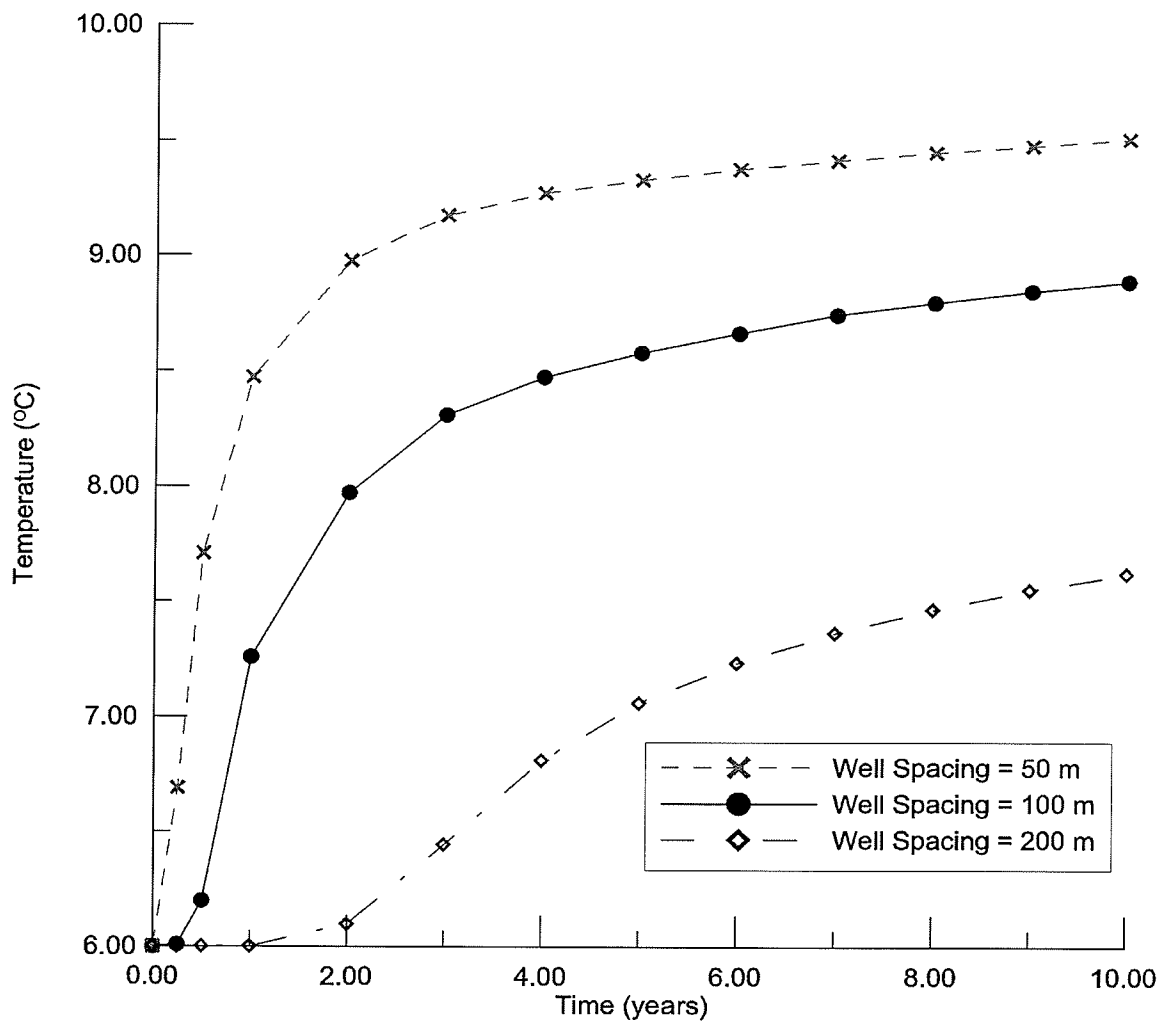
Figure 8.3: Sensitivity of predicted temperatures at the production well to well spacing. The case for 100 metre spacing, shown in black dots, is the base case for all generic porous media models representing the Upper Carbonate Aquifer created in this study.
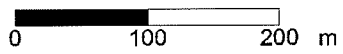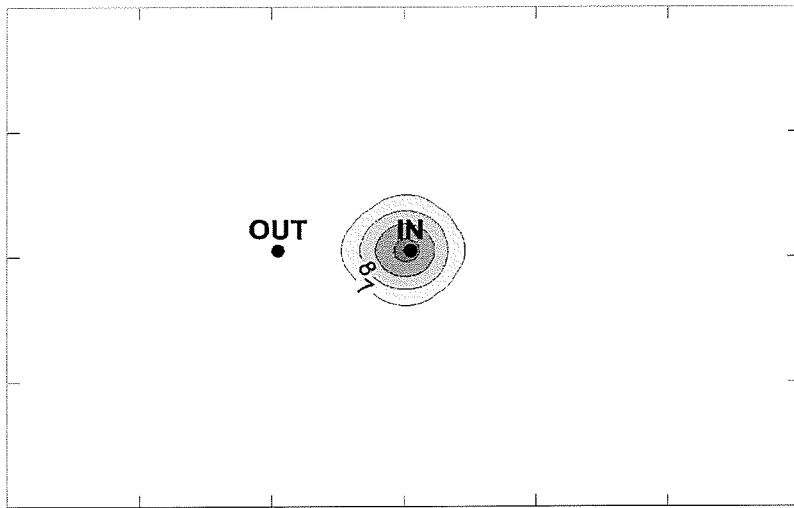
Figure 8.4a: Map of temperatures in the centre of the aquifer for the base case for 0.25 years.
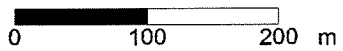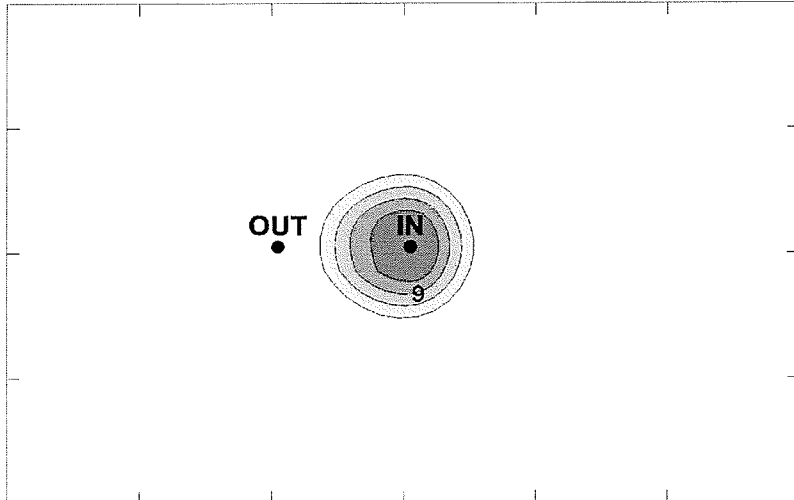
Figure 8.4b: Map of temperatures in the centre of the aquifer for the base case for 0.5 years.
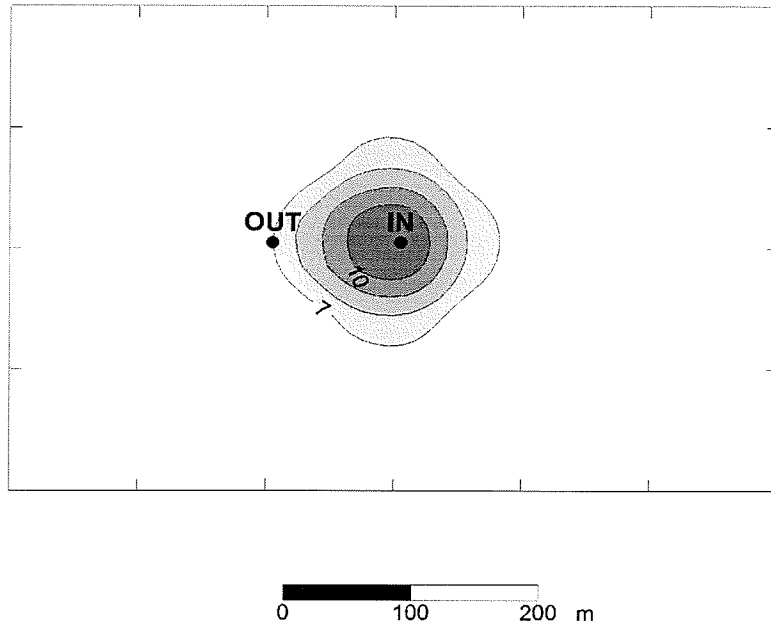
Figure 8.4c: Map of temperatures in the centre of the aquifer for the base case for 1 year.
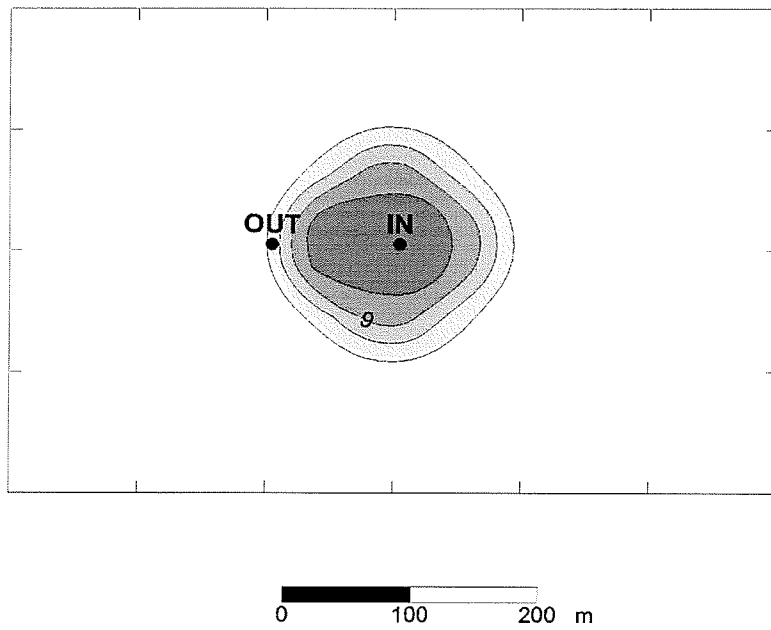
Figure 8.4d: Map of temperatures in the centre of the aquifer for the base case for 2 years.
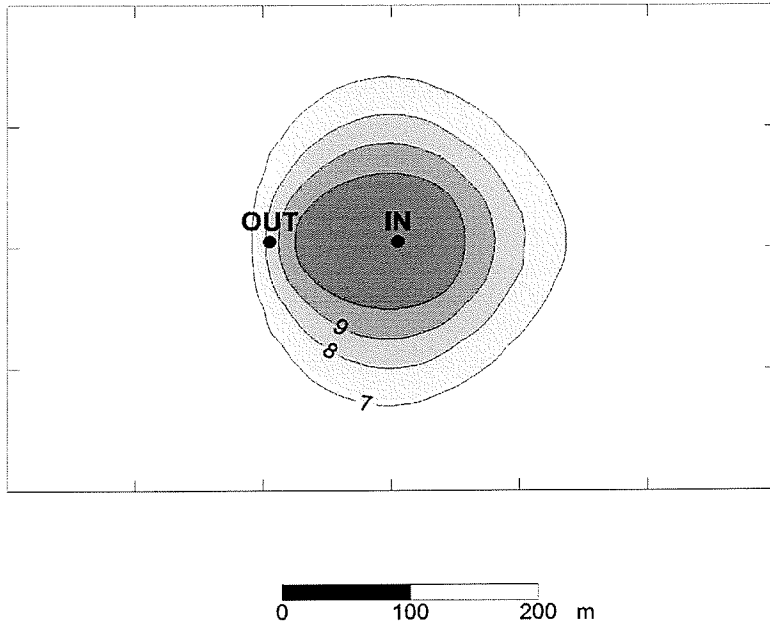
Figure 8.4e: Map of temperatures in the centre of the aquifer for the base case for 5 years.
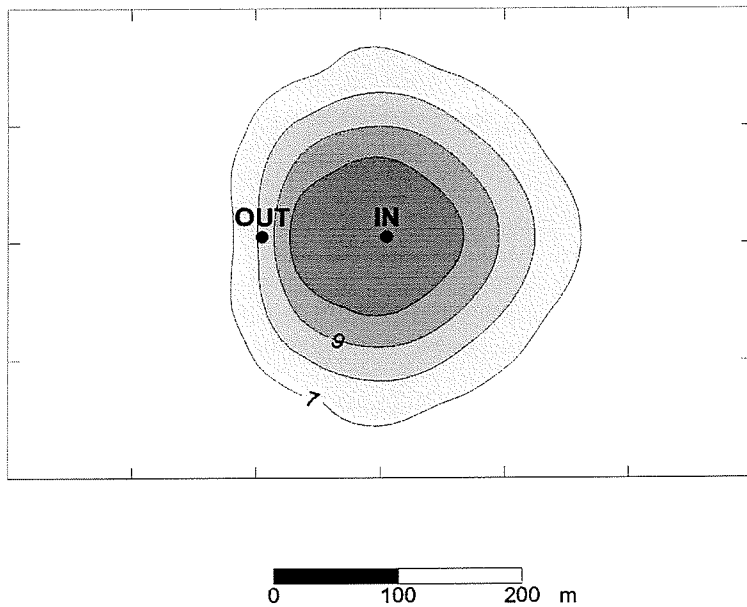
Figure 8.4f: Map of temperatures in the centre of the aquifer for the base case for 10 years
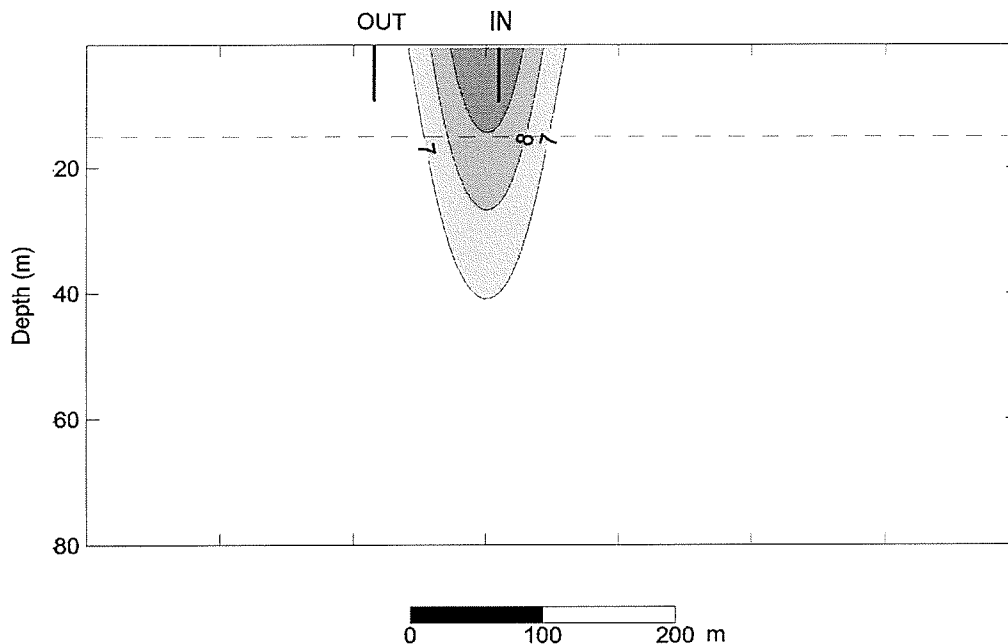
Figure 8.5a: Cross-section of temperature field of generic doublet in porous media for the base model after 0.25 years. Dashed line indicates interface between the upper aquifer and the lower less permeable unit and depth is given in metres below the top of the aquifer.
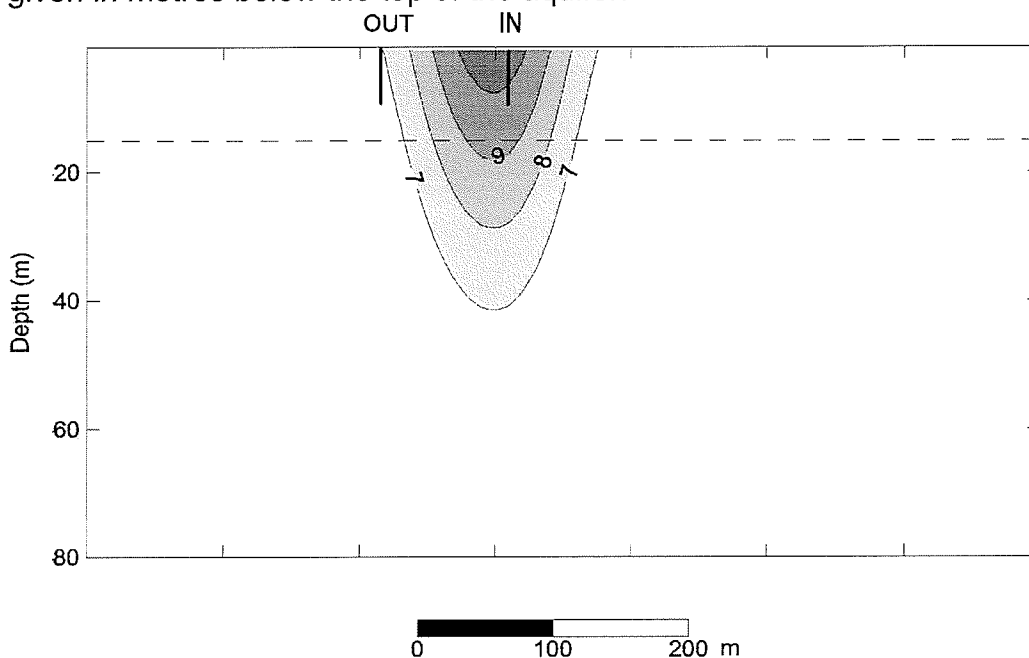
Figure 8.5b: Cross-section of temperature field of generic doublet in porous media for the base model after 0.5 years. Dashed line indicates interface between the upper aquifer and the lower less permeable unit and depth is given in metres below the top of the aquifer.
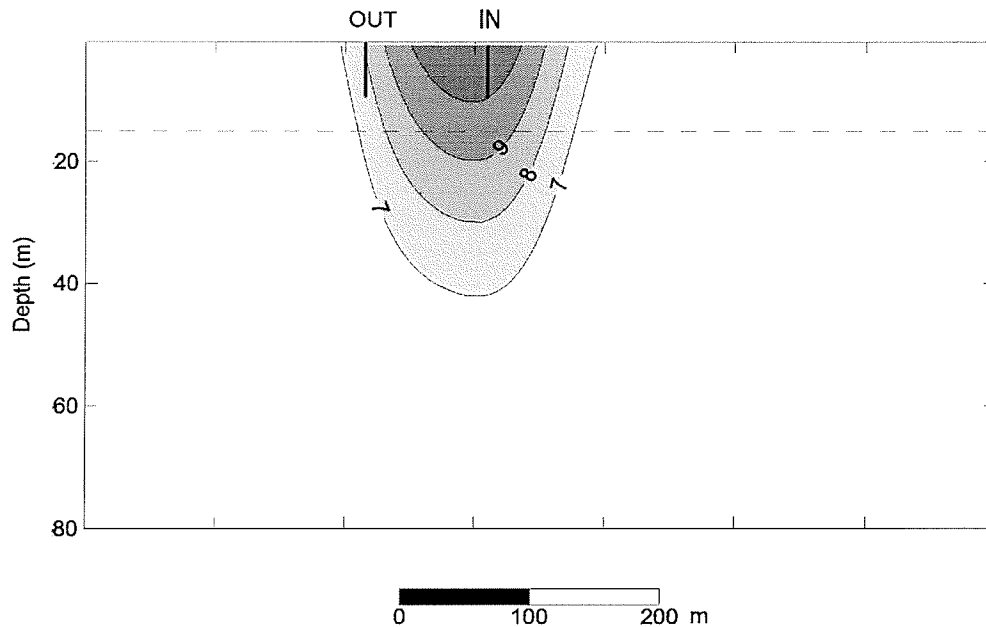
Figure 8.5c: Cross-section of temperature field of generic doublet in porous media for the base model after 1.0 years. Dashed line indicates interface between the upper aquifer and the lower less permeable unit and depth is given in metres below the top of the aquifer.
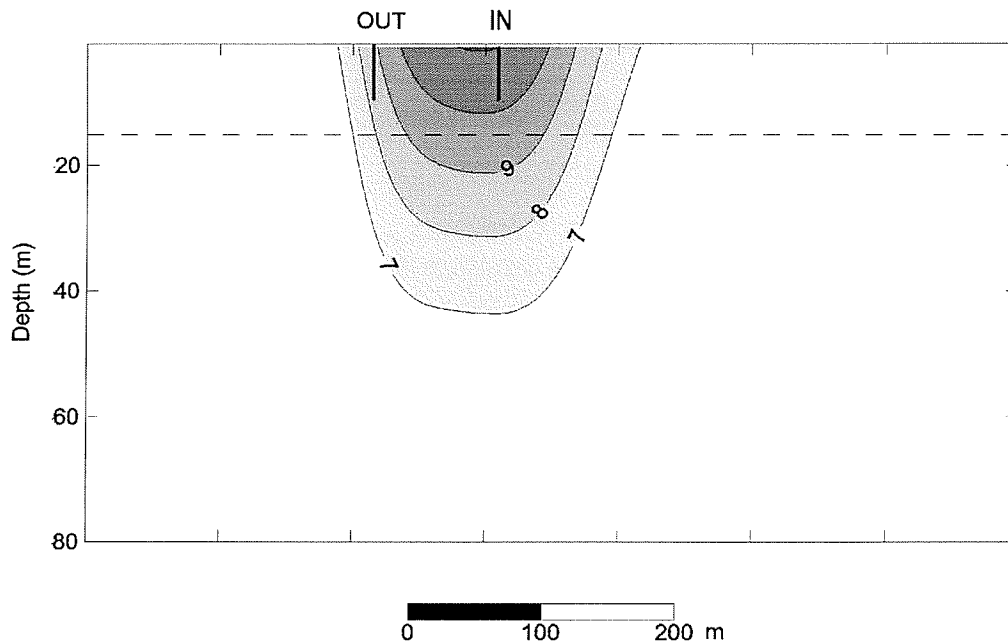
Figure 8.5d: Cross-section of temperature field of generic doublet in porous media for the base model after 2.0 years. Dashed line indicates interface between the upper aquifer and the lower less permeable unit and depth is given in metres below the top of the aquifer.
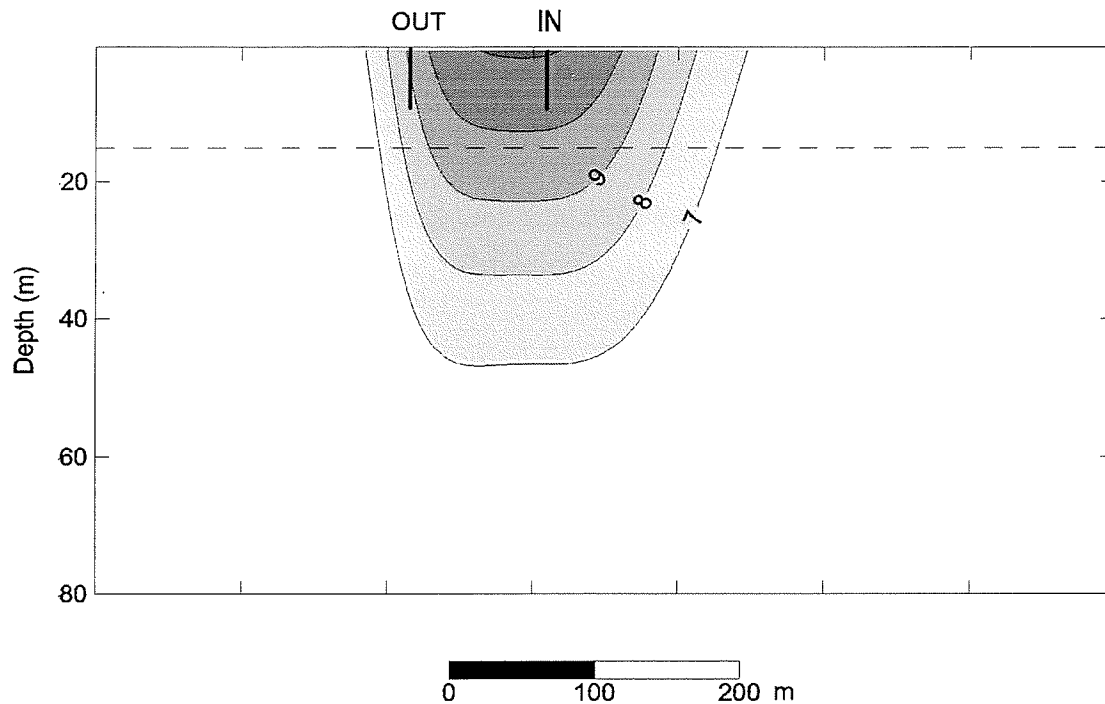
Figure 8.5e: Cross-section of temperature field of generic doublet in porous media for the base model after 5.0 years. Dashed line indicates interface between the upper aquifer and the lower less permeable unit and depth is given in metres below the top of the aquifer.
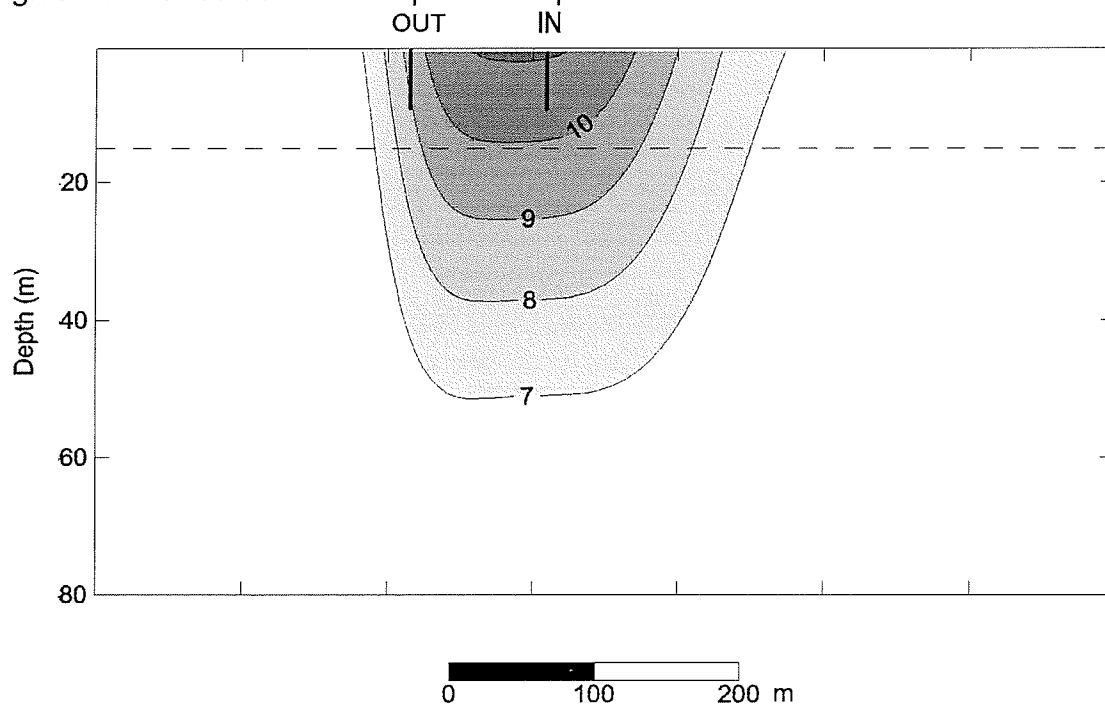
Figure 8.5f: Cross-section of temperature field of generic doublet in porous media for the base model after 10.0 years. Dashed line indicates interface between the upper aquifer and the lower less permeable unit and depth is given in metres below the top of the aquifer.
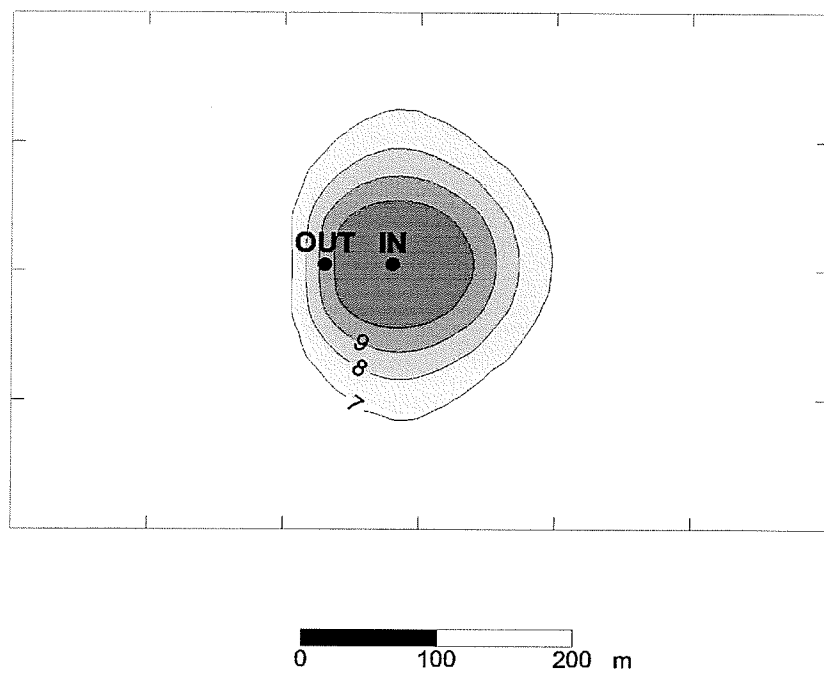
Figure 8.6a: Spatial distribution of temperatures in the generic aquifer after 5 years of production and injection for wells spaced at 200 metres.
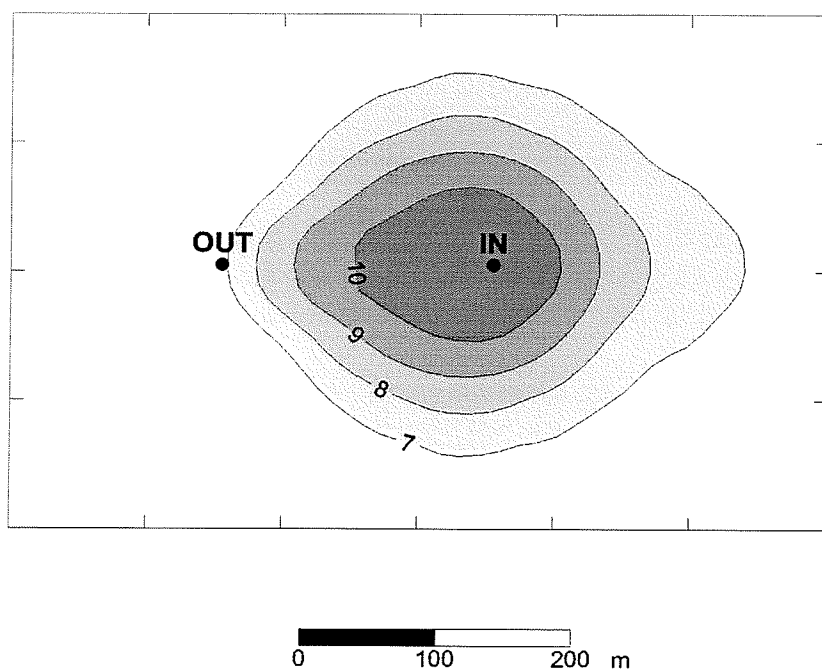
Figure 8.6b: Spatial distribution of temperatures in the generic aquifer after 5 years of production and injection for wells spaced at 200 metres.
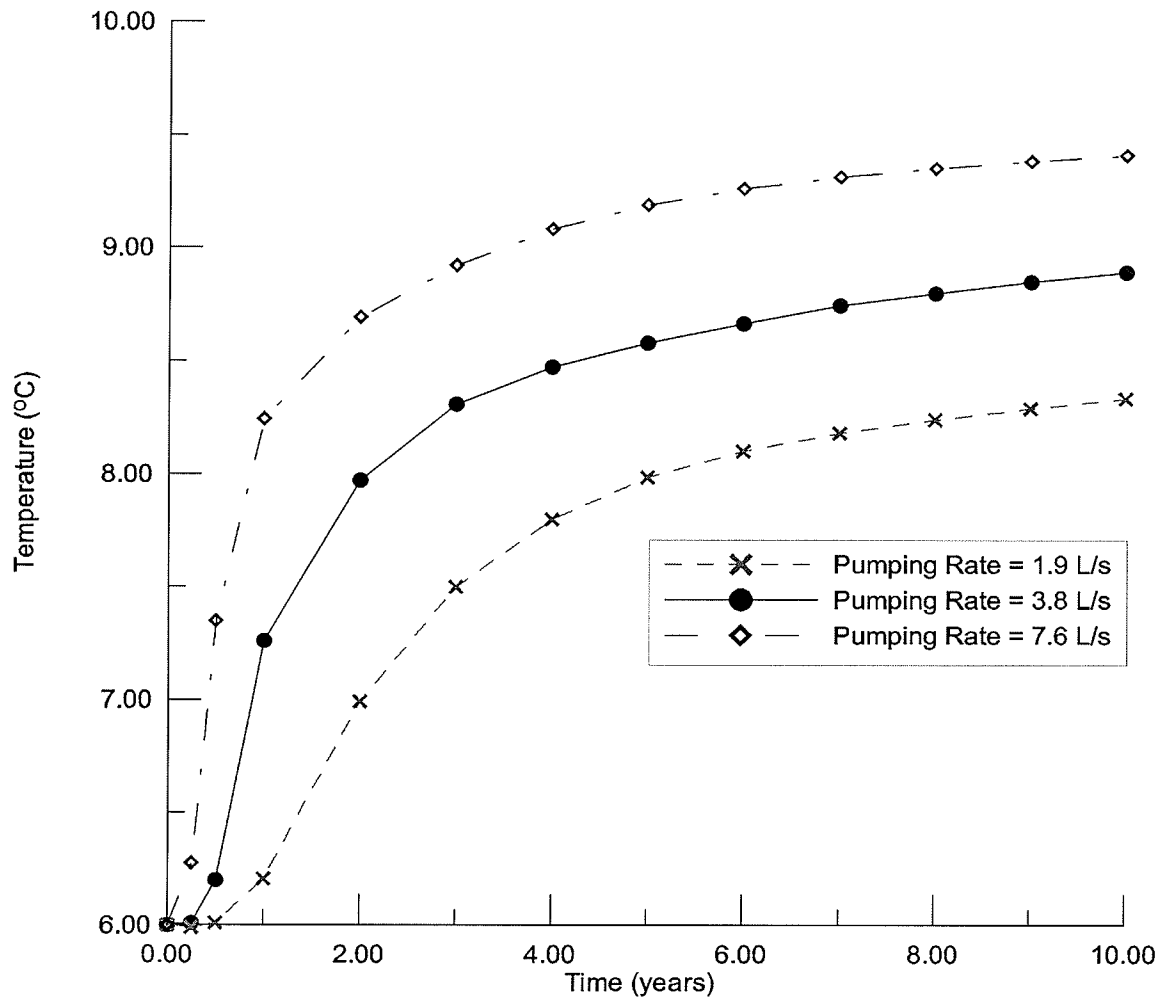
Figure 8.7: Sensitivity of predicted temperatures at the production well for a geological situation typical of the Winnipeg area to pumping rate.
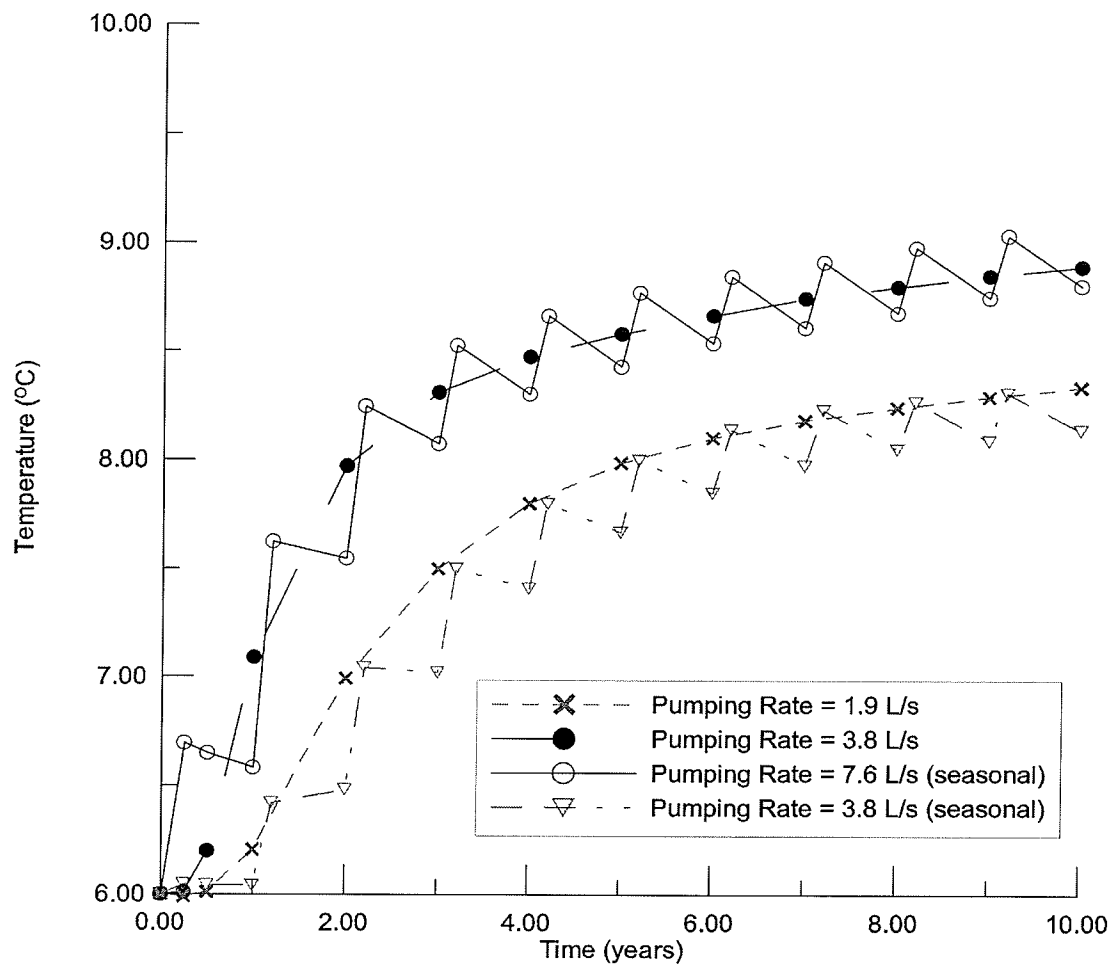
Figure 8.8: Effect of pumping only during the summer. Seasonal pumping rates shown are based on a all production and injection occurring during a three month period.
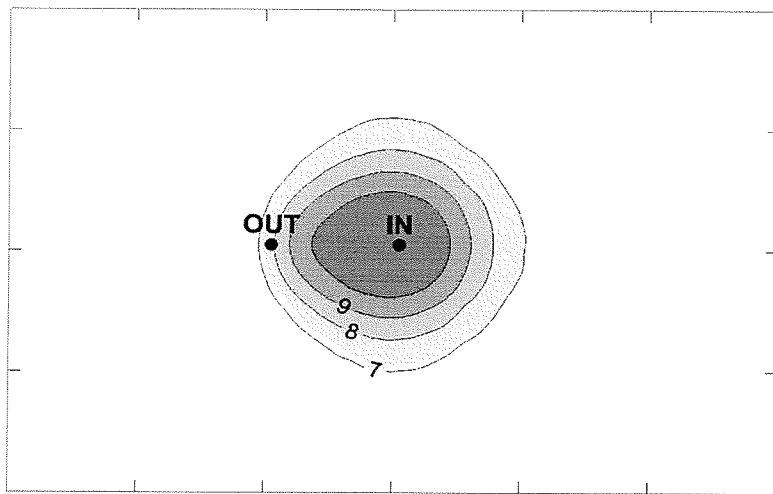
Figure 8.9a: Spatial distribution of temperatures in the generic aquifer after 5 years of production and injection at a rate of 1.9 L/s.
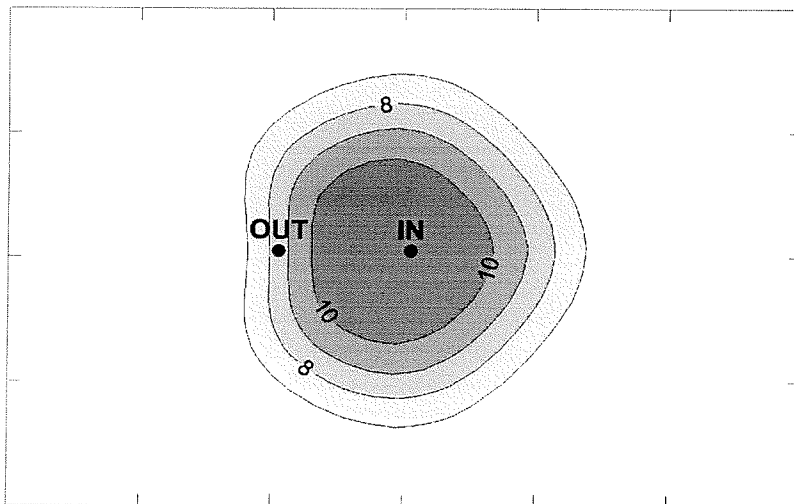
Figure 8.9b: Spatial distribution of temperatures in the generic aquifer after 5 years of production and injection at a rate of 7.6 L/s.
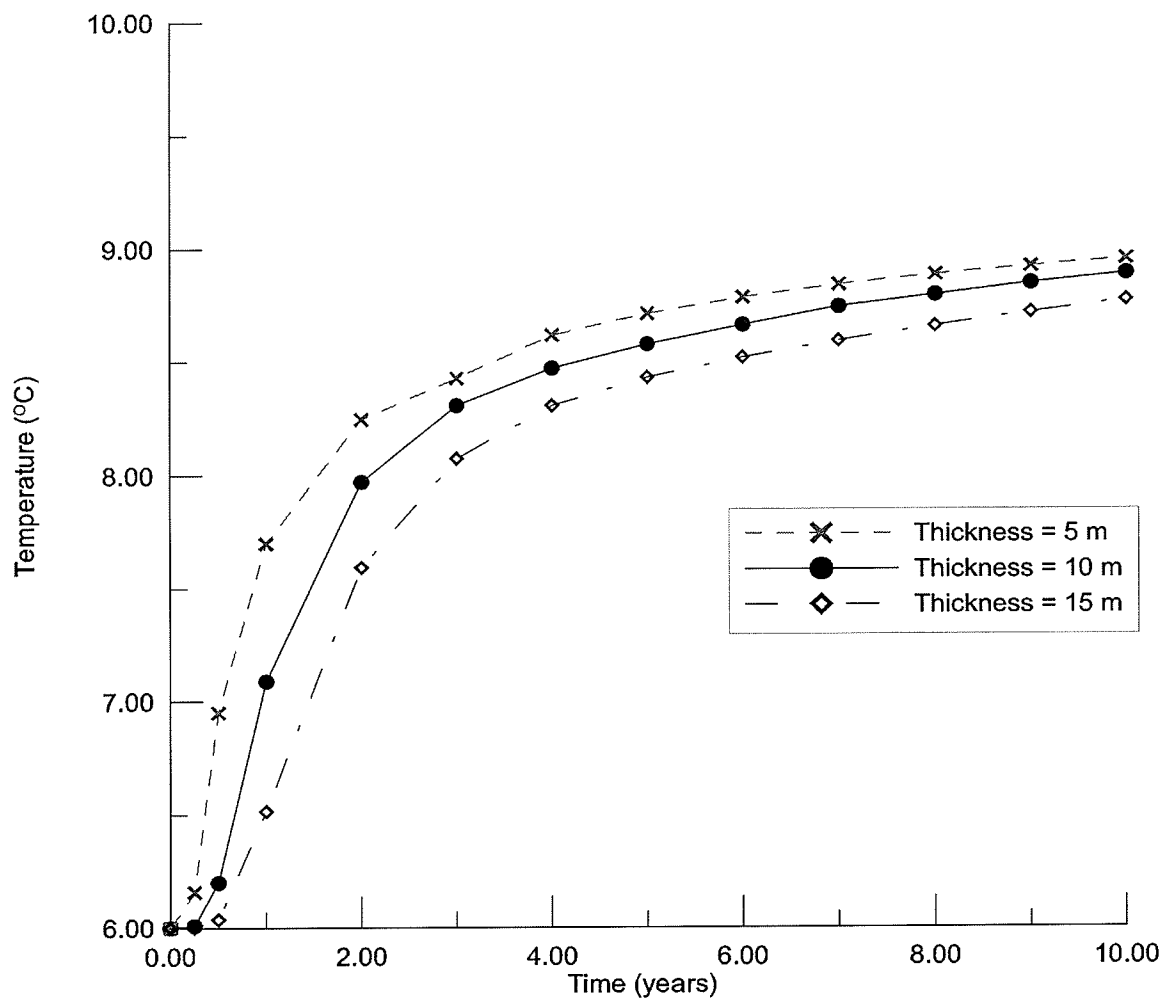
Figure 8.10: Sensitivity of predicted temperatures at the production well for a geological situation typical of the Winnipeg area to variations in aquifer thickness.
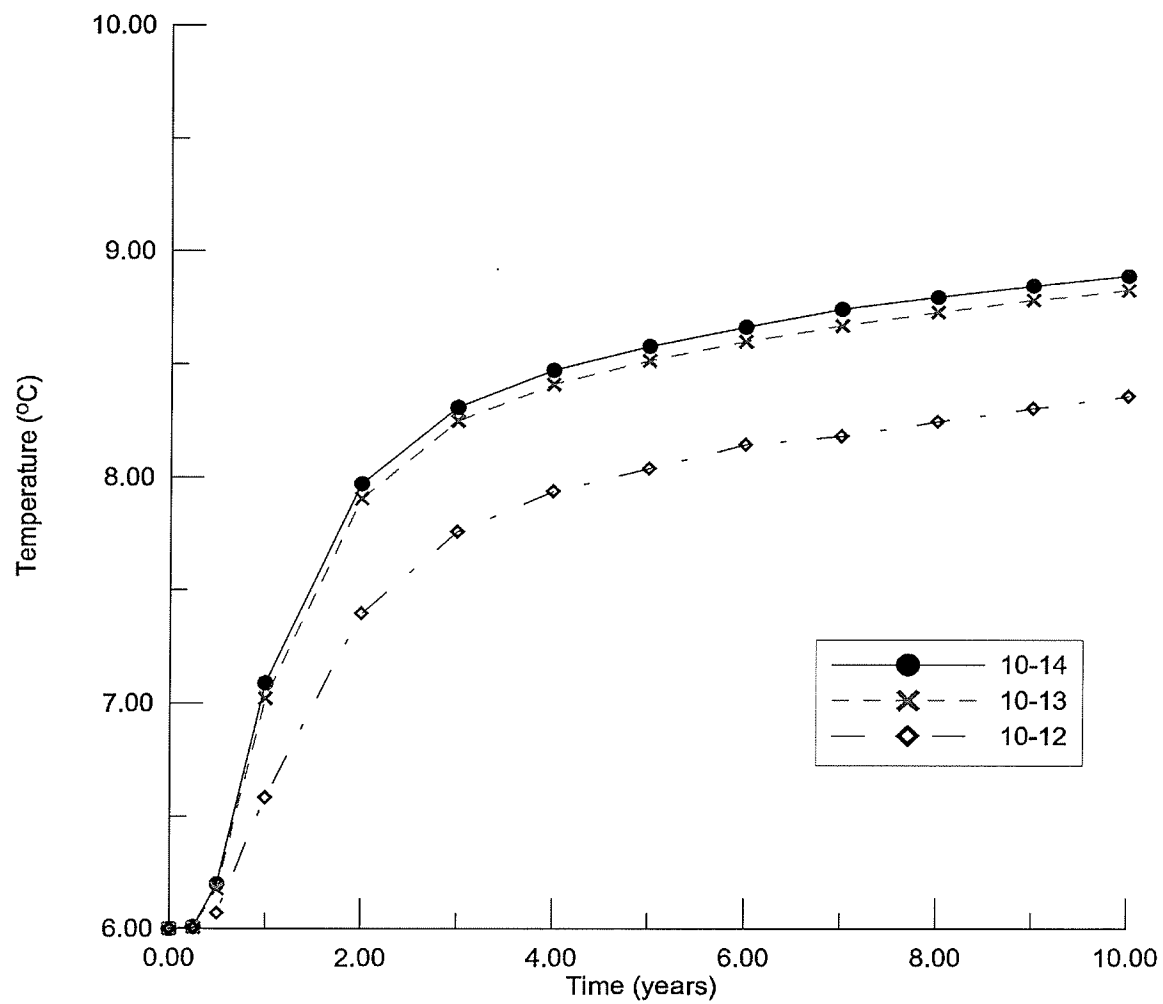
Figure 8.11: Sensitivity of predicted temperatures at the production well to variation in the permeability of the carbonate rock underlying the aquifer. Units of permeability are m^2.
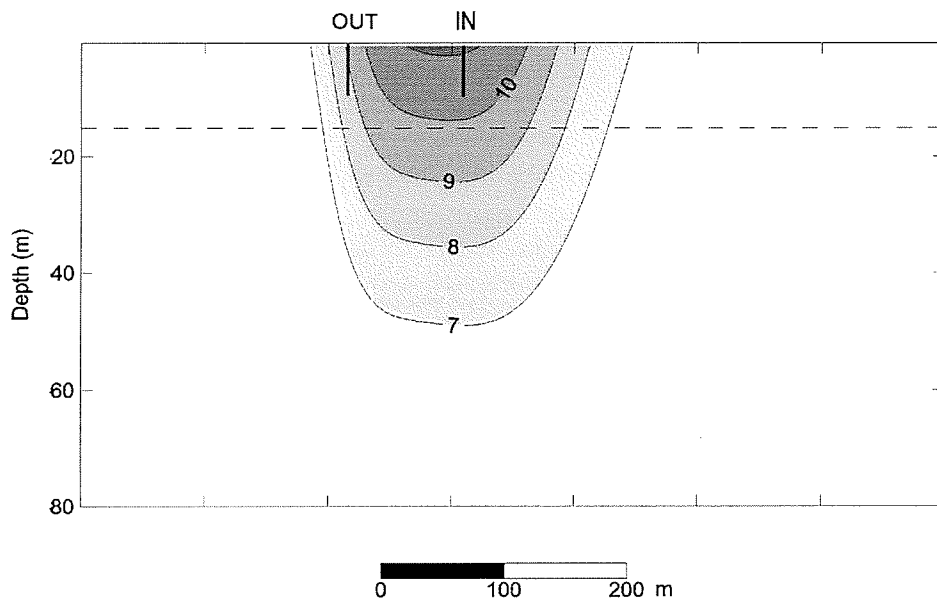
Figure 8.12a: Cross-section of temperature field of generic doublet in porous media after 5 years of production and injection with the permeability of the underlying aquifer decreased to 10^{-12} m^2. Dashed line indicates interface between the upper aquifer and the lower less peremeable unit.
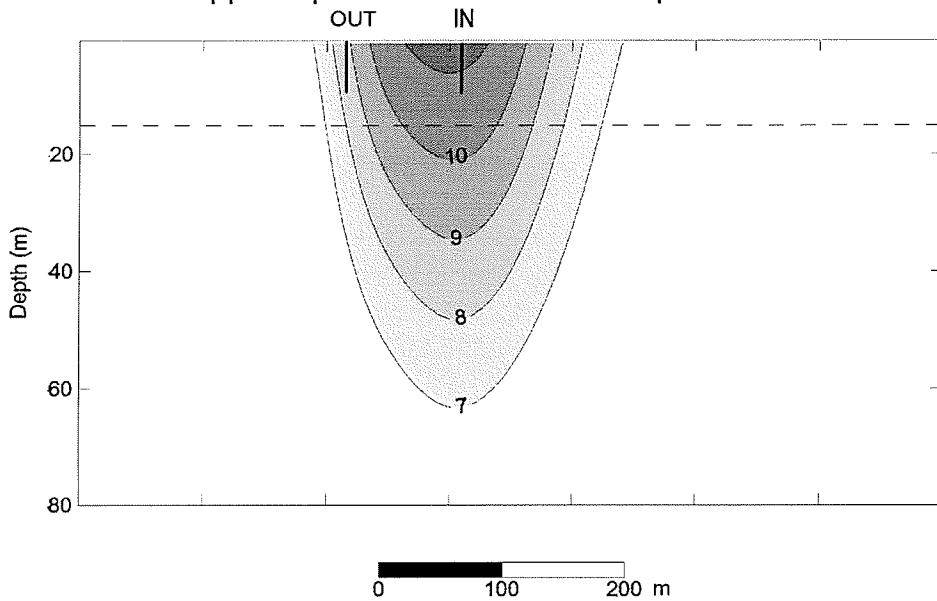
Figure 8.12b: Cross-section of temperature field of generic doublet in porous media after 5 years of production and injection with the permeability of the underlying aquifer increased to 10^{-11} m^2. Dashed line indicates interface between the upper aquifer and the lower less peremeable unit.
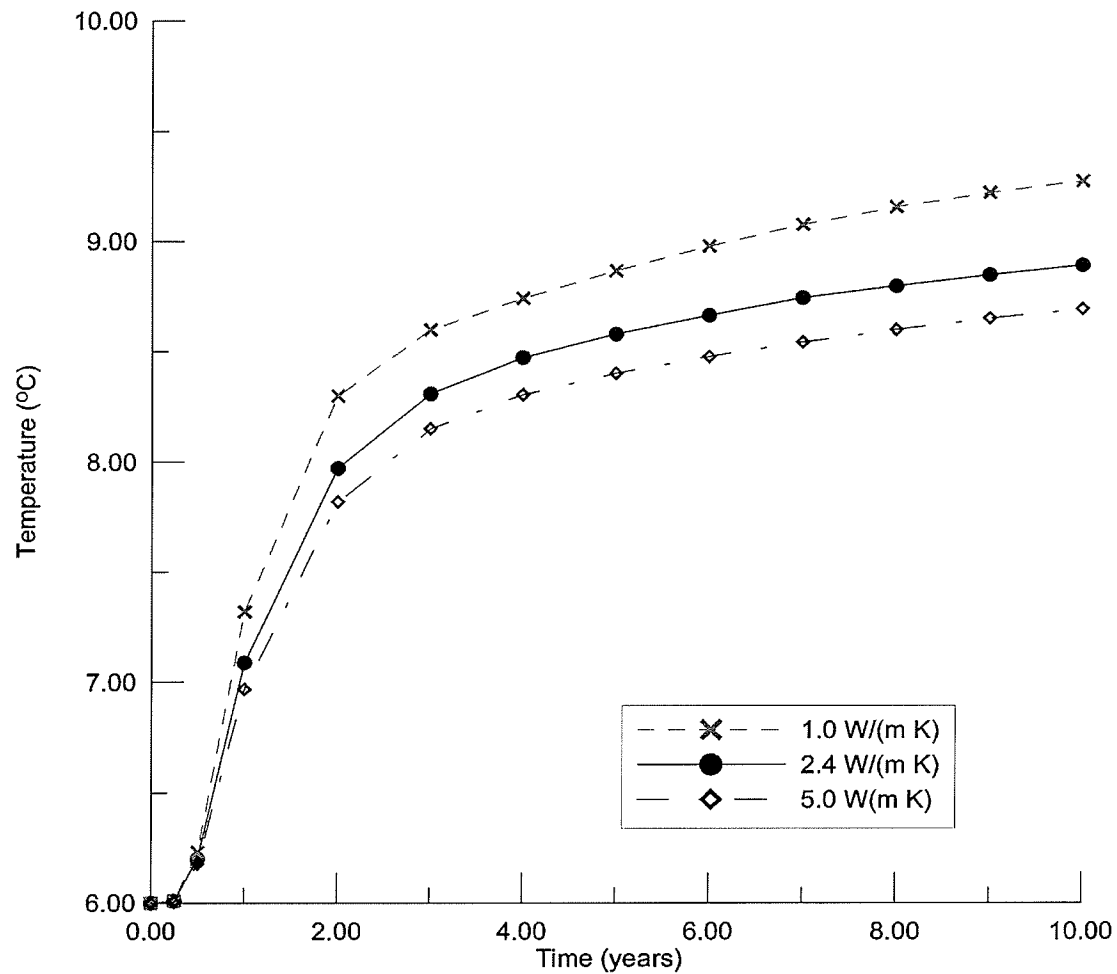
Figure 8.13: Sensitivity of predicted temperatures at the production well for a geological situation typical of the Winnipeg area to the thermal conductivity of the aquifer and underlying carbonate rock.
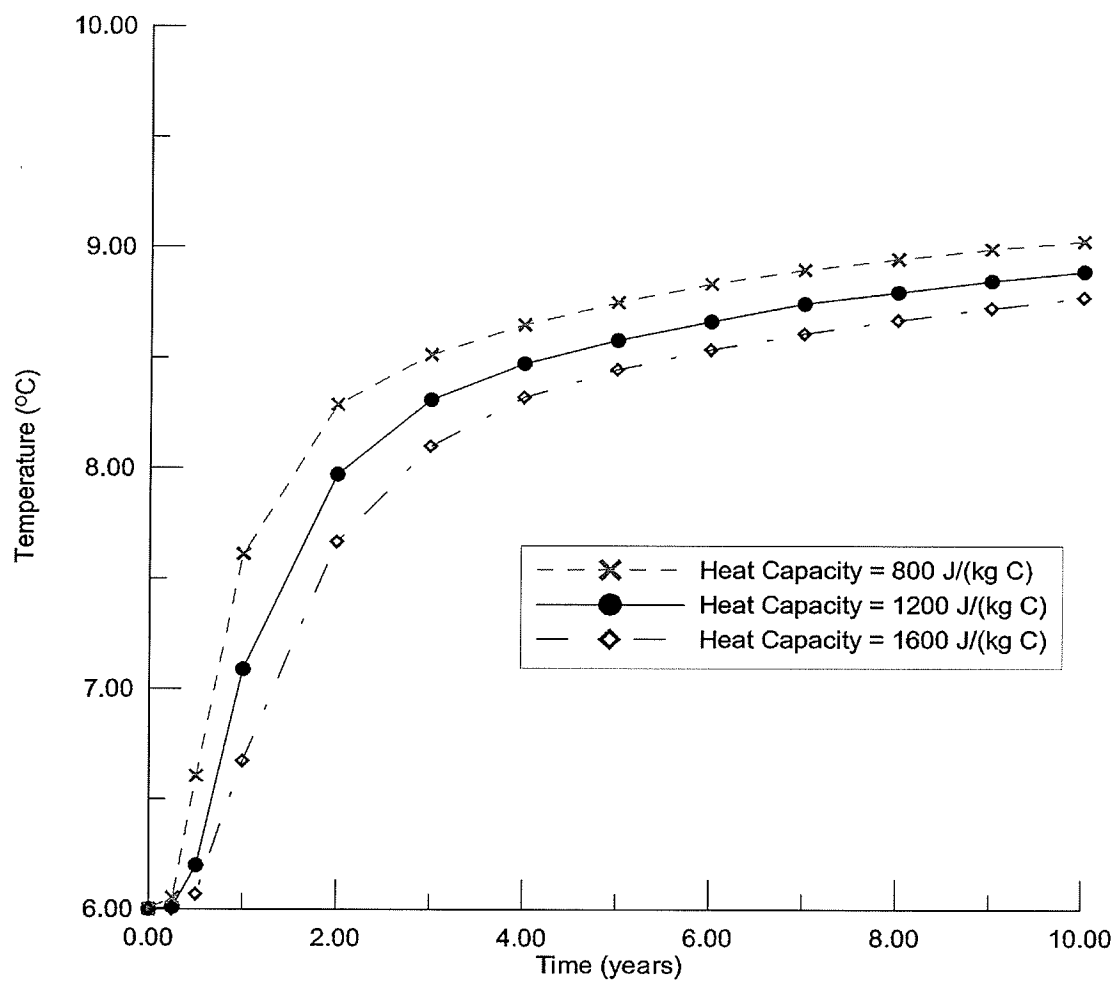
Figure 8.14: Sensitivity of predicted temperatures at the production well for a geological situation typical of the Winnipeg area to the specific heat capacity of the aquifer and underlying carbonate rock.
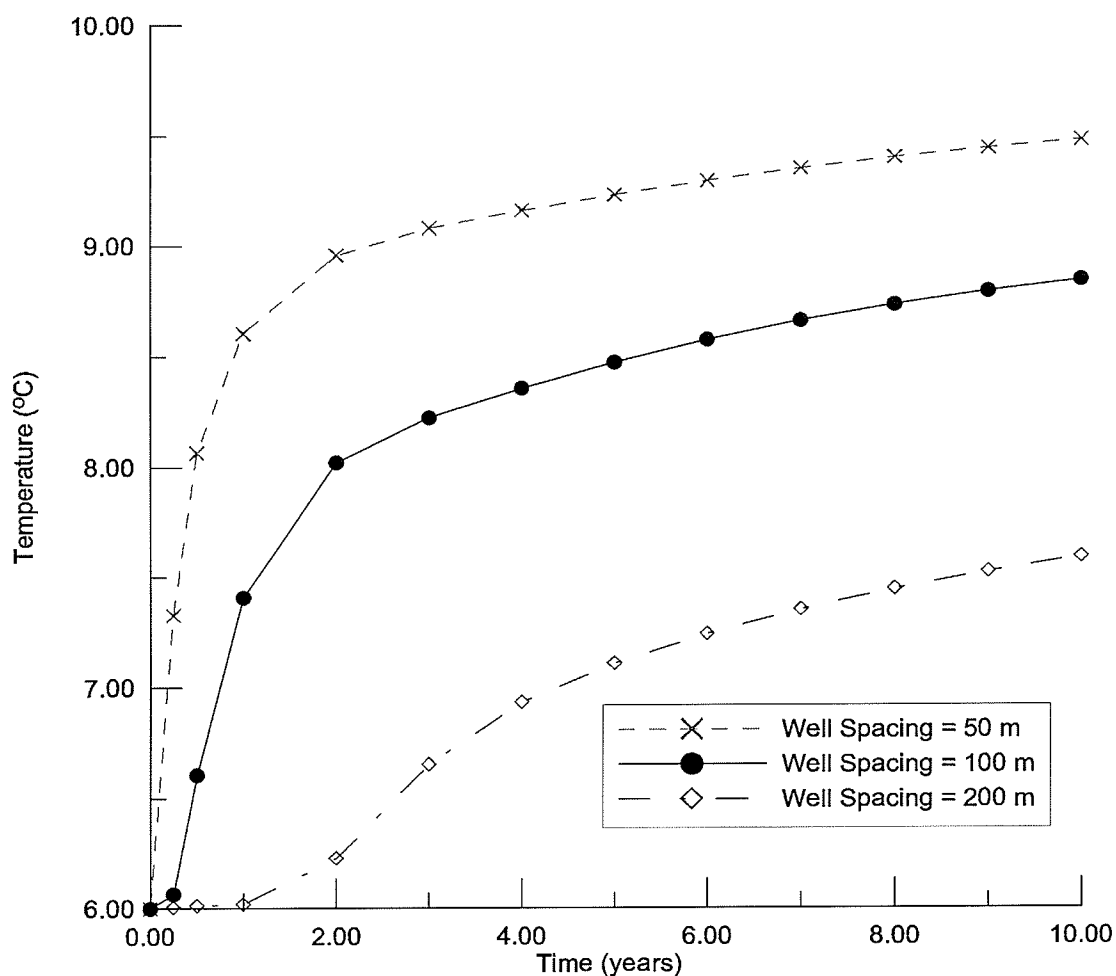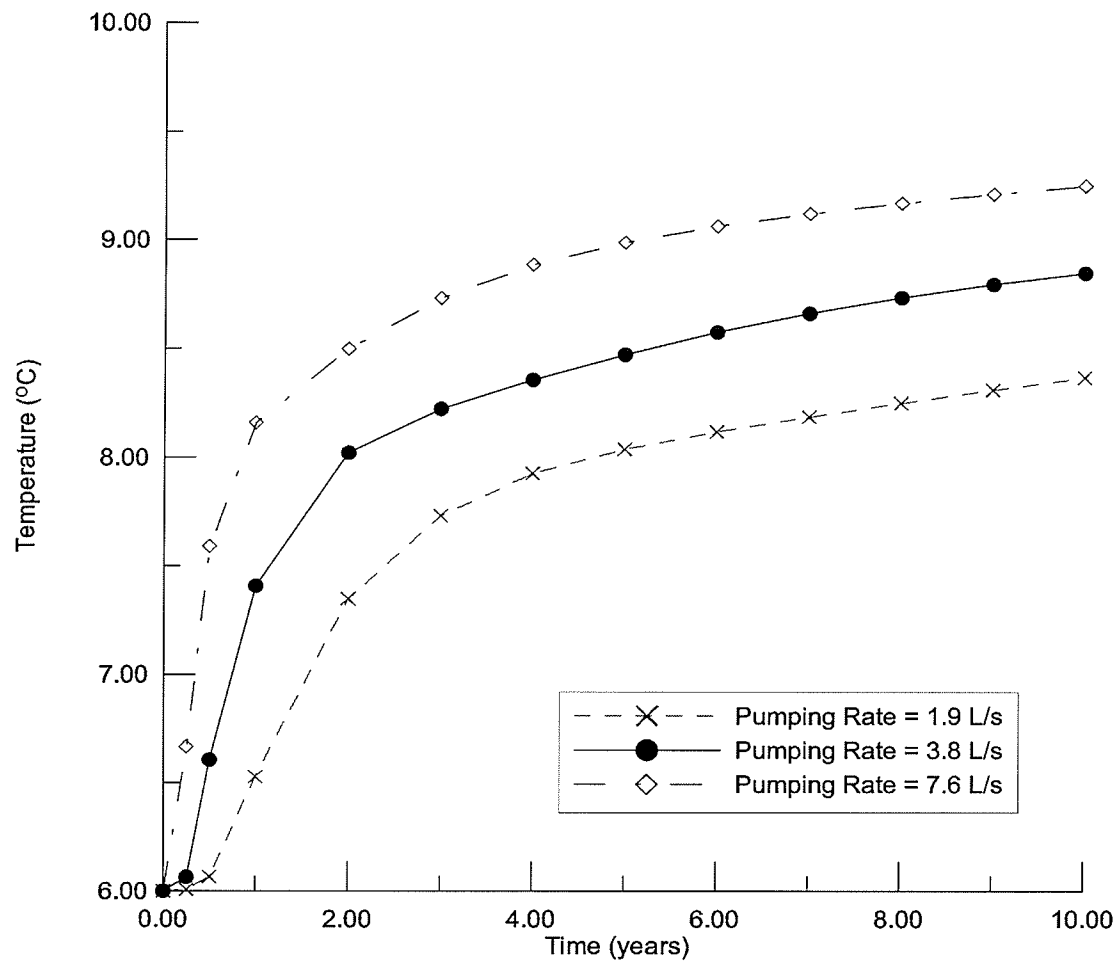
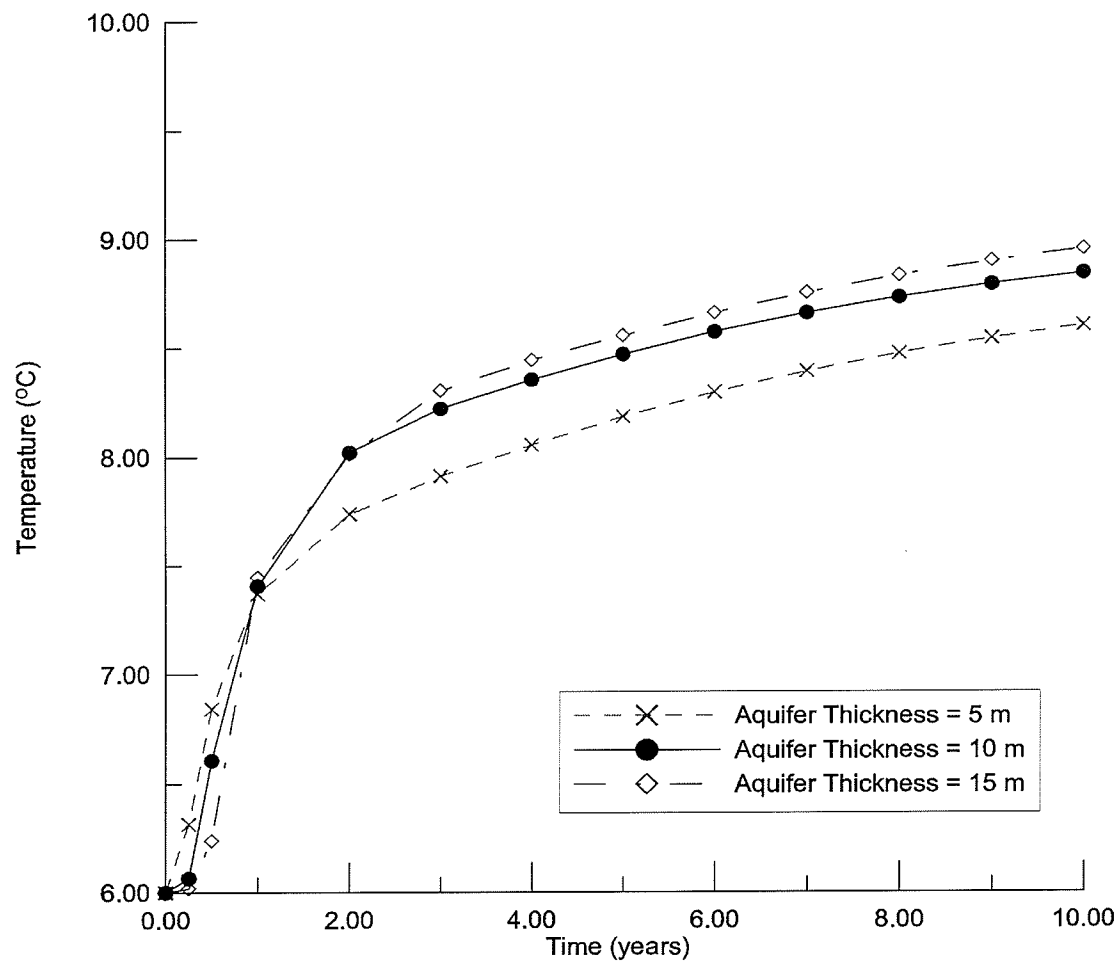Figure 8.15: Sensitivity of predicted temperatures at the production well to changes in well spacing for the generic models created using a dual continuum formulation. The case with the well spacing of 100 metres, shown in black dots, is the base case for all generic dual continuum models conducted in this study.
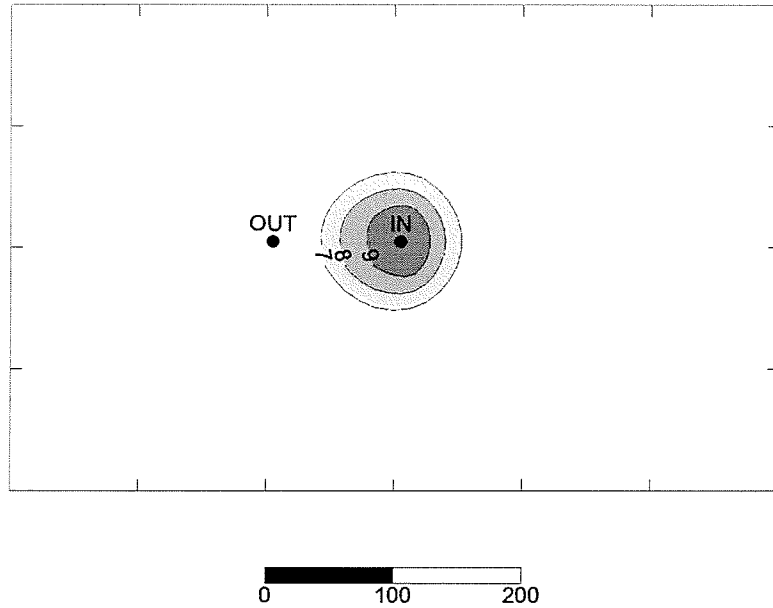
Figure 8.16a: Map of temperatures in the centre of the aquifer for the base case the dual continuum model for 0.25 years. Contours are in °C and scale bar is in metres.
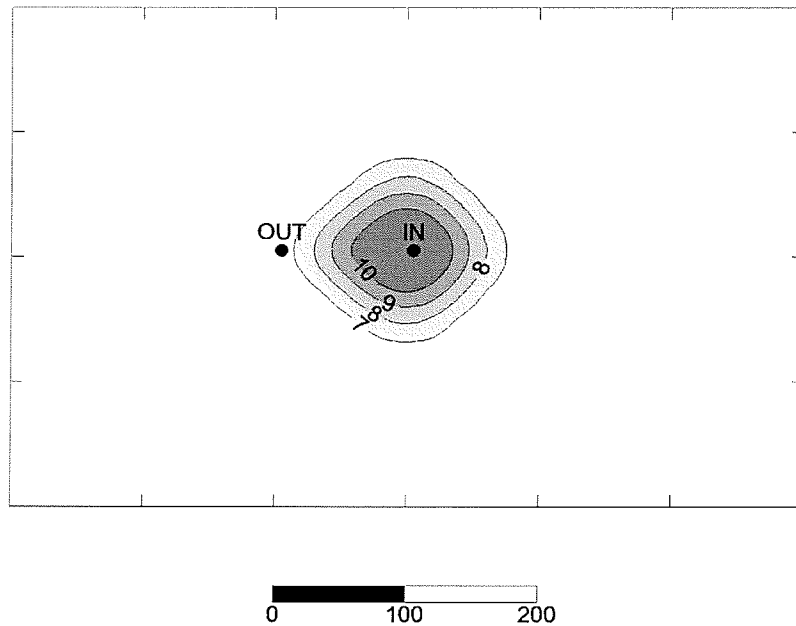
Figure 8.16b: Map of temperatures in the centre of the aquifer for the base case the dual continuum model for 0.5 years. Contours are in °C and scale bar is in metres.
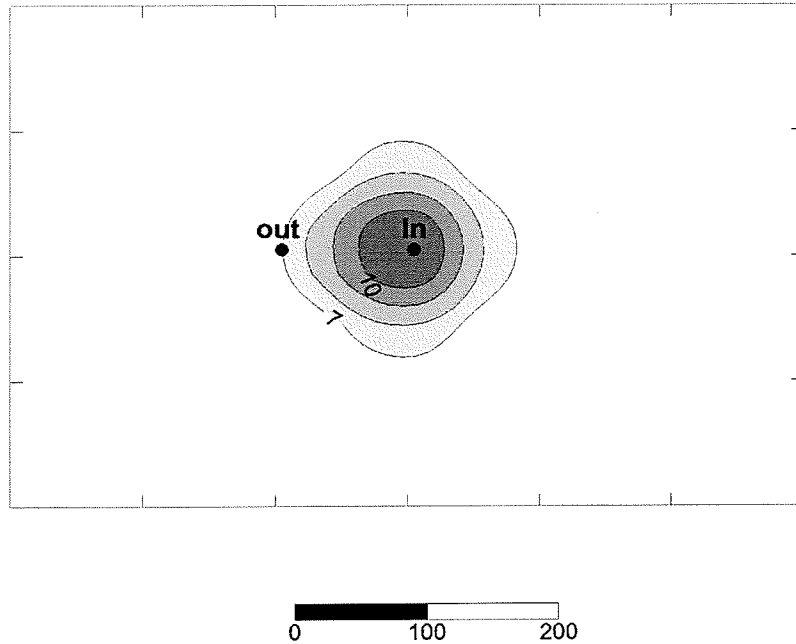
Figure 8.16c: Map of temperatures in the centre of the aquifer for the base case the dual continuum model for1 year. Contours are in °C and scale bar is in metres.
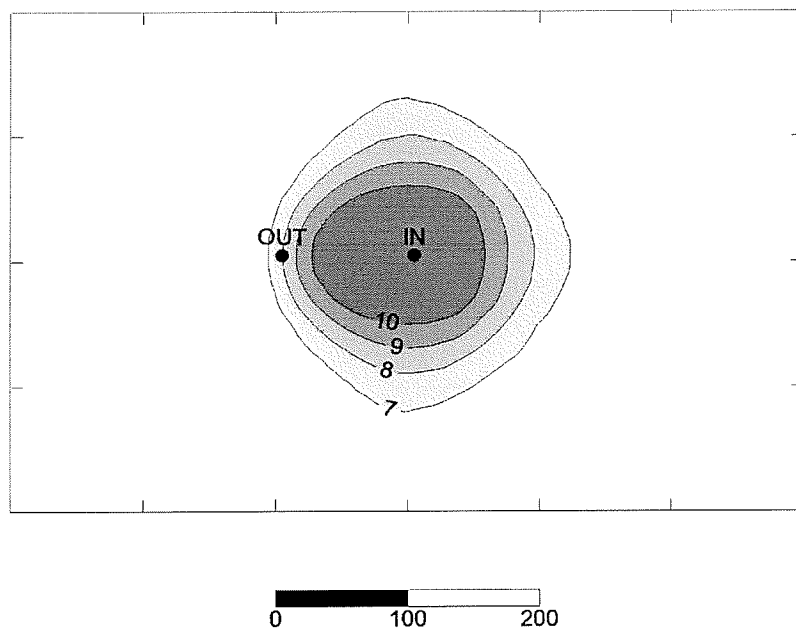
Figure 8.16d: Map of temperatures in the centre of the aquifer for the base case the dual continuum model for 2 years. Contours are in °C and scale bar is in metres.

207
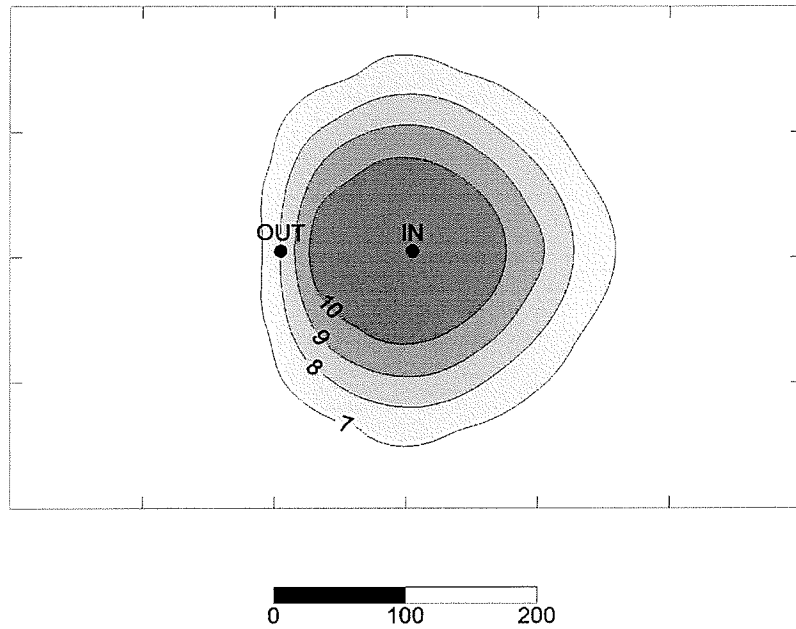
Figure 8.16e: Map of temperatures in the centre of the aquifer for the base case the dual continuum model for 5 years. Contours are in °C and scale bar is in metres.

Figure 8.17: Sensitivity of predicted temperatures at the production well to changes in pumping rate for the generic model hydrogeologic model created using a dual continuum formulation.

Figure 8.18: Effect of aquifer thickness on predicted temperatures at the production well for the generic models created using a dual continuum formulation.
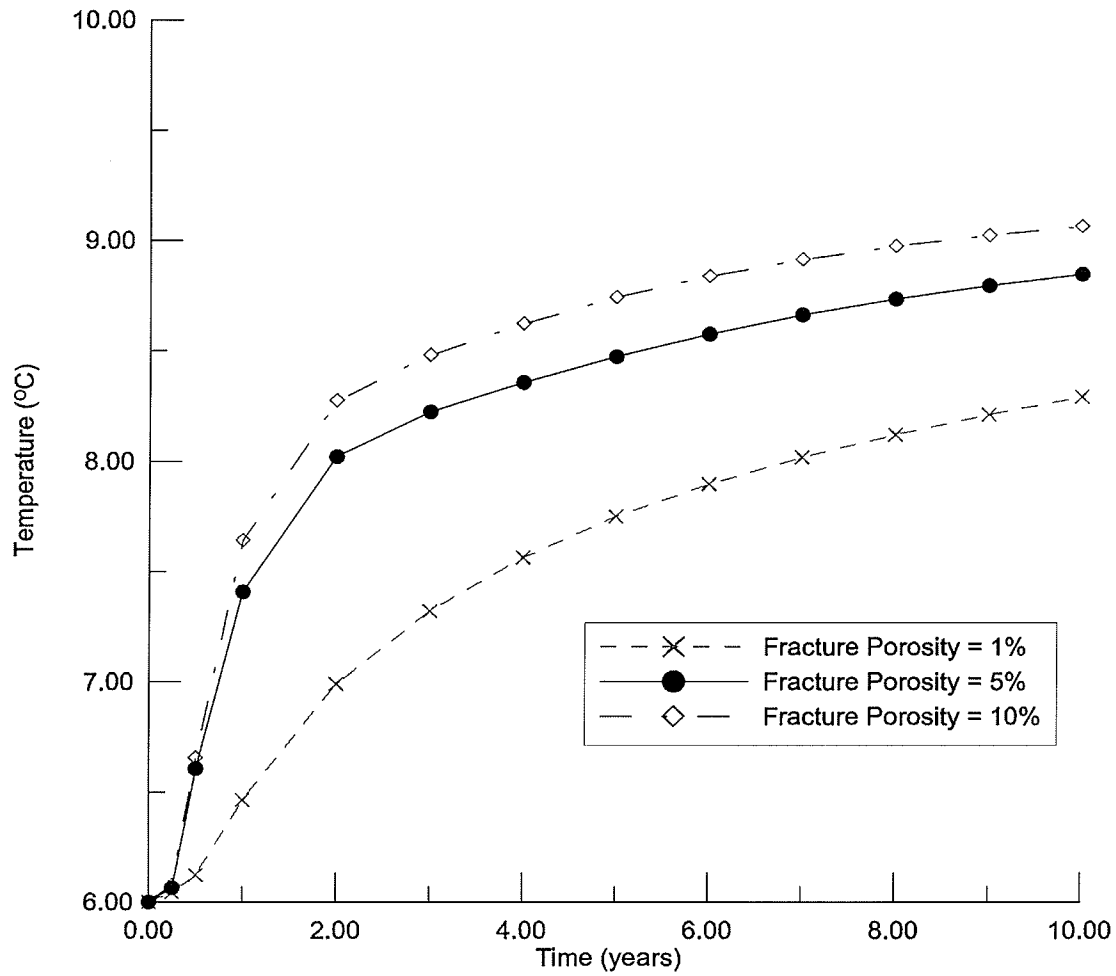
Figure 8.19: Effect of fracture porosity in the aquifer on predicted temperatures at the production well in the generic dual continuum models created in this study.
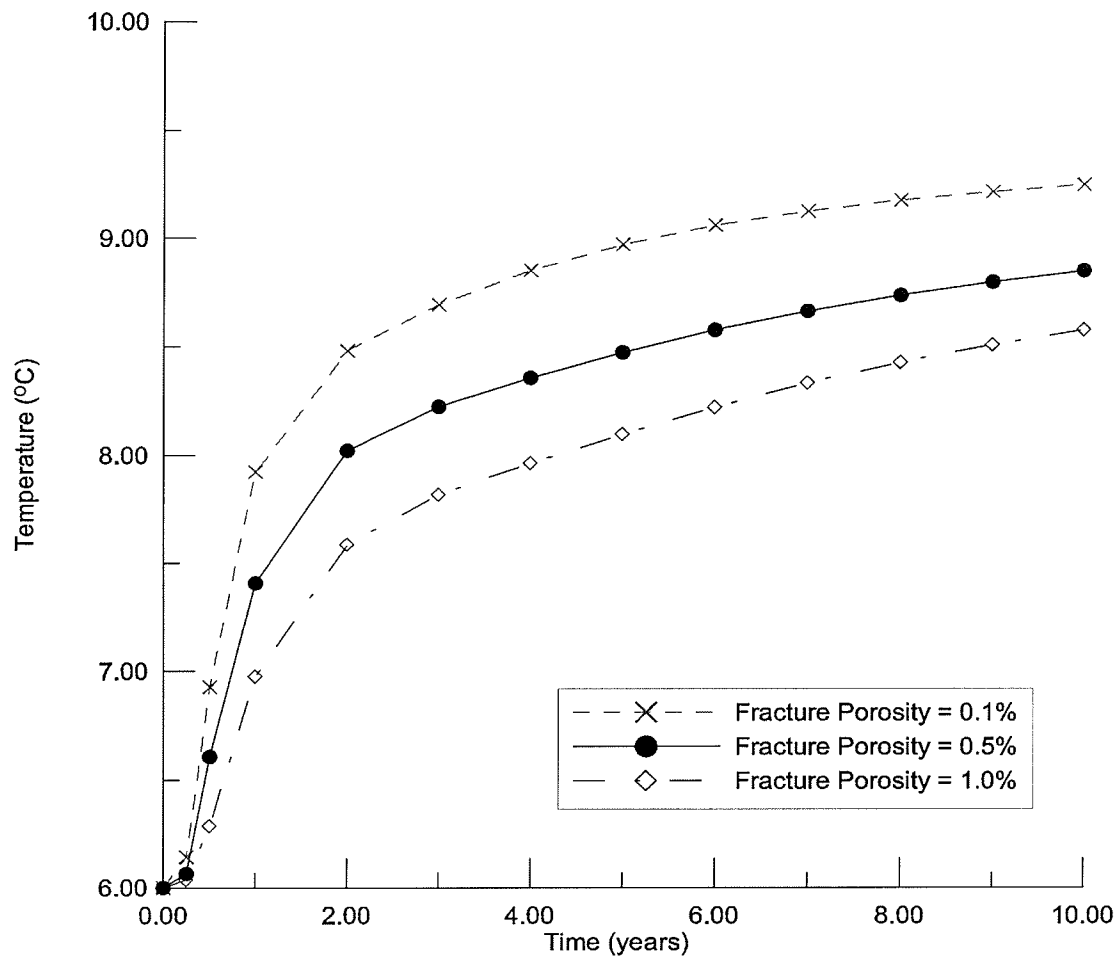
Figure 8.20: Effect of fracture porosity in the rock underlying the aquifer on predicted temperatures at the production well in the generic dual continuum models created in this study.
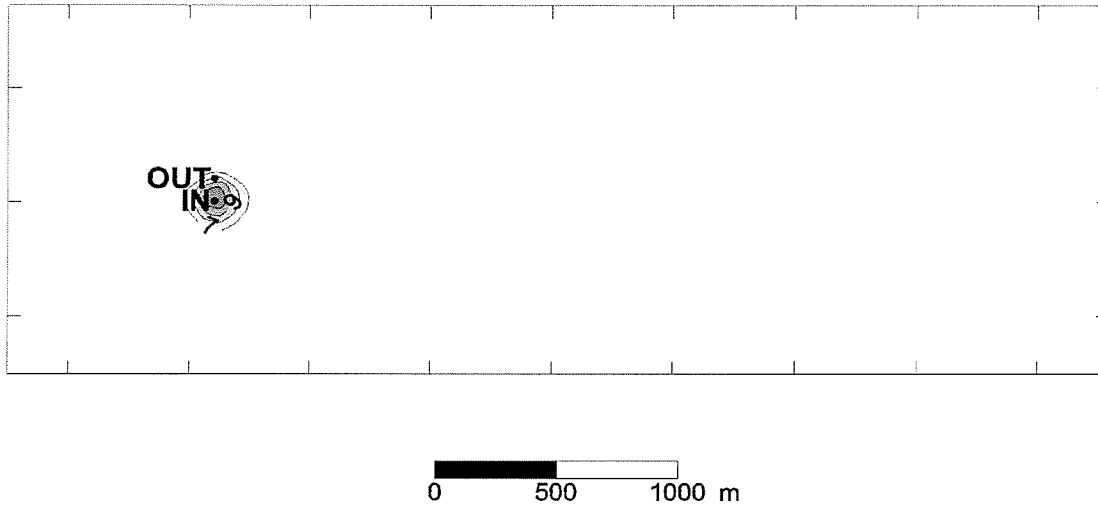
0   500   1000 m
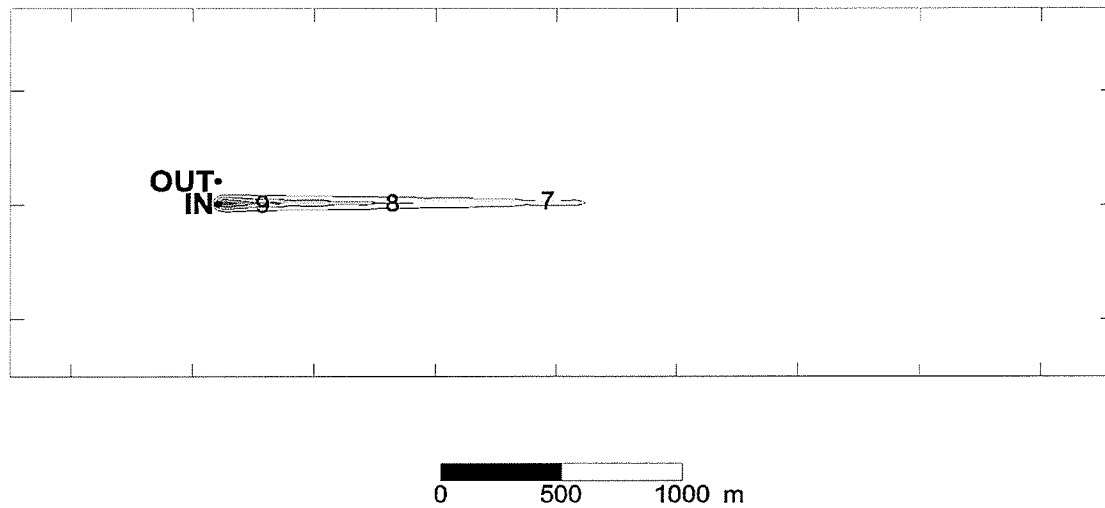
Figure 8.21a: Areal view of aquifer after 5 years of operation of a doublet injecting water at 11 °C at 3.8 L/s for an aquifer with a permeability of 10^{-8} m^2. The head drops by 1 metre from the eastern end of the modeled domain to the western end and this is prescribed by fixed head boundary conditions at each end.
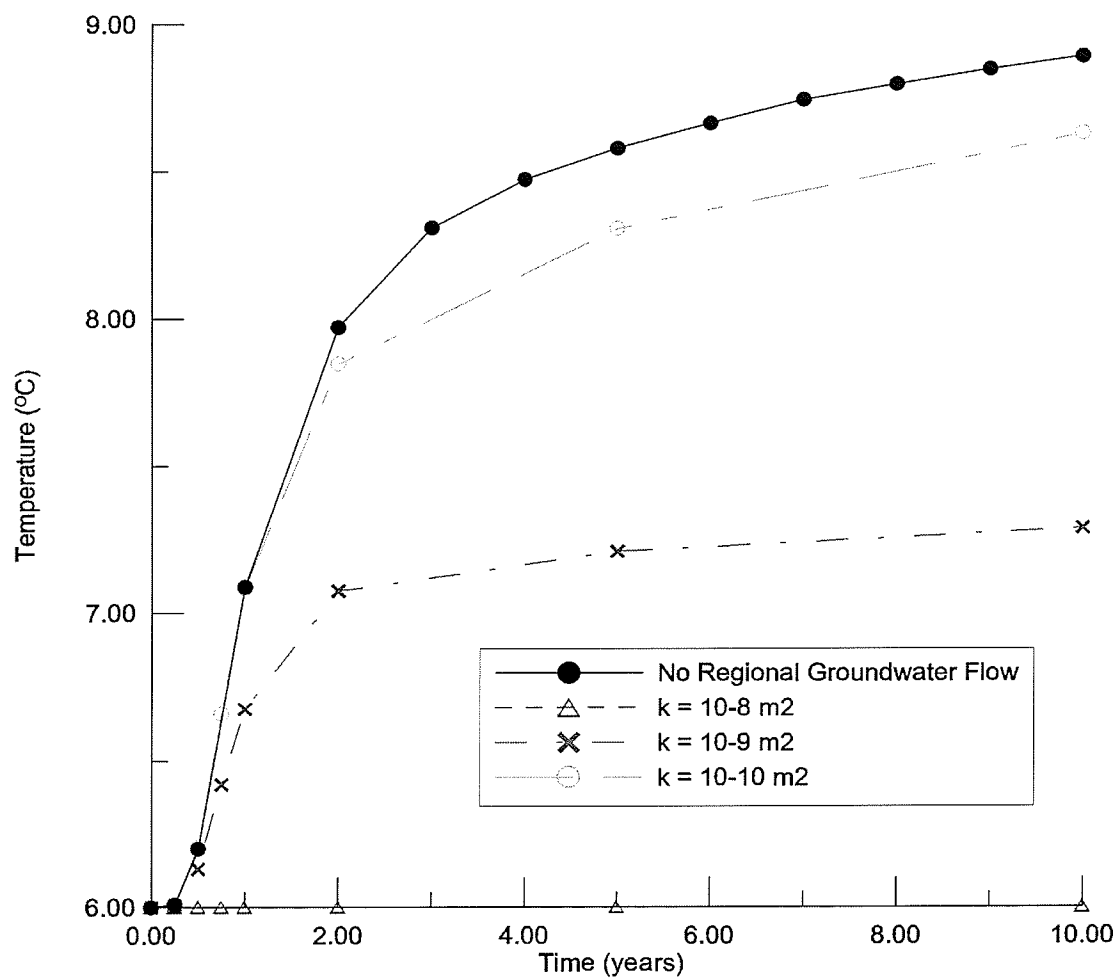

0   500   1000 m
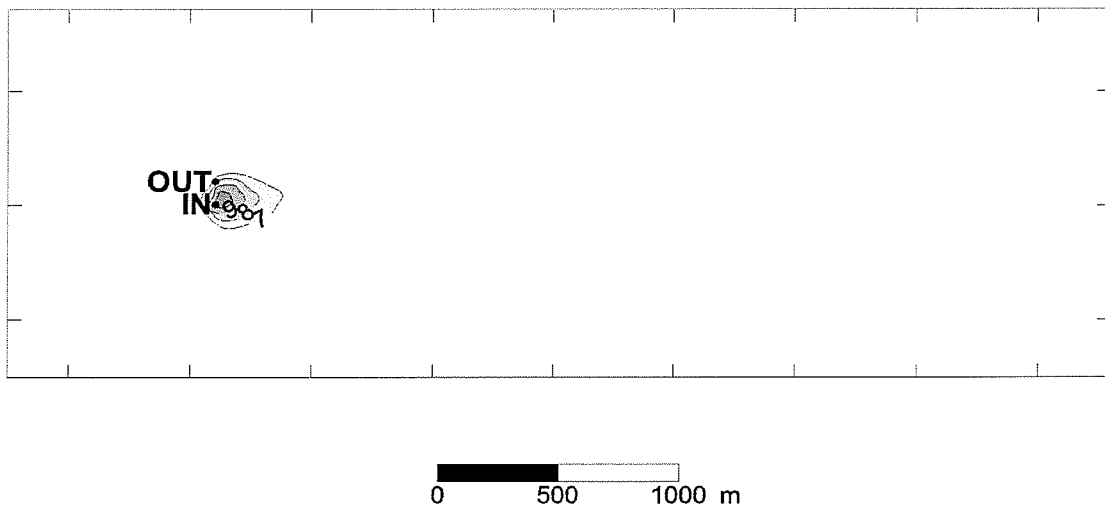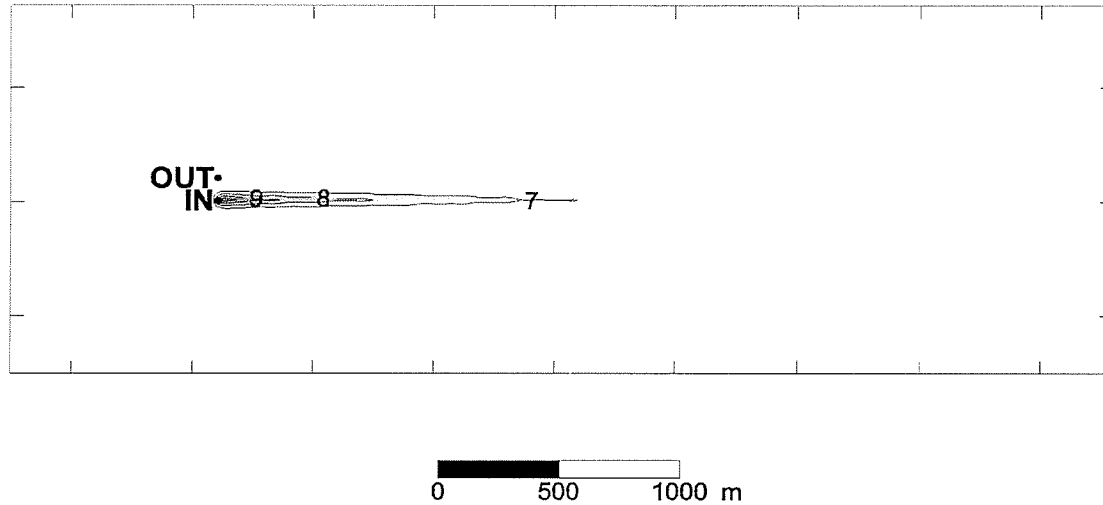
Figure 8.21b: Areal view of aquifer after 5 years of operation of a doublet injecting water at 11 °C at 3.8 L/s for an aquifer with a permeability of 10^{-9} m^2. The head drops by 1 metre from the eastern end of the modeled domain to the western end and this is prescribed by fixed head boundary conditions at each end.

0   500   1000 m

Figure 8.21c: Areal view of aquifer after 5 years of operation of a doublet injecting water at 11 °C at 3.8 L/s for an aquifer with a permeability of 10^{-10} m^2. The head drops by 1 metre from the eastern end of the modeled domain to the western end and this is prescribed by fixed head boundary conditions at each end.

Figure 8.22: Predicted temperatures at the production well as a function of time for a 10 metre thick aquifer that can be treated as a conventional porous medium for various aquifer permeabilities.

Figure 8.23a: Areal view of aquifer after 10 years of operation of a doublet injecting water at 11 °C at 3.8 L/s for an aquifer with a matrix permeability of 10^{-13} and fractures with a permeability of $10^{-7} m^2$. The head drops by 1 metre from the eastern end of the modeled domain to the western end and this is prescribed by fixed head boundary conditions at each end.
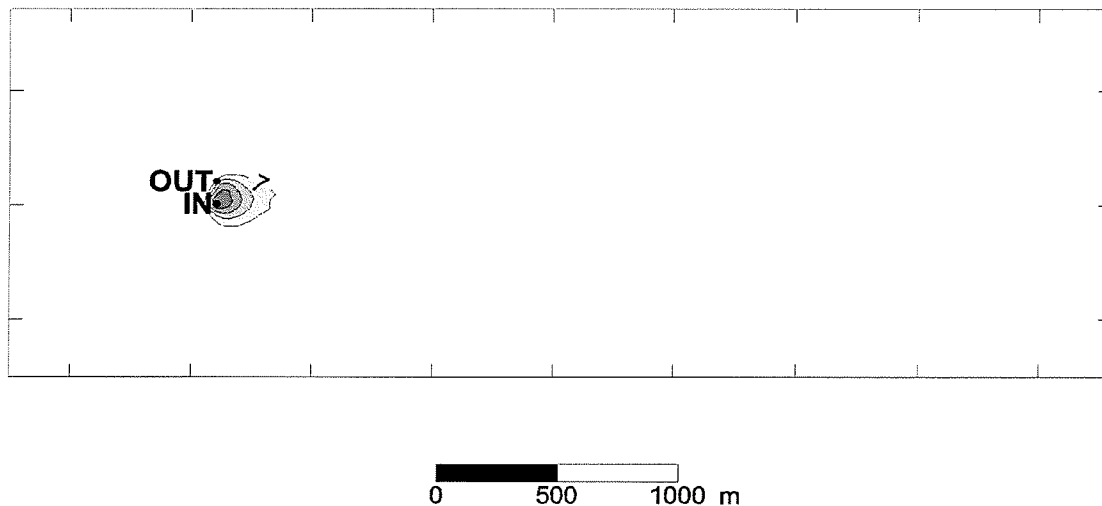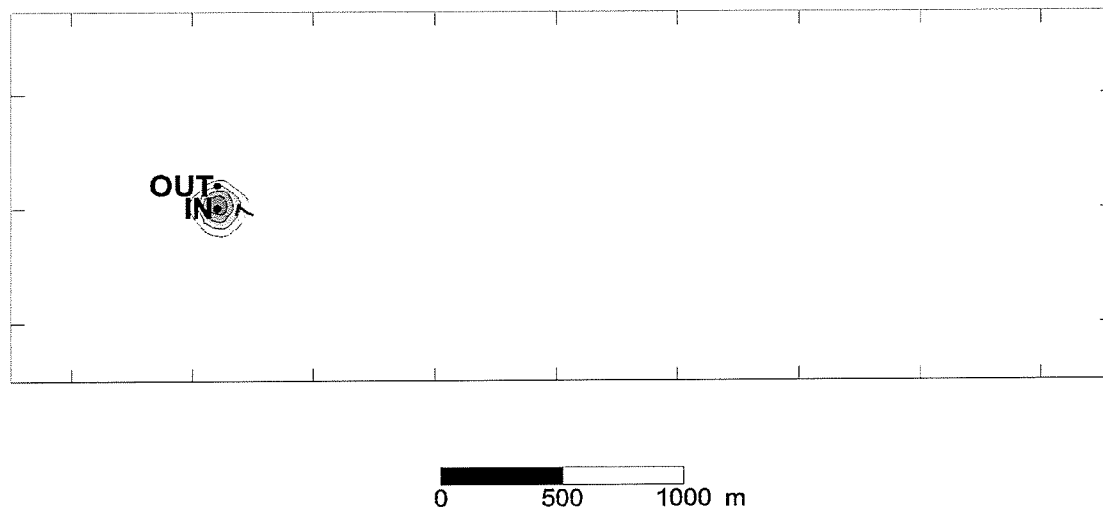

Figure 8.23b: Areal view of aquifer after 10 years of operation of a doublet injecting water at 11 °C at 3.8 L/s for an aquifer with a matrix permeability of 10^{-13} and fractures with a permeability of $10^{-8} m^2$. The head drops by 1 metre from the eastern end of the modeled domain to the western end and this is prescribed by fixed head boundary conditions at each end.
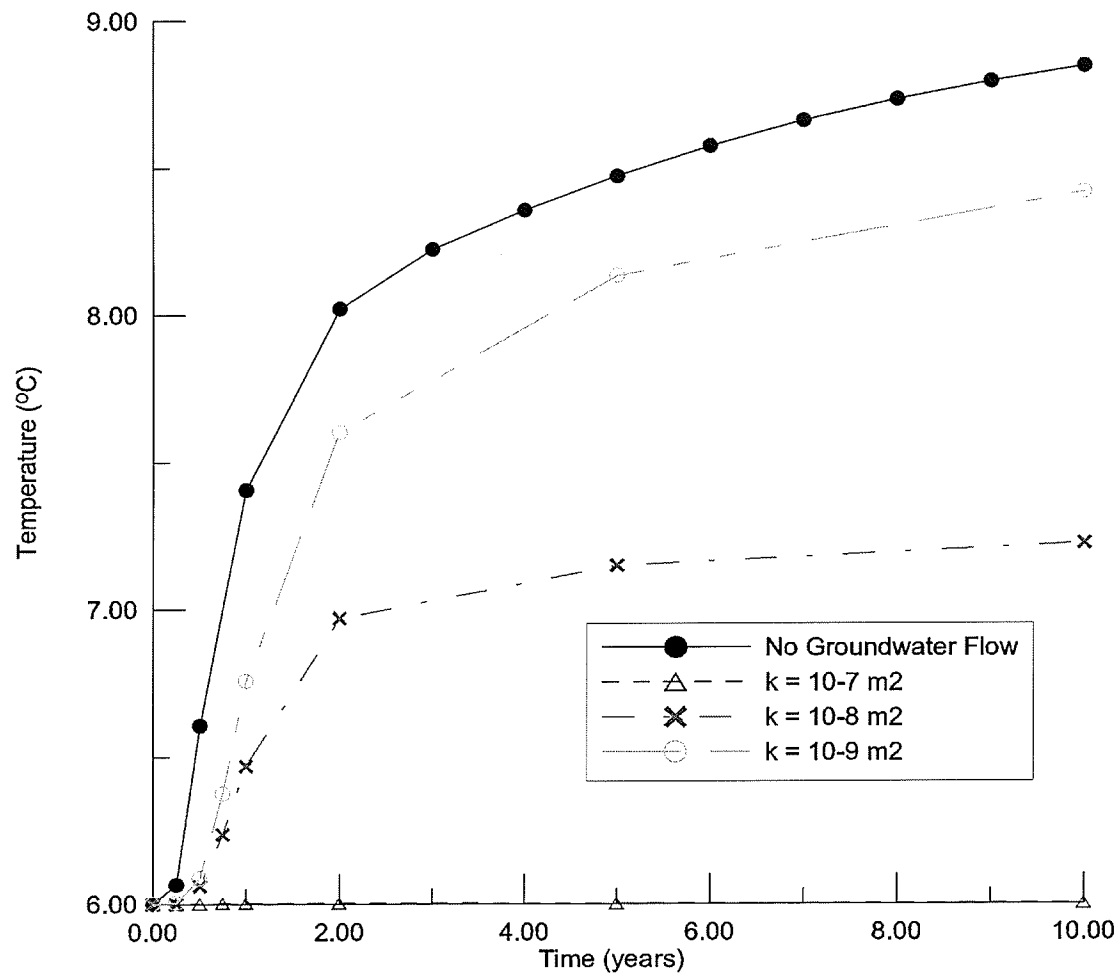
Figure 8.23c: Areal view of aquifer after 10 years of operation of a doublet injecting water at 11 °C at 3.8 L/s for an aquifer with a matrix permeability of 10^{-13} and fractures with a permeability of $10^{-9}m^2$. The head drops by 1 metre from the eastern end of the modeled domain to the western end and this is prescribed by fixed head boundary conditions at each end.

Figure 8.24: Predicted temperatures at the production well as a function of time for a 10 metre thick fractured aquifer. The "no groundwater flow" case refers to the base case from the previous set of dual continuum models where there was regional groundwater flow present.
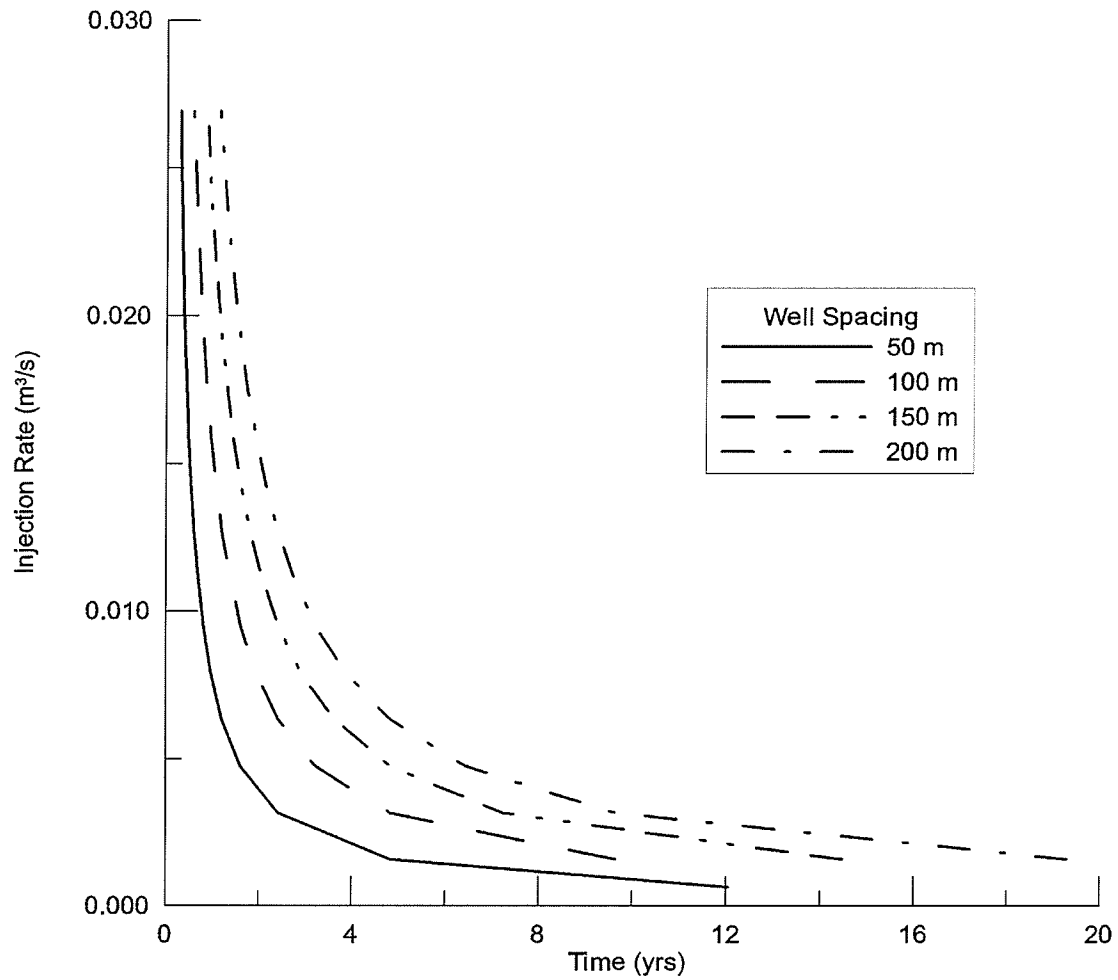
218

Figure 8.25: Breakthrough times in the Winnipeg Formation predicted by Gringarten's method (1978) as a function of injection rate plotted for various well spacings.
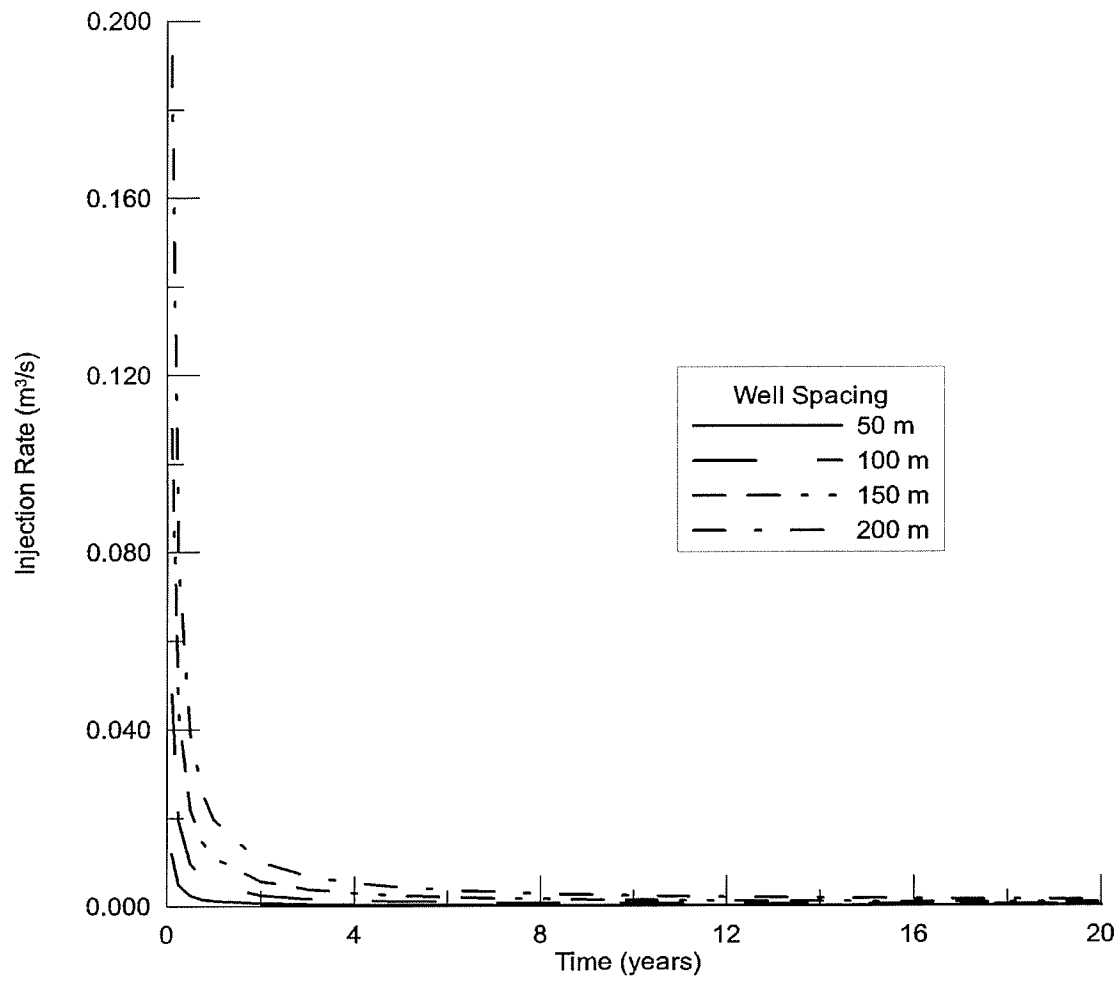
Figure 8.26: Breakthrough times in the Winnipeg Formation predicted by Gringarten and Sauty's method (1975) not considering regional groundwater flow as a function of injection rate plotted for various well spacings.
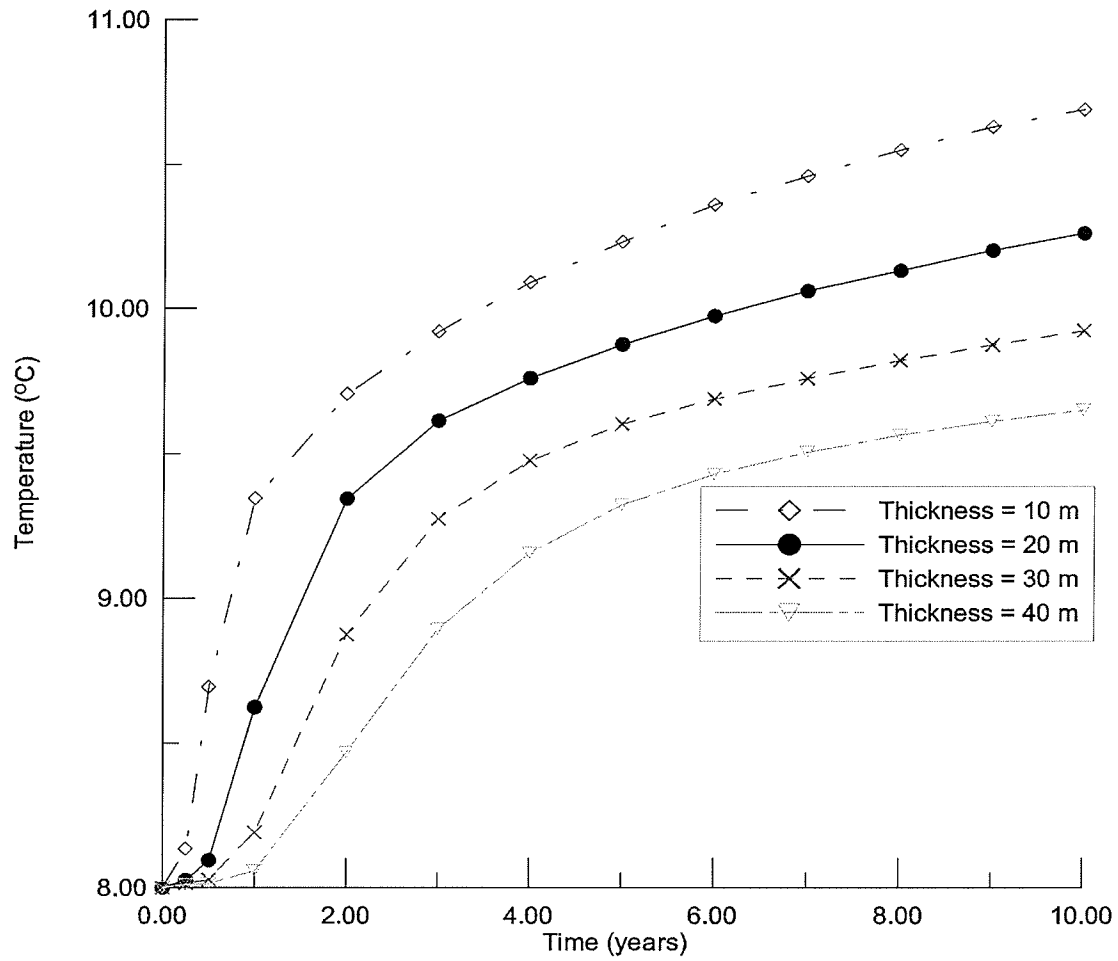
Figure 8.27: Predicted temperatures for a production well in the Winnipeg Formation as a function of time for various aquifer thicknesses.
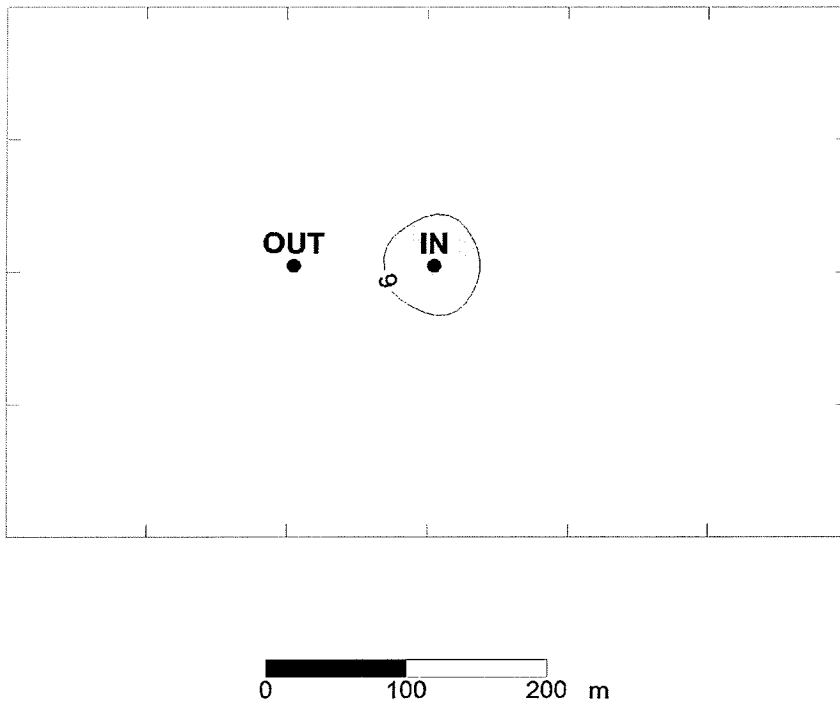
Figure 8.28a: Predicted temperatures for the generic aquifer with a 30 metres thickness representing the Winnipeg Formation after 0.25 years of operation.
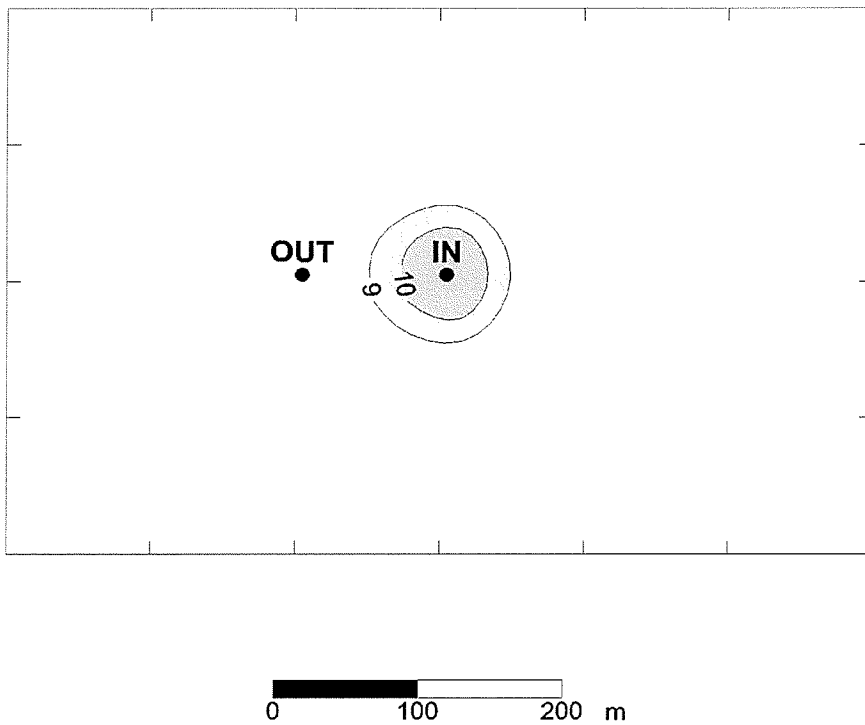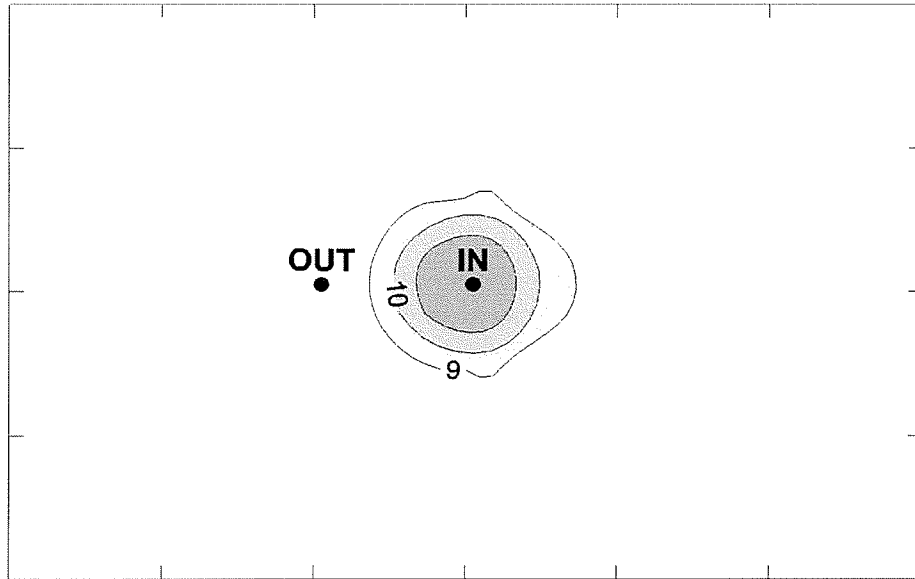

Figure 8.28b: Predicted temperatures for the generic aquifer with a 30 metres thickness representing the Winnipeg Formation after 0.5 years of operation.

222

Figure 8.28c: Predicted temperatures for the generic aquifer with a 30 metres
thickness representing the Winnipeg Formation after 1.0 years of operation.
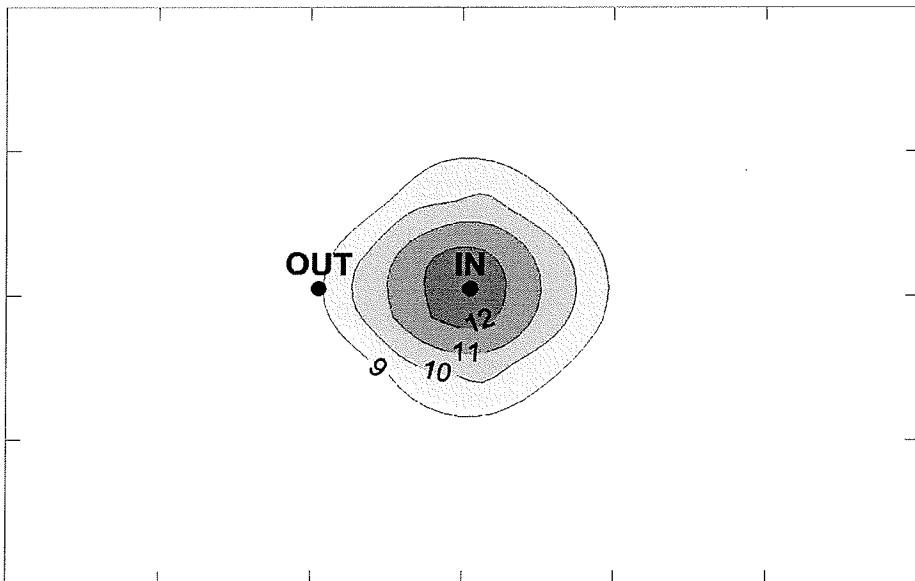

Figure 8.28d: Predicted temperatures for the generic aquifer with a 30 metres
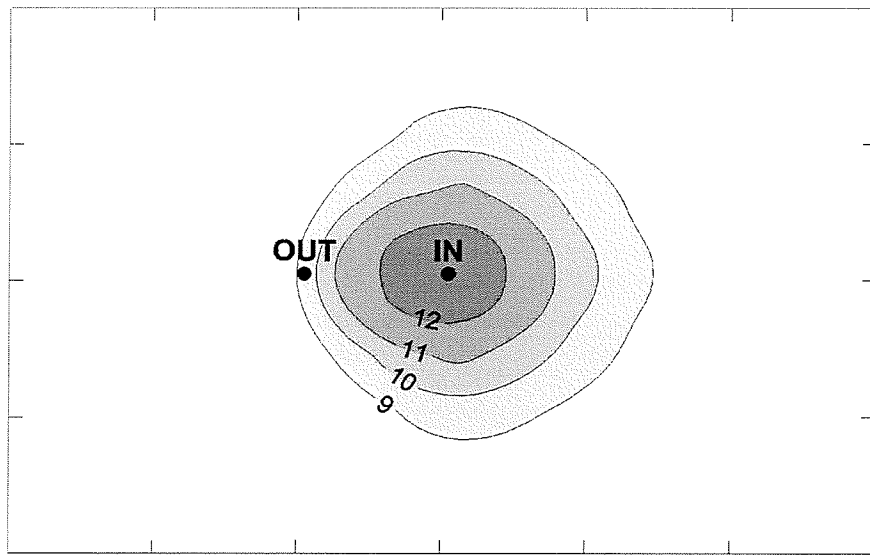thickness representing the Winnipeg Formation after 2.0 years of operation.

Figure 8.28e: Predicted temperatures for the generic aquifer with a 30 metres thickness representing the Winnipeg Formation after 5.0 years of operation.
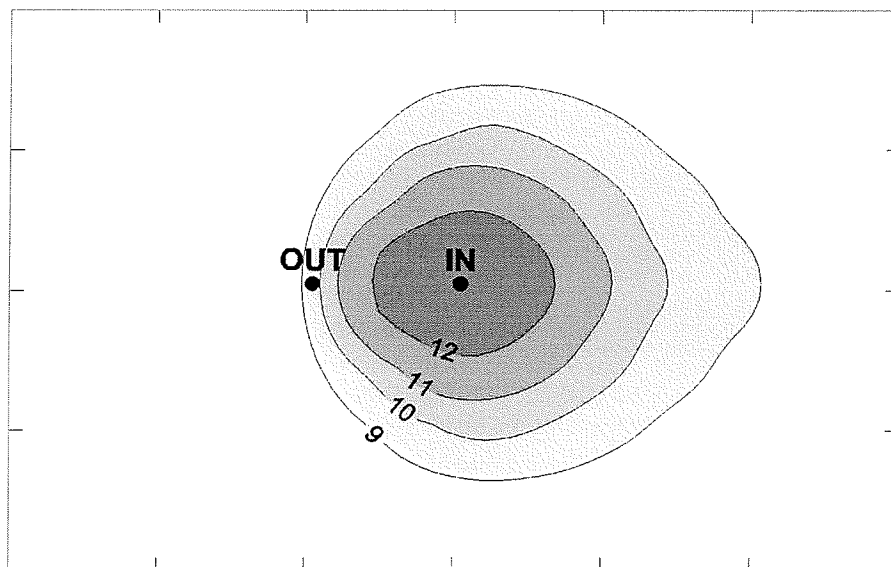

Figure 8.28f: Predicted temperatures for the generic aquifer with a 30 metres thickness representing the Winnipeg Formation after 10.0 years of operation.

CHAPTER 9: CASE STUDIES OF GROUNDWATER SOURCE COOLING

9.1 Introduction

Models of heat transport in the Carbonate Rock Aquifer under the stress of thermal development are required to understand the behaviour of the aquifer. The generic models created in the previous chapter have provided an indication of the relative importance of key variables in the behaviour of heat flow in the Carbonate Rock Aquifer under the stress of thermal development. However, the distribution of hydrogeologic properties in these generic models was relatively simple and may not be able to provide realistic results for actual situations due to the level of heterogeneity present in the aquifer. Also, the variability in the temperature records for production wells in thermal developments (Figures 7.3 to 7.6) suggest that the characterisation of usage patterns may be a significant challenge in the modeling of real situations.

Case studies will be conducted in the current chapter to build upon the findings of the generic models created in the previous chapter. Examining actual sites provides a "reality" check for the generic models, which were laterally homogeneous and had constant pumping rates and injection temperatures. Both conventional porous media models and dual continuum models will be created and their validity will be critiqued.

Two sites were chosen for investigation: 1) an industrial site operating in the St. Boniface area of eastern Winnipeg that has two production wells and one injection well; and 2) the Birchwood area of western Winnipeg where

several systems are operating in close proximity (Figure 9.1). These sites were chosen primarily due to the availability of temperature data and existing knowledge on the hydrogeology of those areas. In both of these cases, pumping rate variability is not well characterised and is estimated from rates licensed by Manitoba Water Branch along with bulk annual usage. Other model parameters are estimated from pump tests, drill logs and values from other hydrogeological studies conducted in the Winnipeg area. Other than a few point measurements made in pumping wells, very little hydraulic head data exist for either site. As a result, hydraulic head will only be used as an approximate guideline for model calibration. Instead, calibration of the models will be based on production well temperatures. The purpose of this modeling is to improve our understanding of heat flow in the Carbonate Rock Aquifer and not to predict the behaviour of these sites in the future, which is largely dependent on future usage patterns. Therefore, no attempt will be made to validate these models.

9.2 St. Boniface Industrial Area

9.2.1 History of Development

An industrial site in St. Boniface operates two production wells (labelled "north" and "south" as per their records in GWDrill) and one injection well (labelled "in") as part of a system utilising groundwater for industrial cooling (Figure 9.2). In this system, the two production wells are approximately the same distance from the injection well (Figure 9.2). The system is estimated to use groundwater at a rate of approximately 13 L s^{-1} for

8 hours per day on Monday through Friday basis. The temperature records for this user shows an increase in the temperature in the northern production well of several degrees Celsius since the start of operation (Figure 9.3). The southern production well has experienced temperature increases of less than 2.0°C since operation of the system began (Figure 9.4).

Another large user of groundwater, with a licensed maximum instantaneous injection rate of 31 L s^{-1}, is present approximately 1 kilometre east of the system in question. This larger system operated as a non-consumptive user until 1999, when injection stopped. At this time no obvious change in the temperature record occurs at either of the production wells at the property of interest, suggesting that it is possible to model the temperature field beneath this property without considering this other nearby user.

Of the four observation wells in the vicinity of this property, anomalous temperatures indicative of advective heat transport are only obvious at W1 (Figure 9.5). Temperatures exceed 11°C at this location over an interval of less than one metre and decrease sharply both above and below this interval, suggesting flow of warm water in a highly permeable zone. The temperature profile observed at CANPAC has a temperature of approximately 8.0°C over a large interval (Figure 9.5). Establishing whether this is due to injection of thermal wastewater or heat loss from buildings at the surface is difficult because both sources of heat were present in the past. Injection of thermal wastewater ceased in the late 1980's and buildings present on the property

were abandoned shortly after. These buildings were demolished in 2002. Temperatures measured north and south of the area at W2 and OJ92 are just over 6°C. The lower temperatures measured at these wells relative to CANPAC and OH12 likely reflect differences in heat loading from the surface related to the age and density of buildings in these areas.

9.2.2 Hydrogeology of the St. Boniface Area

The Carbonate Rock Aquifer in eastern St. Boniface is highly permeable, having transmissivities of approximately 620 m^2 day^{-1} (Render, 1970). Over the entire 120 metre thickness of the aquifer this corresponds to an average permeability of approximately 10^{-11} m^2. However, the bulk of this permeability is considered to be present in the upper few metres of the Red River Formation, which contains the Upper Carbonate Aquifer. Drill logs present in the GWDrill database for the northern production well and the injection well indicated that the upper 2 metres of the Red River Formation are highly fractured. In the log for the southern production well present in the GWDrill database, similar fractures were not noted. However, fractures were noted at this depth at observation well W1, which is located just north of this property. This observation well was drilled as part of this study and the upper few metres of the bedrock were extremely fractured and highly permeable. Circulation was lost immediately after the bedrock was reached during drilling. In all three wells on the industrial property, additional fractures were noted at a depth of approximately 23 metres, sporadically between 30 and 70 metres and at a spacing of approximately 5 metres between 70 and 90 metres. This

fracture distribution is consistent with geophysical logs recorded at a well on the former Canada Packers property (Mwenifumbo et al., 1993), which is less than 1 kilometre away. These geophysical logs suggest that the Upper Carbonate Aquifer is present between 15 and 20 metres depth and another zone of elevated permeability is also present between 70 and 90 metres depth.

Single well pump tests were performed for both production wells and the injection well during the development of the site (Figures 9.6, 9.7 and 9.8). The drawdown responses observed in these tests were quite complex compared to that which would be encountered in aquifers of simple geometry and homogeneous properties and do not lend themselves to an easy interpretation. The well loss term is unknown for these wells; complicating the analysis of the tests which would already be quite difficult judging from the shapes of the drawdown curves. The test for the injection well (Figure 9.6) has at least three distinct portions, which appear to be related to the increasing effect of impermeable or less permeable boundaries as pumping progresses or due to a delayed response of the matrix. The test for the northern production well (Figure 9.7) also appears to have two or three portions to the drawdown response curve, which may also be related to impermeable boundaries, differences between fracture and matrix permeabilities or spatial variations in the fracture network. During the specific capacity test at the southern production well (Figure 9.8), hydraulic head increased during the first few hours of the test. Following this increase,

hydraulic head appears to have a more typical response. The interpretation of these data is difficult because this response may be the result of both pumping and recovery due to a cessation or decrease in pumping elsewhere in the aquifer. These results, in combination with the drill logs and temperatures observed at the production wells suggest that the southern production well and injection well are connected by a fracture network. There could also be an increase in the density or permeability of the fracture network, which is essentially a local feature. The northern production well does not appear to intersect the same fracture network and this idea is supported by the lack of production capacity at the northern production well.

9.2.3 Model Development

On the basis of the pump tests, driller's logs and geophysical data, a conceptual model of the area was created (Figure 9.9). This model consisted of a an upper aquifer in the upper 2 metres of the Red River Formation, which is underlain by 70 metres of less permeable carbonate rock. Underneath this less permeable rock was 25 metres of more permeable rock. A closed zone of enhanced permeability in an area encompassing the northern production well and the injection well was included to account for the lateral differences in permeability suggested by the driller's logs and the hydraulic behaviour of the wells. Parameters used in this model are outlined in Table 9.1. Permeabilities used in this model are similar to those given for the area by Render (1970) and sources for other parameters are outlined in Table 8.1.

A dual continuum model was also created using the same geometries as the conventional porous media model. The concept of a closed fracture network of limited extent was incorporated into this model by including a network of fractures with a spacing of 1 metre in all directions and a permeability of 10^{-9} m^2 in the upper 2 metres of the Carbonate Rock Aquifer over an area including the northern production well and the injection well. The rest of the modeled area was given a fracture permeability of 10^{-10} m^2, with fracture spacing varying from 5 to 20 metres depending on depth (Table 9.1). Fracture spacing was estimated from the well logs for the three wells on the property provided in GWDrill and information provided by Mwenifumbo et al. (1993). Other parameters used in the dual continuum model are outlined in Table 9.1.

Constant head boundary conditions were placed along all lateral boundaries of the model, with no lateral hydraulic gradients imposed by these boundary conditions. A constant head of 10 metres above the top of the aquifer was chosen for these boundaries. This value is probably only accurate to within a few metres but changes in head were of more interest than absolute head values because heat flow is the primary focus of this study as opposed to groundwater supply. The upper and lower boundaries of the model were treated as impermeable boundaries to reflect the positions of the till-carbonate rock interface at the top and the position of the carbonate rock-shale interface at the bottom of the Paleozoic carbonate sequence. Conductive heat losses were allowed at these boundaries. The initial

temperature used in the model was 8.3 °C (Little, personal communication[1]). This temperature was assigned to the entire model domain, neglecting the variability of the background temperature field due to heat losses from the surface and the natural geothermal gradient. The size of the blocks in the integrated finite difference model ranged from 10 x10 metres in the immediate vicinity of the wells to a few hundred metres across near the edges of the model domain.

Pumping rates used in the model were continuous, with injection occurring at 3.9 L s^{-1} and production at 1.3 and 2.6 L s-^{1} in the northern and southern production wells, respectively. These rates were estimated assuming the maximum instantaneous licensed rate occurred for eight hours per day for five days per week. The operator of this cooling system stated that the injection temperature would only be a few degrees Celsius greater than the production temperature in the original licensing file but current production temperatures clearly indicate that this is not the case. Three measurements of injection temperature were available for this site but due to the variability of injection temperature, they were not very useful. At the start of operation an estimated injection temperature of 13.3 °C was used in the model. This temperature represents a 5°C increase over background temperatures and was used as the injection temperature until thermal breakthrough occurred in the model. After thermal breakthrough, a constant

---

[1] Little, J., Manitoba Conservation, Water Branch, July 2003

temperature of 15.3°C was used to reflect the increase in the temperature of the produced water.

9.2.4 Model Results

The porous media model for the site was able to recreate the general trends in the observed temperature records of both production wells (Figures 9.3 and 9.4). The best-fit line for the scatterplot between observed and predicted results (Figure 9.10) has the following equation:

$$T_{predicted} = 0.795T_{observed} + 1.10 \qquad (9.1)$$

The R^2 correlation coefficient for this line is 0.855 and the RMS error produced by the model was 0.07°C. However, this line is significantly different at the 95% level from a line with a slope of one that passes through the origin. This difference likely occurs because the temperatures predicted at the production wells were generally less than those in the observed record, particularly at later times (Figure 9.11). Much of the variability in the temperature record is not explained and this is probably a result of the constant injection temperatures and production rates used in the model as compared to their actual values.

The dual continuum model also recreated the general trends observed in both production wells (Figures 9.3 and 9.4). The scatterplot of predicted versus observed temperatures (Figure 9.12) has a best-fit line of:

$$T_{predicted} = 0.747T_{observed} + 2.89 \qquad (9.2)$$

The R^2 correlation coefficient for this line was 0.856 and the RMS error between the predicted and observed temperature in this model was 0.08 °C.

The temperatures predicted by the dual continuum model are generally less than the observed temperatures but the average difference between predicted and observed temperatures is closer to zero than the difference in the conventional porous media model (Figure 9.13). However, the line described by equation 9.2 is also significantly different from a line with a slope of one passing through the origin at 95% confidence level. As in the porous media model, the variability present in the observed temperature record is not explained, perhaps due to the manner that was used to assign pumping rates and injection temperatures in this model.

Sensitivity analyses were conducted for the conventional porous media and dual continuum models of the industrial site in St. Boniface by examining the changes in predicted temperatures at the southern production well after 1.5 years associated with varying key model parameters. The parameters of interest were the variations in permeability and porosity in the four hydrostratigraphic units of the model. These parameters were multiplied by a factor (referred to as a scaling factor in all sensitivity analyses conducted in this chapter), which examined increases and decreases in permeability of up to an order of magnitude and slightly smaller ranges for changes in porosity. Sensitivity of model results to increases or decreases in pumping rates were also examined. Thermal parameters were not examined in the sensitivity analysis because they are thought to be subject to smaller ranges of variability in the Paleozoic carbonate sequence. Injection temperatures were also not examined as they are relatively well constrained at this site. The

temperature of interest in the sensitivity analysis was the temperature at the southern production well 1.5 years after the start of operation. This point was selected because it occurs late in breakthrough curve, where the results of the model should be reasonably sensitive to changes in model parameters.

In the conventional porous media model, differences in the permeability of the zone of high permeability in the upper reaches of the Red River Formation and in the surrounding rock were found to be the most important to the model (Figure 5.14). By decreasing the permeability of the zone of high permeability by an order of magnitude the predicted temperature at the southern production well decreased by over a 1.0°C from the calibrated model. An increase in the permeability of the surrounding rock of one order of magnitude resulted in a drop in the predicted temperature at the same well of approximately 0.8°C. Changes in the permeability of the middle and lower units of the model produced little change in the temperature of the southern production well. The conventional porous media model was also sensitive to changes in porosity in middle and lower units of the model (Figure 9.15). A decrease in temperature of approximately 0.3 °C was predicted for the southern production well if the porosity of this unit is decreased to 0.05 and an increase in temperature of over 0.2 °C was estimated for an increase in the porosity of this zone to 0.15. Temperature changes of a similar magnitude are predicted for changes in porosity of the middle zone but predicted temperatures at the southern production well increase with decreasing porosity for this unit. Changes in the porosity of the upper zone of

235

enhanced permeability and the upper unit had little impact on the temperatures at the southern production well.

In the dual continuum model, the range of predicted temperatures in the sensitivity analysis was smaller than that observed in the analysis conducted for the conventional porous media model. The hydrostratigraphic unit that was most sensitive to changes in permeability was the upper zone (Figure 5.16). If the permeability of the fractures in this unit was increased by a factor of 5, the predicted temperature at the production well rises by approximately 0.3°C relative to the calibrated model. However, a slightly smaller temperature increase is predicted if the permeability of the fractures in this unit is increased by a factor of 10. A similar trend is observed with increases in the permeability of fractures in the lower unit while decreases in the permeability of the fractures in the same unit result in an increase in predicted temperatures of approximately 0.2°C. Decreases in permeability of all other units result in changes in temperature at the southern production well of less than 0.1 °C. Changing the fracture porosity or matrix porosity in the dual continuum model had little effect on the predicted temperature at the southern production well after 1.5 years (Figure 5.17). The maximum change in temperature predicted in this part of the sensitivity analysis was approximately 0.2 °C. The most notable trends present were an increase in temperature that was related to an increase in the fracture porosity in the middle unit and a decrease in temperature associated with increasing fracture porosities in the upper zone.

The effect of changing pumping rates was examined for both the conventional porous media and dual continuum models. The responses of the models to increasing or decreasing pumping rates were similar in both formulations (Figure 9.18). In both cases, the temperature at the southern production well after 1.5 years of operation was predicted to be approximately 0.5°C less if the pumping rates were reduced by 20%. Increasing the pumping rate by the same percentage is predicted to increase temperatures at the southern production well by approximately 0.4°C at the same location and time.

The spatial distributions of temperature in the aquifer predicted by both models are very similar and as a result only dual continuum results are discussed, because this model is likely a better conceptual representation of the aquifer. The predicted size of the temperature anomaly resulting from injection of thermal wastewater is approximately 200 metres across after 15.2 years of operation as defined by the 9°C isotherm (Figure 9.18). The anomaly is somewhat elongated along a line connecting the injection well and the southern production well and although the majority of the temperature changes take place during the first five years (Figures 9.18a to e), the estimated anomaly continued to grow outward during the 1990's (Figures 9.18e, f and g). The anomaly does not extend very far north of the injection well but the observed temperature at monitoring well W1 is in agreement with the predicted temperature for the summer of 2002 (after 15.2 years of

operation) (Figure 9.18g). However, the timing of the temperature increase at this location cannot be verified because W1 was installed in 2001.

As previously stated, there are no head data available for the property in question other than measurements taken during the specific capacity tests conducted prior to the start of production and injection. Based on these tests, the drawdown at the southern and northern production wells should be approximately 1 and 3 metres, respectively. The porous media model predicts drawdowns of 0.1 and 1.0 metres at these wells, while the drawdowns predicted by the dual continuum model are 0.7 and 3.5 metres. The hydraulic head changes predicted by the model will be different than those actually occurring at this property because of the manner in which pumping rates were assigned to the wells in the models. A constant average pumping rate was used in these rather than the actual rates, which in a typical week occur Monday through Friday for eight hours per day. This treatment of pumping rates will cause the model to predict smaller changes in head than those which likely occur at this site. It should also be noted that similar temperature predictions were possible in other models that predicted very different hydraulic head distributions.

9.2.5 Model Discussion

The difference in the response of temperatures in the northern and southern production wells on this property, which are nearly the same distance away from the injection well, indicate that lateral heterogeneity of the Upper Carbonate Aquifer has had an important influence on heat transport

during thermal development at this location.   When an injection and production well are located in a closed area of enhanced permeability, the magnitude of the temperature increase in the produced water will be greater. The increase in temperature at the production well will also occur more quickly than in situations where the aquifer is laterally homogeneous. This relationship occurs primarily because the flowlines between the two wells become more concentrated in this zone of enhanced permeability, which reduces fluid travel times and also reduces the potential for conductive heat losses and mixing with native groundwaters.

The results of the sensitivity analyses indicate that in a conventional porous medium representation of this system, the most important feature in the model is the difference between the permeability of the zone connecting the southern production well and the injection well and other areas of the Upper Carbonate Aquifer. As these permeabilities become more similar, the temperature at the southern production well decreases. Variations in porosity between the four units used in the model also have a significant effect. This is likely due to the volume of injected water than can occupy the lower and middle units.   If more of this water enters the lower unit, more of the introduced heat is emplaced in the subsurface at a greater distance from the shallower southern production well. Conversely, if more of this introduced heat occupies the middle unit, the transport distance to the southern production well is decreased.

The results of the dual continuum model indicate that this is perhaps a more stable model as estimated temperatures change less with varying material properties. However, less is known about the fracture properties than the effective properties of the carbonate rock at this site. Variation of the permeability and porosity beyond the ranges used in the sensitivity analysis are more likely in this model than in the conventional porous media model.

The models created for this site used a constant injection temperature and this is not representative of reality. The file maintained by the Manitoba Water Branch for this property states that the operator felt that the injected water would only be a few degrees warmer than the in situ groundwater. However, this is obviously not the case as production well temperatures have increased by more than 5°C. Increases in injection temperature following thermal breakthrough are clearly a problem and this will lead to progressively higher temperatures in the aquifer. This effect could render the aquifer useless for some cooling applications, and in the case of cooling for high temperature industrial processes, aquifer temperatures could potentially become quite high.

The lack of hydraulic head measurements at this site makes calibration of a heat transport model difficult. Parameter estimation problems in hydrogeology are inherently ill-posed and any additional data are helpful in constraining the parameters used for modeling. In addition to head measurements made during operation, better quality and more extensive hydraulic testing prior to installation of this system would be useful in

assessing the material properties, particularly with respect to lateral heterogeneity. Given that three wells were installed at this site, it would have been possible to conduct a pump test in one of these wells while making head measurements in the other two. This type of pump tests would be useful in the design of the withdrawal and injection schemes at this location because greater temperature increases and more rapid breakthrough times would have been predicted for the northern well, suggesting that an alternate development scheme be devised.

9.3 Birchwood Area, Western Winnipeg

9.3.1 History of Development

Along Portage Avenue in the vicinity of Moray Street, four buildings use large amounts of groundwater for cooling purposes (Figure 9.20; Table 9.2). This area is commonly referred to as the Birchwood area of Winnipeg. The first of these systems was installed in 1965 at the Birchwood Terrace apartment building. This system is a consumptive user as the thermal wastewater is discharged to the Assiniboine River. In 1973, two non-consumptive systems were installed at the apartment complexes 2600/2610 Portage Avenue and Pinewood Place. Four years later another system was installed at the Birchwood Inn. However, this system is somewhat different from those at 2600/2610 Portage Avenue and Pinewood Place in that it operates throughout the year and is only a partially consumptive system. Render (1981) reported that problems were encountered with the injection well of this system during the first few years of operation, including excessive

hydraulic head in the aquifer and air entrainment in the injected water. These problems were addressed discharging a portion of the thermal wastewater to a storm sewer and by providing better maintenance of the seals in the injection system by. All of the wells installed in the Birchwood area are completed as open holes in the carbonate rock at depths between approximately 23 metres and 122 metres.

9.3.2 Hydrogeology of the Birchwood Area

Render (1981) conducted a study of the sustainability of using groundwater in cooling systems in the Birchwood area by mapping the potentiometric surface in the area, conducting pump tests in all production well in the area and examining available temperature data. Results of pump tests conducted during that study suggested that transmissivities in the area ranged from 228 to 1022 m^2 day^{-1}, which corresponds to a permeability of approximately 10^{-11} m^2 if it is assumed that the entire thickness of carbonate rock in the area is equally permeable. The analysis conducted by Render (1981) used the Theis (1935) solution. However, Render (1981) also notes that there were several discrete fracture zones that may be responsible for most of the permeability. The presence of fractures is also supported data from these pump tests, which shows a departure from the Theis solution at late times. This response may be related to the delayed response of matrix permeability in this fractured medium (Moench, 1984). Although the location of a few of the major fractures is known, their hydraulic characteristics are not.

9.3.3 Model Development

Two numerical models of the Birchwood area were produced to develop a better understanding of the sustainability of the use of groundwater in cooling systems in this area. The hydrostratigraphic model of the area has a uniform cross-section with an upper aquifer, an intermediate zone of lower permeability, a lower aquifer and a lower zone of low permeability (Figure 9.21). Both conventional porous medium and dual continuum models were created using this hydrostratigraphic model using parameters outlined in Table 9.3.

The location of the modeled area is shown covered an area extending from the Assiniboine River to an area north of Ness Avenue and from Sturgeon Creek in the west to an area several hundreds of metres west of Olive Street (Figure 9.20). Fixed head boundary conditions were placed along the Assiniboine River at the south end of the modeled area, along Sturgeon Creek in the southwest of the modeled area and along the northern boundary of the study area, which was placed 1400 metres north of the Assiniboine River. The hydraulic head used for the constant head boundary was 222 m, which is approximately the elevation of the Assiniboine River. The eastern boundary and the section of the western boundary north of Sturgeon Creek were assigned impermeable boundaries based on the assumption that regional groundwater flow is from north to south in this area. The upper and lower bounds of the carbonate rock unit were also treated as impermeable boundaries based on the relatively low permeability of the overlying till and

underlying shale compared to the carbonate rock. Conductive heat losses were allowed at all boundaries. The size of the blocks in the model ranged from 25 metres across for the entire southern portion of the model, where injection and production wells were present, to 200 metres across in the northern portion of the model, where injection and production wells were absent.

Injection and production rates were assigned based on the estimated rates (Table 9.2) and it was assumed that all wells, with exception of those at the Birchwood Inn, were in operation over a four month period from the middle of May to the middle of September but the temporal variability the injection rates are not well constrained. The wells at Birchwood Inn are in operation throughout the year (Render, 1981). Partial records of injection temperature exist for the systems at 2600 Portage Avenue (Figure 9.22) and Pinewood Place (Figure 9.23) but injection temperatures at some times and locations had to be estimated. These estimates were based on Manitoba Water Branch guidelines and injection temperature data at other times. Modeling was further complicated by a period during which operation of the system at the Birchwood Inn decreased over a four year period in the late 1980's. Consequently, an injection rate of zero was assigned from the fall of 1985 to the summer of 1990.

9.3.4 Model Results

The porous media model of the Birchwood area predicted temperatures that were generally less than the observed temperatures

(Figures 9.24 and 9.25). A reasonable fit was obtained for the calibrated model, with an R^2 correlation coefficient of 0.748 for a best-fit line between the predicted and observed temperatures described by the following equation:

$$T_{predicted} = 0.82T_{observed} + 1.16 \qquad (9.3)$$

The RMS error between the predicted and observed temperature in this model was 0.14 °C. The line described by equation 9.4 is significantly different at the 95% level from a line passing through the origin with a slope of one. Both models did a reasonable job of recreating both the general trends observed in the temperature records and the magnitude of temperature increases at each of the production wells with long-term records but are unable to reproduce the highest temperatures observed in the model (Figures 9.26, 9.27 and 9.28).

The dual continuum model created for the Birchwood area was able to reproduce most of the general trends observed in the three production wells in the area (Figures 9.26, 9.27 and 9.28). An overall R^2 correlation coefficient of 0.76 was achieved between the predicted and observed temperatures (Figure 9.29) and the best-fit line between the observed and predicted data has the following equation:

$$T_{predicted} = 0.846T_{observed} + 0.963 \qquad (9.4)$$

The RMS error between the predicted and observed temperature in this model was 0.14 °C. The line described by equation 9.4 is significantly different at the 95% level from a line passing through the origin with a slope of one. This difference occurs because the majority of predicted temperatures

245

by this model were less than the observed temperatures (Figure 9.30). This difference is more apparent at later times in the model.

The conventional porous media model and dual continuum model produced the same general trends for the Birchwood Terrace production well (Figure 9.26). Predicted temperatures are approximately 0.3 °C greater in the dual continuum model during the first few years of the model. At later times, the conventional porous media model produced slightly greater temperatures. The predicted temperature increase at the Birchwood Inn's production well was similar to the magnitude of the observed temperature increase. However, an interruption in the injection of water to the aquifer during the late 1980's produced a drop in predicted temperatures in the model, which was not observed in the actual temperature record. Instead, the observed temperatures continued to increase during this period. Temperatures increased throughout the 1990's in both the observed and predicted temperatures but the predicted temperatures were generally less than 1.0°C during this period.

The conventional porous media and dual continuum models predict similar trends for the production well at 2610 Portage Avenue (Figure 9.27). The conventional porous media model predicts temperatures that are approximately 0.1°C greater throughout the model following thermal breakthrough, which occurred circa 1975. The magnitude of the temperature increase observed in both the predicted and observed records for the production well at 2610 Portage Avenue is similar. However, it is difficult to

246

determine whether the breakthrough times agree between the modeled and observed temperatures because no observations are available until after breakthrough, with the exception of the temperature measurement made immediately after the well was completed. The observed temperatures are generally greater than the predicted temperatures at this location by a few tenths of a degree Celsius and the amount of variability is less than that present in the modeled record.

There is little difference between predicted temperatures in the conventional porous media and dual continuum models for the production well at Pinewood Place (Figure 9.28). Breakthrough time and the magnitude of the temperature increase are in good agreement for the production well at Pinewood Place. The model also recreates the cooling trend observed in the late 1980's but the response to the interruption of injection at the Birchwood Inn is slower and has a less dramatic effect on predicted temperatures than in measured temperatures. The model is not able to reproduce the temperatures measured in 1981 and 1984, which occur prior to the beginning of temperature measurements in the injection well. These temperatures exceed the Province of Manitoba's maximum injection temperature requirements.

Sensitivity analyses were conducted for both the conventional porous media and dual continuum models created for the Birchwood area to assess the importance of the permeabilities and porosities assigned to the various units in these models. The effect of these variations in porosity and

permeability on the predicted temperature at the production well in the Pinewood Place system three years after operation of this system began was examined. This calibration point was selected because it was the earliest temperature measurements made at the production well in this system and it occurs shortly after thermal breakthrough, where the model will be reasonably sensitive to changes in model parameters.

In the conventional porous media model, the predicted temperature at the production well at Pinewood Place increased by nearly 0.2°C when the permeability of the lower aquifer was increased by an order of magnitude (Figure 9.31). Decreasing the permeability of this unit by the same amount was not possible due to numerical instability. However, reducing the permeability by a factor of two cased a decrease in the predicted temperature of over 0.1°C. Increasing the permeability of either the middle unit or the lower unit in this model by ten times led to a decrease in the predicted temperature at the southern production well of approximately 0.3°C. A decrease in the predicted temperature at the Pinewood Place production well in 1976 is expected if thee permeability of either of these units is decreased by an order of magnitude. Increasing or decreasing the permeability of the upper aquifer by ten times had little effect on the predicted temperatures at the point of interest. However, changes in porosity in the upper aquifer have a more pronounced effect on the predicted temperatures at the Pinewood Place production model than changes in porosity in any other unit. If the porosity of the upper aquifer is reduced to 20% of the value used in the

calibrated model, the predicted temperature decreases by approximately 0.2°C and an increase in predicted temperature of approximately 0.1°C occurs if the porosity is doubled. Changes in the porosity assigned to the middle unit and lower aquifer have a similar effect on the predicted temperature at the Pinewood Place production well. A decrease in the porosity to 20% of the calibrated model value in either of these units results in an increase in predicted temperature of approximate 0.1°C. Predicted temperatures decrease by a similar magnitude is observed if the porosity is increased to 200% of the calibrated model value. The model is not very sensitive to changes in the porosity of the lower aquifer.

The dual continuum model appears to be much less sensitive to changes in permeability (Figure 9.33) and porosity (Figure 9.34). The maximum change in predicted temperature was less than 0.1°C and this was caused by an increase in matrix permeability of an order of magnitude over the entire model domain.

The sensitivity of the model to increases or decreases in pumping rates was also examined. This analysis also used the temperature of the production well at Pinewood Place three years after it began to operate as a basis for comparison. In the conventional porous media model, the predicted temperature decreased by over 0.4°C if the pumping rates of all wells were reduced by 20% (Figure 9.35). An increase in the pumping rates by 20% resulted in an increase in predicted temperature of approximately 0.3°C. Similar trends were observed in the dual continuum model.

The spatial distribution of the predicted temperature anomaly was essentially the same in the conventional porous media and dual continuum model and as a result only maps of temperatures predicted by the dual continuum model are presented (Figure 9.36). Small anomalies are predicted to first appear in the vicinity of the wells at Pinewood Place and 2600 Portage Avenue in 1973 (Figure 9.36a). The predicted anomaly around Pinewood Place is approximately symmetric, as it appears to be affected by production at both Pinewood Place and Birchwood Terrace. The anomaly at 2600 Portage Avenue is also slightly skewed in the direction of the production wells to the east. The next major change in the predicted temperature field occurs after the Birchwood Inn system begins to operate in 1977 (Figure 9.36d). After only a few months of operation, the predicted temperature anomaly due to injection at the Birchwood Inn has coalesced with the anomaly from Pinewood Place. The interior of these estimated anomalies appear to reach a near equilibrium state by 1978 (Figure 9.36e) and afterwards, only slight outward growth occurs. By 1985 (Figure 9.36i), the temperature anomaly from 2600 Portage Avenue is predicted to have coalesced with the anomaly associated with the other four systems. The predicted temperature anomaly has a different shape in 1990 (Figure 9.36j) following an absence of production and injection at the Birchwood Terrace and the subsequent resumption of operation. Predicted temperatures in 1999 (Figure 9.36k), which marks the end of the modeled period, were very similar to those observed in 1985, suggesting that this is a quasi-equilibrium state for the

250

system. These predicted temperatures appear to adequately simulate what occurs in this area for the systems at 2600 Portage Avenue, the Birchwood Inn and Pinewood Place. The predicted temperatures shown in the vicinity of Birchwood Terrace are not in good agreement with the temperature record at Birchwood Terrace or with the measured temperature at W5, which was approximately 9.0°C in 2002. Acquiring more data on the distribution of permeability in this area may assist in rectifying this discrepancy.

Little hydraulic head data are available for the Birchwood area. Render (1981) provides a map of the potentiometric surface from 1980 but these data are likely not accurate as it was derived from production and injection wells that were in operation at the time. These measurements are subject to error because the well efficiency term for these wells is unknown and this can lead to significant decreases (or in the case of injection increases) in the water level measured in a well. Also, hydraulic heads are known to vary significantly throughout the year in the Upper Carbonate Aquifer due to natural influences (Render, 1970; Rutulis, 1989; Ferguson and St. George, 2003) and these forcing mechanisms are not considered in this model. Finally, actual rates in these systems will vary depend on the demand for air conditioning which will be quite variable during the summer. This level of variability is not represented in the pumping rates used in model and this would likely cause difficulties in calibrating the model to measured hydraulic head data, if a sufficient amount were available.

9.3.5 Model Discussion

The porous media and dual continuum models perform similarly in their estimation of temperature the Birchwood area. The predicted temperatures at 2610 Portage Avenue and Pinewood Place are reasonable representations of the conditions at the sites but some of the trends present at Birchwood Terrace are not explained by the model. Temperatures are predicted to decrease during a period in the late 1980's at Birchwood Terrace as a result of changes in production and injection patterns at the Birchwood Inn. However, temperatures actually increased slightly during this time. This effect may be due to discontinuities in the fracture network between the injection well at Pinewood Place and Birchwood Terrace. There is little hydrogeological or geological data available to support this idea but it seems likely given the difference in observed temperatures. A discontinuity in the fracture network is also supported by the difference between observed and predicted temperature at W5. Future development of the Carbonate Rock Aquifer for thermal purposes should make a better attempt to characterize variations in the fracture network in the aquifer. This characterisation could include more detailed multiple well pump tests, tracer tests and geophysical logging. An improved record of injection and production rates and temperatures would also assist in the creation of a better model.

From the observed and predicted temperatures in the Birchwood area, temperatures at the production well at Pinewood Place appear to be influenced by injection that is occurring at the neighbouring property to the

west and this influence is most apparent during the period in the later 1980's where operational patterns change. The models predict that temperatures at the Birchwood Terrace should also be affected by this lack of production and injection but the observed temperatures do not support this prediction.

In an earlier study of these cooling systems in the Birchwood area, Render (1981) suggests that failure may be inevitable. However, there appears to have been relatively little change in temperature since that time. Temperature changes occur most rapidly during the first few years of operation in these systems and subsequent changes in temperature appear to be related to changes in the operation of production and injection wells. The size of the overall thermal anomaly is also predicted to grow in areal extent after the initial increase in temperature is observed at the production wells. This is likely due to horizontal conductive heat transport occurring perpendicular to the direction groundwater flow.

Render (1981) also suggested that any model of the Birchwood area would have to incorporate conduits to accurately represent groundwater and heat flow processes in the area. Fractures are clearly important in the model but they seem to have a high enough frequency, at least in some areas, that their overall effect can be represented with a conventional porous media or dual continuum approach. The results of the numerical models in the Birchwood area also suggest that it may be more critical to locate areas where fractures are absent rather than delineating areas where they are present. More complete knowledge of a fracture network's distribution would

allow for more reliable predictions of advective heat transport in the Carbonate Rock Aquifer.

9.4 Summary of Results of Case Studies

Dual continuum models do not appear to perform significantly better than conventional porous media models in the prediction of subsurface heat flow in either of the two case studies presented. This might be due to our state of knowledge of the Carbonate Rock Aquifer, which is relatively poor with respect to the properties at specific depths within the carbonate rock underlying Winnipeg. Sensitivity analyses do indicate that dual continuum models are less sensitive to changes in material properties than conventional porous media models. However, this must be weighed against the greater uncertainty in fracture and matrix properties compared to effective properties measured over large intervals of the aquifer. Generally only transmissivities are known but the incorporation of vertical layering of aquifers and aquitards is required to produce reasonable results in some situations. In this study, the location of some of these variations is known but the hydraulic properties were found based on transmissivities, drill logs, geophysical data and trial-and-error style calibration of the models. In addition to vertical heterogeneity, horizontal variations in material properties must also be considered. The presence of lateral variations in material properties is known to have affected temperatures at a production well in the industrial property in St. Boniface and is suspected to have caused a discrepancy between predicted and observed temperatures in the Birchwood area.

The extent of the temperature anomaly resulting from the injection of thermal wastewater was is approximately 200 metres in all cases. The highest temperatures within these anomalies are present between the injection and production wells and the majority of the increase in this area occurs in the first few years of operation. After this time, the size of the anomaly is predicted to increase outward but there are no long-term records from monitoring wells at an appropriate distance that corroborate this idea.

	Porous Media Model				Dual Continuum Model			
	Upper Aquifer	Upper	Middle	Lower	Upper Aquifer	Upper	Middle	Lower
Matrix Permeability (m^2)	1.0×10^{-9}	1.0×10^{-10}	5.0×10^{-13}	1.0×10^{-11}	1.0×10^{-13}	1.0×10^{-13}	1.0×10^{-13}	1.0×10^{-13}
Fracture Permeability ($m^{2)}$)	N/A	N/A	N/A	N/A	5.0×10^{-8}	2.0×10^{-10}	2.0×10^{-10}	1.0×10^{-9}
Matrix Porosity	0.10	0.10	0.10	0.10	0.10	0.10	0.10	0.10
Fracture Porosity	N/A	N/A	N/A	N/A	0.05	0.01	0.001	0.005
Fracture Spacing (m)	N/A	N/A	N/A	N/A	0.5	10.0	10.0	5.0
Thermal Conductivity ($W\ m^{-1}\ ^{\circ}C^{-1}$)	2.4	2.4	2.4	2.4	2.4	2.4	2.4	2.4
Heat Capacity ($J\ kg^{-1}\ ^{\circ}C^{-1}$)	1200	1200	1200	1200	1200	1200	1200	1200

Table 9.1: Thermal and hydrogeologic properties used in the conventional porous media and dual continuum models of the industrial property in eastern St. Boniface.

Well	Withdrawal Well I.D.	Injection Well I.D.	Estimated Withdrawal Rate (L/s)	Year System Installed	Year Temperature Recording Began
2600/2610 Portage Avenue	GM231	GM232	16	1973	1976
Birchwood Inn	GM225	GM226	28.5*	1977	2002
Pinewood Place	GM227	GM228	19	1673	1976 (1986 for injection)
Birchwood Terrace	GM125	No injection well	19	1965	None

*Birchwood Inn recharges only a portion of the water withdrawn and it is estimated that the injection rate is only 22.2 L/s.

Table 9.2: Records available from Manitoba Water Branch for groundwater use in the Birchwood area (after Render, 1981).

	Porous Media Model				Dual Continuum Model			
	Upper Aquifer	Middle Unit	Lower Aquifer	Lower Unit	Upper Aquifer	Middle Unit	Lower Aquifer	Lower Unit
Matrix Permeability (m^2)	1.0×10^{-10}	1.0×10^{-12}	1.0×10^{-11}	1.0×10^{-12}	1.0×10^{-12}	1.0×10^{-13}	1.0×10^{-13}	1.0×10^{-13}
Fracture Permeability ($m^{2)}$)	N/A	N/A	N/A	N/A	1.0×10^{-9}	1.0×10^{-9}	1.0×10^{-9}	1.0×10^{-9}
Matrix Porosity	0.05	0.05	0.05	0.05	0.05	0.05	0.05	0.05
Fracture Porosity	N/A	N/A	N/A	N/A	0.05	5.0×10^{-5}	5.0×10^{-3}	5.0×10^{-5}
Fracture Spacing (m)	N/A	N/A	N/A	N/A	5.0	10.0	5.0	20.0
Thermal Conductivity (W m^{-1} °C^{-1})	2.4	2.4	2.4	2.4	2.4	2.4	2.4	2.4
Heat Capacity (J kg^{-1} °C^{-1})	1200	1200	1200	1200	1200	1200	1200	1200

Table 9.3: Thermal and hydrogeologic properties used in the conventional porous media and dual continuum models of the Birchwood area of Winnipeg.

258
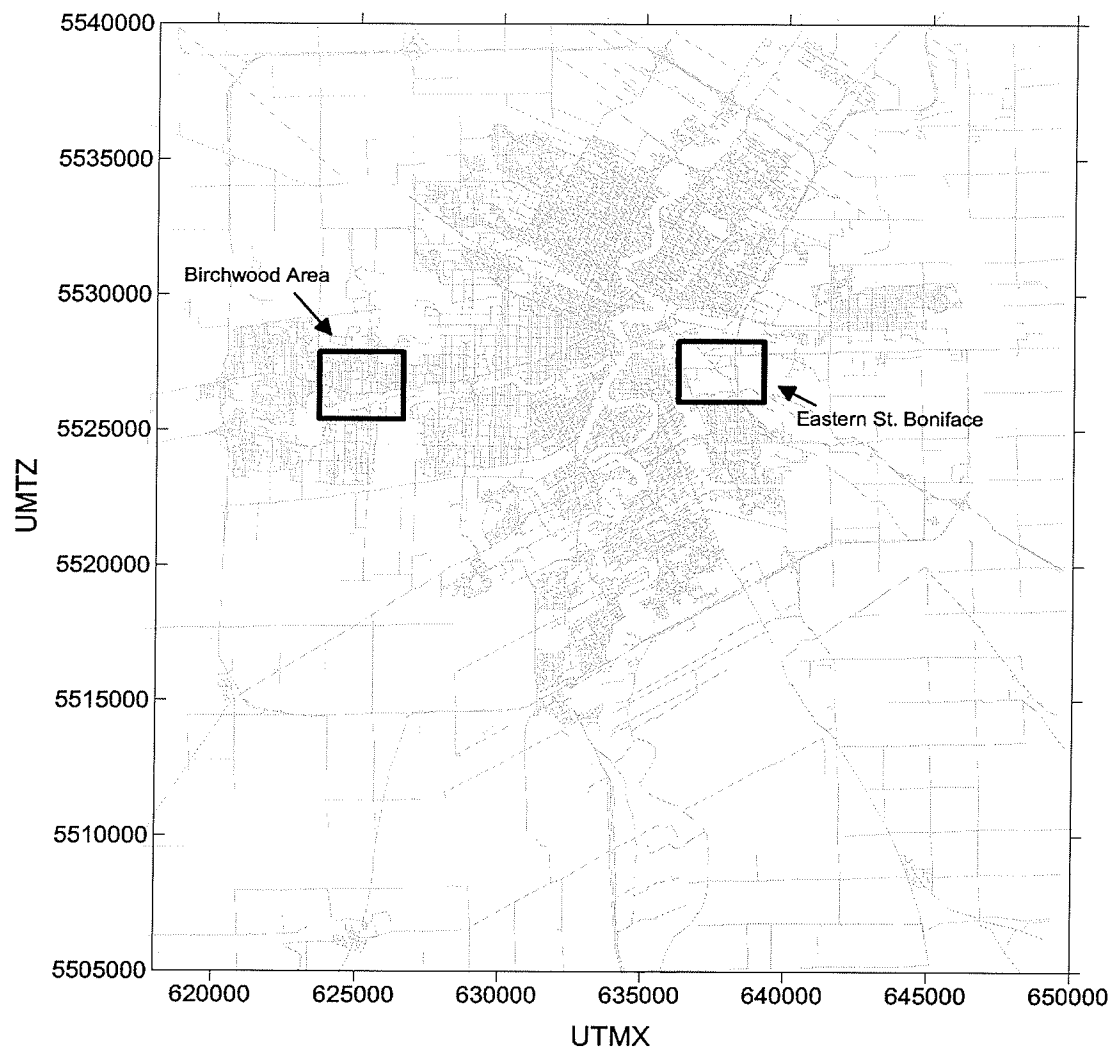
Figure 9.1: Location of case studies in Winnipeg.
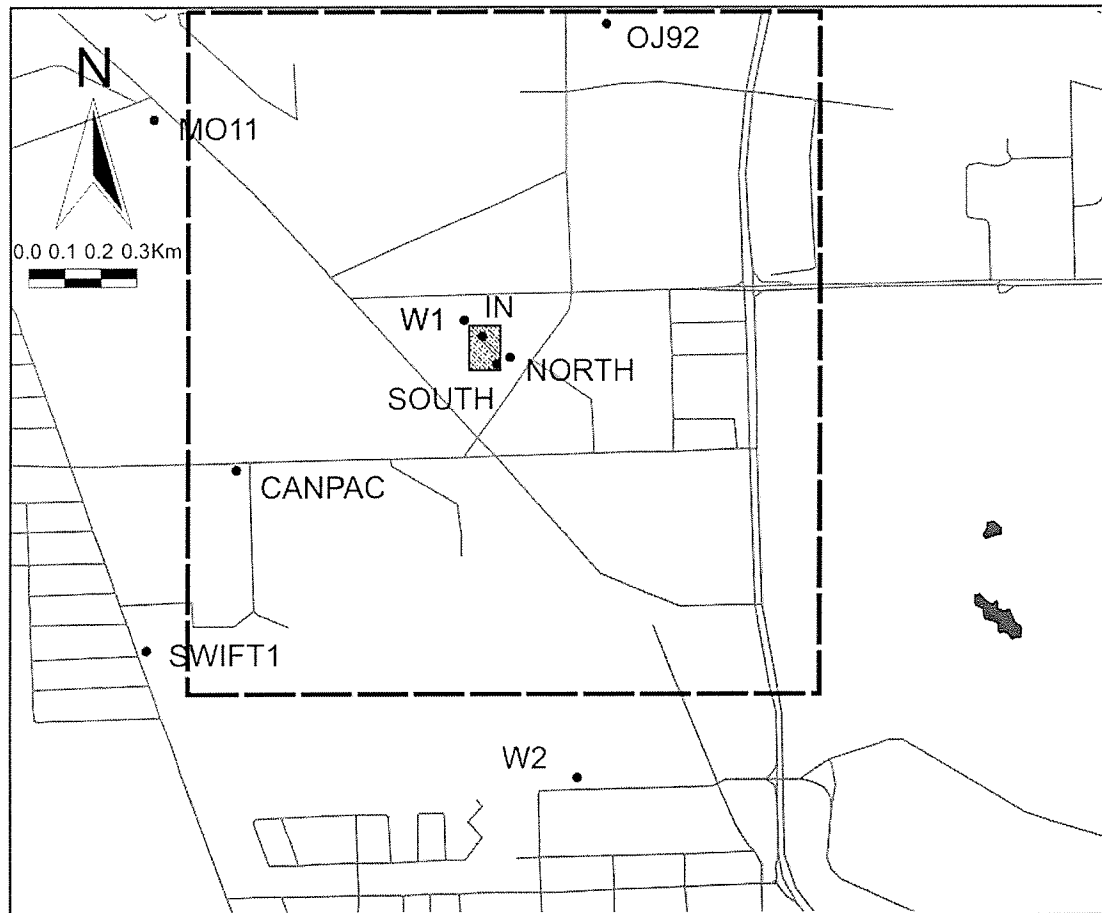
Figure 9.2: Map of the St. Boniface area of Winnipeg showing the location of observation wells and the property to investigated in this study. Wells "IN", "SOUTH" and "NORTH" represent the injection well, southern production well and northern production well on the property of interest. Shaded area around wells "IN" and "SOUTH" represents zone of increased permeability.
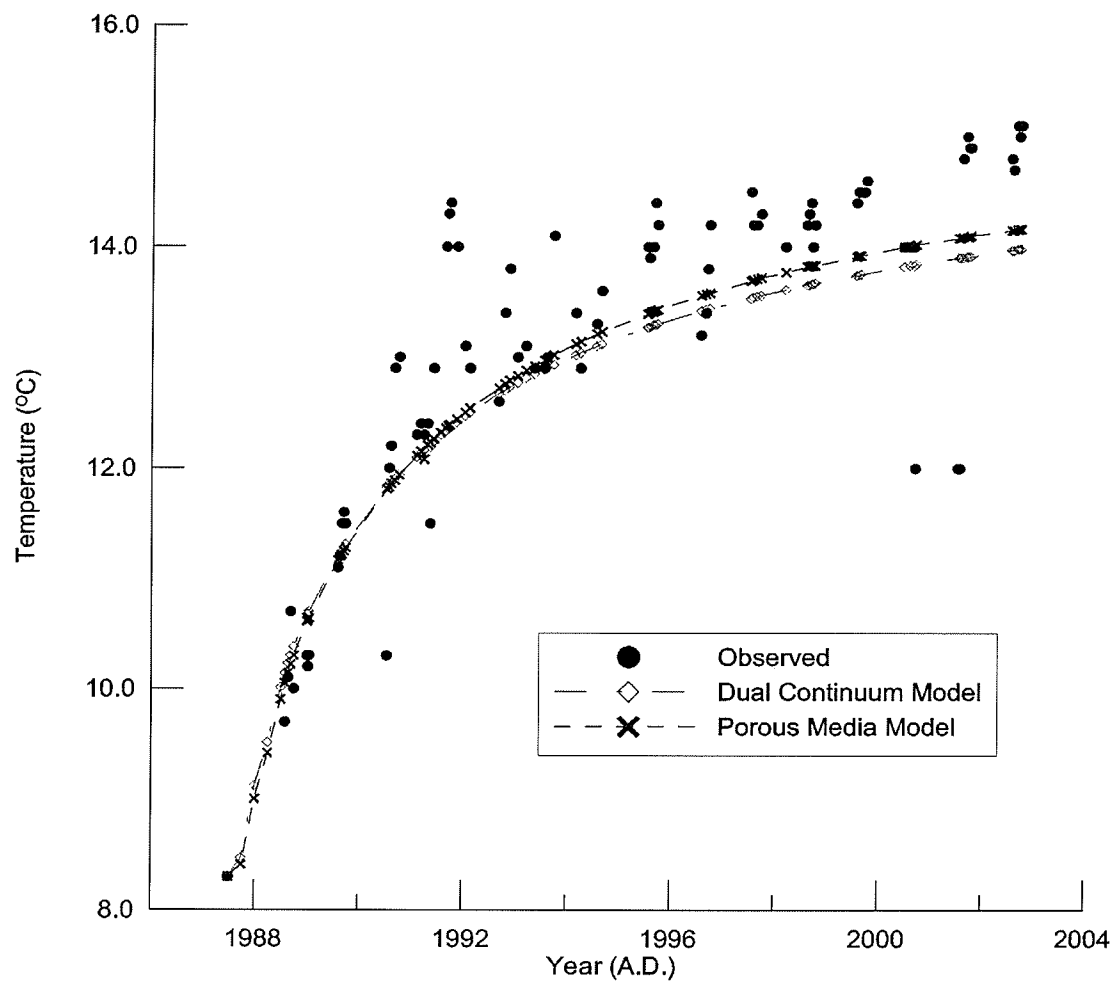
Figure 9.3: Measured and modeled temperatures at the northern production well at the industrial site in St. Boniface.
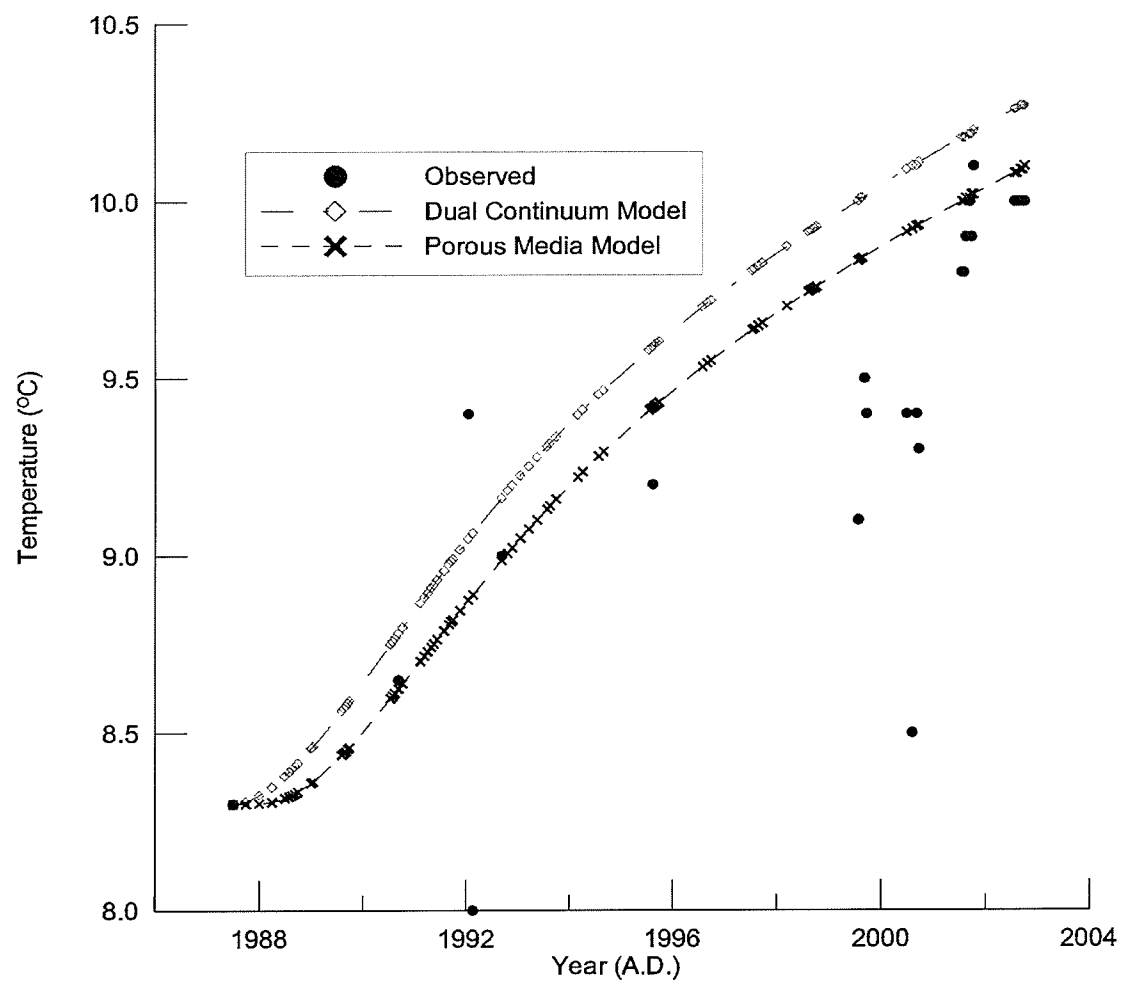
Figure 9.4: Measured and modeled temperatures at the northern production well at the industrial site in St. Boniface.
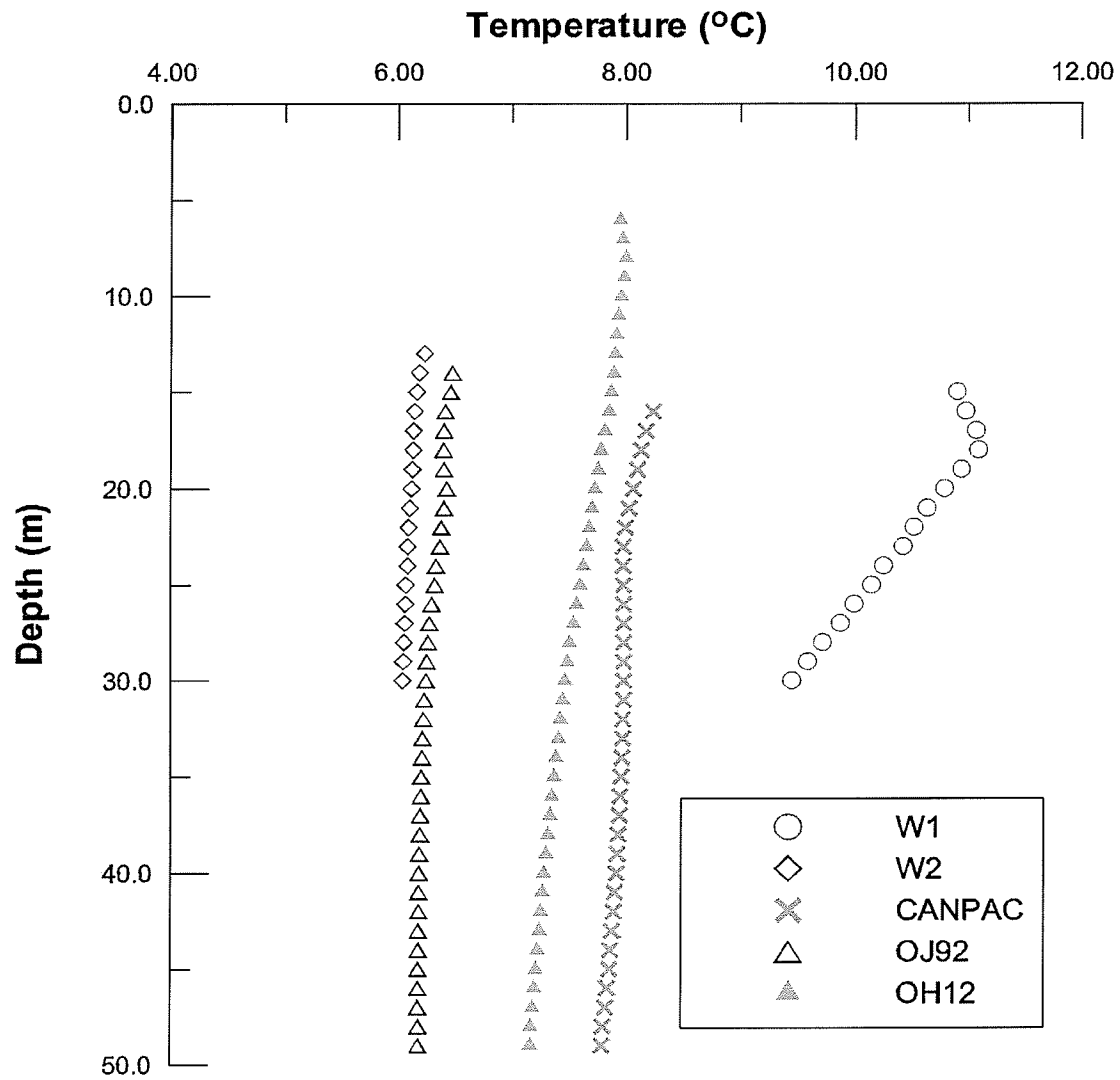
Figure 9.5: Temperature profiles at observation wells in the St. Boniface area of Winnipeg.

263
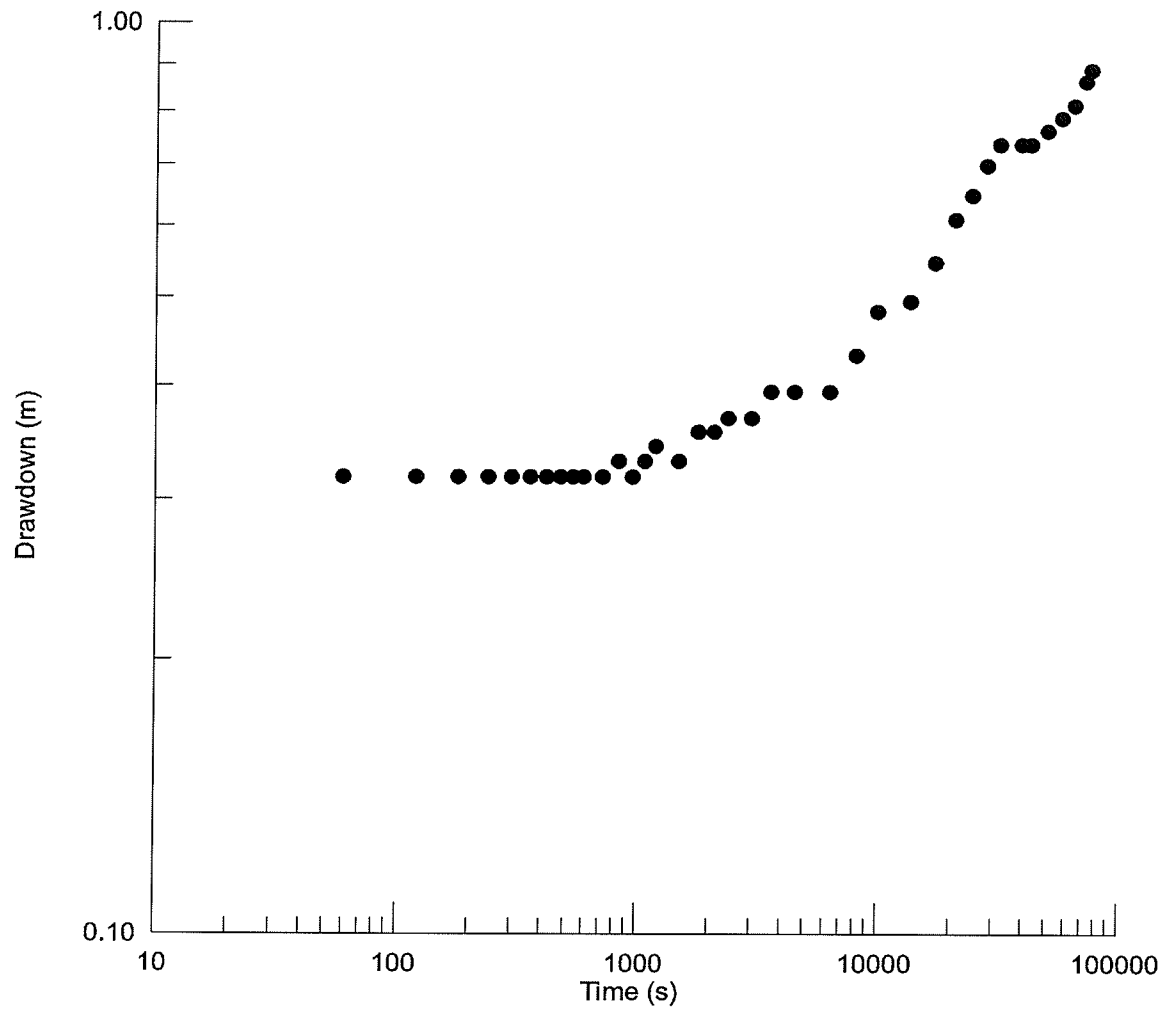
Figure 9.6: Specific capacity test data for injection well on the modeled industrial property in eastern St. Boniface.

Figure 9.7: Specific capacity test data for the northern production well on the modeled industrial property in eastern St. Boniface.
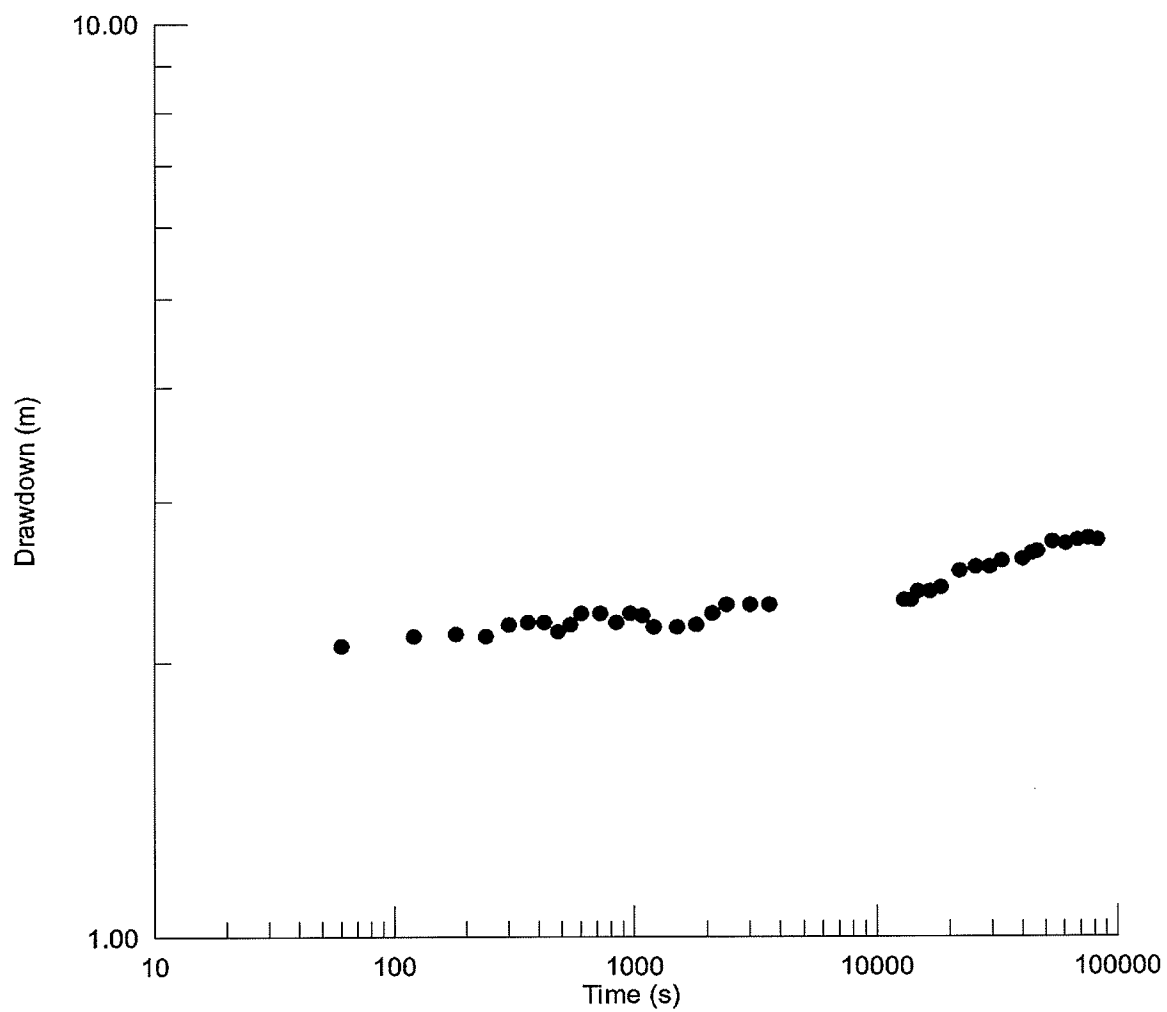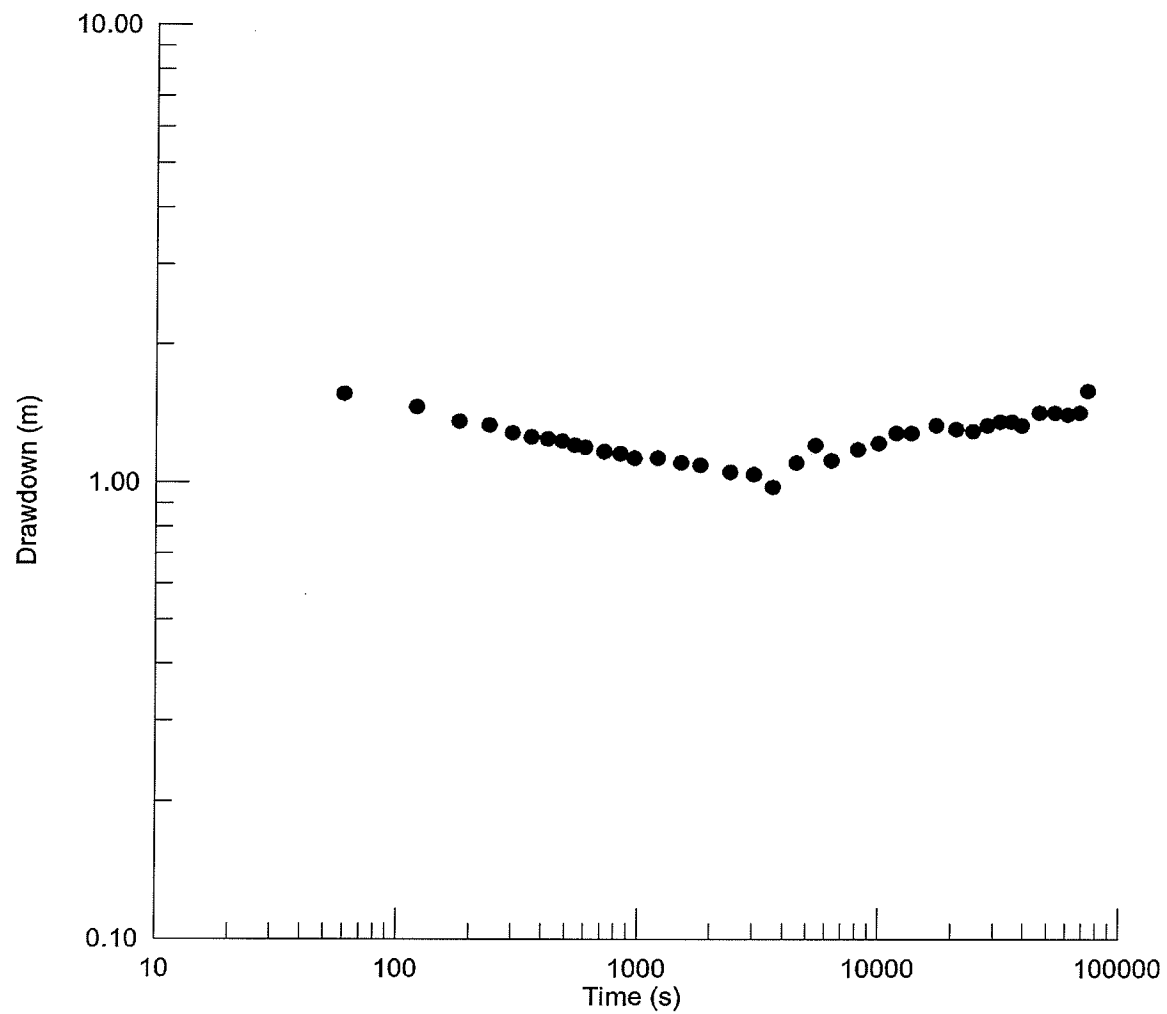
Figure 9.8: Specific capacity test data for the southern production well on the modeled industrial property in eastern St. Boniface.
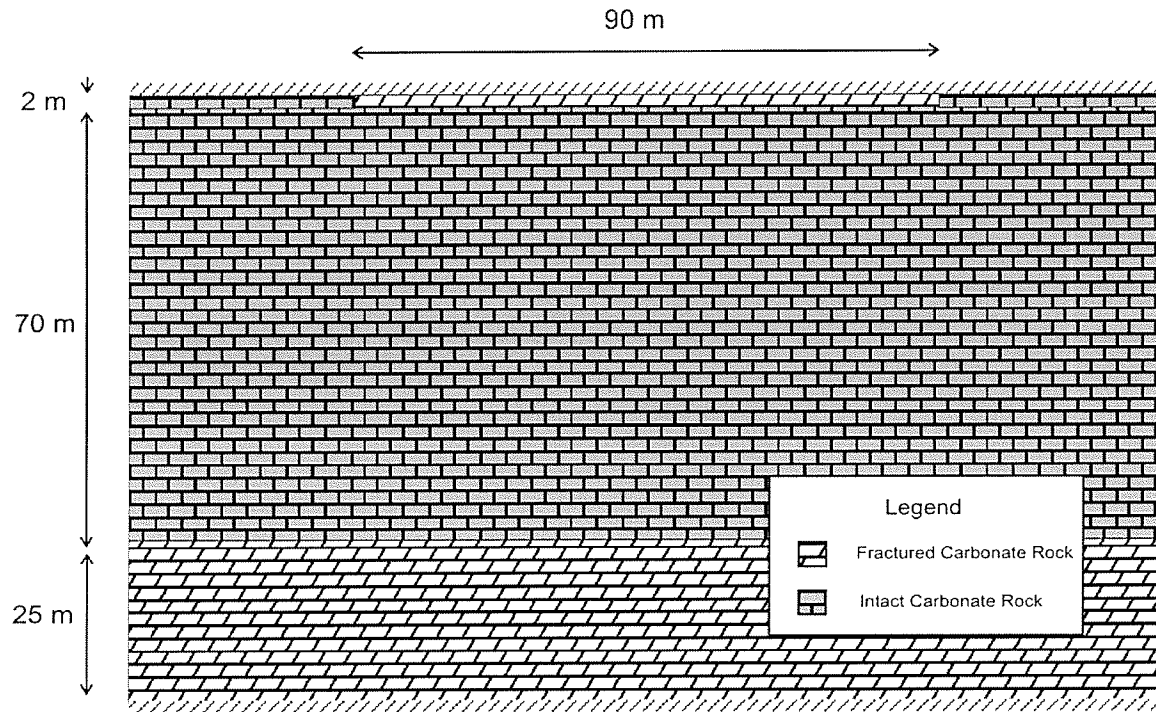
Figure 9.9: Cross-section used in the conceptual model of industrial property in St. Boniface.
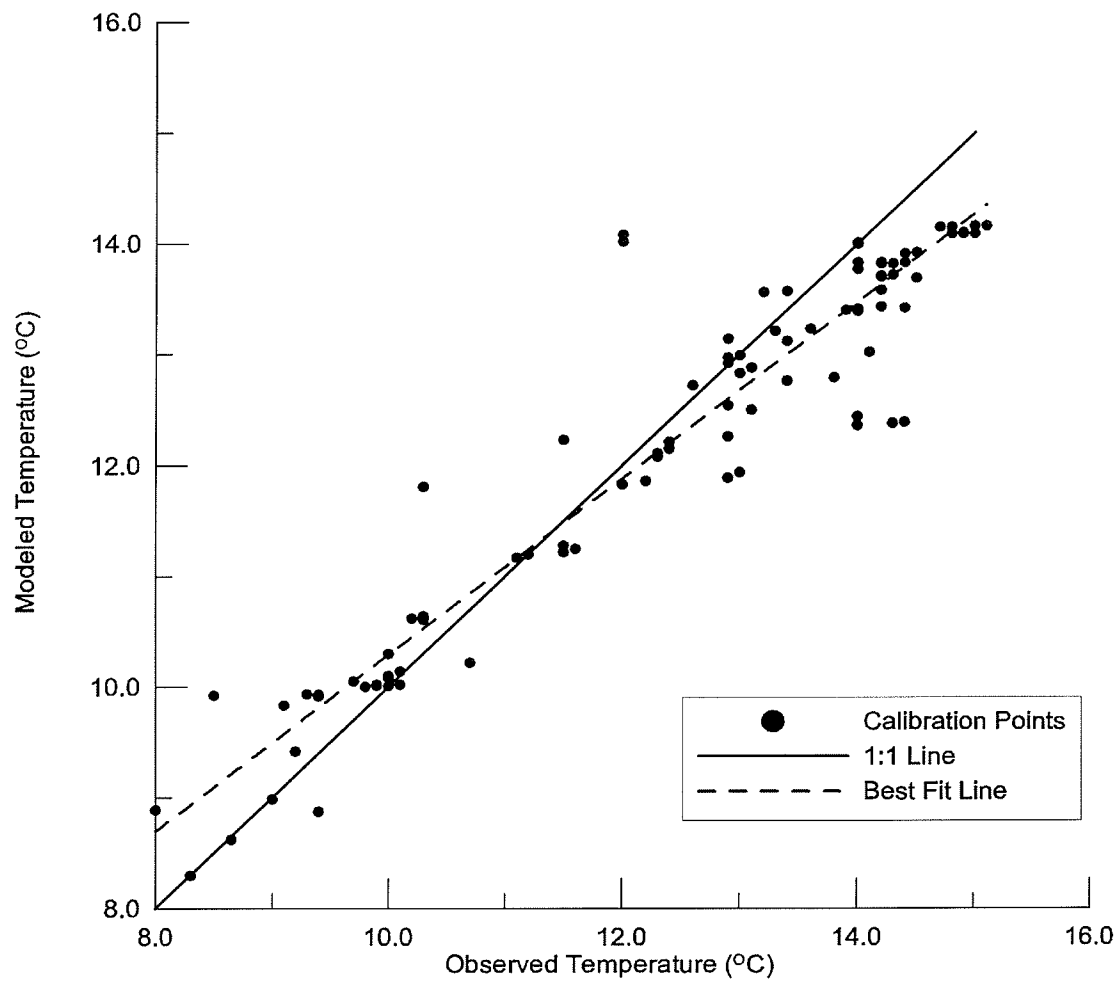
Figure 9.10: Measured versus predicted temperatures in the porous media model of an industrial site in St. Boniface.
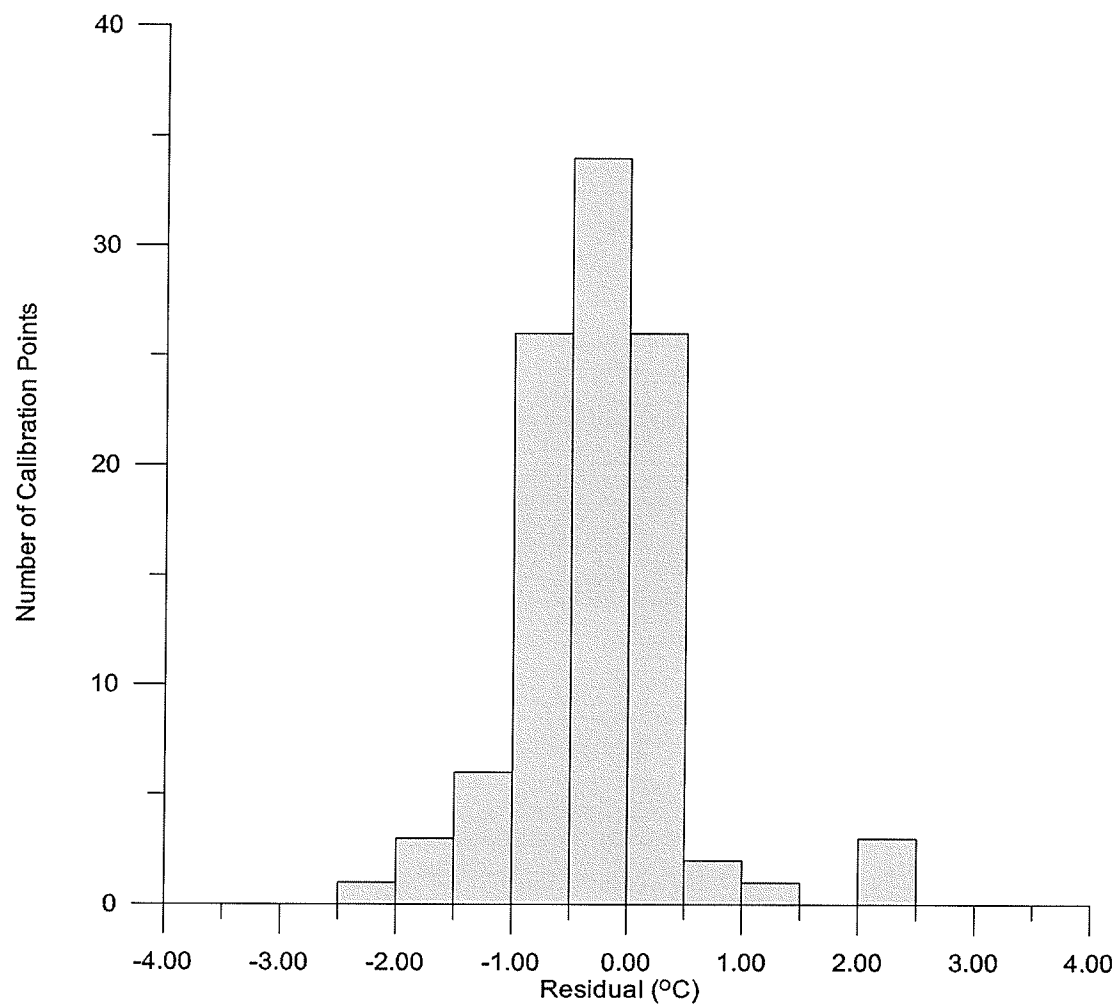
Figure 9.11: Distribution of residual temperatures in the porous media model of an industrial site in St. Boniface.
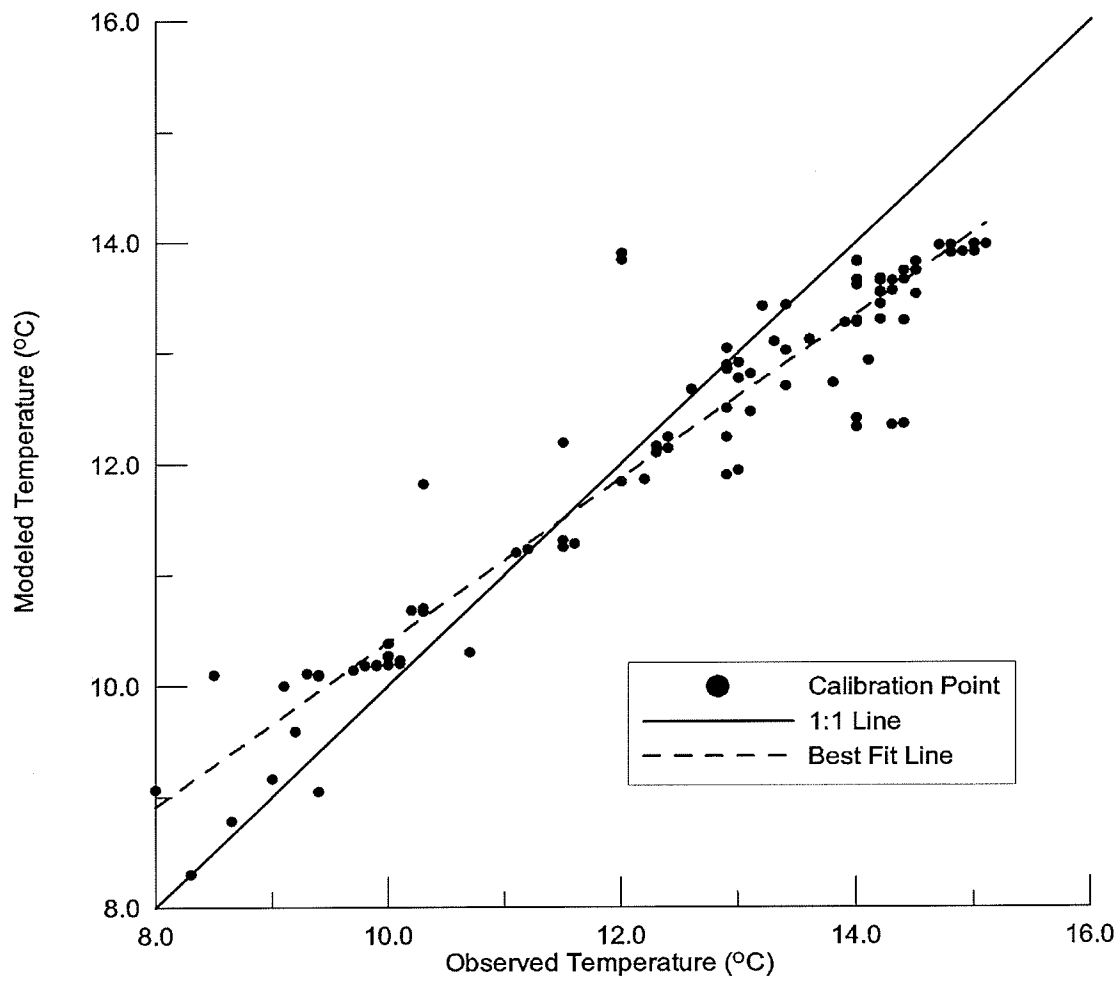
Figure 9.12: Measured versus predicted temperatures in the dual continuum model of an industrial site in St. Boniface.
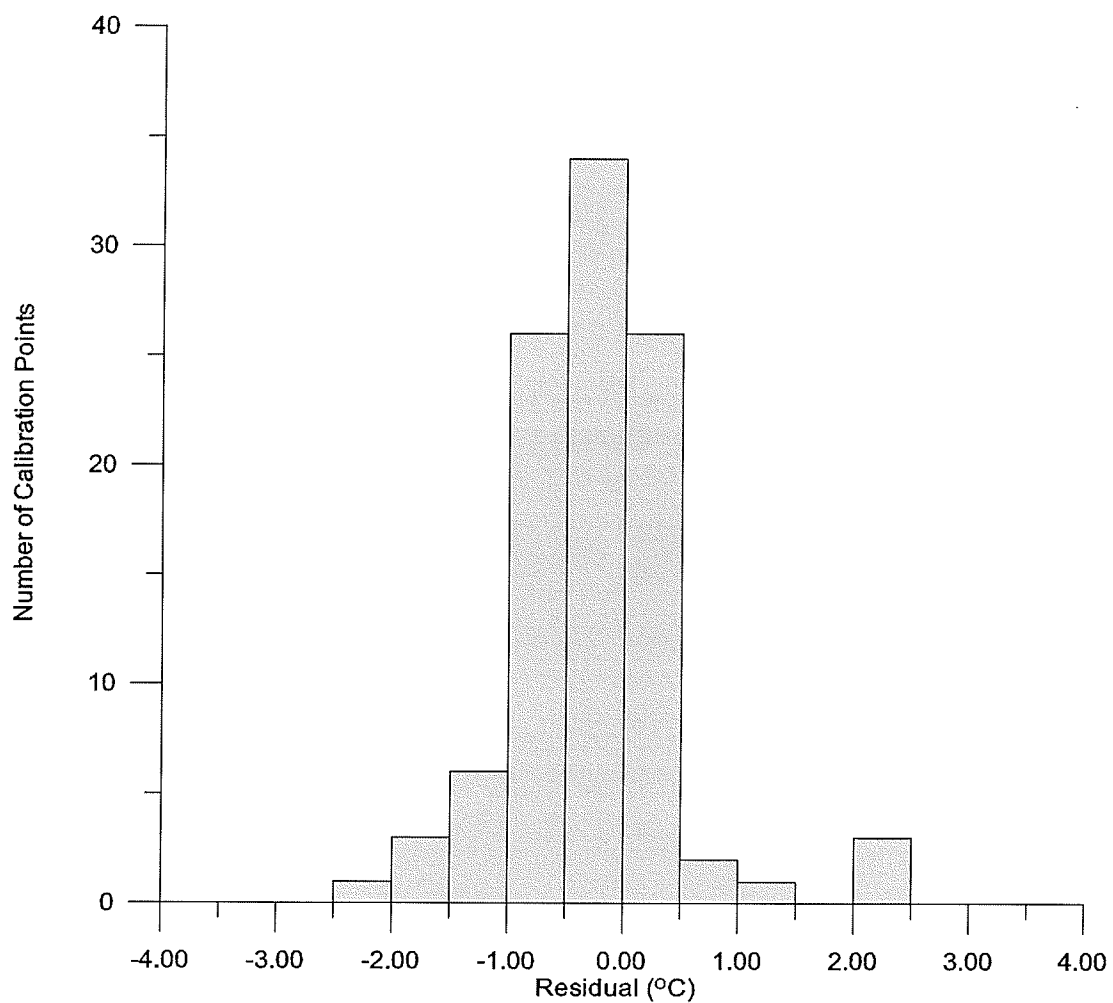
Figure 9.13: Distribution of residual temperatures in the dual continuum model of an industrial site in St. Boniface.
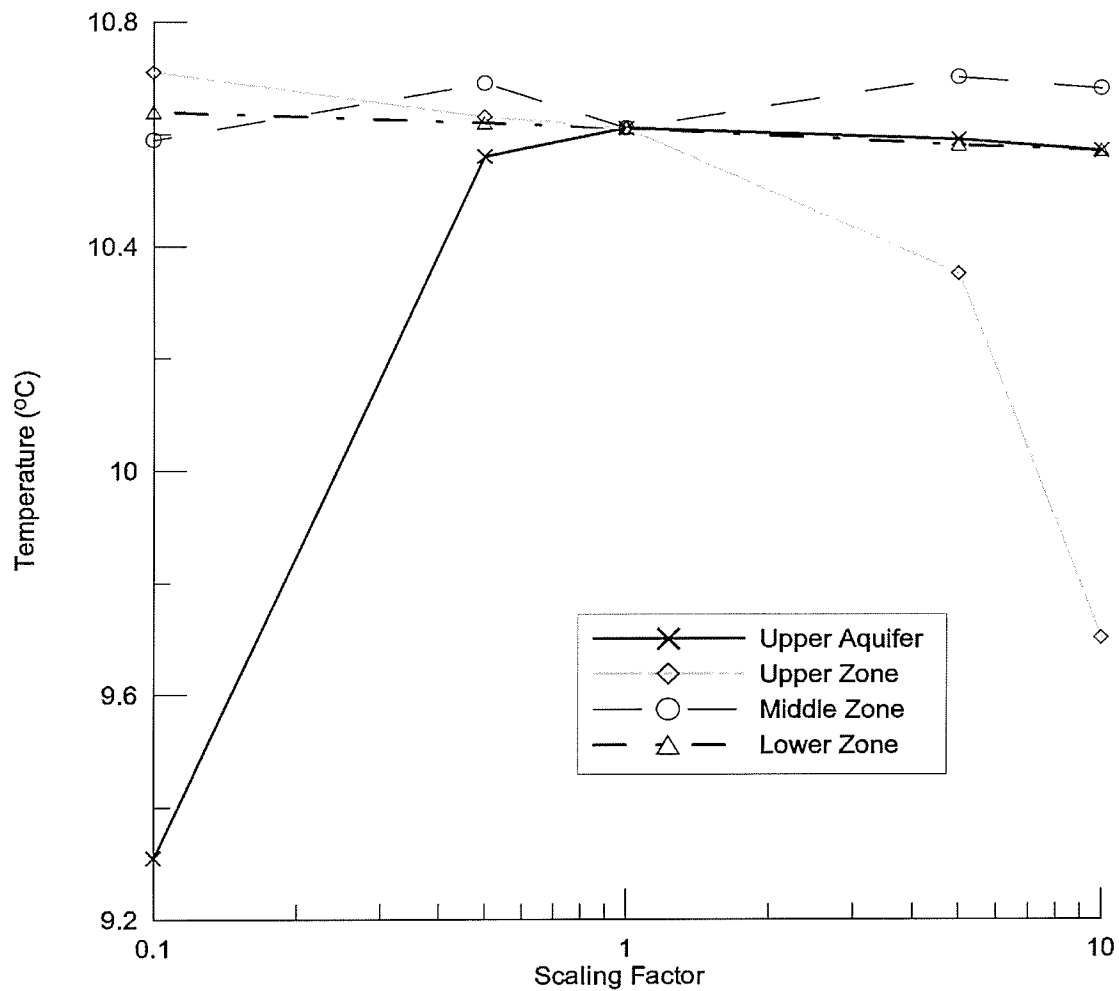
Figure 9.14: Sensitivity of the conventional porous media model of St. Boniface area industrial model to changes in permeability. Scaling factor refers to the number that the permeability of a given unit is multiplied by in a variant of the calibrated model.
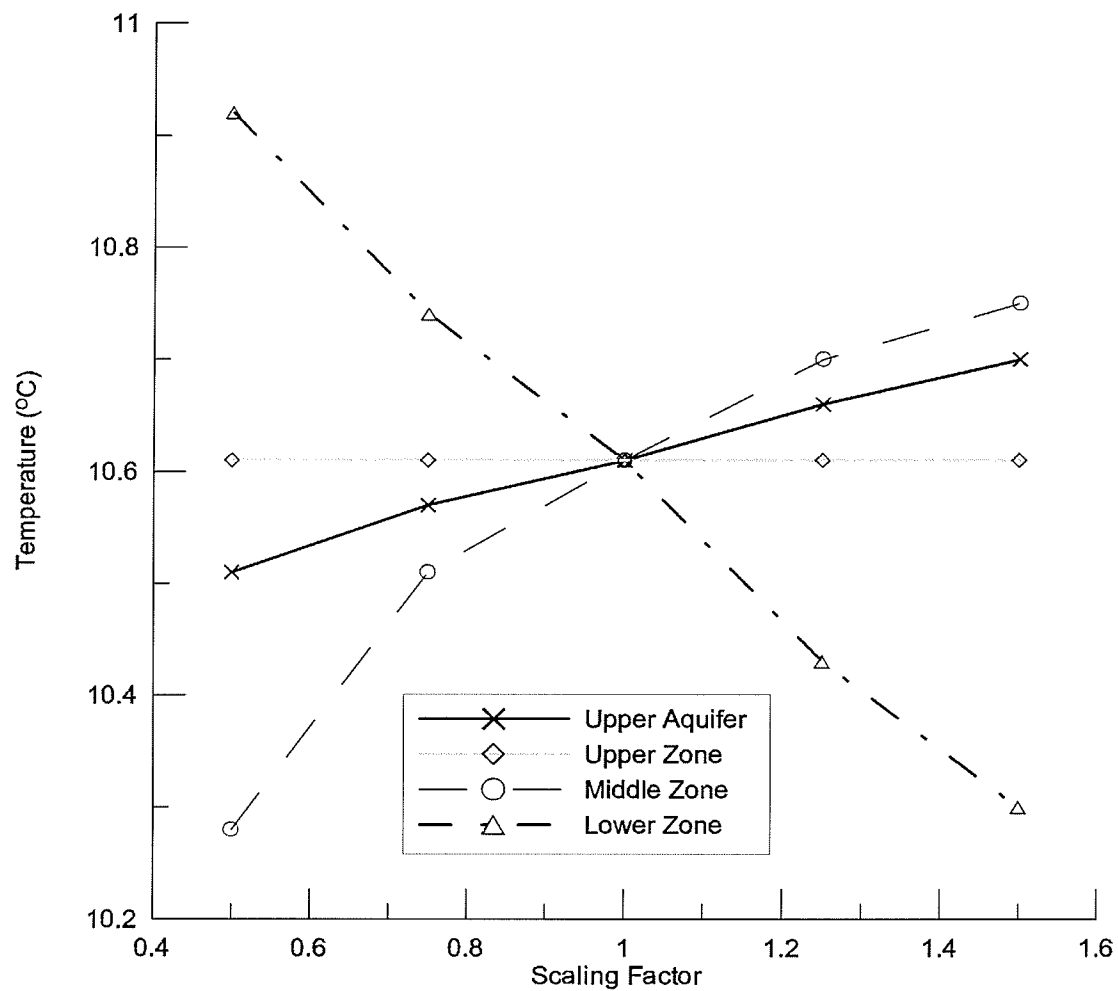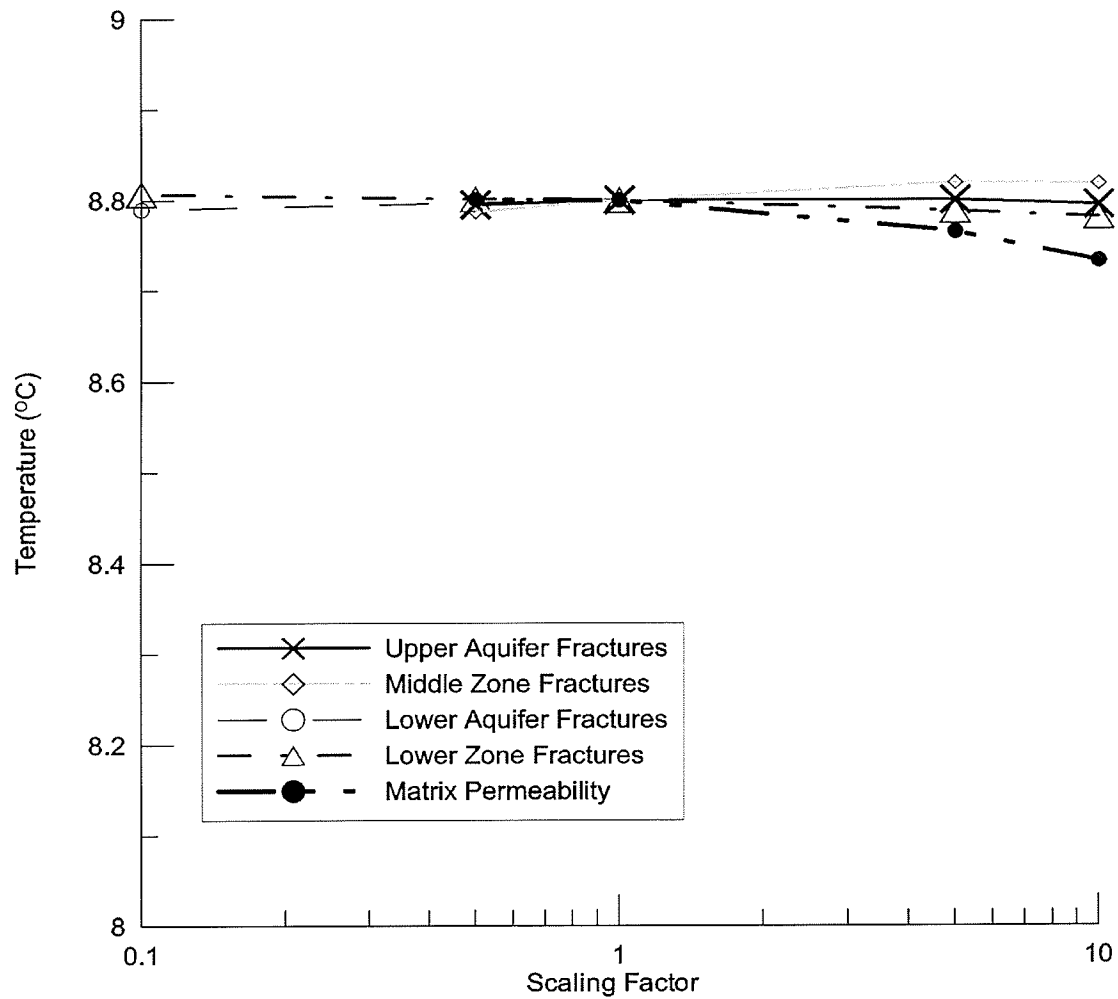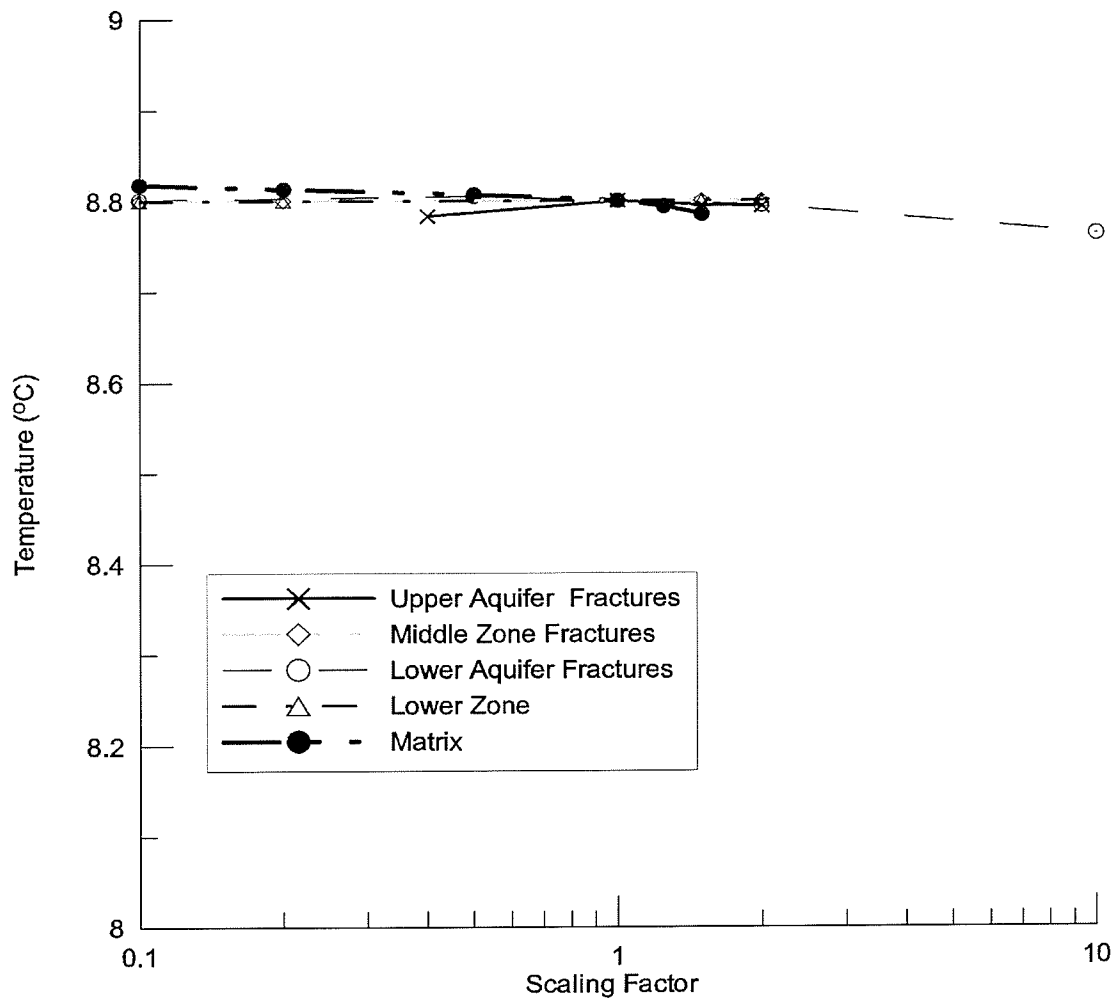
Figure 9.15: Sensitivity of the conventional porous media model of St. Boniface area industrial model to changes in porosity. Scaling factor refers to the number that the porosity of a given unit is multiplied by in a variant of the calibrated model.
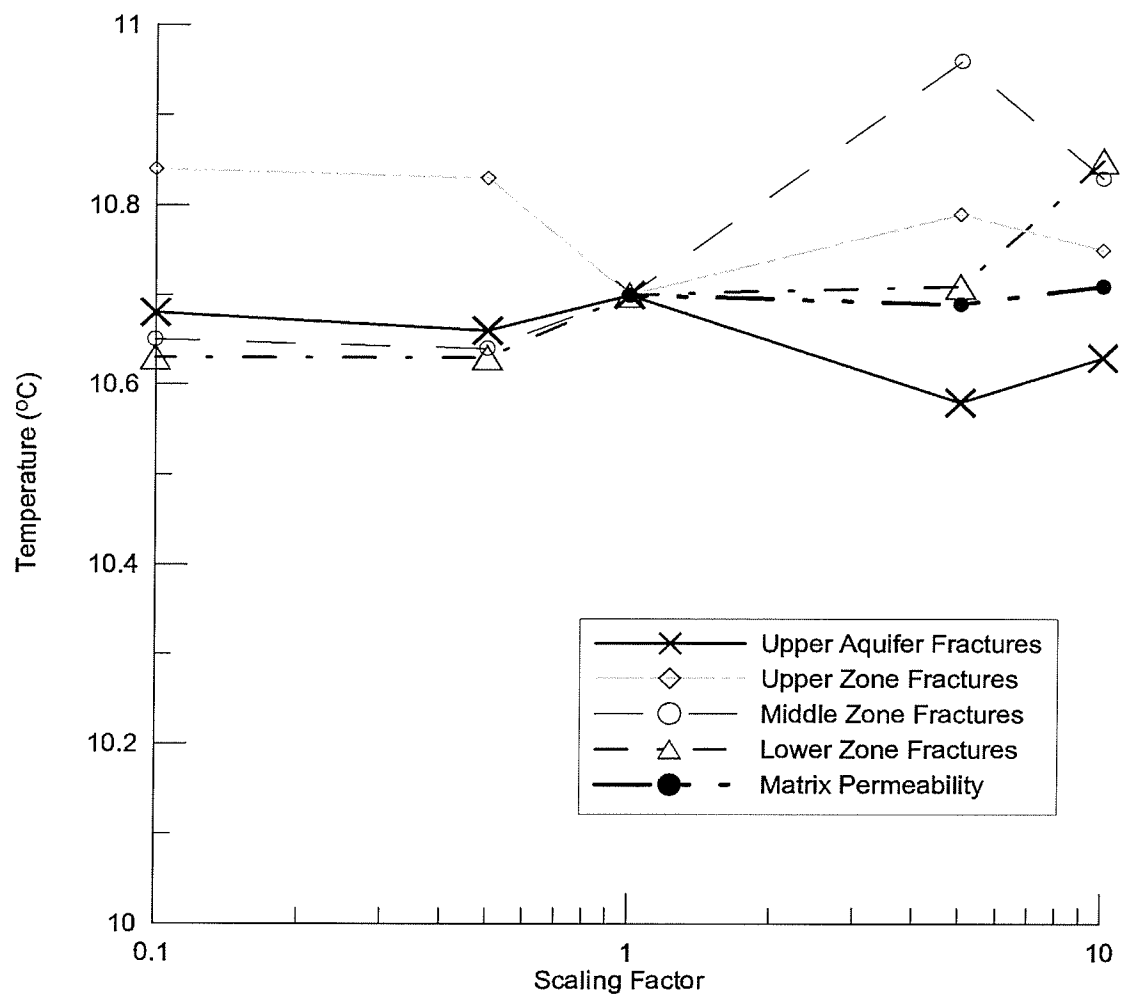
Figure 9.16: Sensitivity of the dual continuum model of St. Boniface area industrial model to changes in permeability. Scaling factor refers to the number that the permeability of a given unit is multiplied by in a variant of the calibrated model.
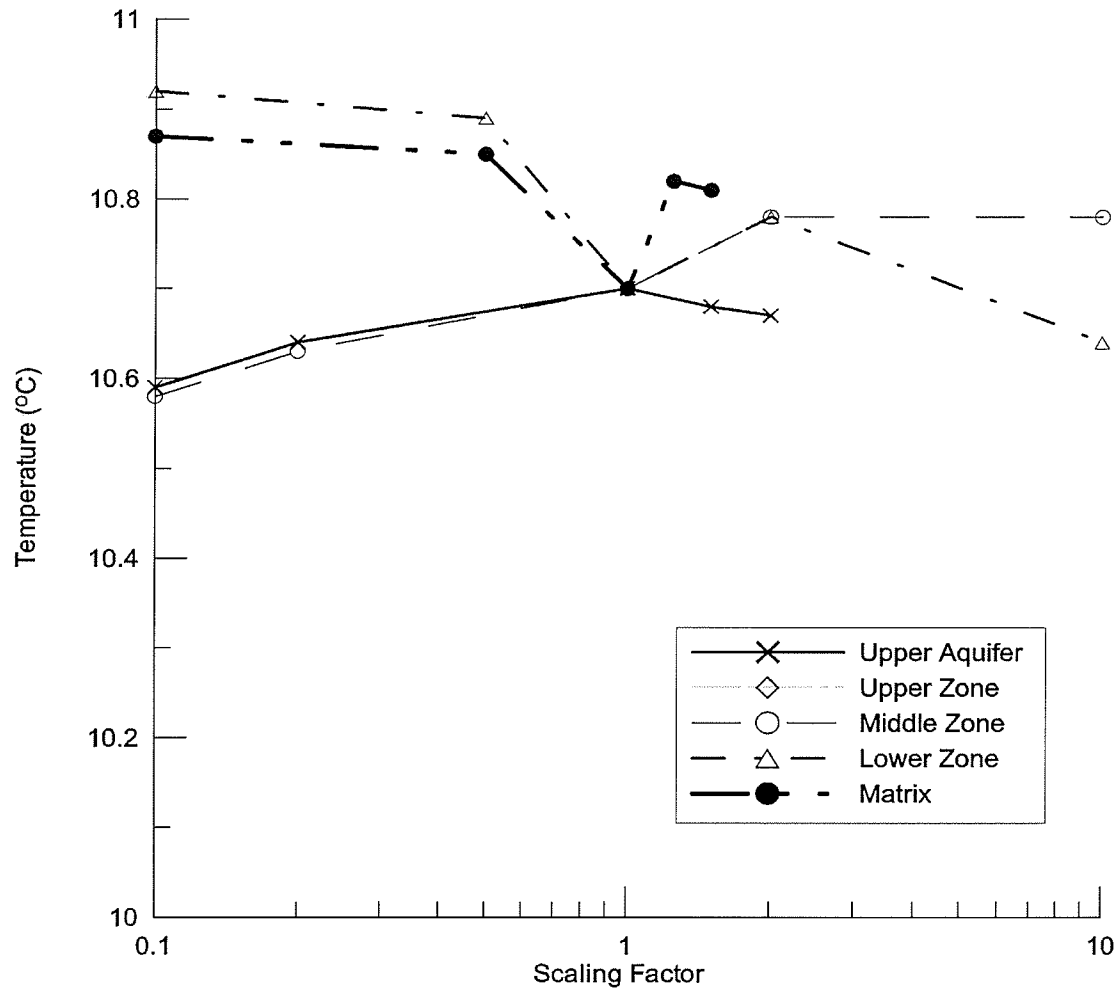
Figure 9.17: Sensitivity of the conventional dual continuum model of St. Boniface area industrial model to changes in porosity. Scaling factor refers to the number that the porosity of a given unit is multiplied by in a variant of the calibrated model.

275
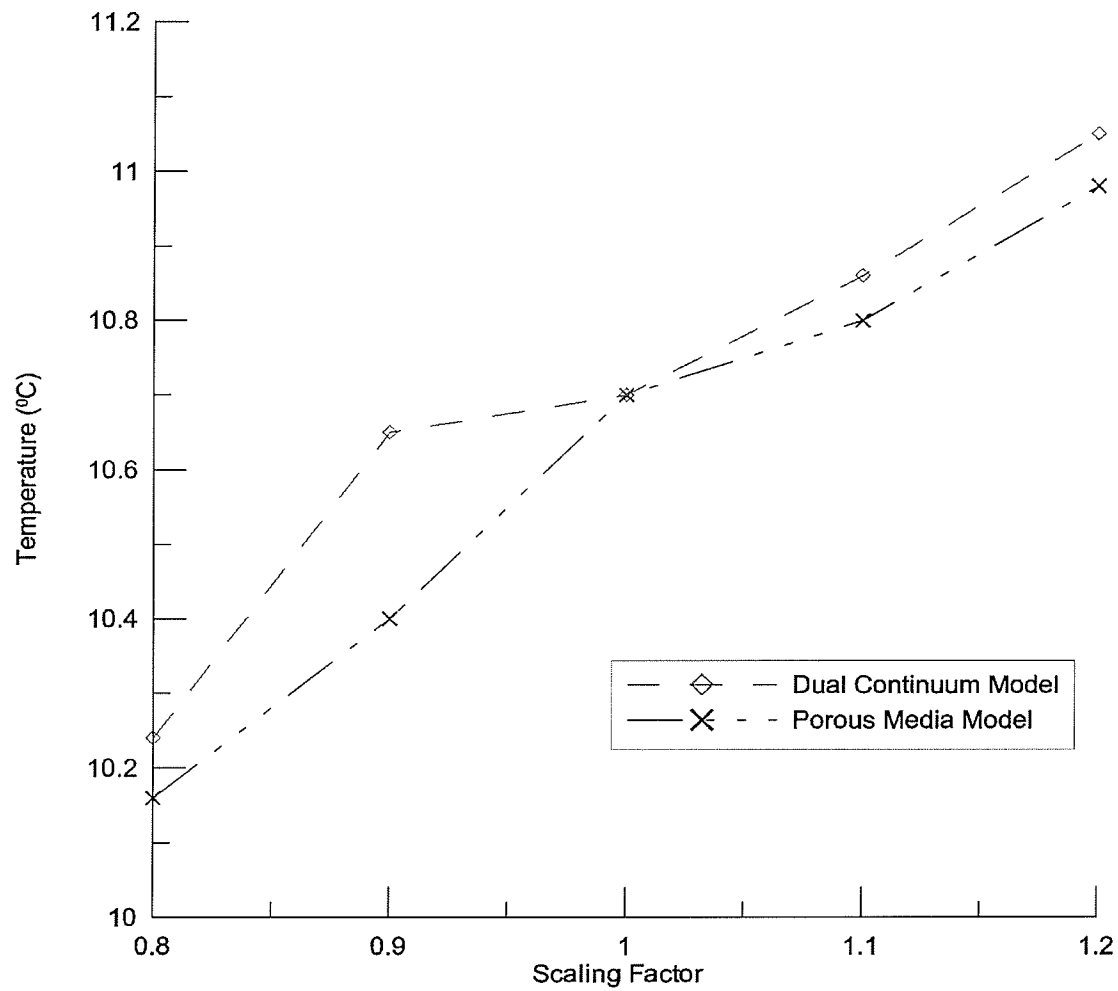
Figure 9.18: Sensitivity of the porous media and dual continuum models of St. Boniface area industrial site to changes in pumping rates. Scaling factor refers to the number that the pumping rates are multiplied by in a variant of the calibrated model.
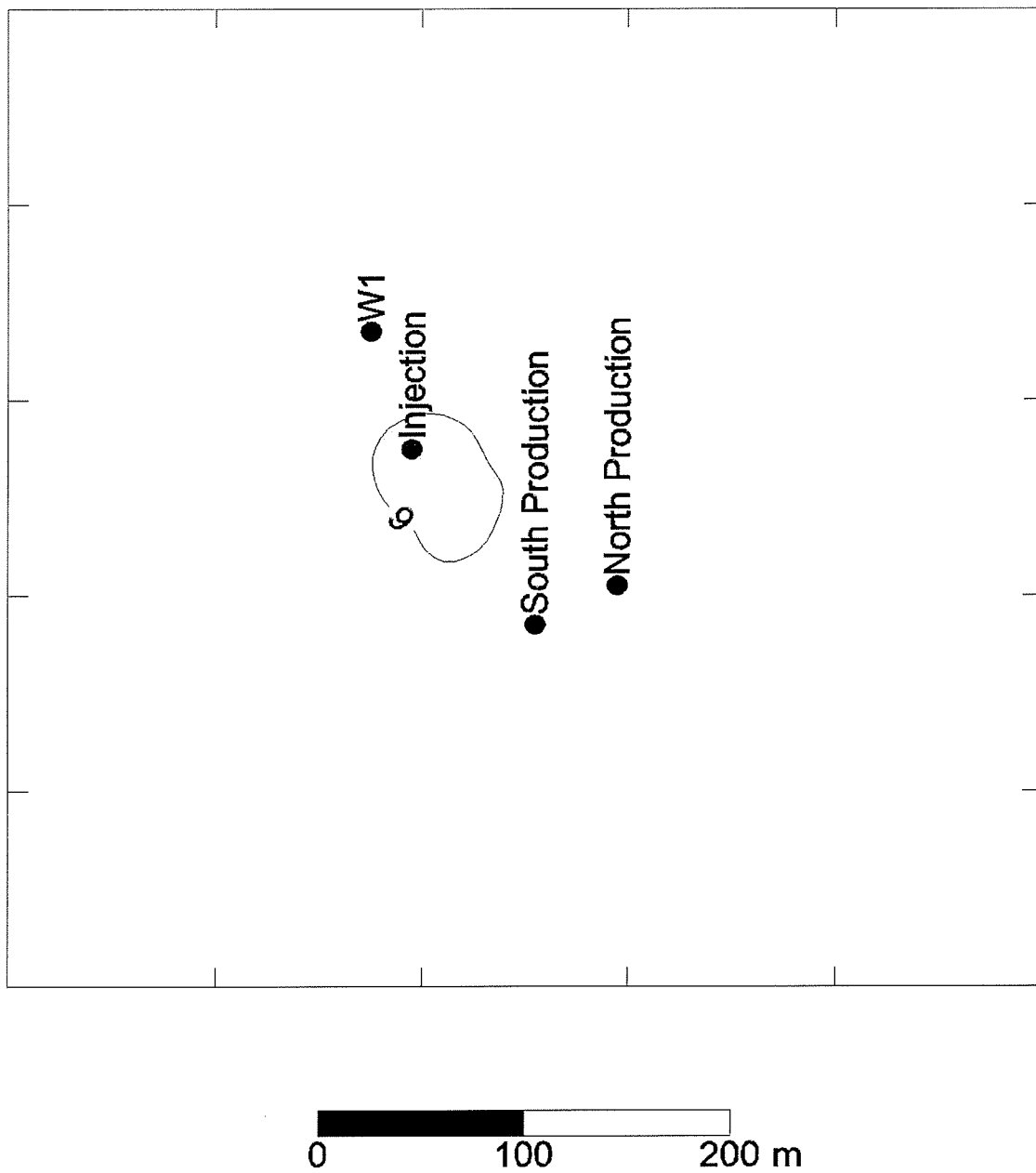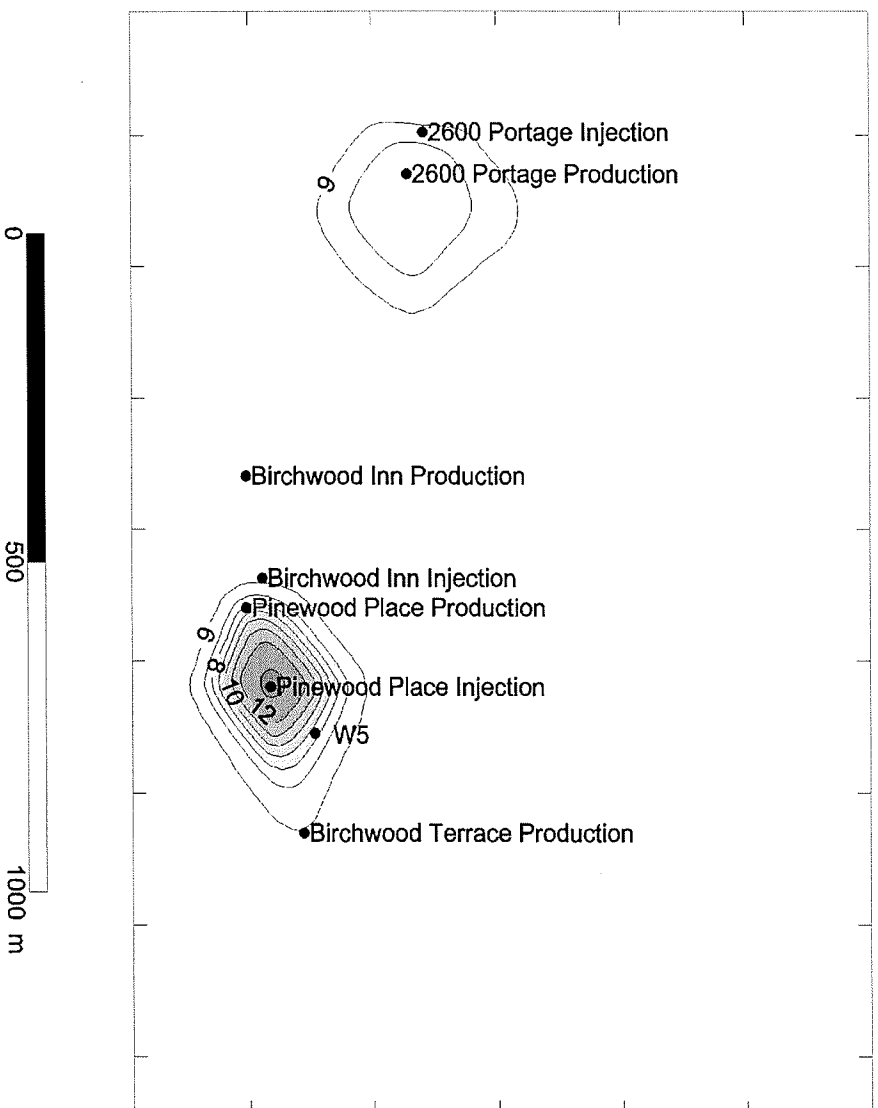
Figure 9.19a: Temperatures predicted by the dual continuum model for the upper 2 metres of the aquifer for at the modeled industrial site in St. Boniface for 0.25 years.
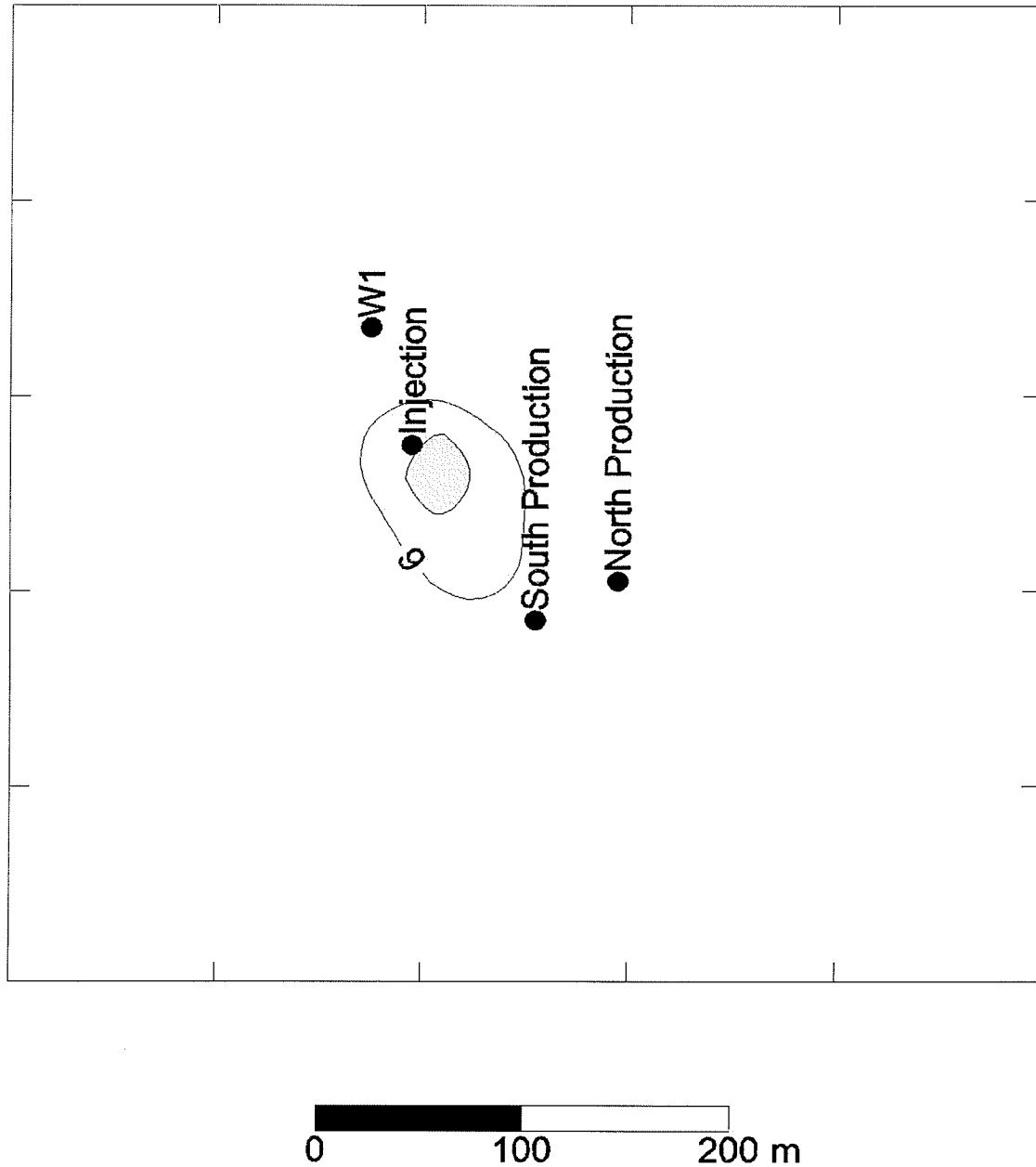
Figure 9.19b: Temperatures predicted by the dual continuum model for the upper 2 metres of the aquifer for at the modeled industrial site in St. Boniface for 0.5 years.
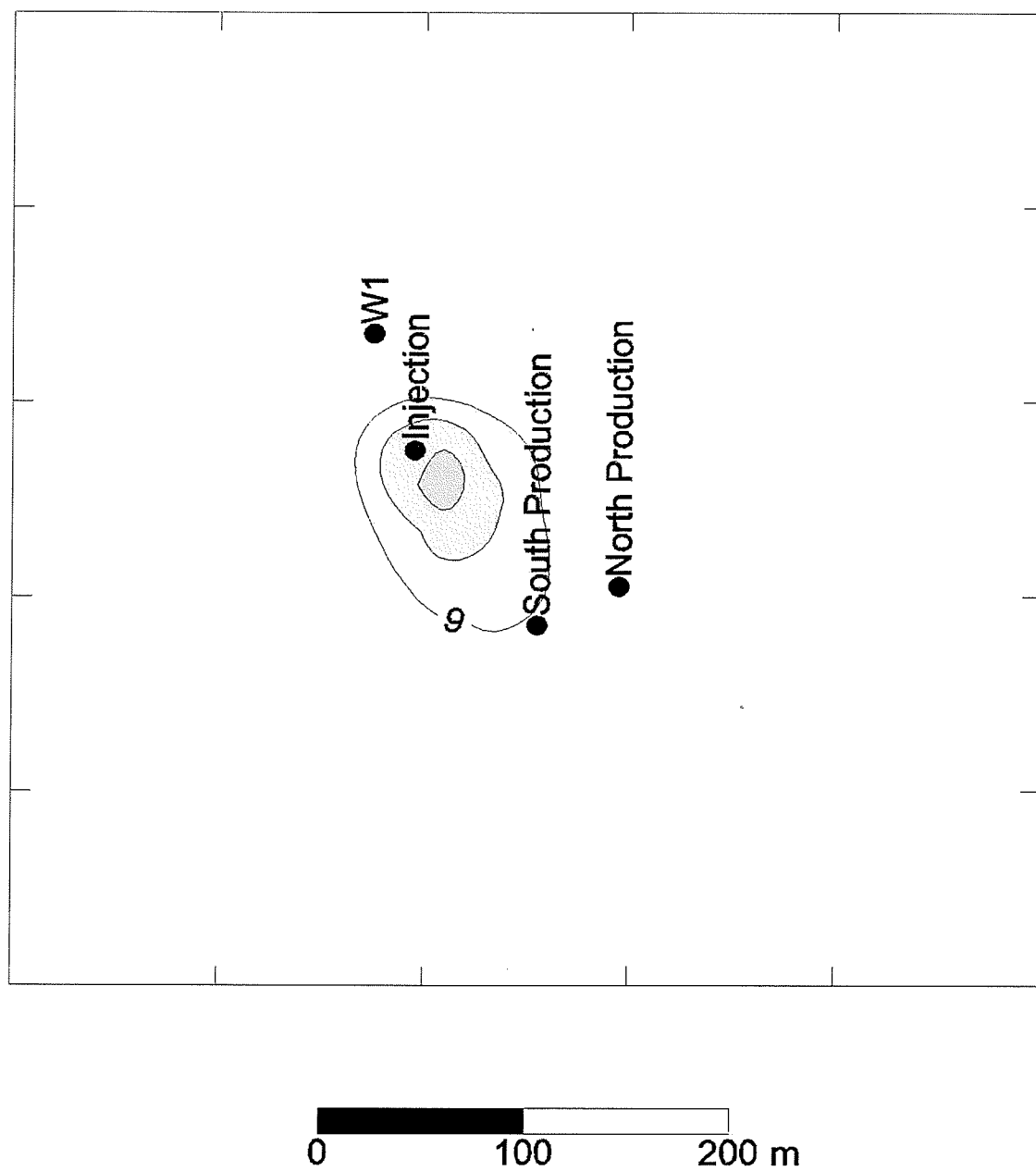
Figure 9.19c: Temperatures predicted by the dual continuum model for the upper 2 metres of the aquifer for at the modeled industrial site in St. Boniface for 0.75 years.
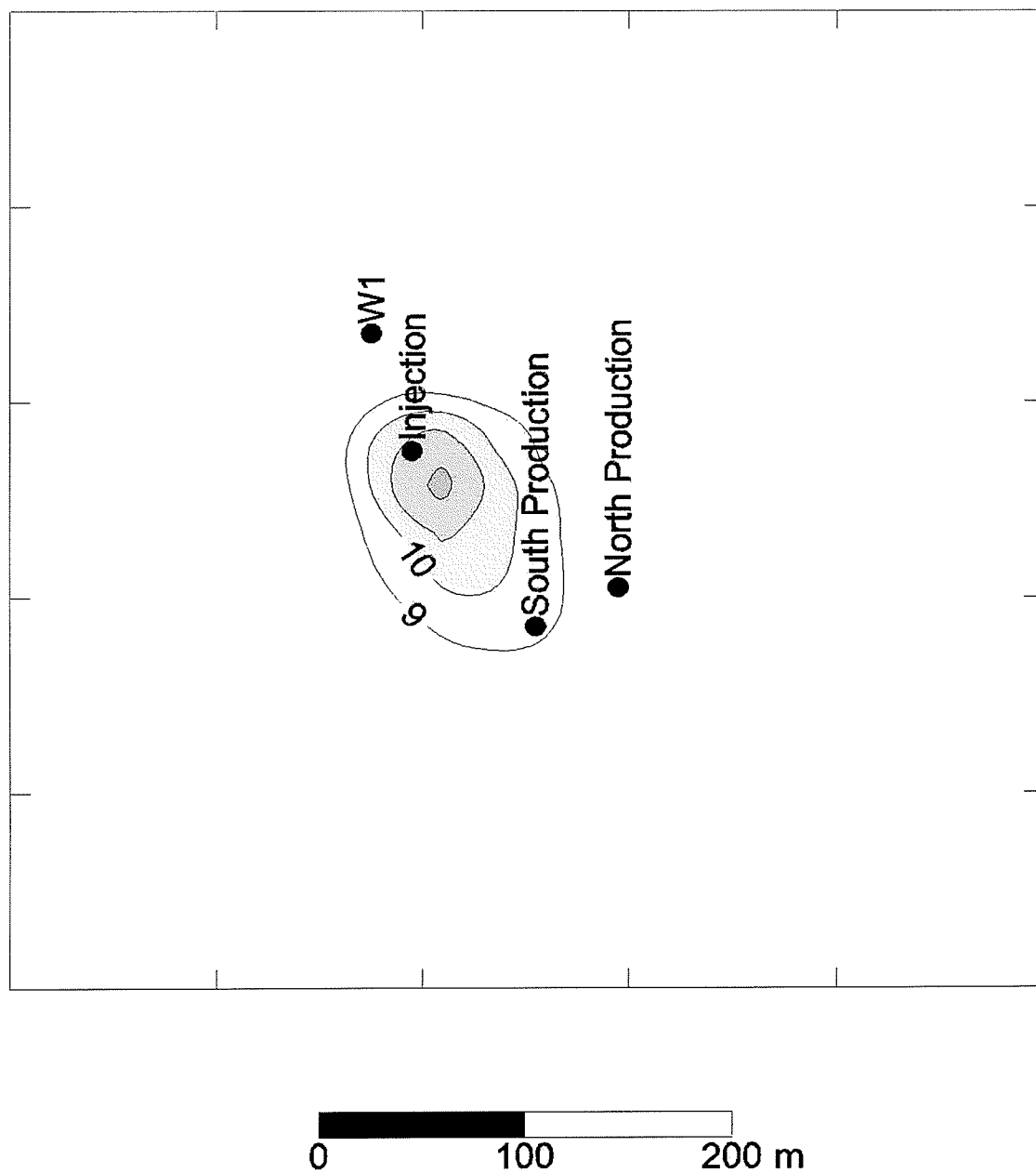
Figure 9.19d: Temperatures predicted by the dual continuum model for the upper 2 metres of the aquifer for at the modeled industrial site in St. Boniface for 1.0 years.
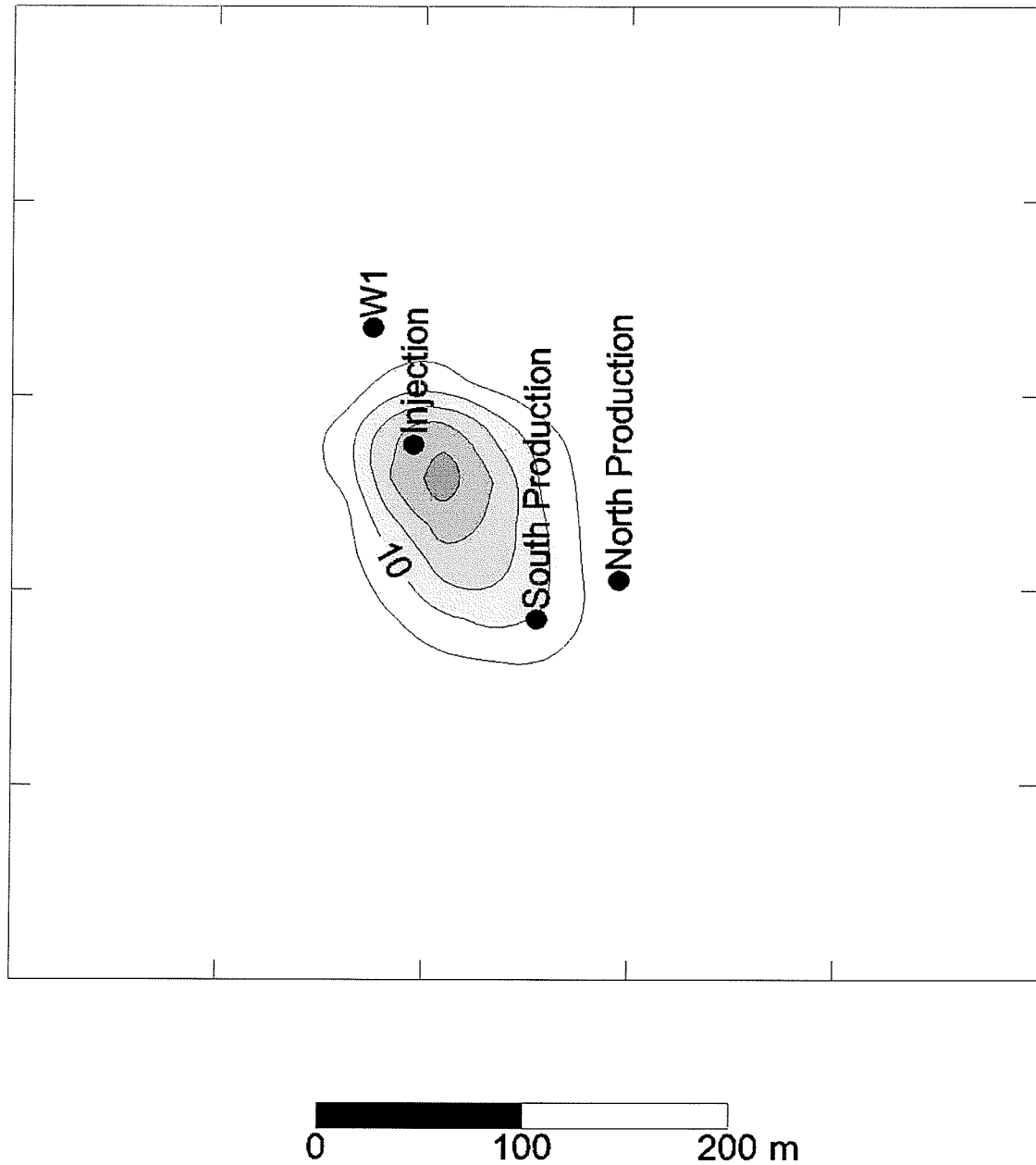
Figure 9.19e: Temperatures predicted by the dual continuum model for the upper 2 metres of the aquifer for at the modeled industrial site in St. Boniface for 2.1 years.
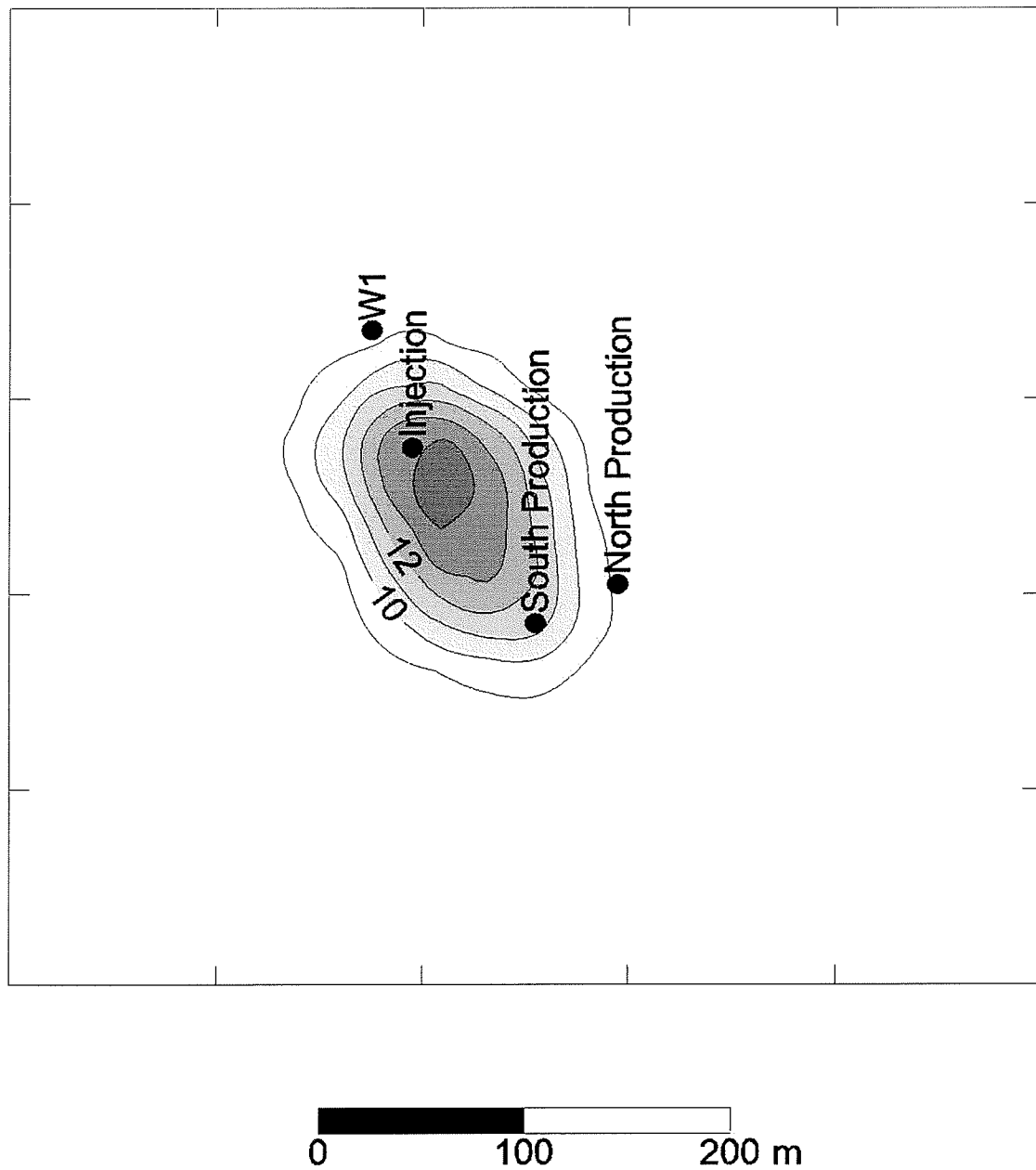
Figure 9.19f: Temperatures predicted by the dual continuum model for the upper 2 metres of the aquifer for at the modeled industrial site in St. Boniface for 5.2 years.
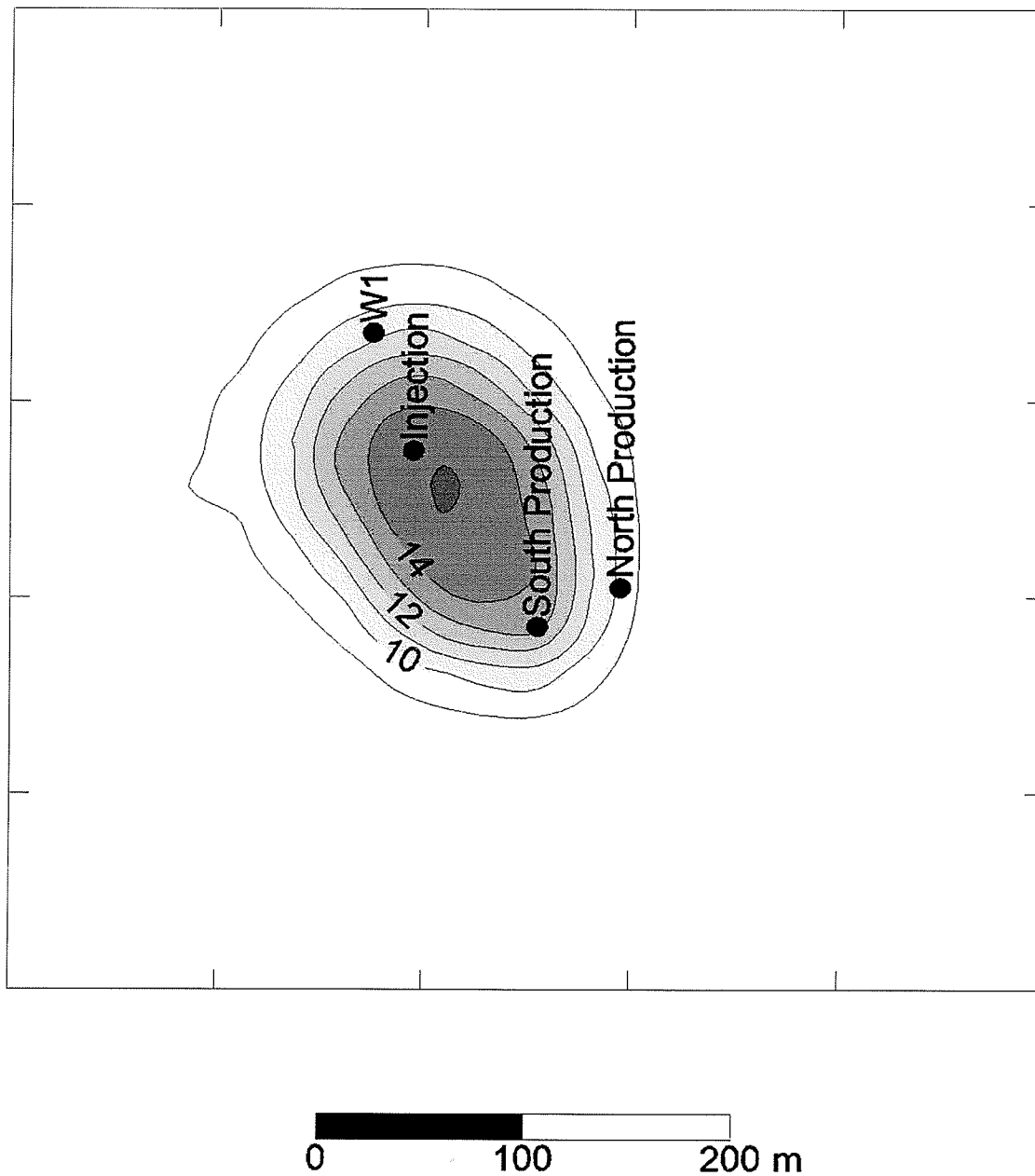
Figure 9.19g: Temperatures predicted by the dual continuum model for the upper 2 metres of the aquifer for at the modeled industrial site in St. Boniface for 15.2 years.
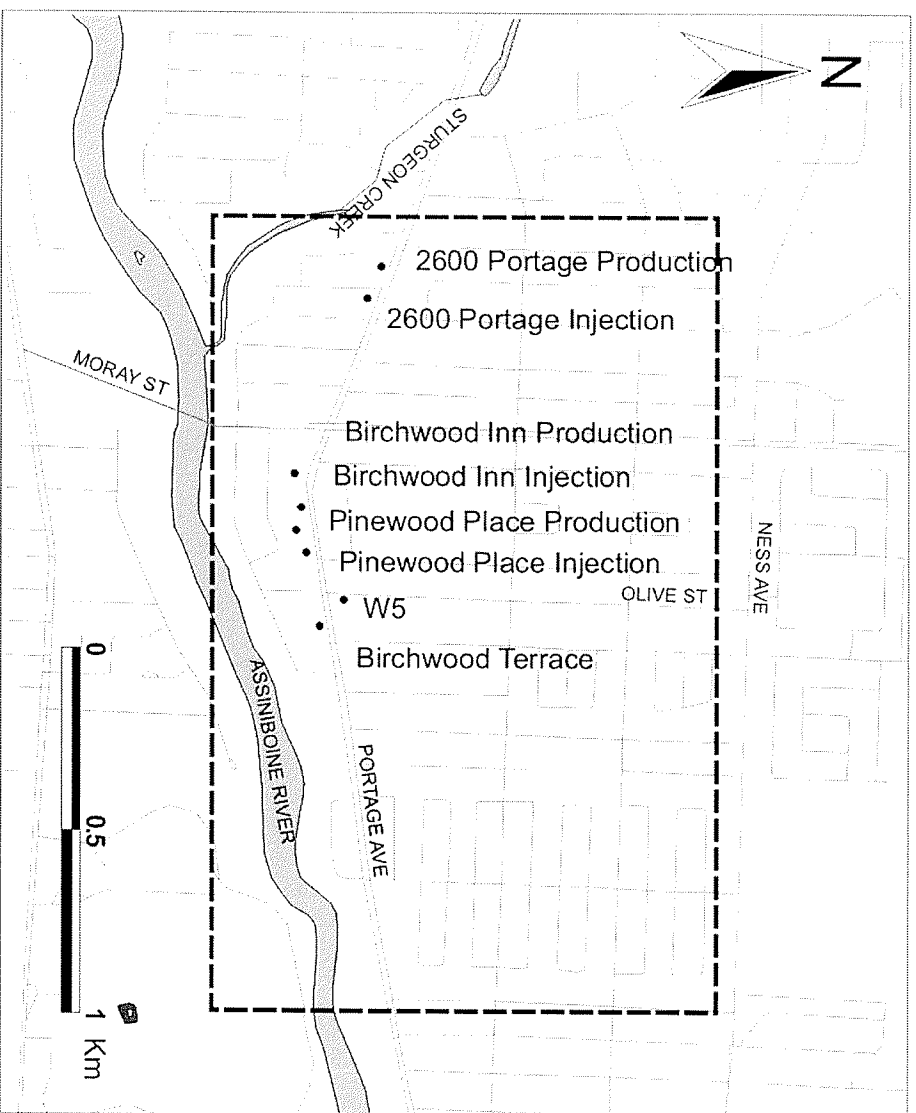
Figure 9.20: Location of production and injection wells in the Birchwood area of Winnipeg. The dashed line indicates the boundaries of the modeled area.
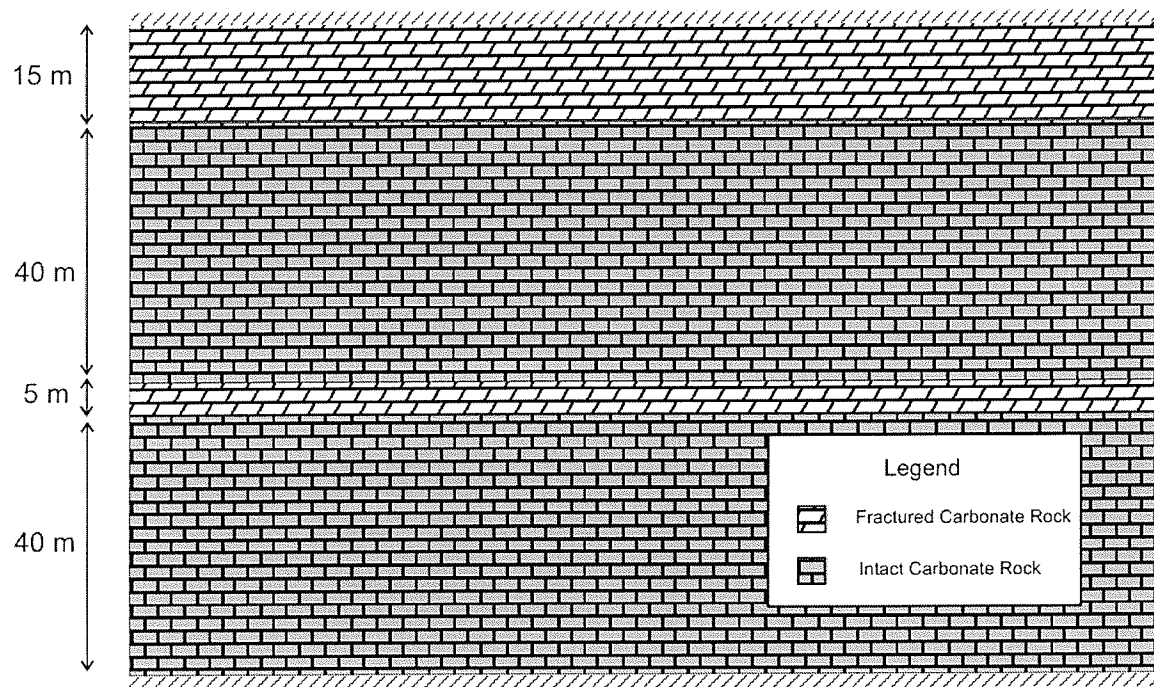
Figure 9.21: Cross-section used in the conceptual model of the Birchwood area.
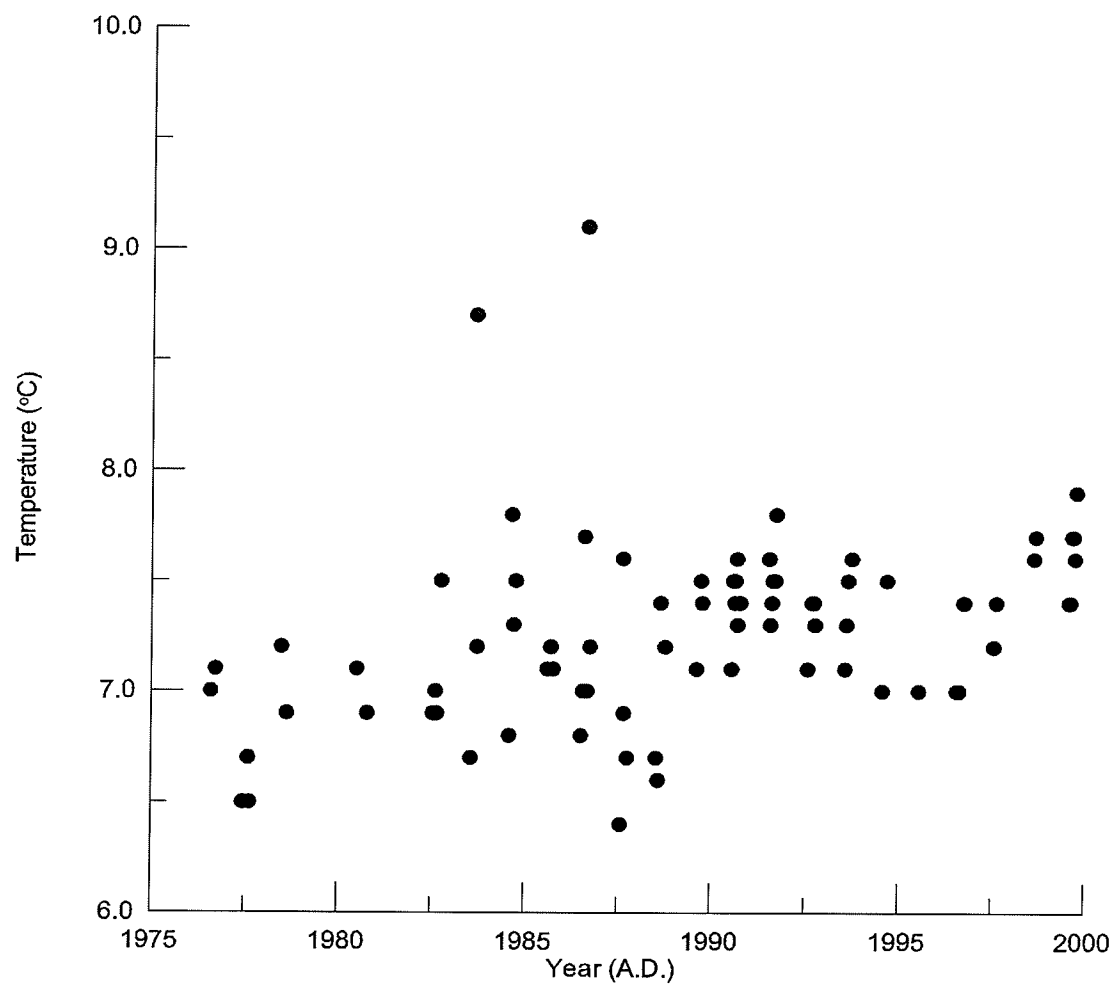
Figure 9.22: Injection temperatures recorded at 2600 Portage Avenue.
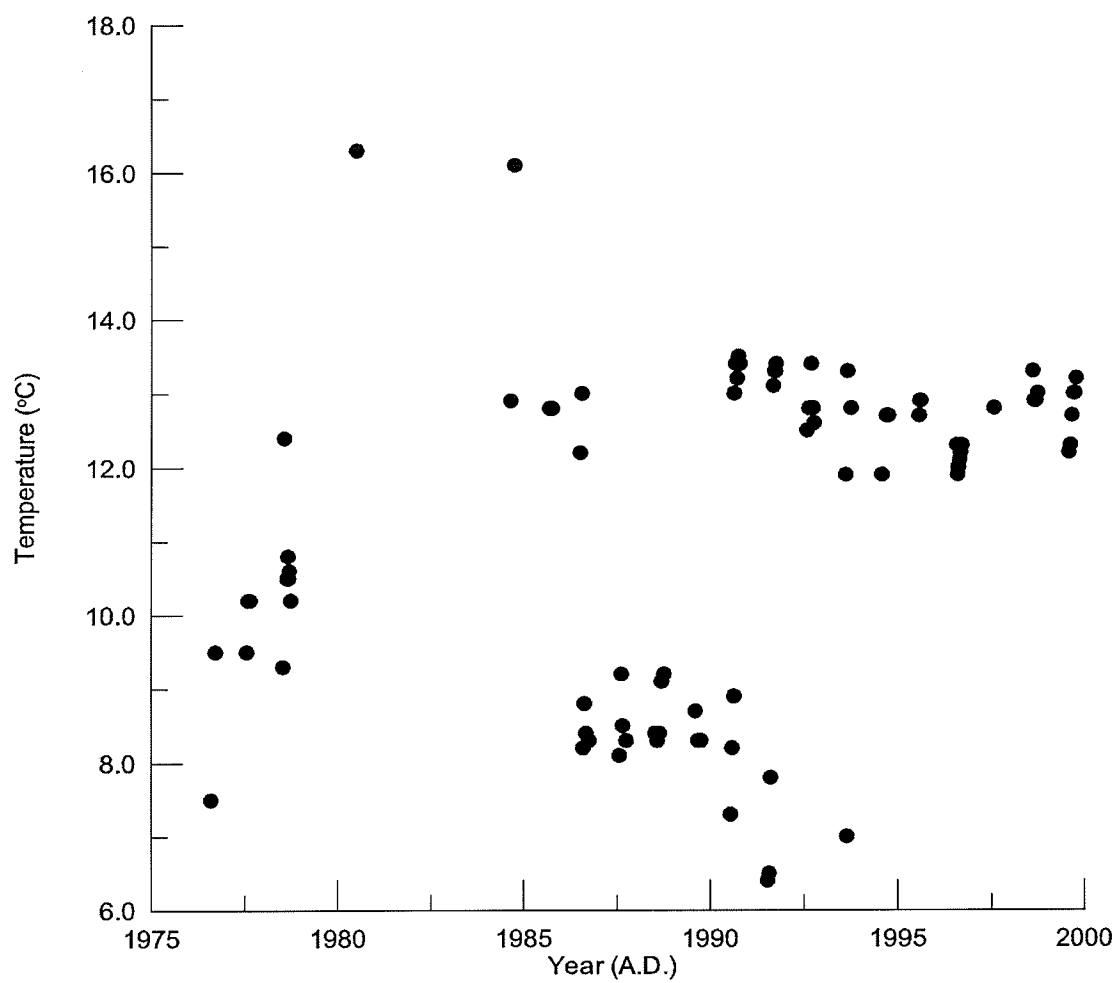
Figure 9.23: Injection temperatures recorded at Pinewood Place.
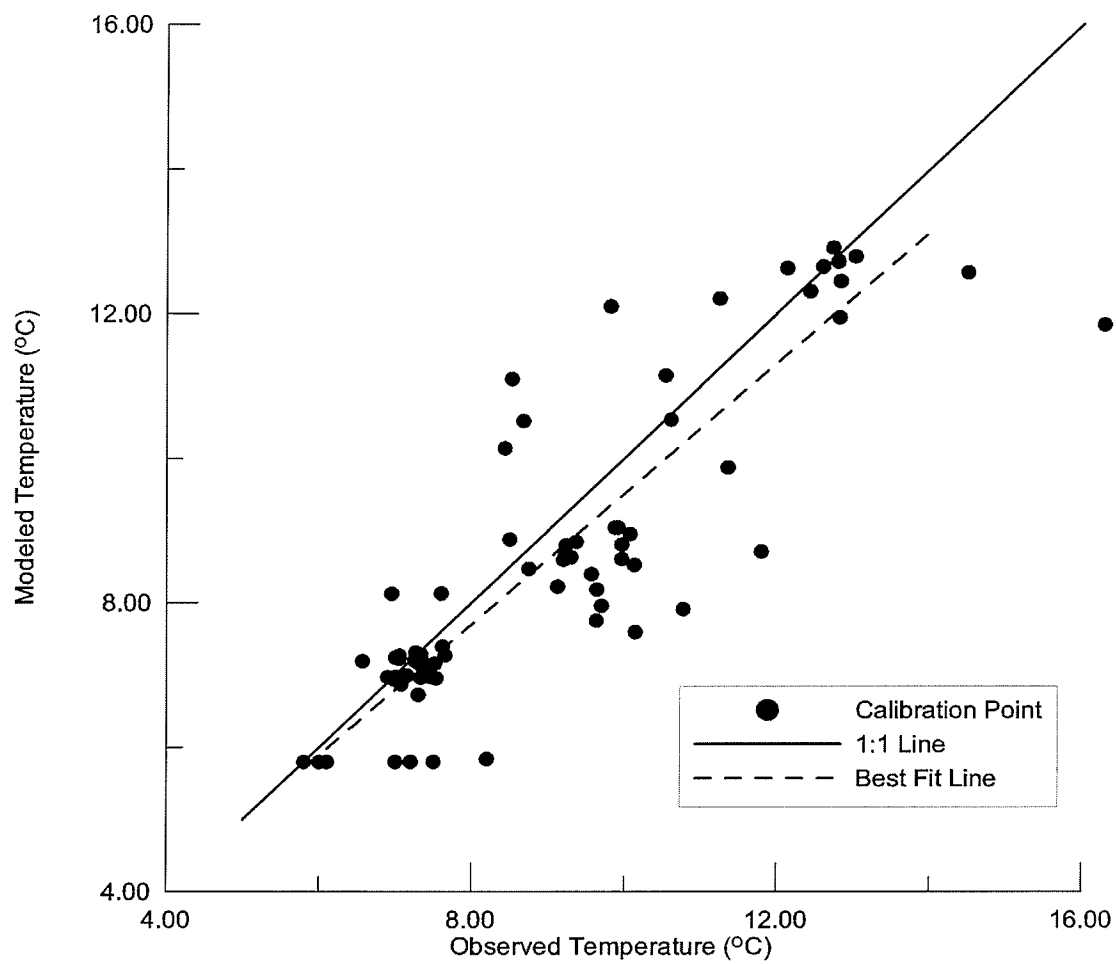
Figure 9.24: Measured versus predicted temperatures in the porous media model of the Birchwood area.
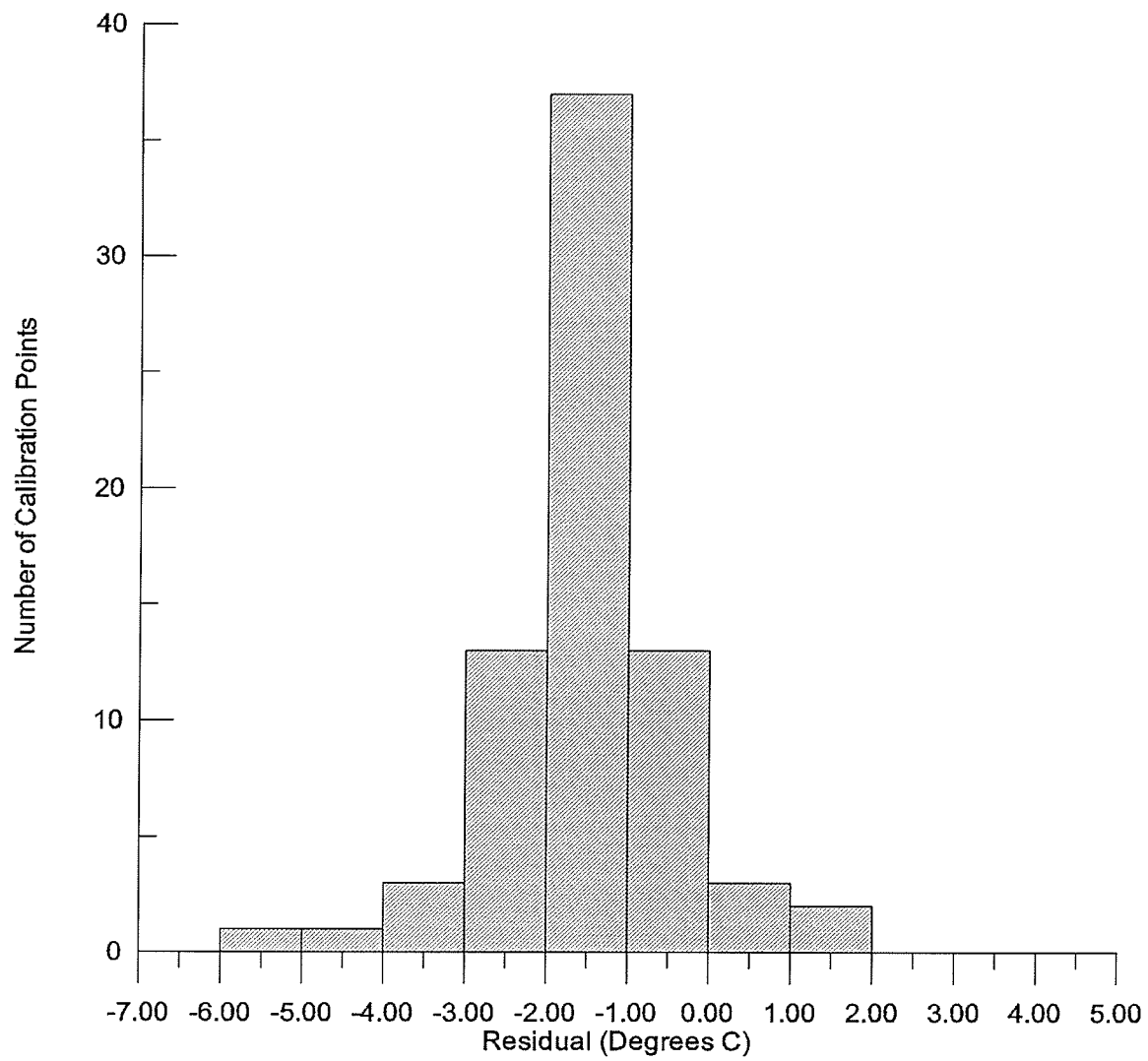
Figure 9.25: Distribution of residual temperatures in the porous media model of the Birchwood area.
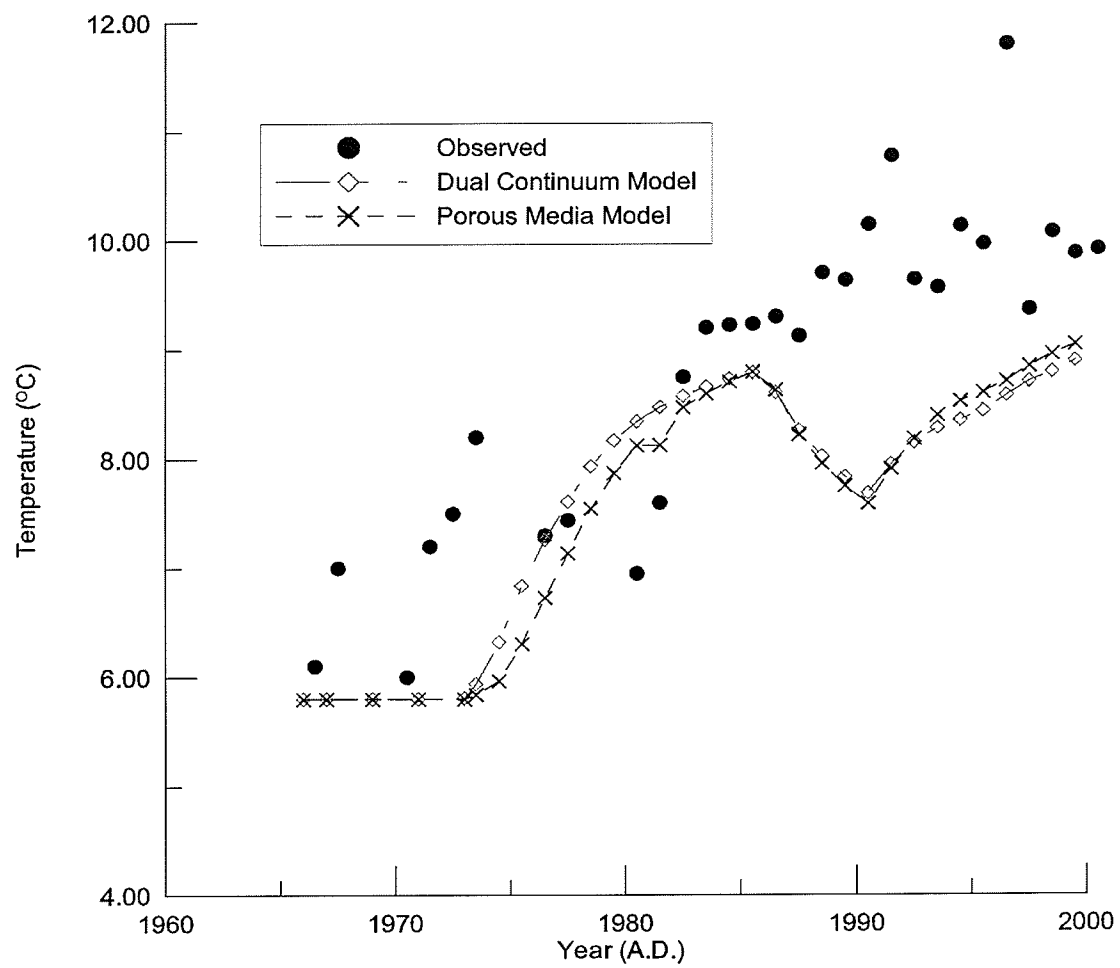
Figure 9.26: Measured and modeled temperatures at the production well at Birchwood Terrace.
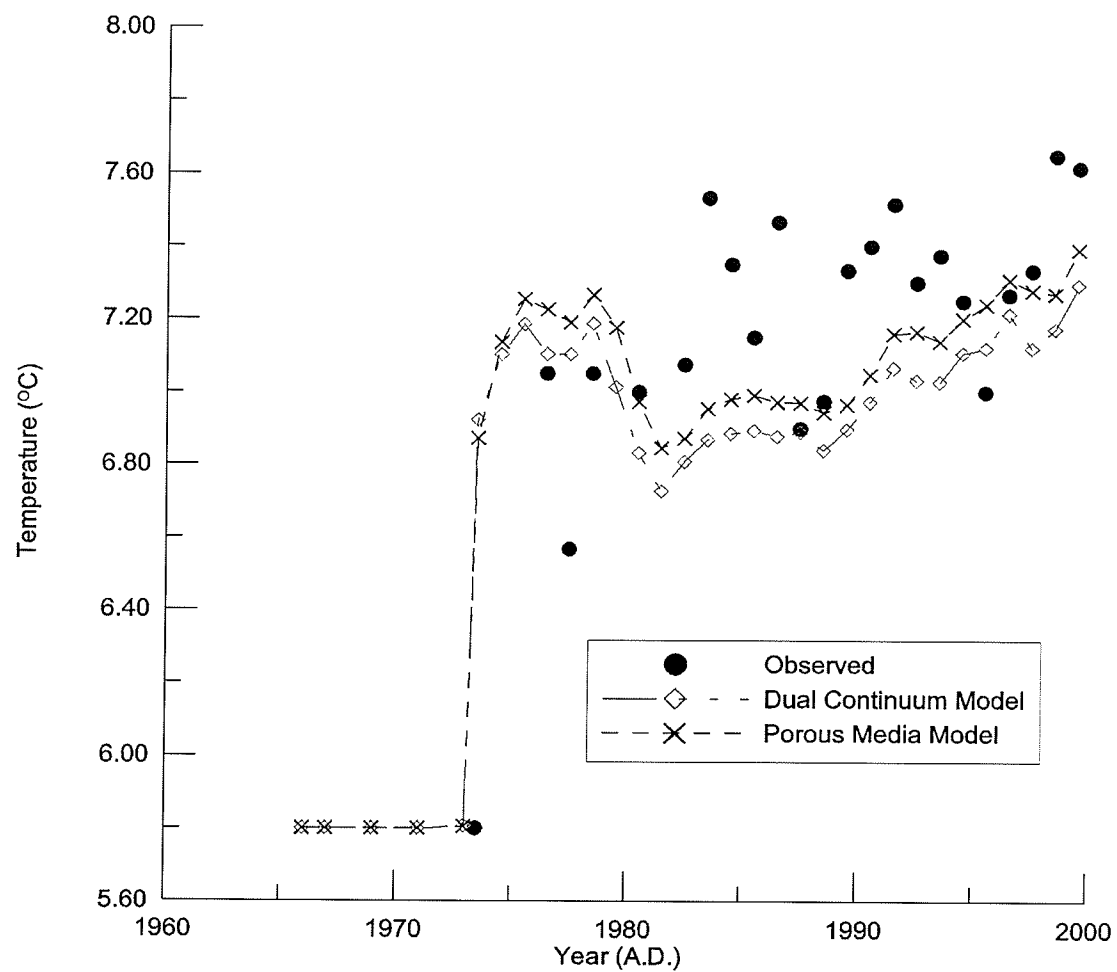
Figure 9.27: Measured and modeled temperatures at the production well at 2610 Portage Avenue.
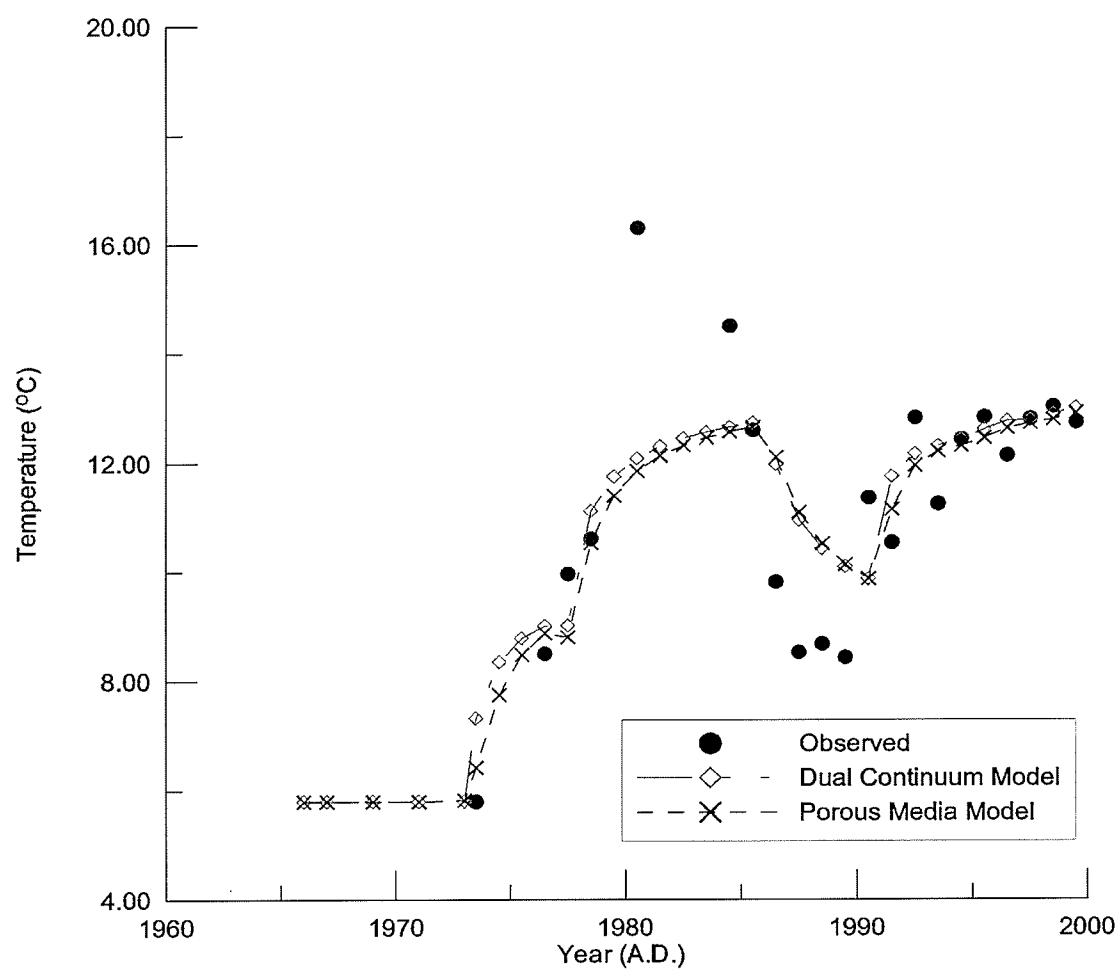
Figure 9.28: Measured and modeled temperatures at the production well at Pinewood Place.
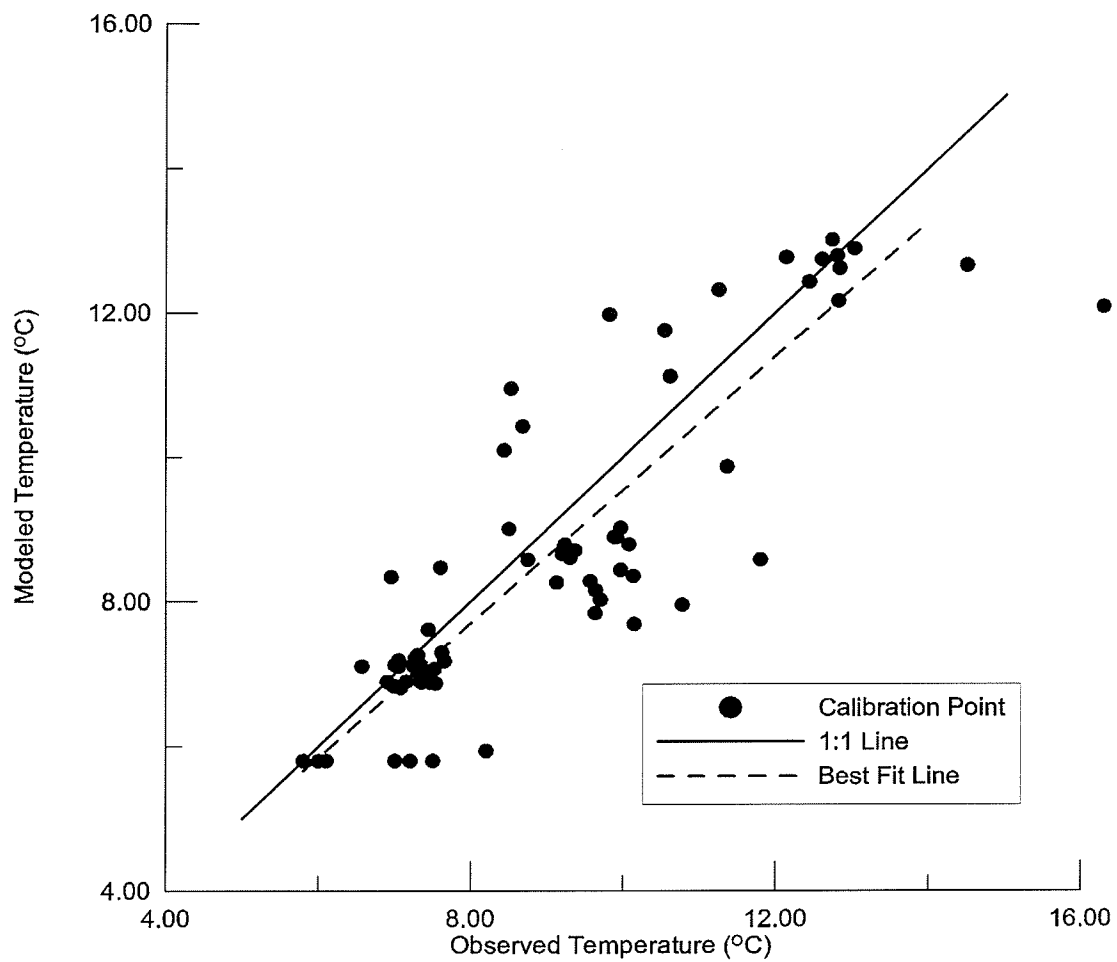
Figure 9.29: Measured versus predicted temperatures in the dual continuum model of the Birchwood area.
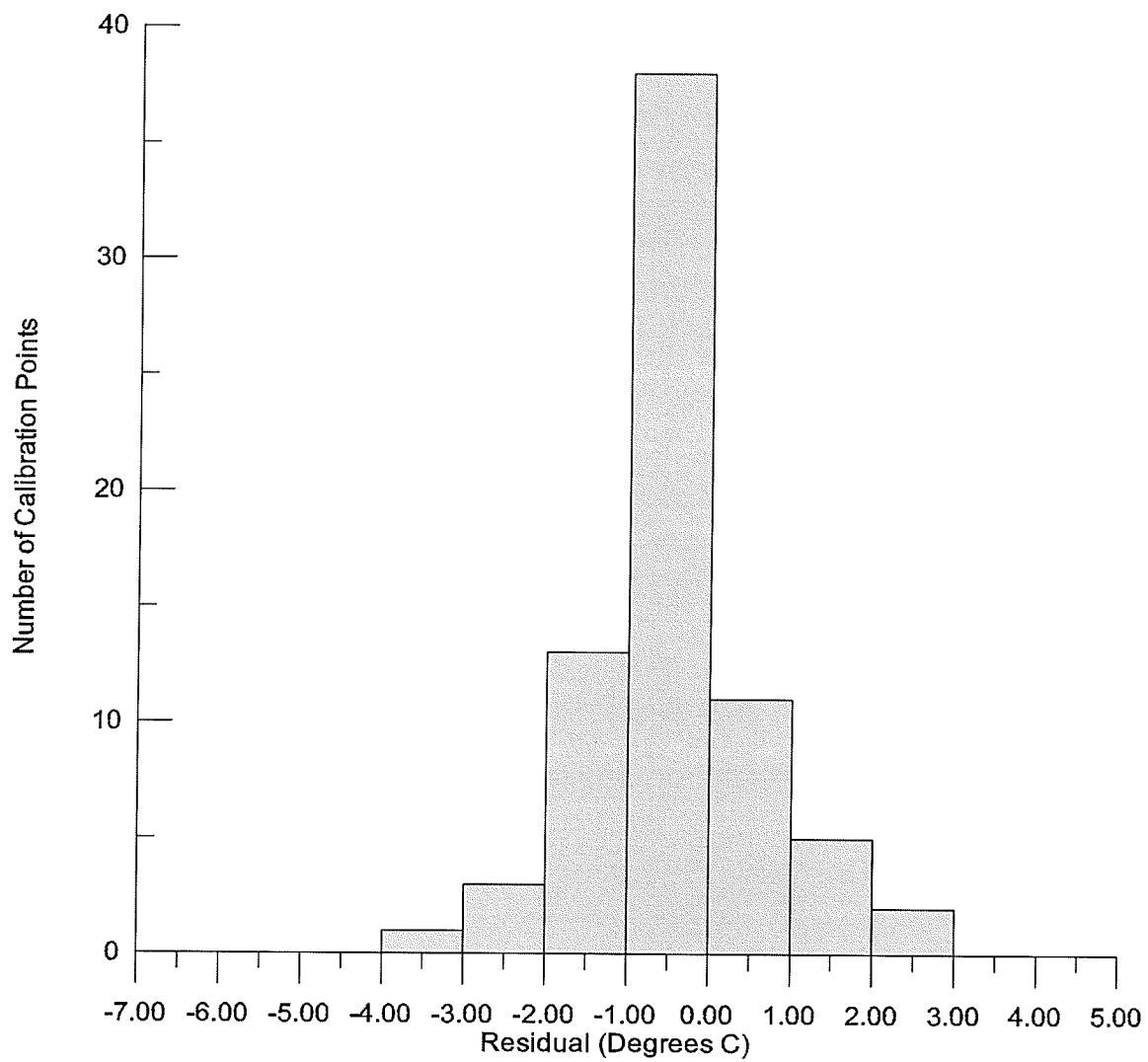
Figure 9.30: Distribution of residual temperatures in the dual continuum model of the Birchwood area.
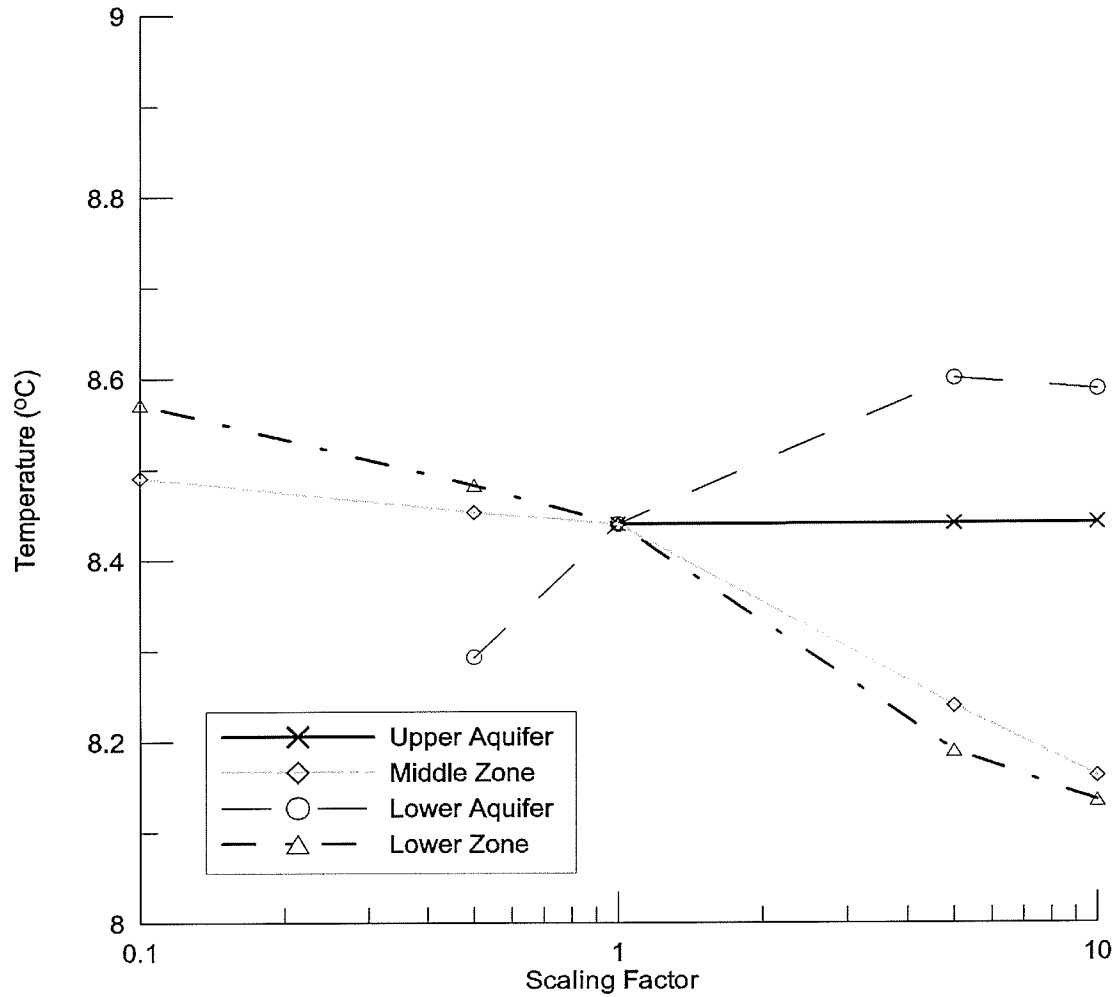
Figure 9.31: Sensitivity of the predicted temperature at Pinewood place after 3 years of operation in the conventional porous media model to changes in permeability. Scaling factor refers to the number that the permeability of a given unit is multiplied by in a variant of the calibrated model.
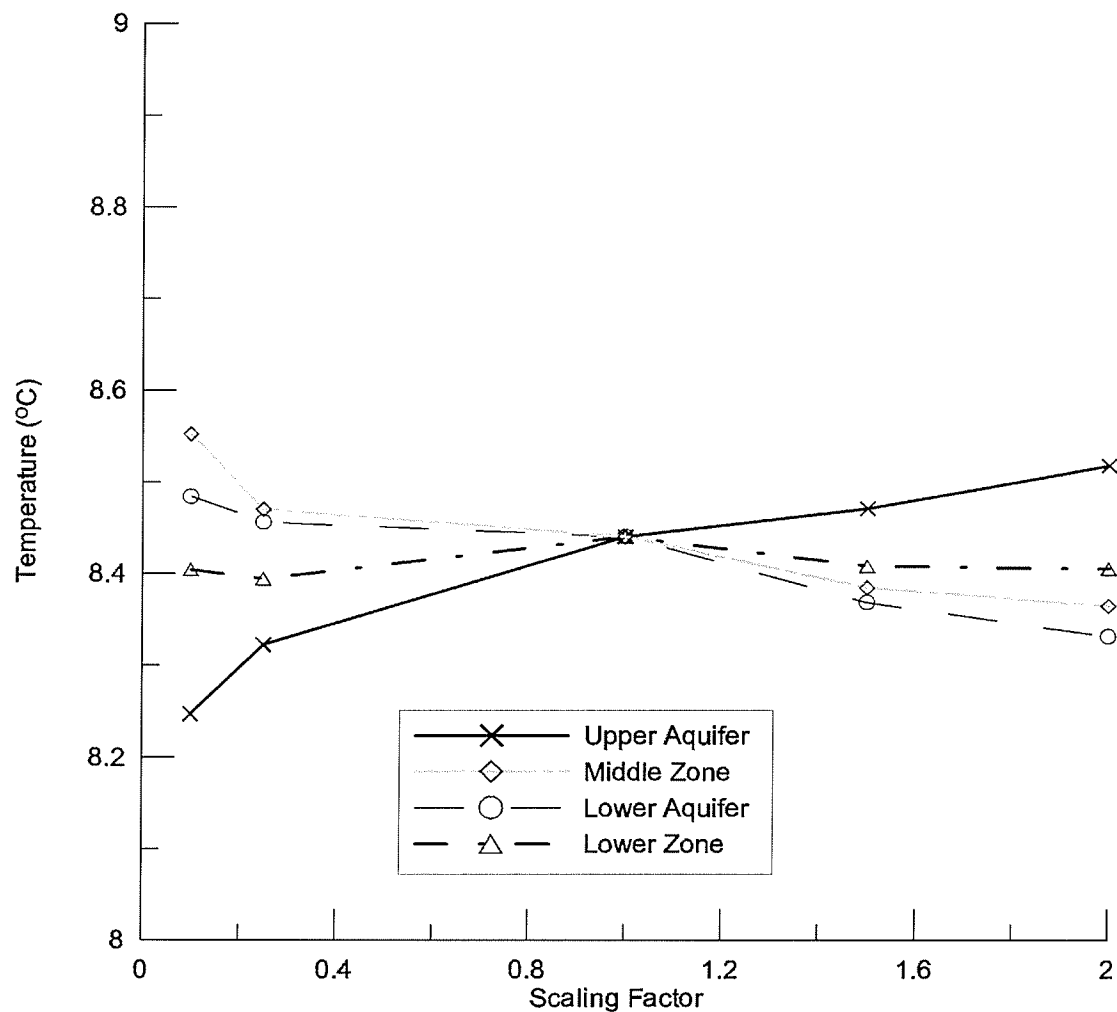
Figure 9.32: Sensitivity of the predicted temperature at Pinewood place after 3 years of operation in the conventional porous media model to changes in porosity. Scaling factor refers to the number that the permeability of a given unit is multiplied by in a variant of the calibrated model.

Figure 9.33: Sensitivity of the predicted temperature at Pinewood place after 3 years of operation in the dual continuum model to changes in permeability. Scaling factor refers to the number that the permeability of a given unit is multiplied by in a variant of the calibrated model.

Figure 9.34: Sensitivity of the predicted temperature at Pinewood place after 3 years of operation in the dual continuum model to changes in porosity. Scaling factor refers to the number that the permeability of a given unit is multiplied by in a variant of the calibrated model.
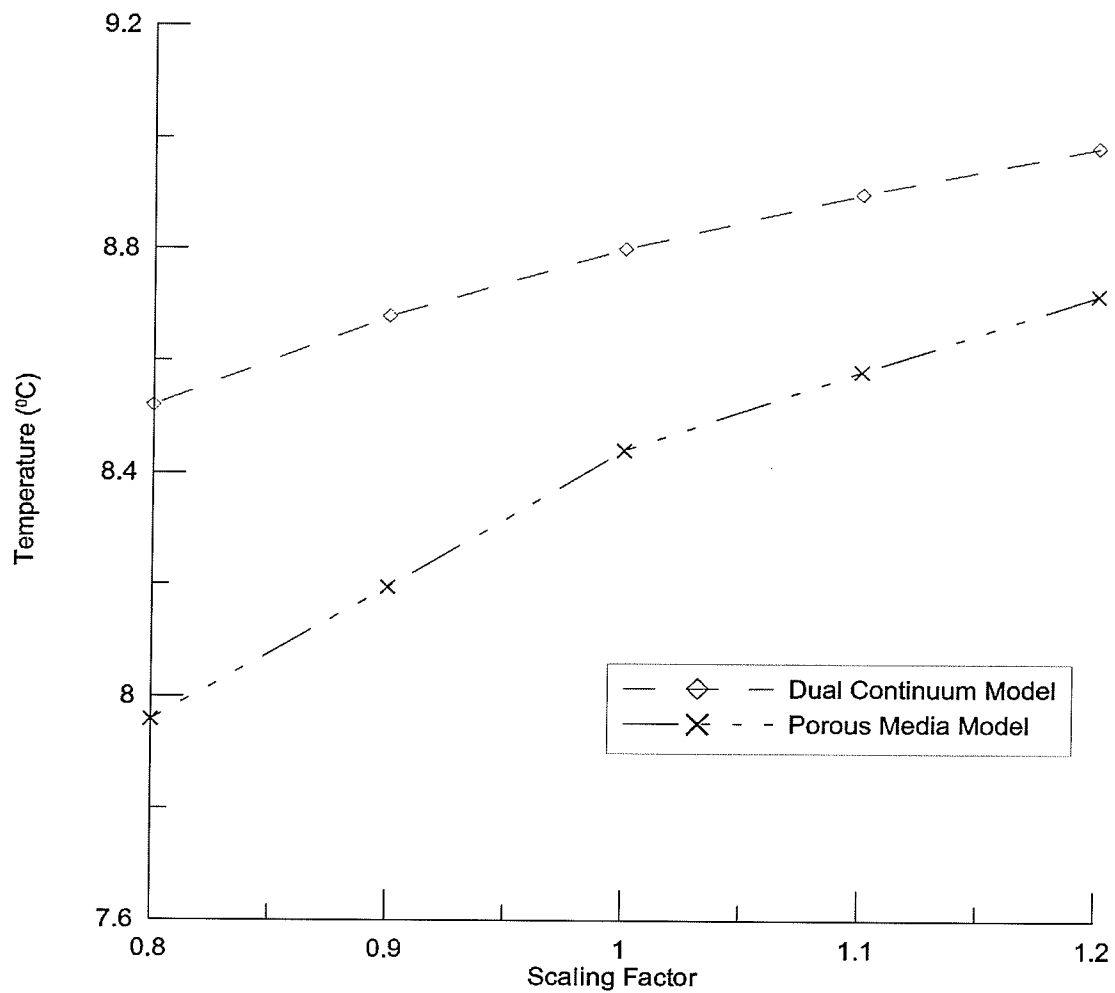
Figure 9.35: Sensitivity of the porous media and dual continuum models of the Birchwood area to changes in pumping rates. Scaling factor refers to the number that the pumping rates are multiplied by in a variant of the calibrated model.

Figure 9.36a: Temperatures predicted in the Upper Carbonate Aquifer by the calibrated dual continuum model for 1973.
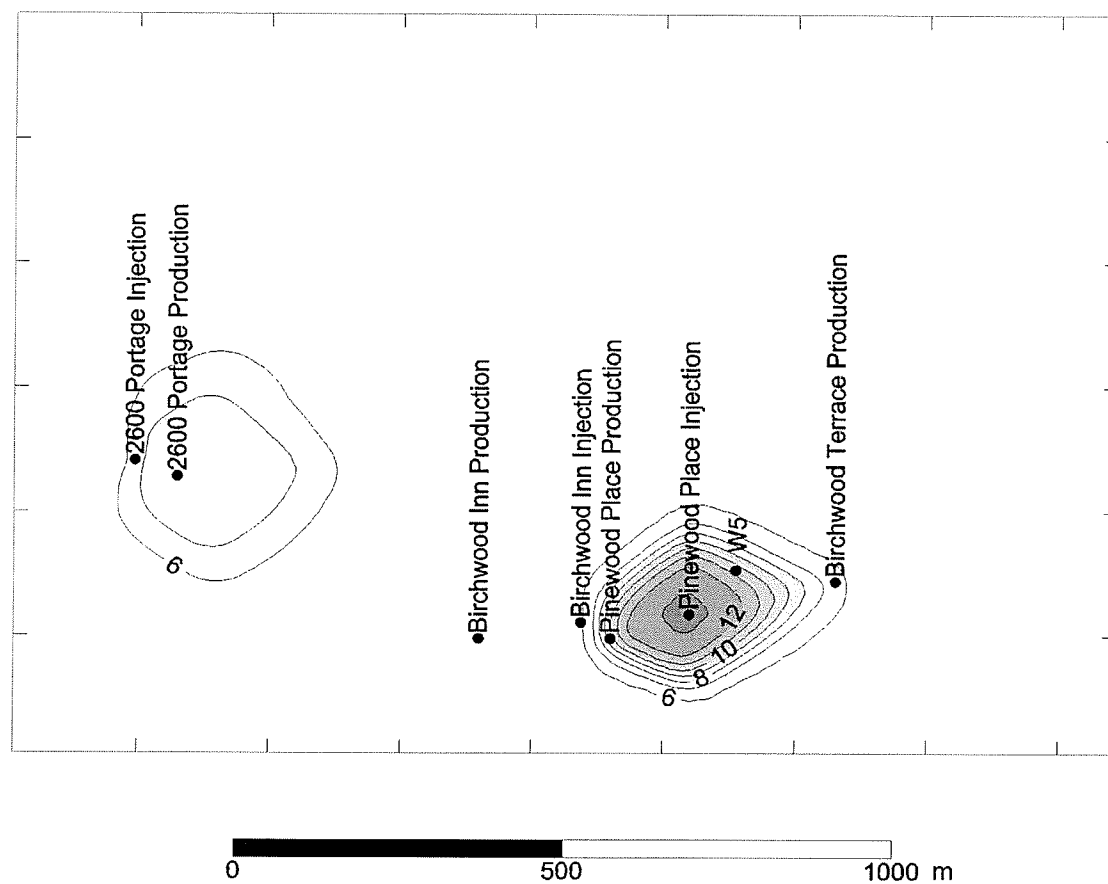
Figure 9.36b: Temperatures predicted in the Upper Carbonate Aquifer by the calibrated dual continuum model for 1974.
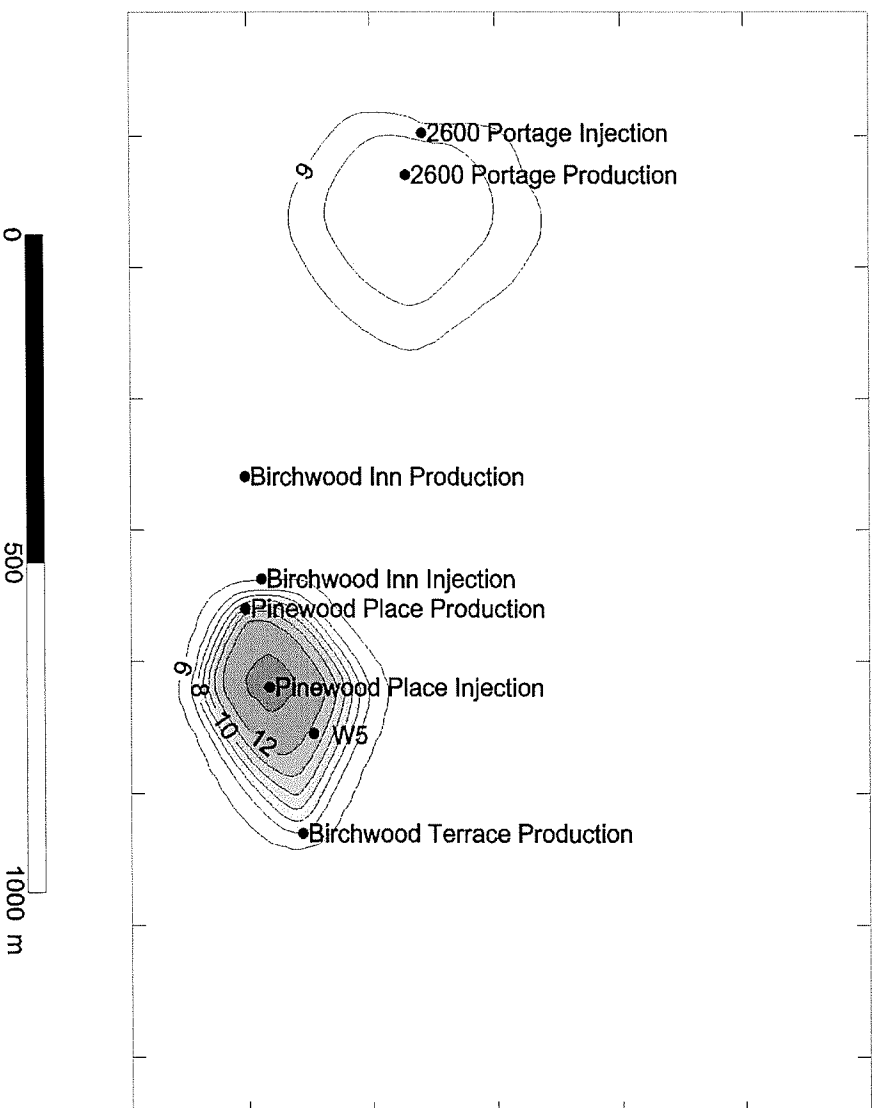
Figure 9.36c: Temperatures predicted in the Upper Carbonate Aquifer by the calibrated dual continuum model for 1975.

302
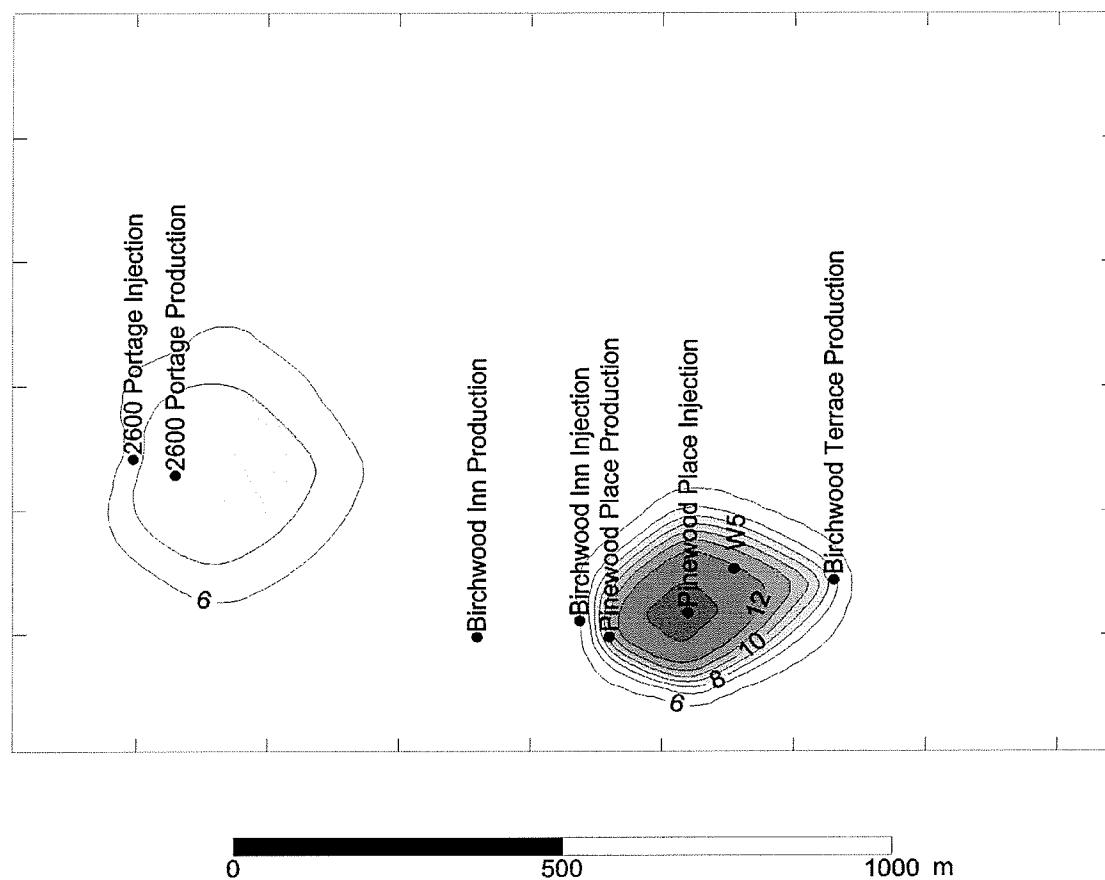
Figure 9.36d: Temperatures predicted in the Upper Carbonate Aquifer by the calibrated dual continuum model for 1976.
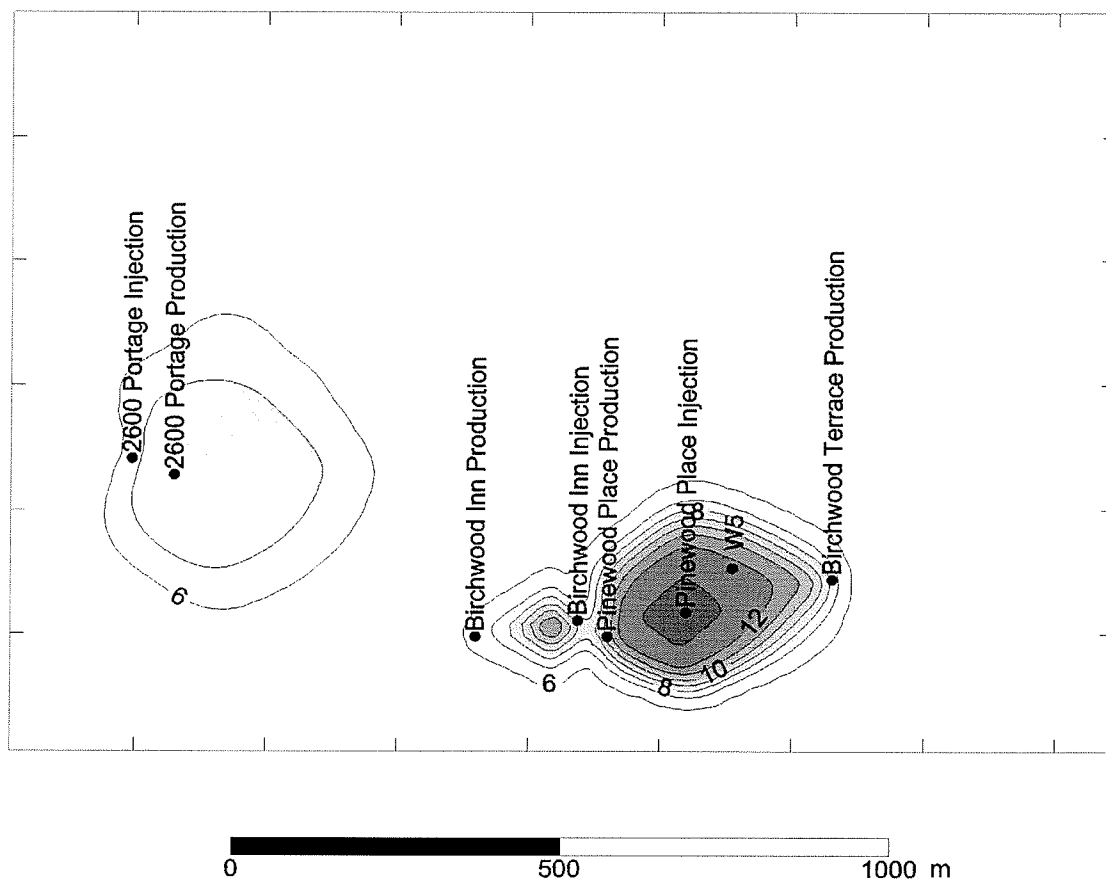
Figure 9.36e: Temperatures predicted in the Upper Carbonate Aquifer by the calibrated dual continuum model for 1977.
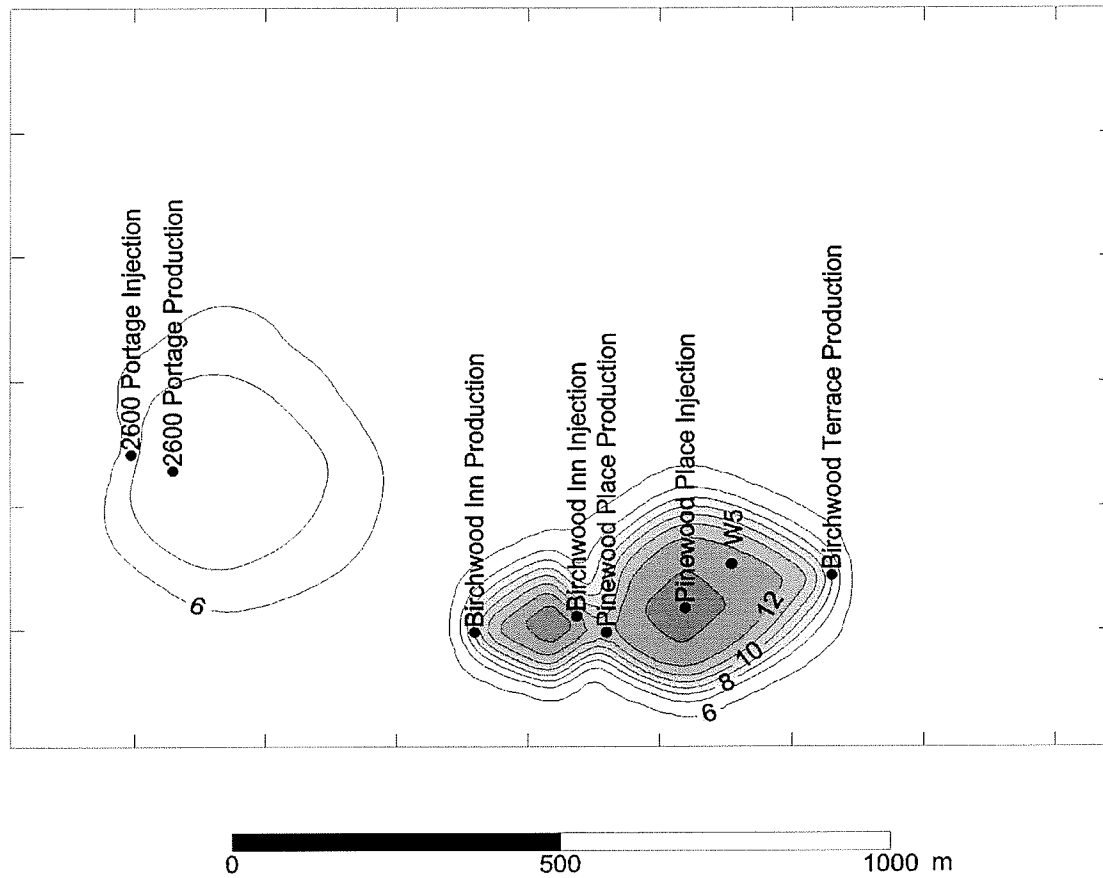
Figure 9.36f: Temperatures predicted in the Upper Carbonate Aquifer by the calibrated dual continuum model for 1978.
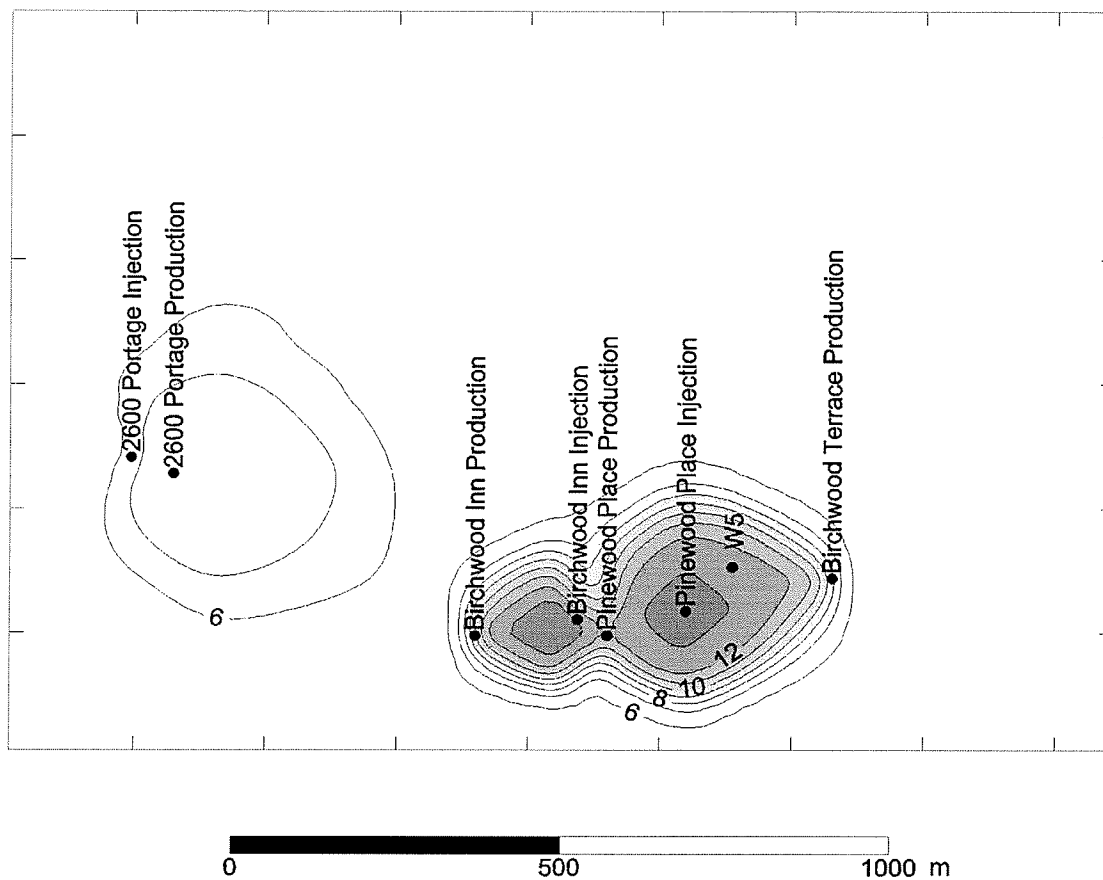
Figure 9.36g: Temperatures predicted in the Upper Carbonate Aquifer by the calibrated dual continuum model for 1979.
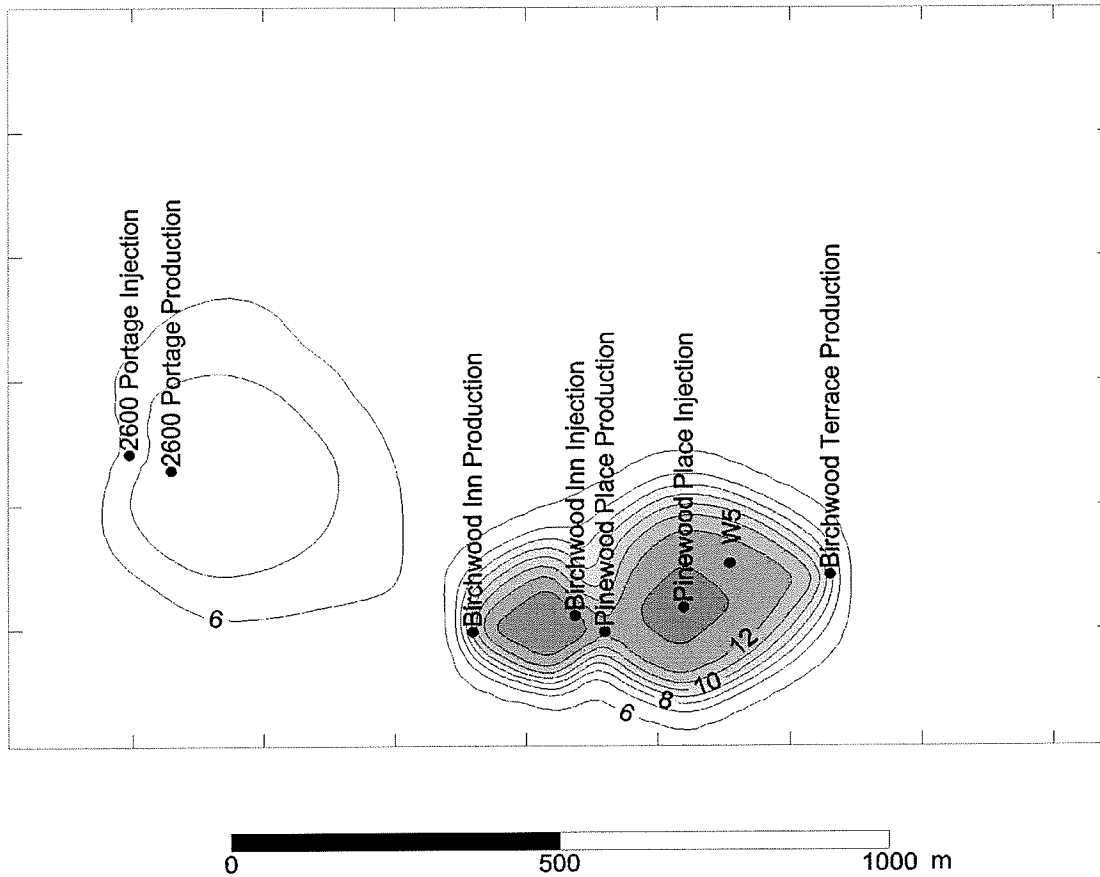
Figure 9.36h: Temperatures predicted in the Upper Carbonate Aquifer by the calibrated dual continuum model for 1980.
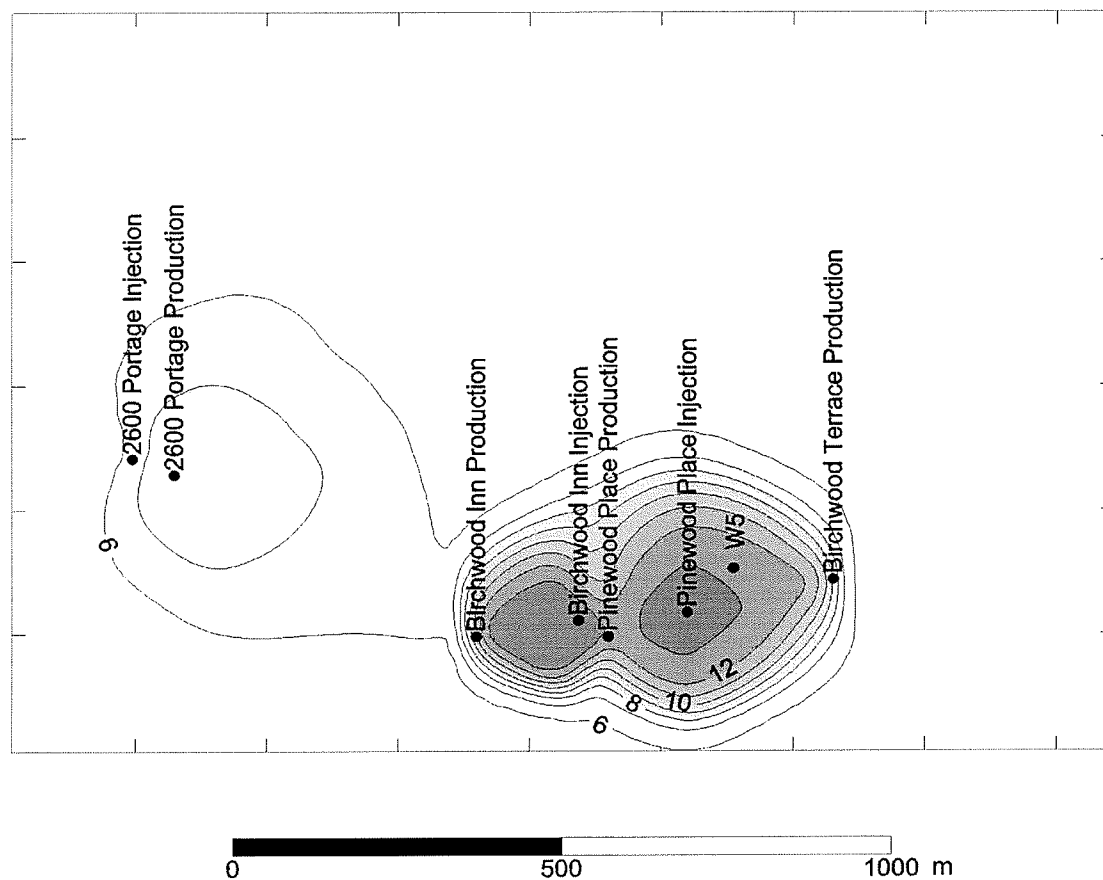
Figure 9.36i: Temperatures predicted in the Upper Carbonate Aquifer by the calibrated dual-continuum model for 1985.
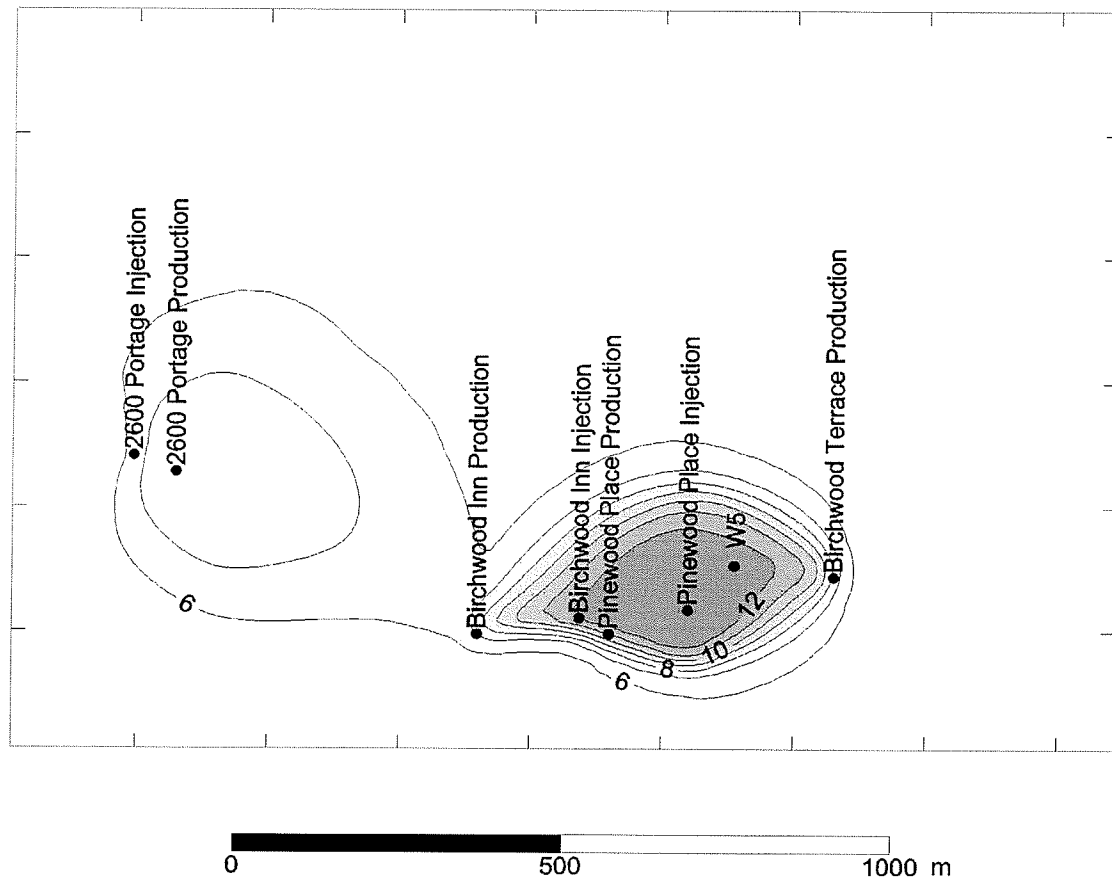
Figure 9.36j: Temperatures predicted in the Upper Carbonate Aquifer by the calibrated dual-continuum model for 1990.
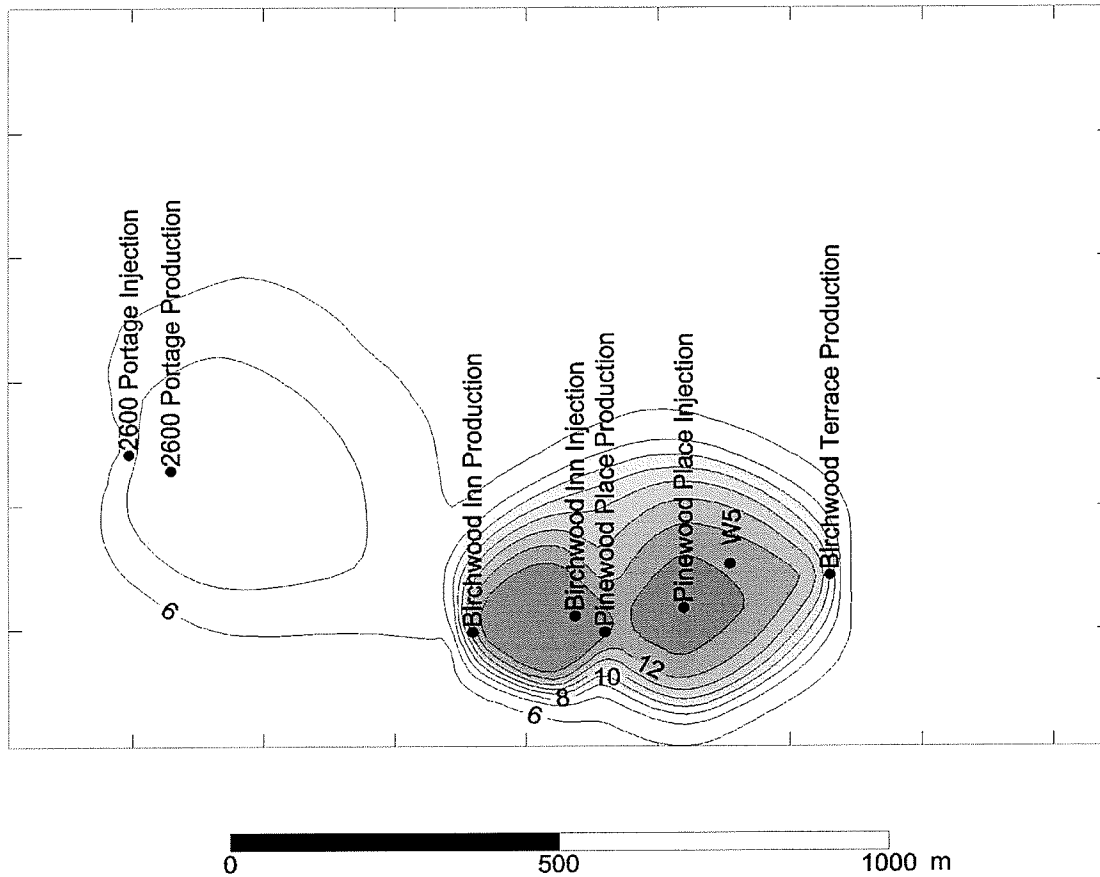
Figure 9.36k: Temperatures predicted in the Upper Carbonate Aquifer by the calibrated dual-continuum model for 1999.

CHAPTER 10: DISCUSSION

10.1 Geothermal Energy Development

10.1.1 Sustainability of Current Practises

Thermal use of groundwater in the Winnipeg area is predominantly for cooling. Typically a withdrawal-injection well doublet is used and thermal breakthrough at production wells most often occurs in the first few years of operation. Temperature increases of several degrees have been observed following thermal breakthrough, reducing the efficiency of groundwater as a coolant. Following thermal breakthrough, injection temperatures are maintained at a nearly constant level in some cases but increase in other situations where the constant temperature increase required for the cooling application. For some industrial processes, where groundwater is being used as a coolant in high temperature processes, a rise in groundwater temperature of a few degrees Celsius at the production well is negligible. Where groundwater is used for air conditioning or refrigeration, a rise in groundwater temperature of a few degrees Celsius can drastically reduce the efficiency of the system. In some of these systems, groundwater is being produced at nearly 15 °C and is being returned to the aquifer at approximately the same temperature. Little heat is being absorbed by the groundwater in these systems and it is doubtful that they are providing much benefit to the operator.

Additional increases in aquifer temperature in areas affected by heat loss from buildings are further decreasing the efficiency of groundwater as a coolant. Observed temperature profiles and numerical modeling suggest that a new equilibrium temperature of approximately 8 to 11°C, depending on the proximity to a building, is reached in the upper few metres of the Carbonate Rock Aquifer after a few decades. These temperatures already exist beneath many areas of the City of Winnipeg and it is conceivable that the temperature in the top of the aquifer will be at least 8°C throughout most areas of Winnipeg within a few decades. This increase represents a noteworthy reduction in the efficiency of groundwater as a coolant, particularly for air conditioning and refrigeration purposes. The magnitude of this increase in temperature is approximately the same increase in temperature suggested by Manitoba Water Branch guidelines for injection wells in systems that use groundwater for cooling and if an additional 5 °C increase is allowed, the use of the aquifer for cooling will be jeopardised. Numerical modeling conducted in the previous two chapters suggest that over the range of hydrogeologic conditions observed in the Winnipeg area, these temperature increases cannot be avoided in current development schemes. Overall, the prospect of future use of groundwater for cooling purposes is bleak if current practises are continued.

10.1.2 Recommendations for Future Development

The current practise of using groundwater for cooling only and injecting the resulting thermal wastewater back into the Carbonate Rock Aquifer is

unsustainable because of the inevitability of the breakthrough of injected wastewater at production wells. Future developments must seek to avoid these rises in temperature at the production well. There are several ways in which sustainability can be accomplished and all of these seek to eliminate the presence of excess heat in the aquifer. This methods include: 1) avoiding discharging thermal wastewater to the aquifer; 2) imposing further limitations on injection rates and temperatures; 3) utilising the excess heat in the aquifer for heating to avoid interference with cooling applications; 4) injecting cold water during the winter to balance thermal loading of the aquifer; and 5) stripping excess heat from thermal wastewater prior to injecting it back into the aquifer. In some cases, it may also be possible to extend the time prior to thermal breakthrough by increasing the spacing of the wells. However, even at a spacing of 1000 metres, thermal breakthrough will likely occur in less than 10 years for a system producing and injecting at 3.8 L s^{-1}, if typical parameters for the Carbonate Rock Aquifer are present.

A limited number of operations in the Winnipeg area do not inject their thermal wastewater back into the Carbonate Rock Aquifer and instead pump this water into a surface water body or storm sewer. Under this scheme, groundwater temperatures are not affected but loss of hydraulic head in the aquifer could potentially be a problem. However, the cumulative drawdown cone in the Carbonate Rock Aquifer beneath Winnipeg has recovered by several metres in some areas since the 1960's (Render, 1970; Kennedy, 2002; Ferguson and St. George, 2003). This observation may allow for some

consumptive use of groundwater in the Winnipeg area, but this practise is not recommended on a wide scale because the potentiometric surface in the Carbonate Rock Aquifer would likely drop by several metres if all users of groundwater for thermal purposes stopped recharging their thermal wastewater. Such a drop would be consistent with the potentiometric surface that existed during the 1960's (Render, 1970), when groundwater use in the Winnipeg area was primarily consumptive. Discharging of thermal wastewater to surface water bodies is not recommended because of the relatively poor water quality in the aquifer beneath many areas of the city (Grasby and Betcher, 2002). Discharging to surface water bodies also requires that the property is in close proximity to a water body and this is not the case for many operations. The City of Winnipeg generally does not allow discharge of thermal wastewater to the sewer system, primarily because the sewer system does not have the capacity to accept large volumes of additional water.

Reducing the injection temperature and rate provides a sustainable option in some conditions. Smaller buildings that do not require large volumes of water for air conditioning may be able to operate for long periods of time without experiencing significant increases in temperature at their production wells. However, this may rule out the use of groundwater for cooling for users with greater cooling demands.

Gringarten and Sauty (1975) suggest that it is theoretically possible to situate production and injection wells so that the injected water never reaches

the production well.   Numerical modeling indicates that this type of arrangement is probably not possible in the Winnipeg area because regional groundwater flow appears to be negligible in most cases.   In rare cases, the Carbonate Rock Aquifer may have the right combination of permeability and regional hydraulic gradients to make it possible to locate the injection and withdrawal wells in a manner that prevents introduced heat from reaching the production well.   However, the design of such as system would be quite difficult because regional groundwater flow velocities and their directions, on the scale required for thermal projects in the Winnipeg area, are poorly understood.

Removing the introduced heat from the aquifer is perhaps the most attractive option for making the use of groundwater as a coolant sustainable. The practise of using groundwater for only cooling or heating and then injecting it back into the same aquifer is referred to as "pump-and-dump" by Michel and Allen (2003) and this practise creates an imbalance on the thermal loading of the aquifer.   To ensure the sustainability of the use of aquifers for thermal purposes, methods of balancing the energy within the aquifer, such as using groundwater for heating in the winter should be examined.   In a situation where thermal loads are balanced or partially balanced, the subsurface is being used for storage rather than as a source or sink of heat.   This is essentially an ATES system where heat generated by either industrial cooling or air conditioning is used for space heating during the winter. The ATES concept may be difficult to apply in practise due to

differences in heating and cooling demands. Energy requirements for air conditioning needs in Manitoba are generally less than heating needs and this may require complex designs and use of other energy sources for space heating in addition to the energy stored in the ATES system. However, even some use of the heat present in thermal wastewater will be beneficial.

The practise of injecting thermal wastewater into aquifers has resulted in an increase in the overall energy content of the subsurface in Winnipeg. Other factors in the urban environment have also contributed to this increase in subsurface energy. This increase in temperature creates an interesting situation where groundwater source heat pumps may be more efficient. A study in Ireland found that shallow aquifers beneath cities that have experienced an increase in temperature of 3 to 4°C can provide an increase in the efficiency and output of heat pumps (Allen et al. 2003). This feature is notable for the Winnipeg area because of the low temperatures and low heat fluxes present naturally. The presence of higher temperatures may also be advantageous during the initial stages of possible ATES projects. Sauty et al. (1982) stated that the initial cycle of the injection of warm water into an aquifer may have to be longer than other cycles to ensure that enough energy can be withdrawn during the first production cycle. Initial cycles may not have to be lengthened as much in the Winnipeg area because the Carbonate Rock Aquifer has been inundated with additional thermal energy for several decades in some locations.

10.2 The Heterogeneity of the Carbonate Rock Aquifer: Implications for Other Studies

10.2.1 Heterogeneity in the Carbonate Rock Aquifer

The current study has examined the response of the Carbonate Rock Aquifer to the production and injection of water on a local scale. Knowledge of the fracture network in the Carbonate Rock Aquifer and its variability has been shown to be important in determining the behaviour of advective heat transport. During thermal exploitation of the aquifer, heterogeneities on the scale of tens of metres can have a significant effect on advective heat transport. This was noted in the case study of the industrial site in St. Boniface and may also play a role in the behaviour of heat flow in the Birchwood area. These heterogeneities are largely due to variations in the fracture network, with respect to the size, permeability, interconnectedness and spatial distribution of the fractures.

Heterogeneities on this scale are less important to regional studies of the aquifer. Kennedy (2002) was able to create a finite element groundwater flow model of the Carbonate Rock Aquifer using elements on the scale of a few kilometres across. Either of the case studies examined in this study would fit within an individual element of that model and there is great deal of detail that is filtered out in that regional model. However, the geostatistics given by Kennedy (2002) do indicate the presence of large variations in permeability. The semi-variance of log transmissivity values located less than a few kilometres apart was nearly 2.0, indicating a lack of correlation for closely

spaced measurements. This finding is in agreement with typical behaviour of the Carbonate Rock Aquifer, where zones of extremely high and extremely low permeability have been found within very small areas. These areas should have little effect on regional flow. Groundwater most likely flows preferentially around low permeability areas and flow in high permeability areas is restricted by the surrounding lower permeability areas of the aquifer. An equivalent permeability model of the Carbonate Rock Aquifer is perhaps best described with the use of a dispersed model similar to equation 4.2, where zones of high permeability are dispersed in a lower permeability medium.

10.2.2 Geotechnical Projects

Geotechnical projects have encountered difficulties at many sites in the Winnipeg area due to variations in the permeability of the Carbonate Rock Aquifer. Render (1970) provided a brief overview of many of these projects. High inflows from the Carbonate Rock Aquifer during foundation installations are a common problem encountered; this has occurred at several bridges and an overpass in the Winnipeg area. Among the largest estimated inflows encountered during a construction project occurred during the installation of an underground storage tank at the Rockwood Propellant Plant. A volumetric discharge of over 200 L s^{-1} from the aquifer into the excavation was estimated at this site (Render, 1970). These inflows are not easily predicted from regional studies due to the degree of variability present in the aquifer. More detailed studies of individual sites are needed to characterise possible

318

inflows. The potential for large inflows from the Carbonate Rock Aquifer should be considered during the planned expansion of the Red River Floodway.

10.2.3 Solute and Contaminant Transport

Solute and contaminant transport studies also need to consider the variability of permeability on a scale similar to geothermal energy projects. There are only a few published accounts of contamination of the Carbonate Rock Aquifer but these cases do suggest that areas of extremely high and low permeability can have notable effects on solute transport in the aquifer.

In most cases solute transport occurs in accordance with regional scale flow, where zones of extremely high and low permeability are of lesser importance. Zones of high permeability can become important when large quantities of water are discharged from the aquifer, either due to pumping or removal of the confining layer. This occurred during the construction of the inlet structure for the Red River Floodway (Betcher et al., 1995) during a short period of time due to dewatering. During this time the saline water-fresh water boundary moved eastward by a few kilometres. The movement in the boundary eastward suggests that the bulk of the water flowing into the excavation was coming from the west, likely due to the existence of a more developed fracture network and possible conduits in that area.

Variations in the fracture network may have caused unexpected behaviour of contaminant plumes at the Rockwood Propellant Plant. At this site two separate plumes both containing trichloroethylene (TCE) and 1,1,1-

trichlorethane (TCA) are present as a result of leaching of degreasing agents into the aquifer beginning in the 1960's. This is the same property where Render (1970) noted high inflows during the installation of an underground storage tank. Regional mapping of the potentiometric surface and geophysical logging (UMA Engineering, 1993) indicated that this highly fractured area extends throughout the property but not far beyond it. The plumes appear to be largely restricted to this highly permeability area, implying that the fracture network may be controlling transport. The direction of plume propagation also suggests that variations in permeability may be affecting transport as the two plumes appear to be moving in slightly different directions, which do not agree with the distribution of hydraulic head. However, these facts may be coincidental as other factors, such as sorption and biodegradation, may be limiting the rate of TCE and TCA transport.

In both cases discussed above, the role of variations in the fracture network on the behaviour of solute and contaminant transport is not well understood. Future investigations should attempt to better account for this variability by conducting more pump tests and possibly tracer tests. In many studies, increasing the number of test holes may greatly increase the amount of certainty that can be placed on both models and design.

CHAPTER 11: CONCLUSIONS AND RECOMMENDATIONS FOR FUTURE RESEARCH

11.1 Summary and Conclusions

Basal heat flow and subsurface temperatures in Southern Manitoba are quite low and as a result there is very little potential for direct-use geothermal energy. These low temperatures also detract from the efficiency of heat pumps. Modeling results indicate that the regional aquifers of southern Manitoba appear to have little impact on heat flow in the region, largely due to the low groundwater velocities present and the geometries of the regional groundwater flow systems. However, groundwater flow does have a large enough impact on the temperature in the Sandilands area to provide an estimate of groundwater recharge. Groundwater recharge in the tills underlying the moraine is estimated to occur at a rate of approximately 10^{-9} to 10^{-8} m s^{-1} in this area and recharge appears to be restricted areas of higher elevation where sands and gravels are present near the surface.

Thermal conductivity of the Red River Formation has a mean value of approximately 2.4 W °C^{-1} m^{-1} based on analyses performed in this study. The use of an empirical model or simple deterministic model to estimate thermal conductivities in other areas of the Paleozoic carbonate sequence in the Winnipeg area is not recommended, due to poor correlations between thermal conductivity and other petrophysical parameters. A stochastic treatment of thermal conductivity suggests that the mean sample value is the best estimate to use in this situation.

321

The temperature field beneath Winnipeg is significantly different than that measured in surrounding areas. This difference is largely due to heat loss from buildings in the area and, to a lesser extent, due to injection of thermal wastewater, changes in surface cover and climate change. Temperatures in the Carbonate Rock Aquifer are greater than 5°C above background temperatures have been observed outside of areas affected by the injection of thermal wastewater. Numerical modeling indicates that after 30 to 40 years of heat loss from a building does the upper portion of the Carbonate Rock Aquifer attains this 5° C increase in temperature and therefore under most older areas of the Winnipeg no further increases in temperature are expected. Further temperature increases are expected beneath the newer areas of Winnipeg. This increase in temperature creates an interesting situation where heat pumps are more efficient in Winnipeg than in surrounding rural areas.

The current practice of using groundwater from the Carbonate Rock Aquifer for cooling is unsustainable due to rises in subsurface temperatures associated with the injection of thermal wastewater. Heat introduced by the injection of thermal wastewater reaches the production well during the first few years of operation for current well spacings and production rates. In many cases the production temperature is nearly the same as the injection temperature shortly after thermal breakthrough. At this point, the efficiency of the system is compromised and operators must accept this lack of efficiency or choose to ignore Manitoba Water guidelines and increase injection

temperatures. Both of these outcomes are undesirable and usage schemes must change to allow for sustainable thermal use of the Carbonate Rock Aquifer. There is an increase in demand for clean energy sources and the use of the waste heat contained in thermal wastewater for space heating could be used to meet a portion of this demand. This task can be accomplished either by stripping the excess heat from the wastewater prior to injecting it back into the aquifer or by storing the heat in the aquifer for use during the winter season. Alternatively, thermal wastewater could be discharged to a surface water body or the sewer. The latter option is less environmentally friendly as it wastes heat, causes drawdown in the aquifer, strains the capacity of the sewer system and can introduce poor quality water into surface water bodies. This practice is not recommended due to the environmental benefits of using the waste heat for space heating.

11.2 Recommendations for Future Research

Regional heat flow in southern Manitoba is relatively poorly constrained outside the Winnipeg area. This is especially true for an area between the Red River and the oil producing areas near Virden and Wascada, where few measurements exist. Also, there is a lack of data for the Precambrian basement throughout much of southern Manitoba. More measurements in these areas may help to provide additional insight into regional groundwater flow and the potential for geothermal energy use in other parts of Manitoba. Also, the treatment of the interaction between regional groundwater flow and heat flow was treated somewhat heuristically

in this thesis, as it was done primarily to assess the background temperature distributions and to look at the relative importance of conduction and advection. However, there is additional potential to constrain regional groundwater flow models with the temperature measurements made in this study and with future temperature measurements. This may be particularly useful in the creation of a numerical model of the Sandilands area. A numerical model of this area would also be of interest as it could help to summarize the findings of recent studies using tritium and chlorofluorocarbons (Cherry, 2000; Hinton, 2003) and the findings of the current study, which were based on heat flow. Additional temperature measurements in the Sandilands area over the next several years or even decades will assist in addressing the effect of variations in climate on estimates of recharge from temperature profiles.

The findings of this study also suggest that the Carbonate Rock Aquifer can be treated as a porous medium in most cases. However, there are important exceptions to this idea and detailed studies that have high frequency records of temperature, hydraulic head and pumping rates may help to provide insight into this problem. These studies should be accompanied by detailed geological and hydrogeological investigations that quantify the hydraulic properties of the matrix and fractures and their spatial distribution. A comparison of the transport of conservative solutes, especially those that could be used as a tracer, and heat flow would also be of use. By establishing this relationship it may be possible to better estimate thermal

breakthrough times, which is an important consideration in both the current

usage schemes and in ATES systems.

REFERENCES

Aitken, J.D. 1989. The Sauk Sequence; Cambrian to Lower Orodovician migeocline and platform. *In* Ricketts, B.D. (ed.). The Western Canadian Sedimentary Basin; A case history, p. 105-119. Canadian Society of Petroleum Geologists, Calgary, Alberta.

Allen, A., Milenic, D. and Sikora, P. 2003. Shallow gravel aquifers and the urban 'heat island' effect: a source of low enthalpy geothermal energy. Geothermics 32: 569-578.

Allen, D.M, Ghomshei, M.M., Sadler-Brown, T.L., Dakin, A. and Holtz, D. 2000. The current status of geothermal exploration and development in Canada. World Geothermal congress 2000, Japan.

Anderson, M.P. and Woessner, W.W. Applied groundwater modeling; simulation of flow and advective transport. Academic Press, San Diego, USA.

Bachu, S. 1991. On the effective thermal and hydraulic conductivity of binary heterogeneous sediments. Tectonophysics 190: 299-314.

Baracos, A., Shields, D.H. and Kjartanson, B.1983. Geological Engineering Maps & Report. Cantext Publications, Winnipeg, Manitoba.

Bear, J. 1972. Dynamics of Fluids in Porous Media, Dover Publications Inc., New York, New York.

Bear, J. 1993. Modeling flow and contaminant transport in fractured rocks. In Bear, J., Tsang, C. and de Marsily, G (eds.). Flow and contaminant transport in fractured rock, p. 1-37. Academic Press, San Diego.

Beck, A.E. 1965. Techniques of Measuring Heat Flow on Land., In Lee,

    W.H.K. (ed.). Terrestrial Heat Flow., Geophysical Monograph No. 8.,

    p. 24-51. American Geophysical Union, Washington, D.C.

Beck, A.E. 1976. An improved method of computing the thermal conductivity

    of fluid-filled sedimentary rocks. Geophysics 41 (1): 133-144.

Beltrami, H. 2001. On the relationship between ground temperature histories

    and meteorological records: a report on the Pomquet station. Global

    and Planetary Change 29 (3-4), 327-348.

Beltrami, H. and Harris, R.N. 2001. Foreword: Inference of climate change

    from geothermal data. Global and Planetary Change 29 (3-4),149-152.

Beltrami, H., Gosselin, C. and Mareschal, J.C. 2003. Ground surface

    temperatures in Canada: Spatial and temporal variability.

    Geophysical Research Letters 30(10): 1499, doi:

    10.1020/2003GL017144.

Berkowitz, B. 2002. Characterizing flow and transport in fractured geological

    media: A review. Advances in Water Resources 25: 861-884.

Betcher, R.N. 1977. Temperature distributions in deep groundwater flow

    systems; a finite element model. M.Sc. Thesis. University of Waterloo,

    Waterloo, Ontario.

Betcher, R.N. 1986. Regional Hydrogeology of the Winnipeg Formation in

    Manitoba. Proceedings of the Third Canadian Hydrogeological

    Conference. International Association of Hydrogeologists, Saskatoon,

    Saskatchewan, pp. 159-174.

Betcher, R., Grove, G. and Pupp, C. 1995. Groundwater in Manitoba: Hydrogeology, Quality Concerns, Management. National Hydrology Research Institute, Saskatoon, Saskatchewan.

Birch, F. 1948. The effects of Pleistocene climatic variations on upon geothermal gradients. American Journal of Science 246, 729-760.

Blackwell, D.D. and Steele, J.L. 1989. Thermal Conductivity of Sedimentary Rocks: Measurement and Significance, In Naeser, N.D. and T.H. McCulloh (eds). Thermal History of Sedimentary Basins: Methods and Case Histories, pp. 13-36, Springer-Verlag, New York, New York.

Bloomquist, R.G. 2003. Geothermal space heating. Geothermics 32: 513-526.

Brailsford, A.D. and Major, K.G. 1964. The thermal conductivity of aggregates of several phases including porous materials, British Journal of Applied Physics 15: 313-319.

Bredehoeft, J.D. and Papadopulos, I.S. 1965. Rates of vertical groundwater movement estimated from the Earth's thermal profile. Water Resources Research 1, no. 2: 325-328.

Brigaud, F. and Chapman, D.S., Le Douaran, S. 1990. Estimating Thermal Conductivity in Sedimentary Basins Using Lithologic Data and Geophysical Well Logs. The American Association of Petroleum Geologists Bulletin 74(9): 1459-1477.

Bruntland, G. (ed.), (1987). Our common future: The World Commission on Environment and Development. Oxford University Press, Oxford, U.K.

Bullard, E.C. 1965. Techniques of Measuring Heat Flow on Land., In Lee, W.H.K. (ed.). Terrestrial Heat Flow., Geophysical Monograph No. 8., p. 1-6. American Geophysical Union, Washington, D.C.

Card, K.D. and Poulsen, K.H. 1998. Geology and Mineral Deposits of the Canadian Shield. In Lucas, S.B. and St-Onge, M.R. (eds.). Geology of the Precambrian Superior and Grenville Provinces and Precambrian Fossils in North America. Geology of Canada, no. 7. Geological Survey of Canada, Ottawa, Ontario, pp. 15-204.

Carslaw, H.S. and Jaeger, J.C. 1959. Conduction of heat in solids. Clarendon Press, Oxford, U.K.

Cartwright, K. 1970. Groundwater discharge in the Illinois Basin as suggested by temperature anomalies. Water Resources Research 6, no. 3: 912-918.

Cermak, V. and Rybach, L. 1982. Thermal properties. In Hellwedge, K. (ed.). Numerical Data and Functional Relationships in Science and Technology, New Series; Group V. Geophysics and Space Research, Volume 1 Physical Properties of Rocks, Subvolume a, pp. 305-371. Springer-Verlag, Berlin, Germany.

Cermak, V., Bodri, L. and Safanda, J. 1992. Underground temperature fields and changing climate; evidence from Cuba. Global and Planetary Change 5 (4); 325-337.

Chapman, D.S. 1995. Climate change inferred from borehole temperatures: an overview. IUGG, XXI. General Assembly, p. A286.

Chen, Z., Grasby, S.E. and Osadetz, K.G. 2002. Predicting average annual groundwater levels from climatic variables; an empirical model. Journal of Hydrology 260: 102-117.

Cherry, A.J. 2000. A Multi-tracer estimation of groundwater recharge in a glaciofluvial aquifer in Southeastern Manitoba. M.Sc. diss, Department of Earth Sciences, University of Ottawa.

Conway, J.G. and Beck, A.E. 1977. Fine-scale correlation between t emperature gradient logs and litnology. Geophysics 42 (7): 1401-1410.

Day, M. J. 1978. Movement and hydrochemistry of groundwater in fractured clayey deposits in the Winnipeg area. M.Sc. Thesis, University of Waterloo, Waterloo, Ontario.

Domenico, P.A and Palciauskas, V.V. 1973. Theoretical Analysis of Forced Convective Heat Transfer in Regional Ground-water Flow. Geological Society of America Bulletin 84 (12): 3803-3814.

Domenico, P.A. and Schwartz, F.W. 1998. Physical and Chemical Hydrogeology, 2nd ed. New York: John Wiley and Sons.

Dortman, N.B. 1976. Physical properties of rocks and mineral deposits; geophysical handbook (in Russian). Moscow, Russia, Izdat Nedla.

Doughty, C. and Karasaki, K. 2002. Flow and transport in hierarchiacally fractured rock. Journal of Hydrology 263: 1-22.

Ferguson, G. and St. George, S. 2003. Historical and Estimated Ground Water Levels Near Winnipeg, Canada, and Their Sensitivity to Climatic

Variability. Journal of the American Water Resources Association 39 (5): 1249-1259.

Ford, D.C. 1983. Karstic interpretation of the Winnipeg aquifer. Journal of Hydrology 61: 177-180.

Freeze, R.A. and Cherry, J.A. 1979. Groundwater. Englewood Cliffs, N.J. : Prentice Hall.

Gelhar, L.W. 1993. Stochastic Subsurface Hydrology. Prentice-Hall Inc. Englewood Cliffs, New Jersey.

Grasby, S.E. and Betcher, R.N.. 2002. Regional Hydrogeochemistry of the Carbonate Rock Aquifer. Canadian Journal of Earth Sciences 39 (7):1053 -1063.

Grasby, S., Osadetz, K., Betcher, R. and Render, F. 2000. Reversal of the regional-scale flow system of the Williston Basin in response to Pleistocene glaciation. Geology 28, no. 7: 635-638.

Gretener, P. E. 1967. On the thermal instability of large diameter wells; an observational report. Geophysics 32, no. 4: 727-738.

Gretener, P.E. 1981. Geothermics: Using Temperature in Hydrocarbon Exploration. AAPG Continuing Education Short Course Note Series. San Francisco, California: American Association of Petroleum Geologists.

Gringarten, A.C. 1978. Reservoir Lifetime and Heat Recovery Factor in Geothermal Aquifers used for Urban Heating. Pure and Applied Geophysics 117 (1-2): 295-308.

Gringarten, A.C. and Sauty, J.P. 1975. A Theoretical Study of Heat Extraction From Aquifers With Uniform Regional Flow. Journal of Geophysical Research 80 (35): 4956-4962.

Grove, D.B., Beetem, W.A. and Sower, F.B. 1970. Fluid travel time between a recharging and discharging well pair in an aquifer having a uniform regional flow field. Water Resources Research 6 (5): 1404-1407.

Guillou-Frottier, L., Mareshcal, J.C. and Musset, J. Ground surface temperature history in central Canada inferred from 10 selected borehole temperature profiles. Journal of Geophysical Research 103 (B4), 7385-7397.

Hales, A.L. Convection Currents in Geysers. 1937. Monthly Notices of the Royal Astronomical Society, Geophysics Supplement 4, no. 1: 122-132.

Harris, R.N. and Chapman, D.S. 1997. Borehole temperatures and a baseline for 20th century global warming estimates. Science 275, no 5306: 1618-1621.

Harris, R.N. and Gosnold, W.D. 1998. Comparisons of borehole temperature-depth profiles and surface air temperatures in the northern plaines of the USA. Geophysical Journal International 138 (2): 541-548.

Hinton, M.J. Comparison of Groundwater CFC Sampling Methods for Measuring Recharge. 4th Joint IAH CNC-CGS Conference, Winnipeg, Manitoba.

Hitchon, B. 1969. Fluid flow in the western Canada sedimentary basin; 1.
Effect of topography. Water Resources Research 5(1): 186-195.

Hoffman, P.F.1989. Precambrian geology and tectonic history of North
America. In Bally, A.W. (ed.). The geology of North America; an
overview. Geological Society of America, Boulder, U.S.A., pp. 447-
512.

Horai. K. 1971. Thermal conductivity of rock-forming minerals. Journal of
Geophysical Research 76 (5): 1278-1308.

Hubbert, M.K. 1940. On the theory of ground-water motion. Journal of
Geology 48: 785-944.

Hubbert, M.K. 1956. Darcy's law and the field equations of the flow of
underground fluids. Petroleum Transactions – AIME 207: 222-235.

Hutchence, K., Weston, J.H., Law, A.G., Vigrass, L.W. and Jones, F.W. 1986.
Modeling of a liquid phase geothermal doublet system at Regina,
Saskatchewan, Canada. Water Resources Research 22: 1469-1479.

Huttrer. G.W. 2001. The status of world geothermal power generation 1995-
2000. Geothermics 30 (1), 1-27.

Jessop, A.M. 1989. Hydrological distortion of heat flow in sedimentary
basins. Tectonophysics 164:211-218.

Jessop, A.M. 1990. Thermal Geophysics. Developments in Solid Earth
Geophysics. Elsevier, Amsterdam, The Netherlands.

Jessop, A.M. and A.M. Judge. 1971. Five measurements of heat flow in
southern Canada. Canadian Journal of Earth Sciences 8 (6): 711-716.

Karl, T.R., Diaz, H.F., and Kukla, G. 1988. Urbanization: Its Detection and Effect in the United States Climate Record. Journal of Climate 1: 1099-1123.

Kennedy, P.L. 2002. Groundwater flow and transport model of the Red River/Interlake area in southern Manitoba. Ph.D. diss, Department of Civil and Geological Engineering, University of Manitoba.

Konikow, L.F. and Bredehoeft, J.D. 1993. Ground water models; validate or invalidate. Ground Water. 31 (2): 178-179.

Lachenbruch, A. and Marshall, B.V. 1986. Changing climate: geothermal evidence from permafrost in the Alaskan Arctic. Science 234, 689-696.

Lachenbruch, A.H. and Sass, J.H. 1977. Heat flow in the United States. In The Earth's Crust. Geophysical Monograph Series 20. Ed. Heacock, G. American Geophysical Union, Washington, D.C.

Landsberg, H.E. 1981. The Urban Climate. International Geophysics Series 28. Academic Press, Toronto, Ontario.

Lewis, T.J. and Beck. A.E. 1977. Analysis of heat-flow data – detailed observations in many holes in a small area. Tectonophysics 41: 41-59.

Li, D. and Lake, L.W. 1994. A moving window semivariance estimator, Water Resources Research 30 (5): 1479-1489.

Lichtner, P.C. Multiphase reactive transport in partially saturated porous media; application to the proposed high-level nuclear waste repository

at Yucca Mountain, Nevada. Abstracts with Programs – Geological

Society of America 28 (7): 48.

Lichtner, P.C., Seth, M.S. and Painter, S. 2000. MULTIFLO User's Manual;

MULTIFLO Version 1.2. Southwest Research Institute. San Antonio,

Texas.

Lowrie, W. 1997. Fundamentals of Geophysics. Cambridge University

Press, Cambridge, U.K.

Lu, N. and Ge, S. 1996. Effect of horizontal heat and fluid flow on the

vertical temperature distribution in a semiconfining layer. Water

Resources Research 32, no. 5 : 1449-1453.

Lund, J.W. and Freeston, D.H. 2000. World-wide direct uses of geothermal

energy 2000. Proceedings World Geothermal Congress 2000.

Kyushu-Tohoku, Japan, pp. 1-21.

MacLeod, J.M. 1997. Instructions for operating the divided bar apparatus for

thermal conductivity measurement at the GSC, Calgary. Geological

Survey of Canada, Open File 3444.

Majorowicz, J.A. and Jessop, A.M. 1981. Regional heat flow patterns in the

Western Canadian sedimentary basin. Tectonophysics 74 (3-4): 209-

238.

Majorowicz, J.A., Jones, F.W. and Jessop, A.M. 1986. Geothermics of the

Williston Basin in Canada in relation to hydrodynamics and

hydrocarbon occurrences. Geophysics 51(3): 767-779.

Majorowicz, J.A., Safanda, J, Harris, R.N., and Skinner, W. 1999. Large

ground surface temperature changes in the last three centuries

inferred from borehole temperatures in the Southern Canadian

Prairies, Saskatchewan. Global and Planetary Change 20: 227-241.

Manley, G. 1958. On the frequency of snowfall in metropolitan England.

Quarterly Journal of the Royal Meteorological Society 84, 70-72.

McBean, G.A., Weaver, A.J. and Roulet, N. 2001. The Science of Climate

Change: What do we know? ISUMA: Canadian Journal of Policy

Research 2(4): 16-25.

McCabe, H. R. 1971. Stratigraphy of Manitoba, an introduction and review,

Geoscience studies in Manitoba. Special Paper - Geological

Association of Canada, 9, pp. 167-187.

McCabe, H.R. 1978. Reservoir potential of the Winnipeg and Deadwood

Formations in Manitoba. Manitoba Energy and Mines Geological

Paper 78-3.

McCabe, H.R., Betcher, R.N. and Render, F.W. 1993. The Fort Garry Aquifer

in Manitoba. Manitoba Energy and Mines, Geological Services.

Geological Report GR93-1.

McMillan, R.J., Betcher, R.N. and Woodbury, A.D. 2001. Studies of Seepage

Beneath Earthen Manure Storages and Cattle Pens in Manitoba.

Proceedings of the Livestock Options for the Future Conference.

Winnipeg, Manitoba, pp. 100-116.

Michel, F.A. and Allen, D.M. 2003. Identification and Management of Potential Problems in Aquifer Thermal Energy Storage Systems. 4th Joint IAH CNC-CGS Conference, Winnipeg, Manitoba.

Moench, A.F. 1984. Double-Porosity Models for a Fissured Groundwater Reservoir With Fracture Skin. Water Resources Research 20(7): 831-846.

Molz, F.J., Warman, J.C., Jones, T.E. 1978. Aqufier storage of heated water; Part 1, A field experiment. Ground Water 16: 234-241.

Murtha, G.G. and J. Williams. 1986. Measurement, prediction and interpolation of soil temperature for use is soil taxonomy: Tropical Australian experience. *Geoderma* 37: 189-206.

Mwenifumbo, C. J., Bezys, R., Betcher, R. N., Killeen, P. G. 1992. Borehole geophysical logs, Manitoba. Open-File Report - Geological Survey of Canada, 2734.

Oke, T.R. 1979. Review of Urban Climatology. *WMO Tech Note No. 169.*

Osadetz, K.G. and Haidl, F.M. Tippecanoe Sequence; Middle Ordovician to Lowest Devonian; vestiges of a great epeiric sea. *In* Ricketts, B.D. (ed.). The Western Canadian Sedimentary Basin; A case history, p. 121-137. Canadian Society of Petroleum Geologists, Calgary, Alberta.

Pach, J.A. 1994. Hydraulic and solute transport characteristics of a fractured glacio-lacustrine clay; Winnipeg, Manitoba. Ph.D. Thesis, University of Waterloo, Waterloo, Ontario.

Painter, S., Winterle, J.R. and Armstrong, A. 2001. Using temperature data to constrain models of groundwater flow near Yucca Mountain, Nevada. Abstracts with Program – Geological Society of America 33(6): 107.

Palmer, C.D. and Cherry, J.A. 1984. Geochemical reactions associated with low-temperature thermal energy storage in aquifers. Canadian Geotechnical Journal 21: 475-488.

Parsons, M.L. 1970. Groundwater thermal regime in a glacial complex. Water Resources Research 6, no. 6: 1701-1720.

Perlinger, J.A., Almendinger, J.E., Urban, N.R. and Eisenreich, S.J. 1987. Groundwater geochemistry of aquifer thermal energy storage; long-term cycle. Water Resources Research 23: 2215-2226.

Pollack, H.N. and Chapman, D.S. 1993. Underground records of changing climate. Scientific American 268, 44-50.

Porter, J.W., Price, R.A. and McCrossan, R.G. 1982. The Western Canada sedimentary basin. In Kent, P., Botts, M.H.P. and McKenzie, D.P. (eds.). Evolution of sedimentary basins. Philosophical Transactions of the Royal Society of London, Series A: Mathematical and Physical Sciences 305(1489): 169-193.

Prest, V.K. 1967. Nomenclature of Moraines and Ice-Flow Features as Applied to the Glacial Map of Canada. Geological Survey of Canada Paper 67-57.

Reiter, M. 2001. Using precision temperature logs to estimate horizontal and

vertical groundwater flow components. Water Resources Research
37, no. 3: 663-674.

Render, F.W. 1970. Geohydrology of the Metropolitan Winnipeg Area as
related to groundwater supply and construction. Canadian
Geotechnical Journal 7, 243-27.

Render, F.W. 1981. Hydrogeologic aspects of suppy well – recharge well air
conditioning in the Birchwood Area of Winnipeg. Manitoba Department
of Natural Resources, Water Resources Branch, Winnipeg, Manitoba,
44pp.

Render, F.W. 1983. Hydrogeology of the Winnipeg Area. In: Baracos, A.,
Shields, D.H. and Kjartanson, B. (Eds.) Geological Engineering Maps
& Report for Urban Development of Winnipeg, Cantext Publications,
Winnipeg, Manitoba, pp. 29-40.

Rutulis, M. 1989. Groundwater drought sensitivity of southern Manitoba.
Canadian Water Resources Journal 14 (1): 18-33.

Rybach, L. 2003. Geothermal energy: sustainability and the environment.
Geothermics 32: 463-470.

Sauty, J.P., Gringarten, A.C., Menjoz, A. Landel, P.A. 1982. Sensible energy
storage in aquifers; 1. Theoretical study. Water Resources Research
18: 245-252.

Scanlon, B.R. and P.G. Cook. 2002. Preface, Theme Issue on Groundwater
Recharge. Hydrogeology Journal 10, no.1: 3-4.

Schmidt, W.L and Gosnold, W.D. and Enz, J. 2001. A decade of air-ground temperature exchange from Fargo, North Dakota. Global and Planetary Change 29 (3-4), 311-325.

Schon, J.H. 1996. Physical Properties of Rocks: Fundamentals and Principles of Petrophysics. Handbook of Geophysical Exploration Volume 18. Pergamon, Trowbridge, U.K.

Shen, P.Y., Pollack, H.N., Huang, S. and Wang, K. 1995. Effects of subsurface heterogeneity on the inference of climate change from borehole temperature data: Model studies and field examples from Canada. Journal of Geophysical Research 100(4): 6383-6396.

Simpson, F, McCabe, H.R. and Barchyn, D. 1987. Subsurface disposal of wastes in Manitoba. Part 1: Current status and potential of subsurface disposal of fluid industrial wastes in Manitoba. Manitoba Geological Survey Geological Paper GP83-1.

Slattery, J.C. 1972. Momentum, Energy and Mass Transfer in Continua. McGraw-Hill, New York, U.S.A.

Smith, L. and Chapman, D.S. 1983. On the Thermal Effects of Groundwater Flow 1. Regional Scale Systems. Journal of Geophysical Research 88 (B1), 593-608.

Snow, D.T. 1969. Anisotropic permeability of fractured media. Water Resources Research 5: 1272-1289.

Spitz, K. and Moreno, J.L. 1996. A practical guide to groundwater and solute transport modeling. John Wiley and Sons, New York, USA.

Stallman, R.W. 1963. Computation of vertical groundwater velocity from temperature data. U.S. Geological Survey Water Supply Paper 1544H.

Taniguchi, M., Shimada, J., Tanaka, T., Kayane, I., Sakura, Y., Shimano, Y., Dapaah-Siakwan, S. and Kawashima, S.. Disturbances of temperature-depth profiles due to surface climate change and subsurface water flow: 1. An effect of linear increase in surface temperature caused by global warming and urbanization in the Tokyo metropolitan area, Japan. Water Resources Research 35 (5), 1507-1517.

Teller, J.T. and M.M. Fenton.1980. Late Wisconsinan glacial stratigraphy and history of southeastern Manitoba. Canadian Journal of Earth Sciences 17, no. 1: 19-35.

Teller, J.T. and Clayton, L. 1983. An Introduction to Glacial Lake Agassiz. In Teller, J.T. and Clayton, L. Glacial Lake Agassiz. Geological Association of Canada Special Paper, pp. 1-3.

Theis, C.V. 1935. The relation between the lowering of the piezometric surface and the rate and duration of discharge of a well using groundwater storage. Transactions of the American Geophysical Union 2: 519-524.

Toth, J. 1962. A theory of groundwater in small drainage basins in central Alberta, Canada. Journal of Geophysical Research 67(11): 4375-4387.

UMA Engineering Ltd. 1993. Bristol Aerospace Limited Rockwood Propellant Plant. Unpublished report.

Woodbury, A.D., and Smith, L. 1985. On the thermal effects of three dimensional groundwater flow, Journal of Geophysical Research 90(B1): 759-767.

Woodbury, A.D., Smith, L and Dunbar, W.S. 1988. Simultaneous inversion of hydrogeologic data; 1. Theory and application using hydraulic head data. Water Resources Research, 23(8): 1586-1606.

Woodbury, A. D., Narod, B., Chandra, B., and B. Bennist. 1991. Temperature measurements in geotechnical studies using low-noise high-resolution digital techniques. Canadian Geotechnical Journal, 28(5): 639-649.

Woodside, W., and Messmer, J.H. 1961.Thermal conductivity of porous media, 1. Unconsolidated sands, 2, Consolidated rocks, Journal of Applied Physics., 32: 1688-1706.

Appendix A: Petrophysical Data

Borehole	Sample Number	Depth (m)	Porosity	Average thermal conductivity (W m^{-1} °C^{-1})	Orientation of Thermal Conductivity Measurements	Saturated Density (kg m^{-3})	Mineral Density (kg m^{-3})
W8	59A	17.98	0.11	2.35	Vertical	2570	2761
W8	59B	18.01	0.05	2.94	Vertical	2740	2825
W8	59C	18.04	0.05	2.84	Vertical	2703	2791
W8	59D	18.07	0.05			2718	2801
W8	63A	19.20	0.03	3.15	Vertical	2747	2807
W8	64HA	19.51	0.05			2729	2816
W8	65A	19.81	0.06			2698	2801
W8	65C	19.87	0.07	2.61	Vertical	2612	2729
W8	65D	19.81	0.05	2.80	Vertical	2695	2793
W8	68A	20.73	0.07	2.32	Vertical	2641	2756
W8	68B	20.76				2665	
W8	68B2	20.76	0.09	2.79	Vertical	2668	2837
W8	68C	20.79				2633	2238
W8	69B	21.06	0.09			2622	2777
W8	69C	21.09	0.10	2.47	Vertical	2634	2809
W8	69D	21.12	0.13	1.01	Vertical	2592	2834
W8	69HA	21.03	0.10	1.66	Horizontal	2626	2804
W8	69HB	21.03	0.10	2.14	Horizontal	2617	2792
W8	69HC	21.03	0.09	1.96	Horizontal	2619	2787
W8	70.5A	21.49	0.10	1.84	Vertical	2574	2757
W8	70.5B	21.52	0.12			2638	2859
W8	70.5C	21.55	0.11	2.34	Vertical	2606	2815
W8	72HA	21.95	0.11	2.42	Horizontal	2582	2784
W8	73A	22.25	0.13			2584	2816
W8	73B	22.28	0.10	2.27	Vertical	2563	2736
W8	73C	22.31	0.14			2611	2863
W8	74A	22.56	0.11			2633	2827
W8	74B	22.59	0.08			2681	2828
W8	74HA	22.56	0.12				
W8	75A	22.86	0.15			2529	2801
W8	75B	22.89	0.16	1.77	Vertical	2531	2816
W8	76A	23.16	0.12			2571	2783
W8	76B	23.20	0.13			2585	2813
W8	76C	23.23	0.11			2568	2765
W8	77A	23.47	0.12	1.71	Vertical	2577	2791
W8	77B	23.50	0.12	2.43	Vertical	2571	2786
W8	78A	23.77	0.15	1.89	Vertical	2549	2825
W8	78B	23.77	0.16			2541	2836
W8	78HA	23.80	0.14	2.05	Horizontal	2538	2784
W8	80.5A	24.54	0.14	1.58	Vertical	2565	2825
W8	80.5B	24.57	0.12			2555	2772
W8	80.5C	24.60	0.11			2575	2777
W8	81.5HB	24.84	0.12	1.92	Horizontal	2564	2786

Borehole	Sample Number	Depth (m)	Porosity	Average thermal conductivity (W m^{-1} °C^{-1})	Orientation of Thermal Conductivity Measurements	Saturated Density (kg m^{-3})	Mineral Density (kg m^{-3})
W8	83A	25.30	0.11			2593	2797
W8	83B	25.33	0.11	2.27	Vertical	2596	2795
W8	83C	25.36	0.11			2559	2759
W8	83D	25.39	0.08			2566	2705
W8	84.5HA	25.76	0.14	0.87	Horizontal	2552	2799
W8	85A	25.94	0.17			2505	2818
W8	85B	25.97	0.14			2463	2697
W8	85HA	25.91	0.13	2.58	Horizontal	2571	2815
W8	85HB	25.91	0.13			2570	2802
W8	86A	26.21	0.09	2.51	Vertical	2631	2787
W8	86B	26.24	0.05			2650	2733
W8	86C	26.27	0.07	2.58	Vertical	2670	2799
W8	87A	26.52	0.07	3.56	Vertical	2620	2750
W8	87B	26.55	0.07			2643	2769
W8	87C	26.58	0.07			2641	2760
W8	87HA	26.61	0.07	1.91	Horizontal	2681	2815
W8	87HB	26.52	0.08	1.89	Horizontal	2680	2828
W8	87HC	26.52	0.08	1.74	Horizontal	2674	2814
W8	88.5C	27.04	0.14	1.87	Vertical	2545	2788
W8	89A	27.13	0.05			2734	2828
W8	89B	27.16	0.05	2.60	Vertical	2726	2814
W8	89C	27.19	0.05	2.50	Vertical	2724	2815
W8	89D	27.22		2.13	Vertical		
W8	89HA	27.13	0.05			2678	2775
W8	90A	27.43	0.06	1.86	Vertical	2691	2802
W8	92A	28.04	0.05			2672	2761
W8	92B	28.07	0.06	1.45	Vertical	2669	2773
W8	92C	28.10	0.08	2.66	Vertical	2646	2790
W8	94A	28.65	0.06	2.42	Vertical	2681	2781
W8	94B	28.68	0.05	1.79	Vertical	2710	2804
W8	94C	28.71	0.05			2688	2774
W8	94D	28.74	0.06	2.81	Vertical	2715	2819
GSC7001	N/A	122.22		1.71	Vertical		
GSC7001	N/A	63.70		1.84	Vertical		
GSC7001	N/A	107.29		1.85	Vertical		
GSC7001	N/A	63.70		2.00	Vertical		
GSC7001	N/A	122.20		2.15	Vertical		
GSC7001	N/A	137.16		2.23	Vertical		
GSC7001	N/A	46.94		2.39	Vertical		
GSC7001	N/A	20.12		2.45	Vertical		
GSC7001	N/A	76.20		2.55	Vertical		
GSC7001	N/A	20.40		2.60	Vertical		
GSC7001	N/A	137.20		2.70	Vertical		
GSC7001	N/A	46.90	0.065	2.74	Vertical		
GSC7001	N/A	20.10	0.13	2.85	Vertical		

Borehole	Sample Number	Depth (m)	Porosity	Average thermal conductivity (W m^{-1} $^\circ$C^{-1})	Orientation of Thermal Conductivity Measurements	Saturated Density (kg m^{-3})	Mineral Density (kg m^{-3})
GSC7001	N/A	24.10		2.97	Vertical		
GSC7001	N/A	20.42		3.21	Vertical		
GSC7001	N/A	107.30		3.21	Vertical		
GSC7001	N/A	24.08		3.77	Vertical		
GSC7001	N/A	167.60		5.54	Vertical		
PB	P1A	25.00	0.05	1.943	Vertical		
PB	P2A	25.00	0.06	2.412	Vertical		
PB	P3A	25.00	0.06	1.591	Vertical		
PB	P3B	25.00	0.07	2.470	Vertical		
PB	P4A	25.00	0.07	5.539	Vertical		
PB	P4B	25.00	0.07				

Appendix B: Temperature Data

B.1 Well Locations and Aquifer Temperatures

Well Identification	Description	UTMX (m)	UMTY (m)	Upper Carbonate Aquifer Temperature (°C)	Winnipeg Formation Temperature (°C)	Source
G050C018	Pembina Hwy and Hwy 100	632620	5515230	6.2	N/A	Ferguson
G050G003	Oak Bluff MO-5	623605	5514130	6	N/A	Ferguson
G050H003	St Annes Rd RRF 02	639810	5516930	6	N/A	Ferguson
G050J022	Route 90 and Hwy 101	626700	5538300	5.9	N/A	Ferguson
G05MJ077	611 Academy Rd	629500	5526300	7.5	N/A	Ferguson
G050H013	Swift 1 Archibald St	636870	5526590	7.5	N/A	Ferguson
G05MJ006	Assiniboine River and Hwy 100	620420	5525290	6.7	N/A	Ferguson
G050H019	Canada Packers	637200	5527000	8	N/A	Ferguson
G05MJ008	Sturgeon Creek and Perimeter	620510	5529850	5.7	N/A	Ferguson
G050C049	Rue des Trappistes and Pembina Hwy	633000	5513800	6.5	N/A	Ferguson
G050H010	Murdock Rd and Dugald Rd RRF 055	645000	5527860	5.6	N/A	Ferguson
G050J030	Murdock Rd and Dugald Rd	645000	5527800	5.6	N/A	Ferguson
G050J003	Deacon Rd and Cedar Lake Rd	648300	5529010	5.9	N/A	Ferguson
G050J103	M-187 Grassmere	637420	5538890	6	N/A	Ferguson
G050J009	Grassie Blvd and Hwy 59 RRF 045	640230	5531980	6.3	N/A	Ferguson
G050J014	Gunn Rd RRF 052	644500	5531000	5.8	N/A	Ferguson
G050H012	MO-11 GWWD	636540	5528540	7.7	N/A	Ferguson
G050J028	Hudson Bay House MO-15	634020	5527905	9.6	7.4	Ferguson
G050H011	Hwy 1 and Floodway RRF 061	647210	5521860	5.8	N/A	Ferguson
G050H009	Ile de Chenes	646000	5508300	5.7	N/A	Ferguson

346

Well Identification	Description	UTMX (m)	UMTY (m)	Upper Carbonate Aquifer Temperature (°C)	Winnipeg Formation Temperature (°C)	Source
G05MJ007	Inkster Blvd and Hwy 101 MO-7	620800	5534400	5.6	N/A	Ferguson
G05MJ037	Air Canada (Winnipeg Airport)	625700	5529300	6	N/A	Ferguson
G05MJ005	Wilkes Ave and Hwy 101	620220	5522020	6	N/A	Ferguson
G05MJ076	Grace Hospital	623700	5526800	6.4	N/A	Ferguson
G050C003	Norwood Bridge	634200	5527300	7.7	N/A	Ferguson
G050C008	Taylor Ave near PanAm Pool	632020	5524150	7.9	N/A	Ferguson
G050C001	St Marys Rd Near Floodway Inlet RRF 040	634970	5513340	6.2	N/A	Ferguson
G050H005	Symington Rd and Hwy 1 RRF 043	643600	5524000	5.9	N/A	Ferguson
G050J092	Riverside Quarries (Panet)	638420	5528800	6.4	N/A	Ferguson
G060G020	Turnbull Drive and Hwy 75	633500	5512800	6.4	N/A	Ferguson
UM2	University Stadium	633440	5518680	6	N/A	Ferguson
G050C022	St Marys Rd north of Hwy 100	635650	5517680	6.6	N/A	Ferguson
G050J004	CNR Keewatin Bridge RRF 14	646720	5532420	5.8	N/A	Ferguson
GF1	Dawson Rd east of Dugald	637650	5527670	11.1	N/A	Ferguson
GF2	De Bourmont	637930	5526340	6.1	N/A	Ferguson
GF3	Des Meurons south of Provencher	635580	5528550	8.8	N/A	Ferguson
GF4	Goulet St	635790	5527540	7.1	N/A	Ferguson
GF5	Olive St and Portage Ave	625310	5526250	8.9	N/A	Ferguson
GF6	McPhillips St and Selkirk Ave	632330	5534130	8	N/A	Ferguson
GF7	St Annes Rd and Bishop Grandin	637150	5522690	6.4	N/A	Ferguson
GF8	McGillivray and Fennel	631850	5522230		N/A	Ferguson

Well Identification	Description	UTMX (m)	UMTY (m)	Upper Carbonate Aquifer Temperature (°C)	Winnipeg Formation Temperature (°C)	Source
G050H004	Mazenod Rd north of Symington Yard RRF 025	640140	5526870	6	N/A	Ferguson
G050J025	McPhillips Pumping Station	632090	5533720	7	N/A	Ferguson
G050J026	McPhillips Pumping Station MO-12	632100	5533730	7	7.1	Ferguson
G05MJ009	Portage and Perimeter	620650	5527290	6.9	N/A	Ferguson
GM127	Production Well	628502	5529139	11.6	N/A	WRB
GM155	Production Well	637905	5527192	10.3	N/A	WRB
GM163	Production Well	622430	5526795	7.9	N/A	WRB
GM198	Production Well	627290	5525510	6.7	N/A	WRB
GM199	Production Well	633030	5519007	8.3	N/A	WRB
GM203	Production Well	631315	5523751	11.5	N/A	WRB
GM225	Production Well	624915	5526052	9.6	N/A	WRB
GM227	Production Well	625330	5526230	13.8	N/A	WRB
GM229	Production Well	630960	5520405	7.5	N/A	WRB
GM231	Production Well	624357	5526314	7.2	N/A	WRB
GM233	Production Well	624972	5528314	10.8	N/A	WRB
GM234	Production Well	630820	5532777	9.6	N/A	WRB
GM242	Production Well	628970	5528050	8.1	N/A	WRB
GM245	Production Well	624777	5529144	8.4	N/A	WRB
GM247	Production Well	629903	5534230	9	N/A	WRB
GM251	Production Well	635564	5518260	9.9	N/A	WRB
GM252	Production Well	624986	5528843	9.6	N/A	WRB
GM256	Production Well	624772	5529144	9.6	N/A	WRB
GM259	Production Well	637990	5527391	10	N/A	WRB
GM262	Production Well	643647	5531673	7.1	N/A	WRB
GM65	Production Well	629950	5527110	7.6	N/A	WRB

348

Well Identification	Description	UTMX (m)	UMTY (m)	Upper Carbonate Aquifer Temperature (°C)	Winnipeg Formation Temperature (°C)	Source
GM67	Production Well	630961	5523697	8.4	N/A	WRB
GSC7001	University of Manitoba Fitzgerald Bldg	633900	5518680	8.2	7.2	GSC
GSC9901	St. Labre Rd	701891	5475650	N/A	7.9	Ferguson
GSC9902	East of PR210, on rd south of 404 jct	697724	5779676	N/A	N/A	Ferguson
G050E005	Zhoda1A (deep)	682206	5460882	5.9	N/A	Ferguson
G050E006	Zhoda1B (shallow)	682206	5460882	5.9	N/A	Ferguson
Woodridge1	Woodridge 1 Across PR210 from fire tower	707193	5466096	N/A	N/A	Ferguson
TH1	West of PR210, south of St Labre Jct	700891	5475123	N/A	N/A	Ferguson
TH2	West of PR210 north of Woodridge	705345	5467979	N/A	N/A	Ferguson
G050H036	Richer1	686261	5493556	5.7	N/A	Ferguson
G050H031	Giroux1	661230	541264	6	N/A	Ferguson
G050E004	Pansy1	673240	5494076	6.1	N/A	Ferguson
G050E003	Grunthal1	654664	5474699	6.1	N/A	Ferguson
G050E004	Dugald RRF 047	655615	5526058	4.7	N/A	Ferguson
G050H008	St. Anne	671634	5510039	5	N/A	Ferguson
G050E029	Steinbach2	673240	5486240	5.3	N/A	Ferguson
G050H020	East of La Broquerie OH20	690541	5488235	6.1	N/A	Ferguson
G05SA003	Ross	682688	5513933	5.4	N/A	Ferguson
G050E038	SILA 97-4	675802	5468453	5.6	N/A	Ferguson
G050E030	Steinbach3	667475	5486068	5.1	N/A	Ferguson
G050E032	Steinbach5	666834	5487670	5.1	N/A	Ferguson

Appendix B.2 Measured Temperature Profiles Spring 2000
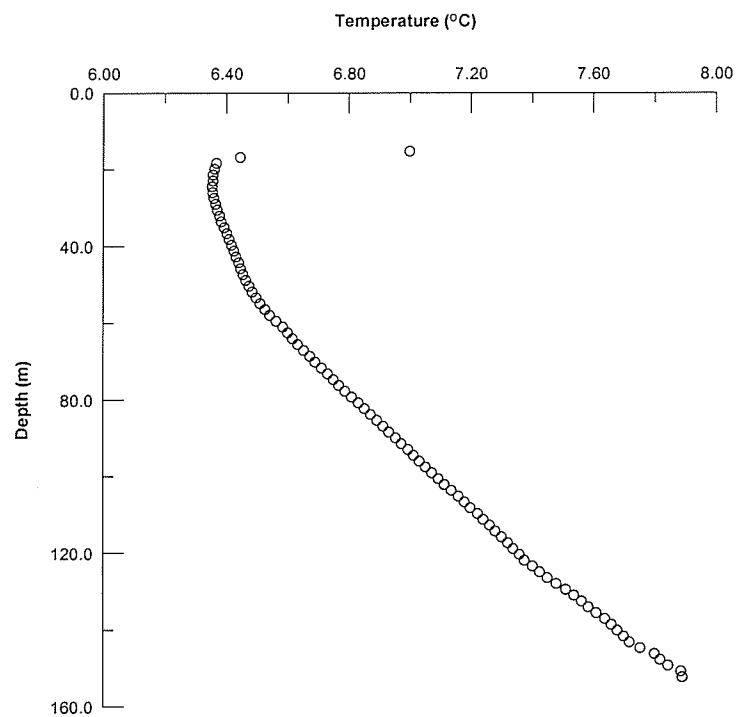
GSC9901 May 2000
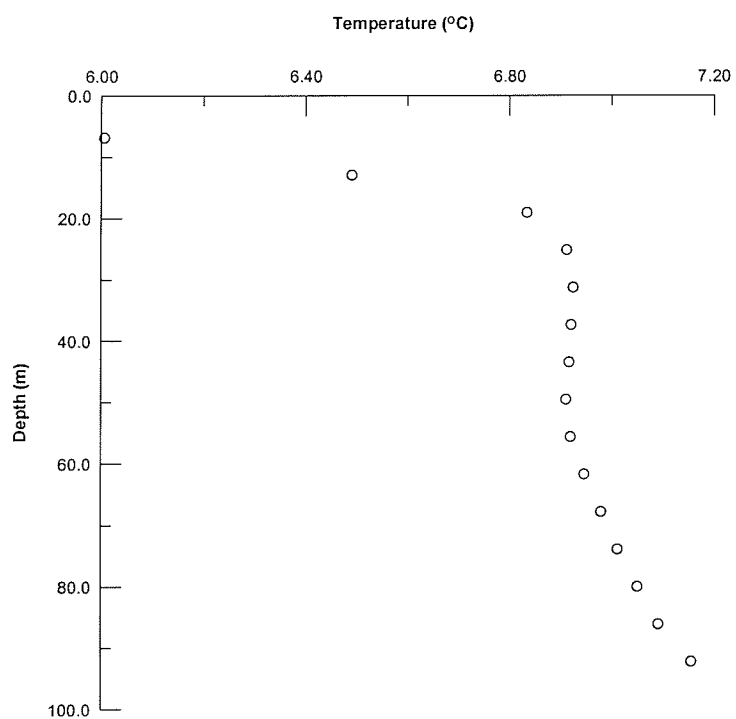
GSC9902 May 2000
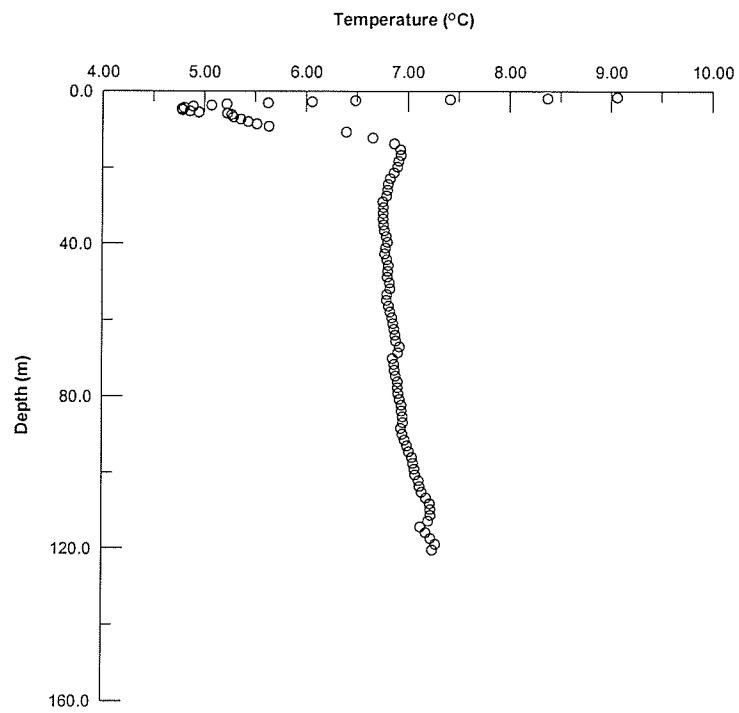
G050E005 Zhoda1A
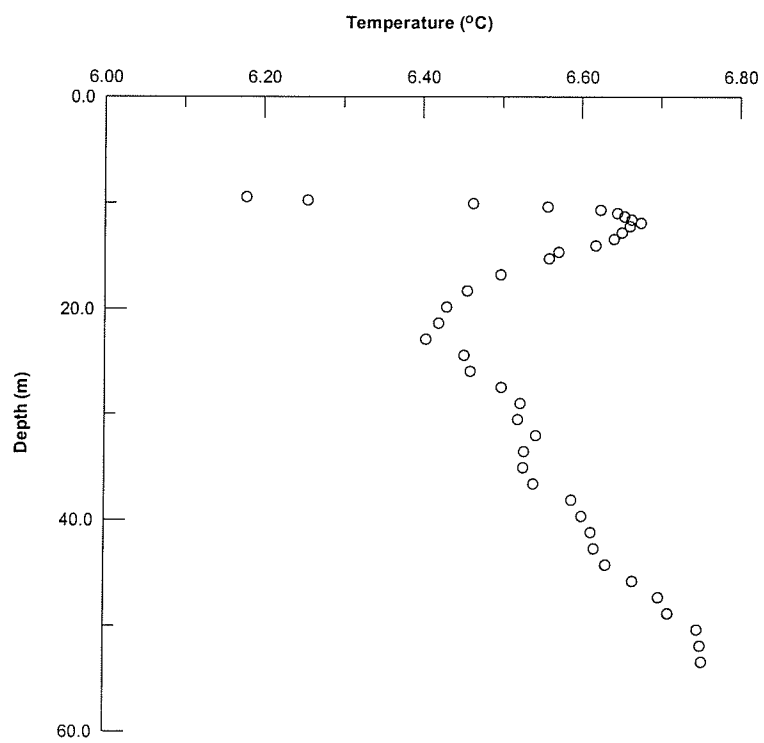
Woodridge 1 May 2000
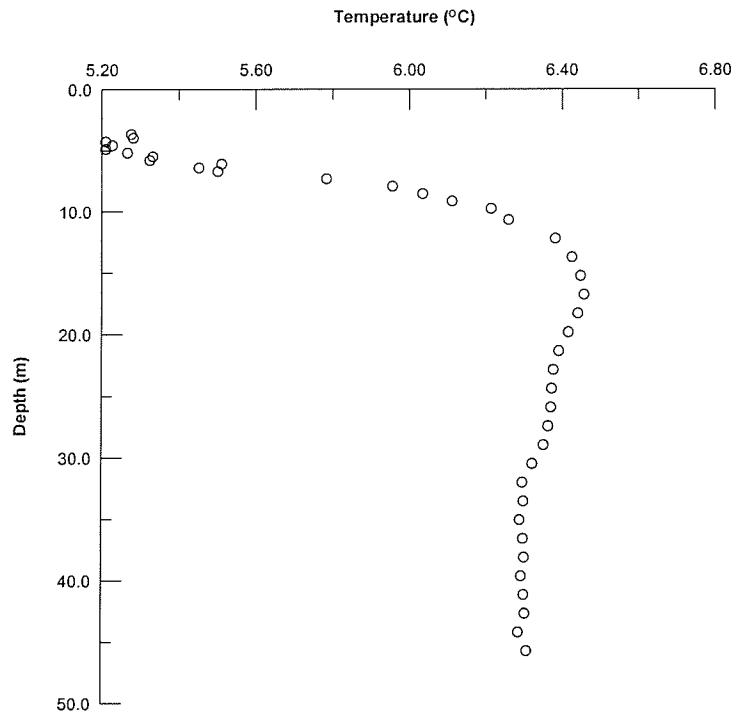
G050H036 Richer 1 May 2000

G050E004 Pansy1

352
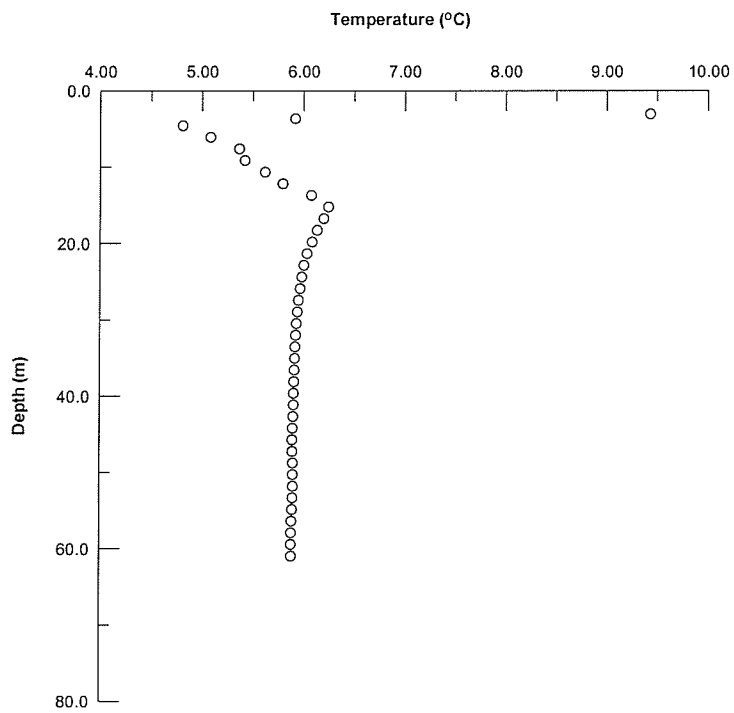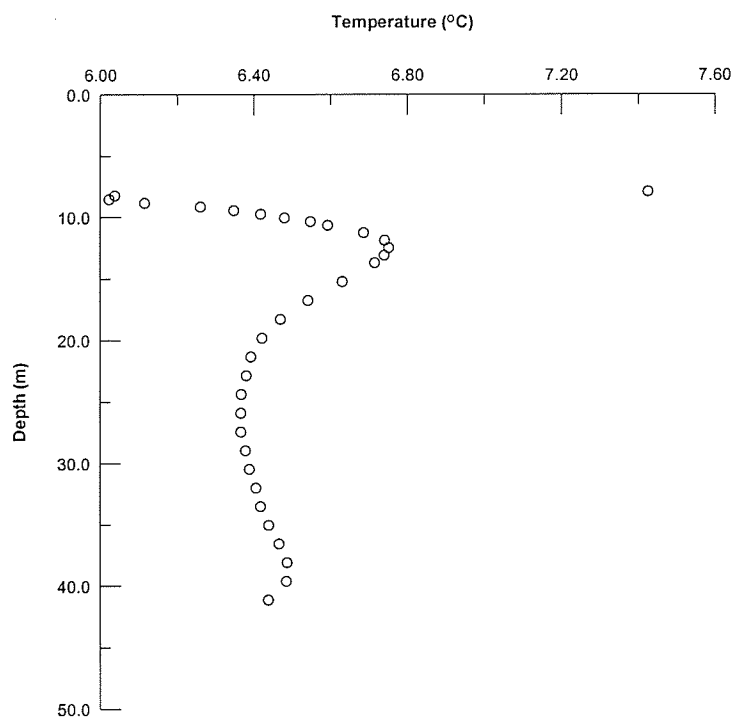
G050E003 Grunthal 1 May 2000
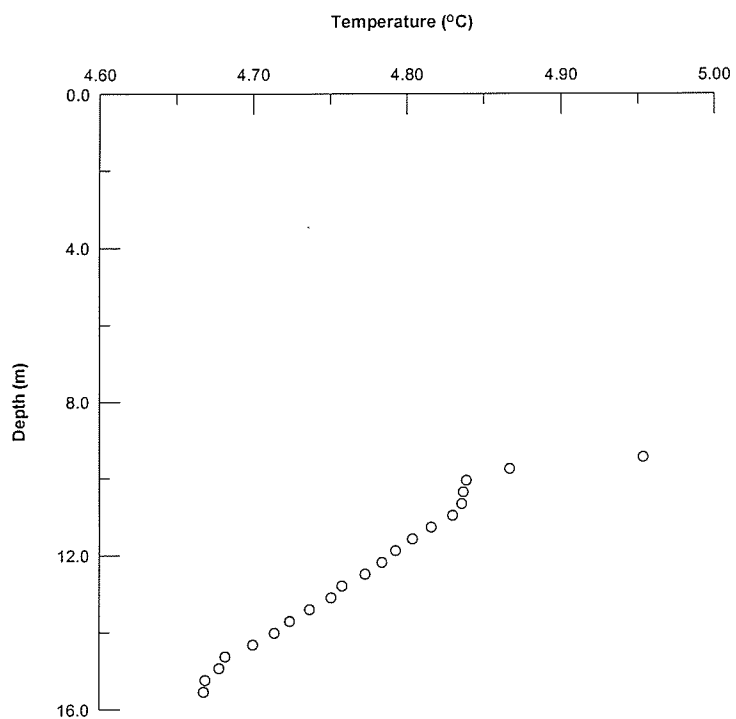
G050E004 Dugald May 2000

353
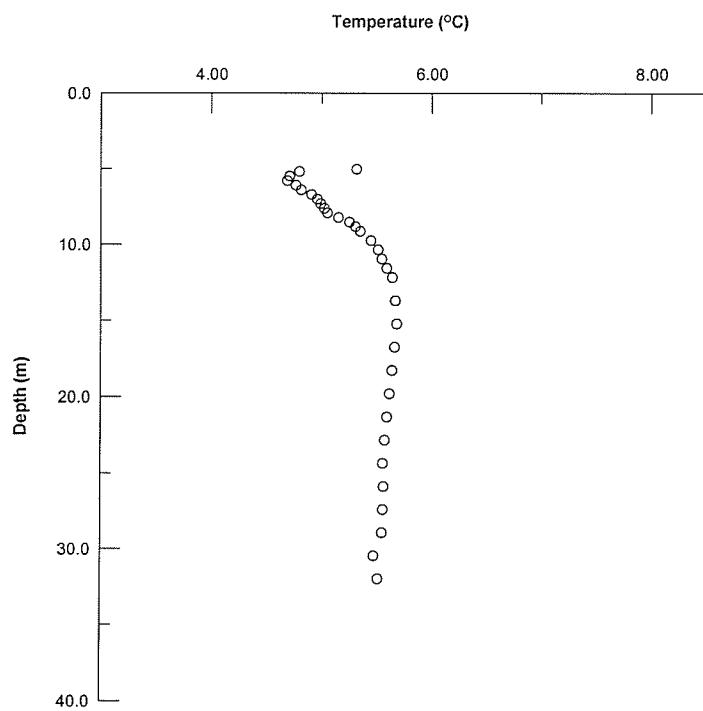
G050H008 Ste. Anne May 2000
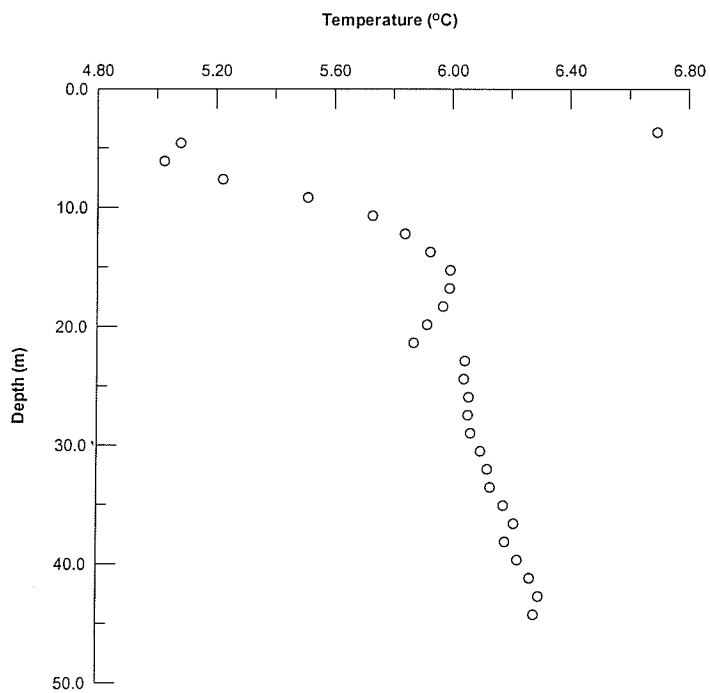
G050E029 Steinbach 2 May 2000
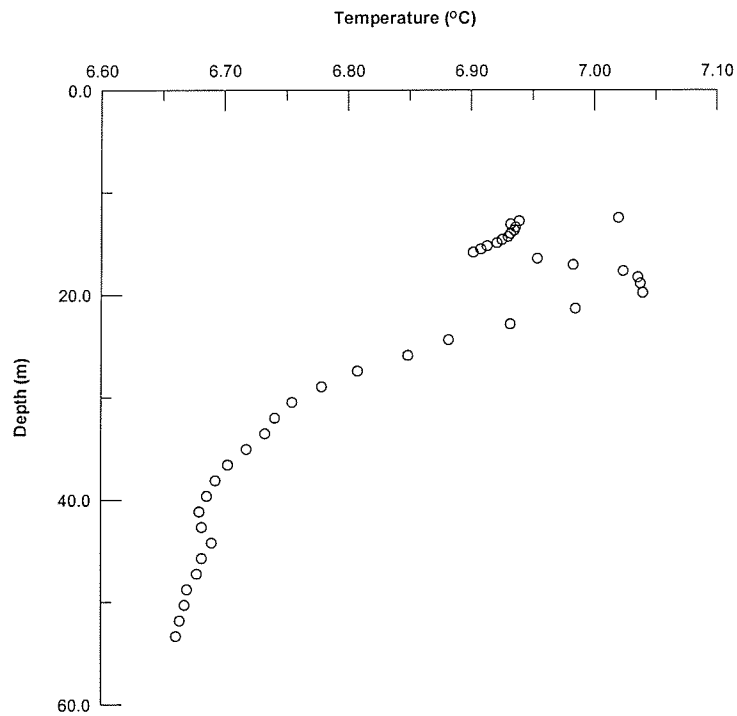
G050H020 June 2000
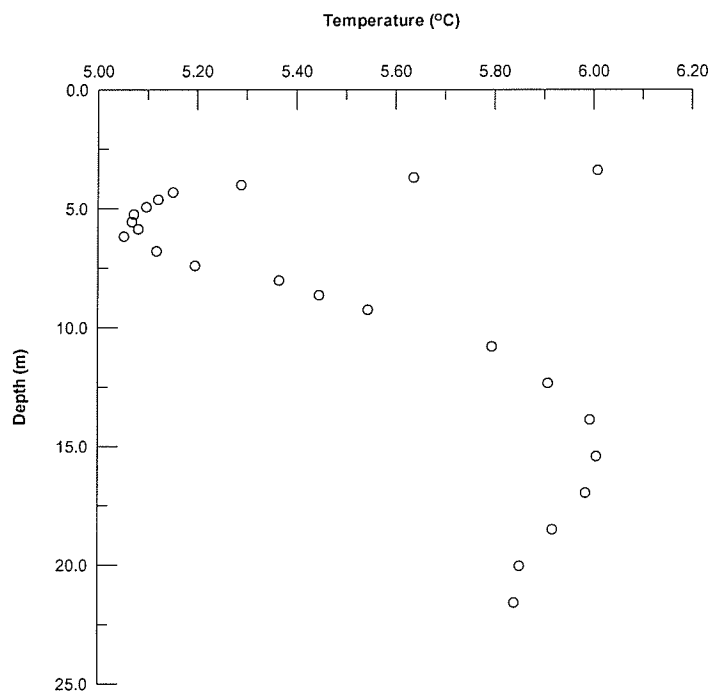
G05SA003 Ross May 2000
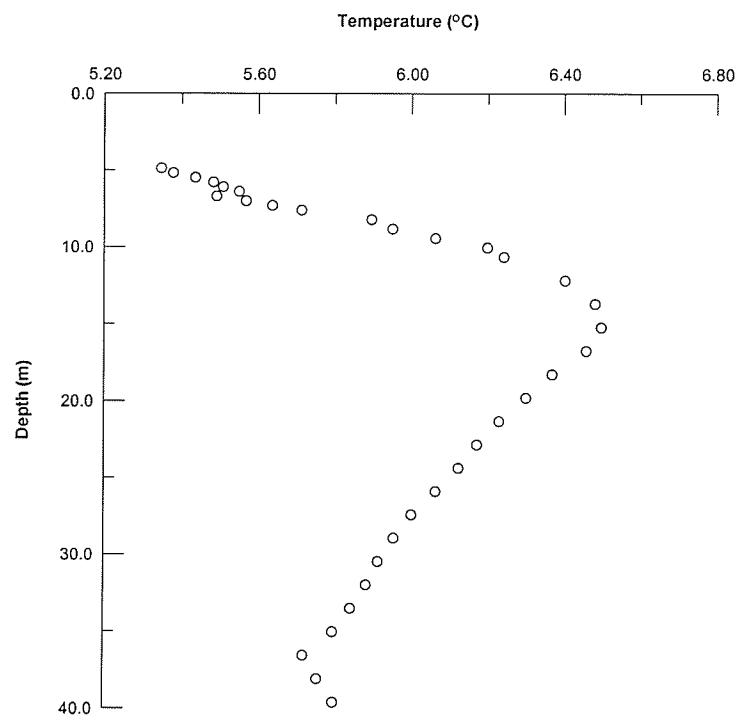
G05OE030 Steinbach 3 May 2000
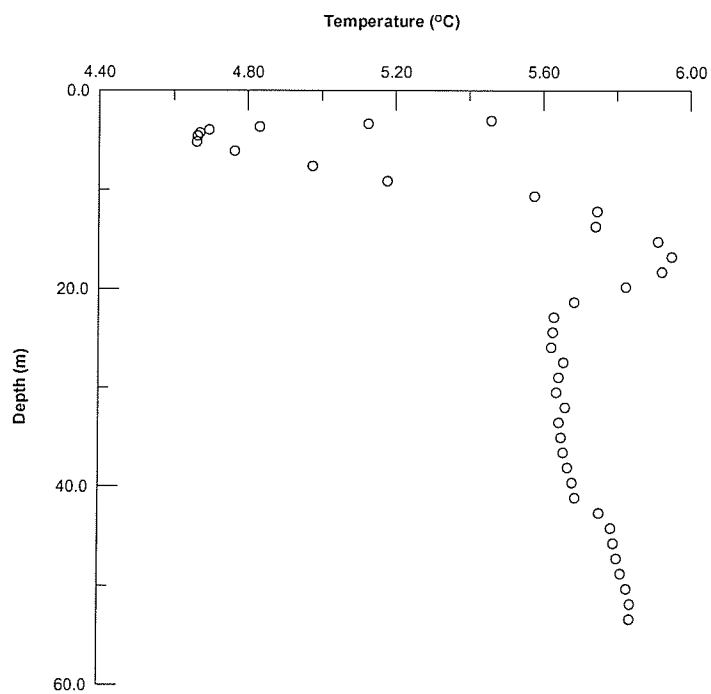
G050E032 Steinbach 5 May 2000

Appendix B.3 Measured Temperature Profiles Summer 2000
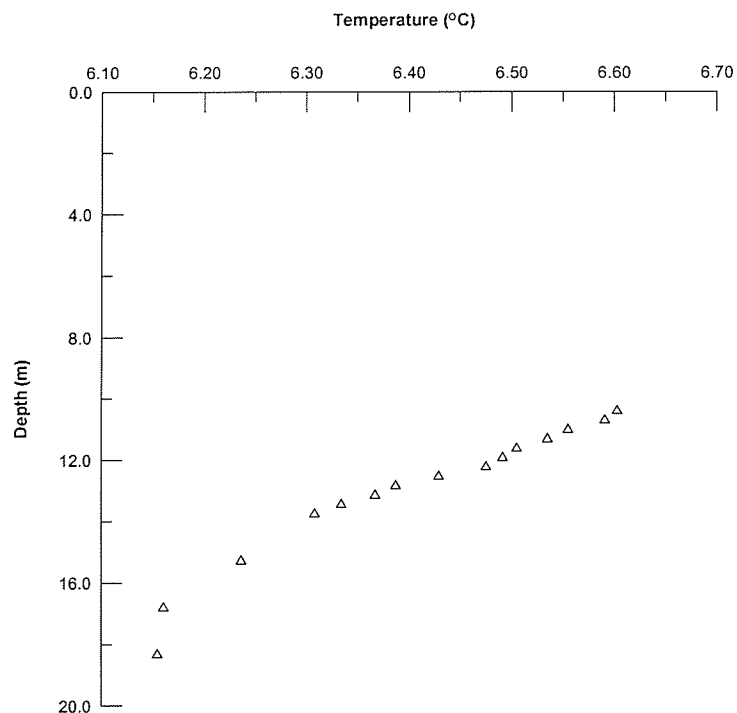
G050C018 Pembina Hwy and Hwy 100 August 2000
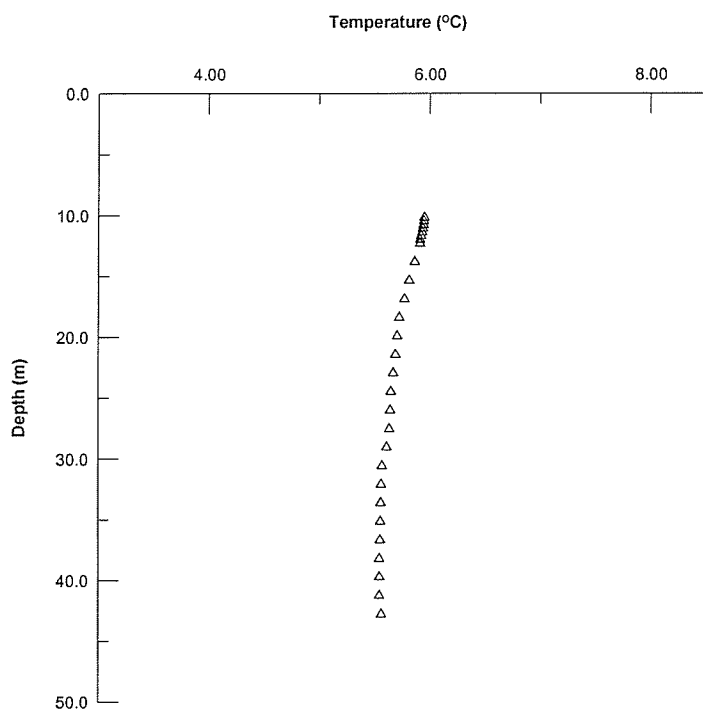
G050G003 Oak Bluff August 2000
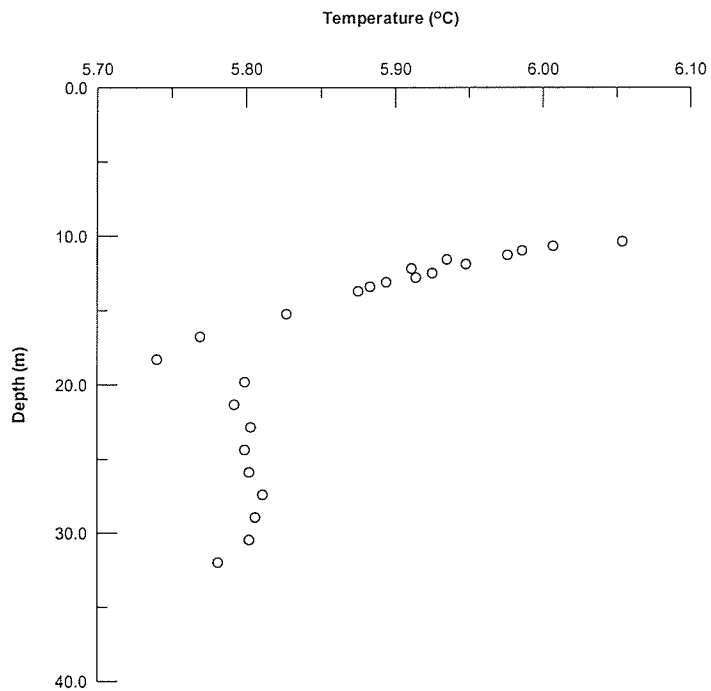
G05OH003 St Annes Rd RRF02 August 2000
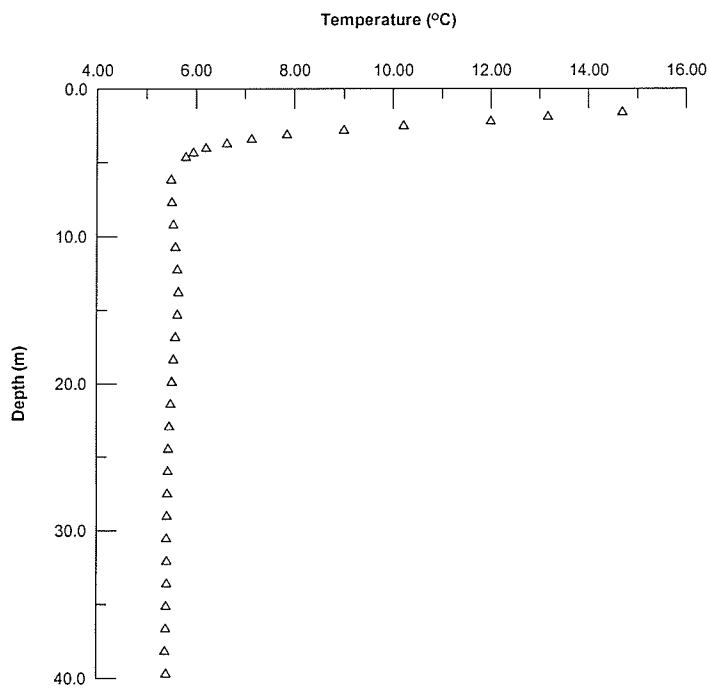
G05OJ022 Route 90 and Hwy 101 August 2000
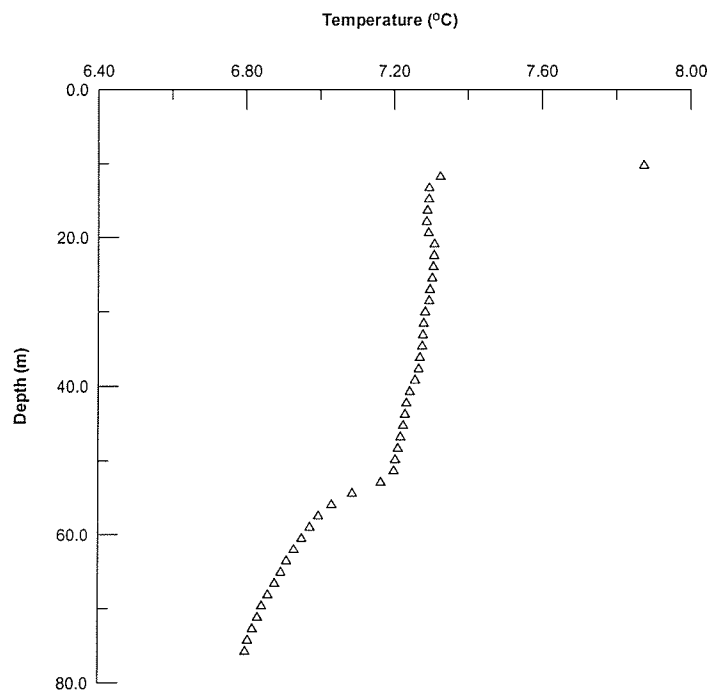
G05MJ077 611 Academy Rd August 2000
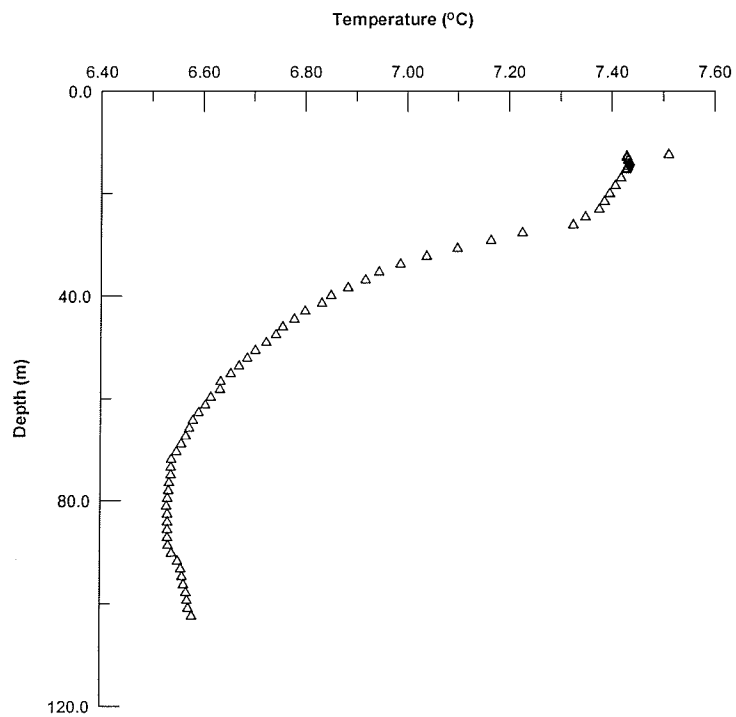
G05OJ013 Swift 1 August 2000

Temperature (°C)

G05MJ006 Assiniboine River and Hwy 100 August 2000

Temperature (°C)
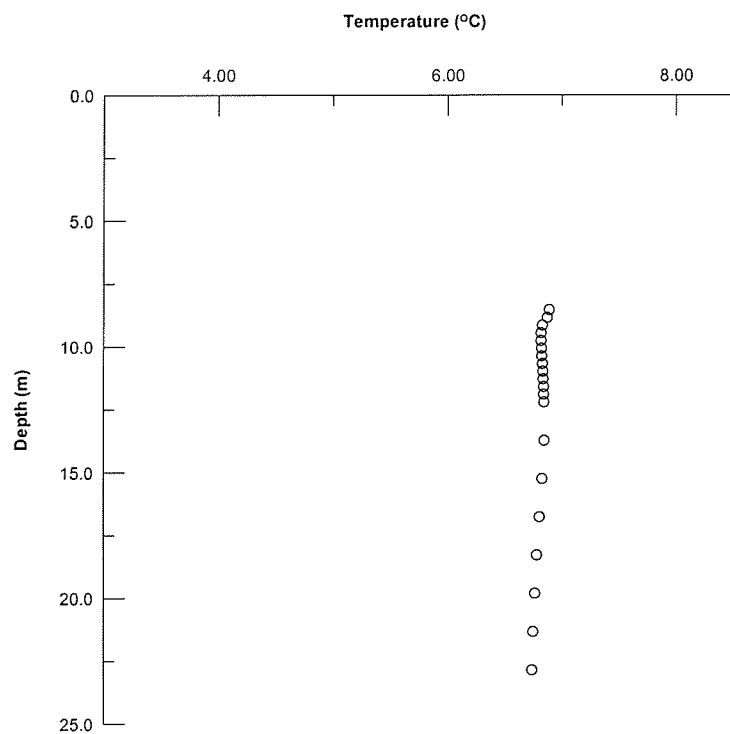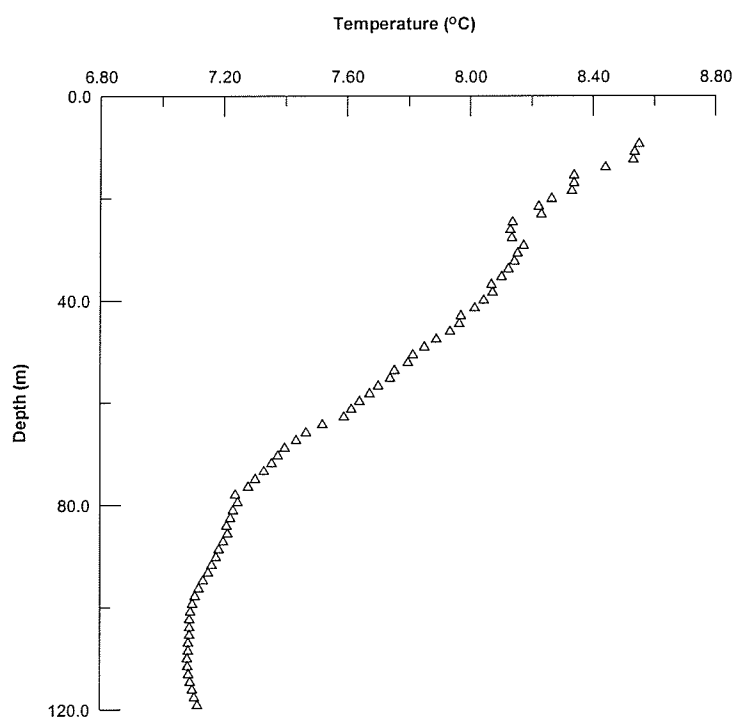
G05OH019 Canada Packers August 2000
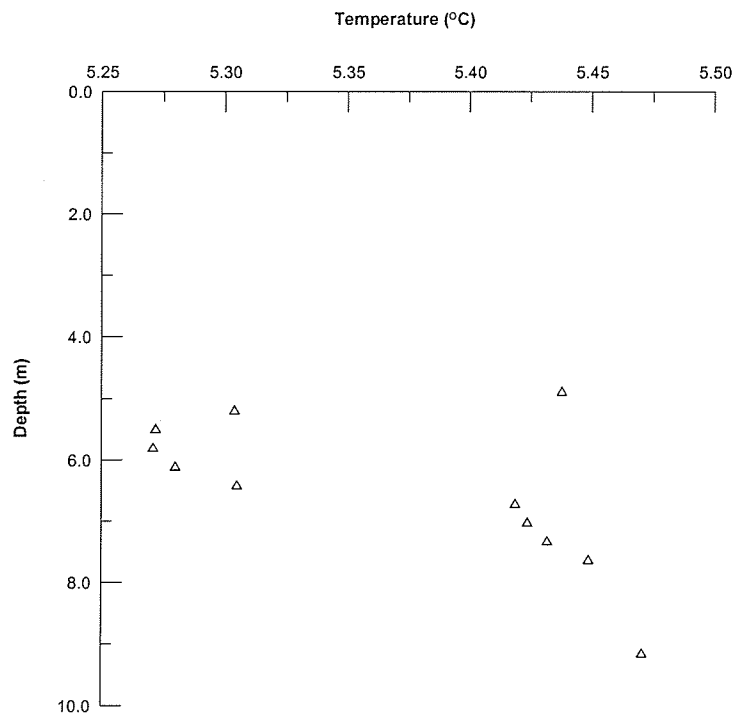
G05MJ008 Sturgeon Creek and Hwy 101 August 2000
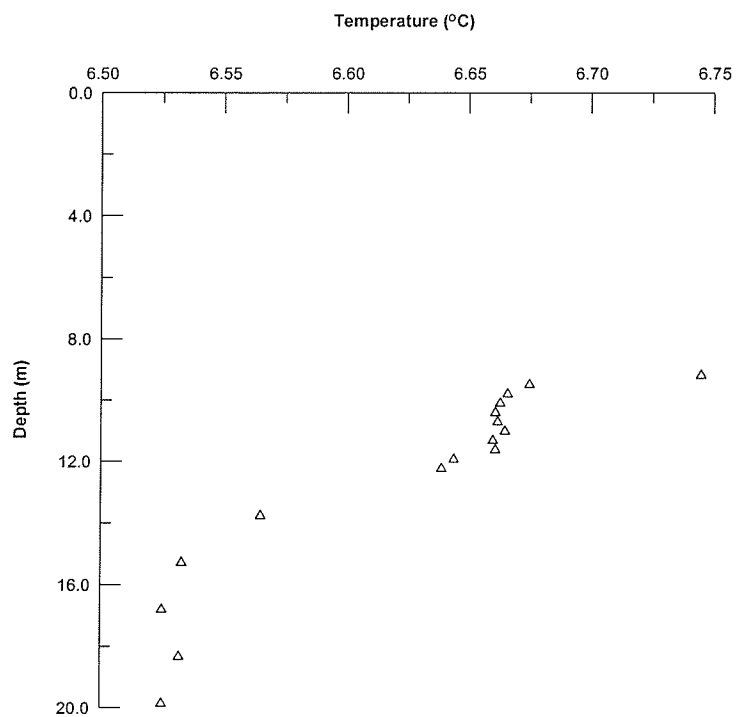
G05OC049 Rue des Trappistes and Pembina Hwy August 2000
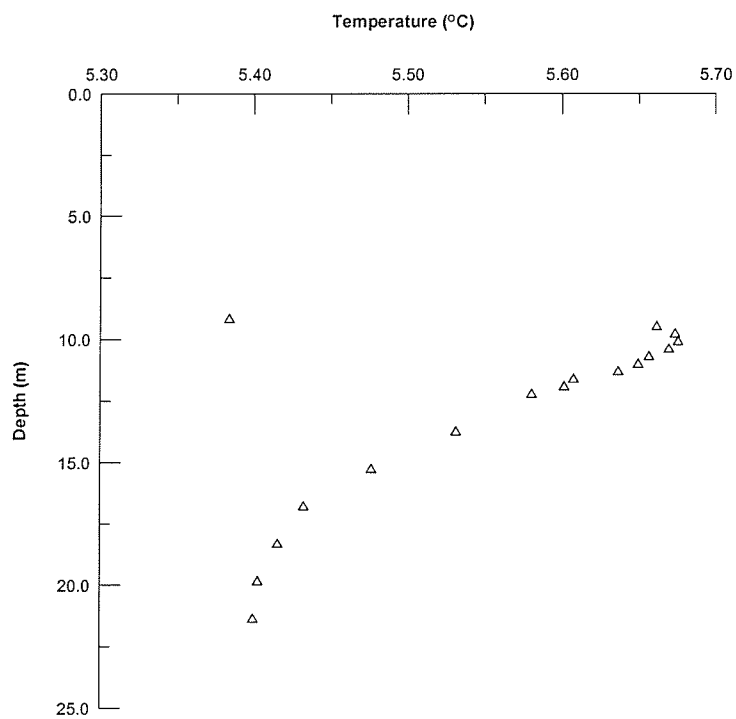
G05OH010 Murdock Rd and Dugald Rd RRF 055 August 2000
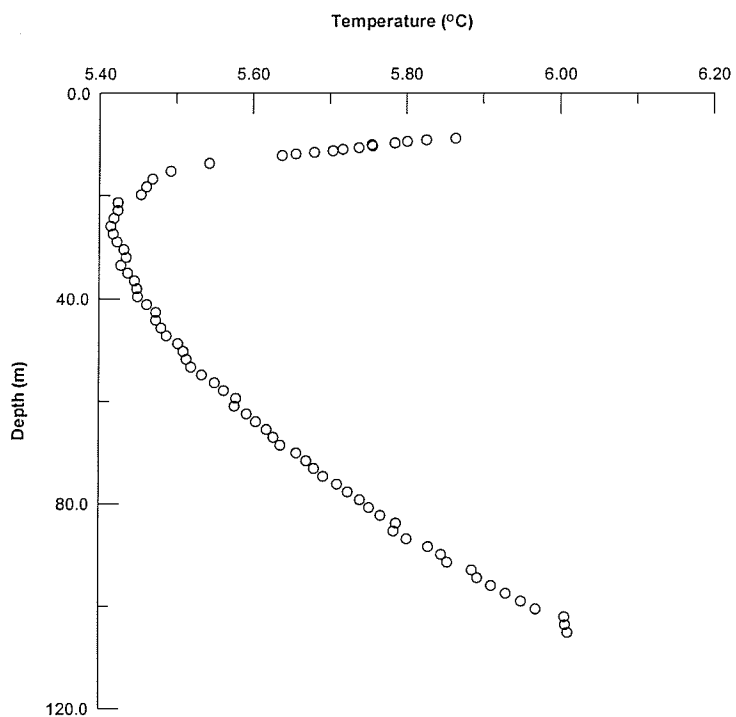
G05OJ030 Murdock Rd and Dugald Rd August 2000

362
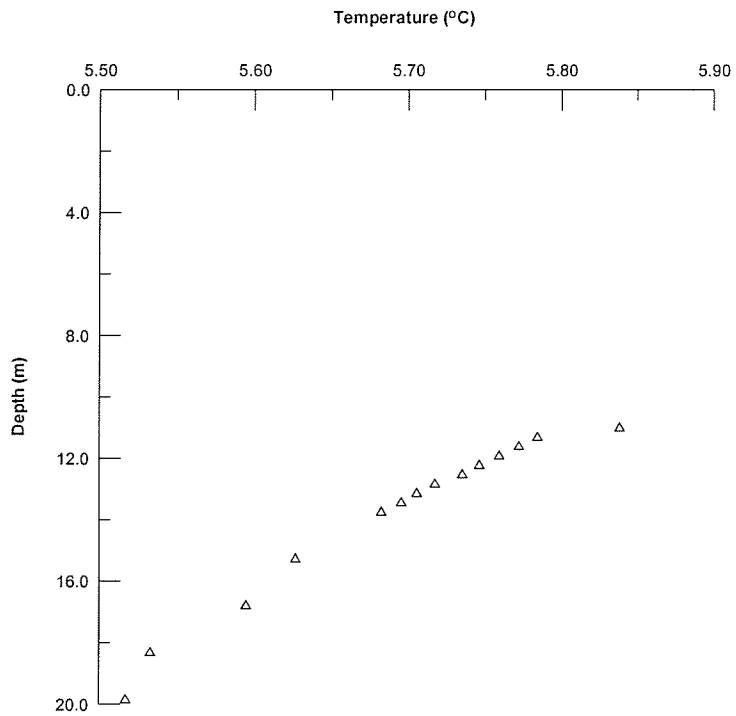
G05OJ003 Deacon Rd and Cedar Lake Rd August 2000
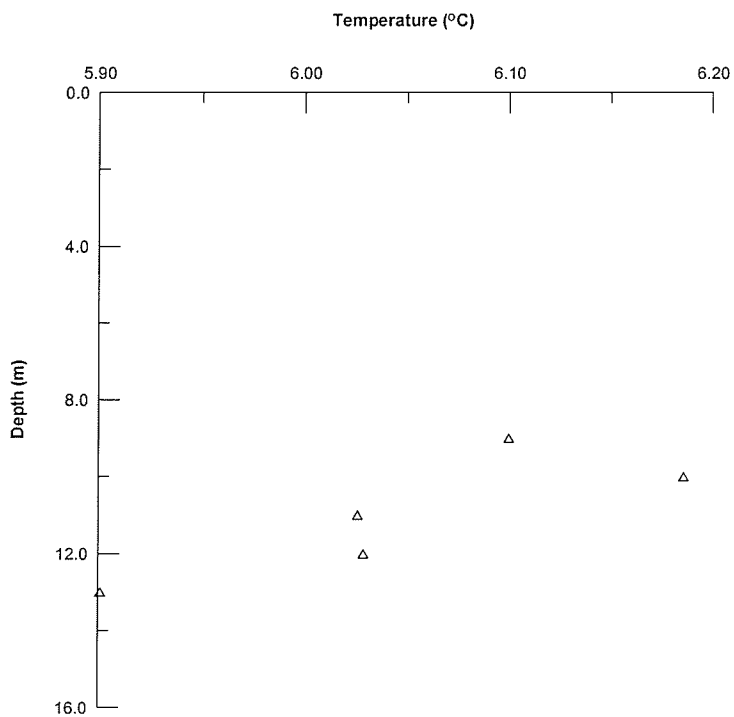
G05OJ103 Grassmere August 2000
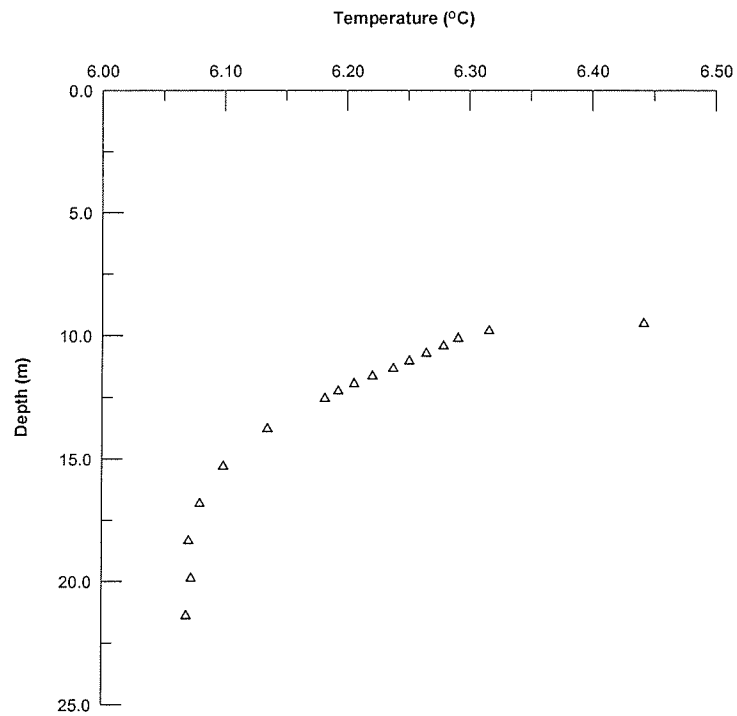
G05OJ009 Grassie Blvd and Hwy 59 RRF 045
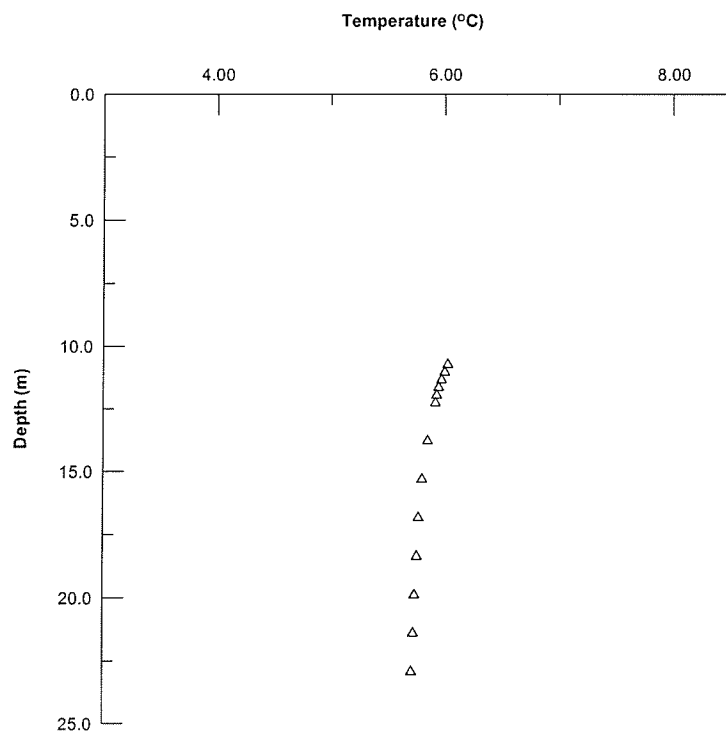
G05OJ014 Gunn Rd August 2000
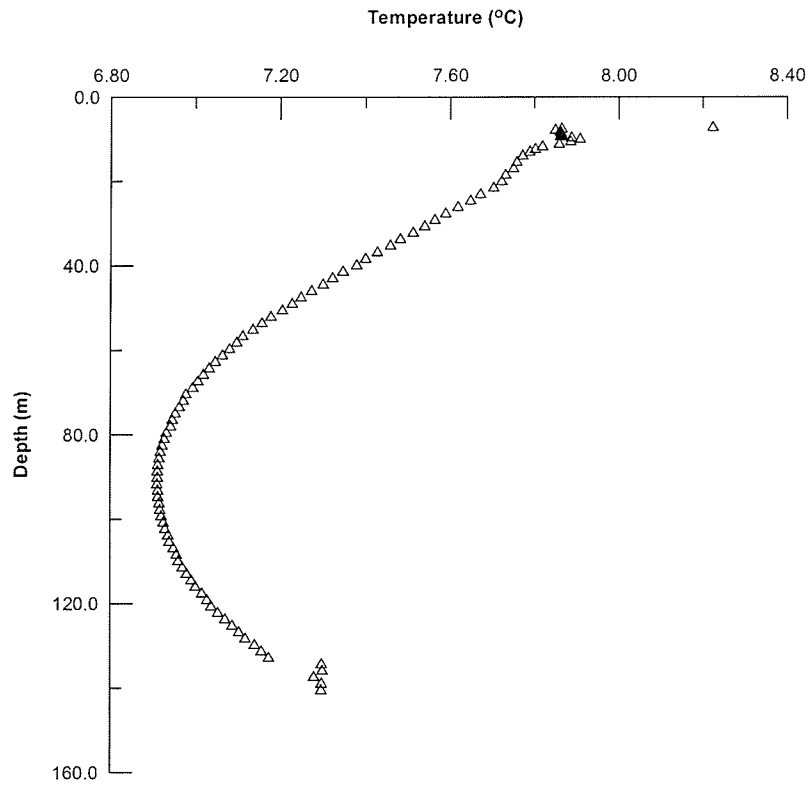
G05OH012 GWWD August 2000
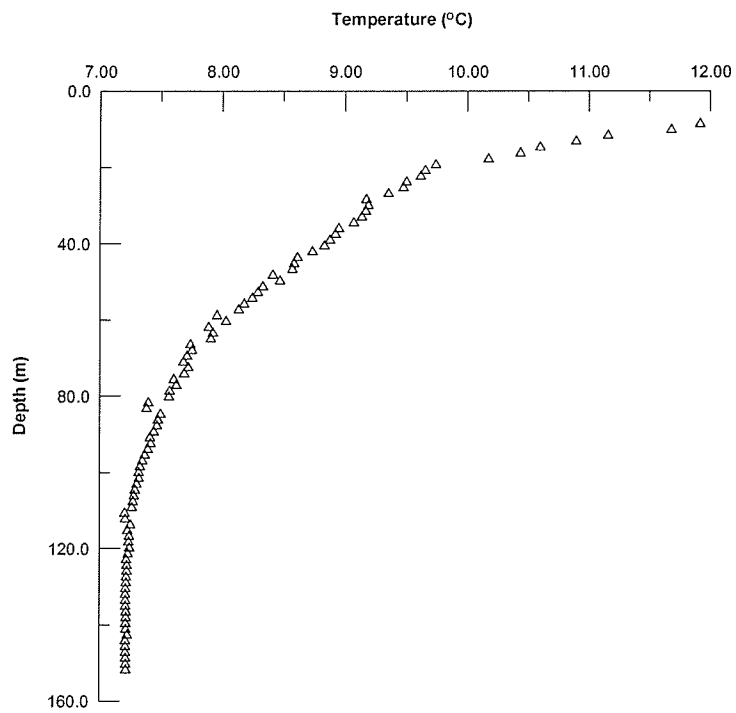
G05OJ028 Hudson Bay House August 2000

365
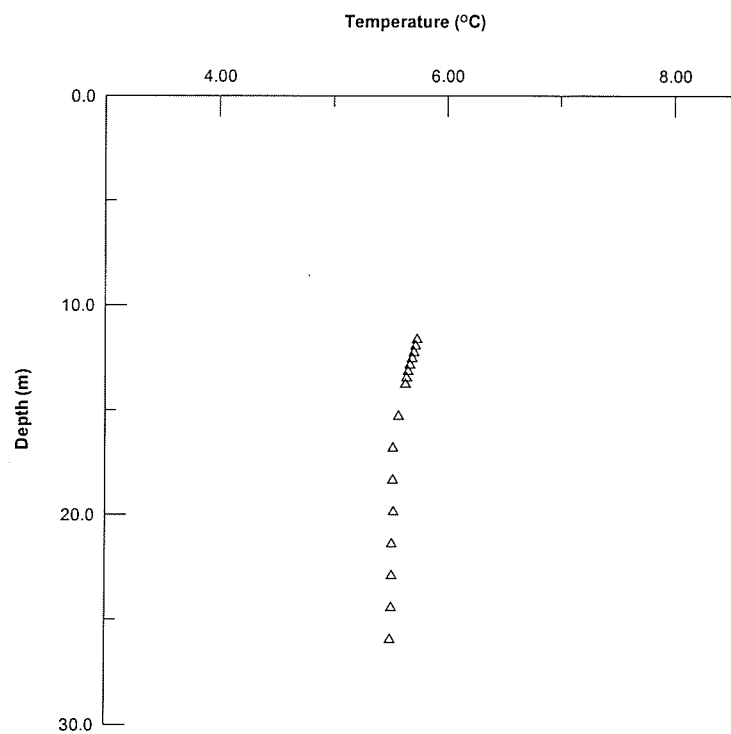
G05OH011 Hwy 1 and Floodway RRF 061 August 2000
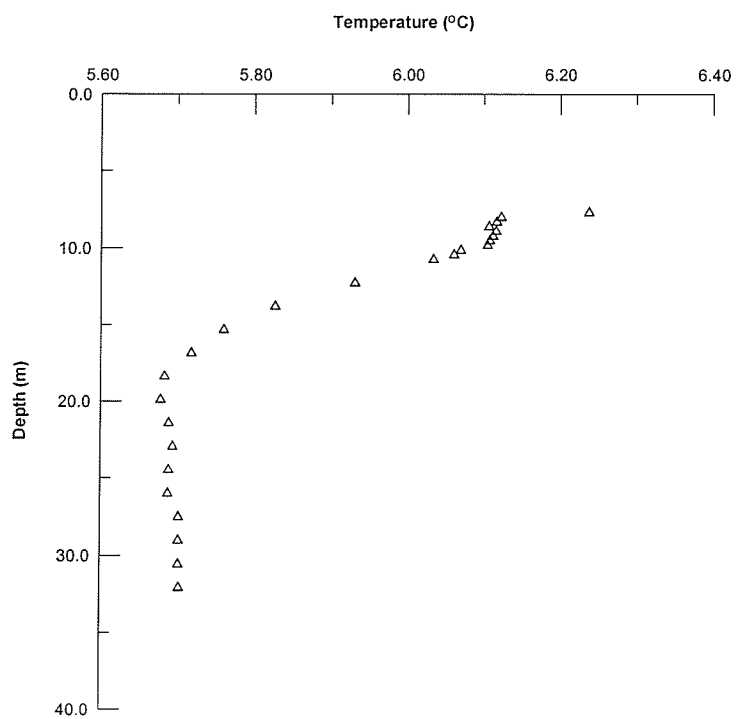
G05OH009 Ile des Chenes August 2000
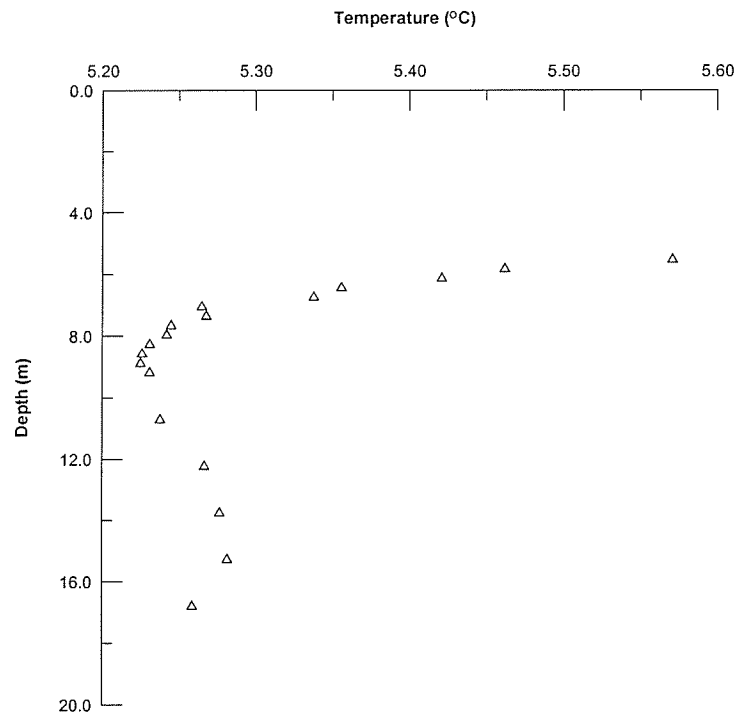
G05MJ007 Inkster Blvd and Hwy 101 August 2000
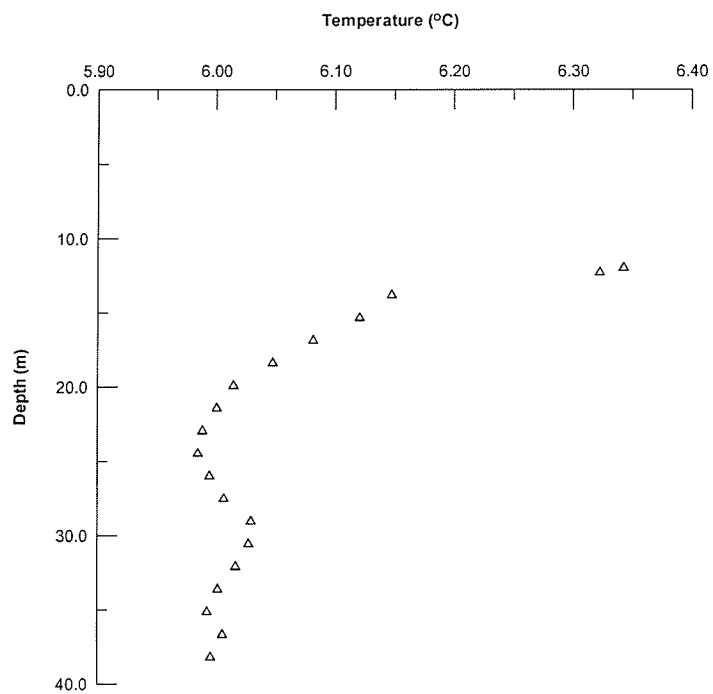
G05MJ037 Air Canada August 2000
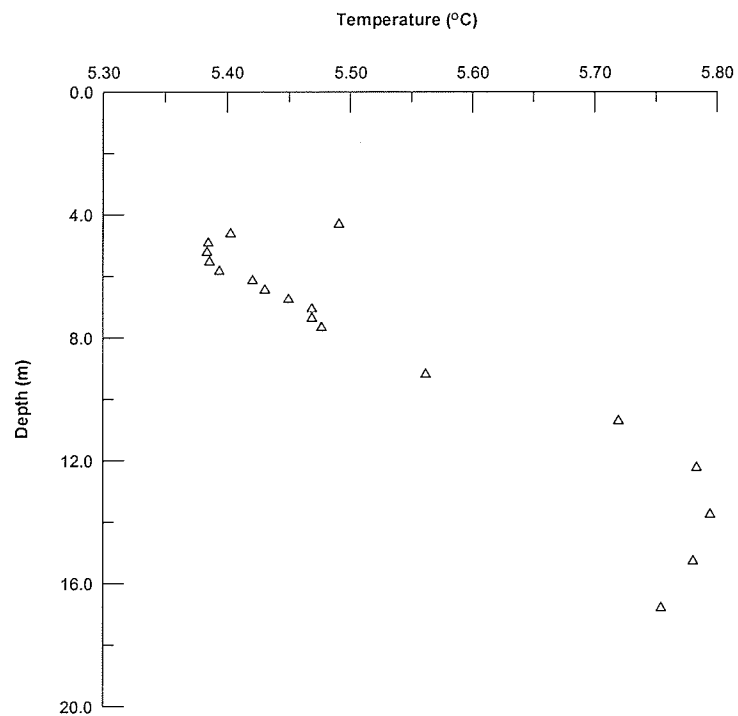
G05MJ005 Wilkes Ave and Hwy 100 August 2000

G05MJ076 Grace Hospital August 2000

Temperature (°C)
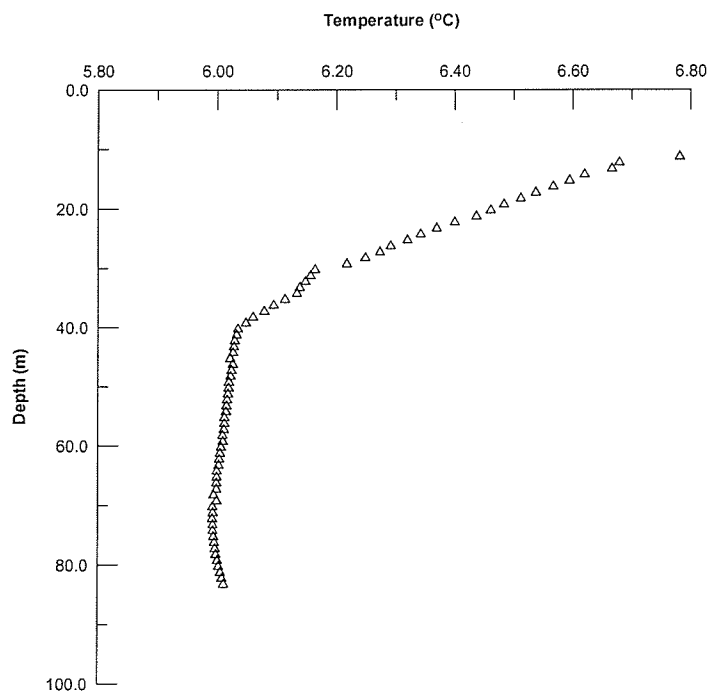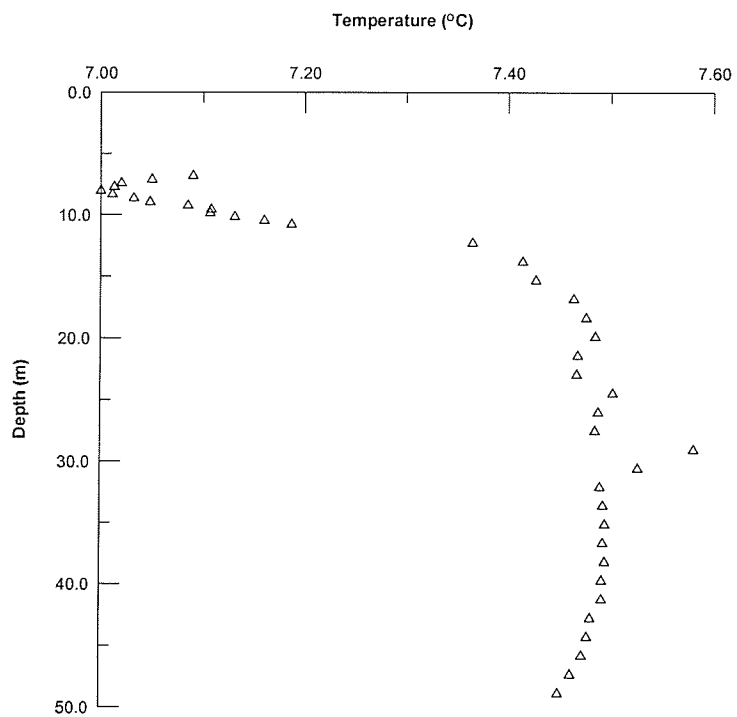
G05OC003 Norwood Bridge August 2000

Temperature (°C)
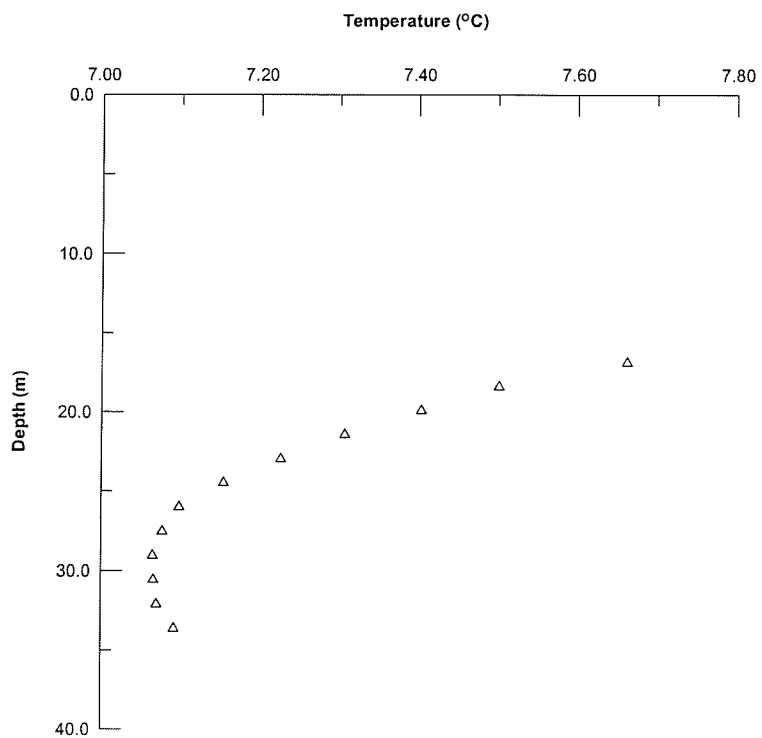
G05OC008 Taylor Ave August 2000

Temperature (°C)
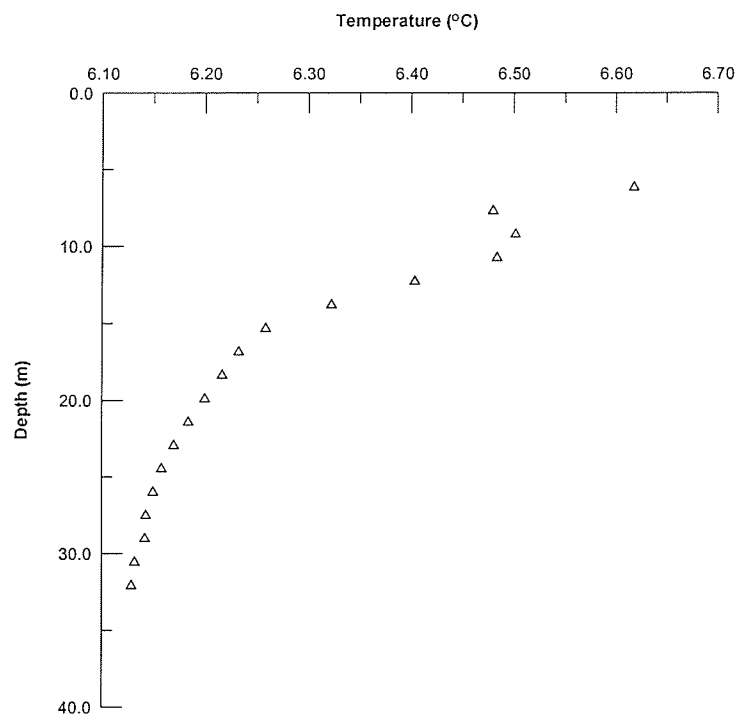
G05OC001 St. Mary's Rd and Floodway Inlet Structure RRF 040 August 2000

Temperature (°C)
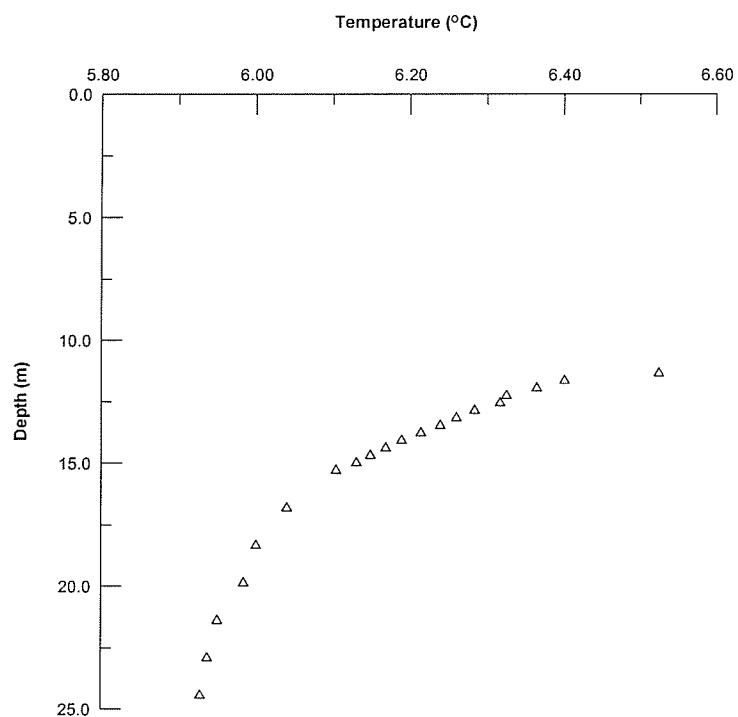
GOH005 Symington Rd and Hwy 1 RRF 043 August 2000
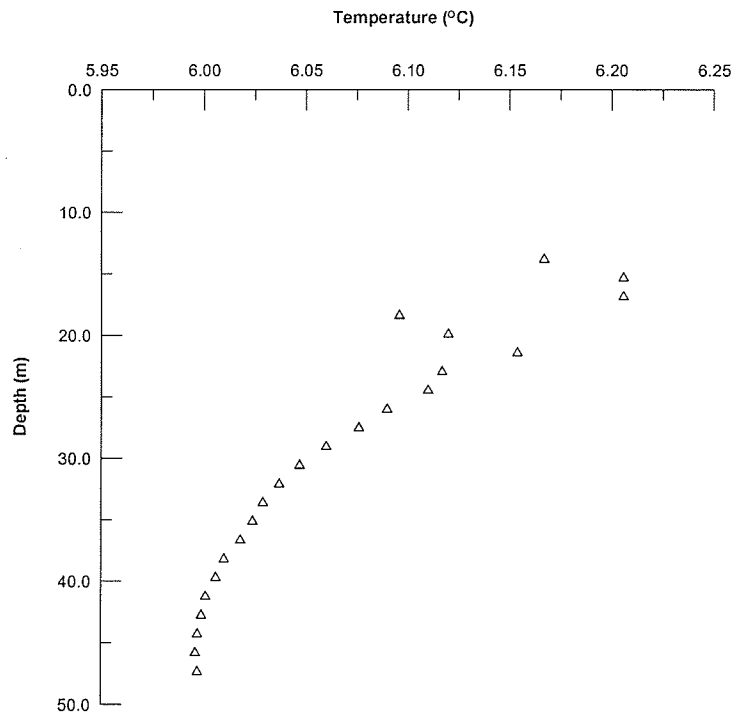
G05OJ092 Riverside Quarries August 2000
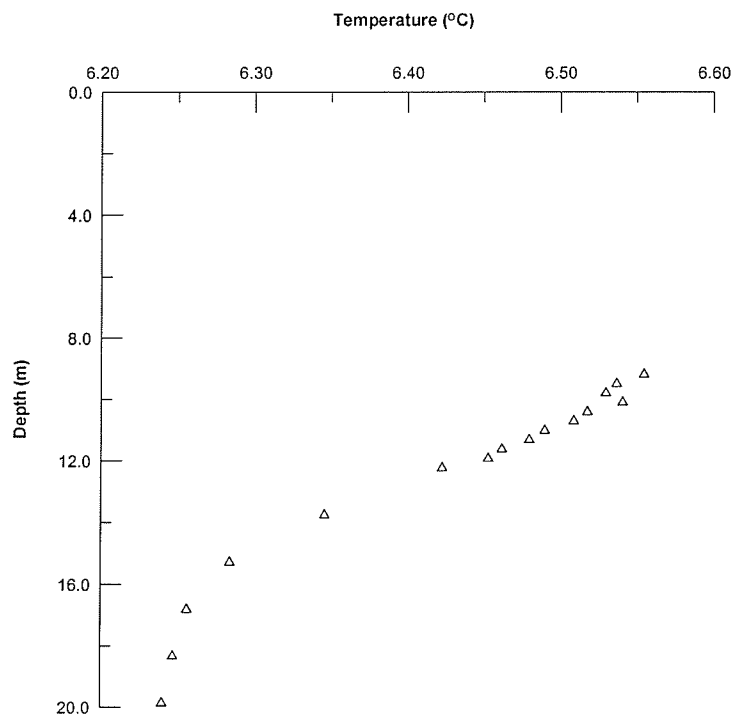
G06OG020 Turnbull Dr and Hwy 75 August 2000
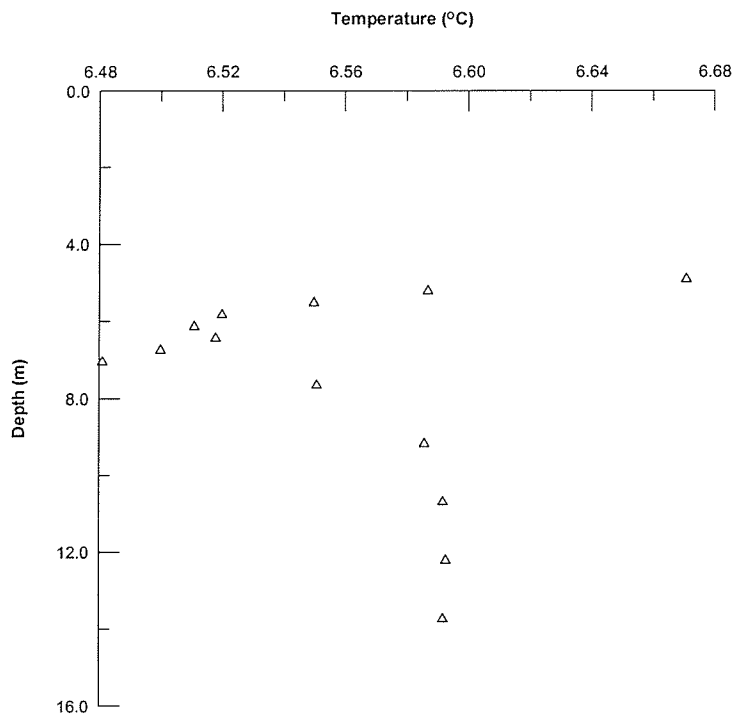
G05MJ009 Portage Ave and Hwy 101 August 2000
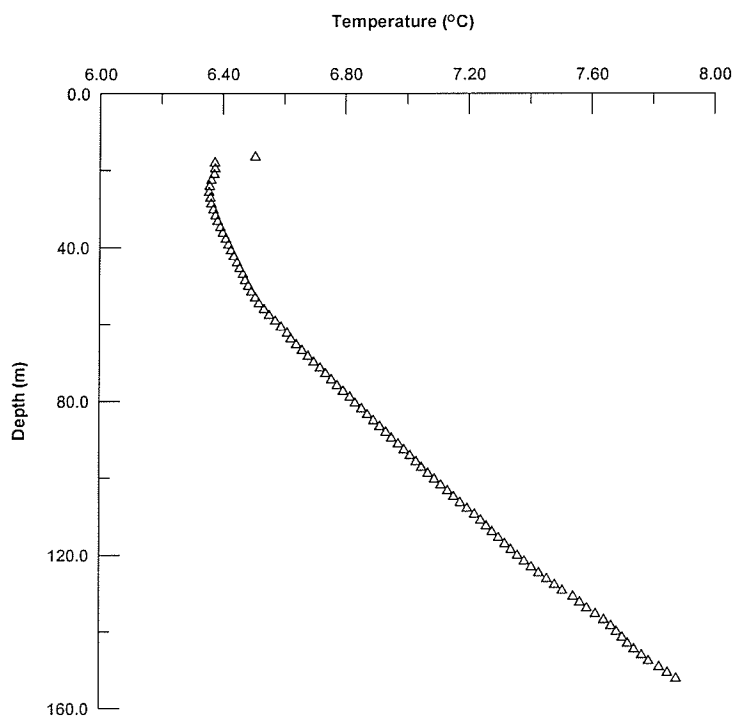
GSC9901 August 2000

Temperature (ºC)

Depth (m)
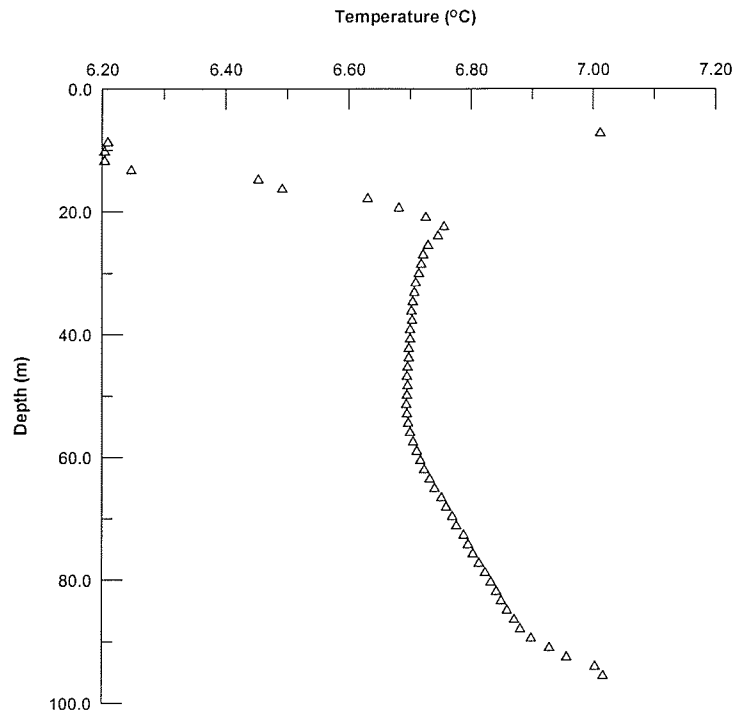
GSC9902 August 2000

Temperature (ºC)

Depth (m)
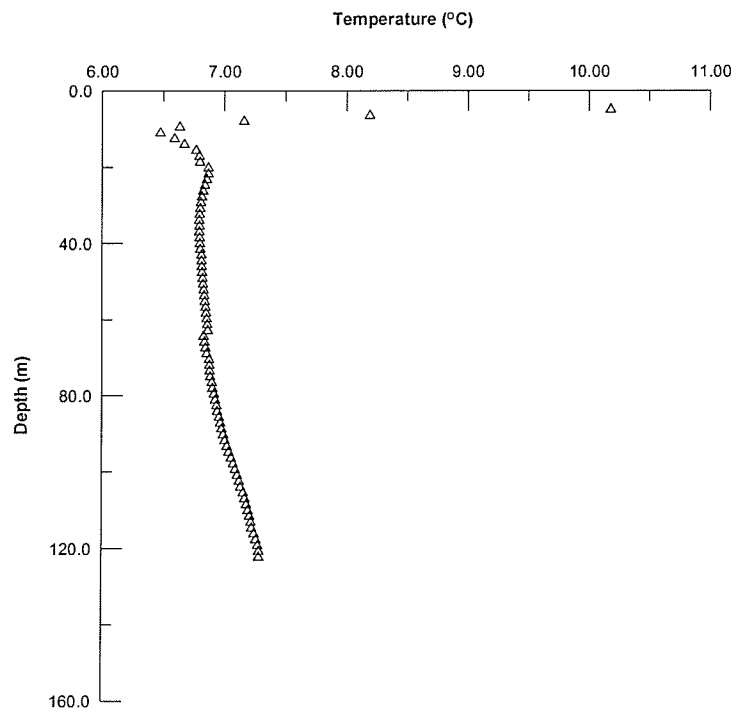
G05OE005 Zhoda 1A August 2000
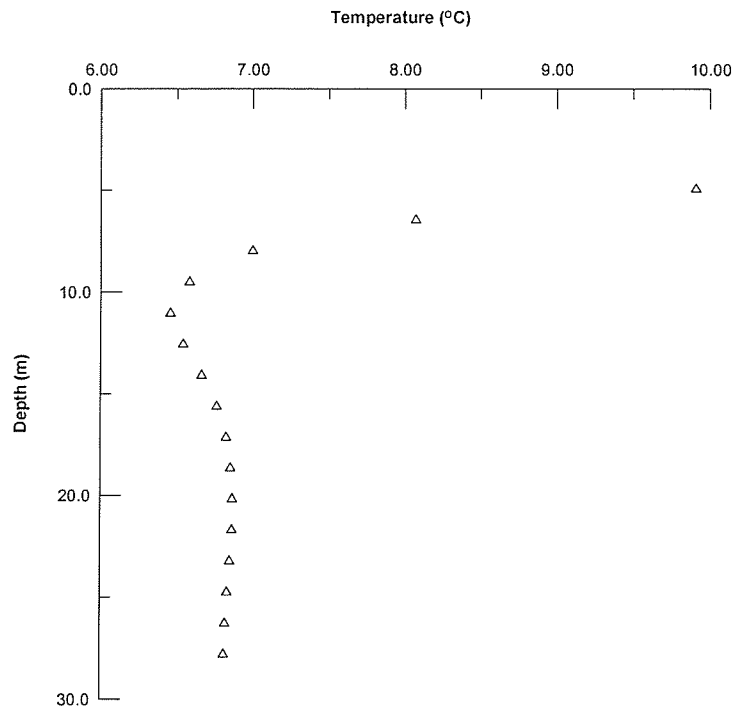
G05OE006 Zhoda 1B August 2000
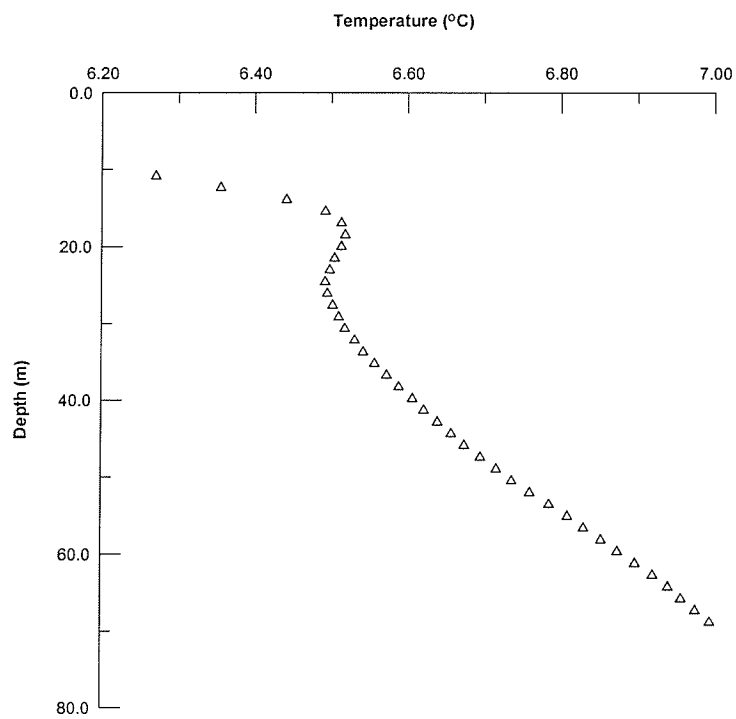
Woodridge 1 August 2000
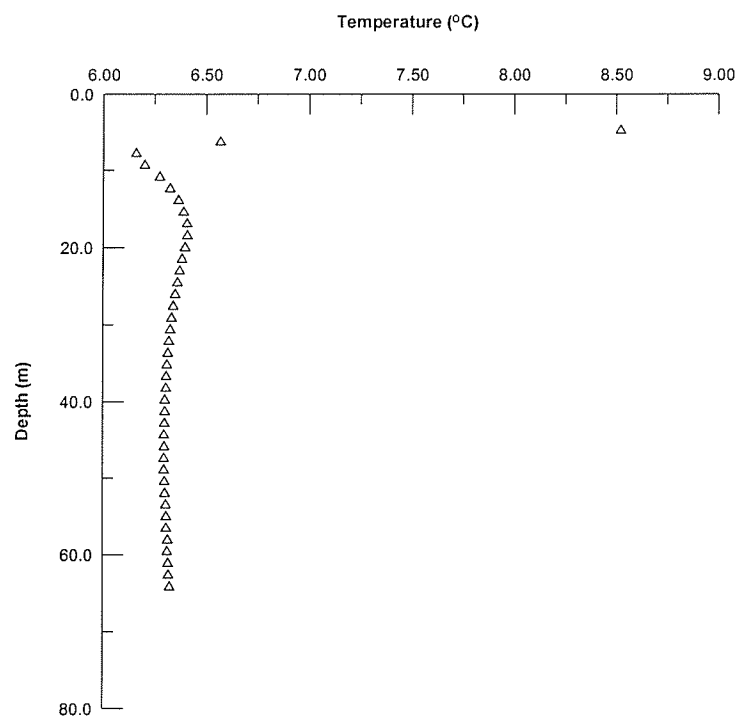
G05OH036 Richer 1 August 2000
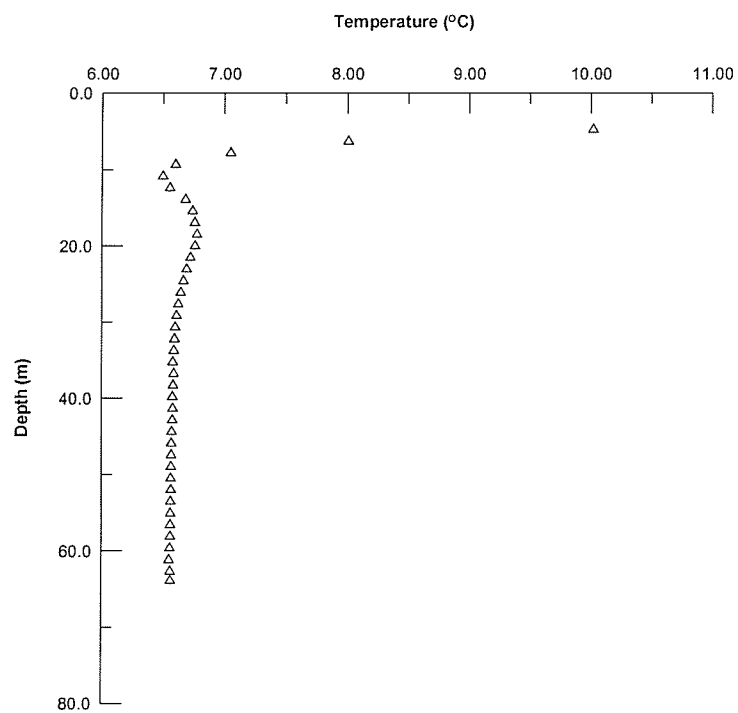
G05OH031 Giroux 1 August 2000
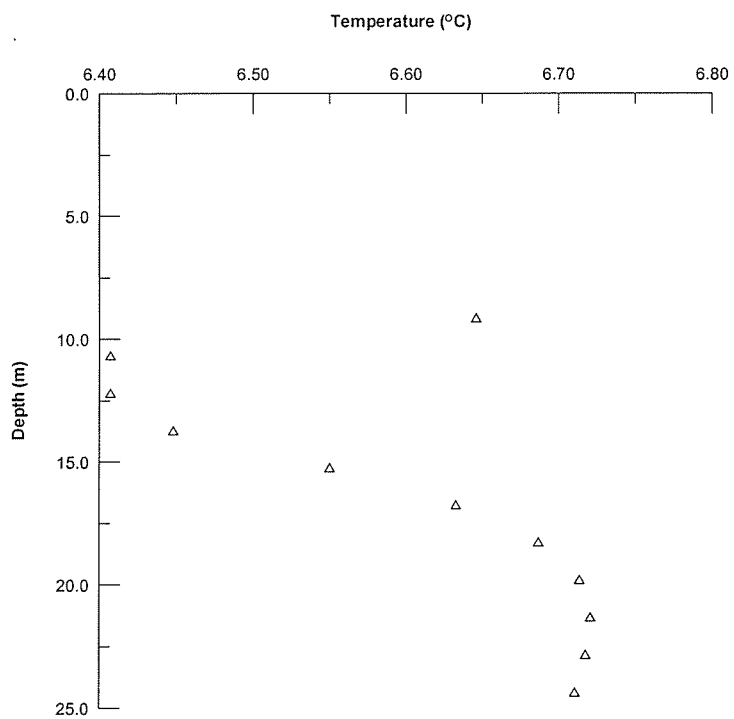
G05OE004 Pansy1 August 2000
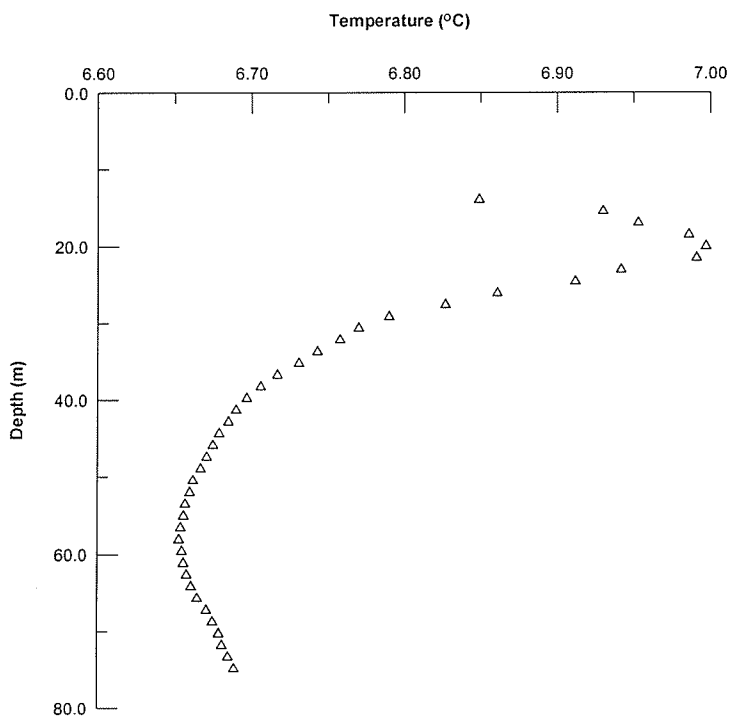
G05OH020 East of La Broquerie August 2000
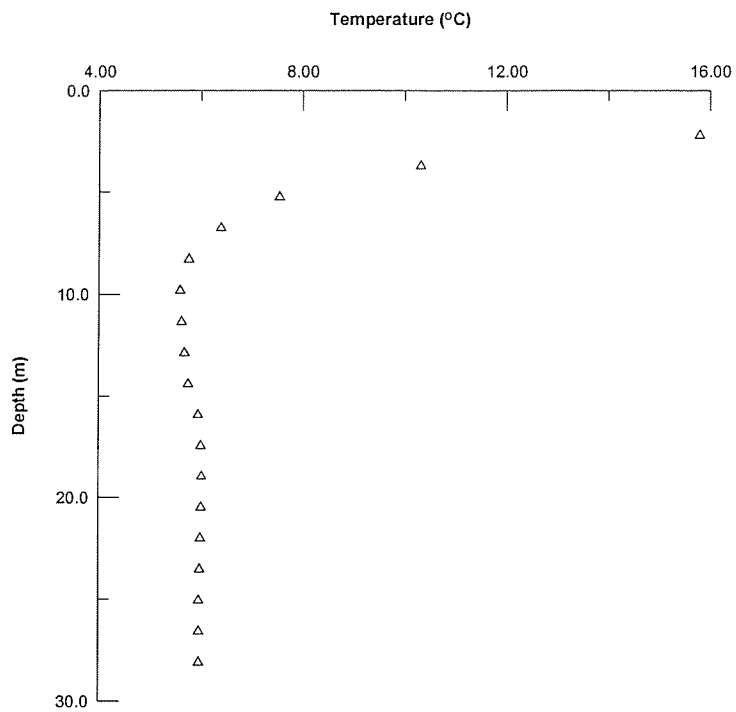
G05SA003 Ross August 2000
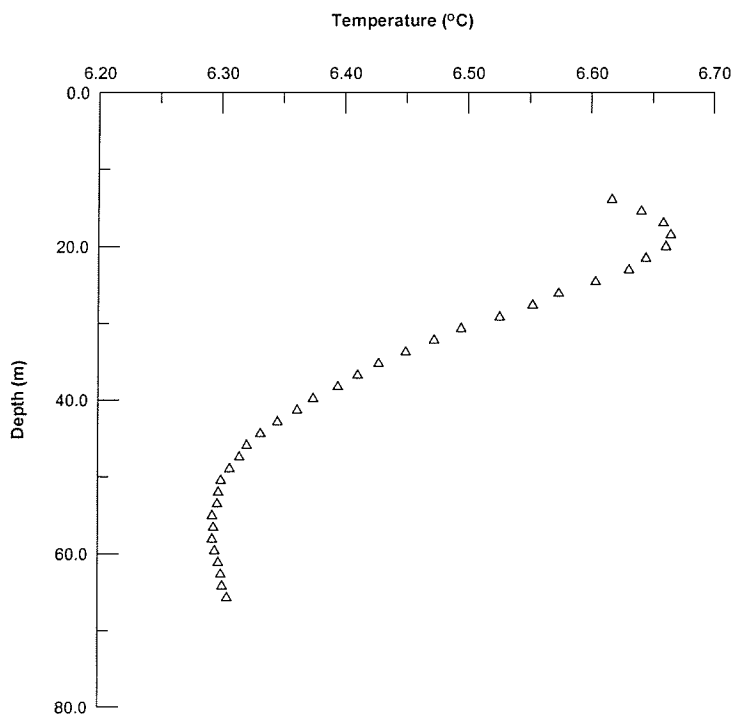
G05OE038 SILA 97-4 August 2000

Appendix B.4 Measured Temperature Profiles Fall 2001
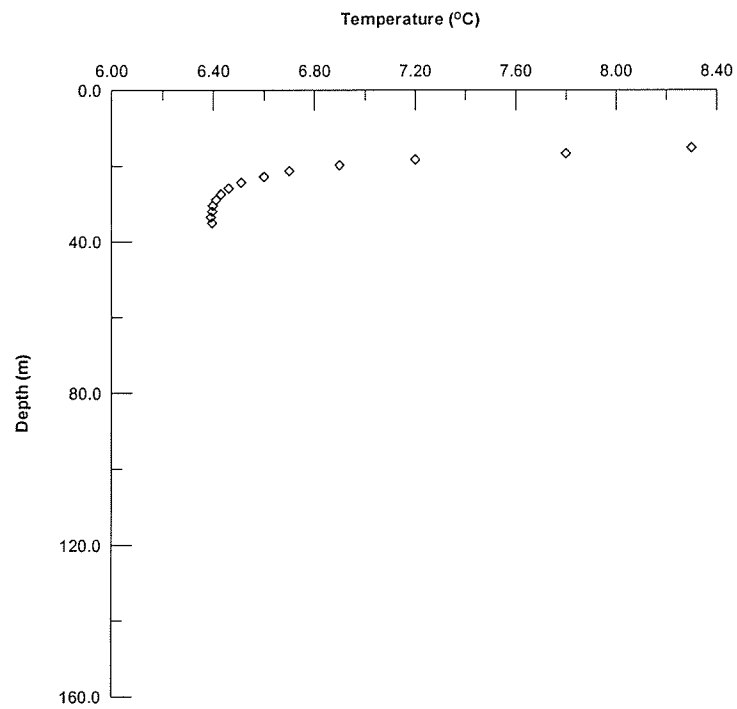
GSC9901 November 2001
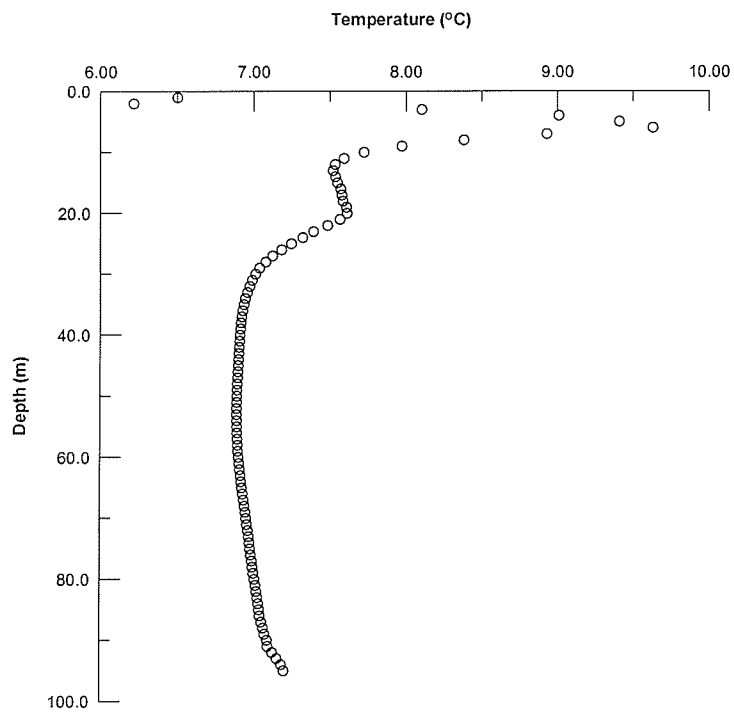
GSC9902 November 2001
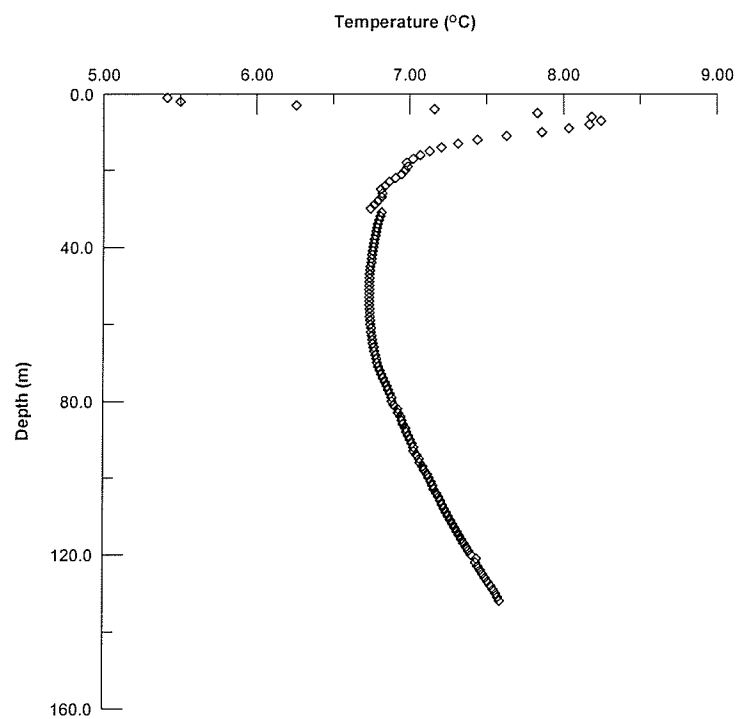
TH1 November 2001
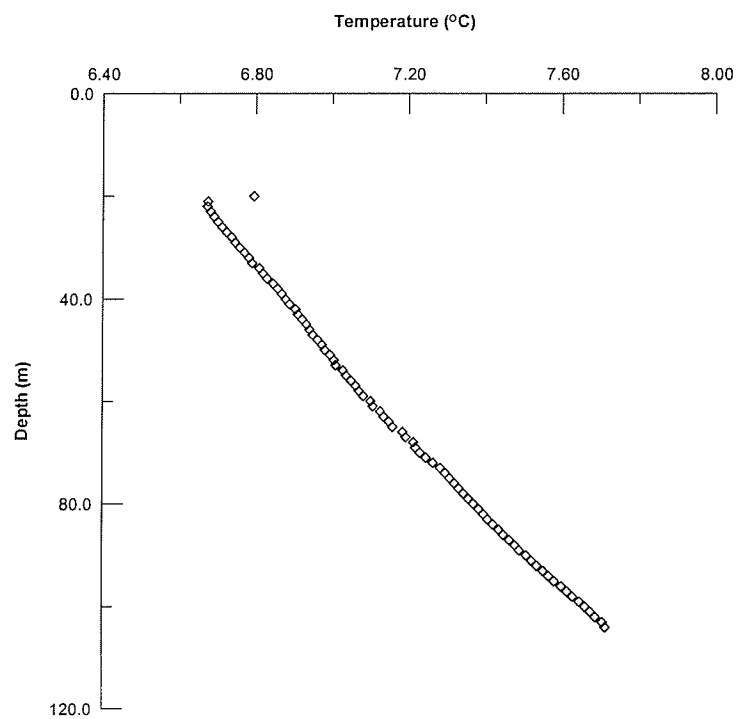
TH2 November 2001

Appendix B.5 Measured Temperature Profiles Summer 2002
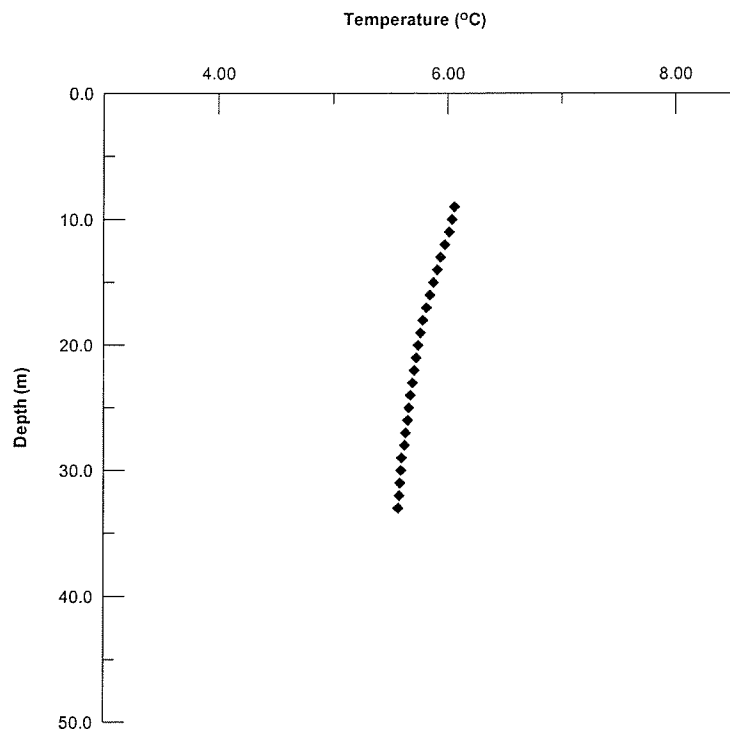
G05OC003 Oak Bluff July 2002
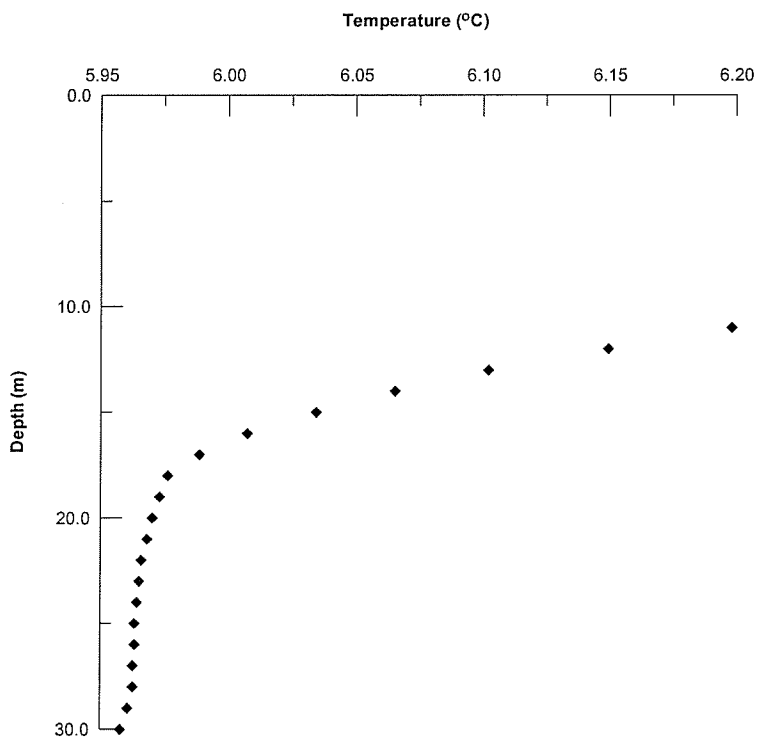
G05OH003 St. Annes Rd RRF 02 July 2002
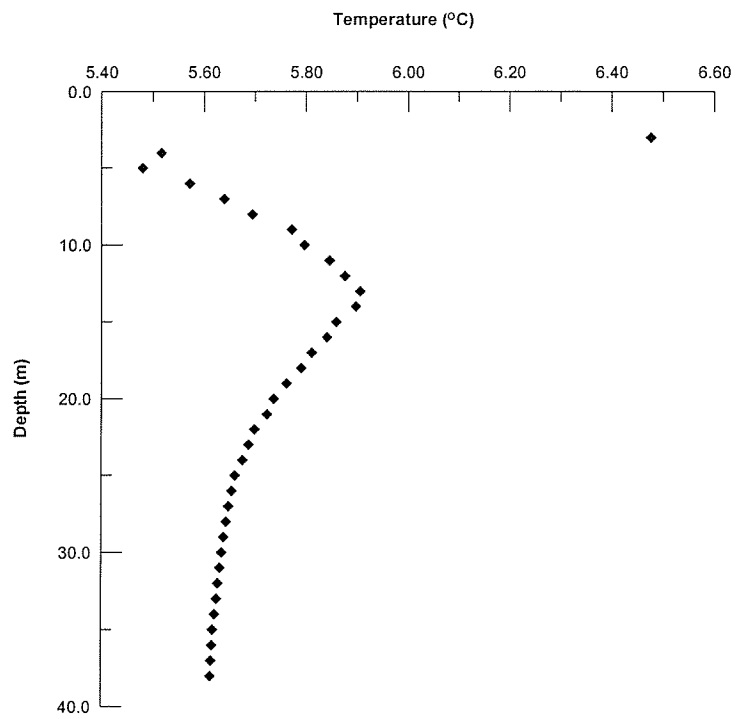
G05OJ022 Route 90 and Hwy 101 August 2002
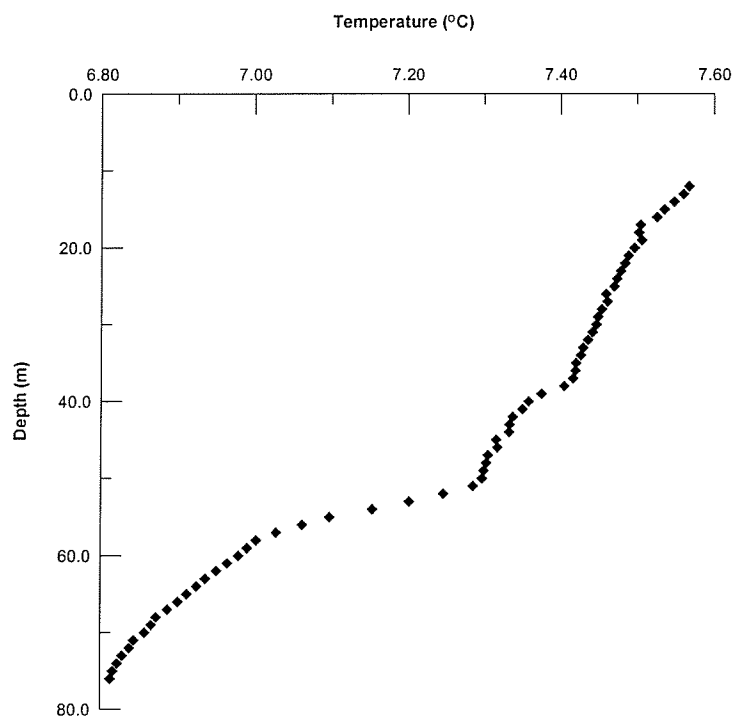
G05MJ077 611 Academy Rd August 2002

Temperature (°C)
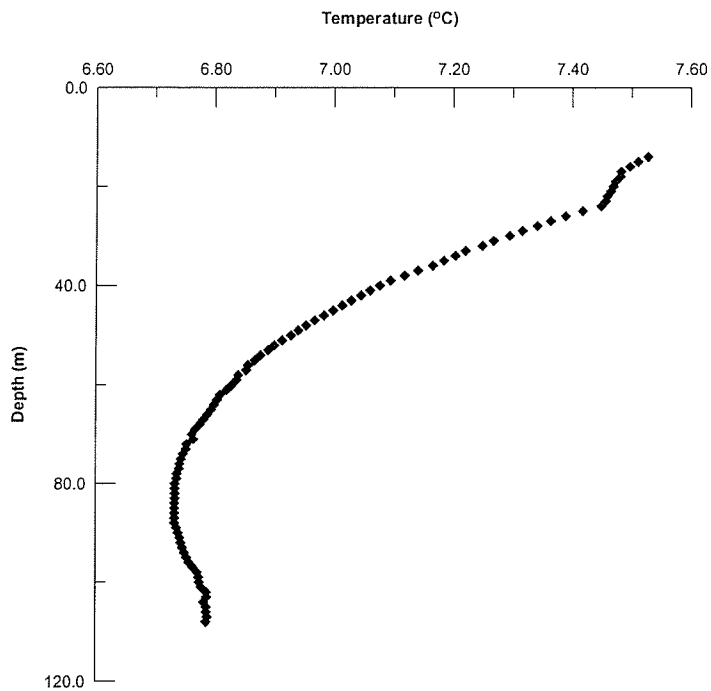
G05OH013 Swift1 July 2002

Temperature (°C)
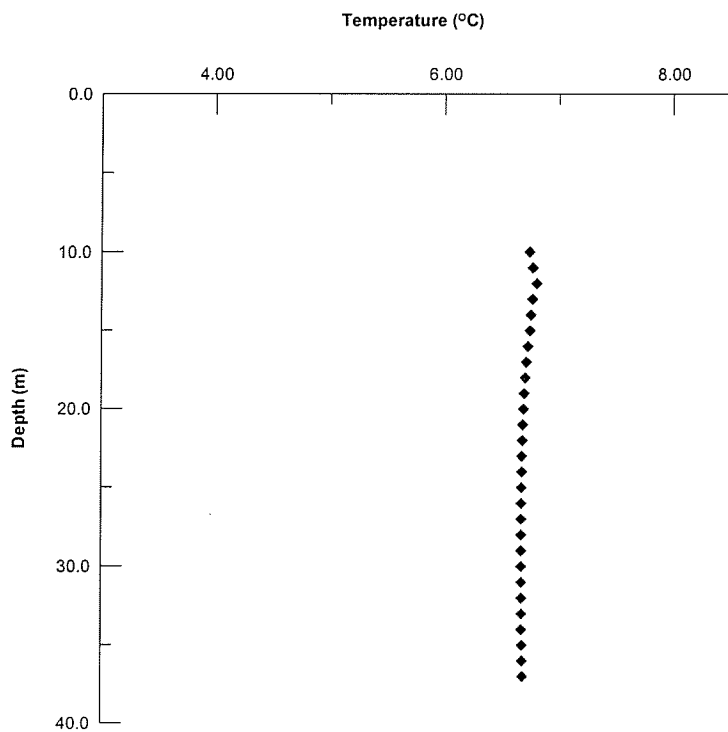
G05MJ006 Assiniboine River and Hwy 100 August 2002
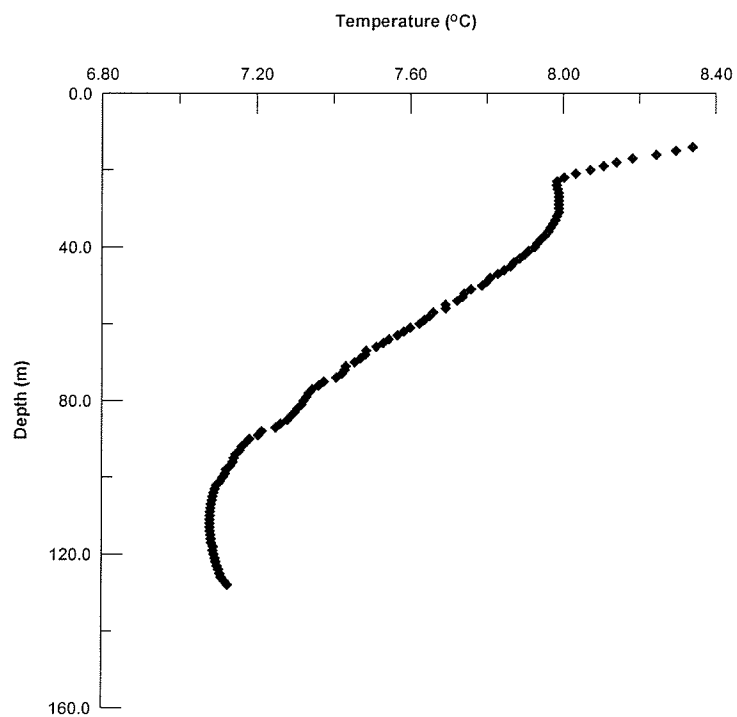
G05OH019 Canada Packers July 2002
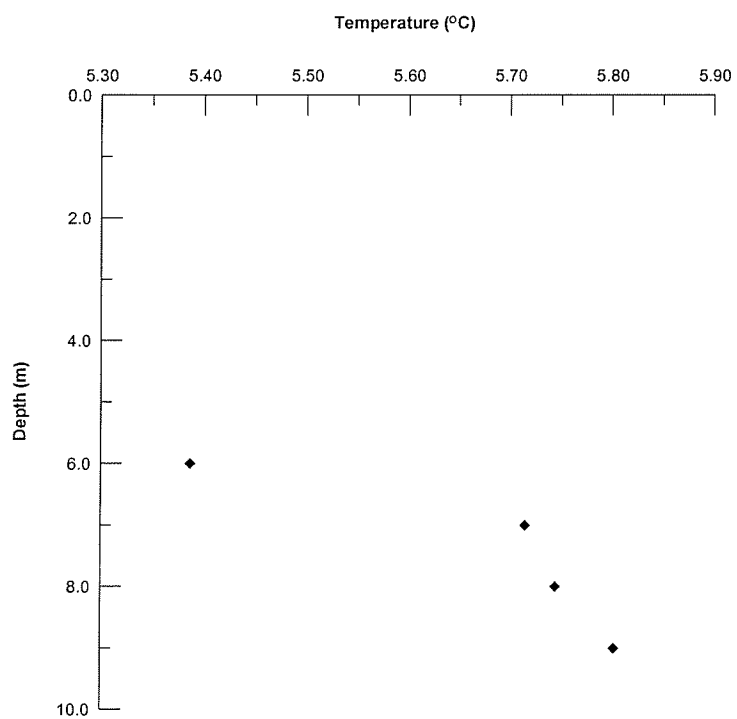
G05MJ008 Sturgeon Creek and Hwy 101 August 2002
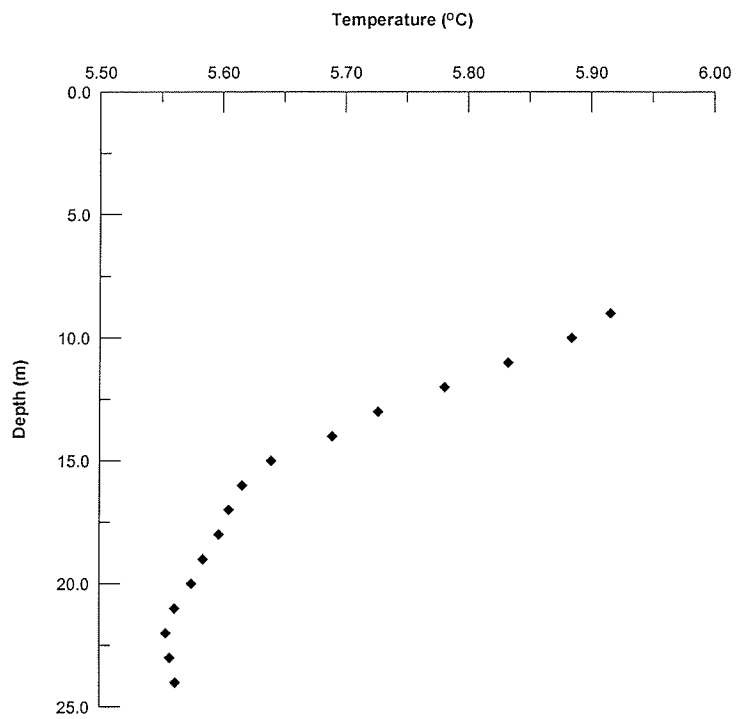
Temperature (°C)

Depth (m)

G05OH010 Murdock Rd and Dugald Rd RRF 055 August 2002

Temperature (°C)

Depth (m)

G05OJ003 Deacon Rd and Cedar Lake Rd August 2002

Temperature (°C)

Depth (m)
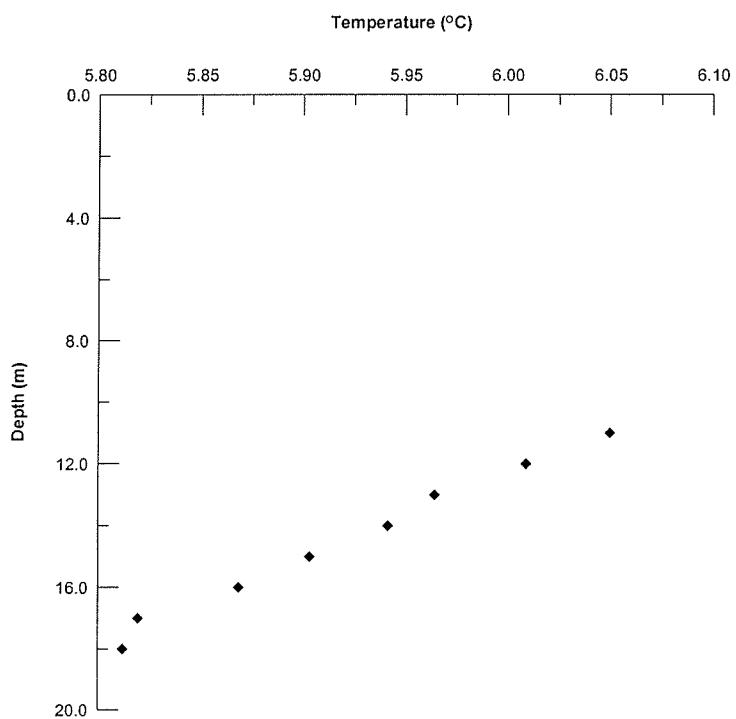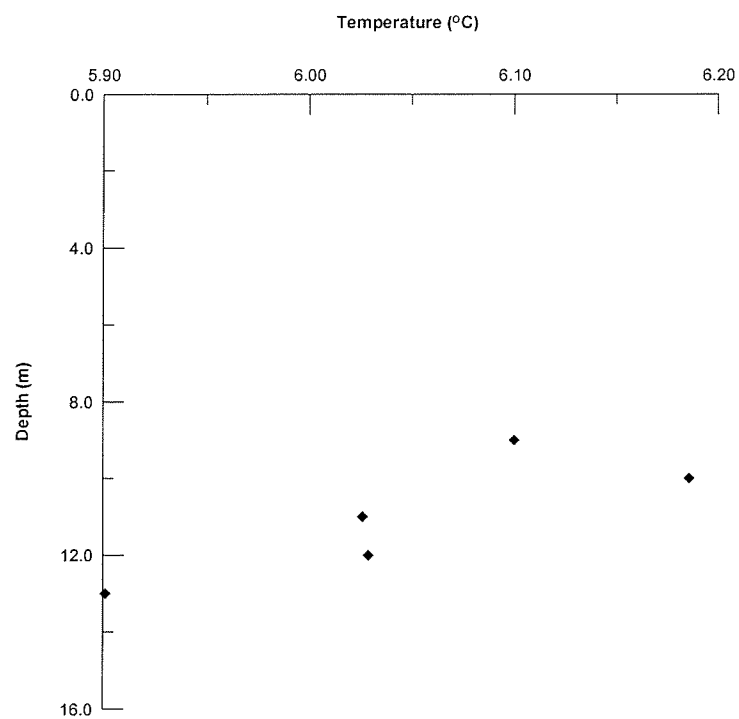
G05OJ103 Grassmere August 2002

Temperature (°C)

Depth (m)
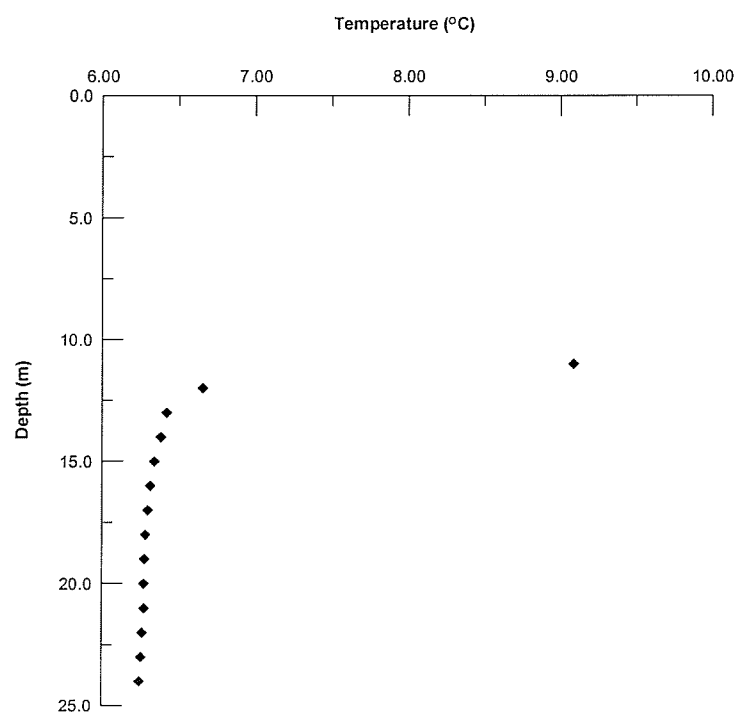
G05OJ009 Grassie Blvd and Hwy 59 RRF 045
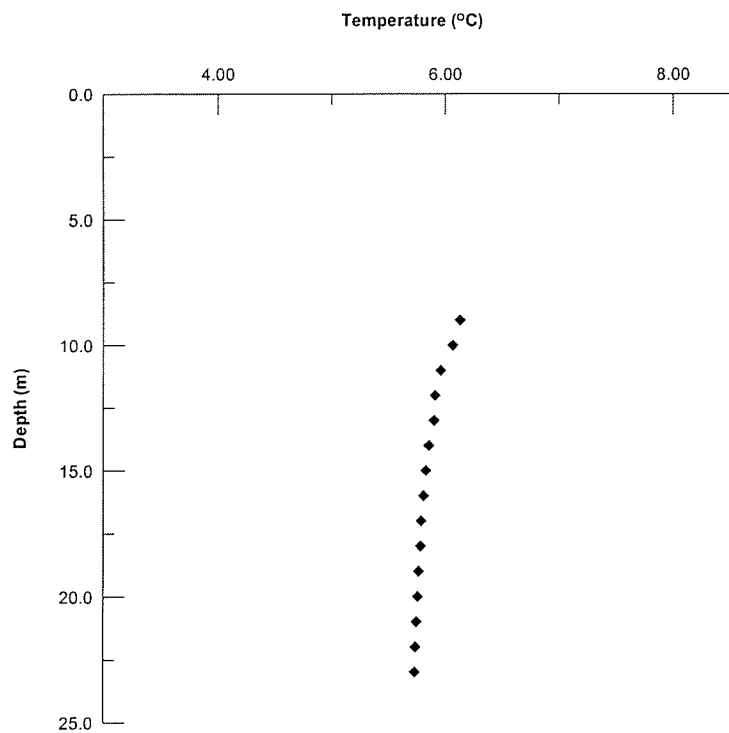
G05OJ014 Gunn Rd RRF 014 July 2002
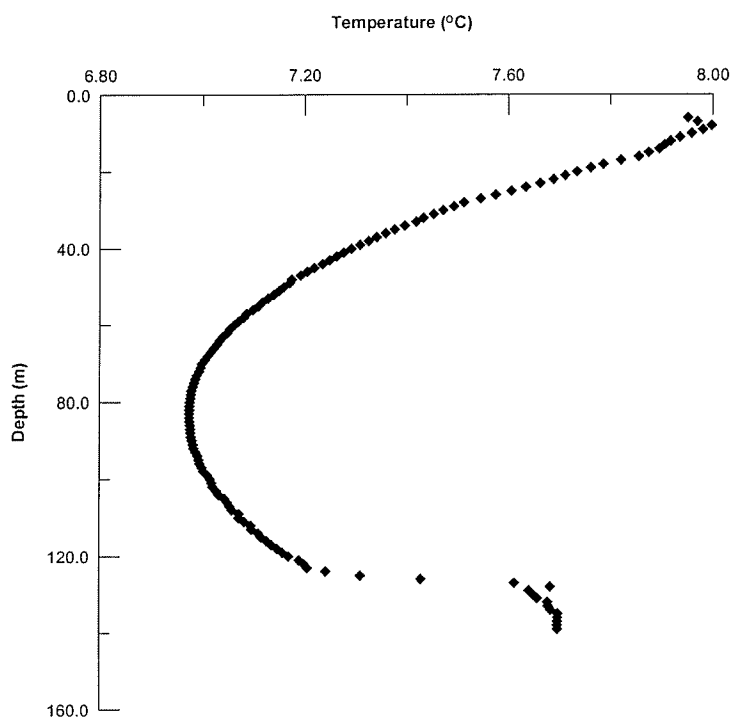
G05OH012 GWWD July 2002
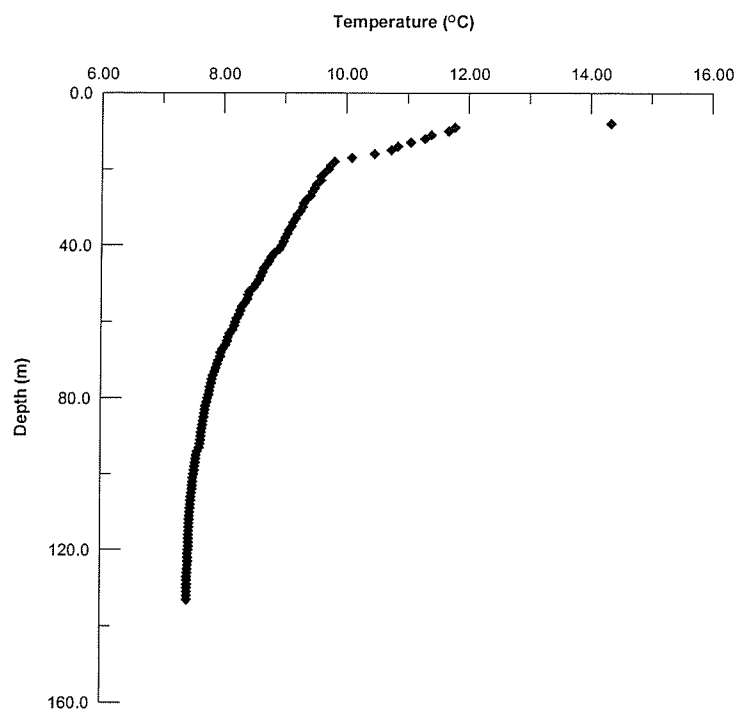
G05OJ028 Hudson Bay House July 2002
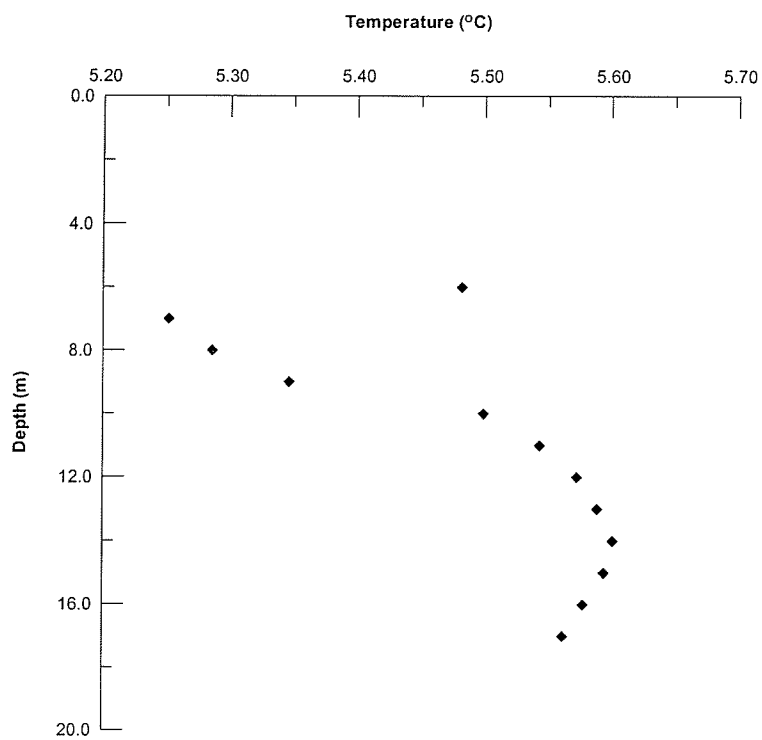
G05MJ009 Inkster Blvd and Hwy 101 August 2002

Temperature (°C)
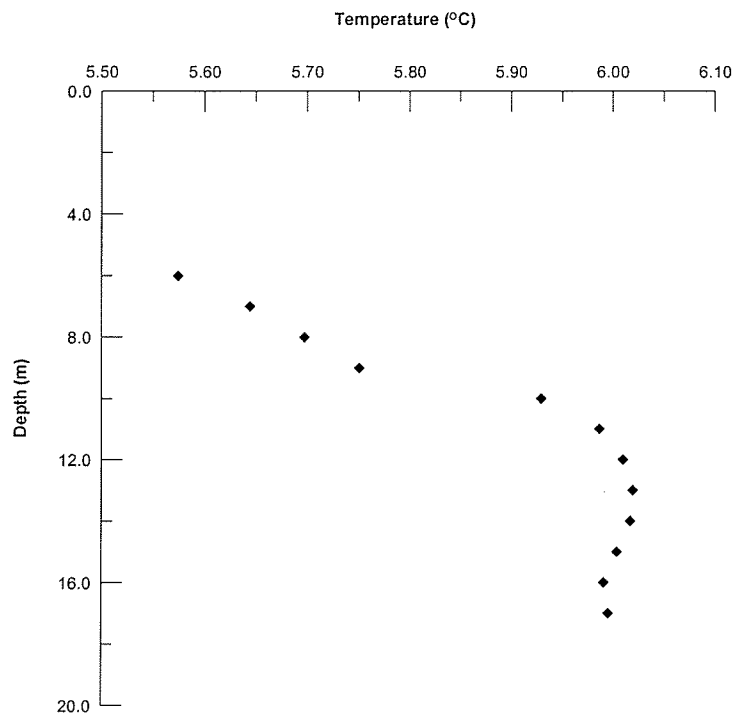
G05MJ005 Wilkes Ave and Hwy 100 July 2002

Temperature (°C)
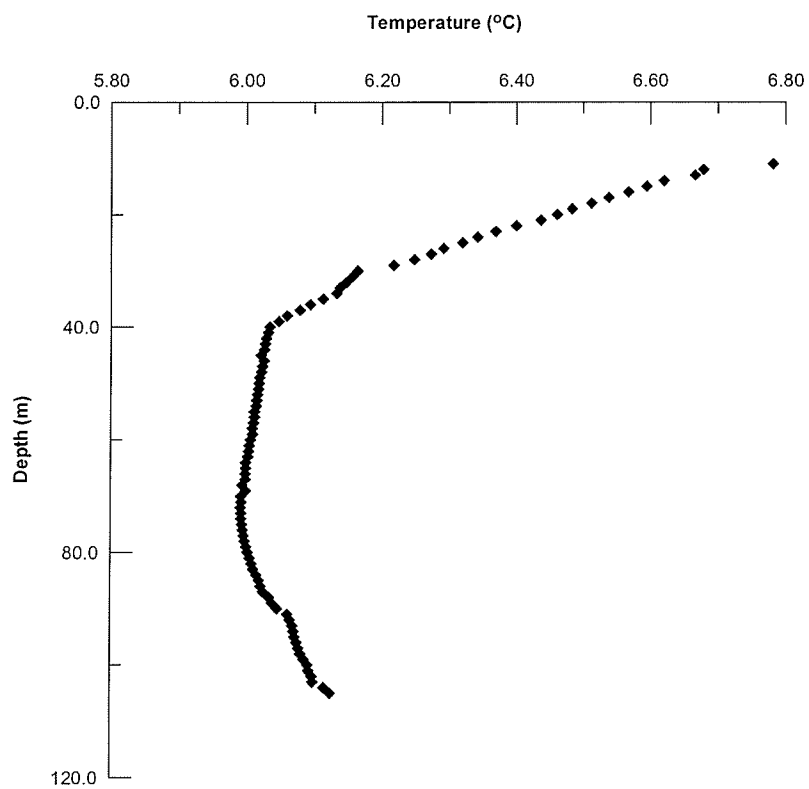
G05MJ076 Grace Hospital August 2002

388
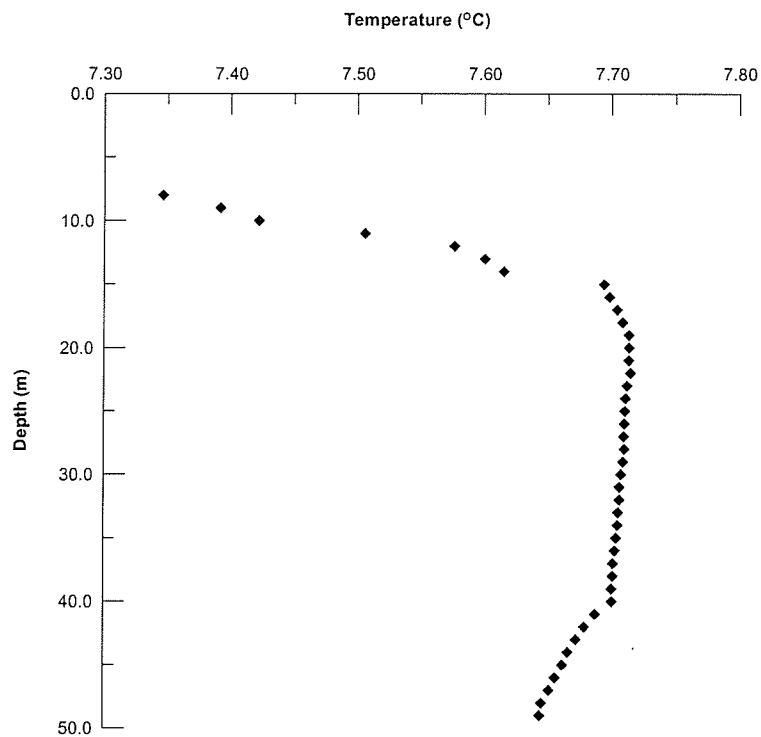
G05OC003 Norwood Bridge August 2002
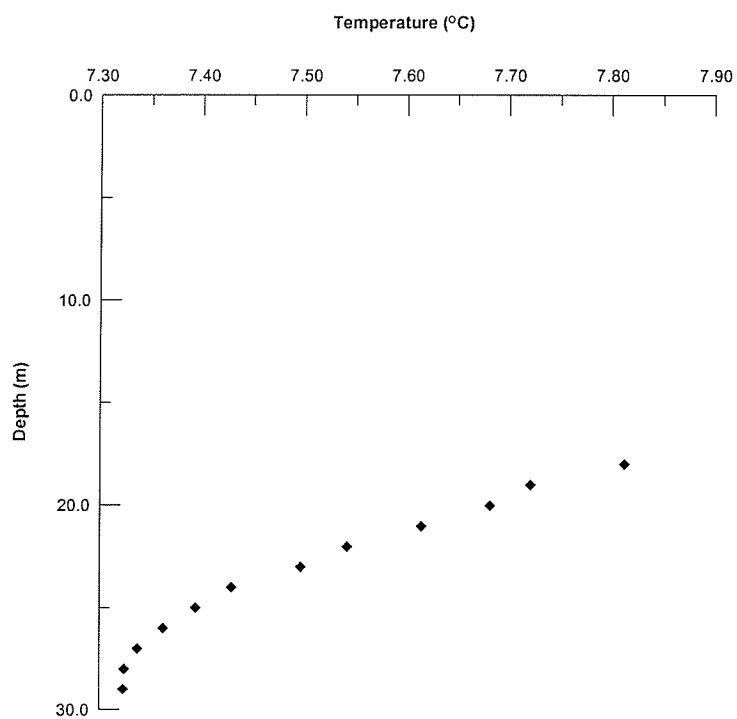
G05OC008 Taylor Ave July 2002
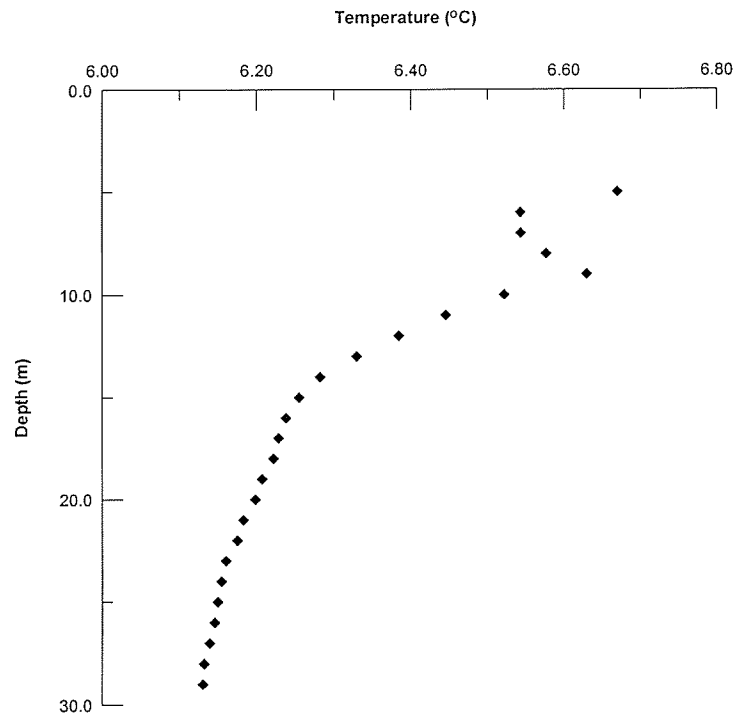
G05OC001 St. Mary's Rd and Floodway Inlet Structure RRF 040 June 2002
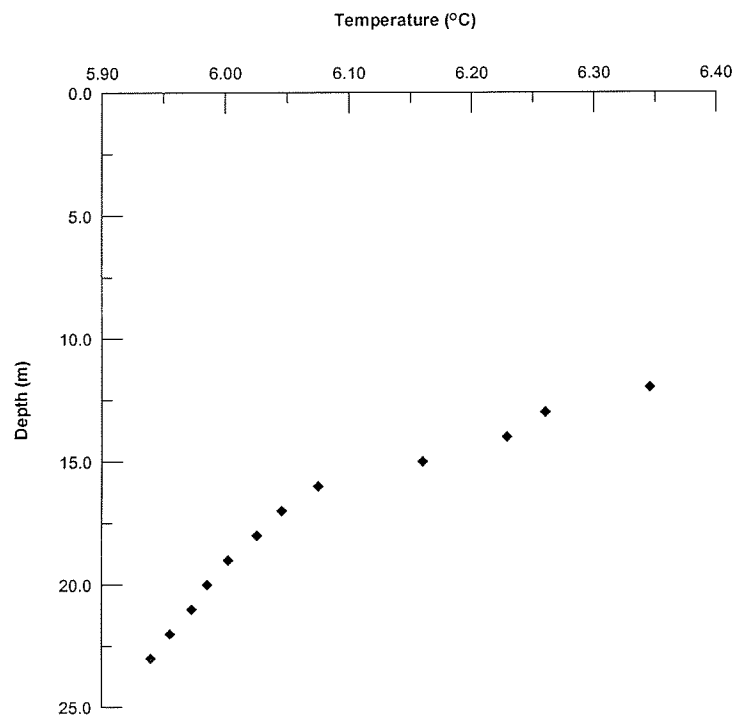
G05OH005 Symington Rd and Hwy 1 RRF 043 July 2002

Temperature (°C)

Depth (m)
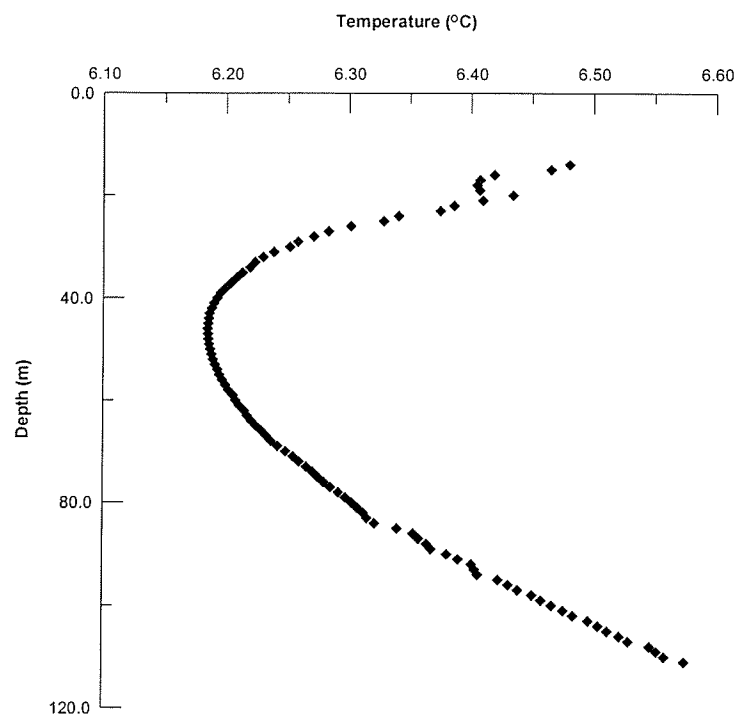
G05OJ092 Riverside Quarries June 2002

Temperature (°C)

Depth (m)
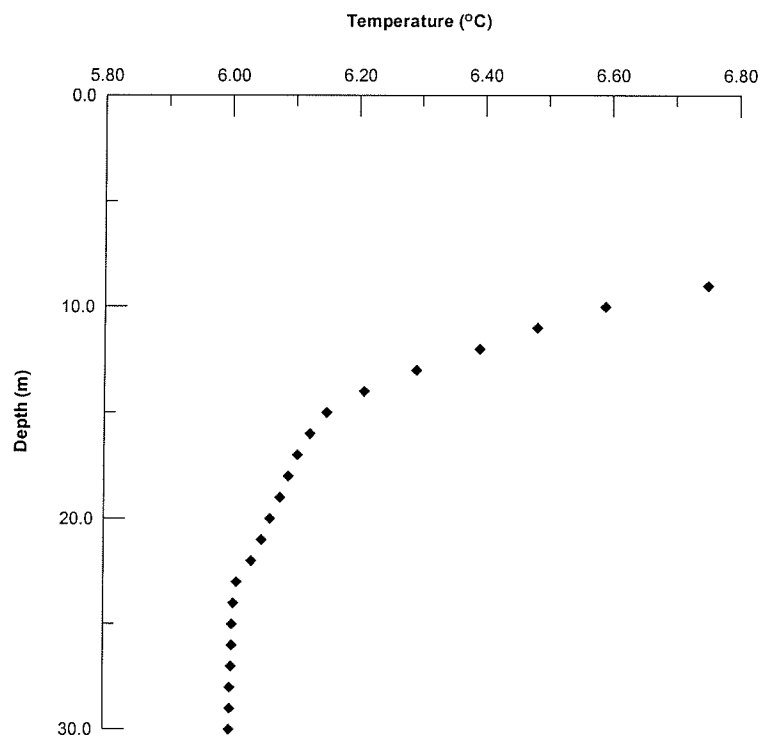
UM2 University Stadium March 2002
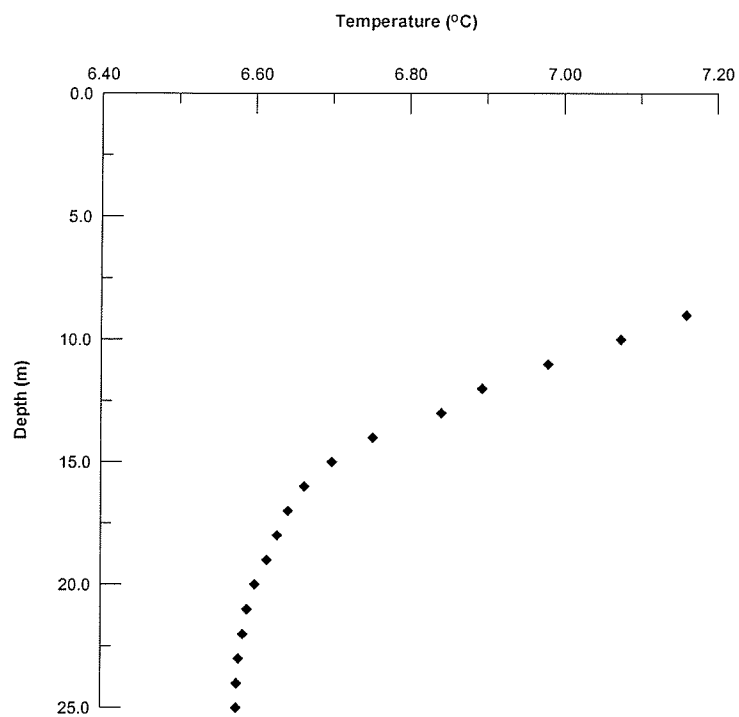
G050OC022 St. Mary's Rd north of Hwy 100 June 2002
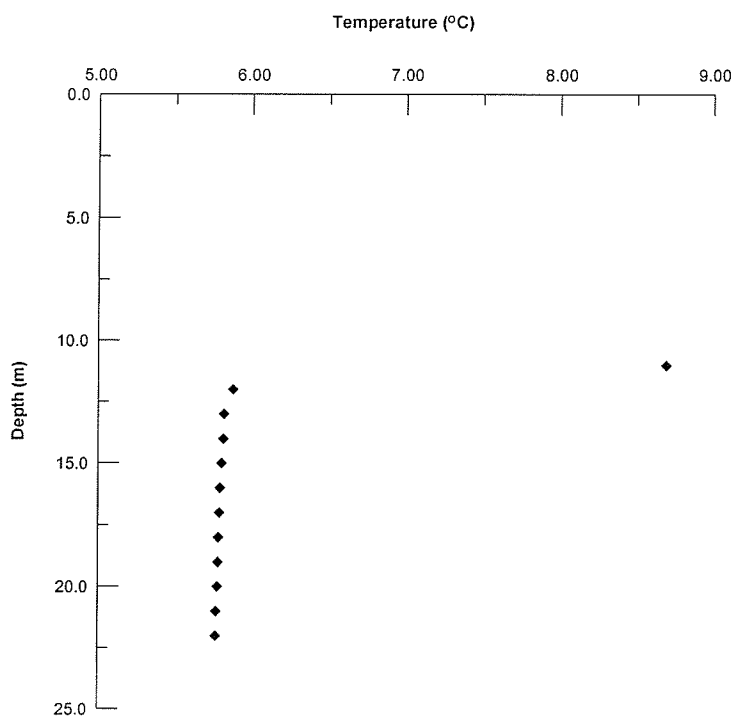
G05OJ004 CNR Keewatin Bridge August 2002

Temperature (°C)
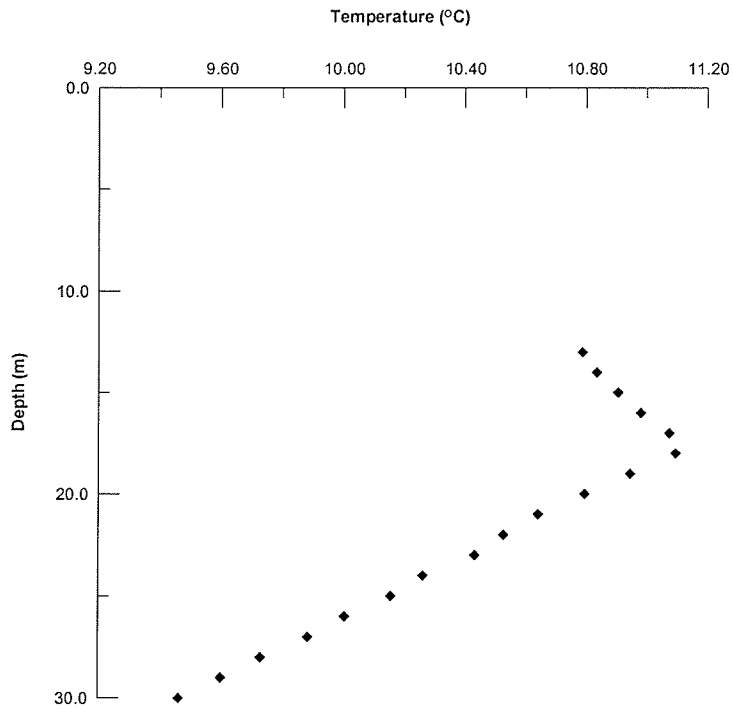
GF1 Dawson Rd and Dugald Rd June 2002

Temperature (°C)
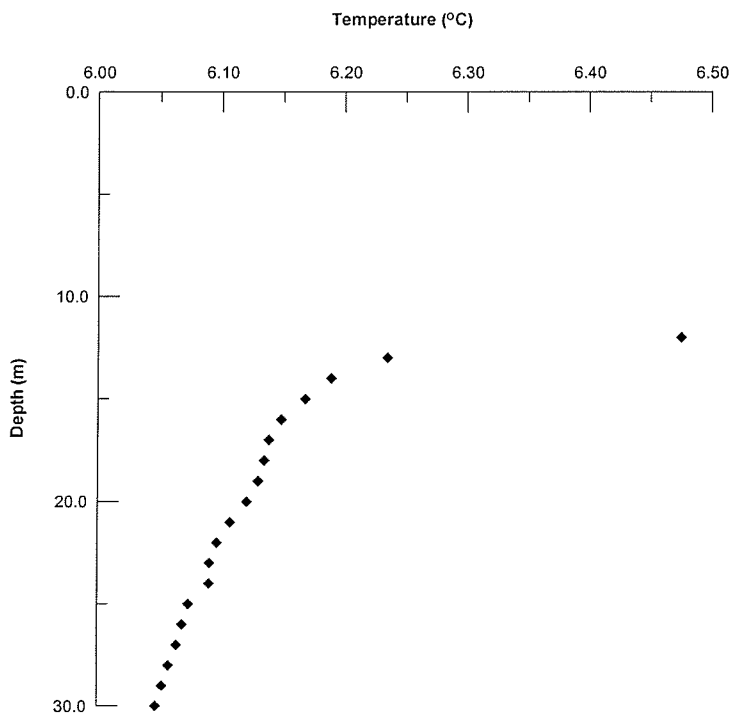
GF2 Maginot St June 2002
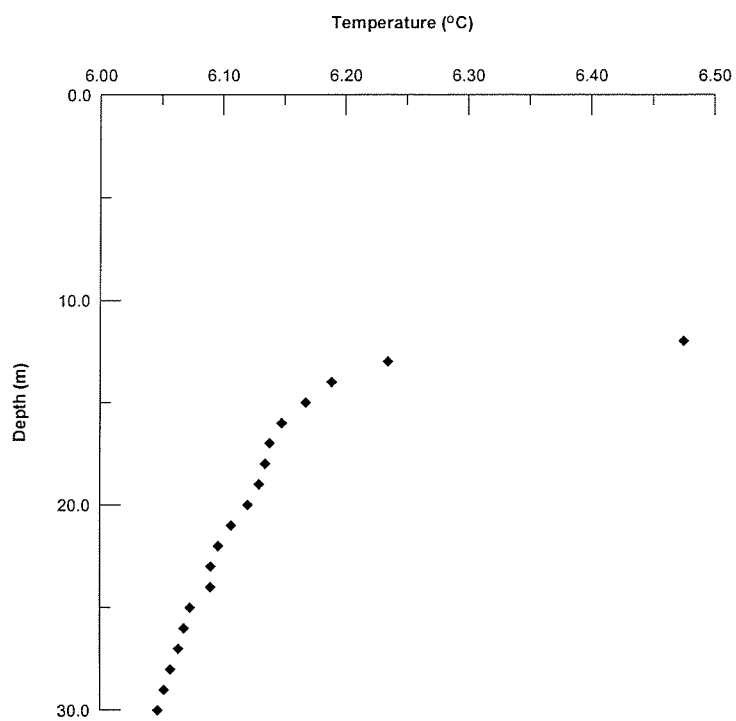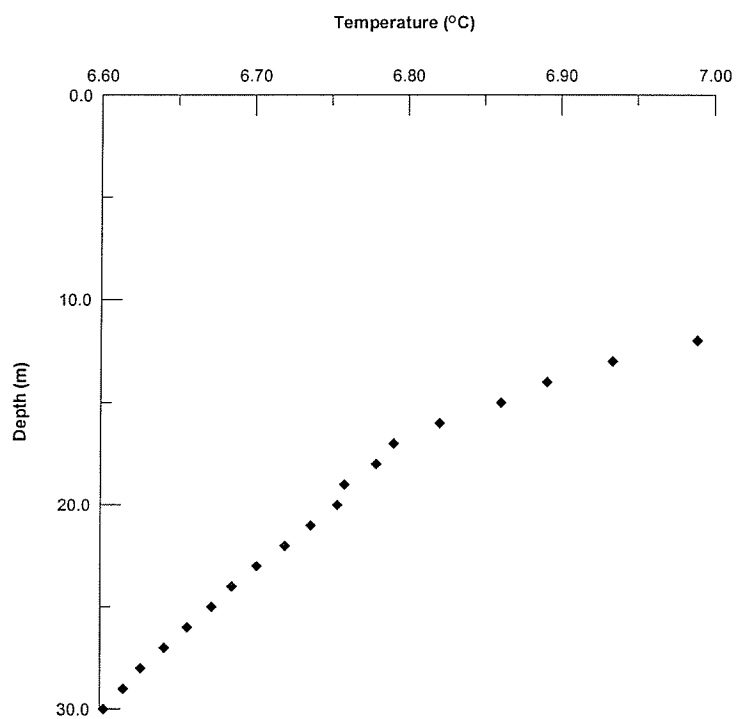
GF3 Goulet St July 2002
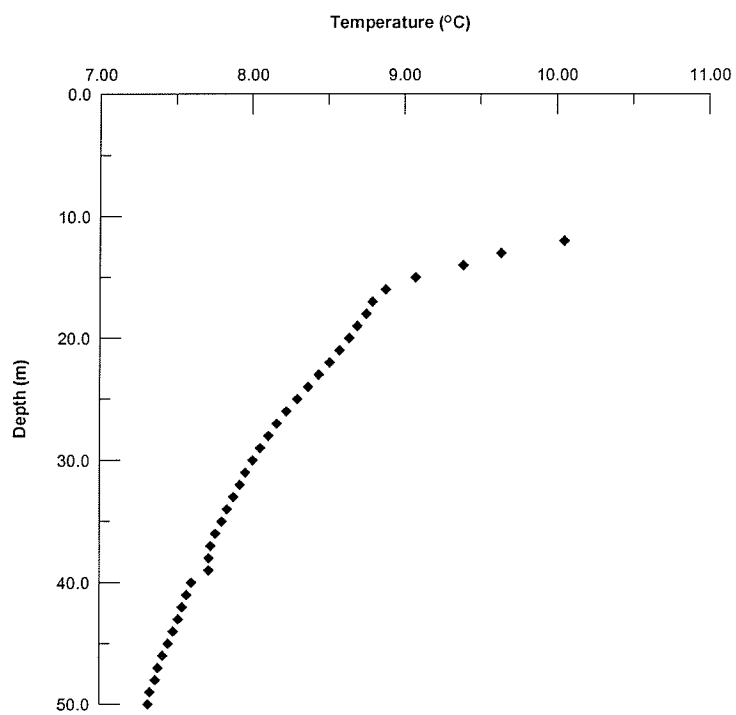
GF4 Des Meurons St July 2002
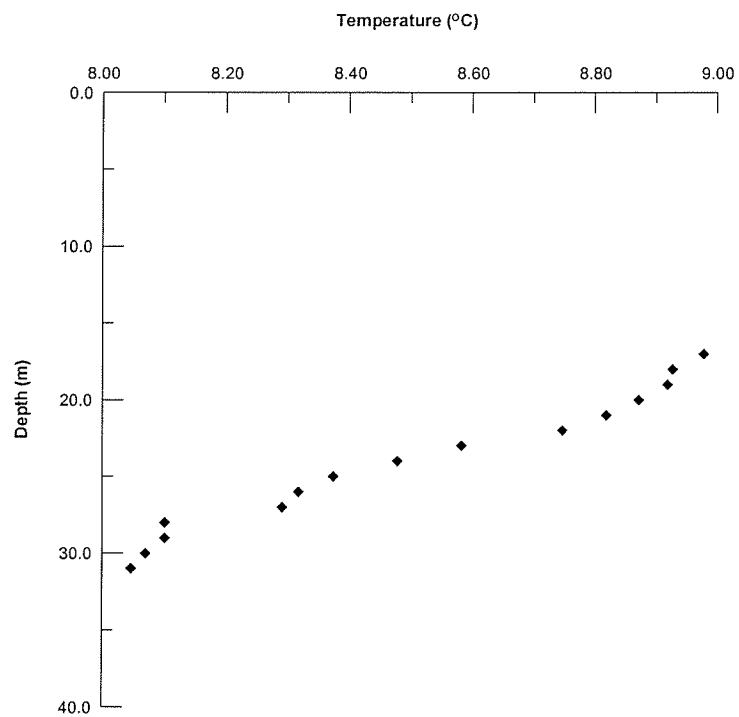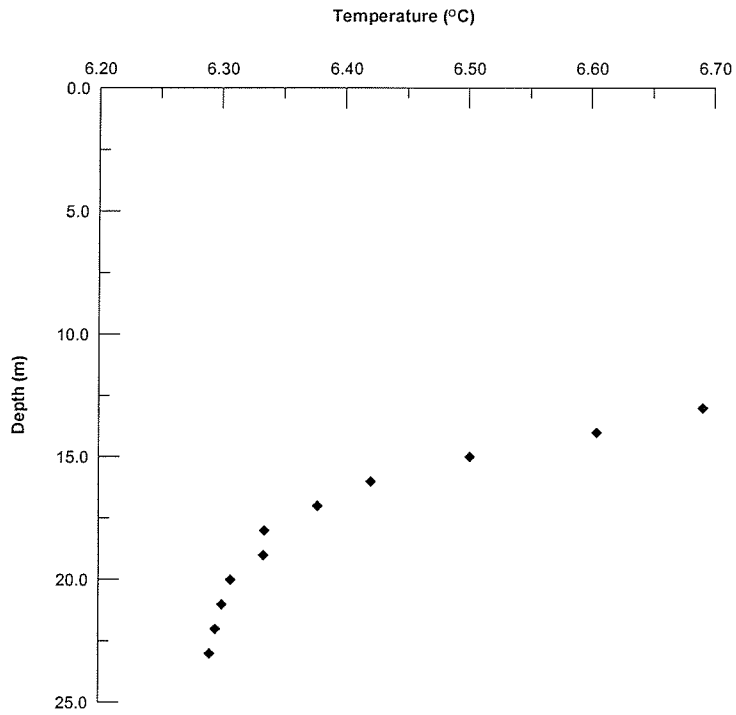
GF5 Olive St July 2002
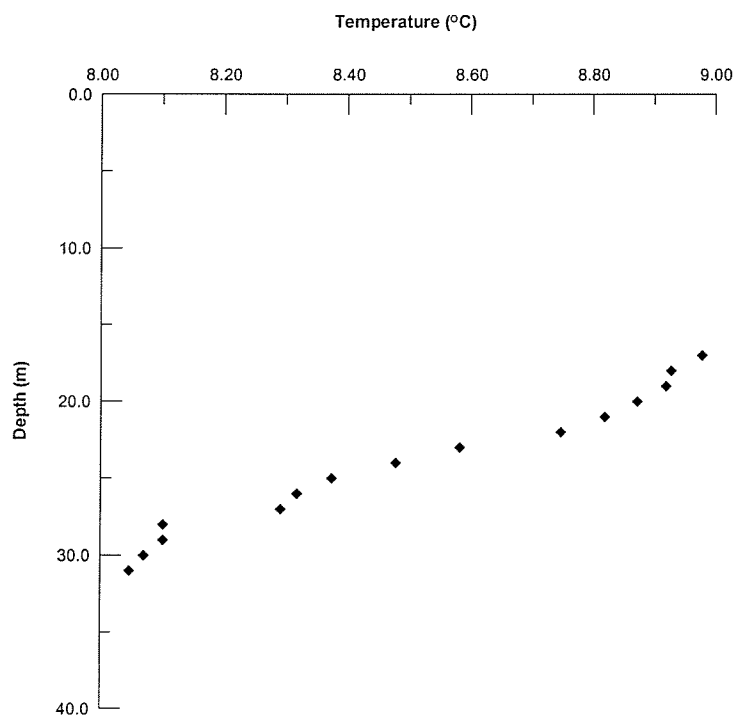
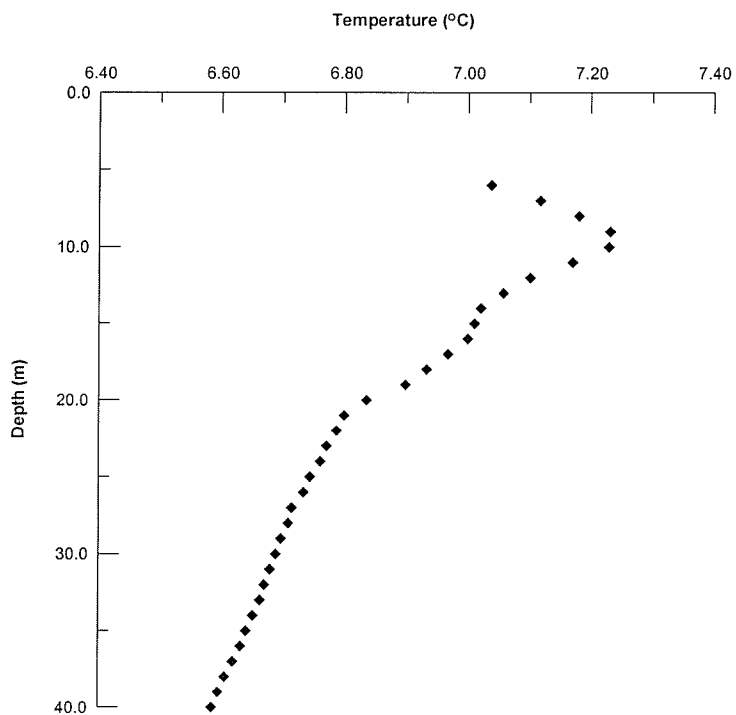GF6 McPhillips St and Selkirk Ave July 2002
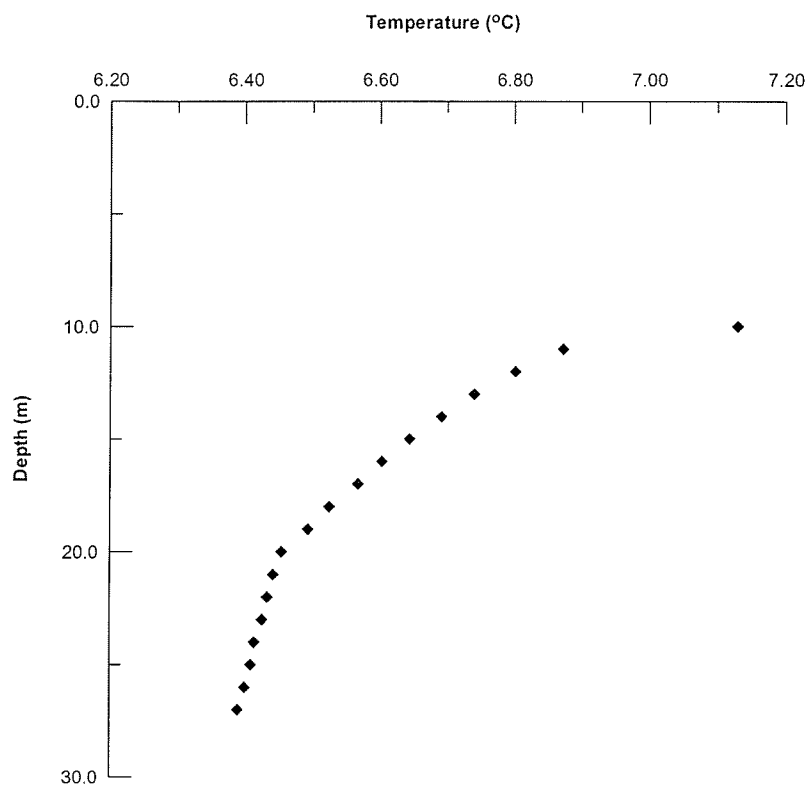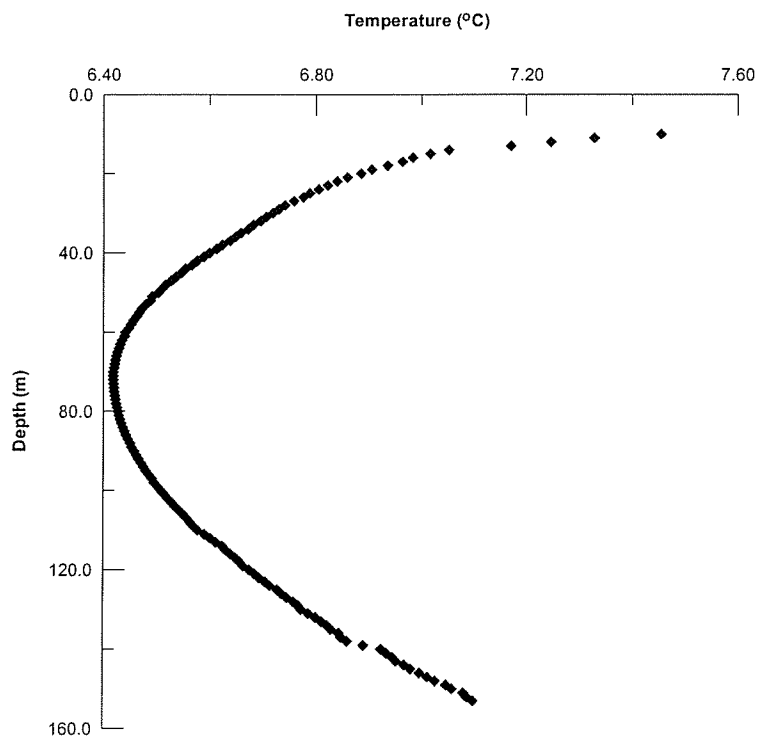
GF7 St. Anne's Rd June 2002

GF8 McGillivray Blvd August 2002

G05OH004 Mazenod Rd north of Symington Yard August 2002

G05OJ025 McPhillips Pumping Station July 2002

G05OJ026 McPhillips Pumping Station July 2002